frontiers | Research Topics

Mechanism and pharmacodynamic material basis of neurodegenerative disease therapies

Edited by
Zhi Sun, Erxi Wu and Yi Wang

Published in
Frontiers in Pharmacology
Frontiers in Neuroscience

ISSN 1664-8714
ISBN 978-2-8325-3166-2
DOI 10.3389/978-2-8325-3166-2

About Frontiers

Frontiers is more than just an open access publisher of scholarly articles: it is a pioneering approach to the world of academia, radically improving the way scholarly research is managed. The grand vision of Frontiers is a world where all people have an equal opportunity to seek, share and generate knowledge. Frontiers provides immediate and permanent online open access to all its publications, but this alone is not enough to realize our grand goals.

Frontiers journal series

The Frontiers journal series is a multi-tier and interdisciplinary set of open-access, online journals, promising a paradigm shift from the current review, selection and dissemination processes in academic publishing. All Frontiers journals are driven by researchers for researchers; therefore, they constitute a service to the scholarly community. At the same time, the *Frontiers journal series* operates on a revolutionary invention, the tiered publishing system, initially addressing specific communities of scholars, and gradually climbing up to broader public understanding, thus serving the interests of the lay society, too.

Dedication to quality

Each Frontiers article is a landmark of the highest quality, thanks to genuinely collaborative interactions between authors and review editors, who include some of the world's best academicians. Research must be certified by peers before entering a stream of knowledge that may eventually reach the public - and shape society; therefore, Frontiers only applies the most rigorous and unbiased reviews. Frontiers revolutionizes research publishing by freely delivering the most outstanding research, evaluated with no bias from both the academic and social point of view. By applying the most advanced information technologies, Frontiers is catapulting scholarly publishing into a new generation.

What are Frontiers Research Topics?

Frontiers Research Topics are very popular trademarks of the *Frontiers journals series*: they are collections of at least ten articles, all centered on a particular subject. With their unique mix of varied contributions from Original Research to Review Articles, Frontiers Research Topics unify the most influential researchers, the latest key findings and historical advances in a hot research area.

Find out more on how to host your own Frontiers Research Topic or contribute to one as an author by contacting the Frontiers editorial office: frontiersin.org/about/contact

Mechanism and pharmacodynamic material basis of neurodegenerative disease therapies

Topic editors

Zhi Sun — First Affiliated Hospital of Zhengzhou University, China
Erxi Wu — Baylor Scott and White Health, United States
Yi Wang — Zhejiang University, China

Citation

Sun, Z., Wu, E., Wang, Y., eds. (2023). *Mechanism and pharmacodynamic material basis of neurodegenerative disease therapies*. Lausanne: Frontiers Media SA.
doi: 10.3389/978-2-8325-3166-2

Table of contents

frontiers | Frontiers in Neuroscience

TYPE Editorial
PUBLISHED 21 July 2023
DOI 10.3389/fnins.2023.1254881

OPEN ACCESS

EDITED AND REVIEWED BY
Nicholas M. Barnes,
University of Birmingham, United Kingdom

*CORRESPONDENCE
Erxi Wu
✉ Erxi.Wu@BSWHealth.org

RECEIVED 07 July 2023
ACCEPTED 11 July 2023
PUBLISHED 21 July 2023

CITATION
Wu E, Ke R, Qi D and Huang JH (2023) Editorial: Mechanism and pharmacodynamic material basis of neurodegenerative disease therapies. *Front. Neurosci.* 17:1254881. doi: 10.3389/fnins.2023.1254881

Editorial: Mechanism and pharmacodynamic material basis of neurodegenerative disease therapies

Erxi Wu[1,2,3,4]*, Ronghu Ke[1], Dan Qi[1] and Jason H. Huang[1,2,5]

[1]Department of Neurosurgery and Neuroscience Institute, Baylor Scott and White Health, Temple, TX, United States, [2]Department of Medical Education, Texas A&M University School of Medicine, Temple, TX, United States, [3]Department of Pharmaceutical Science, Texas A&M University School of Pharmacy, College Station, TX, United States, [4]Department of Oncology, Livestrong Cancer Institutes, Dell Medical School, The University of Texas at Austin, Austin, TX, United States, [5]Department of Neurosurgery, Baylor College of Medicine, Temple, TX, United States

KEYWORDS

neurodegenerative disease, Alzheimer's disease, Parkinson's disease, therapies, natural compounds, metabolism, multiomics

Editorial on the Research Topic
Mechanism and pharmacodynamic material basis of neurodegenerative disease therapies

Neurodegenerative disorders exert a profound global impact, causing a gradual deterioration of the nervous system and leading to the progressive loss of neurons. These conditions disrupt vital communication pathways, resulting in impaired cognition, memory, behavior, sensory perception, and motor function (Wilson et al., 2023). The high prevalence of neurodegenerative diseases, such as Alzheimer's disease (AD) and Parkinson's disease (PD), among the aging population underscores the urgent need for effective treatments. Currently, available treatments for neurodegeneration are limited or non-existent, imposing significant socioeconomic and personal burdens.

In recent years, the emergence of "omic" approaches, such as genomics, transcriptomics, epigenomics, and metabolomics, has provided unprecedented insights into the understanding of neurodegenerative diseases (Badhwar et al., 2020). Despite these advancements, therapeutic interventions capable of curing these conditions are still lacking. Therefore, it is imperative to actively pursue new drug candidates and effective treatment strategies. The primary focus of this Research Topic is to utilize "omics" in studying biomarkers, pathogenesis, and disease progression, while also identifying novel therapeutic targets for neurodegenerative diseases and related conditions. This issue accepted 10 exceptional papers, including original research articles and reviews. Through these contributions, we aim to shed light on the latest advancements and discoveries in the field, fostering a deeper understanding of neurodegenerative diseases and providing a platform for the development of novel treatment modalities.

Exploring potential therapeutic natural compounds for neurodegenerative diseases such as AD

Currently, effective therapies for neurodegenerative diseases such as AD remain elusive. AD is the most prevalent neurodegenerative disorder and the leading cause of dementia among the elderly (Alzheimer's Association, 2023). Clinical treatment of AD focuses primarily on syndrome control and lacks effective therapy. Although the recent approval of two drugs, aducanumab and lecanemab, by the United States FDA for treating AD has sparked controversy, there is growing interest in exploring natural compounds as a promising avenue for AD treatment (Zhang et al., 2012; Xia et al., 2017). An important aspect of this issue is the significant number of studies dedicated to investigating novel approaches for the treatment of AD, with a particular emphasis on utilizing natural compounds. These studies delve into the exploration of alternative therapeutic strategies, aiming to identify potential interventions that harness the power of nature. By dedicating considerable attention to this aspect, this issue contributes to the growing body of research dedicated to advancing AD treatment through the exploration of natural compounds.

Zhou et al. investigated the therapeutic effects of Alpiniae oxyphyllae Fructus (AOF) on AD using metabolomics. They found that treatment with AOF in APP/PS1 transgenic mice with AD reversed significant alterations in 31 metabolites in plasma, including notable changes in bile acids, indicating the potential of AOF to ameliorate AD symptoms by modulating bile acid metabolism and highlighting the need for further research into its therapeutic mechanisms.

Liu et al. found that Ginkgo biloba L. leaf extract (GBLE) reversed the significant alterations in 60 metabolites observed in APP/PS1 mice with AD, similar to the response seen with donepezil, an established AD medication. This suggests that GBLE restores lipid metabolic balance and may contribute to its neuroprotective effects in AD treatment, providing insights into AD pathogenesis and the therapeutic potential of GBLE.

Li et al. demonstrated that total saikosaponins (TS) from Radix bupleuri (Chaihu) improved cognitive function, reduced amyloid-beta (Aβ) generation and plaque deposition, enhanced autophagy, downregulated β-secretase 1 (BACE1), nuclear factor-κB (NF-κB), and inflammatory factors, activated nuclear factor 2 (Nrf2), and potentially regulated gut microbiota while alleviating oxidative stress, suggesting TS as a potential therapeutic strategy for AD pending further investigation into the underlying mechanisms.

Wang et al. investigated the therapeutic effect and mechanism of Anemarrhenae Rhizoma (AR) on AD using a rat model induced by D-galactose and aluminum chloride ($AlCl_3$). Metabolomics analysis using mass spectrometry identified 32 significantly affected metabolites in the serum, indicating the influence of AR on various metabolic pathways. The findings from behavior studies, histopathological observations, and biochemical analyses supported the therapeutic potential of AR in AD prevention and treatment, providing valuable insights into its therapeutic mechanism.

Wu et al. identified phenylpropanoid sucrose esters from Fallopia dentatoalata that exhibited moderate inhibitory effects against acetylcholinesterase (AChE) and potential inhibitory effects against butyrylcholinesterase (BuChE), with certain compounds acting as non-competitive inhibitors of AChE and others acting as competitive inhibitors of BuChE, suggesting their potential as anticholinesterase therapeutics for AD.

Song et al. investigated the protective effects of matrine (MAT) on retinal ganglion cells (RGCs) in optic neuritis (ON), a condition associated with vision loss and inflammation. The study found that MAT treatment reduced inflammation and demyelination, and promoted RGC survival by upregulating the expression of Sirtuin 1 (SIRT1) and its downstream molecules Nrf2 and PGC-1α, suggesting its potential as a therapeutic intervention for optic neuritis.

Investigating immune infiltration in AD for developing therapeutic targets

Zhang et al. analyzed the immune cell composition in the entorhinal cortex of AD patients and identified 81 immune-related differentially expressed genes. They found decreased lymphocyte scores and increased myeloid cell scores in AD patients and identified 37 genes involved in innate immunity, with eight genes being potential drug targets. These findings provide insights into potential therapeutic targets relevant to the immune components in AD, contributing to the understanding and treatment of the disease.

Highlighting the roles of exosomes in AD development and diagnosis

The review by Zou et al. offers a comprehensive overview of the roles of exosomes in AD, highlighting their involvement in AD development, their potential as biomarkers in various body fluids, and their significance in AD diagnosis and treatment. This review underscores the potential of exosomes as valuable tools for AD diagnosis, treatment, and clinical management of AD-related dementia.

Identifying BAG5 as a potential diagnostic biomarker for PD with the PINK1 R492X mutation

In their study, Fu et al. found lower expression levels of Bcl2-associated athanogene 5 (BAG5) in the skin tissues of PD patients with the R492X PINK1 mutation than healthy controls. They also discovered that BAG5 interacts with the R492X mutated PINK1 protein and

facilitates its degradation through the ubiquitin/proteasome-dependent pathway. These findings highlight the potential of BAG5 as a diagnostic biomarker and provide insights into therapeutic targets for PD patients with the R492X PINK1 mutation.

Targeting ferroptosis for the treatment of ischemic stroke

Wei et al.'s review highlights the role of the neurovascular unit (NVU) in ischemic stroke and underscores ferroptosis as a significant factor in stroke progression and NVU regulation, suggesting that targeting ferroptosis holds promise as a therapeutic strategy to prevent severe brain damage and reduce the risk of neurodegenerative conditions associated with ischemic stroke.

Perspectives

The primary objective of this Research Topic was to provide the scientific community with valuable insights into recent advancements in studying the mechanisms and pharmacodynamic material basis of therapies for neurodegenerative diseases. By doing so, we aimed to contribute to the development of more effective therapeutic strategies, with the ultimate goal of benefiting patients worldwide who are affected by these debilitating conditions. Through this collective effort, we aspire to make significant strides toward improving the lives of individuals suffering from neurodegenerative diseases.

Author contributions

All authors listed have made a substantial, direct, and intellectual contribution to the work and approved it for publication.

Funding

This work was funded by grants from two Corbett Estate Funds [Nos. 62285-531021-41800 (Cross-talking between oncogenesis and neurodegenerative diseases) and 62285-531021-61800 (Natural Products): recipient EW].

Conflict of interest

The authors declare that the research was conducted in the absence of any commercial or financial relationships that could be construed as a potential conflict of interest.

Publisher's note

All claims expressed in this article are solely those of the authors and do not necessarily represent those of their affiliated organizations, or those of the publisher, the editors and the reviewers. Any product that may be evaluated in this article, or claim that may be made by its manufacturer, is not guaranteed or endorsed by the publisher.

References

Alzheimer's Association (2023). *2023 Alzheimer's Disease Facts and Figures.* Available online at: https://www.alz.org/media/documents/alzheimers-facts-and-figures.pdf

Badhwar, A., McFall, G. P., Sapkota, S., Black, S. E., Chertkow, H., Duchesne, S., et al. (2020). A multiomics approach to heterogeneity in Alzheimer's disease: focused review and roadmap. *Brain* 143, 1315–1331. doi: 10.1093/brain/awz384

Wilson, D. M. III, Cookson, M. R., Van Den Bosch, L., Zetterberg, H., Holtzman, D. M., and Dewachter, I. (2023). Hallmarks of neurodegenerative diseases. *Cell* 186, 693–714. doi: 10.1016/j.cell.2022.12.032

Xia, Z., Wang, F., Zhou, S., Zhang, R., Wang, F., Huang, J. H., Wu, E., Zhang, Y., and Hu, Y. (2017). Catalpol protects synaptic proteins from beta-amyloid induced neuron injury and improves cognitive functions in aged rats. *Oncotarget* 8, 69303–69315. doi: 10.18632/oncotarget.17951

Zhang, R., Wang, Z., Howson, P. A., Xia, Z., Zhou, S., Wu, E., Xia, Z., and Hu, Y. (2012). Smilagenin attenuates beta amyloid (25-35)-induced degeneration of neuronal cells via stimulating the gene expression of brain-derived neurotrophic factor. *Neuroscience* 210, 275–285. doi: 10.1016/j.neuroscience.2012.03.017

frontiers | Frontiers in Pharmacology

ORIGINAL RESEARCH
published: 11 July 2022
doi: 10.3389/fphar.2022.905708

In Vitro and *in Silico* Analysis of Phytochemicals From *Fallopia dentatoalata* as Dual Functional Cholinesterase Inhibitors for the Treatment of Alzheimer's Disease

Yichuang Wu[1†], Xiangdong Su[1†], Jielang Lu[1], Meifang Wu[1], Seo Young Yang[2], Yang Mai[1], Wenbin Deng[1] and Yongbo Xue[1*]*

[1]School of Pharmaceutical Sciences (Shenzhen), Sun Yat-sen University, Shenzhen, China, [2]Department of Pharmaceutical Engineering, Sangji University, Wonju, South Korea

OPEN ACCESS

Edited by:
Yi Wang,
Zhejiang University, China

Reviewed by:
Junwei He,
Jiangxi University of Traditional Chinese Medicine, China
Angel Agis-Torres,
Universidad Complutense de Madrid, Spain
Qinshi Zhao,
Kunming Institute of Botany (CAS), China

***Correspondence:**
Wenbin Deng
dengwb5@mail.sysu.edu.cn
Yongbo Xue
xueyb@mail.sysu.edu.cn

[†]There authors have contributed equally to this work and shared first authorship

Specialty section:
This article was submitted to Neuropharmacology, a section of the journal Frontiers in Pharmacology

Received: 27 March 2022
Accepted: 20 June 2022
Published: 11 July 2022

Citation:
Wu Y, Su X, Lu J, Wu M, Yang SY, Mai Y, Deng W and Xue Y (2022) In Vitro and in Silico Analysis of Phytochemicals From Fallopia dentatoalata as Dual Functional Cholinesterase Inhibitors for the Treatment of Alzheimer's Disease. Front. Pharmacol. 13:905708. doi: 10.3389/fphar.2022.905708

Current studies have found that butyrylcholinesterase (BuChE) replaces the biological function of acetylcholinesterase (AChE) in the late stage of Alzheimer's disease. Species in the genus of Fallopia, rich in polyphenols with diverse chemical structures and significant biological activities, are considered as an important resource for screening natural products to against AD. In this study, thirty-four compounds (1–34) were isolated from Fallopia dentatoalata (Fr. Schm.) Holub, and their inhibitory effects against AChE and BuChE were assessed. Compounds of the phenylpropanoid sucrose ester class emerged as the most promising members of the group, with 31–33 displaying moderate AChE inhibition (IC50 values ranging from 30.6 ± 4.7 to 56.0 ± 2.4 μM) and 30–34 showing potential inhibitory effects against BuChE (IC50 values ranging from 2.7 ± 1.7 to 17.1 ± 3.4 μM). Tacrine was used as a positive control (IC50: 126.7 ± 1.1 in AChE and 5.5 ± 1.7 nM in BuChE). Kinetic analysis highlighted compounds 31 and 32 as non-competitive inhibitors of AChE with Ki values of ~30.0 and ~34.4 μM, whilst 30–34 were revealed to competitively inhibit BuChE with Ki values ranging from ~1.8 to ~17.5 μM. Molecular binding studies demonstrated that 30–34 bound to the catalytic sites of BuChE with negative binding energies. The strong agreement between both *in vitro* and in silico studies highlights the phenylpropanoid sucrose esters 30–34 as promising candidates for use in future anti-cholinesterase therapeutics against Alzheimer's disease.

Keywords: *Fallopia dentatoalata*, Alzheimer's disease, cholinesterase (AChE, BChE), polyphenols, phenylpropanoid sucrose esters, kinetic—spectrophotometric method, molecular docking

INTRODUCTION

Alzheimer's disease (AD) is a chronic and occult neurodegenerative disease featured by permanent memory loss and progressive cognitive impairments, which is relatively prevalent in the elder population (Wang and Zhang, 2019). The progression of AD believes to involve with multiple complicated pathogenesis and etiologies, and the cholinergic hypothesis is the earliest and most widely studied pathogenetic mechanism of AD (Du et al., 2018; Wang and Zhang, 2019). According to the cholinergic hypothesis, acetylcholine (ACh) is an essential neurotransmitter which acts as a chemical messenger

when secreted by nerve cells (Du et al., 2018). This signaling is important for numerous biological processes, including the support of cognitive functions and memory in the central nervous system (CNS), and activating muscles in the peripheral nervous system (PNS) (Krátký et al., 2018). The cholinesterases, including acetylcholinesterase (AChE, EC 3.1.1.7) and butyrylcholinesterase (BuChE, EC 3.1.1.8), are a group of esterases that catalyze the hydrolysis of cholinergic neurotransmitters into choline and their corresponding acids, which results in the return of the activated cholinergic neuron back to its resting state (Nicolet et al., 2003). AChE is regarded as a high-performance cholinesterase with highly specific catalytic activity towards ACh (80%), while BuChE, a substitute for AChE, is a non-selective cholinesterase, which can degrade both ACh and butyrylcholine (Nicolet et al., 2003; Dvir et al., 2010). Previous studies have demonstrated that ACh deficiency can cause several neurological disorders in the cortical cholinergic sites of the brain among patients with AD (Martinez and Castro, 2006). Several pharmacotherapeutics that act as acetylcholinesterase inhibitors (AChEIs) have been demonstrated to increase the concentration of ACh and thereby contribute to the alleviation the symptoms of AD (Martinez and Castro, 2006). Although AChEIs hitherto still remain the most prevailing drugs for the treatment of AD, those drugs demonstrate the limited clinical outcomes and fail to prevent the disease progression (Wang and Zhang, 2019). Research into the pathological mechanisms of the disease has revealed that AChE levels accumulate at a much higher rate than those of BChE during the early stages of AD, whereas towards the later stages of the disease, the levels of BChE increase and ultimately substitute the function of AChE (Mesulam et al., 2002; Martinez and Castro, 2006). Whilst a number of AChE inhibitors that originate from natural sources have been developed into therapeutic agents for the treatment of AD, the number of BChE inhibitory therapeutics from the natural pool is substantially lower (Clive et al., 2005). The phytochemical study outlined herein aims to address this deficiency through the characterization and biological evaluation of the natural constituents isolated from *F. dentatoalata*.

F. dentatoalata is an annual plant with wing-shaped flowers which belongs to the genus *Fallopia*. It is naturally distributed throughout several East Asian countries, including China, Japan, and India. *F. dentatoalata* is a popular cultivated species in China, especially in the Jiangsu, Hubei, and Jilin provinces (Meng et al., 2021a). In recent decades, a substantial number of phytochemical studies have led to the isolation of various chemical constituents from *F. dentatoalata*, including anthraquinones, stilbenes, amides, and flavonoids (Meng et al., 2021a). *Fallopia multiflora* is the most popular *Fallopia* species and its roots enjoy use as a traditional Chinese medicine, mainly to boost immunity and prevent aging (Lin et al., 2015). Moreover, recent studies have demonstrated its preventive and curative effects in the treatment of neurodegenerative diseases (Qian et al., 2020). Some evidence indicates that the chemical constituents of *F. dentatoalata* share a similar profile to those of *F. multiflora*. Emodin (**21**) and tetrahydroxystilbene-2-*O*-β-D-glucoside (**26**), for example, are two major compounds isolated from *F. dentatoalata* and *F. multiflora* which exhibit a wide range of neurobiological properties including neuroprotection and anti-neuroinflammation (Fakhri et al., 2021; Semwal et al., 2021). In adidtion, extracts from *F. multiflora* have been reported to show inhibitory activity against AChE (IC_{50}: 9.11 μg/ml) and BuChE (IC_{50}: 4.83 μg/ml) (Li et al., 2017). By contrast, the chemical extracts from *F. dentatoalata* have yet to have their inhibitory activities agaisnt AChE and BuChE assessed.

Our ongoing program to discover natural anti-cholinergic candidates from *Fallopia* species has resulted the isolation of thirty-four compounds from the aerial parts of *F. Dentatoalata*, which are disclosed for the first time herein. The chemical structures of these isolates were elucidated based on extensive methods of characterization, including 1D- and 2D-NMR, HR-FAB-MS spectroscopic analyses, and by comparison with previously reported data. Enzymatic assays were conducted to evaluate their inhibitory activities against AChE and BuChE.

MATERIALS AND METHODS

General Experimental Procedures

Column chromatographic procedures were performed using silica gel (80–120 mesh and 200–300 mesh, Qingdao Marine Chemical Co. Ltd., Qingdao, China) and Sephadex™ LH-20 gel (40–70 μm; Merck, Darmstadt, Germany), whereas precoated silica gel (GF254, Qingdao Marine Chemical Co. Ltd., Qingdao) plates were used for TLC analyses. Spots were visualized by heating silica gel plates sprayed with 10% H_2SO_4 in EtOH. UV spectra were recorded using a Waters UV-2401A spectrophotometer equipped with a DAD and a cell of 1 cm pathlength. Methanolic samples were scanned from 190 to 400 nm in 1 nm steps. Semipreparative HPLC was performed on an Agilent 1120 apparatus equipped with a UV detector and a reversed-phase C_{18} column (5 μm, 10 × 250 mm, Welch Ultimate XB-C18). 1D (^1H, ^{13}C) spectra of all compounds were recorded on Bruker AM-600, AM-500, and AM-400 NMR spectrometers (Bruker, Karlsruhe, Germany), with TMS as the internal reference. |Enzymatic activity experiments were performed using SpectraMax i3x (Molecular Devices, Austria).

Chemicals and Reagents

All HPLC solvents were purchased from Guangdong Guanghua Sci-Tech Co. Ltd. (Guangzhou, China). Acetylcholinesterase (C3389), acetylthiocholine iodide (A5751), butyrylcholinesterase (C1057), butyrylthiocholine iodide (B3253), and 5,5-dithiobis (2-nitrobenzoic acid) (DTNB), tacrine and dimethylsulfoxide (DMSO) were purchased from Sigma-Aldrich Co. (St. Louis, Missouri, United States). All chemicals and solvents used in column chromatography and assays were acquired from commercial sources.

Plant Material

The dried aerial parts of *F. dentatoalata* were collected from Nanyang City of Henan Province in China and taxonomically identified by Prof. Zulin Ning (Key Laboratory of Plant Resources Conservation and Sustainable Utilization, Chinese Academy of Sciences). A voucher specimen (SYSUSZ-2019-X3) was deposited at the Department of Natural Medicines, School of Pharmaceutical Sciences (Shenzhen), Sun Yat-sen University.

Extraction and Isolation

The air-dried aerial parts of *F. dentatoalata* (9.3 kg) were extracted using 70% aqueous ethanol (15 L × 4 × 2 h at room temperature) with ultrasonic assistance. The combined extracts were filtered and evaporated under reduced pressure to yield a brown residue (1.6 kg). The residue was suspended in H_2O and successively partitioned with petroleum ether (PE) (10 L), ethyl acetate (EA) (10 L), and *n*-butanol (10 L), yielding petroleum ether (121.3 g), ethyl acetate (93.0 g) and *n*-BuOH (311.3 g) extracts.

The ethyl acetate layer was subjected to silica gel (100–200 mesh) column chromatography (CC) (CH_2Cl_2–MeOH, 100:1–1:1 v/v) to obtain seven fractions (Fr. 1–7). Fr. 2 (10.0 g) was decolorized using MCI gel CC (MeOH–H_2O, 20–100%, v/v) to afford three subfractions (Fr. 2A–2C). Fr. 2B was subjected to silica gel CC (PE–EA, 20:1–5:1, v/v) to yield compound **21** (18.0 mg). Compound **22** (15.0 mg) was purified from Fr. 2C by silica gel CC (PE-EA, 20:1–5:1, v/v). Fr. 3 (8.3 g) was decolorized using MCI gel CC (MeOH–H_2O, 20–100%, v/v) to afford three subfractions (Fr. 3A–3C). Fr. 3A was successively separated *via* Sephadex LH-20 CC (CH_2Cl_2–MeOH, 1:1, v/v) and silica gel CC (CH_2Cl_2–MeOH, 50:1–10:1, v/v) to afford compound **5** (5.0 mg) and **17** (10.0 mg). Compounds **1** (15.0 mg), **3** (8.0 mg), and **16** (13.0 mg) were purified from Fr. 3B by silica gel CC (CH_2Cl_2-MeOH, 50:1–10:1, v/v). Fr. 4 (7.0 g) was subjected to silica gel CC (CH_2Cl_2–MeOH, 50:1–10:1, v/v) to afford four subfractions (Fr. 4A–4D). Fr. 4D was successively separated via MCI CC (MeOH–H_2O, 20–100%, v/v) and Sephadex LH-20 CC (CH_2Cl_2–MeOH, 1:1, v/v) to afford compounds **28** (16.0 mg) and **29** (26.0 mg). Fr. 5 (17.5 g) was subjected to silica gel CC (CH_2Cl_2–MeOH, 50:1–1:1, v/v) to afford six subfractions (Fr. 5A–5F). Fr. 5D was successively separated *via* Sephadex LH-20 CC (CH_2Cl_2–MeOH, 1:1, v/v) and silica gel CC (CH_2Cl_2–MeOH, 50:1–30:1, v/v) to afford **7** (26.0 mg). Fr. 5E was successively separated *via* silica gel CC (CH_2Cl_2–MeOH, 30:1–2:1, v/v), Sephadex LH-20 CC (CH_2Cl_2–MeOH, 1:1, v/v), and semi-preparative HPLC (MeOH–H_2O, 30:70 to 80:20, v/v, 3 ml/min) to afford **18** (10.0 mg, t_R 6.3 min) and **19** (2.0 mg, t_R 6.6 min). Fr. 5F was successively separated *via* Sephadex LH-20 CC (CH_2Cl_2–MeOH, 1:1, v/v) and semi-preparative RP-HPLC (MeCN–H_2O, 20:80–60: 40, v/v, 3 ml/min) to afford **30** (4.0 mg, t_R 7.1 min), **31** (7.0 mg, t_R 8.1 min), and **32** (5.0 mg, t_R 7.3 min). Fr. 6 (35.0 g) was subjected to silica gel CC (CH_2Cl_2–MeOH, 50:1–1:1, v/v) to afford six subfractions (Fr. 6A–6F). Fr. 6C was successively separated *via* Sephadex LH-20 CC (CH_2Cl_2–MeOH, 1:1, v/v) and silica gel CC (CH_2Cl_2–MeOH, 30:1–5:1, v/v) to afford compounds **26** (16.0 mg) and **27** (8.0 mg). Fr. 6D was successively separated *via* silica gel CC (CH_2Cl_2–MeOH, 30:1–2:1, v/v), Sephadex LH-20 CC (CH_2Cl_2–MeOH, 1:1, v/v), and semi-preparative RP-HPLC (MeOH–H_2O, 40:60 to 80:20, v/v, 3 ml/min) to afford compounds **4** (10.0 mg, t_R 8.9 min), **8** (5.0 mg, t_R 5.7 min), **9** (15.0 mg, t_R 11.7 min), **11** (2.0 mg, t_R 10.1 min), and **24** (15.0 mg, t_R 13.6 min). Similarly, compounds **10** (12.0 mg, t_R 15.1 min), **12** (74.0 mg, t_R 11.5 min), **13** (24.0 mg, t_R 12.7 min), **20** (6.0 mg, t_R 16.6 min), **33** (6.0 mg, t_R 17.4 min), and **34** (7.0 mg, t_R 19.6 min) were obtained from Fr. 6E and Fr. 6F by semi-preparative RP-HPLC (MeOH–H_2O, 20:80–80:20, v/v, 3 ml/min). Fr. 7 (7.0 g) was successively separated *via* silica gel CC (CH_2Cl_2–MeOH, 20:1–0:1, v/v) and semipreparative RP-HPLC (MeOH–H_2O, 20:80–100:0, v/v, 3 ml/min) to afford two subfractions (Fr. 7A–7B). Fr. 7B was successively separated *via* Sephadex LH-20 CC (CH_2Cl_2–MeOH, 1:1, v/v), silica gel CC (CH_2Cl_2–MeOH, 20:1–1:1, v/v), and semipreparative RP-HPLC (MeOH–H_2O, 50:50–100:0, v/v, 3 ml/min) to afford **2** (10.0 mg, t_R 4.6 min), **6** (7.0 mg, t_R 6.3 min), **14** (10.0 mg, t_R 7.6 min), **15** (10.0 mg, t_R 8.7 min), **23** (6.0 mg, t_R 12.6 min), and **25** (10.0 mg, t_R 9.1 min).

Lapathoside B (30)

Yellowish amorphous solid. UV (MeOH): λ_{max} (log ε) 217 (2.70), 323 (3.20) nm, see **Supplementary Figure S6**. ^{1}H (600 MHz, CD_3OD-d_4) and ^{13}C-NMR (151 MHz, CD_3OD-d_4) data, see **Supplementary Table S1**; HR-FAB-MS *m/z* 1039.2842 $[M+Na]^+$ (calcd for $C_{51}H_{52}NaO_{22}^+$ 1039.2848), see **Supplementary Figure S1**.

Vanicoside B (31)

Yellowish amorphous solid. UV (MeOH): λ_{max} (log ε) 213 (3.00), 318 (5.10) nm, see **Supplementary Figure S7**. ^{1}H (600 MHz, CD_3OD-d_4) and ^{13}C NMR (151 MHz, CD_3OD-d_4) data, see **Supplementary Table S1**; HR-FAB-MS *m/z* 1011.2840 $[M+Na+CH_3OH]^+$ (calcd for $C_{50}H_{52}NaO_{21}^+$ 1011.2899), see **Supplementary Figure S2**.

Lapathoside A (32)

Yellowish amorphous solid. UV (MeOH): λ_{max} (log ε) 215 (4.70), 322 (5.80) nm, see **Supplementary Figure S8**. ^{1}H (600 MHz, CD_3OD-d_4) and ^{13}C NMR (151 MHz, CD_3OD-d_4) data, see **Supplementary Table S1**; HR-FAB-MS *m/z* 1004.3183 $[M+NH_4]^+$ (calcd for $C_{50}H_{54}NO_{21}^+$ 1004.3188), see **Supplementary Figure S3**.

Smilaside J (33)

Yellowish amorphous solid. UV (MeOH): λ_{max} (log ε) 2218 (4.70), 235.7 (3.20), 332 (5.80) nm, see **Supplementary Figure S9**. ^{1}H (400 MHz, CD_3OD-d_4) and ^{13}C NMR (101 MHz, CD_3OD-d_4) data, see **Supplementary Table S2**; HR-FAB-MS *m/z* 858.2823 $[M+NH_4]^+$ (calcd for $C_{41}H_{48}NO_{19}^+$ 858.2821), see **Supplementary Figure S4**.

Smilaside G (34)

Yellowish amorphous solid. UV (MeOH): λ_{max} (log ε) 229 (2.70), 314 (4.70) nm, see **Supplementary Figure S10**. ^{1}H (600 MHz, CD_3OD-d_4) and ^{13}C NMR (150 MHz, CD_3OD-d_4) data, see **Supplementary Table S2**; HR-FAB-MS *m/z* 833.2271 $[M+Na]^+$ (calcd for $C_{40}H_{42}NaO_{18}^+$ 833.2263), see **Supplementary Figure S5**.

AChE and BuChE Assays

In vitro cholinesterase assays were performed using a modified version of previously published methods (Kim et al., 2016). Briefly, 130 μL of enzyme (acetylcholinesterase and butyrylcholinesterase: 0.05 Unit/mL) in 50 mM potassium

phosphate buffer (pH 7.4) was mixed with 20 μL of compounds (1–0.002 mM) dissolved in methanol in a 96-well plate. 25 μL of 1 mM DTNB [5,5′-dithiobis (2-nitrobenzoic acide)] and 25 μL of 5 mM substrate, acetylthiocholine iodide (A5751), and butyrylthiocholine iodide (B3253) were sequentially added to wells in the plate. Plates were incubated at 37°C for 30 min then monitored with a Microplate reader (SpectraMax i3x) (405 nm). Tacrine was used as positive control. The inhibition ratio was calculated using the equation:

$$\text{Inhibitory activity}\,(\%) = [(\Delta C - \Delta I)/\Delta C] \times 100$$

Where C and I are the intensity of control and inhibitor after 20 min, respectively.

Molecular Docking Simulation

Autodock package 4.2 (La Jolla, CA. United States) was used for the molecular docking of receptor with ligand. Ligands were built as 3D structures and minimized with MM2 charge using Chem3D Pro 17.1. For flexible ligands, single bonds were assigned using AutoDockTools. The 3D structures of BuChE (pdb ID: 1P0I) was derived using the RCSB protein data bank. Hydrogens were added to both, then each were assigned with computed gasteiger charges. To simulate docking, a grid containing the active site was set (grid points X.Y.Z 80.80.100 for AChE, and X.Y.Z 60.80.70 for BuChE) with 0.375 Å spacing. Docking simulations of protein structures and newly built ligands were performed using the Lamarckian Genetic Algorithm. Finally, ligands were docked into the box 25,000,000 times, then the results of the top 50 ranks were extracted. Data were presented in figures using Discovery Studio and Ligpot (Cambridge, United Kingdom) and Chimera (San Francisco, CA, United States).

Statistical Analysis

All inhibitory concentration data was obtained from independent experiments carried out in triplicate. Results are shown as the mean ± standard error of the mean (SEM). The results were subjected to analysis using Sigma plot 14.5 (Systat Software Inc., San Jose, CA, United States).

RESULTS AND DISCUSSION

Isolation and Identification

In this study, thirty-four compounds (**1**–**34**) were isolated from the aerial parts of *F. dentatoalata via* extensive column chromatography. These were identified as apigenin (**1**) (Ha et al., 2012), isovitexin (**2**) (Jayasinghe et al., 2004), kaempferol (**3**) (Fukai and Nomura, 1988), afzelin (**4**) (Xu et al., 2009), astragalin (**5**) (Otsuka et al., 1989), kaempferol-3-rutinoside (**6**) (de Sa de Sousa Nogueira et al., 2013), luteolin (**7**) (Zhang et al., 2015), quercetin (**8**) (Lesjak et al., 2018), guaijaverin (**9**) (Yoshida

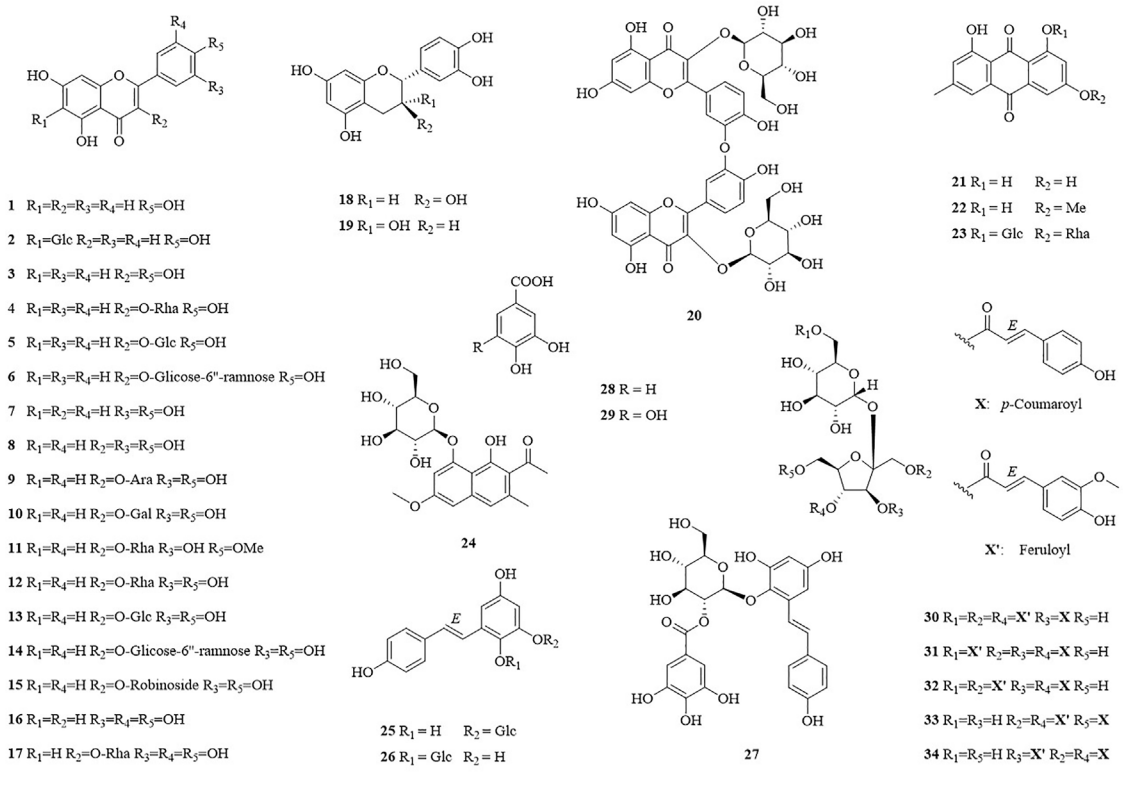

FIGURE 1 | Structure of isolated compounds **1**–**34** from *F. dentatoalata*.

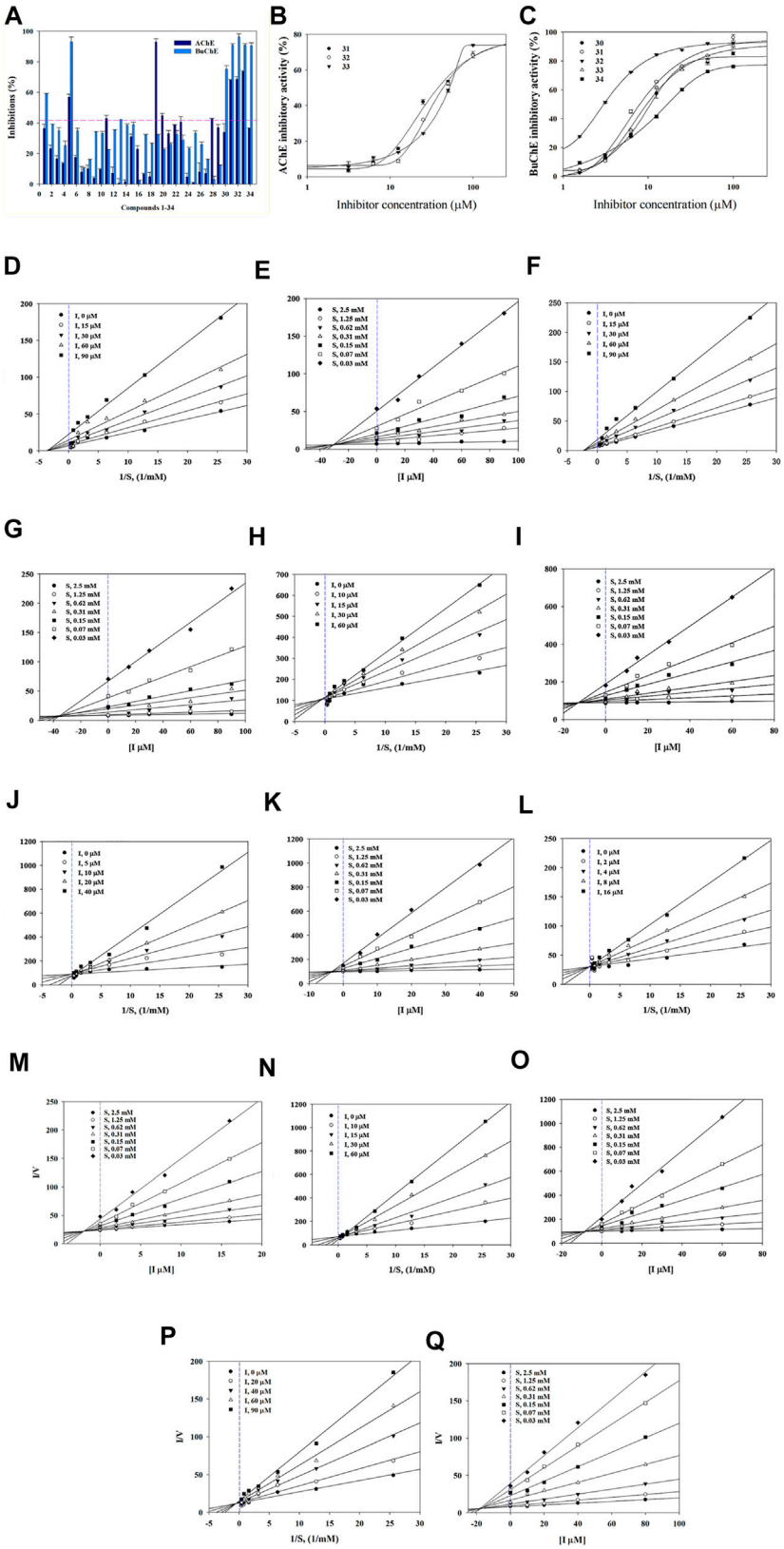

FIGURE 2 | Inhibitory activity of compounds **1**–**34** at 100 μM towards AChE and BuChE **(A)**. IC_{50} values of **31**–**33** on AChE **(B)** and **30**–**34** BuChE **(C)**. Lineweaver-Burk plots **(D,F)** and Dixon plots **(E,G)** of compounds **31** and **32** on AChE. Lineweaver-Burk plots **(H, J, L, N, P)** and Dixon plots **(I, K, M, O, Q)** of compounds **30**–**34** on BuChE.

TABLE 1 | Inhibitory activity of compounds **30**–**34** against AChE and BuChE.

Comp	AChE[a]			BuChE[a]		
	IC_{50} (μM)	Inhibition type	K_i (μM)	IC_{50} (μM)	Inhibition type	K_i (μM)
30	>100	–	–	10.9 ± 4.9	Competitive	~12.1
31	32.3 ± 4.7	Non-Competitive	~30.0	7.5 ± 4.1	Competitive	~3.5
32	30.6 ± 4.7	Non-Competitive	~34.4	2.7 ± 1.7	Competitive	~1.8
33	56.0 ± 2.4	–	–	10.1 ± 4.6	Competitive	~8.5
34	>100	–	–	17.1 ± 3.4	Competitive	~17.5
Tacrine[b]	126.7 ± 1.1 nM	–	–	5.5 ± 1.7 nM	–	–

[a]*All compounds were examined in triplicate.*
[b]*Positive control.*
(–) Not tested.

TABLE 2 | Binding site residues and docking scores of compounds **30**–**34** bound to BuChE obtained using Autodock 4.2.

Comp	Binding energy (kcal/mol)	Hydrogen bond interaction	Van der Waals	Hydrophobic interactions			Other interactions	
				π-π stacked	π-σ	π-alkyl	π-anion/ cation	π-amide
30	–7.13	Asn83, Ser287, Asn289, Tyr282, Gln270	Val288, Trp82, Ser79, Tyr332, Leu273, Thr284, Leu274	Phe278		Ile356	Asp70	
31	–7.36	Gly78, Trp430, Ser72, Asn289, Gly116	Gln71, Asp70, Thr284, Ile69, Thr120, Met437, Tyr440, Trp82, Ser79			Ala328, Ala277		Gly283
32	–7.55	Ala277, His438, Pro285, Val331, Gln71	Ile69, Tyr440, Met437, Trp430, Leu286, Asp70, Thr284	Phe278		Ala328, Trp82, Ala277		
33	–5.33	His438, Ser198, Asp70, Thr120, Gly283	Phe398, Ile356, Gly117, Gln119, Asn83, Ser79, Trp82, Tyr332, Ser72	Phe329	Trp231	Pro285		Thr284 Gly116
34	–5.23	Ile69, Ser72, Thr284, Pro281	Asp70, Tyr332, Gln119, Thr120, Leu286, Gln71, Gly117, Phe278	Phe329 Trp231		Pro285 Ile356		Gly116

et al., 1992), hyperoside (**10**) (Isaza et al., 2001), tamarixetin-3-rhamnoside (**11**) (Norman et al., 2021), quercitrin (**12**) (Chen et al., 2008), isoquercitrin (**13**) (Jin et al., 2009), rutin (**14**) (Kazuma et al., 2003), quercetin-3-*O*-robinoside (**15**) (Dossou et al., 2021), myricetin (**16**) (Zhang et al., 2004), myricitrin (**17**) (Kil et al., 2019), (+)-catechin (**18**) (Foo et al., 1997), (-)-epicatechin (**19**) (Lin and Lee, 2010), zizyflavoside B (**20**) (Yang et al., 2020), emodin (**21**) (Meselhy, 2003), physcion (**22**) (Jo et al., 2011), glucofrangulin A (**23**) (Bezabih and Abegaz, 1998), torachrysone-8-*O*-β-D-glucoside (**24**) (Zhao et al., 2017), polydatin (**25**) (Yi et al., 2020), tetrahydroxystilbene-2-*O*-β-D-glucoside (**26**) (Tsai et al., 2018), (*E*)-2,3,5,4′-tetrahydroxystilbene-2-*O*-(2″-*O*-galloyl)-β-D-glucoside (**27**) (Nguyen et al., 2020), protocatechuic acid (**28**) (Meng et al., 2021b), gallic acid (**29**) (Chen et al., 2021), lapathoside B (**30**) (Takasaki et al., 2001), vanicoside B (**31**) (Kumagai et al., 2005), lapathoside A (**32**) (Takasaki et al., 2001), smilaside J (**33**) (Zhang et al., 2008), and smilaside G (**34**) (Takasaki et al., 2001). Identification was enabled by comparison of their spectroscopic data with those reported previously, see **Supplementary Table S3–S13** (**Figure 1**).

Enzyme Assays

Compounds were first evaluated *in vitro* for their inhibitory activities against AChE and BuChE at a concentration of 100 μM. The amount of 5-thio-2-nitrobenzoic acid produced from the substrates (acetylthiocholine iodide and butyrylthiocholine iodide) was quantified in the presence or absence of compounds using a SpectraMax i3x model at 405 nm. Tacrine was used as a positive control (IC_{50}: 126.7 ± 1.1 in AChE and 5.5 ± 1.7 nM in BuChE). Compounds **1**–**34** exhibited inhibitory effects on AChE and BuChE with different ratios, ranging from 0.9 ± 0.3% to 73.8 ± 0.4%, and from 2.3 ± 0.3% to 96.3 ± 2.0% of the control value at 100 μM, respectively (**Figure 2A**). Among them, compounds 31–33 exhibited more than 60% inhibition in a dose-dependent manner on AChE, with IC_{50} values of 32.3 ± 4.7, 30.6 ± 4.7, and 56.0 ± 2.4 μM, respectively (**Figure 2B**; **Table 1**). Compounds 30–33 displayed potent inhibitory activities against BuChE with IC_{50} values of 2.7 ± 1.7 and 10.9 ± 4.9 μM, while compound 34 exhibited a moderate inhibition on BuChE with an IC_{50} value of 17.1 ± 3.4 μM (**Figure 2C**; **Table 1**).

Structure-activity relationships (SAR) of compounds **30**–**34** were guided by their IC_{50} values in order to better understand their respective pharmacophores (**Supplementary Figure S11**). Compound **33** (IC_{50}:10.1 μM) with a *p*-coumaroyl motif linked to the C-4 position of fructose, demonstrated an inhibitory effect comparable with compound **30** (IC_{50}:10.9 μM), while compound **31** (IC_{50}: 7.5 μM), which has a feruloyl group linked to the C-6′ position of glucose and a *p*-coumaroyl linked to the C-3 position of fructose, exhibited an inhibitory activity over 2-fold higher than that of Compound **34** (IC_{50}:17.1 μM). In addition, the

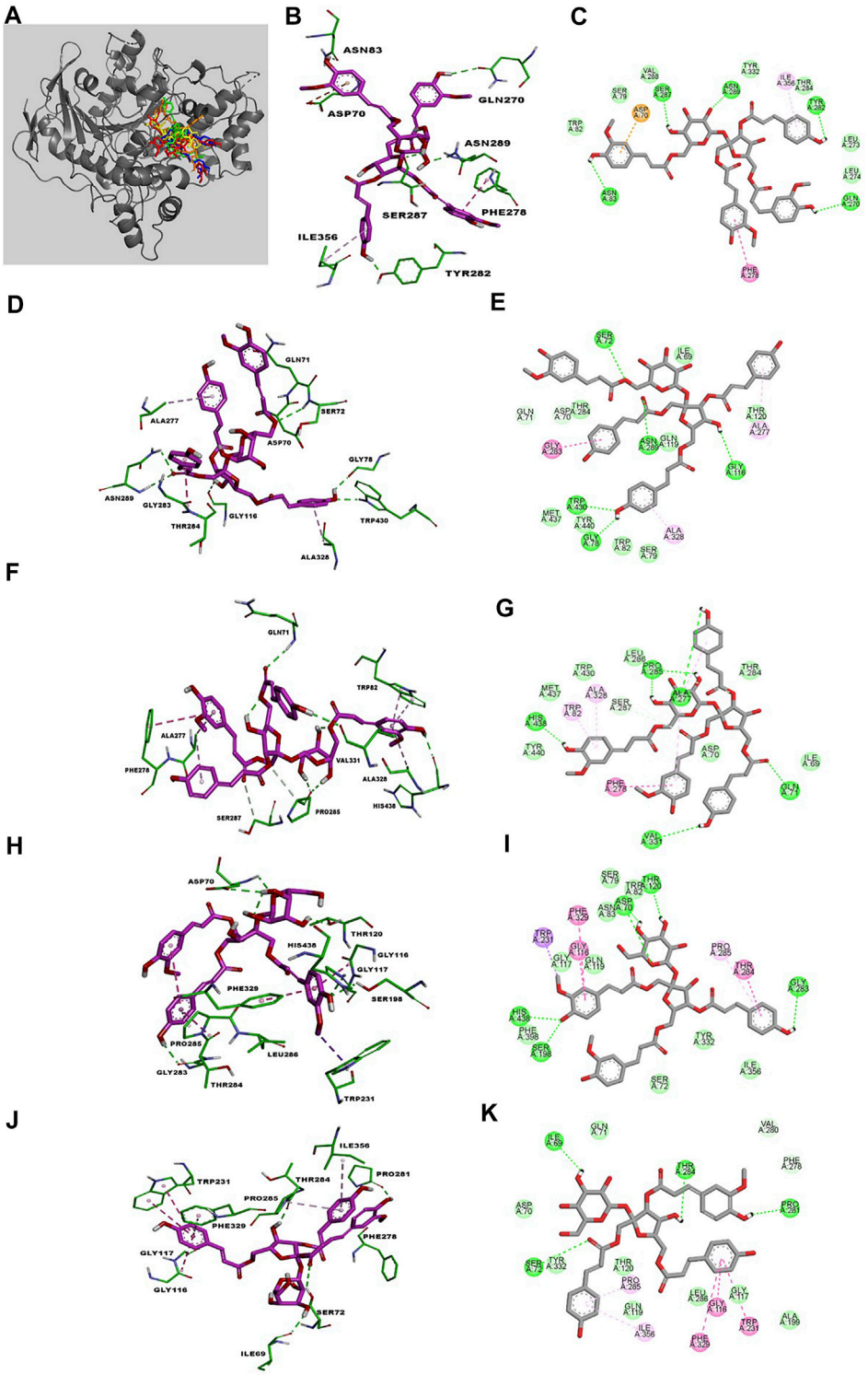

FIGURE 3 | The best poses of compounds **30**–**34** (**30**, red; **31**, green; **32**, orange; **33**, yellow; **34**, blue) docked with BuChE **(A)**. Molecular docking models **(B, D, F, H, J)** and 2D ligand interaction diagrams **(C, E, G, I, K)** of BuChE inhibition at the catalytic pocket by compounds **30**–**34**, respectively. Different interactions between compounds and amino acid residues in the catalytic site are designated by the following: thick light purple stick models represent compounds **30**–**34**, green dotted lines represent hydrogen bonds, light green lines represent Van der Waals interactions, dark pink lines represent π–π and π–σ interactions, and light pink lines represent π–alkyl interactions.

presence of a feruloyl group at C-6′, a *p*-coumaroyl group at C-6, and a feruloyl group linked to the C-1 position of fructose such as those found in compound **32** (IC_{50}: 2.7 μM), are likely to be the structural units most responsible for the observed anti-cholinesterase activities. Consequently, the inhibitory activities decreased in the order **32** > **31** > **33** > **30** > **34**, with compound **32** being the most potent of the series.

Enzyme Kinetics Study

The binding mechanisms of isolated compounds which displayed IC_{50} values less than 50 μM against cholinesterase were investigated. This was achieved by performing enzyme kinetic studies on AChE/BuChE in the presence of different concentrations of compounds **30**–**34** (2–90 μM) at various steady-state substrate concentrations (0.07–5 mM). The interactions between compounds and cholinesterase are represented using classic double-reciprocal Lineweaver-Burk and Dixon plots (Lineweaver and Burk, 1934; Dixon, 1953). Compounds **31** and **32** were revealed to have various V_{max} values and a K_m value, which confirmed both were non-competitive inhibitors that docked with both AChE and substrate-bound AChE (**Figures 2D,F**) (Lee et al., 2018). The resulting linear equations for compounds **30**–**34** with BuChE led to a series of lines with different slopes that crossed at similar intercepts on the vertical axis and different points on the horizontal axis. Compounds **30**–**34** were therefore designated as competitive inhibitors of BuChE (**Figures 2H,J,L,N,P**) (Kim et al., 2016). Furthermore, the intersections of the lines on the Dixon plots indicated that the inhibition constants (K_i) of compounds **31** and **32** towards AChE were ~30.0 and ~34.4 μM, respectively (**Figures 2E,G**; **Table 1**). The K_i values of compounds **30**–**34** for the inhibition of BuChE were ~12.1, ~3.5, ~1.8, ~8.5 and 17.5 μM, respectively (**Figures 2I,K,M,O,Q**; **Table 1**).

Molecular Docking of BuChE Inhibition

Kinetic studies demonstrated that compounds **30**–**34** significantly downregulated the catalytic activity of BuChE by competitively binding to its active site. Previous researches demonstrated that the active site gorge of BuChE include: catalytic triad (Ser198-His438-Glu325), acyl loop (Ala277-Leu286-Val288), π-cation site (Tyr82-Ala328), □-loop (Ile69-Ser79), oxyanion hole (Ala199-Gly116-Gly117), and peripheral site (Asn68-Glu70-Tyr332) (Nicolet et al., 2003; Vyas et al., 2010). Molecular docking simulations were subsequently performed in order to confirm and identify their binding energies and outline the binding interactions (i.e. hydrogen-bonding, Van der Waals, and hydrophobic interactions) between ligands **30**–**34** and BuChE (**Table 2**). Full docking views of each phenylpropanoid sucrose ester bound to the catalytic site of BuChE are shown in **Figure 3**.

Compound **30** achieved and Autodock score of –7.13 kcal/mol (**Table 2**). Hydroxyl and carboxyl groups displayed hydrogen bonding with the key amino acids Asn83 (2.72 Å), Ser287 (2.66 Å), Asn289 (2.61 Å), Tyr282 (2.83 Å), and Gln270 (3.19 Å) (**Figures 3B,C**). An aromatic ring of the feruloyl group attached to C-1 of fructose exhibited π-π stacking with Phe278 at a distance of 4.59 Å. Other residues from different active sites, including Val288, Trp82, Ser79, Tyr332, Leu273, Leu274, Thr284, Ile356, and Asp70, showed bonding with **30** *via* Van der Waals, π-alkyl and π-anion interactions (**Figures 3B,C**).

Compounds **31** and **32** displayed stable binding energies of –7.36 and –7.55 kcal/mol when bound to the active site, which arose as a result of interactions with five (Gly78 at 2.09 Å, Trp430 at 2.31 Å, Ser72 at 2.90 Å, Asn289 at 2.38 and 2.68 Å, Gly116 2.78 Å) and six (Ala277 at 2.02 Å, His438 at 2.03 Å, Pro285 at 2.01 and 2.50 Å, Val331 at 2.48 Å, Gln71 at 2.41 Å) hydrogen bonds to amino acid residues in the BuChE active site, respectively (**Figures 3D,E**; **Table 2**). Both **31** and **32** shared the same catalytic residues of Tyr440, Met437, Asp70, Ile69 (*via* Van der Waals interactions) and Ala328 and Ala277 (*via* π-alkyl interactions) (**Figures 3D–G**; **Table 2**). Furthermore, compound **31** exhibited additional Van der Waals interactions with Gln71, Thr284, Thr120, Trp82, Ser79, and a π-amide interaction with Gly283, which further confirmed its interaction with BuChE (**Figures 3D,E**; **Table 2**). The remaining residues of Trp430, Leu286, Thr284, and Trp82 from the active site formed Van der Waals and π-alkyl interactions with compound **32** (**Figures 3F,G**; **Table 2**).

Compounds **33** and **34** bound to the catalytic region of BuChE with a relatively large binding energies of –5.33 and –5.23 kcal/mol respectively, which suggests that the number of phenylpropanoids affects the binding energy. As shown in **Figures 3H–K**, compounds **33** and **34** formed five hydrogen bonds (His438 at 2.35 Å, Ser198 at 2.16 Å, Asp70 at 2.36 and 2.58 Å, Thr120 at 2.02 Å, Gly283 at 2.12 Å), meanwhile **34** formed four (Thr284 at 1.74, Pro281 at 2.02 Å, Ile69 at 2.11 Å and Ser72 at 3.04 Å), respectively (**Table 2**). Additionally, **33** and **34** shared the same residues of Tyr332, Gly117, and Gln119 (*via* Van der Waals interactions), Phe329 and Trp231 (*via* π-π and π-σ interactions), Pro285 and Gly116 (*via* π-alkyl and π-amide interactions), respectively (**Table 2**). The other residue interactions of **33** and **34** are similar with those of compounds **30**–**32** (**Figure 3**; **Table 2**). The molecular docking results are consistent with the those from the kinetic studies, which confirm compounds **30**–**34** to be competitive inhibitors binding at the catalytic active site of BuChE. Furthermore, molecular docking simulations between these isolates and BuChE enzyme suggest that phenylpropanoid sucrose esters represent a novel molecular architecture in the development of BuChE inhibitors.

CONCLUSION

Thirty-four previously reported compounds were isolated from the MeOH extracts of the aerial parts of *F. dentatoalata*. These compounds were further classified into seventeen flavonoids and their glycosides (**1**–**17**), two flavan-3-ols (**18**–**19**), a biflavone (**20**), three anthraquinones (**21**–**23**), a naphtolic glycoside (**24**), three stilbenoid derivatives (**25**–**27**), two phenolic acids (**28**–**29**), and five phenylpropanoid sucrose esters (**30**–**34**). The inhibitory activities of all compounds

against AChE and BuChE were evaluated. To the best of our knowledge, this is the first phytochemical investigation on potential anti-cholinesterase candidates from *F. dentatoalata*. However, several compounds already have been evaluated for their potential anti-cholinesterase effects before, especially flavonoids (Wu et al., 2017; Borowiec et al., 2022). For examples, compounds **1**, **5** and **19** showed over 50% inhibitions against AChE and BuChE, which further proved to be comparable with reported values (Kim et al., 2016; Nugroho et al., 2018; Islam et al., 2021; Karatas et al., 2022). In addition, compounds **31**–**33** showed moderate inhibition of AChE, and were determined to be non-competitive inhibitors. Compounds **30**–**34** significantly suppressed the activity of BuChE and were identified as competitive inhibitors. *In vitro* and *in silico* results indicate that the phenylpropanoid sucrose esters **30**–**34** from *F. dentatoalata* hold potential as candidates for future development as anti-cholinesterase therapeutics against AD.

DATA AVAILABILITY STATEMENT

The original contributions presented in the study are included in the article/**Supplementary Material**, further inquiries can be directed to the corresponding authors.

AUTHOR CONTRIBUTIONS

YW and XS: writing original draft, isolation and structural elucidation, enzymatic assays, and molecular docking. YW and JL: isolation and structural elucidation. MW, SY, and YM: enzymatic assays and molecular docking. WD and YX: review and editing, and supervision.

FUNDING

This research was financially supported by the National Natural Science Foundation of China (Nos. 21977120 and 31770379), the China Postdoctoral Science Foundation (2020M673027), Science, Technology and Innovation Commission of Shenzhen Municipality (JCYJ20200109142215045 and JCYJ20180307154653332), and Shenzhen Science and Technology Program (KQTD20190929173853397).

SUPPLEMENTARY MATERIAL

The Supplementary Material for this article can be found online at: https://www.frontiersin.org/articles/10.3389/fphar.2022.905708/full#supplementary-material

REFERENCES

Bezabih, M., and Abegaz, B. M. (1998). Glucofrangulin A Diacetate from the Fruits of Rhamnus Prinoids. *Bull. Chem. Soc. Eth.* 12 (1), 45–48. doi:10.4314/bcse.v12i1.21033

Borowiec, K., Stachniuk, A., Szwajgier, D., and Trzpil, A. (2022). Polyphenols Composition and the Biological Effects of Six Selected Small Dark Fruits. *Food Chem.* 391, 133281. doi:10.1016/j.foodchem.2022.133281

Chen, K., Qu, J., Chen, H., Wang, J., Hua, H., Li, J., et al. (2021). Investigating the Medicinal Potential, Material Basis and Mechanism of *Polygoni Orientalis* Fructus Based on Multi-Technology Integrated Network Pharmacology. *Phytomedicine* 91, 153685. doi:10.1016/j.phymed.2021.153685

Chen, Z., Liu, Y. M., Yang, S., Song, B. A., Xu, G. F., Bhadury, P. S., et al. (2008). Studies on the Chemical Constituents and Anticancer Activity of *Saxifraga Stolonifera* (L) Meeb. *Bioorg. Med. Chem.* 16 (3), 1337–1344. doi:10.1016/j.bmc.2007.10.072

Clive, G. B., Nigel, H. G., Angela, L. G. B., Albert, E., and Sultan, D. (2005). Cholinesterases: Roles in the Brain during Health and Disease. *Curr. Alzheimer Res.* 2 (3), 307–318. doi:10.2174/1567205054367838

de Sá de Sousa Nogueira, T. B., de Sá de Sousa Nogueira, R. B., E Silva, D. A., Tavares, J. F., de Oliveira Lima, E., de Oliveira Pereira, F., et al. (2013). First Chemical Constituents from *Cordia Exaltata* Lam and Antimicrobial Activity of Two Neolignans. *Molecules* 18 (9), 11086–11099. doi:10.3390/molecules180911086

Dixon, M. (1953). The Determination of Enzyme Inhibitor Constants. *Biochem. J.* 55 (1), 170–171. doi:10.1042/bj0550170

Dossou, S. S. K., Xu, F., Cui, X., Sheng, C., Zhou, R., You, J., et al. (2021). Comparative Metabolomics Analysis of Different Sesame (*Sesamum indicum* L.) Tissues Reveals a Tissue-specific Accumulation of Metabolites. *Bmc Plant Biol.* 21 (1), 352. doi:10.1186/s12870-021-03132-0

Du, X., Wang, X., and Geng, M. (2018). Alzheimer's Disease Hypothesis and Related Therapies. *Transl. Neurodegener.* 7 (1), 2. doi:10.1186/s40035-018-0107-y

Dvir, H., Silman, I., Harel, M., Rosenberry, T. L., and Sussman, J. L. (2010). Acetylcholinesterase: From 3D Structure to Function. *Chem. Biol. Interact.* 187 (1), 10–22. doi:10.1016/j.cbi.2010.01.042

Fakhri, S., Gravandi, M. M., Abdian, S., Akkol, E. K., Farzaei, M. H., and Sobarzo-Sánchez, E. (2021). The Neuroprotective Role of Polydatin: Neuropharmacological Mechanisms, Molecular Targets, Therapeutic Potentials, and Clinical Perspective. *Molecules* 26 (19), 5985. doi:10.3390/molecules26195985

Foo, L. Y., Lu, Y., McNabb, W. C., Waghorn, G., and Ulyatt, M. J. (1997). Proanthocyanidins from *Lotus Pedunculatus*. *Phytochemistry* 45 (8), 16891696. doi:10.1016/s0031-9422(97)00198-2

Fukai, T., and Nomura, T. (1988). Seven Prenylated Flavonol Glycosides from Two *Epimedium* Species. *Phytochemistry* 27 (1), 259–266. doi:10.1016/0031-9422(88)80627-7

Ha, T. J., Lee, J. H., Lee, M. H., Lee, B. W., Kwon, H. S., Park, C. H., et al. (2012). Isolation and Identification of Phenolic Compounds from the Seeds of Perilla Frutescens (L.) and Their Inhibitory Activities against α-glucosidase and Aldose Reductase. *Food Chem.* 135 (3), 1397–1403. doi:10.1016/j.foodchem.2012.05.104

Isaza, J. H., Ito, H., and Yoshida, T. (2001). A Flavonol Glycoside-Lignan Ester and Accompanying Acylated Glucosides from *Monochaetum Multiflorum*. *Phytochemistry* 58 (2), 321–327. doi:10.1016/S0031-9422(01)00247-3

Islam, M. A., Zaman, S., Biswas, K., Al-Amin, M. Y., Hasan, M. K., Alam, A. H. M. K., et al. (2021). Evaluation of Cholinesterase Inhibitory and Antioxidant Activity of Wedelia Chinensis and Isolation of Apigenin as an Active Compound. *BMC Complement. Med. Ther.* 21 (1), 204. doi:10.1186/s12906-021-03373-4

Jayasinghe, U. L., Balasooriya, B. A., Bandara, A. G., and Fujimoto, Y. (2004). Glycosides from *Grewia Damine* and *Filicium Decipiens*. *Nat. Prod. Res.* 18 (6), 499–502. doi:10.1080/14786410310001620538

Jin, H. Z., Chen, G., Li, X. F., Shen, Y. H., Yan, S. K., Zhang, L., et al. (2009). Flavonoids from *Rhododendron Decorum*. *Chem. Nat. Compd.* 45 (1), 85–86. doi:10.1007/s10600-009-9245-x

Jo, G., Shin, S. Y., Lee, Y., Hyun, J., Dong, K. S., Park, J. C., et al. (2011). A Compound Isolated from *Rumex Japonicus* Induces Early Growth Response Gene-I Expression. *J. Korean Soc. Appl. Bi.* 54 (4), 637–643. doi:10.3839/jksabc.2011.097

Karatas, D. D., Oz, V., Yener, I., Akdeniz, M., Erek, F., Aydin, I., et al. (2022). Phytochemical Contents of Different Parts of the Seeded Raisins from the South-East Anatolia: Enzyme Inhibitory Potential of Pulp Extracts. *Chem. Biodivers.* 19 (3), e202100844. doi:10.1002/cbdv.202100844

Kazuma, K., Noda, N., and Suzuki, M. (2003). Malonylated Flavonol Glycosides from the Petals of *Clitoria Ternatea*. *Phytochemistry* 62 (2), 229–237. doi:10.1016/s0031-9422(02)00486-7

Kil, H. W., Rho, T., and Yoon, K. D. (2019). Phytochemical Study of Aerial Parts of *Leea Asiatica*. *Molecules* 24 (9), 1733. doi:10.3390/molecules24091733

Kim, J. H., Lee, S. H., Lee, H. W., Sun, Y. N., Jang, W. H., Yang, S. Y., et al. (2016). (-)-Epicatechin Derivate from *Orostachys Japonicus* as Potential Inhibitor of the Human Butyrylcholinesterase. *Int. J. Biol. Macromol.* 91, 1033–1039. doi:10.1016/j.ijbiomac.2016.06.069

Krátký, M., Štěpánková, Š., Vorčáková, K., and Vinšová, J. (2018). Investigation of Salicylanilide and 4-Chlorophenol-Based N-Monosubstituted Carbamates as Potential Inhibitors of Acetyl- and Butyrylcholinesterase. *Bioorg. Chem.* 80, 668–673. doi:10.1016/j.bioorg.2018.07.017

Kumagai, H., Kawai, Y., Sawano, R., Kurihara, H., Yamazaki, K., and Inoue, N. (2005). Antimicrobial Substances from Rhizomes of the Giant Knotweed *Polygonum Sachalinense* against the Fish Pathogen *Photobacterium Damselae* Subsp. *Piscicida*. *Z Naturforsch C J. Biosci.* 60 (1-2), 39–44. doi:10.1515/znc-2005-1-208

Lee, J. S., Kim, J. H., Han, Y. K., Ma, J. Y., Kim, Y. H., Li, W., et al. (2018). Cholinesterases Inhibition Studies of Biological Active Compounds from the Rhizomes of *Alpinia Officinarum* Hance and In Silico Molecular Dynamics. *Int. J. Biol. Macromol.* 120, 2442–2447. doi:10.1016/j.ijbiomac.2018.09.014

Lesjak, M., Beara, I., Simin, N., Pintać, D., Majkić, T., Bekvalac, K., et al. (2018). Antioxidant and Anti-inflammatory Activities of Quercetin and its Derivatives. *J. Funct. Foods* 40, 68–75. doi:10.1016/j.jff.2017.10.047

Li, Q., Tu, Y., Zhu, C., Luo, W., Huang, W., Liu, W., et al. (2017). Cholinesterase, β-amyloid Aggregation Inhibitory and Antioxidant Capacities of Chinese Medicinal Plants. *Industrial Crops Prod.* 108, 512–519. doi:10.1016/j.indcrop.2017.07.001

Lin, H. C., and Lee, S. S. (2010). Proanthocyanidins from the Leaves of *Machilus Philippinensis*. *J. Nat. Prod.* 73 (8), 1375–1380. doi:10.1021/np1002274

Lin, L., Ni, B., Lin, H., Zhang, M., Li, X., Yin, X., et al. (2015). Traditional Usages, Botany, Phytochemistry, Pharmacology and Toxicology of *Polygonum Multiflorum* Thunb.: a Review. *J. Ethnopharmacol.* 159, 158–183. doi:10.1016/j.jep.2014.11.009

Lineweaver, H., and Burk, D. (1934). The Determination of Enzyme Dissociation Constants. *J. Am. Chem. Soc.* 56 (3), 658–666. doi:10.1021/ja01318a036

Martinez, A., and Castro, A. (2006). Novel Cholinesterase Inhibitors as Future Effective Drugs for the Treatment of Alzheimer's Disease. *Expert Opin. Investig. Drugs* 15 (1), 1–12. doi:10.1517/13543784.15.1.1

Meng, L., Sun, C., Gao, L., Saleem, M., Li, B., and Wang, C. (2021b). Hydroxybenzoate Hydroxylase Genes Underlying Protocatechuic Acid Production in *Valsa mali* Are Required for Full Pathogenicity in Apple Trees. *Mol. Plant Pathol.* 22 (11), 1370–1382. doi:10.1111/mpp.13119

Meng, L., Qi, W., Zhang, X., Zhang, D., Huang, Y., Shi, M., et al. (2021a). Phytochemical and Chemotaxonomic Study on Fallopia Dentatoalata (Fr. Schm.) Holub. *Biochem. Syst. Ecol.* 98, 104331. doi:10.1016/j.bse.2021.104331

Meselhy, M. (2003). Constituents from Moghat, the Roots of *Glossostemon Bruguieri* (Desf.). *Molecules* 8 (8), 614–621. doi:10.3390/80800614

Mesulam, M. M., Guillozet, A., Shaw, P., Levey, A., Duysen, E. G., and Lockridge, O. (2002). Acetylcholinesterase Knockouts Establish Central Cholinergic Pathways and Can Use Butyrylcholinesterase to Hydrolyze Acetylcholine. *Neuroscience* 110 (4), 627–639. doi:10.1016/s0306-4522(01)00613-3

Nguyen, T. A., Ha, M. T., Park, S. E., Choi, J. S., Min, B. S., and Kim, J. A. (2020). Stilbenes with Potent Protein Tyrosine Phosphatase-1B Inhibitory Activity from the Roots of *Polygonum Multiflorum*. *J. Nat. Prod.* 83 (2), 323–332. doi:10.1021/acs.jnatprod.9b00777

Nicolet, Y., Lockridge, O., Masson, P., Fontecilla-Camps, J. C., and Nachon, F. (2003). Crystal Structure of Human Butyrylcholinesterase and of its Complexes with Substrate and Products. *J. Biol. Chem.* 278 (42), 41141–41147. doi:10.1074/jbc.M210241200

Norman, E. O., Tuohey, H., Pizzi, D., Saidah, M., Bell, R., Brkljača, R., et al. (2021). Phytochemical Profiling and Biological Activity of the Australian Carnivorous Plant, *Drosera Magna*. *J. Nat. Prod.* 84 (4), 964–971. doi:10.1021/acs.jnatprod.0c00869

Nugroho, A., Choi, J. S., Seong, S. H., Song, B.-M., Park, K.-S., and Park, H.-J. (2018). Isolation of Flavonoid Glycosides with Cholinesterase Inhibition Activity and Quantification from *Stachys Japonica*. *Nat. Prod. Sci.* 24 (4), 259. doi:10.20307/nps.2018.24.4.259

Otsuka, H., Yamasaki, K., and Yamauchi, T. (1989). Alangifolioside, a Diphenylmethylene Derivative, and Other Phenolics from the Leaves of *Alangium Platanifolium* Var. *Trilobum*. *Phytochemistry* 28 (11), 3197–3200. doi:10.1016/0031-9422(89)80306-1

Qian, J., Hou, M., Wu, X., Dai, C., Sun, J., and Dong, L. (2020). A Review on the Extraction, Purification, Detection, and Pharmacological Effects of 2,3,5,4'-Tetrahydroxystilbene-2-O-β-D-Glucoside from Polygonum Multiflorum. *Biomed. Pharmacother.* 124, 109923. doi:10.1016/j.biopha.2020.109923

Semwal, R. B., Semwal, D. K., Combrinck, S., and Viljoen, A. (2021). Emodin - A Natural Anthraquinone Derivative with Diverse Pharmacological Activities. *Phytochemistry* 190, 112854. doi:10.1016/j.phytochem.2021.112854

Takasaki, M., Kuroki, S., Kozuka, M., and Konoshima, T. (2001). New Phenylpropanoid Esters of Sucrose from *Polygonum Lapathifolium*. *J. Nat. Prod.* 64 (10), 1305–1308. doi:10.1021/np010222q

Tsai, P. W., Lee, Y. H., Chen, L. G., Lee, C. J., and Wang, C. C. (2018). *In Vitro* and *In Vivo* Anti-osteoarthritis Effects of 2,3,5,4'-Tetrahydroxystilbene-2-O-β-D-Glucoside from Polygonum Multiflorum. *Molecules* 23 (3), 571. doi:10.3390/molecules23030571

Vyas, S., Beck, J. M., Xia, S., Zhang, J., and Hadad, C. M. (2010). Butyrylcholinesterase and G116H, G116S, G117H, G117N, E197Q and G117H/E197Q Mutants: A Molecular Dynamics Study. *Chem. Biol. Interact.* 187 (1), 241–245. doi:10.1016/j.cbi.2010.04.004

Wang, H., and Zhang, H. (2019). Reconsideration of Anticholinesterase Therapeutic Strategies against Alzheimer's Disease. *ACS Chem. Neurosci.* 10 (2), 852–862. doi:10.1021/acschemneuro.8b00391

Wu, H. K., Sun, T., Zhao, F., Zhang, L. P., Li, G., and Zhang, J. (2017). New Diterpenoids Isolated from *Leonurus Japonicus* and Their Acetylcholinesterase Inhibitory Activity. *Chin. J. Nat. Med.* 15 (11), 860–864. doi:10.1016/s1875-5364(18)30020-7

Xu, G. H., Ryoo, I. J., Kim, Y. H., Choo, S. J., and Yoo, I. D. (2009). Free Radical Scavenging and Antielastase Activities of Flavonoids from the Fruits of *Thuja Orientalis*. *Arch. Pharm. Res.* 32 (2), 275–282. doi:10.1007/s12272-009-1233-y

Yang, Y.-y., Lin, M.-m., Wang, Y.-x., and Chen, Y.-g. (2020). Compounds from the Pods of *Albizia Julibrissin*. *Chem. Nat. Compd.* 56 (2), 328–330. doi:10.1007/s10600-020-03021-2

Yi, S., Kuang, T., Miao, Y., Xu, Y., Wang, Z., Dong, L.-B., et al. (2020). Discovery and Characterization of Four Glycosyltransferases Involved in Anthraquinone Glycoside Biosynthesis in *Rubia Yunnanensis*. *Org. Chem. Front.* 7 (17), 2442–2448. doi:10.1039/d0qo00579g

Yoshida, T., Maruyama, T., Nitta, A., and Okuda, T. (1992). Eucalbanins A,B and C, Monomeric and Dimeric Hydrolyzable Tannins from Eucalyptus Alba REINW. *Chem. Pharm. Bull.* 40 (7), 1750–1754. doi:10.1248/cpb.40.1750

Zhang, L., Liao, C. C., Huang, H. C., Shen, Y. C., Yang, L. M., and Kuo, Y. H. (2008). Antioxidant Phenylpropanoid Glycosides from *Smilax Bracteata*. *Phytochemistry* 69 (6), 1398–1404. doi:10.1016/j.phytochem.2008.01.002

Zhang, X. F., Du, J. L., Ren, J., Ye, F. M., Xie, Y. G., Cheng, X. R., et al. (2015). Three New Sesquiterpene Lactones from *Inula Britannica*. *Arch. Pharm. Res.* 38 (5), 666–672. doi:10.1007/s12272-014-0388-3

Zhang, Y., DeWitt, D. L., Murugesan, S., and Nair, M. G. (2004). Novel Lipid-Peroxidation- and Cyclooxygenase-Inhibitory Tannins from *Picrorhiza Kurroa* Seeds. *Chem. Biodivers.* 1 (3), 426–441. doi:10.1002/cbdv.200490036

Zhao, Y., Chen, M. X., Kongstad, K. T., Jäger, A. K., and Staerk, D. (2017). Potential of Polygonum Cuspidatum Root as an Antidiabetic Food: Dual High-Resolution α-Glucosidase and PTP1B Inhibition Profiling Combined with HPLC-HRMS and NMR for Identification of Antidiabetic Constituents. *J. Agric. Food Chem.* 65 (22), 4421–4427. doi:10.1021/acs.jafc.7b01353

Conflict of Interest: The authors declare that the research was conducted in the absence of any commercial or financial relationships that could be construed as a potential conflict of interest.

Publisher's Note: All claims expressed in this article are solely those of the authors and do not necessarily represent those of their affiliated organizations, or those of the publisher, the editors and the reviewers. Any product that may be evaluated in this article, or claim that may be made by its manufacturer, is not guaranteed or endorsed by the publisher.

frontiers | Frontiers in Pharmacology

TYPE Original Research
PUBLISHED 21 July 2022
DOI 10.3389/fphar.2022.940999

OPEN ACCESS

EDITED BY
Zhi Sun,
First Affiliated Hospital of Zhengzhou University, China

REVIEWED BY
Sachchida Nand Rai,
University of Allahabad, India
Yuqing Yan,
West Virginia University, United States

*CORRESPONDENCE
Yao Yao,
20070007@nxmu.edu.cn
Ji-Xiang Tian,
jxtian@icmm.ac.cn

†These authors have contributed equally to this work

SPECIALTY SECTION
This article was submitted to Neuropharmacology, a section of the journal Frontiers in Pharmacology

RECEIVED 10 May 2022
ACCEPTED 28 June 2022
PUBLISHED 21 July 2022

CITATION
Li J, Zou B, Cheng X-Y, Yang X-H, Li J, Zhao C-H, Ma R-X, Tian J-X and Yao Y (2022), Therapeutic effects of total saikosaponins from Radix bupleuri against Alzheimer's disease. *Front. Pharmacol.* 13:940999. doi: 10.3389/fphar.2022.940999

Therapeutic effects of total saikosaponins from *Radix bupleuri* against Alzheimer's disease

Juan Li[1,2†], Bin Zou[1†], Xiao-Yu Cheng[3†], Xin-He Yang[1], Jia Li[1], Chun-Hui Zhao[4], Rui-Xia Ma[1], Ji-Xiang Tian[4*] and Yao Yao[5*]

[1]School of Pharmacy, Ningxia Medical University, Yinchuan, China, [2]Ningxia Engineering and Technology Research Center for Modernization of Characteristic Chinese Medicine, and Key Laboratory of Ningxia Ethnomedicine Modernization, Ministry of Education, Ningxia Medical University, Yinchuan, China, [3]Department of Neurology and Clinical Research Center of Neurological Disease, The Second Affiliated Hospital of Soochow University, Suzhou, China, [4]Institute of Chinese Materia Medica, China Academy of Chinese Medical Sciences, Beijing, China, [5]School of Basic Medical Sciences, Ningxia Medical University, Yinchuan, China

Alzheimer's disease (AD) is a neurodegenerative disease characterized by memory loss and cognitive dysfunction in the elderly, with amyloid-beta (Aβ) deposition and hyperphosphorylation of tau protein as the main pathological feature. Nuclear factor 2 (Nrf2) is a transcription factor that primarily exists in the cytosol of hippocampal neurons, and it is considered as an important regulator of autophagy, oxidative stress, and inflammation. Total saikosaponins (TS) is the main bioactive component of *Radix bupleuri* (Chaihu). In this study, it was found that TS could ameliorate cognitive dysfunction in APP/PS1 transgenic mice and reduce Aβ generation and senile plaque deposition via activating Nrf2 and downregulating the expression of β-secretase 1 (BACE1). In addition, TS can enhance autophagy by promoting the expression of Beclin-1 and LC3-II, increasing the degradation of p62 and NDP52 and the clearance of phosphorylated tau (*p*-tau), and reducing the expression of *p*-tau. It can also downregulate the expression of nuclear factor-κB (NF-κB) to inhibit the activation of glial cells and reduce the release of inflammatory factors. *In vitro* experiments using PC12 cells induced by Aβ, TS could significantly inhibit the aggregation of Aβ and reduce cytotoxicity. It was found that Nrf2 knock-out weakened the inhibitory effect of TS on BACE1 and NF-κB transcription in PC12 cells. Moreover, the inhibitory effect of TS on BACE1 transcription was achieved by promoting the binding of Nrf2 and the promoter of BACE1 ARE1. Results showed that TS downregulated the expression of BACE1 and NF-κB through Nrf2, thereby reducing the generation of Aβ and inhibiting neuroinflammation. Furthermore, TS can ameliorate synaptic loss and alleviate oxidative stress. In gut microbiota analysis, dysbiosis was demonstrated in APP/PS1 transgenic mice, indicating a potential link between gut microbiota and AD. Furthermore, TS treatment reverses the gut microbiota disorder in APP/PS1 mice, suggesting a therapeutic strategy by remodeling the gut microbe. Collectively, these data shows that TS may serve as a potential approach for AD treatment. Further investigation is

needed to clarify the detailed mechanisms underlying TS regulating gut microbiota and oxidative stress.

KEYWORDS

total saikosaponins, Alzheimer's disease, Aβ, p-tau, Nrf2, autophagy, gut microbiota

1 Introduction

Alzheimer's disease (AD) is a progressive and multifaceted neurodegenerative disorder of the central nervous system with dementia, loss of memory, and cognitive disturbance (Luo et al., 2016). At present, cholinesterase inhibitors (ChEIs) and N-methyl-D-aspartate receptor antagonists such as donepezil, rivastin, galantamine, and memantine have been approved for clinical treatment of AD, which are single-target drugs that can only show mild and temporary improvement in learning and memory dysfunction accompanied by hepatotoxicity or cholinergic crisis, indicating that improving cognitive function through a single target is not a feasible therapeutic approach (Yang et al., 2017; Liu et al., 2018; Osama et al., 2020; Scheltens Philip, 2021). Therefore, developing multi-target, low-toxicity, and effective drugs for the treatment of AD is necessary.

The neuropathological features of AD include the deposition of Aβ plaques in the neocortex and neurofibrillary tangles (primarily composed of tau aggregates) in the marginal and cortical joint areas (Busche & Hyman, 2020). Genetic studies have shown that mutations in amyloid precursor protein (APP) or enzymes that produce Aβ can cause autosomal dominant hereditary AD; thus, Aβ is considered as the key initiator of the disease. The Aβ cascade hypothesis indicates that Aβ can induce a series of harmful responses, including increased inflammation, synaptic dysfunction, and neuronal loss, and promote tau protein phosphorylation (Tsai et al., 2015; Pereira et al., 2019; Busche & Hyman, 2020; Zetterberg & Bendlin, 2021). The hyperphosphorylation of tau protein (a microtubule-associated protein) is related to the tangles of nerve fibers, which can also aggravate the inflammation of the nervous system, affect the mitochondrial function of neurons, and promote the decline of cognitive function (Tsai et al., 2015; Wang Z. Y. et al, 2016). Recently, the therapeutic effect of Nrf2 on AD has been reported: Nrf2 is highly expressed in astrocytes, providing a neuroprotective effect (Cuadrado et al., 2018; Osama et al., 2020). In NRF2-deficient mice, the levels of insoluble *p*-tau and Aβ increased significantly, which aggravated cognitive impairment in APP/PS1 mice (Branca et al., 2017; Rojo et al., 2017; Osama et al., 2020). In addition, considerable literature has shown that NRF2 promotes the clearance of APP and tau by upregulating the expression of autophagy genes, which plays an important role in maintaining cellular redox dynamic balance and regulating neuroinflammation (Pajares et al., 2016; Pajares et al., 2018; Osama et al., 2020). Therefore, Nrf2 plays a central role in the pathological process of AD.

Recently, several studies have focused on elucidating the two-way communication pathway between intestinal bacteria and the central nervous system: microbe–gut–brain axis. Clinical and laboratory studies have revealed the changes in intestinal flora and its metabolites related to the occurrence and development of AD (Wang Z. Y. et al, 2016; Cryan et al., 2020), and some studies have proven that abnormal microbiota may cause AD. Based on previous reports, the level of trimethylamine N-oxide produced by dietary choline metabolism is increased in patients with dementia, which is positively correlated with *p*-tau, a biomarker of AD (Vogt et al., 2018). In addition, intestinal microbiota-bile acid (BA) can significantly decrease the concentration of primary bile acid (CA) in patients with AD, which is closely related to cognitive decline (MahmoudianDehkordi et al., 2019). Furthermore, scientists have transplanted feces of AD animals into aseptic APP transgenic mice. The accumulation of Aβ is accelerated after transplantation, demonstrating that intestinal microflora contributes to the development of AD pathology. Considering the vital role of intestinal flora in AD, more studies have focused on the intervention of AD based on microbiota. For example, *Clostridium butyricum* (CB) could improve cognitive impairment and Aβ deposition in APP/PS1 mice, reduce neuroinflammation mediated by microglia, and reverse the abnormal changes of gut microbiota (GM) and butyric acid, indicating that CB can play the role of anti-AD by regulating the GM–gut–brain axis (Sun et al., 2020). Therefore, the therapy based on intestinal microbiota may provide a new direction for the treatment of AD (Harach et al., 2017).

Radix bupleuri (Chaihu) is a traditional Chinese medicine widely used to treat fever, influenza, inflammation, chronic hepatitis, cancer, nephrotic syndrome and other diseases (Park et al., 2015; Lin et al., 2016). It was recorded that Chaihu show ability to nourish liver and blood, promote blood circulation and Qi flow in the brain (Liang et al., 2012), thus it could be used to treat brain disease. Many traditional prescriptions with Chaihu as the main drug such as Chaihu Shugan San and Xiaochaihu Tang have been used in AD treatment and reported to show potent anti-AD effects (Zhao et al., 2012; Liu et al., 2019a; Zeng et al., 2019; Sohn et al., 2021). Saikosaponins, a group of oleanane triterpenoid saponins, are the main bioactive component in Chaihu. More than 100 different saikosaponins have been identified, of which the main components are saikosaponin a and d. Saikosaponins show various bioactivities such as anticancer, antiviral, antipyretic, hepatoprotective, neuroprotective, immunomodulatory, and antibacterial effects

(Park et al., 2015; Lee et al., 2016; Lin et al., 2016; Kim, 2018; Li et al., 2020). Recent studies have shown that saikosaponins have multiple effects on inflammation, antioxidant balance, and injury: SSd can inhibit the production of reactive oxygen species (ROS) and upregulate the expression of antioxidant enzymes, namely, superoxide dismutase (SOD) and malondialdehyde (MDA); SSa and SSd can also inhibit the expression of inflammatory factors in mouse macrophages induced by LPS, indicating that saikosaponins may be used to treat AD through antioxidation and inhibition of neuroinflammation (Kim, 2018). At present, few studies have been conducted on the use of saikosaponins in the treatment of AD. Lee et al. have shown that SSc can inhibit the secretion of $A\beta_{1\text{-}40}$ and $A\beta_{1\text{-}42}$ and the phosphorylation of tau and promote nerve growth factor-mediated axonal growth (Lee et al., 2016; Kim, 2018). Based on these evidence, total saikosaponins (TS) may have a therapeutic effect in AD treatment, but the effect and mechanism need to be further elucidated.

The present study aimed to investigate the therapeutic effect of TS on APP/PS1 transgenic mice and underlying mechanisms. The results reveal that TS downregulated the transcription and expression level of BACE1 through the Nrf2 pathway to reduce Aβ production and senile plaque deposition. The inhibitory effect of TS on BACE1 transcription was achieved by promoting the binding of Nrf2 and the promoter of BACE1 ARE1. In addition, TS promoted autophagy by regulating the expression of autophagic proteins, thereby reducing the level of *p*-tau. In the aspect of neuroinflammation, TS could downregulate NF-κB transcription and expression through Nrf2, thus inhibiting the activation of glial cells and reducing the production of inflammatory factors. TS was found to ameliorate synaptic loss and alleviate oxidative stress. Furthermore, TS could reverse the GM disorder in APP/PS1 mice and improve the diversity of GM. Collectively, this study can provide a new insight and potential approach for the treatment of AD.

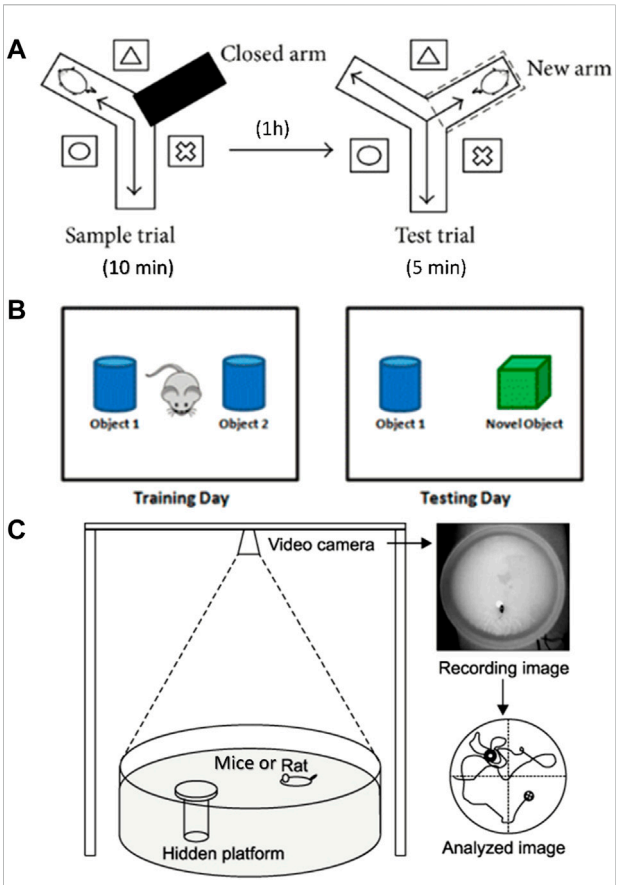

FIGURE 1
Diagram of behavioral experimental equipment. **(A)** Schematic diagram of Y-maze experimental device. **(B)** Schematic diagram of NOR experiment. **(C)** Schematic diagram of Morris water maze device.

2 Materials and methods

2.1 Preparation of total saikosaponins

Radix Bupleuri was purchased from the Chinese Medicinal Material market in Bozhou, China (Lot No. 20190311). Total saikosaponins were prepared using a modified method based on previous report (Li et al., 2013). Briefly, 3 kg air-dried roots were sliced and reflux-extracted by 80% ethanol (adjusted to pH 9 with KOH) for two times, 90 min each. The extract solution was concentrated under vacuum to 3 L, and then subjected to column chromatography using 4.5 L AB-8 macroporous absorption resin. It was eluted with water, 30% ethanol, 70% ethanol and 95% ethanol successively. The 70% ethanol elution was collected and evaporated under vacuum, and then dried using vacuum freeze dryer to yield TS. Three main monomeric saponins in TS were determined using HPLC, and the content of SSa, SSd, SSc was 17.11, 12.52, 3.36%, respectively.

2.2 Animal experiment procedure

Eight-month-old APP/PS1 mice and wild-type (WT) C57BL/6J mice (half male and half female, weighing 25 ± 5 g) were purchased from Beijing Huafukang Experimental Animal Technology Co., Ltd. All animal procedures were performed in accordance with the Provision and General Recommendation of Chinese Experimental Animals Administration Legislation and approved by the Ethic Committee of Ningxia Medical University (No. 2016–037). Throughout the study, all mice were kept in a pathogen-free environment with a light/dark cycle of 12 h and free access to food and water under constant temperature and humidity (22 ± 1°C and 45–55%, respectively). APP/PS1 mice were randomly divided into five groups (n = 10): model group; low, middle, and high-dose TS

groups; and donepezil group (positive control). C57BL/6J WT mice were used as blank control. The mice of TS groups were intragastrically administrated with different doses of TS (20, 40, and 80 mg/kg), and the positive group was given donepezil (5 mg/kg). The blank group and model group were given the same amount of normal saline as control. The administration lasted for 30 days, and behavioral tests including Y maze test, novel object recognition (NOR) test, and Morris water maze test were performed on days 22–30. Then, mice were sacrificed by cervical dislocation on day 31, and samples were collected for further assessment.

2.3 Behavioral experiments

One month after drug treatment, Y-maze test was performed to evaluate the working memory ability as previously described (Liu et al., 2019b). The Y maze consists of three identical arms, each with an angle of 120° and a size of 30 cm × 8 cm × 15 cm (length × width × height). A movable partition was placed in the center, and different geometric figures were affixed to each arm of the maze as a visual marker. The three arms of the Y maze were randomly set as the novel arm, the start arm, and the other arm. A camera was placed 1.5 m above the maze to record the movement track of the mice. The diagram of the Y maze is shown in Figure 1A. The Y maze experiment consists of two stages with an interval of 1 h. The first stage is the training period. After blocking the new arm with a partition, the mice were placed into the starting arm to move freely for 10 min in the maze. After 1 h, during the second stage of detection, a new different arm septum was opened, and similarly, the mice were placed into the starting arm to move freely for 5 min in the three arms. Before each trial, the maze was thoroughly cleaned with 75% ethanol to eliminate scent cues. The residence time of mice in the new arm was recorded.

The NOR test was conducted to evaluate the ability to distinguish new object as previously reported (Scott et al., 2017). The schematic diagram of the NOR test is shown in Figure 1B. During habituation, each mouse was allowed to explore freely for 5 min in the test box (50 cm × 50 cm × 30 cm). During training, which started 24 h later, two identical objects were placed in the test box. Each mouse was placed in the box and allowed to explore freely for 5 min, and the touching times of mice to each object were recorded. After 24 h, one of the original objects was replaced by a new object similar in size but different in shape and color. Each mouse was placed in the test box and allowed to explore freely for 5 min. The touching times of mice to each object were recorded. After each test, the test box and objects were cleaned with 75% ethanol. The times of exploring new and old objects were statistically analyzed, and the discrimination index (DI) was calculated. DI = (TN−TF)/(TN+TF), where TN is the number of times to explore new objects, and TF is the number of times to explore old objects.

Morris water maze test was carried out to evaluate spatial learning and memory ability as previously described (Liu et al., 2019). In brief, the test was carried out in a round stainless-steel pool with a diameter of 1.2 m, which was divided into four quadrants. A 10 cm diameter hidden platform was placed at the center of the IV quadrant, 1 cm below the water surface. The water temperature was kept at 22–24°C. The schematic diagram of the water maze system is shown in Figure 1C. The experiment lasted for 5 days, and each mouse was trained two times a day. During the place navigation test, mice were released into the water facing the pool wall from the edge of each quadrant and allowed to swim freely for 60 s until they found the hidden platform. If a mouse could not find the platform within 60 s, then it will be placed onto the platform and stayed for 30 s. Mice were trained two times a day for 3 days. Twenty-4 hours after the training period, the place navigation test was carried out. The time each mouse spent to find the hidden platform was recorded as escape latency. Afterward, the spatial probe test was performed, in which the platform was removed, and the mice were released into the water to swim freely for 60 s. The following data were recorded: 1) latency, the time mouse spent to reach the hidden platform area for the first time; 2) number of crossing, the number of times the mouse passed through the hidden platform area; 3) time in the target quadrant, the time mouse spent in the quadrant of the former hidden platform. All experimental data were analyzed using the WMT-100S analysis system (Techman Software, Chengdu, China).

2.4 Brain tissue preparation

After the behavioral test, the mice were anesthetized and perfused with PBS containing heparin (10 U/mL) precooled at 4°C. The brain was removed and divided into two parts along the sagittal plane. The left hemisphere was fixed with 4% paraformaldehyde, and paraffin-embedded sections were prepared for immunohistochemical experiments. The right hemisphere was stored at −80°C for further ELISA and Western blot experiments.

2.5 Immunohistochemical staining

The brain tissue soaked in 4% paraformaldehyde (Solebo) was trimmed, dehydrated, waxed, and then embedded. The repaired wax block was cut into a cross-section with a thickness of 4 μm and then dewaxed and rehydrated after baking. Antigen repair was performed with 0.01 m sodium citrate solution (pH 6.0). Endogenous peroxidase was blocked with 3% hydrogen peroxide solution (Solebo) and then blocked with 3%BSA for 30 min. The slices were then incubated overnight at 4°C with antibodies *p*-tau (Ser396, 1:200, Affinity, AF3148), Iba-1 (1:200, GeneTex, GTX101495), GFAP (1:200, CST, 3670),

Synaptophysin (1:200, Abcam, ab32127), PSD-95 (1:200, Abcam, ab12093), and NeuN (1:200, Abcam, ab177487). On the second day, after washing with PBS three times, the slices were incubated with HRP-sheep and rabbit anti-IgG (1:200, Abbkine, A21020), HRP-sheep anti-mouse IgG (1:200, Beijing Zhongshan Biological Engineering Co., Ltd.), Alexa Fluor 488-donkey anti-rabbit IgG secondary antibody (1:200, Abcam, ab150073), and Alexa Fluor 594-donkey anti-sheep IgG (1:200, Abcam, ab150132), followed by coloration with DAB (Beijing Zhongshan Jinqiao Biotechnology Co., Ltd.), and finally dehydrated. The second anti-rabbit IgG antibody was incubated with the second antibody of donkey anti-rabbit IgG (1:200, Beijing Zhongshan Bio-Engineering Co., Ltd.), followed by coloration by DAB (Beijing Zhongshan Jinqiao Biotechnology Co., Ltd.), and then sealed using a neutral gum (Beijing Zhongshan Jinqiao Biotechnology Co., Ltd.). All sections were observed by using an optical microscope (DP73-ST-SET, Olympus, Japan) or sealed with an anti-fluorescence quenching agent.

2.6 Quantification of cerebral Aβ levels

Aβ40 and Aβ42 are markers of amyloid deposition in the cerebral cortex of patients with AD (Olsson et al., 2016). The levels of Aβ in mouse brain were determined using Aβ40 and Aβ42 Elisa kits (China Peptide Biochemistry Co., Ltd. and IBL Co., Ltd.) according to the instructions of the manufacturer. The sample to be tested was properly diluted with dilution buffer and coated in an ELISA plate at 100 μL per hole at 4°C overnight, and the coating solution was discarded the next day and washed nine times for 60 s each time. In addition, the labeled antibody working solution, 100 μL per well, was incubated at 4°C for 1 h, and the plate was washed nine times for 60 s each time. Afterward, TMB substrate chromogenic solution was added, 100 μL per well, and light reaction was avoided for 20 min at 37°C. Finally, absorbance was determined at 450 nm after termination.

2.7 Measurement of oxidative stress and inflammatory cytokines

TNF-α, IL-6, and IL-1β in the samples were evaluated using ELISA kit according to the manufacturer's protocol (Biolegend), and oxidative stress was assessed by using MDA, SOD, and GSH kits according to the manufacturer's protocol (Shanghai Biyuntian Biotechnology Co., Ltd.).

2.8 Cell culture

PC12 cells from the Library of Chinese Academy of Sciences cells were incubated in DMEM (Basal Media, J210908) containing 10% fetal bovine serum (Gibco, 10099141C) and 1% penicillin/streptomycin (Hyclone) at 37°C. The cells were cultured in a Petri dish or cell culture plate to 70–80% fusion.

2.9 Cell viability assay

The cells were seeded in a 96-well plate (5×10^4 cells/well) and treated with different concentrations of TS (0.01, 0.1, 0.1, and 10 μg/ml), 1 μM of Aβ, 10 μM of CQ (MCE), or 0.1–3.2 μM of Rapa (MCE) for 24 h. Then, the cells were incubated with 5 mg/ml of MTT (50 μL/well) for 4 h. The supernatant was removed, and 150 μL of DMSO was added. The absorbance was measured at 570 nm using a microplate reader. The absorbance values of each group were normalized to the ratio in the control group.

2.10 Thioflavin T fluorescence assay

Thiosulfonate T (ThT) was used for immunofluorescence assay of amyloid fibers *in vitro*. In addition, 10 μM of Aβ42 was mixed with 0.2 μg/ml of TS and incubated at 37°C. Then, 180 μL of ThT (5 μM) and 20 μL of samples were mixed in a 96-well plate. The fluorescence value of ThT in the solution was detected at different time points using a fluorescence microplate reader (excitation wavelength of 448 nm and emission wavelength of 485 nm).

2.11 Small ribonucleic acid interference

PC12 cells were cultured in a six-well cell culture plate (3×10^5 cells/well). The liposome transfection reagent (LipoFiterTM3, HB-TRLF3) and Nrf2-siRNA (Santa Cruz, sc-155128) were mixed at 1:1 and added to the serum-free DMEM. After incubation in the six-well plate for 6 h, total RNA was extracted and incubated with fresh DMEM containing serum for 36 h. Then, RT-qPCR was performed as described in Section 2.13.

2.12 Chromatin immunoprecipitation

The ChIP was performed using ChIP Assay kit (Beyotime Biotechnology, P2078) according to the manufacturer's protocol. Briefly, PC12 cells treated with TS were cross-linked for 10 min in 10 ml of 1% formaldehyde solution at room temperature and then quenched for 5 min with glycine solution. Cells were washed two times with cold PBS containing PMSF. Then, the cells were scraped, collected, and centrifuged at 4°C and 1000 g for 2 min, and the supernatant was removed. The precipitate was re-suspended with SDS lysis buffer containing PMSF and incubated on ice for 10 min for full cleavage. Chromatin

fragments were treated with SONICS (1 min, 5 s on/5 s off) ultrasound. Then, the ultrasonically treated sample was centrifuged at 4°C and 12000 g for 5 min. The supernatant was placed in an ice bath, and the ChIP dilution buffer containing 1 mM PMSF in 1.8 ml was added to dilute the sample to a 2 ml final volume. A 50 μL sample solution was used as Input for follow-up detection. The rest of the sample solution was mixed with 70 μL Protein A+G Agarose/Salmon Sperm DNA and rotated slowly at 4°C for 30 min to reduce the non-specific binding to the target protein or target DNA sequence. Then, the sample was centrifuged at 4°C and 1000 g for 1 min, and the supernatant was transferred to a new centrifuge tube. Subsequently, 1.43 μL of Nrf2 antibody was added and rotated slowly at 4°C to mix overnight. Afterward, 60 μL of Protein A+G Agarose/Salmon Sperm DNA was added and mixed slowly at 4°C for 60 min to precipitate the protein or the corresponding complex recognized by the primary antibody. Then, the solution was centrifuged at 4°C and 1000 g for 1 min. The supernatant was removed carefully, and low-salt immune complex wash buffer, high-salt immune complex wash buffer, and LiCl immune complex wash buffer were used to wash the precipitate once; TE buffer was used to wash the precipitate two times. Then, the solution was centrifuged for 1 min at 4°C and 1,000 g, and the supernatant was removed carefully. The freshly prepared 250 μL of elution buffer was added, vortexed, mixed well, rotated at room temperature, and continuously eluted for 5 min. Afterward, the solution was centrifuged for 1 min at 1,000 *g*, and the supernatant was removed and combined, obtaining a total of 500 μL of supernatant. Twenty microliters of 5M NaCl was added to 500 μL of supernatant and 2.5 μL of 15M NaCl to obtain a 50 μL input and then heated at 65°C for 4 h to remove the cross-linking between protein and genomic DNA. The 520 μL sample was purified by DNA. Forty microliters of TE was used to re-suspend DNA precipitates for qPCR detection of the target gene.

2.13 Quantitative real-time polymerase chain reaction

After homogenization of PC12 cells, total RNA was extracted using a total RNA extraction reagent (RNAsimple Total RNA Kit, TIANGEN, DP419) and homogenized in accordance with the regulations of manufacturers, and Promega deoxyribonuclease I (Promega) was used to remove pollution. Five hundred nanogram of each sample were used for first-strand cDNA synthesis (RevertAid First-strand cDNA Synthesis Kit, Thermo, K1622). Then, CFX connect (Biorad) were used for real-time RT-PCR. PCR amplification was performed with SYBR PreMix Ex TaqTMII (Takara). The amplification conditions of all genes were as follows: amplification at 95°C for 30 s, 40 times amplification at 95°C, amplification for 5s, and amplification for 30 s at 60°C. The differences between the Ct values for experimental and reference genes were calculated as ΔΔCt. The qRT-PCR primer sequences are listed in Table 1.

2.14 Western blot analysis

Tissue and cell lysates were obtained using a whole protein extraction kit (Key GEN, Nanjing, China). The protein concentration in the supernatant was determined by bicinchoninic acid assay (Key GEN, Nanjing, China). Then, the proteins were separated by SDS-polyacrylamide gel electrophoresis and electro-transferred to polyvinylidene fluoride. After blocking with 5% skimmed milk powder, the film was incubated at 4°C overnight with different primary antibodies: Nrf2 (1:1,000, Proteintech, 16396-1-AP), BACE1 (1:1,000, Proteintech, 12807-1-AP), *p*-tau (Ser 396, 1:500, Affinity, AF3148), NDP52/CALCOCO2 (1:1,000, Proteintech, 12229-1-AP), p62 (1:200, Santa Cruz, sc-48402), LC3 (1:200, Santa Cruz, sc-398822), Beclin-1 (1:200, Santa Cruz, sc-48341), mTOR (1:200, Santa Cruz, sc-517464), *p*-TFEB (1:1,000, Affinity, AF3708) and β-actin (1:1,000, Affinity, AF7018). The membrane was washed in TBST (0.5% Tween-20) three times, incubated with anti-rabbit or anti-mouse IgG second antibody (1:20,000, Abbkine, A21010) at room temperature for 1 h, and developed using an enhanced chemiluminescence kit (Key GEN, Nanjing, China). Imprinting was captured using an image analyzer (Amersham Imager 600, General Electric Company, United States), and the relative intensity of the bands was quantified by ImageJ software.

2.15 Fecal sample collection and deoxyribonucleic acid extraction

After intragastrical administration for 4 weeks, mouse fecal samples were collected in a clean cage. Uncontaminated feces were collected and placed in a sterile and enzyme-free EP tube, immediately stored in dry ice, and then frozen at −80°C. A Total DNA was isolated using the MagPure Soil DNA LQ Kit (D6356-03, Personal Biotechnology Co., Ltd., Shanghai, China). The NanoDrop 2000ultraviolet spectrophotometer was used to measure the quality of the DNA. The purified samples were stored at −20°C for further analysis.

2.16 16S rRNA gene high-throughput sequencing and sequencing data analysis

16S rRNA can be used as the characteristic nucleic acid sequence of species, and it is considered as the most suitable index for bacterial phylogenetic and taxonomic identification. In this experiment, bacterial 16S rRNA at the V3-V4 region was amplified using gene universal primers: 338F (5′-ACTCCTACG

TABLE 1 qPCR primer information.

Primer name	Sequence (Forward)	Sequence (Reverse)
BACE1	GTCCTTCCGCATCACCATCCTTC	ACTGTGAGACGGCGAACTTGTAAC
BACE1 ARE1	ACAGGTTCAGATGGGAGAAGACC	AGGAGTAGGGATTTTGGAGGGAC
NF-κB	GGATGGCTTCTATGAGGCTGAACTC	CTTGCTCCAGGTCTCGCTTCTTC

GGAGGCAGCA-3′) and 806R (5′-GGACTACHVGGGTWTCTAAT-3′). The amplification products were recovered by 2% agarose gel electrophoresis method and quantified by Quant-iT PicoGreen dsDNA Assay Kit. The sequencing libraries were constructed on the Illumina Nova Seq system (Personal Biotechnology Co., Ltd., Shanghai, China).

2.17 Analysis of gut microbiota

ASVs (amplicon sequence variants) were clustered and dereplicated by DADA2, and the similarity was 100% (Callahan et al., 2016) (Personal Biotechnology Co., Ltd., Shanghai, China). Compared with Greengenes database (Release13.8, http://greengenes.secondgenome.com/), ASVs were annotated with a taxonomic identifier. QIIME2 (2019.4) software was used to show the specific composition of each group at different species taxonomic levels. Chao1 index and Observed species index were used as indicators to measure Alpha diversity according to species richness. R programming language was used to count the number of ASVs in each group according to the grouping of samples, and bray-curtis clustering algorithm and average clustering method was used to calculate the distance matrices of each sample to evaluate the similarity between samples. The clustering results of each sample were calculated and presented in the form of heat map. Finally, the importance index of marker species was analyzed by Random Forest algorithm. The random forest analysis and nested hierarchical cross test were used in QIIME2 and https://www.genescloud.cn/home online software.

2.18 Statistical analysis

All the experiments were repeated three times, and all the data in each experiment were represented as means ± SEM and processed using GraphPad Prism (version 8, GraphPad Software Inc., CA, United States). Using one-way ANOVA or two-way ANOVA with Dunnett's multiple comparison post hoc test to compare the differences among the groups. For comparisons between two groups, the significance of difference between means was determined by Student's t-test. A p value of <0.05 was considered as statistical significance.

3 Results

3.1 Total saikosaponins treatment alleviates cognitive impairment in APP/PS1 mice

The effect of TS on spatial memory ability impairment in APP/PS1 mice was evaluated by MWM test (Figures 2A–C). Compared with WT mice, the escape latency of APP/PS1 mice in the place navigation test was significantly increased (Figure 2A, $p < 0.0001$), and the number of crossing platform and the time spent in the target quadrant were significantly decreased (Figure 2B, $p < 0.0001$; Figure 2C, $p < 0.001$), indicating that the spatial memory ability of APP/PS1 mice was seriously impaired. Compared with APP/PS1 mice, the escape latency in the middle and high-dose TS treatment group was remarkably shortened (Figure 2A, $p < 0.05$ and $p < 0.01$ respectively), and the number of crossing platform and time spent in the target quadrant were significantly increased after high-dose TS treatment (Figure 2B, $p < 0.05$; Figure 2C, $p < 0.01$), indicating that 80 mg/kg TS treatment could significantly improve the spatial memory impairment of APP/PS1 mice.

The effect of TS on spatial working memory ability impairment in APP/PS1 mice was evaluated by Y-maze test. APP/PS1 mice showed less residence time in the new arm than WT mice (Figure 2D, $p < 0.01$), whereas middle and high-dose TS treatment significantly increased the residence time (Figure 2D, $p < 0.01$ and $p < 0.0001$, respectively), indicating that TS could effectively improve the spatial working memory ability of APP/PS1 mice.

The effect of TS on the NOR ability impairment in APP/PS1 mice was evaluated by NOR test. The results showed that compared with WT mice, the DI of APP/PS1 mice was significantly lower than that of WT mice (Figure 2E, $p < 0.0001$). After middle and high-dose TS treatment, the DI significantly increased, indicating that TS could improve NOR ability in APP/PS1 mice (Figure 2E, $p < 0.01$ and $p < 0.0001$ respectively). Collectively, these data indicated that TS treatment could significantly alleviate cognitive impairment in APP/PS1 mice.

3.2 Total saikosaponins treatment reduces Aβ level and senile plaque in APP/PS1 mice brain

The levels of soluble and insoluble Aβ40 and Aβ42 in brain tissue were measured by ELISA. Compared with WT mice, the

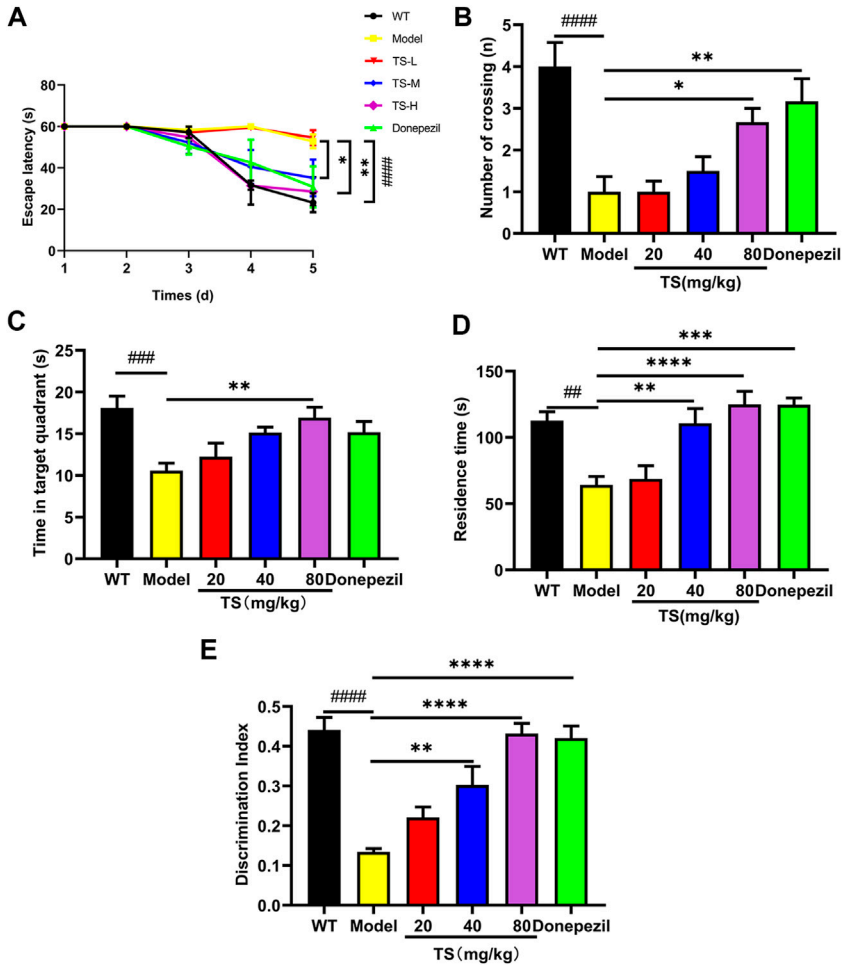

FIGURE 2
TS ameliorated cognitive impairment in APP/PS1 mice. **(A)** The effect of TS on the escape latency in APP/PS1 mice was investigated by Morris water maze ($^{\#\#\#\#}p < 0.0001$, $^{*}p = 0.0277$, $^{**}p = 0.0010$). **(B)** The effect of TS on the number of crossing platform in APP/PS1 mice was investigated by Morris water maze ($^{\#\#\#\#}p < 0.0001$, $^{*}p = 0.0353$, $^{**}p = 0.0044$). **(C)** The effect of TS on the time spent in the target quadrant in APP/PS1 mice by Morris water maze ($^{\#\#\#}p = 0.0007$, $^{**}p = 0.0042$). **(D)** The effect of TS on the residence time in APP/PS1 mice was evaluated by Y-maze test ($^{\#\#}p = 0.0015$, $^{**}p = 0.0024$, $^{***}p = 0.001$, $^{****}p < 0.0001$). **(E)** The effect of TS on the discrimination index in APP/PS1 mice was investigated by NOR test ($^{\#\#\#\#}p < 0.0001$, $^{**}p = 0.0021$, $^{****}p < 0.0001$). $^{\#}$ Compared with WT group; * Compared with model group. Data are presented as mean ± S.E.M. ($n = 10$).

levels of soluble and insoluble Aβ40 and Aβ42 in the brain of APP/PS1 mice significantly increased (Figures 3A–D, $p < 0.0001$), which were remarkably decreased after high-dose TS treatment (Figures 3A–D, $p < 0.0001$). Medium-dose TS treatment reduced the soluble Aβ42 level (Figure 3B, $p < 0.01$) and insoluble Aβ40 and Aβ42 levels (Figure 3C, $p < 0.001$; Figure 3D, $p < 0.0001$). Low-dose TS treatment only reduced the levels of insoluble Aβ40 and Aβ42 (Figure 3C, $p < 0.05$; Figure 3D, $p < 0.0001$). These results indicated that TS significantly reduced the level of Aβ in the brain of AD mice.

Thioflavine S (ThS) is a fluorescent dye with β-folding binding properties, which is widely used to observe the aggregation of amyloid plaques (Shin et al., 2021; Zhao et al., 2021). The ThS staining results showed no senile plaque in the brain of WT mice, and the number and area of senile plaques in the brain of APP/PS1 mice were significantly increased (Figures 3E,F, $p < 0.0001$), which were remarkably declined after TS treatment (Figures 3E,F). Collectively, these data showed that TS treatment was effective in reducing the production of Aβ and formation of senile plaques in the brain of APP/PS1 mice.

3.3 Total saikosaponins inhibits the expression of BACE1 via promoting the Nrf2 pathway in APP/PS1 mice to reduce Aβ deposition

Aβ peptide is produced by sequential cleavage of APP mediated by BACE1 and γ-secretase, and the increase of BACE1 will lead to a sharp increase in Aβ production

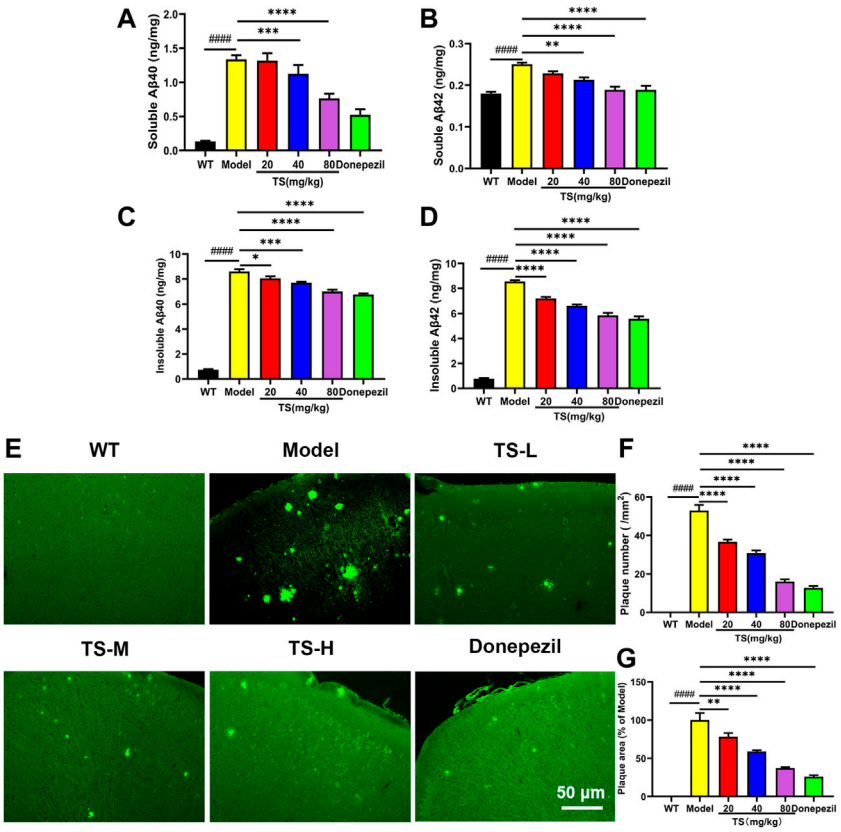

FIGURE 3
TS treatment decreased the levels of Aβ and senile plaque in the brain of APP/PS1 mice. **(A)** The effect of TS on the levels of soluble Aβ40 in the brain of APP/PS1 mice was measured by ELISA ($^{\#\#\#\#}p < 0.0001$, $^{***}p = 0.0003$, $^{****}p < 0.0001$). **(B)** The effect of TS on the levels of soluble Aβ42 in the brain of APP/PS1 mice was measured by ELISA ($^{\#\#\#\#}p < 0.0001$, $^{**}p = 0.0015$, $^{****}p < 0.0001$). **(C)** The effect of TS on the levels of insoluble Aβ40 in the brain of APP/PS1 mice was measured by ELISA ($^{\#\#\#\#}p < 0.0001$, $^{*}p = 0.0220$, $^{***}p = 0.0002$, $^{****}p < 0.0001$). **(D)** The effect of TS on the levels of insoluble Aβ42 in the brain of APP/PS1 mice was measured by ELISA ($^{\#\#\#\#}p < 0.0001$, $^{****}p < 0.0001$). **(E)** The effect of TS on the senile plaque in the brain of APP/PS1 mice was investigated by ThS fluorescence. **(F)** Quantitative analysis of the number of senile plaques in the brain of APP/PS1 mice ($^{\#\#\#\#}p < 0.0001$, $^{****}p < 0.0001$). **(G)** Quantitative analysis of the positive area of senile plaques in the brain of APP/PS1 mice ($^{\#\#\#\#}p < 0.0001$, $^{**}p = 0.0069$, $^{****}p < 0.0001$). $^{\#}$Compared with WT group; *Compared with model group. Data are presented as mean ± SEM ($n = 6$).

(Osama et al., 2020). Therefore, the effects of TS on the expression of BACE1 and Nrf2 were examined to explore the mechanism of TS-mediated reduction of Aβ production. First, MTT experiments were performed, and results revealed that TS could significantly inhibit the cytotoxicity induced by Aβ in PC12 cells (Figure 4A, $p < 0.0001$). Subsequently, the effects of TS on Nrf2 and BACE1 protein expression *in vivo* and *in vitro* were investigated using the APP/PS1 mouse model and Aβ-induced PC12 cell model. The results showed that compared with WT mice and blank PC12 cells, the expression level of Nrf2 protein in the model group decreased *in vivo* (Figures 4B,C, $p < 0.05$) and *in vitro* (Figures 4E,F, $p < 0.05$), and the expression of BACE1 protein increased *in vivo* (Figures 4B,D, $p < 0.05$) and *in vitro* (Figures 4E,G, $p < 0.001$). After TS treatment, the expression of Nrf2 protein increased *in vivo* (Figures 4B,C) and *in vitro* (Figures 4E,F). Similarly, the expression of BACE1 protein decreased *in vivo* (Figures 4B,D) and *in vitro* after TS treatment (Figures 4E,G).

PC12 cells were transfected with Nrf2-siRNA to silence the Nrf2 gene to explore the role of Nrf2 in the anti-AD effect of TS. The transfection efficiency reached more than 50% based on the results of Western blot analysis (Figures 4H,I, $p < 0.05$). QPCR was used to investigate the effect of TS on BACE1 transcription after Nrf2 silencing (Figure 4J). The result showed that the transcription level of BACE1 in the model group increased significantly (Figure 4J, $p < 0.0001$) compared with the blank group, which was decreased after TS treatment (Figure 4J, $p < 0.05$). After Nrf2 gene silencing, the inhibitory effect of TS on BACE1 transcription was remarkably attenuated, indicating that TS inhibits the transcription of BACE1 through Nrf2.

Next, ChIP assay was performed to study whether TS can promote the binding of Nrf2 to BACE1 promoter. Nrf2 binding to ARE1 in rat BACE1 ARE1 promoter was increased in

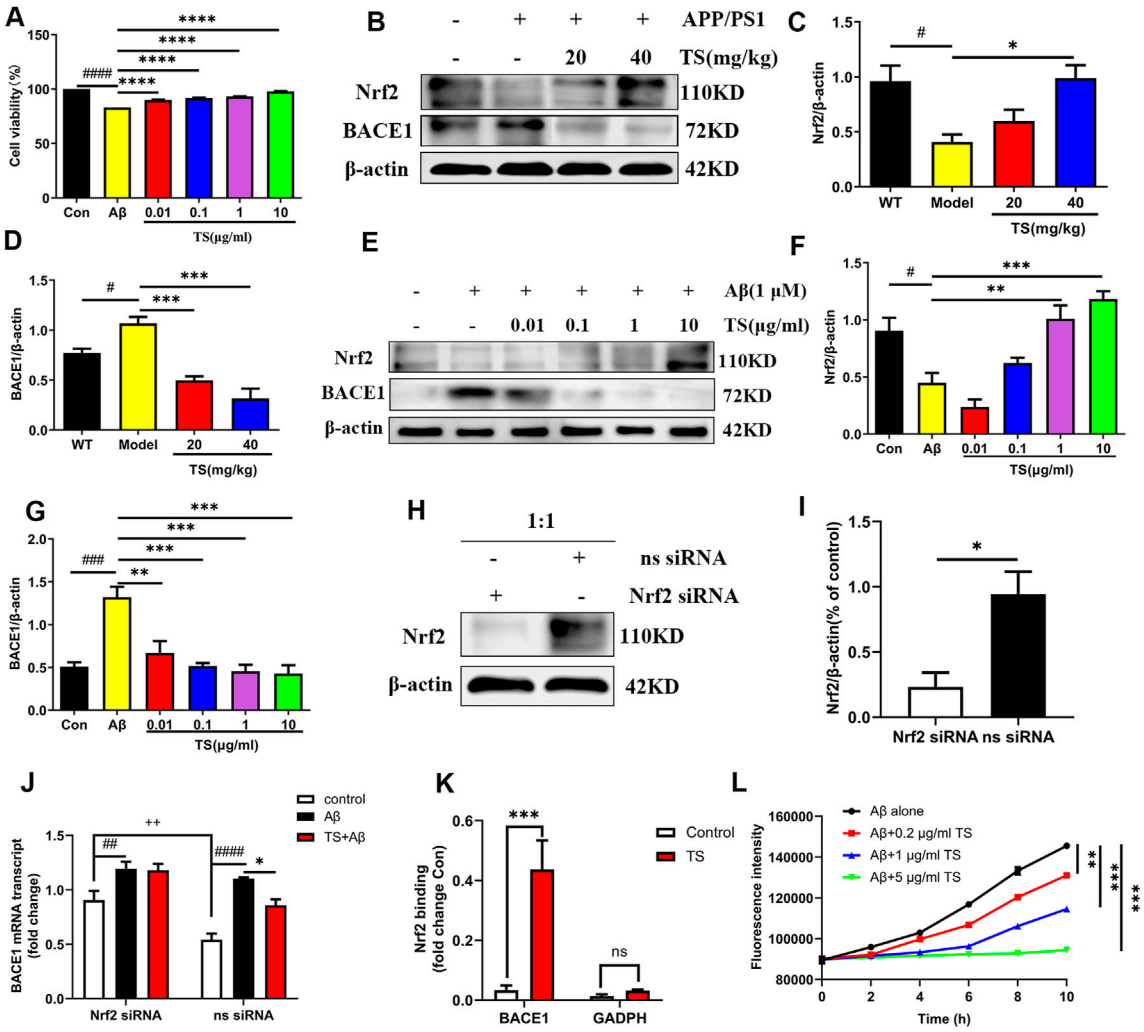

FIGURE 4
TS treatment promoted Nrf2 to inhibit the expression of BACE1 in the brain of APP/PS1 mice. **(A)** The effect of TS on the survival rate of Aβ-induced PC12 cells for 24 h was evaluated by MTT assay ($^{\#\#\#\#}p < 0.0001$, $^{****}p < 0.0001$). **(B)** The effect of TS on Nrf2 and BACE1 proteins in the brain of APP/PS1 mice were detected by Western blot. **(C)** Quantitative analysis of the relative expression level of Nrf2 protein in each group ($^{\#}p = 0.0195$, $^{*}p = 0.0151$). **(D)** Quantitative analysis of the relative expression level of BACE1 protein in each group ($^{\#}p = 0.0343$, $^{***}p = 0.0008$, $^{***}p = 0.001$). **(E)** The effect of TS on Nrf2 and BACE1 protein in Aβ-induced PC12 cells were detected by Western blot. **(F)** Quantitative analysis of the relative expression concertation of Nrf2 protein in each group ($^{\#}p = 0.0119$, $^{**}p = 0.0027$, $^{***}p = 0.0003$). **(G)** Quantitative analysis of the relative expression concertation of BACE1 protein in each group ($^{\#\#\#}p = 0.0003$, $^{**}p = 0.0016$, $^{***}p = 0.0003$, $^{***}p = 0.0002$, $^{***}p = 0.0001$). **(H)** PC12 cells were transfected with Nrf2-siRNA and transfection reagent at 1:1 for 36h, and the expression of Nrf2 was detected by Western blotting. **(I)** Quantitative analysis of the relative expression level of Nrf2 protein in Nrf2-siRNA and ns-siRNA groups ($^{*}p = 0.0199$). **(J)** The effect of TS on transcription the level of BACE1 in Nrf2$^{-/-}$ PC12 cells was investigated by qPCR ($^{\#\#}p = 0.0093$, $^{\#\#\#\#}p < 0.0001$, $^{*}p = 0.0234$, $^{++}p = 0.0030$). **(K)** The effect of TS on the level of Nrf2 and BACE1 promoter binding was investigated by CHIP experiment ($^{***}p = 0.0008$). **(L)** The effect of TS on the level of Aβ aggregation was detected by ThT fluorescence method ($^{**}p = 0.0058$, $^{***}p = 0.0003$, $^{***}p = 0.0002$). $^{\#}$: Comparing with WT group; *: Compared with model group; $^{+}$: Compared with ns siRNA group. Data are presented as mean ± SEM ($n = 3$).

TS-treated PC12 cells compared with controls (Figure 4K, $p < 0.001$), but the negative primers on rat GAPDH promoter had no significant change. Therefore, Nrf2 can directly bind to the ARE1 region of BACE1 promoter, and TS can promote the binding of Nrf2 and BACE1 promoter.

ThT fluorescence assay was used to evaluate the effect of TS on Aβ aggregation. The results showed that Aβ gradually accumulates from monomer to fibril formation with time, which was indicated by the increasing fluorescence density of ThT. TS incubation could inhibit Aβ aggregation in a concentration-dependent manner (Figure 4L). Co-incubation of 5 μg/ml of TS with 10 μM of Aβ could inhibit the aggregation of Aβ (Figure 4L, $p < 0.001$). Collectively, these results showed that TS could reduce the level of BACE1 by activating the expression of Nrf2, thereby reducing the formation and aggregation of Aβ.

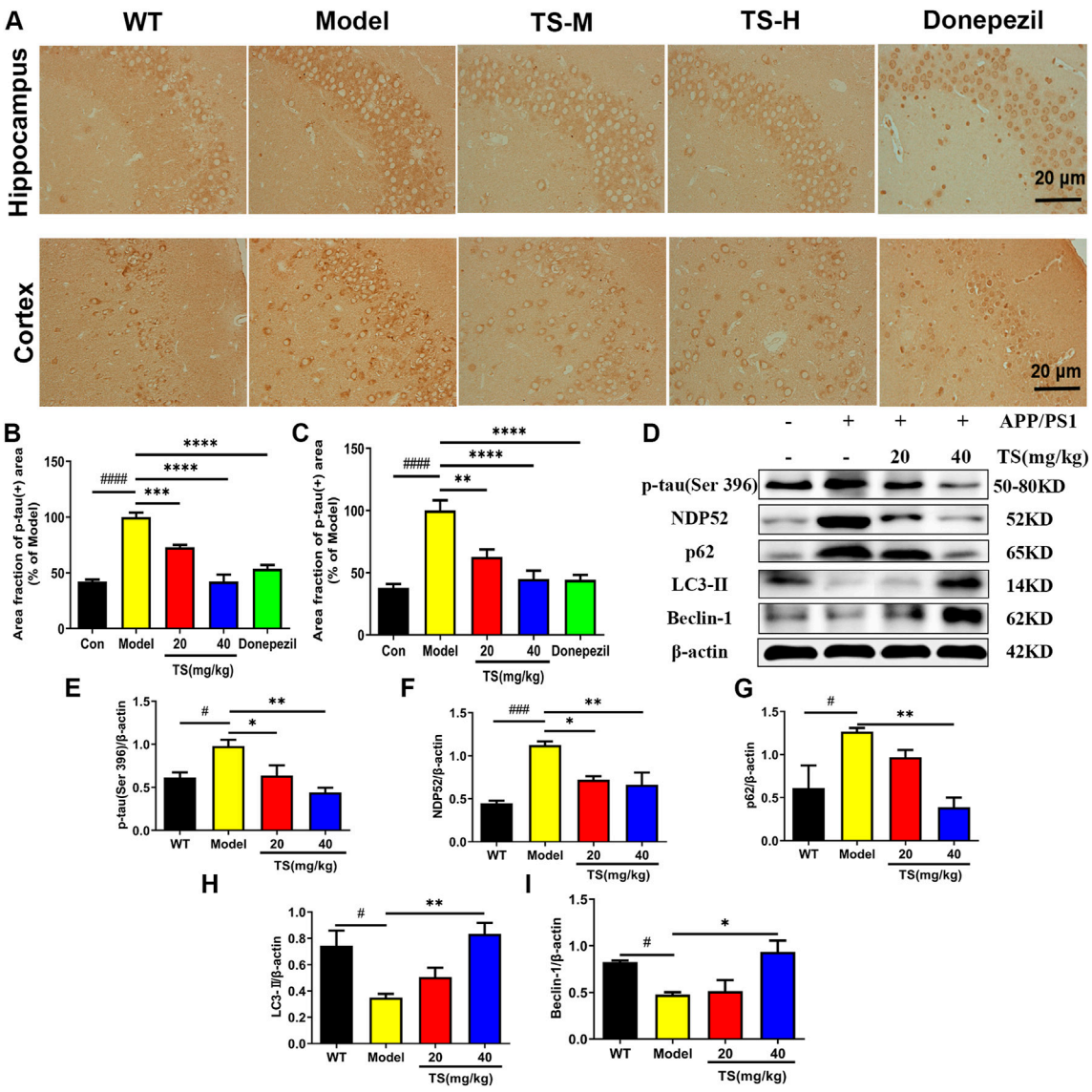

FIGURE 5
Effects of TS on expressions of *p*-tau, NDP52, p62 and LC3-II proteins in APP/PS1 mice. **(A)** The effect of TS on *p*-tau (ser396) in hippocampus and cortex of APP/PS1 mice was investigated by immunohistochemistry. **(B)** Quantitative analysis of the percentage of *p*-tau (Ser396) positive area in the hippocampus of APP/PS1 mice ($^{\#\#\#\#}p < 0.0001$, $^{***}p = 0.0007$, $^{****}p < 0.0001$). **(C)** Quantitative analysis of the percentage of *p*-tau (Ser396) positive area in the cortex of APP/PS1 mice ($^{\#\#\#\#}p < 0.0001$, $^{**}p = 0.0016$, $^{****}p < 0.0001$). **(D)** The effects of TS on expressions of *p*-tau (Ser 396), NDP52, p62 and LC3-II proteins in the brain of APP/PS1 mice were detected by Western blot. **(E)** Quantitative analysis of the relative expression level of *p*-tau (Ser 396) protein in each group ($^{\#}p = 0.0332$, $^{*}p = 0.0436$, $^{**}p = 0.0042$). **(F)** Quantitative analysis of the relative expression level of NDP52 protein in each group ($^{\#\#\#}p = 0.0008$, $^{*}p = 0.0177$, $^{**}p = 0.0086$). **(G)** Quantitative analysis of the relative expression level of p62 protein in each group ($^{\#}p = 0.0379$, $^{**}p = 0.0086$). **(H)** Quantitative analysis of the relative expression level of LC3-II protein in each group ($^{\#}p = 0.0216$, $^{**}p = 0.0073$). **(I)** Quantitative analysis of the relative expression level of Beclin-1 protein in each group ($^{\#}p = 0.0496$, $^{*}p = 0.0136$). $^{\#}$Compared with WT group; *Compared with model group. Data are presented as mean ± SEM ($n = 3$).

3.4 Total saikosaponins treatment reduces *p*-tau protein level via inducing autophagy

Hyperphosphorylation of tau protein leads to formation of neurofibrillary tangles and cognitive impairment. The effect of TS on the level of *p*-tau (Ser396) in the hippocampus and cortex of APP/PS1 mice was evaluated by immunohistochemical staining. Compared with WT mice, the levels of *p*-tau in the hippocampus and cerebral cortex of the model group mice were significantly higher (Figures 5A,B, $p < 0.0001$; Figures 5A,C, $p < 0.0001$), whereas the levels of *p*-tau in the low and middle-dose TS treatment groups were significantly lower than those in the

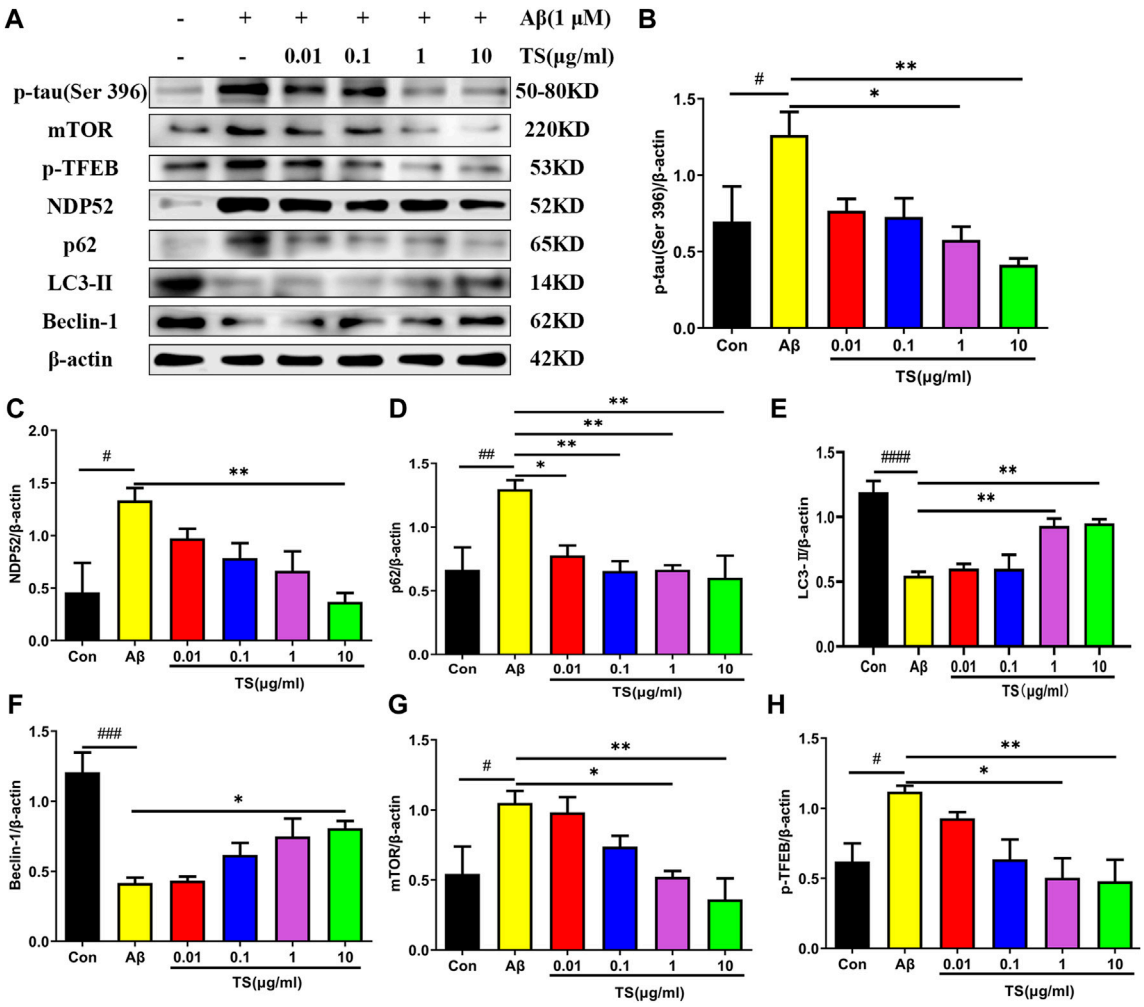

FIGURE 6
TS treatment promoted autophagy and clear *p*-tau. **(A)** The effect of TS on *p*-tau (Ser 396), NDP52, p62 and LC3-II and Beclin-1 proteins in the Aβ-induced PC12 cells were detected by Western blot. **(B)** Quantitative analysis of the relative expression concertation of *p*-tau (Ser 396) protein in each group ($^{\#}p = 0.0409$, $^{*}p = 0.0130$, $^{**}p = 0.0029$). **(C)** Quantitative analysis of the relative expression concertation of NDP52 protein in each group ($^{\#}p = 0.0113$, $^{**}p = 0.0057$). **(D)** Quantitative analysis of the gray value of p62 protein bands in each group ($^{\#\#}p = 0.0093$, $^{*}p = 0.0312$, $^{**}p = 0.0084$, $^{**}p = 0.0093$, $^{**}p = 0.0047$). **(E)** Quantitative analysis of the relative expression concertation of LC3-II protein in each group ($^{\#\#\#\#}p < 0.0001$, $^{**}p = 0.0053$, $^{**}p = 0.0037$). **(F)** Quantitative analysis of the relative expression concertation of Beclin-1 protein in each group ($^{\#\#\#}p = 0.0002$, $^{*}p = 0.0356$). **(G)** Quantitative analysis of the relative expression level of mTOR protein in each group ($^{\#}p = 0.0450$, $^{*}p = 0.0359$, $^{**}p = 0.0068$). **(H)** Quantitative analysis of the relative expression level of *p*-TFEB protein in each group ($^{\#}p = 0.0435$, $^{*}p = 0.0129$, $^{**}p = 0.0099$). $^{\#}$Compared with WT group; *Compared with model group. Data are presented as mean ± SEM ($n = 3$).

model group (hippocampus: Figures 5A,B, $p < 0.001$ and $p < 0.0001$, respectively; cerebral cortex: Figures 5A,C, $p < 0.01$ and $p < 0.0001$, respectively). The effect of TS on the level of *p*-tau protein *in vivo* and *in vitro* was further investigated by Western blot. The level of *p*-tau in the brain of APP/PS1 mice was higher than that of WT mice (Figures 5D,E, $p < 0.05$), whereas low and middle-dose TS treatment significantly decreased the level of *p*-tau in the brain of APP/PS1 mice (Figures 5D,E, $p < 0.05$ and $p < 0.01$ respectively). These data indicated that TS treatment could reduce *p*-tau level in the brain of APP/PS1 mice.

In exploring the mechanism of TS reducing *p*-tau protein level, the effects of TS on autophagy were examined. The changes in the expression of autophagic proteins were assessed by Western blot assay. The results showed that compared with WT mice, the expression of LC3-II and Beclin-1 in the model group decreased (Figures 5D,H, $p < 0.05$; Figures 5D,I, $p < 0.05$), whereas the expression of NDP52 and p62 increased (Figures 5D,F, $p < 0.001$; Figures 5D,G, $p < 0.05$), indicating that autophagy was inhibited. After treatment with TS, the expression of LC3-II and Beclin-1 increased significantly (Figures 5D,H,I), whereas the

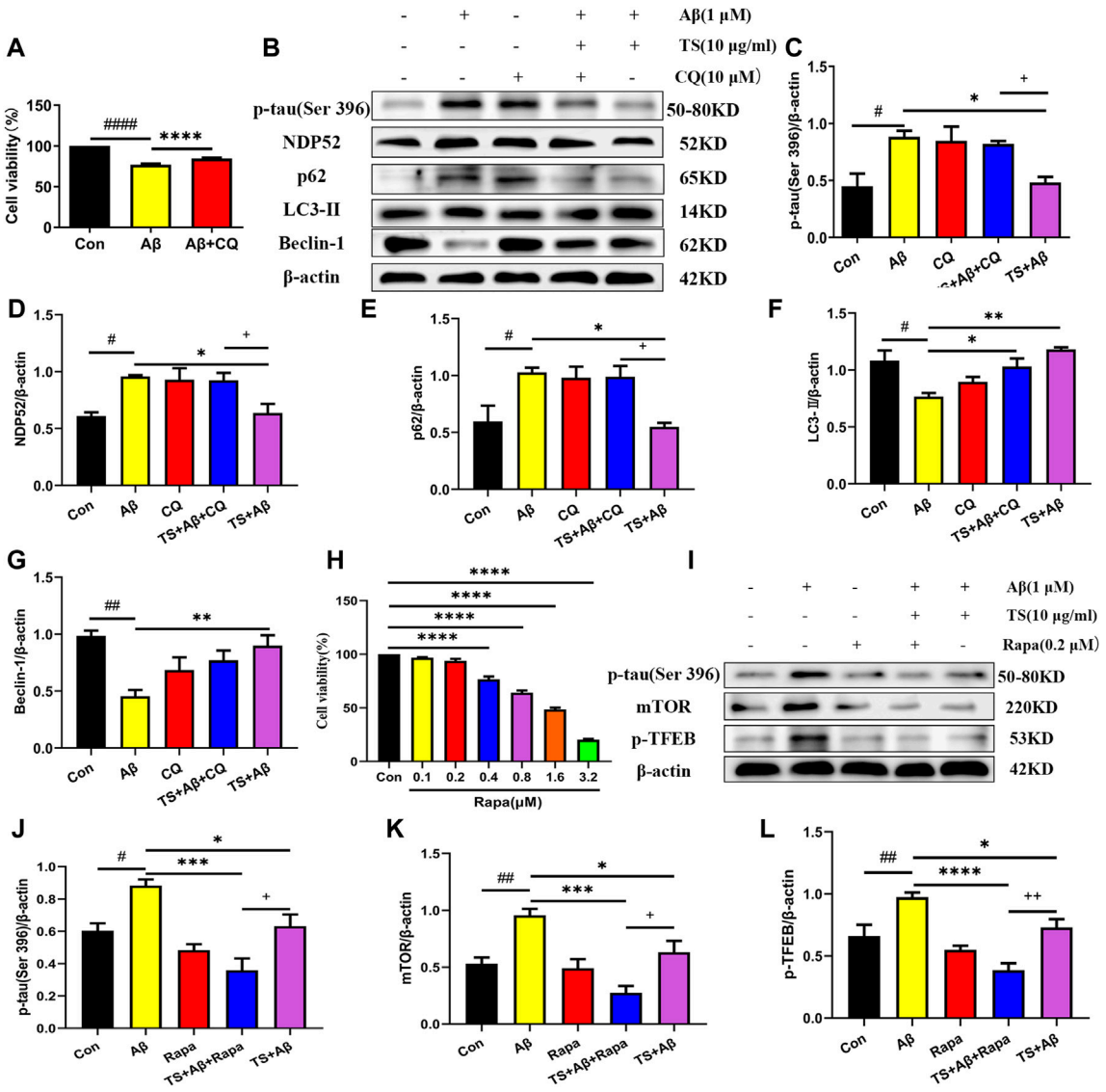

FIGURE 7
TS promoted autophagy in Aβ-induced PC12 cells to clear *p*-tau. **(A)** The effect of CQ on the survival rate of Aβ-induced PC12 cells for 24 h was evaluated by MTT assay ($^{\#\#\#\#}p < 0.0001$, $^{****}p < 0.0001$). **(B)** The effects of CQ on expression of *p*-tau (Ser 396), NDP52, p62, LC3-II and Beclin-1 proteins in the Aβ-induced PC12 cells after TS treatment were detected by Western blot. **(C)** Quantitative analysis of the relative expression level of *p*-tau (Ser 396) protein in each group ($^{\#}p = 0.0128$, $^{*}p = 0.0205$, $^{+}p = 0.0495$). **(D)** Quantitative analysis of the relative expression level of NDP52 protein in each group ($^{\#}p = 0.0134$, $^{*}p = 0.0217$, $^{+}p = 0.0386$). **(E)** Quantitative analysis of the relative expression level of p62 protein bands in each group ($^{\#}p = 0.0226$, $^{*}p = 0.0124$, $^{+}p = 0.0200$). **(F)** Quantitative analysis of the relative expression level of LC3-II protein in each group ($^{\#}p = 0.0101$, $^{*}p = 0.0277$, $^{**}p = 0.0016$). **(G)** Quantitative analysis of the relative expression level of Beclin-1 protein in each group ($^{\#\#}p = 0.0013$, $^{**}p = 0.0056$). **(H)** MTT assay was used to test the effect of Rapa on PC12 cells for 24 h ($^{****}p < 0.0001$). **(I)** The effects of Rapa on expression of *p*-tau (Ser 396), mTOR and *p*-TFEB proteins in the Aβ-induced PC12 cells after TS treatment were detected by Western blot. **(J)** Quantitative analysis of the relative expression level of *p*-tau (Ser 396) protein in each group ($^{\#}p = 0.00175$, $^{***}p = 0.0002$, $^{*}p = 0.0315$, $^{+}p = 0.0442$). **(K)** Quantitative analysis of the relative expression level of mTOR protein in each group ($^{\#\#}p = 0.0062$, $^{***}p = 0.0002$, $^{*}p = 0.0305$, $^{+}p = 0.0250$). **(L)** Quantitative analysis of the relative expression level of *p*-TFEB protein in each group ($^{\#\#}p = 0.0041$, $^{****}p < 0.0001$, $^{*}p = 0.0288$, $^{++}p = 0.0081$). $^{\#}$: Compared with WT group; *Compared with model group; $^{+}$Comparing with TS+Aβ group. Data are presented as mean ± SEM ($n = 3$).

expression of NDP52 and p62 decreased in a dose-dependent manner (Figures 5D,F,G).

Consistent results were obtained in *in vivo* experiments using Aβ-induced PC12 cells. As shown in Figure 6, the level of *p*-tau in the model group was increased compared with the blank group (Figures 6A,B, $p < 0.05$), whereas TS treatment could reduce the level of *p*-tau in Aβ-induced PC12 cells (Figures 6A,B, $p < 0.05$ and $p < 0.01$, respectively). Meanwhile, levels of autophagy-related proteins also changed in Aβ-induced PC12 cells. Compared with the blank group, the expression of LC3-II and Beclin-1 in the model group was

decreased (Figures 6A,E, $p < 0.0001$; Figures 6A,F, $p < 0.001$), whereas the expression of NDP52, P62, mTOR and *p*-TFEB was increased (Figures 6A,C, $p < 0.05$; Figures 6A,D, $p < 0.01$; Figures 6A,G, $p < 0.05$; Figures 6A,H, $p < 0.05$), which indicated that autophagy was suppressed. TS treatment could significantly increase the expression of LC3-II and Beclin-1 (Figures 6A,E,F) and reduce the expression of NDP52, P62, mTOR and *p*-TFEB (Figures 6A,C,D,G,H), indicating that TS may reduce the *p*-tau protein level by promoting autophagy.

Subsequently, CQ, an inhibitor of autophagic degradation, was employed to further clarify the mechanism of TS on autophagy and the relationship between autophagy inhibiting and *p*-tau reducing effects of TS. The MTT experiment results showed that CQ treatment could protect PC12 cells from Aβ-induced reduction in cell viability (Figure 7A). The levels of *p*-tau and autophagic proteins were detected using western blot analysis. It was found that compared with the TS group without CQ treatment, the *p*-tau level of the TS group treated with CQ was higher (Figures 7B,C, $p < 0.05$), indicating that CQ could inhibit *p*-tau reducing effect of TS. Western blotting results of autophagic proteins showed that compared with the TS dose group without CQ treatment, the level of NDP52 in the TS group treated with CQ increased (Figures 7B,D, $p < 0.05$), and the expression of Beclin-1 decreased (Figures 7B,E, $p < 0.05$), indicating that CQ inhibited the degradation of autophagosomes. No significant difference in the expression of p62 and LC3-II was observed. Furthermore, Rapamycin (Rapa), an mTOR inhibitor and autophagy inducer, was employed to further clarify the mechanism of TS on *p*-tau clearance through lysosome and autophagy. MTT results showed that Rapa treatment had no significant effect on cell viability at 0.1 or 0.2 μM (Figure 7H). We then examined the levels of *p*-tau and lysosome-associated proteins via western bolt analysis. It was found that compared with the TS group without Rapa treatment, the level of *p*-tau, mTOR and *p*-TFEB in the TS group treated with Rapa was decreased (Figures 7I–K, $p < 0.05$; Figures 7I,L, $p < 0.01$), indicating that Rapa could prompt *p*-tau clearance effect of TS through increasing the number of lysosomes and promoting the degradation of autophagosomes. Taken together, TS could reduce *p*-tau protein level by promoting autophagy, and the increase of autophagy flux is positively correlated with the clearance of *p*-tau.

3.5 Total saikosaponins treatment attenuates oxidative stress and inflammation in brain tissue of APP/PS1 mice

Considering the key role of oxidative stress and inflammation in the etiology of AD, the levels of key biomarkers of oxidative stress and inflammation in mice brain were evaluated using ELISA. Firstly, the levels of inflammatory factors were detected. The results showed that compared with the WT mice, the levels of TNF-α, IL-1βand IL-6 in the brain of the model group mice were significantly increased (Figures 8A–C, $p < 0.0001$). While high dose of TS could significantly reduce the levels of TNF-α, IL-1β and IL-6 (Figures 8A–C, $p < 0.01$, $p < 0.0001$, $p < 0.05$, respectively) in the brain of AD mice. Middle dose of TS only decreased the level of TNF-α (Figure 8A, $p < 0.05$).

Then the levels of oxidative stress markers in mice brain were measured, including the levels of MDA, SOD and GSH. The results showed that compared with WT mice, the levels of MDA and GSSG in the brain of APP/PS1 mice were increased (Figures 8D,G, $p < 0.0001$, $p < 0.05$, respectively), while the levels of SOD, GSH and the ratio of GSH/GSSG were significantly decreased (Figures 8E,F,H, all $p < 0.0001$). Compared with the model group, different dose of TS treatment significantly reduced the content of MDA in the brain of APP/PS1 mice (Figure 8D, $p < 0.0001$). High-dose TS treatment could significantly increase the content of antioxidant SOD, GSH and the ratio of GSH/GSSG (Figures 8E,F,H, $p < 0.05$, $p < 0.01$, $p < 0.01$, respectively), and decrease the content of GSSG (Figure 8G, $p < 0.05$) in the brain of AD mice. Medium dose of TS can increase the level of GSH and the ratio of GSH/GSSG (Figures 8F,H, $p < 0.05$). These results suggested that TS treatment could inhibit oxidative stress and neuroinflammation in the brain of AD mice.

3.6 Total saikosaponins inhibits neuroinflammation through Nrf2/NF-κB pathway

The activation of astrocytes and microglia is considered as key event in the progression of AD, which was evaluated using Iba-1 and GFAP immunohistochemical staining. The results of GFAP immunostaining showed that compared with WT mice, the activation of astrocytes in the brain of model group mice was significantly increased (Figures 9A,B, $p < 0.0001$), while TS could significantly reduce the positive staining area of GFAP (Figures 9A,B), suggesting that TS could inhibit the excessive activation of astrocytes in the brain of AD mice. The results of Iba-1 immunostaining showed that the activation of microglia in the brain of model mice was significantly increased than that of WT mice (Figures 9A,C, $p < 0.0001$), and TS treatment could significantly reduce the activation of microglia (Figures 9A,C, $p < 0.0001$). The above results suggested that TS treatment could significantly inhibit the activation of glial cells including astrocytes and microglia in the brain of APP/PS1 mice.

In order to investigate the mechanism of TS in inhibiting neuroinflammation, the expression of Nrf2 and NF-κB protein in the brain of APP/PS1 mice and Aβ-induced PC12 cells were examined. The results showed that compared with blank group, the expression level of NF-κB protein in the model group increased both *in vivo* (Figures 9D,E, $p < 0.01$) and *in vitro* (Figures 9F,G, $p < 0.01$). After treatment with TS, the expression of NF-κB protein decreased in high dose of TS *in vivo* (Figures 9D,E, $p < 0.05$) and in 10 μg/ml of TS *in vitro* (Figures 9F,G, $p < 0.05$), suggesting that TS could inhibit the expression of NF-κB in the brain of APP/PS1 mice and Aβ-induced PC12 cells.

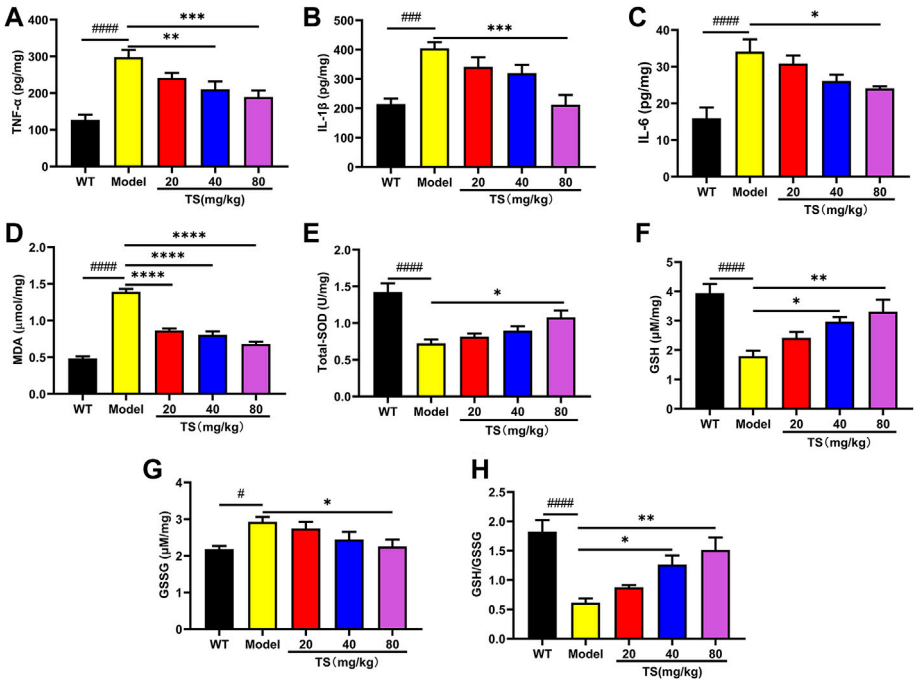

FIGURE 8
TS treatment inhibited cerebral inflammation and oxidative stress in APP/PS1 mice. **(A)** The effect of TS on the levels of TNF-α in the brain of APP/PS1 mice was measured by ELISA ($^{####}p < 0.0001$, $^{**}p = 0.0065$, $^{***}p = 0.0008$). **(B)** The effect of TS on the levels of IL-1β in the brain of APP/PS1 mice was measured by ELISA ($^{###}p$ 0.0002, $^{***}p = 0.0002$). **(C)** The effect of TS on the levels of IL-6 in the brain of APP/PS1 mice was measured by ELISA ($^{####}p < 0.0001$, $^{*}p = 0.0209$). **(D)** The effect of TS on the levels of MDA in the brain of APP/PS1 mice was measured by ELISA ($^{####}p < 0.0001$, $^{****}p < 0.0001$). **(E)** The effect of TS on the levels of SOD in the brain of APP/PS1 mice was measured by ELISA ($^{####}p < 0.0001$, $^{*}p = 0.0129$). **(F)** The effect of TS on the levels of GSH in the brain of APP/PS1 mice was measured by ELISA ($^{####}p < 0.0001$, $^{*}p = 0.0177$, $^{**}p = 0.0020$). **(G)** The effect of TS on the levels of GSG in the brain of APP/PS1 mice was measured by ELISA ($^{#}p = 0.0123$, $^{*}p = 0.0248$). **(H)** Quantitative analysis of the ratio of GSH/GSSG ($^{####}p < 0.0001$, $^{*}p = 0.0178$, $^{**}p = 0.0010$). $^{\#}$Compared with WT group; *Compared with model group. Data are presented as mean ± SEM ($n = 6$).

Nrf2-siRNA transfected PC12 cells were employed to further explore the role of Nrf2 in the down-regulation of NF-κB expression induced by TS. It was found that compared with the blank group, the transcription level of NF-κB in the model group increased significantly (Figure 9H, $p < 0.001$), which was decreased after treatment with TS (Figure 9H, $p < 0.05$). After Nrf2 gene silencing, the inhibitory effect of TS on NF-κB transcription was remarkably attenuated, suggesting that TS inhibits the transcription of NF-κB through Nrf2.

3.7 Total saikosaponins treatment ameliorate synaptic loss in APP/PS1 mice

Synaptic loss is an important pathological feature of AD, which is highly correlated with cognitive function impairment in AD patients or animal models (John & Reddy, 2021). Presynaptic protein synaptophysin and postsynaptic protein PSD-95 are two synaptic marker proteins (John & Reddy, 2021). Postsynaptic density protein PSD-95 is the main scaffold protein of dendritic spine coordinating the relationship between neurotransmitters and receptors, and ultimately determining the synaptic response (Savioz et al., 2014; John & Reddy, 2021). Synaptophysin and PSD-95 immunofluorescence assay was performed to verify the effect of TS on synaptic loss. The results of immunofluorescence staining in mice brain showed that the levels of synaptophysin (Figures 10A,B, $p < 0.0001$) and PSD-95 (Figures 10A,C, $p < 0.0001$) in the brain of AD mice were significantly lower than those of WT mice. While TS treatment could significantly increase the levels of synaptophysin (Figures 10A,B) and PSD-95 (Figures 10A,C), suggesting that TS treatment could effectively prevent synaptic loss in the brain of AD mice.

3.8 Total saikosaponins treatment reverses the microbiota disorder in APP/PS1 mice

16S rRNA gene sequencing was used to analyze and evaluate the effect of TS on GM in APP/PS1 mice. The Chao1 index and

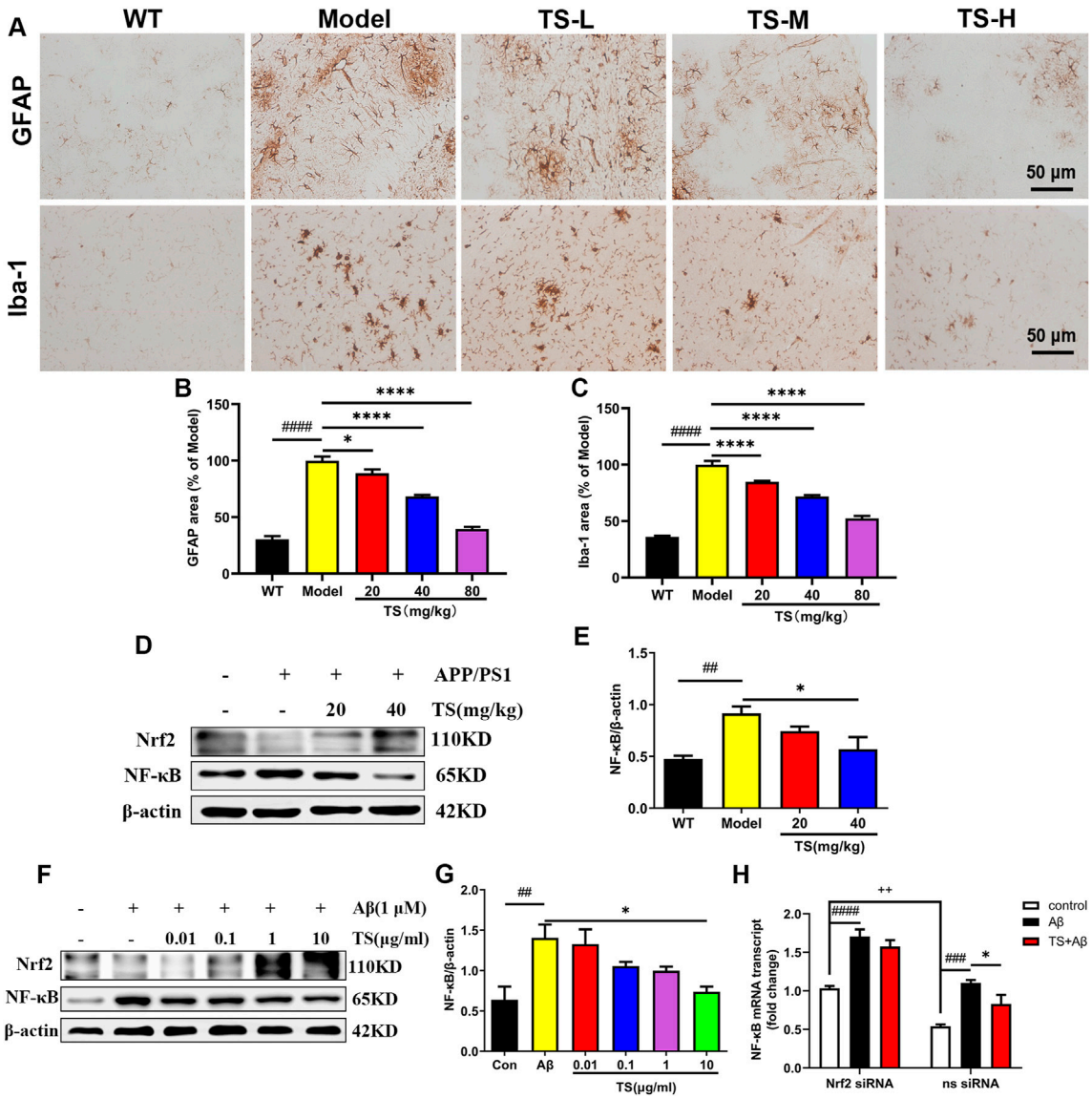

FIGURE 9
TS treatment reduced astrocytes and microglia activation in APP/PS1 mice. **(A)** The effects of TS on the activation of astrocytes and microglia in the brain of APP/PS1 mice were investigated by immunohistochemical staining. **(B)** Quantitative analysis of the percentage of GFAP positive area in the brain of APP/PS1 mice ($^{\#\#\#\#}p < 0.0001$, $^{*}p = 0.0312$, $^{****}p < 0.0001$). **(C)** Quantitative analysis of the percentage of Iba-1 positive area in the brain of APP/PS1 mice ($^{\#\#\#\#}p < 0.0001$, $^{****}p < 0.0001$). **(D)** The effects of TS on expressions of Nrf2 and NF-κB proteins in the brain of APP/PS1 mice were detected by Western blot. **(E)** Quantitative analysis of the relative expression level of NF-κB protein in each group ($^{\#\#}p = 0.0068$, $^{*}p = 0.0243$). **(F)** The effects of TS on expressions of Nrf2 and NF-κB proteins in the Aβ-induced PC12 cells were detected by Western blot. **(G)** Quantitative analysis of the relative expression level of NF-κB protein in each group ($^{\#\#}p = 0.0048$, $^{*}p = 0.0126$). **(H)** The effect of TS on the transcription level of NF-κB in Nrf2$^{-/-}$ PC12 cells was detected by qPCR. ($^{\#\#\#}p = 0.0003$, $^{\#\#\#\#}p < 0.0001$, $^{*}p = 0.0382$, $^{++}p = 0.0013$). $^{\#}$Compared with WT group; *Compared with model group; $^{+}$Compared with ns siRNA group. Data are presented as mean ± SEM ($n = 3$).

observed index show the significant change of bacterial communities in alpha diversity among different groups (Figure 11A), indicating the exits of microbiota dysbiosis in APP/PS1 mice, and TS reverses this pathological change. The Venn diagram showed the difference of ASV numbers detected in three groups of mice (Figure 11B), indicating that the composition of flora changed among the three groups. Then, the gut bacterial composition at the phylum level was profiled. As shown in Figure 11C, the main bacteria in three groups are identified. The result revealed that the microbiome at the phylum level underwent a disorder in APP/PS1 mice, and TS treatment remarkably affected the microbiome composition, indicating a potential mechanism and a therapy target of AD though the gut–brain axis. Heatmaps of most differentially abundant taxa revealed the change trend in three groups. Based on heatmap analysis (Figure 12), the abundance of *Desulfovibrio*,

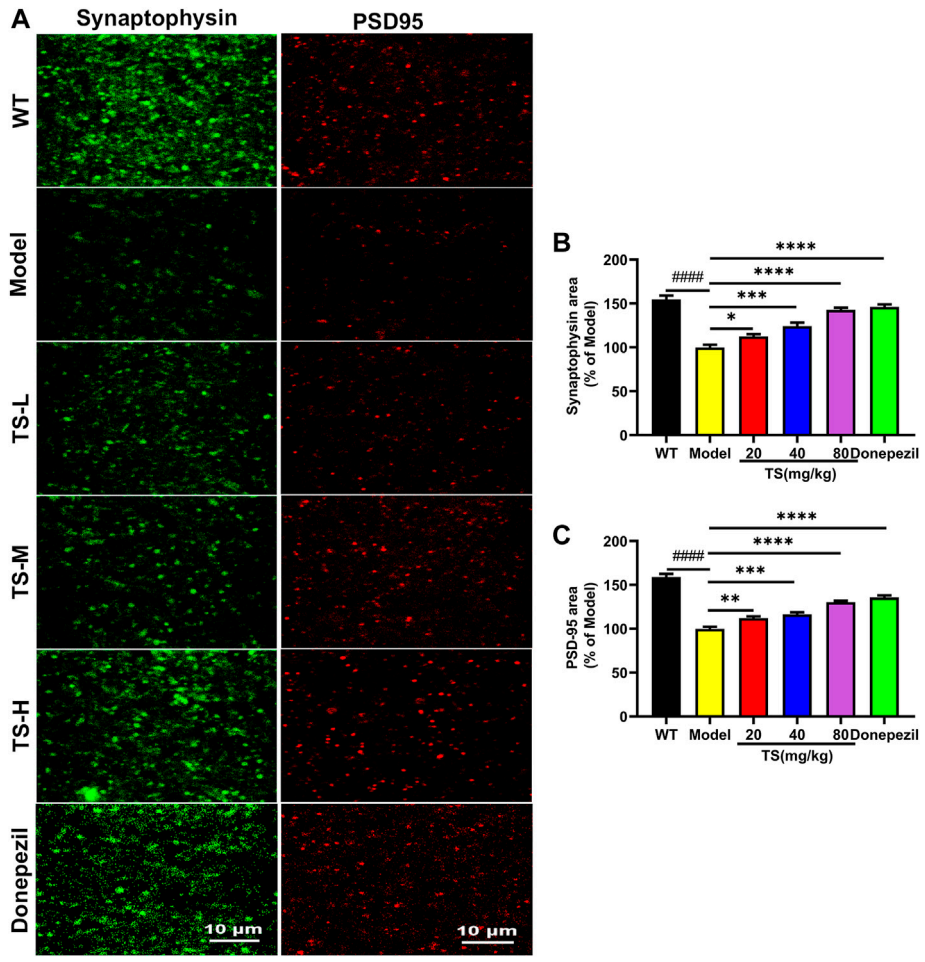

FIGURE 10
TS treatment improved synaptic dysfunction in APP/PS1 mice. **(A)** The effect of TS on the level of synaptophysin and PSD-95 in the brain of APP/PS1 mice was investigated by immunofluorescence assay. **(B)** Quantitative analysis of the percentage of synaptophysin positive area in the brain of APP/PS1 mice ($^{####}p < 0.0001$, $^{*}p = 0.0496$, $^{****}p < 0.0001$). **(C)** Quantitative analysis of the percentage of PSD-95 positive area in the brain of APP/PS1 mice ($^{####}p < 0.0001$, $^{**}p = 0.0059$, $^{***}p = 0.0002$, $^{****}p < 0.0001$). $^{\#}$Compared with WT group; *Compared with model group. Data are presented as mean ± SEM ($n = 6$).

Helicobacter, *Mucispirillum*, *Roseburia*, and *Clostridium* increased in APP/PS1 mice, whereas it was reduced after TS treatment. Random forest analysis suggests that *Helicobacter* and *Mucispirillum* show a significant difference among the groups (Figure 13), indicating that these bacteria were involved in the pathogenesis of AD, and TS prevents cognitive impairment in APP/PS1 mice by remodeling the GM.

4 Discussion

In this study, it was demonstrated that TS has protective effects on cognitive function and neuropathological impairments in APP/PS1 transgenic mice, reducing Aβ production, senile plaque deposition, *p*-tau level, oxidative stress, and inflammatory response; inhibiting glial cell activation; and improving synaptic function. As shown in Figure 14, the underlying mechanism was found to involve reducing Aβ deposition by activating the Nrf2/BACE1 signaling pathway and promoting autophagy by regulating the expression of NDP52 and other autophagy-related proteins, thereby reducing the level of *p*-tau, which has been rarely reported in previous literature. With regard to neuroinflammation, TS can downregulate NF-κB expression through Nrf2, which inhibited the activation of glial cells and reduced the production of inflammatory factors. Moreover, TS could upregulate the expression of anti-oxidative stress factors such as SOD and downregulate the expression of oxidative stress factors such as MDA through Nrf2, thereby exerting an anti-oxidative stress effect. Furthermore, it was found that TS could significantly affect the diversity, composition, and abundance of

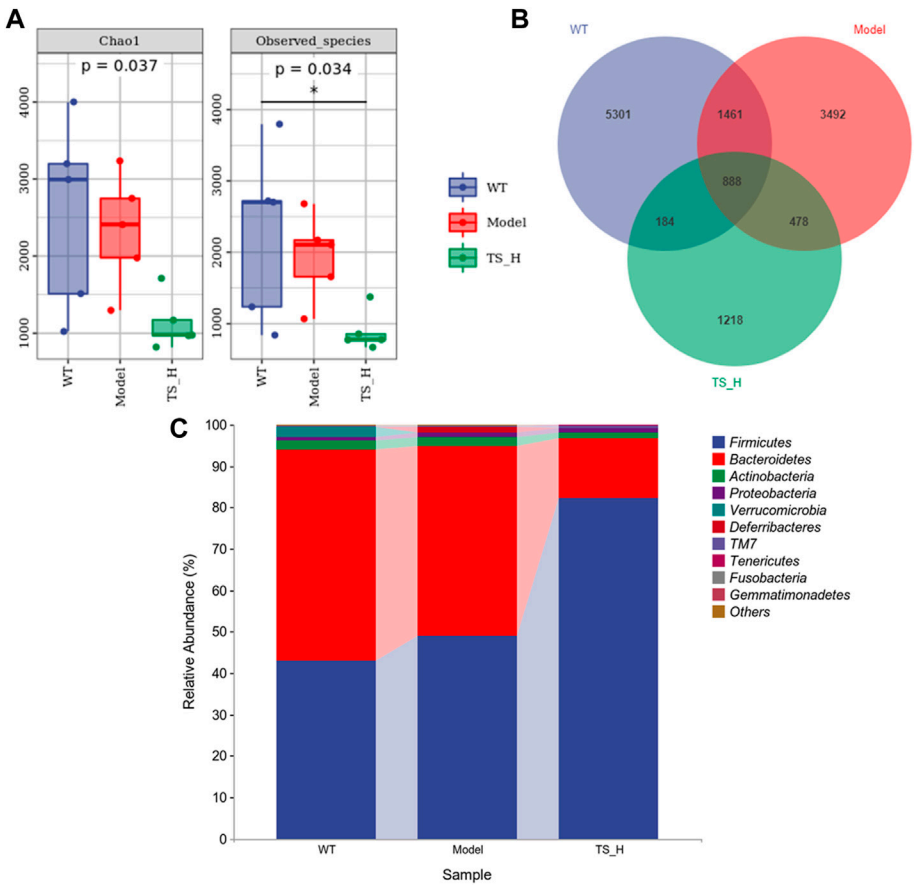

FIGURE 11
Differences in the diversity and composition of gut microbial genes among WT mice, APP/PS1 mice and TS treatment APP/PS1 mice. **(A)** Alpha diversity analysis-Chao1 index and Observed species index box chart. **(B)** Venn diagram. **(C)** Column pictures of relative abundance and composition of gut microbiota at phylum level in each group. *$p < 0.05$ versus WT group ($n = 5$).

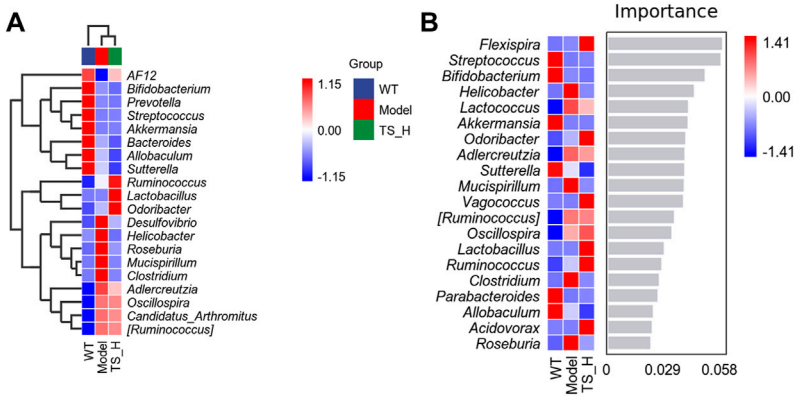

FIGURE 12
Heatmaps of most differentially abundant taxa in WT mice, APP/PS1 mice and TS treatment APP/PS1 mice. **(A)** Heat-map of microbial community composition. **(B)** Random forest analysis map. $n = 5$ for each treatment.

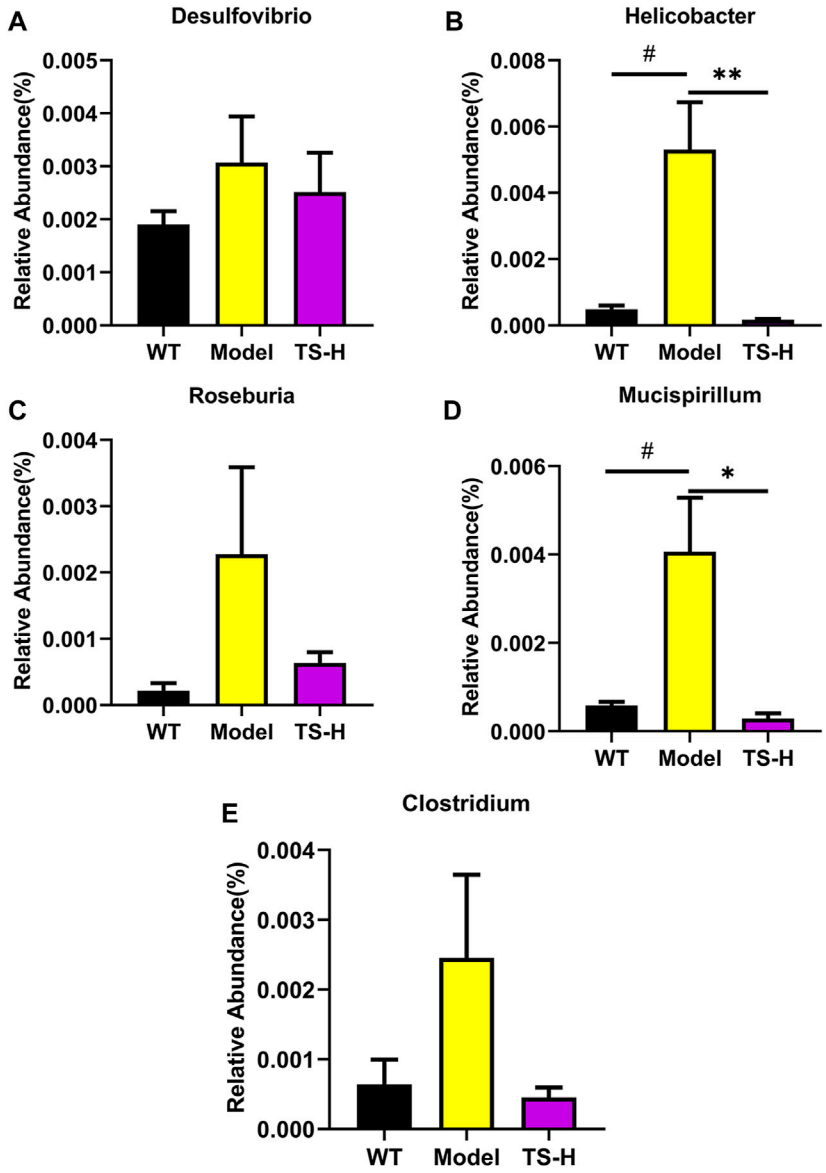

FIGURE 13
Relative abundance of five representative microbial species at the genus levels in WT mice, APP/PS1 mice and TS treatment APP/PS1 mice. **(A)** *Desulfovibrio*. **(B)** *Helicobacter* ($^{\#}p$ = 0.0113, $^{**}p$ = 0.0084). **(C)** *Roseburia*. **(D)** *Mucispirillum* ($^{\#}p$ = 0.0239, $^{*}p$ = 0.0169). **(E)** *Clostridium*. Data were expressed as mean ± SEM. $^{\#}$Compared with WT group; *Compared with model group (n = 3).

intestinal flora and GM. The results showed that TS could significantly downregulate the abnormally increased abundance of *Helicobacter*, *Mucispirillum*, *Roseburia*, and *Clostridium* in APP/PS1 transgenic mice, indicating that TS may have a protective effect on AD by regulating GM.

Three behavioral experiments were used to investigate the effects of TS on the cognitive function of APP/PS1 mice. The results indicated that TS treatment could significantly improve the cognitive function of APP/PS1 mice. APP/PS1 transgenic mice are an AD mouse model expressing mutations in APP and presenilin genes transcribed under the control of a neuron-specific Thy1 promoter. These two genes can lead to early onset of familial AD by jointly exacerbating Aβ or tau pathology (Dodiya et al., 2019; Soto-Faguas et al., 2021). Based on previous studies, APP/PS1 mice develop brain amyloid lesions at 6–8 weeks of age; Aβ accumulates in the cerebral cortex and hippocampus at 8 months, and hyperphosphorylated tau near Aβ plaques and reduced synaptic density are observed (Kosel et al., 2020). Senile plaques are secreted proteins released by stepwise proteolysis

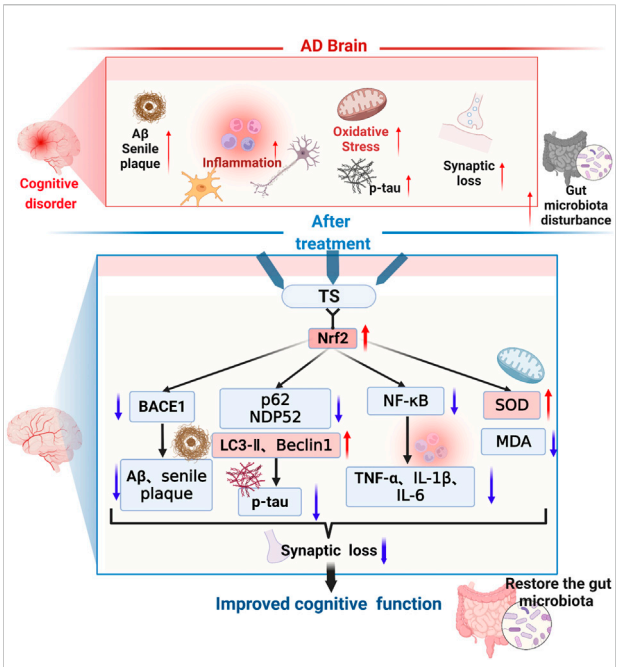

FIGURE 14
The therapeutic effects and related mechanisms of TS against AD. The following pathological phenomena occur in the AD brain: (1) increased Aβ generation, aggregation and increased deposition of senile plaques; (2) enhanced activation of microglia and astrocytes, elevated inflammatory cytokines levels; (3) increased oxidative stress and decreased secretion of antioxidant stress factors; (4) increased synaptic loss; (5) aggravated gut mictobiota dysbiosis and increased the pathogenic bacteria. Finally, these pathological changes led to the cognitive dysfunction of the AD patients. TS treatment could improve cognitive function through multiple mechanisms. Firstly, TS regulated the transcription and expression of BACE1 via Nrf2, reduced the generation and aggregation of Aβ, thus inhibited the deposition of senile plaque. Secondly, TS downregulated the expression of p62 and NDP52 by promoting autophagy, upregulated the expression of LC3-II and Beclin-1, thus promoting the clearance of *p*-tau. Thirdly, TS downregulated the transcription and expression of NF-κB via Nrf2, reduced the levels of inflammatory cytokines, thus ameliorated the neuroinflammation. Fourthly, TS increased the level of SOD and reduced the level of MDA, alleviating oxidative stress. Eventually, TS ameliorated synapse loss and alleviated the gut microbiota dysbiosis. Red arrows represent upregulation and blue arrows represent downregulation. AD, Alzheimer's disease; TS, Total saikosaponins; Nrf2, nuclear factor 2; BACE1, β-secretase 1; Aβ, amyloid-beta; *p*-tau, phosphorylated tau; NF-κB, nuclear factor-κB; TNF-α, tumour necrosis factor α; IL-1β, interleukin-1β; IL-6, interleukin-6; SOD, superoxide dismutase; MDA, malondialdehyde.

of APP, whereas hyperphosphorylation of tau leads to the formation of NFTs in AD (Lee et al., 2016). Therefore, the APP/PS1 mouse model has been widely used in the study of AD, which is a pathological model with Aβ aggregation and senile plaque deposition, tau hyperphosphorylation, and synaptic dysfunction, which is also consistent with our experimental results. In addition, after antibiotic or bacterial treatment, APP/PS1 mice have reduced Aβ deposition, improved cognitive memory function, and reduced inflammatory levels (Cryan et al., 2019). Jing Sun et al. also used this model to study the reduction of microglia-mediated neuroinflammation by probiotic CB in relation to its metabolite butyric-mediated regulation of the brain–gut axis (Sun et al., 2020). These results indicate that the APP/PS1 mouse model achieves the conditions for GM experiments.

Nrf2 is a transcription factor that primarily exists in the cytosol of hippocampal neurons, regulates many antioxidant enzymes, such as heme oxygenase-1 (HO-1) and quinine oxidoreductase 1 (NQO1), and upregulates proinflammatory cytokines through the ARE pathway (Kobayashi et al., 2016; Bahn et al., 2019; Ren et al., 2020). After oxidative stress, Nrf2 translocates into the nucleus in response to this pathway, Keap1/Nrf2/ARE, initiating the transcription of anti-oxidative stress genes such as SOD, upregulating GSH levels, and downregulating peroxidase MDA levels (Tu et al., 2019; Osama et al., 2020; Toma et al., 2021). Therefore, Nrf2 activation can protect our body from harmful stress by upregulating antioxidant defense, inhibiting inflammation, and maintaining protein homeostasis and play a protective role in AD brain (Ren et al., 2020). Nrf2 levels could decrease with age in postmortem human brain and animal models of AD (Ren et al., 2020; Wei et al., 2020). Significantly reduced levels of Nrf2 were also detected in APP/PS1 mice and Aβ-induced cell models. Recent studies have shown a correlation between Nrf2 deficiency and AD because Nrf2 not only reduces oxidative stress and inflammation but also directly or indirectly regulates autophagy *in vivo* and *in vitro* (Pajares et al., 2016; Branca et al., 2017; Jan et al., 2017; Rojo et al., 2017; Ren et al., 2020). Transcriptional analysis suggests that the brain of Nrf2 knockout mice replicates the least normal pathway in the human AD brain (Rojo et al., 2017; Wei et al., 2020). Subsequently, some studies have found that Nrf2 knockout exacerbates cognitive deficits in mouse models of AD, induces multiple stress responses, and aggravates AD pathologies (Branca et al., 2017; Rojo et al., 2017; Ren et al., 2020). This result indicates that Nrf2 can be activated through the genetic or pharmacological pathways to play a neuroprotective effect.

APP is a single-pass transmembrane protein expressed in high levels in the brain, and three enzymes are responsible for cleaving APP: α-secretase, BACE1, and γ-secretase (Lee et al., 2016). Aβ, a derivative of APP, is primarily produced by sequential cleavage of BACE1 and γ-secretase, and deposited in the brains of AD patients in the form of plaques (Lee et al., 2016; Jiang et al., 2020; Han et al., 2021; Ledo et al., 2021). Increased concentration and activity of BACE1 was also observed in AD brain and body fluids (Lee et al., 2016; Hampel et al., 2021). Some ingredients of traditional Chinese medicine have been found to show effects on BACE1. Ginsenosides can reduce the activity and expression of BACE1, but have no effect on the levels of total APP and SAPPα (Cao et al., 2016; Singh et al., 2021). Baicalein shows potent anti-BACE1 activity and can inhibit Aβ-

induced PC12 cytotoxicity (Singh et al., 2021). Thus, the effect of TS on BACE1 expression was investigated. Aβ is a polypeptide composed of 39–42 amino acids, and the most common Aβ fragments contain 40 or 42 amino acids. The levels of soluble and insoluble Aβ40 and Aβ42 in brain tissue were examined (Lee et al., 2016; Fao et al., 2019; Kwak et al., 2020). It was found that high doses of TS significantly reduced the levels of soluble and insoluble Aβ40 and Aβ42 in the brain, whereas different doses of TS significantly reduced the deposition of senile plaques in APP/PS1 mice. It was also found that TS could effectively inhibit Aβ aggregation and diminish cytotoxicity in PC12 cells after Aβ-induced *in vitro* studies by ThT and MTT assays. The abovementioned results indicated that TS treatment significantly reduced Aβ generation and aggregation in AD mice and cells. In the mechanism study, it was found that TS reduced BACE1 expression in APP/PS1 mice *in vivo* and in Aβ-induced PC12 cells *in vitro*, indicating that TS inhibits Aβ formation by reducing BACE1 expression. The results were consistent with previous report, which found that treatment with therapeutic drugs significantly inhibited the expression of BACE1 and reduced the release of SAPPβ in APPswe/PS1ΔE9 mice, but it did not change the expression of full-length APP, PS1, a disintegrin, metalloproteinase 10 (ADAM10), and other cleavage products, including SAPPα, neprilysin, and insulin-degrading enzyme in APPswe/PS1dE9 mice (Wei et al., 2020). Therefore, Aβ was primarily reduced by inhibiting β-secretase-induced amyloid generation but not by increasing non-amyloid production.

Recently, Nrf2 was found to negatively regulate BACE1 expression and improve cognitive deficits in mouse models of AD (Bahn et al., 2019; Ren et al., 2020). Bahn et al. revealed a previously unknown molecular mechanism, in which Nrf2-deficient AD mice had significantly increased BACE1 and BACE1-AS expression and Aβ deposition, and more severe cognitive dysfunction compared with 5xFAD and Nrf2 knockout mice, whereas the activation of Nrf2 inhibited BACE1 and BACE1-AS expression and Aβ production and improved cognitive dysfunction and AD-related pathological characteristics (Bahn et al., 2019). Thus, it was hypothesized whether TS could inhibit BACE1 expression by activating Nrf2, thereby reducing Aβ formation. Subsequently, the changes of Nrf2 and BACE1 and the relationship between them after TS treatment were investigated. The results showed that TS could reduce the expression of BACE1 by activating Nrf2, and when Nrf2 was knocked down, the effect of TS on inhibiting BACE1 expression was attenuated, which indicated that TS negatively regulated the expression of BACE1 by activating Nrf2, thereby inhibiting the production and deposition of Aβ. Moreover, using CHIP assay, it was found that Nrf2 could directly bind to the ARE1 site in the BACE1 promoter, and TS could promote the binding of Nrf2 and BACE1 promoters to inhibit the transcription of BACE1.

Tau primarily accumulates in the medial temporal lobe, and its main function is to bind and stabilize microtubules, which are a major component of the neuronal cytoskeleton, providing structural support to neurons, and binding is regulated by its phosphorylation state (Lee et al., 2016; Maass et al., 2018; Lowe et al., 2019; Kosel et al., 2020; Kwak et al., 2020; Limorenko & Lashuel, 2022). In AD, abnormally phosphorylated tau detaches from microtubules and begins to accumulate with other tau filaments (Lee et al., 2016). This process has two stages: paired helical filament (PHF) stage, in which these aggregated tau filaments form PHF, and neurofibrillary tangle (NFT) stage, in which the formed PHF winds around each other to form insoluble double-fiber NFT in the cell and eventually accumulates in the form of NFT (Jo et al., 2014; Lee et al., 2016; Limorenko & Lashuel, 2022). In this process, microtubule disassembly can cause the collapse of neurons, impairing the ability of neurons to communicate with one another (Jo et al., 2014; Lee et al., 2016). Among the multiple phosphorylation sites associated with AD, tau is phosphorylated at Thr231 and Ser396 during the PHF stage, whereas it is primarily phosphorylated at Ser396 during the NFT stage. In addition, Aβ can induce tau phosphorylation at Thr231 and Ser396 (Lee et al., 2016). Collectively, tau is primarily phosphorylated at Ser396, and it belongs to the C-terminal domain, which plays a key role in regulating tau aggregation (Jo et al., 2014). Thus, the effect of TS on *p*-tau (Ser396) level were examined. The results showed that TS could reduce the accumulation of *p*-tau (Ser396) and reduce the level of *p*-tau (Ser396) in the hippocampus and cerebral cortex of APP/PS1 mice. In the study of Saikosaponin C (SSc) by Lee et al., they found that SSc had an inhibitory effect on *p*-tau but not on the expression of total Tau (Tau5) (Lee et al., 2016). Combined with their study, TS and its monomeric saponin SSc can reduce *p*-tau level in AD brain.

At present, increasing evidence shows that impaired autophagy is closely related to the pathogenesis of AD. The researchers found that autophagosomes and lysosome accumulated in the brains of AD patients by electron microscopy and that autophagic flux was inhibited (Zhang et al., 2021). In addition, autophagy plays an important role in tau pathology. Data have shown that once autophagic flux is blocked, the clearance of Tau is affected, and insoluble tau aggregates accumulate remarkably (Zhang et al., 2021). In the brains of AD patients, hyperphosphorylated tau colocalized with the autophagic marker LC3 and autophagic receptor p62, which was not observed in controls (Piras et al., 2016; Zhang et al., 2021). The turnover of LC3 is an essential process during autophagic activation, in which LC3-I is modified by phosphatidyl ethanolamine and converted to LC3-II (Jiang et al., 2018). Autophagic receptors interact with LC3, including p62, NBR1, and NDP52, of which p62 and NDP52 are the most studied. They can direct autophagic targets to autophagosomes, which then fuse cargo-containing autophagosomes with lysosomal vesicles and promote the

degradation of autophagosomes (Jo et al., 2014; Menzies et al., 2017; Viret et al., 2018). Based on previous results, the downregulation of p62 expression is induced by Nrf2 activation, and the accumulation of hyperphosphorylated tau is observed in p62 knockout mice, and few studies have investigated the effect of NDP52 on tau (Jo et al., 2014). Jo et al. showed that compared with p62, their data strongly indicated that NDP52 may be the main autophagy adaptor that promotes phosphorylated tau degradation (Jo et al., 2014). Based on the abovementioned findings, whether the reduction of *p*-tau level by TS was through the autophagy of p62 and NDP52 was investigated. The changes in the expression levels of autophagic proteins such as p62 and NDP52 and the changes in *p*-tau in APP/PS1 mice and Aβ-induced PC12 cells after TS treatment were examined. The results showed that after TS treatment, the expression of LC3-II and Beclin-1 increased, and the expression of NDP52 and p62 decreased in AD mice and cells, indicating that the autophagic flux increased, whereas the level of *p*-tau significantly decreased; after subsequent administration of the autophagic degradation inhibitor CQ, the levels of NDP52 and p62 increased, and the clearance of *p*-tau decreased, indicating that TS upregulated the expression of autophagy-related proteins such as NDP52 and p62 by promoting autophagy and promoted the formation and degradation of autophagosomes, thereby promoting the clearance of *p*-tau.

Transcription factor EB (TFEB) is also an important autophagic factor, which is highly expressed in the central nervous system and active in neurons and astrocytes (Bao et al., 2016; Sachchida Nand Rai, 2021). TFEB can regulate the expression of genes involved in the autophagy-lysosome pathway (Puertollano et al., 2018; La Spina et al., 2020), and regulate autophagy flux by promoting the occurrence of lysosomes and autophagosomes and regulating autophagy body-lysosome fusion, thus promoting autophagic clearance (Sachchida Nand Rai, 2021). Evidences revealed that TFEB could effectively reduce the nerve fiber entanglement and the level of *p*-tau, thus ameliorating cognitive dysfunction (Wang H. et al, 2016; Sardiello, 2016; Sachchida Nand Rai, 2021). Therefore, TFEB has become a potential therapeutic target for the development of effective drugs. MTOR complex 1 (mTORC1) can negatively regulate TFEB, promote the production of *p*-TFEB and inhibit its nuclear translocation, thus hinder the process of autophagy degradation (Saftig & Haas, 2016; Napolitano et al., 2020). In this study, after treatment with TS, we observed a decrease in the levels of *p*-TFEB and mTOR, indicating that TS can inhibit the expression of mTOR, reduce the production of *p*-TFEB, and promote the nuclear translocation of TFEB to regulate autophagosome-lysosome fusion. After administration of Rapa, the levels of *p*-TFEB, mTOR and *p*-tau decreased, indicating that TS down-regulated the expression of *p*-TFEB and mTOR, accelerated autophagy degradation by promoting autophagosome-lysosome fusion, thus boosting the clearance of *p*-tau.

Oxidative stress can lead to a severe imbalance between the production of ROS and reactive nitrogen species and antioxidant defenses (Butterfield & Halliwell, 2019). Extensive studies have shown that oxidative stress has a great impact on the pathogenesis and progression of AD, and the relationship between oxidative stress and AD neurodegeneration has been widely reported (Cheignon et al., 2018; Butterfield & Halliwell, 2019; Wei et al., 2020). The indicators which were examined to represent changes in oxidative stress included MDA, SOD, GSH, GSSG, and the ratio of GSH/GSSG. MDA is a major aldehyde produced by the peroxidation decomposition of unsaturated fatty acids, a studied indicator of the degrees of lipid peroxidation, reflecting the overproduction of ROS and the ability to surpass the endogenous antioxidant defense system (Liu et al., 2020; Pau et al., 2021). In addition, the antioxidant enzymes SOD and GSH and GSSG play an important role in regulating the balance of the oxidative stress system. SOD, an important free radical scavenging enzyme in organisms, is the first line of defense against oxidative stress, which can catalyze O_2 disproportionation reaction to eliminate oxygen free radicals produced in the body, thereby protecting cells from oxygen free radicals (Balamurugan et al., 2018; Liu et al., 2020). In addition, SOD and MDA can verify the oxidative stress status of cells, and the imbalance between them often leads to pathological factors of neurodegenerative diseases (Liu et al., 2020). Moreover, glutathione peroxidase (GSH) is widely present in the human body, and it specifically catalyzes the reduction of hydrogen peroxide by reducing glutathione to protect the structure and function of cell membrane (Liu et al., 2020). In addition, the ratio of GSSG/GSH is a good marker of oxidative stress, depletion of GSH content, increase of GSSG content, and imbalance of GSH/GSSG ratio in AD patients and animal models (Vida et al., 2017). Our experimental results demonstrated that TS could decrease the content of MDA and GSSG, increase the content of SOD and GSH, and the ratio of GSH/GSSG, indicating that TS could inhibit the oxidative stress state in APP/PS1 mice. The regulation of oxidative stress is closely related to the function of mitochondria. Mitochondrial dysfunction plays an important role in the AD pathogenesis (Rai et al., 2020). Evidence shows that in the pathogenesis of AD, excessive production of ROS leads to oxidative stress, which seriously impairs the function of mitochondria and leads to neuronal damage (Rai et al., 2020). The effect of TS on mitochondrial function was not investigated in this study, which is needed to be further elucidated.

Neuroinflammation processes can produce proinflammatory cytokines (including IL-1β, IL-6, IL-1β, and TNF-α), and the innate immune cells involved in the process primarily include microglia and astrocytes (Leng & Edison, 2021). The release of proinflammatory molecules may lead to synaptic dysfunction, neuronal death, and inhibition of neurogenesis. For example, IL-1β leads to synaptic loss by increasing prostaglandin

E2 production, when the NF-κB pathway is inhibited, TNF-α leads to neuronal death by activating tumor necrosis factor receptor 1 (TNFR 1) (Leng & Edison, 2021). Therefore, the effects of TS on the activation of microglia and astrocytes and the release of proinflammatory cytokines were examined. It was found that TS could reduce the levels of Iba-1 and GFAP and the activation of microglia and astrocytes, thereby reducing the levels of TNF-α, IL-1β, IL-1, and the release of proinflammatory factors in APP/PS1 mice to inhibit neuroinflammation.

The abovementioned results illustrate that TS can inhibit glial activation and neuroinflammation in APP/PS1 transgenic mice, and the underlying mechanism was further investigated. It has been shown that Aβ can activate the NF-κB pathway in astrocytes, which can act on receptors on neurons and microglia, leading to neuronal dysfunction and microglial activation (Leng & Edison, 2021). Numerous studies have shown an interaction between Nrf2 and NF-κB signaling pathways, which regulate the main pathway of inflammatory response (Wardyn et al., 2015; Tom et al., 2019; Sorrenti et al., 2020). The effect of Nrf2 is related to its ability to antagonize NF-κB, and the activation of Nrf2 can inhibit the NF-κB pathway. For example, the Nrf2 agonist SFN can reduce the activity of NF-κB (Sorrenti et al., 2020). Thus, the NF-κB signaling pathway was selected to investigate the effects of TS on inflammatory factors and glial activation to improve the mechanism of TS. It was found that TS treatment significantly inhibited the expression of NF-κB in APP/PS1 mice and Aβ-induced PC12 cells by *in vivo* and *in vitro* experiments. However, in Nrf2 knockout PC12 cells, the transcriptional effect of TS inhibition of NF-κB was weakened, demonstrating that TS improves neuroinflammation by acting on Nrf2 to downregulate the expression of NF-κB.

Synapses, the junctions between two neurons, are important structures for maintaining the normal functional network of neurons, and they are considered as pathologically relevant factors for cognitive decline (Lee et al., 2016; Wei et al., 2020). The presynaptic vesicle protein synaptophysin and postsynaptic protein PSD-95 play crucial roles in synaptic transmission, synaptic maturation, and synaptic plasticity, and if the molecular network between synapses controls the transmission of synaptic signals and synaptic plasticity, then disturbances in synaptic function may lead to long-term neuronal damage and cognitive decline (Lee et al., 2016). In our results, TS increased the expression of synaptophysin and PSD-95 in APP/PS1 mice and alleviated synaptic dysfunction. Similarly, Chao Wei and Lee et al. found that SSc treatment could increase the protein levels of synaptophysin and PSD-95, thus enhancing synaptic integrity (Lee et al., 2016; Wei et al., 2020). Collectively, TS and its monomeric saponin SSc could protect synaptic function via upregulating the expression of synaptophysin and PSD-95.

Considerable evidence shows that AD is closely related to GM. Clinical data and animal experimental studies show intestinal flora imbalance in AD patients and models, which can promote neuroinflammation and amyloidosis, thereby playing a role in the occurrence and development of AD. Moreover, various drugs have been proved to achieve therapeutic effects through flora, such as probiotics, antibiotics and GV-971. In order to comprehensively evaluate the protective effect of TS, we applied 16s rRNA high-throughput sequencing to analyze the structural diversity, composition, and abundance of GM in WT mice, APP/PS1 transgenic mice, and TS intervention mice. Our results showed that the abundance of *Desuflovibrio*, *Helicobacter*, *Mucispirillum*, *Roseburia*, and *Clostridium* in APP/PS1 mice was significantly higher than that in WT mice, which was partly consistent with previous research. Furthermore, we found that TS treatment reversed the abnormal upregulated abundance of these flora, indicating that TS may play a protective role in AD by regulating GM. Further investigation are needed to verify how TS exerts therapeutic effect against AD through GM. Existing studies have shown a close relationship between GM and inflammation (Giau et al., 2018; Garcez et al., 2019; Wang et al., 2019; Sun et al., 2020). Therefore, whether TS can reduce the inflammatory response by regulating GM is a reasonable research direction.

In conclusion, TS plays a comprehensive role in the treatment of AD through the abovementioned ways, which can effectively ameliorate the cognitive impairment in AD mice. How TS plays a protective role by regulating the GM need to be further investigated. Whether GM affect the release of inflammatory factors or the deposition of Aβ through their metabolites, such as short-chain fatty acids, may be the next research direction in the future.

Data availability statement

The original contributions presented in the study are publicly available. This data can be found here: https://www.ncbi.nlm.nih.gov/, PRJNA859675.

Ethics statement

The animal study was reviewed and approved by the Ethic Committee of Ningxia Medical University.

Author contributions

JL, X-YC and YY conceived, planned, and oversaw the studies. BZ and X-HY performed laboratory experiments and analyzed the data. JL and R-XM assisted in data analysis. JL, BZ, X-YC, YY wrote the paper. C-HZ and J-XT revised the paper. All authors have reviewed and approved it for publication.

Funding

This research was supported by National Natural Science Foundation of China (82160759, 82060792, 81660645, 81660673); Key R&D Program of Ningxia (2018BFG02005, 2021BEG03100), Natural Science Foundation of Ningxia (2020AAC03133, 2021AAC03143), the Fourth Batch of Ningxia Youth Talents Supporting Program (TJGC2019091, TJGC2019100).

Conflict of interest

The authors declare that the research was conducted in the absence of any commercial or financial relationships that could be construed as a potential conflict of interest.

Publisher's note

Supplementary material

The Supplementary Material for this article can be found online at: https://www.frontiersin.org/articles/10.3389/fphar.2022.940999/full#supplementary-material

References

Bahn, G., Park, J. S., Yun, U. J., Lee, Y. J., Choi, Y., Park, J. S., et al. (2019). NRF2/ARE pathway negatively regulates BACE1 expression and ameliorates cognitive deficits in mouse Alzheimer's models. *Proc. Natl. Acad. Sci. U. S. A.* 116 (25), 12516–12523. doi:10.1073/pnas.1819541116

Balamurugan, M., Santharaman, P., Madasamy, T., Rajesh, S., Sethy, N. K., Bhargava, K., et al. (2018). Recent trends in electrochemical biosensors of superoxide dismutases. *Biosens. Bioelectron.* 116, 89–99. doi:10.1016/j.bios.2018.05.040

Bao, J., Zheng, L., Zhang, Q., Li, X., Zhang, X., Li, Z., et al. (2016). Deacetylation of TFEB promotes fibrillar Aβ degradation by upregulating lysosomal biogenesis in microglia. *Protein Cell.* 7 (6), 417–433. doi:10.1007/s13238-016-0269-2

Branca, C., Ferreira, E., Nguyen, T. V., Doyle, K., Caccamo, A., Oddo, S., et al. (2017). Genetic reduction of Nrf2 exacerbates cognitive deficits in a mouse model of Alzheimer's disease. *Hum. Mol. Genet.* 26 (24), 4823–4835. doi:10.1093/hmg/ddx361

Busche, M. A., and Hyman, B. T. (2020). Synergy between amyloid-beta and tau in Alzheimer's disease. *Nat. Neurosci.* 23 (10), 1183–1193. doi:10.1038/s41593-020-0687-6

Butterfield, D. A., and Halliwell, B. (2019). Oxidative stress, dysfunctional glucose metabolism and Alzheimer disease. *Nat. Rev. Neurosci.* 20 (3), 148–160. doi:10.1038/s41583-019-0132-6

Cao, G., Su, P., Zhang, S., Guo, L., Zhang, H., Liang, Y., et al. (2016). Ginsenoside Re reduces Aβ production by activating PPARγ to inhibit BACE1 in N2a/APP695 cells. *Eur. J. Pharmacol.* 793, 101–108. doi:10.1016/j.ejphar.2016.11.006

Cheignon, C., Tomas, M., Bonnefont-Rousselot, D., Faller, P., Hureau, C., Collin, F., et al. (2018). Oxidative stress and the amyloid beta peptide in Alzheimer's disease. *Redox Biol.* 14, 450–464. doi:10.1016/j.redox.2017.10.014

Cryan, J. F., O'Riordan, K. J., Cowan, C. S. M., Sandhu, K. V., Bastiaanssen, T. F. S., Boehme, M., et al. (2019). The microbiota-gut-brain Axis. *Physiol. Rev.* 99 (4), 1877–2013. doi:10.1152/physrev.00018.2018

Cryan, J. F., O'Riordan, K. J., Sandhu, K., Peterson, V., and Dinan, T. G. (2020). The gut microbiome in neurological disorders. *Lancet. Neurol.* 19 (2), 179–194. doi:10.1016/s1474-4422(19)30356-4

Cuadrado, A., Kugler, S., and Lastres-Becker, I. (2018). Pharmacological targeting of GSK-3 and NRF2 provides neuroprotection in a preclinical model of tauopathy. *Redox Biol.* 14, 522–534. doi:10.1016/j.redox.2017.10.010

Dodiya, H. B., Kuntz, T., Shaik, S. M., Baufeld, C., Leibowitz, J., Zhang, X., et al. (2019). Sex-specific effects of microbiome perturbations on cerebral Aβ amyloidosis and microglia phenotypes. *J. Exp. Med.* 216 (7), 1542–1560. doi:10.1084/jem.20182386

Fao, L., Mota, S. I., and Rego, A. C. (2019). Shaping the Nrf2-ARE-related pathways in Alzheimer's and Parkinson's diseases. *Ageing Res. Rev.* 54, 100942. doi:10.1016/j.arr.2019.100942

Garcez, M. L., Jacobs, K. R., and Guillemin, G. J. (2019). Microbiota alterations in alzheimer's disease: Involvement of the kynurenine pathway and inflammation. *Neurotox. Res.* 36 (2), 424–436. doi:10.1007/s12640-019-00057-3

Giau, V. V., Wu, S. Y., Jamerlan, A., An, S. S. A., Kim, S. Y., Hulme, J., et al. (2018). Gut microbiota and their neuroinflammatory implications in alzheimer's disease. *Nutrients* 10 (11), E1765. doi:10.3390/nu10111765

Hampel, H., Vassar, R., De Strooper, B., Hardy, J., Willem, M., Singh, N., et al. (2021). The beta-Secretase BACE1 in Alzheimer's Disease. *Biol. Psychiatry* 89 (8), 745–756. doi:10.1016/j.biopsych.2020.02.001

Han, J., Park, H., Maharana, C., Gwon, A. R., Park, J., Baek, S. H., et al. (2021). Alzheimer's disease-causing presenilin-1 mutations have deleterious effects on mitochondrial function. *Theranostics* 11 (18), 8855–8873. doi:10.7150/thno.59776

Harach, T., Marungruang, N., Duthilleul, N., Cheatham, V., Mc Coy, K. D., Frisoni, G., et al. (2017). Reduction of Abeta amyloid pathology in APPPS1 transgenic mice in the absence of gut microbiota. *Sci. Rep.* 7, 41802. doi:10.1038/srep41802

Jan, A., Jansonius, B., Delaidelli, A., Somasekharan, S. P., Bhanshali, F., Vandal, M., et al. (2017). eEF2K inhibition blocks Aβ42 neurotoxicity by promoting an NRF2 antioxidant response. *Acta Neuropathol.* 133 (1), 101–119. doi:10.1007/s00401-016-1634-1

Jiang, R., Wu, X. F., Wang, B., Guan, R. X., Lv, L. M., Li, A. P., et al. (2020). Reduction of NgR in perforant path decreases amyloid-beta peptide production and ameliorates synaptic and cognitive deficits in APP/PS1 mice. *Alzheimers Res. Ther.* 12 (1), 47. doi:10.1186/s13195-020-00616-3

Jiang, S., Zhao, Y., Zhang, T., Lan, J., Yang, J., Yuan, L., et al. (2018). Galantamine inhibits beta-amyloid-induced cytostatic autophagy in PC12 cells through decreasing ROS production. *Cell. Prolif.* 51 (3), e12427. doi:10.1111/cpr.12427

Jo, C., Gundemir, S., Pritchard, S., Jin, Y. N., Rahman, I., Johnson, G. V., et al. (2014). Nrf2 reduces levels of phosphorylated tau protein by inducing autophagy adaptor protein NDP52. *Nat. Commun.* 5, 3496. doi:10.1038/ncomms4496

John, A., and Reddy, P. H. (2021). Synaptic basis of Alzheimer's disease: Focus on synaptic amyloid beta, P-tau and mitochondria. *Ageing Res. Rev.* 65, 101208. doi:10.1016/j.arr.2020.101208

Kim, B. M. (2018). The role of saikosaponins in therapeutic strategies for age-related diseases. *Oxid. Med. Cell. Longev.* 2018, 8275256. doi:10.1155/2018/8275256

Kobayashi, E. H., Suzuki, T., Funayama, R., Nagashima, T., Hayashi, M., Sekine, H., et al. (2016). Nrf2 suppresses macrophage inflammatory response by blocking proinflammatory cytokine transcription. *Nat. Commun.* 7, 11624. doi:10.1038/ncomms11624

Kosel, F., Pelley, J. M. S., and Franklin, T. B. (2020). Behavioural and psychological symptoms of dementia in mouse models of Alzheimer's disease-related pathology. *Neurosci. Biobehav. Rev.* 112, 634–647. doi:10.1016/j.neubiorev.2020.02.012

Kwak, S. S., Washicosky, K. J., Brand, E., von Maydell, D., Aronson, J., Kim, S., et al. (2020). Amyloid-β42/40 ratio drives tau pathology in 3D human neural cell culture models of Alzheimer's disease. *Nat. Commun.* 11 (1), 1377. doi:10.1038/s41467-020-15120-3

La Spina, M., Contreras, P. S., Rissone, A., Meena, N. K., Jeong, E., Martina, J. A., et al. (2020). MiT/TFE family of transcription factors: An evolutionary perspective. *Front. Cell. Dev. Biol.* 8, 609683. doi:10.3389/fcell.2020.609683

Ledo, J. H., Liebmann, T., Zhang, R., Chang, J. C., Azevedo, E. P., Wong, E., et al. (2021). Presenilin 1 phosphorylation regulates amyloid-beta degradation by microglia. *Mol. Psychiatry* 26 (10), 5620–5635. doi:10.1038/s41380-020-0856-8

Lee, T. H., Park, S., You, M. H., Lim, J. H., Min, S. H., Kim, B. M., et al. (2016). A potential therapeutic effect of saikosaponin C as a novel dual-target anti-Alzheimer agent. *J. Neurochem.* 136 (6), 1232–1245. doi:10.1111/jnc.13515

Leng, F., and Edison, P. (2021). Neuroinflammation and microglial activation in alzheimer disease: Where do we go from here? *Nat. Rev. Neurol.* 17 (3), 157–172. doi:10.1038/s41582-020-00435-y

Li, P., Wu, M., Xiong, W., Li, J., An, Y., Ren, J., et al. (2020). Saikosaponin-d ameliorates dextran sulfate sodium-induced colitis by suppressing NF-κB activation and modulating the gut microbiota in mice. *Int. Immunopharmacol.* 81, 106288. doi:10.1016/j.intimp.2020.106288

Li, Z. Y., Guo, Z., Liu, Y. M., Liu, X. M., Chang, Q., Liao, Y. H., et al. (2013). Neuroprotective effects of total saikosaponins of *Bupleurum yinchowense* on corticosterone-induced apoptosis in PC12 cells. *J. Ethnopharmacol.* 148 (3), 794–803. doi:10.1016/j.jep.2013.04.057

Liang, Z. B., Liu, L., and Chao, Z. (2012). Investigation of medicinal *Bupleurum* resources and current situation of Chaihu production. *Lishizhen Med. Materia Medica Redearch* 23 (8), 2011–2013. doi:10.3969/j.issn.1008-0805.2012.08.075

Limorenko, G., and Lashuel, H. A. (2022). Revisiting the grammar of tau aggregation and pathology formation: How new insights from brain pathology are shaping how we study and target tauopathies. *Chem. Soc. Rev.* 51 (2), 513–565. doi:10.1039/d1cs00127b

Lin, X., Wu, S., Wang, Q., Shi, Y., Liu, G., Zhi, J., et al. (2016). Saikosaponin-D reduces H_2O_2-induced PC12 cell apoptosis by removing ROS and blocking MAPK-dependent oxidative damage. *Cell. Mol. Neurobiol.* 36 (8), 1365–1375. doi:10.1007/s10571-016-0336-5

Liu, H. X., Yuan, X. L., Xu, C. Y., and Liu, L. S. (2019a). Yuan's experience in the treatment of alzheimer'S disease by "shugan bushen tiaoshen. *Chin. J. Basic Med. Traditional Chin. Med.* 25 (6), 838–840.

Liu, K., Lin, H. H., Pi, R., Mak, S., Han, Y., Hu, Y., et al. (2018). Research and development of anti-alzheimer's disease drugs: An update from the perspective of technology flows. *Expert Opin. Ther. Pat.* 28 (4), 341–350. doi:10.1080/13543776.2018.1439475

Liu, X. Q., Deng, Y. X., Dai, Z., Hu, T., Cai, W. W., Liu, H. F., et al. (2020). Sodium tanshinone IIA sulfonate protects against Aβ1-42-induced cellular toxicity by modulating Aβ-degrading enzymes in HT22 cells. *Int. J. Biol. Macromol.* 151, 47–55. doi:10.1016/j.ijbiomac.2020.02.040

Liu, Y., Du, T., Zhang, W., Lu, W., Peng, Z., Huang, S., et al. (2019b). Modified huang-lian-jie-du decoction ameliorates Aβ synaptotoxicity in a murine model of alzheimer's disease. *Oxid. Med. Cell. Longev.* 2019, 8340192. doi:10.1155/2019/8340192

Lowe, V. J., Bruinsma, T. J., Wiste, H. J., Min, H. K., Weigand, S. D., Fang, P., et al. (2019). Cross-sectional associations of tau-PET signal with cognition in cognitively unimpaired adults. *Neurology* 93 (1), e29–e39. doi:10.1212/WNL.0000000000007728

Luo, W., Wang, T., Hong, C., Yang, Y. C., Chen, Y., Cen, J., et al. (2016). Design, synthesis and evaluation of 4-dimethylamine flavonoid derivatives as potential multifunctional anti-Alzheimer agents. *Eur. J. Med. Chem.* 122, 17–26. doi:10.1016/j.ejmech.2016.06.022

Maass, A., Lockhart, S. N., Harrison, T. M., Bell, R. K., Mellinger, T., Swinnerton, K., et al. (2018). Entorhinal tau pathology, episodic memory decline, and neurodegeneration in aging. *J. Neurosci.* 38 (3), 530–543. doi:10.1523/JNEUROSCI.2028-17.2017

MahmoudianDehkordi, S., Arnold, M., Nho, K., Ahmad, S., Jia, W., Xie, G., et al. (2019). Alzheimer's Disease Neuroimaging, I. & the Alzheimer Disease Metabolomics, CAltered bile acid profile associates with cognitive impairment in Alzheimer's disease-An emerging role for gut microbiome. *Alzheimers Dement.* 15 (1), 76–92. doi:10.1016/j.jalz.2018.07.217

Menzies, F. M., Fleming, A., Caricasole, A., Bento, C. F., Andrews, S. P., Ashkenazi, A., et al. (2017). Autophagy and neurodegeneration: Pathogenic mechanisms and therapeutic opportunities. *Neuron* 93 (5), 1015–1034. doi:10.1016/j.neuron.2017.01.022

Napolitano, G., Di Malta, C., Esposito, A., de Araujo, M. E. G., Pece, S., Bertalot, G., et al. (2020). A substrate-specific mTORC1 pathway underlies Birt-Hogg-Dube syndrome. *Nature* 585 (7826), 597–602. doi:10.1038/s41586-020-2444-0

Olsson, B., Lautner, R., Andreasson, U., Öhrfelt, A., Portelius, E., Bjerke, M., et al. (2016). CSF and blood biomarkers for the diagnosis of alzheimer's disease: A systematic review and meta-analysis. *Lancet. Neurol.* 15 (7), 673–684. doi:10.1016/s1474-4422(16)00070-3

Osama, A., Zhang, J., Yao, J., Yao, X., and Fang, J. (2020). Nrf2: A dark horse in alzheimer's disease treatment. *Ageing Res. Rev.* 64, 101206. doi:10.1016/j.arr.2020.101206

Pajares, M., Jimenez-Moreno, N., Garcia-Yague, A. J., Escoll, M., de Ceballos, M. L., Van Leuven, F., et al. (2016). Transcription factor NFE2L2/NRF2 is a regulator of macroautophagy genes. *Autophagy* 12 (10), 1902–1916. doi:10.1080/15548627.2016.1208889

Pajares, M., Rojo, A. I., Arias, E., Diaz-Carretero, A., Cuervo, A. M., Cuadrado, A., et al. (2018). Transcription factor NFE2L2/NRF2 modulates chaperone-mediated autophagy through the regulation of LAMP2A. *Autophagy* 14 (8), 1310–1322. doi:10.1080/15548627.2018.1474992

Park, W. H., Kang, S., Piao, Y., Pak, C. J., Oh, M. S., Kim, J., et al. (2015). Ethanol extract of Bupleurum falcatum and saikosaponins inhibit neuroinflammation via inhibition of NF-κB. *J. Ethnopharmacol.* 174, 37–44. doi:10.1016/j.jep.2015.07.039

Pau, M. C., Zinellu, E., Fois, S. S., Piras, B., Pintus, G., Carru, C., et al. (2021). Circulating malondialdehyde concentrations in obstructive sleep apnea (osa): A systematic review and meta-analysis with meta-regression. *Antioxidants (Basel)* 10 (7), 1053. doi:10.3390/antiox10071053

Pereira, C. F., Santos, A. E., Moreira, P. I., Pereira, A. C., Sousa, F. J., Cardoso, S. M., et al. (2019). Is Alzheimer's disease an inflammasomopathy? *Ageing Res. Rev.* 56, 100966. doi:10.1016/j.arr.2019.100966

Piras, A., Collin, L., Gruninger, F., Graff, C., and Ronnback, A. (2016). Autophagic and lysosomal defects in human tauopathies: Analysis of post-mortem brain from patients with familial alzheimer disease, corticobasal degeneration and progressive supranuclear palsy. *Acta Neuropathol. Commun.* 4, 22. doi:10.1186/s40478-016-0292-9

Puertollano, R., Ferguson, S. M., Brugarolas, J., and Ballabio, A. (2018). The complex relationship between TFEB transcription factor phosphorylation and subcellular localization. *EMBO J.* 37 (11), e98804. doi:10.15252/embj.201798804

Rai, S. N., Singh, C., Singh, A., Singh, M. P., and Singh, B. K. (2020). Mitochondrial dysfunction: A potential therapeutic target to treat alzheimer's disease. *Mol. Neurobiol.* 57 (7), 3075–3088. doi:10.1007/s12035-020-01945-y

Ren, P., Chen, J., Li, B., Zhang, M., Yang, B., Guo, X., et al. (2020). Nrf2 ablation promotes alzheimer's disease-like pathology in APP/PS1 transgenic mice: The role of neuroinflammation and oxidative stress. *Oxid. Med. Cell. Longev.* 2020, 3050971. doi:10.1155/2020/3050971

Rojo, A. I., Pajares, M., Rada, P., Nunez, A., Nevado-Holgado, A. J., Killik, R., et al. (2017). NRF2 deficiency replicates transcriptomic changes in Alzheimer's patients and worsens APP and TAU pathology. *Redox Biol.* 13, 444–451. doi:10.1016/j.redox.2017.07.006

Sachchida Nand Rai, N. T., Singh, P., Mishra, D., Singh, A., Hooshmandi, E., Vamanu, E., et al. (2021). Therapeutic potential of vital transcription factors in Alzheimer's and Parkinson's disease with particular emphasis on transcription factor EB mediated autophagy. *Front. Neurosci.* 15, 777347. doi:10.3389/fnins.2021.777347

Saftig, P., and Haas, A. (2016). Turn up the lysosome. *Nat. Cell. Biol.* 18 (10), 1025–1027. doi:10.1038/ncb3409

Sardiello, M. (2016). Transcription factor EB: From master coordinator of lysosomal pathways to candidate therapeutic target in degenerative storage diseases. *Ann. N. Y. Acad. Sci.* 1371 (1), 3–14. doi:10.1111/nyas.13131

Savioz, A., Leuba, G., and Vallet, P. G. (2014). A framework to understand the variations of PSD-95 expression in brain aging and in Alzheimer's disease. *Ageing Res. Rev.* 18, 86–94. doi:10.1016/j.arr.2014.09.004

Scheltens, P., De Strooper, B., Kivipelto, M., Holstege, H., Chételat, G., and Teunissen, C. E. (2021). Alzheimer's disease. *Lancet* 2021 (397), 1577–1590. doi:10.1016/s0140-6736(20)32205-4

Scott, K. A., Ida, M., Peterson, V. L., Prenderville, J. A., Moloney, G. M., Izumo, T., et al. (2017). Revisiting Metchnikoff: Age-related alterations in microbiota-gut-brain axis in the mouse. *Brain Behav. Immun.* 65, 20–32. doi:10.1016/j.bbi.2017.02.004

Shin, J., Park, S., Lee, H., and Kim, Y. (2021). Thioflavin-positive tau aggregates complicating quantification of amyloid plaques in the brain of 5XFAD transgenic mouse model. *Sci. Rep.* 11 (1), 1617. doi:10.1038/s41598-021-81304-6

Singh, A. K., Rai, S. N., Maurya, A., Mishra, G., Awasthi, R., Shakya, A., et al. (2021). Therapeutic potential of phytoconstituents in management of alzheimer's disease. *Evid. Based. Complement. Altern. Med.* 2021, 5578574. doi:10.1155/2021/5578574

Sohn, E., Kim, Y. J., and Jeong, S. J. (2021). Korean traditional herbal formula Soshiho-tang attenuates memory impairment and neuronal damage in mice with amyloid-beta-induced Alzheimer's disease. *Integr. Med. Res.* 10 (3), 100723. doi:10.1016/j.imr.2021.100723

Sorrenti, V., Davinelli, S., Scapagnini, G., Willcox, B. J., Allsopp, R. C., Willcox, D. C., et al. (2020). Astaxanthin as a putative geroprotector: Molecular basis and focus on brain aging. *Mar. Drugs* 18 (7), E351. doi:10.3390/md18070351

Soto-Faguas, C. M., Sanchez-Molina, P., and Saura, C. A. (2021). Loss of presenilin function enhances tau phosphorylation and aggregation in mice. *Acta Neuropathol. Commun.* 9 (1), 162. doi:10.1186/s40478-021-01259-7

Sun, J., Xu, J., Yang, B., Chen, K., Kong, Y., Fang, N., et al. (2020). Effect of Clostridium butyricum against microglia-mediated neuroinflammation in alzheimer's disease via regulating gut microbiota and metabolites butyrate. *Mol. Nutr. Food Res.* 64 (2), e1900636. doi:10.1002/mnfr.201900636

Tom, S., Rane, A., Katewa, A. S., Chamoli, M., Matsumoto, R. R., Andersen, J. K., et al. (2019). Gedunin inhibits oligomeric aβ1-42-induced microglia activation via modulation of nrf2-NF-κb signaling. *Mol. Neurobiol.* 56 (11), 7851–7862. doi:10.1007/s12035-019-1636-9

Toma, C., De Cilla, S., Palumbo, A., Garhwal, D. P., and Grossini, E. (2021). Oxidative and nitrosative stress in age-related macular degeneration: A review of their role in different stages of disease. *Antioxidants (Basel)* 10 (5), 653. doi:10.3390/antiox10050653

Tsai, F. S., Wu, L. Y., Yang, S. E., Cheng, H. Y., Tsai, C. C., Wu, C. R., et al. (2015). Ferulic acid reverses the cognitive dysfunction caused by amyloid beta peptide 1-40 through anti-oxidant activity and cholinergic activation in rats. *Am. J. Chin. Med.* 43 (2), 319–335. doi:10.1142/S0192415X15500214

Tu, W., Wang, H., Li, S., Liu, Q., and Sha, H. (2019). The anti-inflammatory and anti-oxidant mechanisms of the keap1/nrf2/ARE signaling pathway in chronic diseases. *Aging Dis.* 10 (3), 637–651. doi:10.14336/AD.2018.0513

Vida, C., Martinez de Toda, I., Garrido, A., Carro, E., Molina, J. A., De la Fuente, M., et al. (2017). Impairment of several immune functions and redox state in blood cells of alzheimer's disease patients. Relevant role of neutrophils in oxidative stress. *Front. Immunol.* 8, 1974. doi:10.3389/fimmu.2017.01974

Viret, C., Rozieres, A., and Faure, M. (2018). Novel insights into NDP52 autophagy receptor functioning. *Trends Cell. Biol.* 28 (4), 255–257. doi:10.1016/j.tcb.2018.01.003

Vogt, N. M., Romano, K. A., Darst, B. F., Engelman, C. D., Johnson, S. C., Carlsson, C. M., et al. (2018). The gut microbiota-derived metabolite trimethylamine N-oxide is elevated in Alzheimer's disease. *Alzheimers Res. Ther.* 10 (1), 124. doi:10.1186/s13195-018-0451-2

Wang, H., Wang, R., Carrera, I., Xu, S., and Lakshmana, M. K. (2016a). TFEB overexpression in the P301S model of tauopathy mitigates increased PHF1 levels and lipofuscin puncta and rescues memory deficits. *eNeuro* 3 (2), ENEURO.0042–16.2016. doi:10.1523/ENEURO.0042-16.2016

Wang, X., Sun, G., Feng, T., Zhang, J., Huang, X., Wang, T., et al. (2019). Sodium oligomannate therapeutically remodels gut microbiota and suppresses gut bacterial amino acids-shaped neuroinflammation to inhibit Alzheimer's disease progression. *Cell. Res.* 29 (10), 787–803. doi:10.1038/s41422-019-0216-x

Wang, Z. Y., Liu, J. G., Li, H., and Yang, H. M. (2016b). Pharmacological effects of active components of Chinese herbal medicine in the treatment of alzheimer's disease: A review. *Am. J. Chin. Med.* 44 (8), 1525–1541. doi:10.1142/S0192415X16500853

Wardyn, J. D., Ponsford, A. H., and Sanderson, C. M. (2015). Dissecting molecular cross-talk between Nrf2 and NF-κB response pathways. *Biochem. Soc. Trans.* 43 (4), 621–626. doi:10.1042/BST20150014

Wei, C., Fan, J., Sun, X., Yao, J., Guo, Y., Zhou, B., et al. (2020). Acetyl-11-keto-beta-boswellic acid ameliorates cognitive deficits and reduces amyloid-beta levels in APPswe/PS1dE9 mice through antioxidant and anti-inflammatory pathways. *Free Radic. Biol. Med.* 150, 96–108. doi:10.1016/j.freeradbiomed.2020.02.022

Yang, W. T., Zheng, X. W., Chen, S., Shan, C. S., Xu, Q. Q., Zhu, J. Z., et al. (2017). Chinese herbal medicine for Alzheimer's disease: Clinical evidence and possible mechanism of neurogenesis. *Biochem. Pharmacol.* 141, 143–155. doi:10.1016/j.bcp.2017.07.002

Zeng, Q., Li, L., Siu, W., Jin, Y., Cao, M., Li, W., et al. (2019). A combined molecular biology and network pharmacology approach to investigate the multi-target mechanisms of Chaihu Shugan San on Alzheimer's disease. *Biomed. Pharmacother.* 120, 109370. doi:10.1016/j.biopha.2019.109370

Zetterberg, H., and Bendlin, B. B. (2021). Biomarkers for Alzheimer's disease-preparing for a new era of disease-modifying therapies. *Mol. Psychiatry* 26 (1), 296–308. doi:10.1038/s41380-020-0721-9

Zhang, Z., Yang, X., Song, Y. Q., and Tu, J. (2021). Autophagy in Alzheimer's disease pathogenesis: Therapeutic potential and future perspectives. *Ageing Res. Rev.* 72, 101464. doi:10.1016/j.arr.2021.101464

Zhao, L., Duan, Z., Wang, Y., Wang, M., Liu, Y., Wang, X., et al. (2021). Protective effect of Terminalia chebula Retz. extract against Aβ aggregation and Aβ-induced toxicity in *Caenorhabditis elegans*. *J. Ethnopharmacol.* 268, 113640. doi:10.1016/j.jep.2020.113640

Zhao, W., Li, G., Fan, X., Xue, H., Huang, X., Pei, R., et al. (2012). Effect of Chaihu Shugan San on memory function in Alzheimer's disease rats. *Chin. J. Exp. Traditional Med. Formulae* 18 (10), 207–210. doi:10.13422/j.cnki.syfjx.2012.10.064

frontiers | Frontiers in Neuroscience

ORIGINAL RESEARCH
published: 27 July 2022
doi: 10.3389/fnins.2022.903958

Identification of BAG5 as a Potential Biomarker for Parkinson's Disease Patients With R492X *PINK1* Mutation

Yu Fu[1,2], Yongkang Chen[1,2], Haiyan Tian[1,2], Han Liu[1,2], Dan Qi[3], Erxi Wu[3,4,5,6] and Xuejing Wang[1,2]**

[1] Department of Neurology, The First Affiliated Hospital of Zhengzhou University, Zhengzhou, China, [2] Institute of Parkinson's Disease and Movement Disorders, Zhengzhou University, Zhengzhou, China, [3] Neuroscience Institute and Department of Neurosurgery, Baylor Scott & White Health, Temple, TX, United States, [4] Department of Surgery, Texas A&M University Health Science Center College of Medicine, Temple, TX, United States, [5] Department of Pharmaceutical Sciences, Texas A&M University Health Science Center, College of Pharmacy, College Station, TX, United States, [6] Livestrong Cancer Institutes, Dell Medical School, The University of Texas at Austin, Austin, TX, United States

Parkinson's disease (PD) is a degenerative, progressive nervous system disorder with an unknown cause. *PINK1* [phosphatase and tensin homolog deleted on chromosome 10 (PTEN)-induced putative kinase 1] causative mutations R492X may cause autosomal recessive early-onset parkinsonism. In this study, we utilized patient samples and cell line system to investigate roles of Bcl2-associated athanogene 5 (BAG5) in PD patients with R492X *PINK1* mutation. We show that the expression levels of BAG5 in the skin tissues from PD patients with R492X *PINK1* mutation are markedly lower than those from the healthy control subjects in a small cohort of patients, which has not been recognized before. In addition, we demonstrate that BAG5 physically binds to R492X mutated PINK1 protein. Furthermore, we reveal that BAG5 promotes the degradation of R492X mutated PINK1 protein via ubiquitin/proteasome-dependent pathway, suggesting that decreased level of BAG5 may lead to R492X mutated PINK1 protein accumulation. These findings suggest that BAG5 may serve as an early detection biomarker for PD patients with R492X *PINK1* mutation and provide important new insights on how BAG5 affects R492X mutated PINK1 protein, highlighting therapeutic targets for this disease.

Keywords: R492X *PINK1* mutation degradation, Bcl2-associated athanogene 5, ubiquitination, Parkinson's disease, skin

OPEN ACCESS

Edited by:
Habibeh Khoshbouei, University of Florida, United States

Reviewed by:
Yong Li, Baylor College of Medicine, United States
Murali M. Yallapu, The University of Texas Rio Grande Valley, United States

****Correspondence:***
Erxi Wu
Erxi.Wu@BSWHealth.org
Xuejing Wang
fccwangxj2@zzu.edu.cn

Specialty section:
This article was submitted to Neuropharmacology, a section of the journal Frontiers in Neuroscience

Received: *24 March 2022*
Accepted: *09 June 2022*
Published: *27 July 2022*

Citation:
Fu Y, Chen Y, Tian H, Liu H, Qi D, Wu E and Wang X (2022) Identification of BAG5 as a Potential Biomarker for Parkinson's Disease Patients With R492X PINK1 Mutation. Front. Neurosci. 16:903958. doi: 10.3389/fnins.2022.903958

INTRODUCTION

The phosphatase and tensin homologue deleted on chromosome 10 (PTEN)-induced putative kinase 1 (*PINK1*) is a mitochondria-targeted serine/threonine kinase with a mitochondrial localization signal (MLS) domain and a functional serine/threonine kinase domain (Matsuda et al., 2013; Wang et al., 2014; Vizziello et al., 2021; Kakade et al., 2022). MLS parts include a mitochondrial-targeting sequence (MTS) and a putative transmembrane domain (TD), the

Abbreviations: BAG5, Bcl2-associated athanogene 5; BD, BAG domain; CHX, cycloheximide; co-IP, co-immunoprecipitation; EGFP, enhanced green fluorescent protein; FITC, fluorescein isothiocyanate; GFP, green fluorescent protein; HA, haemagglutinin; MG132, carbobenzoxy-Leu-Leu-leucinal; MLS, mitochondrial localization signal; MTS, mitochondrial-targeting sequence; PD, Parkinson's disease; *PINK1*, PTEN-induced kinase 1; *PINK1* R492X, PTEN-induced kinase 1 p.R492X mutation; PTEN, phosphatase and tensin homolog; TD, transmembrane domain; UPS, ubiquitin/proteasome system.

degradation of N-terminal domain was reported to affect the cellular location of *PINK1* (Eldeeb and Ragheb, 2020; Sekine, 2020; Vizziello et al., 2021). *PINK1* has been well-known for the notion of neuroprotective roles, as it protects cells from damage-mediated mitochondrial dysfunction (Brunelli et al., 2020). In addition, *PINK1* is also known to be implicated in various processes like apoptosis and mitophagy (Voigt et al., 2016; Li et al., 2022). The *PINK1* (or *PARK6*) gene was identified to be linked to Parkinson's disease (PD) for the first time by linkage analysis of consanguineous families with early-onset autosomal recessive PD and is recently reported as one of the most commonly mutated genes in early onset PD (Valente et al., 2004; Agarwal and Muqit, 2022; Gan et al., 2022). More than 50 *PINK1* mutations have been found to impair mitochondrial functional throughout the kinase and carboxyl-terminal regulatory domains of *PINK1* (Rochet et al., 2012; Matsuda et al., 2013). The R492X mutation in the *PINK1* gene was identified by Hatano et al. (2004). Despite the neurotoxicity of R492X mutated PINK1 protein, inducing mitochondrial dysfunction and oxidative stress, the underlying molecular mechanisms are still to be explored (Leites and Morais, 2021).

The Bcl-2 associated athanogene (BAG) family is a group of chaperone regulators (Qin et al., 2016). All members of the BAG protein family contain BAG domain (BD), which mediates direct interaction with the ATPase domain of Hsp70/Hsc70 molecular chaperones (Bracher and Verghese, 2015). The BAG family proteins perform diverse functions including apoptosis and protein degradation (Bracher and Verghese, 2015). BAG5 is a unique member of the BAG family with five BDs. Previous studies have reported that BAG5 inhibited both Parkin E3 ligase and Hsp70 chaperone activities thereby enhancing dopaminergic neuron degeneration (Berliner et al., 1986; De Snoo et al., 2019). This suggests that BAG5 is involved in proteasome-mediated protein degradation, which is also associated with Parkinson's disease. In addition, two early studies demonstrated that BAG5 inhibited MPP^+-induced apoptosis through both endogenous and mitochondria-mediated pathways of apoptosis (Peviani et al., 2012; Wang et al., 2014).

In this study, we first found that the expression levels of BAG5 in the skin tissues from a small cohort of PD patients with R492X *PINK1* mutation markedly decreased compared with those from the healthy control subjects. Furthermore, we demonstrated that BAG5 promotes the degradation of R492X mutated PINK1 protein via ubiquitylation-dependent pathway. These data suggest that BAG5 may serve as an early detection biomarker for PD patients with R492X *PINK1* mutation and provide important new insights on how BAG5 affects R492X mutated PINK1 protein, highlighting therapeutic targets for this disease.

MATERIALS AND METHODS

Parkinson's Disease Patients and Skin Biopsy

Skin tissues were obtained from two patients with PD harboring R492X *PINK1* mutation and two healthy controls. Punch biopsy of the skin (3 mm) were elevated with local anesthesia from the left lateral calf. Samples were immediately fixed in 4% paraformaldehyde and kept at 4°C for at least 2 days. The study was performed with the approval of the Institutional Ethics Committee of the Zhengzhou University (2015-81100949).

Plasmid Constructs

Plasmids have been previously described (Wang et al., 2014). Briefly, the mammalian expression plasmid pKH3-HA-PINK1 was a kind gift from Dr. Bin Li (University of Science & Technology of China). Full-length BAG5 cDNA was amplified from a human fetal brain library (Invitrogen) using the primers 5′-cggaattctatgcgtttccattggttaccc-3′ and 5′-cgcggatccgtactcccattcatcaga-3′ and inserted into pcDNA3.1(+)/myc-HisA vector at *Bam*HI/*Eco*RI sites. pEGFP-BAG5 was constructed by subcloning a fragment excised from pcDNA3.1(+)/myc-HisA-BAG5 into pEGFP-N3 vector at *Bam*HI/*Eco*RI sites. All constructs were sequenced to confirm their fidelity. HA-PINK1^{R492X} was constructed similarly with HA-PINK1 (Che et al., 2013).

Cell Culture, Transfections, and RNA Interference

Human embryonic kidney 293 (HEK293) cells (purchased from the Type Culture Collection of the Chinese Academy of Sciences, Shanghai, China) were maintained in DMEM (GIBCO, United States) supplemented with 10% newborn calf serum (GIBCO, United States), 100 U/ml penicillin and 100 mg/ml streptomycin (Invitrogen, United States), at 37°C in a humidified incubator of 5% CO_2. The mammalian expression plasmid enhanced green fluorescent protein (EGFP)-BAG5, haemagglutinin (HA)-PINK1 and HA-PINK1^{R492X} were gifts provided by Professor Guanghui Wang (Che et al., 2013) (Soochow University, China). The HA tag was added to the N-terminal of PINK1 or PINK1 R492X, the expression was confirmed by immunostaining (**Supplementary Figure 1**). Transfections were performed using Lipofectamine 2000 (Invitrogen, United States) according to the instructions. Cycloheximide (CHX) was purchased from Sigma and carbobenzoxy-Leu-Leu-leucinal (MG132), a proteasome inhibitor, was obtained from Calbiochem. Plasmids and Lipofectamine 2000 were premixed in OPTI-medium (GIBCO, United States) for 30 min and then applied to the cells. After transfection for 6 h, the medium was replaced with fresh medium containing 15% FBS, and cells were treated for another 24 h and harvested subsequently. According to the manufacturer's instructions (Invitrogen), 50 pmol of BAG5 siRNA was transfected using Oligofectamine. Oligo RNA was purchased from Gene-Pharma (Shanghai, China) containing the following sequences: siBAG5 sense, 5′-GGAGAUAUUCAGCAAGCUATT-3′, siBAG5 antisense, 5′-UAGCUUGCUGAAUAUCUCCTT-3′; siRNA control sense, 5′-UUCUCCGAACGUGUCACGUdTdT-3′, siRNA control antisense, 5′-ACGUGACACGUUCGGAGAAdTdT-3′.

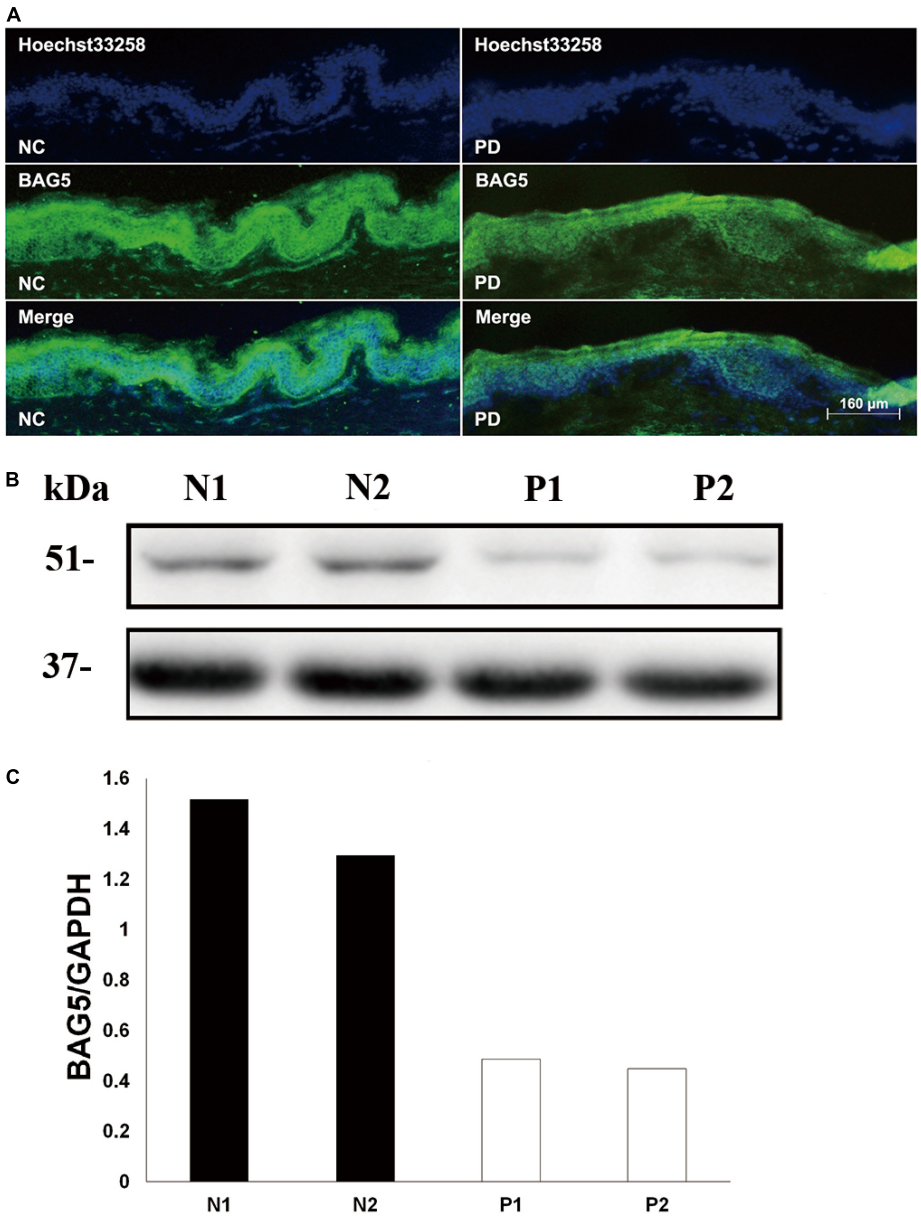

FIGURE 1 | Decreased level of BAG5 in the skin tissue of patients with R492X *PINK1* mutation. **(A)** Immunofluorescence staining for the expression of BAG5 in skin tissues from healthy individuals (NC, left) and patients with PD harboring R492X *PINK1* mutation (PD, right). **(B)** Western blotting was performed using skin tissues from healthy individuals (N1 and N2) and PD patients with R492X *PINK1* mutation (P1 and P2). **(C)** Quantitative data from **(B)** (Density of endogenous BAG5 against GAPDH) using NIH ImageJ. The data represent the intensity of BAG5 band of the healthy individuals (N1 and N2) or PD patients with R492X *PINK1* mutation (P1 and P2), respectively. GAPDH serves as a loading control.

Immunoprecipitation and Western Blotting Analysis

Whole cell lysates were sonicated in lysis buffer [50 mM Tris–HCl (pH 7.5), 150 mM NaCl, 1 mM EDTA, 1 mg/ml aprotinin, 10 mg/ml of leupeptin, 0.5 mM Pefabloc SC, 10 mg/ml of pepstatin, 1% NP-40]. Cellular debris was removed by centrifugation at 12,000 × *g* for 20 min at 4°C. The supernatants were incubated with the antibodies in 0.01% BSA for 4 h at 4°C. After incubation, protein G Sepharose (Roche, Switzerland) was used for precipitation. The beads were washed with 1 × PBS for six times, and proteins were eluted with SDS sample buffer for immunoblot analysis. The samples were subjected to SDS-PAGE. After transferred to nitrocellulose membranes, blots were blocked with 15% non-fat dry milk in TBST (0.25% Triton X-100 in PBS, pH 7.4) for 1 h, and then incubated with primary antibodies overnight at 4°C. After washing three times in TBST, the membrane was incubated with anti-rabbit IgG (Cell Signaling Technology, United States) or anti-mouse IgG

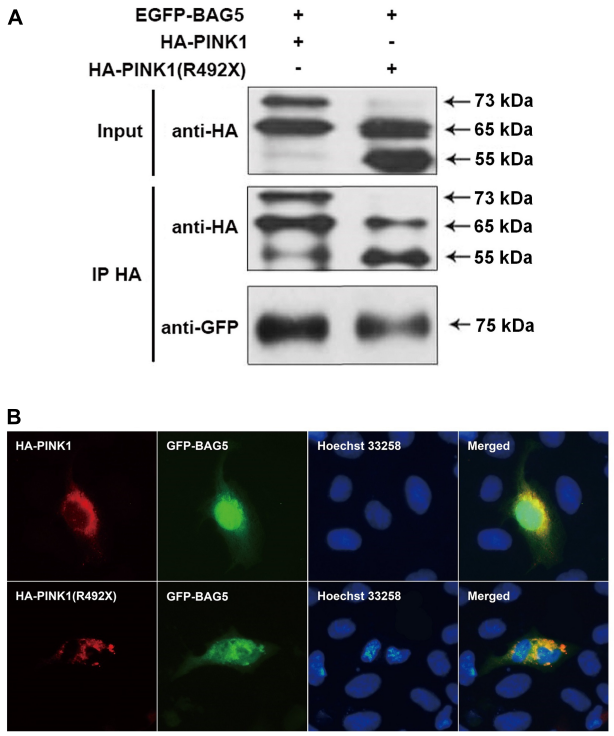

FIGURE 2 | BAG5 interacts with R492X mutated PINK1 protein. **(A)** BAG5 interacts with PINK1 and R492X mutated PINK1 protein. We performed co-IP assays using HEK293 cells expressing GFP-BAG5 and HA-PINK1 or HA-PINK1^{R492X}. Cell lysates were subjected to co-IP with rabbit polyclonal anti-HA tag antibody. The IP and input lysates were analyzed by immunoblotting with mouse monoclonal anti-HA tag antibodies. The results showed that BAG5 interacts with both wild type PINK1 and R492X mutated PINK1 protein. **(B)** Co-localization of GFP-BAG5 and HA-PINK1^{R492X}. HEK293 cells were transfected with EGFP-BAG5 and HA-PINK1 or HA-PINK1^{R492X}. Images show regional co-localization of BAG5 with R492X mutated PINK1 protein.

(Cell Signaling Technology, United States) for 1 h. Membranes were washed for three times and proteins were visualized using an ECL detection kit (Pierce Chemical, United States). The primary antibodies used were mouse monoclonal anti-HA tag antibody (Abcam, United Kingdom), rabbit polyclonal anti-HA tag antibody (Cell Signaling Technology, United States), rabbit polyclonal anti-GAPDH antibody (Cell Signaling Technology, United States), mouse monoclonal anti-BAG5 antibody (Abcam, United Kingdom), rabbit polyclonal anti-green fluorescent protein (GFP) antibody (Abcam, United Kingdom), and rabbit polyclonal anti-ubiquitin antibody (Cell Signaling Technology, United States).

Immunohistochemistry and Immunohistofluorescence

HEK293 cells were washed with 1 × PBS and fixed with 4% paraformaldehyde for 5 min. Then cells were incubated with 0.25% Triton X-100 for 15 min and blocked in 4% FBS for 20 min, subsequently incubated with the primary antibodies overnight at 4°C. Frozen skin tissue sections were washed in 1 × PBS for five times and incubated with 0.3% Triton X-100 at room temperature for 30 min. After blocking the non-specific binding sites using 1 × PBS containing 2% BSA, the skin tissue sections were incubated with the primary antibodies overnight at 4°C. Following three washes with 1 × PBS containing 0.3% Triton-100, fluorescein isothiocyanate (FITC)-conjugated goat anti-mouse IgG was applied as secondary antibody (Vector Laboratories, United States) for 2 h at room temperature. Images were captured by using Nikon Labphoto-2 fluorescence microscope. The human subject studies were approved by the Institutional Ethics Committees of the Zhengzhou University. Written informed consent for skin biopsy was obtained from all patients and healthy individuals participating in the study.

Statistical Analysis

All statistical analyses were performed using Student's *t*-test or one-way ANOVA using SPSS statistical software package (SPSS version 8.0). Data were shown as mean ± SD or mean ± SEM. A *p* value less than 0.05 was considered statistically significant.

RESULTS

Expression of BAG5 in the Skin Tissues From Patients With R492X *PINK1* Mutation Is Lower in Comparison to Health Controls

The BAG family proteins exhibit multiple functions including apoptosis and protein degradation (Bracher and Verghese, 2015), and previous studies have shown that BAG5 inhibited both Parkin E3 ligase and Hsp70 chaperone activities thereby enhancing dopaminergic neuron degeneration (De Snoo et al., 2019; Chen et al., 2020). We then hypothesized that BAG5 is involved in the pathogenesis of R492X *PINK1* mutation in autosomal-recessive PD. To test this hypothesis, we performed skin biopsy from two patients with PD harboring R492X *PINK1* mutation and two healthy controls. We found that the decreased level of BAG5 was detected in patients with R492X *PINK1* mutation compared with healthy control subjects by immunofluorescence (**Figure 1A**) and Western blotting analysis (**Figures 1B,C**). These results suggest that BAG5 is implicated in the pathogenesis of R492X *PINK1* mutation in PD.

BAG5 Interacts With R492X Mutated PINK1 Protein

To determine the relationship between BAG5 and R492X mutated PINK1 protein, we first used co-immunoprecipitation (co-IP) experiments to examine if there is a direct interaction between BAG5 and R492X mutated PINK1 protein. We co-transfected with EGFP-BAG5 and HA-PINK1 or HA-PINK1^{R492X} vectors in HEK293 cells. After immunoprecipitation with a rabbit polyclonal anti-HA tag antibody, the immunoprecipitants were subjected to immunoblot analysis with a mouse monoclonal anti-GFP or anti-HA tag antibody. EGFP-BAG5 was co-precipitated with HA-PINK1^{R492X}, suggesting that BAG5 physically binds to R492 mutated PINK1 protein.

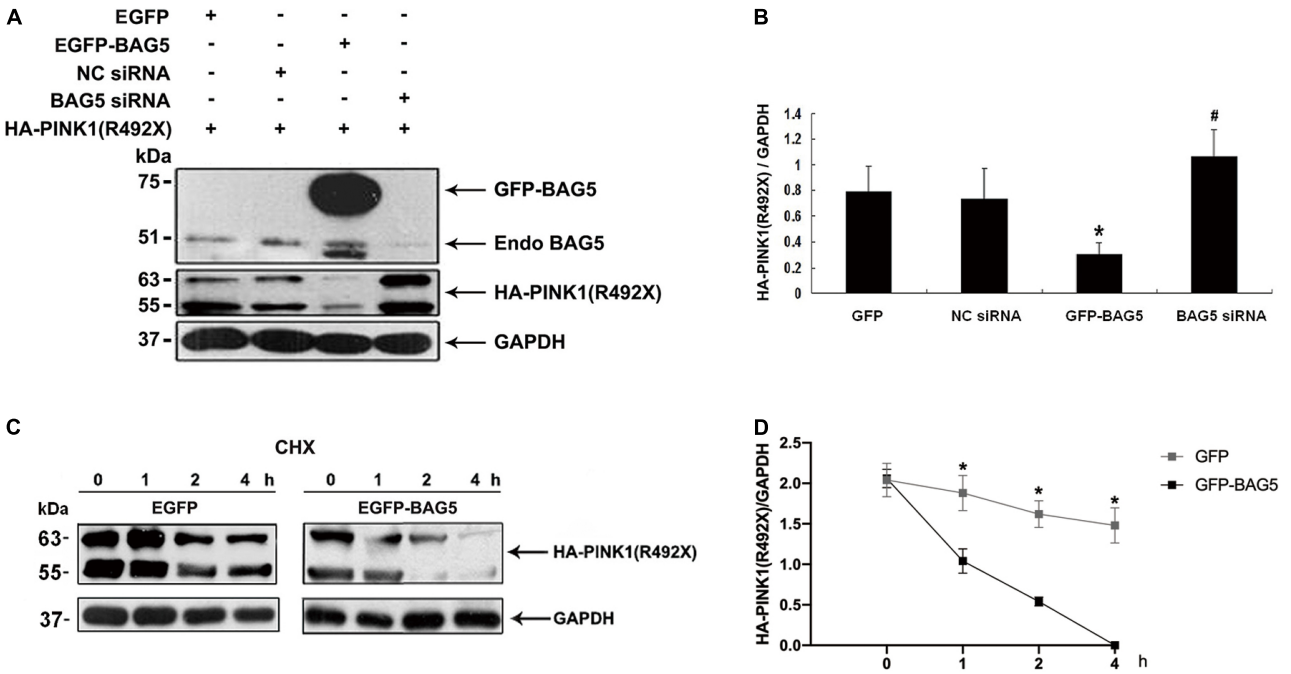

FIGURE 3 | BAG5 promotes R492X mutated PINK1 protein degradation. **(A)** HEK293 cells were transfected with EGFP, EGFP-BAG5, negative control siRNA (NC siRNA), BAG5 siRNA and HA-PINK1^{R492X} for 36 h. Cells extracts were analyzed by immunoblot using the specific antibodies. HA-PINK1^{R492X} was decreased in GFP-BAG5-expressing cells, whereas knockdown of BAG5 increased the level of HA-PINK1^{R492X}. **(B)** Quantitative data from A were shown. Values shown are the means ± SEM from the experiments. Level of statistical significance, $^{*}p < 0.05$, $^{\#}p < 0.01$. **(C)** HEK293 cells were transfected for 36 h with either EGFP or EGFP-BAG5 with HA-PINK^{R492X}, then cells were incubated for the indicated times in the presence of 100 mg/ml CHX. Cells were resuspended in lysis buffer, and the proteins were analyzed by immunoblot using anti-HA tag antibody. **(D)** The expression level of HA-PINK1^{R492X} was significantly lower in GFP-BAG5-overexpressing cells than in GFP-overexpressing cells. Values shown are the means ± SEM, level of statistical significance, $^{*}p < 0.05$. All experiments were performed more than thrice.

The results are shown in **Figure 2A**. Then, we detected subcellular co-localization of GFP-BAG5 with HA-*PINK1* and HA-*PINK1*^{R492X} in HEK293 cells co-transfected with HA-*PINK1* or HA-*PINK1*^{R492X} and EGFP-BAG5. As shown in **Figure 2B**, HA-*PINK1* was distributed most in the mitochondrial-rich perinuclear region (Matsuda et al., 2013; Liu et al., 2017), and GFP-BAG5 was evenly distributed throughout the whole cell. Furthermore, HA-*PINK1* and GFP-BAG5 were co-localized in perinuclear region. HA-*PINK1*^{R492X} was distributed unevenly around the nucleus, and largely co-localized with GFP-BAG5 (**Figure 2B**). These results confirmed that BAG5 interacts with R492X mutated *PINK1* protein.

BAG5 Promotes Degradation of R492X Mutated PINK1 Protein

Previous studies showed that BAG5 was involved in regulating degradation of specific proteins by ubiquitin/proteasome-dependent pathways (Wang et al., 2014). We next investigated the effect of BAG5 on degradation of R492X mutated PINK1 protein. HEK293 cells were co-transfected with HA-PINK1^{R492X} and EGFP-BAG5 or EGFP-N1 (control) for about 36 h. The expression level of HA-PINK1^{R492X} was markedly lower in cells co-transfected with EGFP-BAG5, but not in cells co-transfected with EGFP tag alone (**Figure 3A**). To further confirm the role of BAG5 in degradation of R492X mutated PINK1 protein, we knocked down the expression of endogenous BAG5 by siRNA. As shown in **Figures 3A,B**, the down regulation of BAG5 significantly increases the expression of HA-PINK1^{R492X} in HEK 293 cells. Subsequently, we examined the stability of HA-PINK1^{R492X} in cells stably expressing either GFP or GFP-BAG5 after CHX treatment to block total protein synthesis. The poor expression of HA-PINK1^{R492X} in GFP-BAG5-overexpressing cells provides evidence that overexpression of GFP-BAG5 accelerates cellular degradation of HA-PINK1^{R492X} (**Figures 3C,D**).

BAG5 Increases the Ubiquitination of R492X Mutated PINK1 Protein

Previous studies demonstrated that *PINK1* was mostly degraded by the ubiquitin-proteasome system (UPS) (Whiten et al., 2021). To explore whether overexpression of BAG5 increased the ubiquitination of R492X mutated *PINK1* protein, HEK293 cells were co-transfected with HA-PINK1^{R492X} and EGFP-BAG5 or EGFP-N1 for about 36 h, and then cells were treated with the proteasome inhibitor MG132 for 12 h. Cell lysates were collected and immuno-precipitated using affinity-purified rabbit anti-HA tag antibodies. As shown in **Figure 4**, overexpression of EGFP-BAG5 significantly increased the ubiquitination of HA-PINK1^{R492X} compared with EGFP control in the presence of MG132 (**Figure 4**). Thus, the results show that BAG5 accelerates

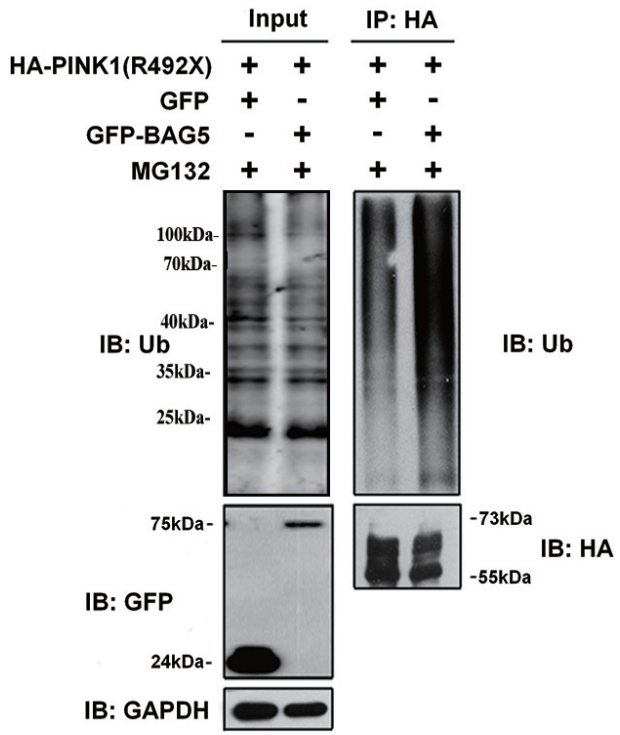

FIGURE 4 | BAG5 increases ubiquitination of R492X mutated PINK1 protein. HEK293 cells were co-transfected with HA-PINK1^{R492X} and EGFP-N1 or EGFP-BAG5. The cells were treated with 10 mM MG132 for 12 h and subjected to immunoprecipitation using rabbit polyclonal antibodies against HA tag. Inputs and immunoprecipitants were subjected to immunoblot analysis using anti-ubiquitin, anti-EGFP, anti-HA tag or anti-GAPDH antibody.

the degradation of R492X mutated PINK1 protein via increasing ubiquitination of R492X mutated PINK1 protein.

DISCUSSION

In this study, we show that the expression level of BAG5 in R492X *PINK1* mutated PD patients is much lower than that in healthy controls. We then demonstrated that BAG5 promoted the degradation of R492X mutated *PINK1*. Moreover, we reveal that BAG5 functions through physically interacting with R492X mutated PINK1 protein. The evidence from this study indicates that BAG5 functions as a modulator controlling the expression level of R492X mutated PINK1 protein. Decreased expression of BAG5 promotes R492X mutated PINK1 protein accumulation and mitochondrial dysfunction, which potentially enhances the cytotoxic effect of R492X mutated PINK1 protein in patients with R492X PINK1 mutation. Although, the interaction between endogenous BAG5 and R492X mutated PINK1 and how BAG5 expression is regulated in PD patients with such mutation need to be further investigated, these data highlight the therapeutic targets for PD patients with R492X *PINK1* mutation.

Bcl-2 associated athanogene family consists of 6 protein members, characterized by the same BAG domain, and is found to participate in cell proliferation and survival, increasing stress tolerance, and cancer development (Pattingre and Turtoi, 2022). BAG5 is exceptional in this group of protein since it consists solely of the five BAG domains (Bracher and Verghese, 2015). Ying et al. (2013) showed that BAG5 reduced the degradation of PTEN and maintained its levels via an ubiquitination-dependent pathway. Che et al. (2015) demonstrated that BAG5 stabilized pathogenic ataxin3-80Q by inhibiting its ubiquitination as determined by western blotting and co-immunofluorescence experiments. Qin et al. (2017) revealed that BAG5 could decrease DJ-1's stability and reduce its function on mitochondrial protection. These studies indicated that BAG5, as a key chaperone regulator of heat shock proteins, regulates ubiquitin-mediated degradation of many other proteins. The authenticity of our results is verified in line with the property above of BAG5. Wang et al. (2014) demonstrated that BAG5 inhibited PINK1 degradation through direct interaction with PINK1 through the UPS and BAG5 protected mitochondria against neurotoxin MPP^+- and rotenone-induced oxidative stress. Here, we show that BAG5 promotes R492X mutated PINK1 protein degradation in this study. Mutations in *PINK1* gene are the second most common cause of autosomal recessive early-onset PD (Wang et al., 2018; Li et al., 2021). In 2004, R492X *PINK1* mutation was first identified in autosomal recessive early-onset parkinsonism (Hatano et al., 2004). Previous study by Yuan et al. (2010) revealed that stable expression of the R492X mutated PINK1 protein, unlike the wild-type PINK1 protein, causes mitochondrial cytochrome C release and cellular apoptosis. The R492X mutation seems to be a dominant-negative or gain-of-function dominant mutation that can induce cellular mitochondrial dysfunction and oxidative stress, especially with the environmental neurotoxin (MPP^+). Therefore, the mechanism by which BAG5 exhibits an opposite effect on the degradation of the two proteins is not clear and remains to be further investigated. A simple explanation might be that BAG5 is involved in cellular mitochondrial and oxidative stress response/modulation and has multiple functions, one of which leads to a change in protein structure. Individual properties and physiological situation of the R492X mutated PINK1 protein might have been changed, which consequently resulted in different reactions to BAG5.

CONCLUSION

In summary, we show that the expression levels of BAG5 decline in the skin tissues from patients with R492X *PINK1* mutation compared with control cases. Further, our results help demonstrate that BAG5 promotes the degradation of R492X mutated PINK1 protein via the UPS pathway *in vitro*. Although further studies on expanded patient samples from a large cohort and on why BAG5 level is decreased in PD patients with R492X *PINK1* mutation are needed, the level of BAG5 in the biopsied skin may be used for an indication of the patients' condition or a diagnostic biomarker of familial juvenile parkinsonism. This study may also highlight potential therapeutic effect of targeted regulation of BAG5 for PD patients with R492X *PINK1* mutation.

DATA AVAILABILITY STATEMENT

The original contributions presented in the study are included in the article/**Supplementary Material**, further inquiries can be directed to the corresponding authors.

ETHICS STATEMENT

The studies involving human participants were reviewed and approved by the Institutional Ethics Committee of the Zhengzhou University, Henan, China. The patients/participants provided their written informed consent to participate in this study.

AUTHOR CONTRIBUTIONS

XW and EW conceived the research design, carried out the experiments, analyzed the data, and wrote the first draft of this manuscript. YF and DQ analyzed the data, wrote, reviewed, and revised this manuscript. YC, HT, and HL provided administrative, technical, and material support. All authors read and approved the final manuscript.

FUNDING

This work was supported by grants from the National Natural Science Foundation of China (Nos. 81671267, 81471307, 81301086, and 81430023).

ACKNOWLEDGMENTS

We thank other members of our laboratories for critical discussions. We also thank Xuebing Ding at The First Affiliated Hospital of Zhengzhou University for her valuable inputs.

SUPPLEMENTARY MATERIAL

The Supplementary Material for this article can be found online at: https://www.frontiersin.org/articles/10.3389/fnins.2022.903958/full#supplementary-material

Supplementary Figure 1 | Expression of C-terminal and N-terminal HA tagged PINK1^{R492X}. The HA tag was added to the C-terminal **(A)** or N-terminal **(B)** PINK1^{R492X}, the expression was confirmed by immunostaining.

REFERENCES

Agarwal, S., and Muqit, M. M. K. (2022). PTEN-induced kinase 1 (PINK1) and Parkin: unlocking a mitochondrial quality control pathway linked to Parkinson's disease. *Curr. Opin. Neurobiol.* 72, 111–119. doi: 10.1016/j.conb.2021.09.005

Berliner, J. A., Territo, M., Almada, L., Carter, A., Shafonsky, E., and Fogelman, A. M. (1986). Monocyte chemotactic factor produced by large vessel endothelial cells in vitro. *Arteriosclerosis* 6, 254–258. doi: 10.1161/01.atv.6.3.254

Bracher, A., and Verghese, J. (2015). GrpE, Hsp110/Grp170, HspBP1/Sil1 and BAG domain proteins: nucleotide exchange factors for Hsp70 molecular chaperones. *Subcell. Biochem.* 78, 1–33. doi: 10.3389/fmolb.2015.00010

Brunelli, F., Valente, E. M., and Arena, G. (2020). Mechanisms of neurodegeneration in Parkinson's disease: keep neurons in the PINK1. *Mech. Ageing Dev.* 189:111277. doi: 10.1016/j.mad.2020.111277

Che, X., Tang, B., Wang, H., Yan, X., Jiang, H., Shen, L., et al. (2015). The BAG2 and BAG5 proteins inhibit the ubiquitination of pathogenic ataxin3-80Q. *Int. J. Neurosci.* 125, 390–394. doi: 10.3109/00207454.2014.940585

Che, X., Tang, B., Wang, X., Chen, D., Yan, X., Jiang, H., et al. (2013). The BAG2 protein stabilises PINK1 by decreasing its ubiquitination. *Biochem. Biophys. Res. Commun.* 441, 488–492. doi: 10.1016/j.bbrc.2013.10.086

Chen, H. Y., Lin, C. H., and Teng, S. C. (2020). Stress-induced p53 drives BAG5 cochaperone expression to control alpha-synuclein aggregation in Parkinson's disease. *Aging* 12, 20702–20727. doi: 10.18632/aging.103998

De Snoo, M. L., Friesen, E. L., Zhang, Y. T., Earnshaw, R., Dorval, G., Kapadia, M., et al. (2019). Bcl-2-associated athanogene 5 (BAG5) regulates Parkin-dependent mitophagy and cell death. *Cell Death Dis.* 10:907.

Eldeeb, M. A., and Ragheb, M. A. (2020). N-degron-mediated degradation and regulation of mitochondrial PINK1 kinase. *Curr. Genet.* 2020, 693–701. doi: 10.1007/s00294-020-01062-2

Gan, Z. Y., Callegari, S., Cobbold, S. A., Cotton, T. R., Mlodzianoski, M. J., Schubert, A. F., et al. (2022). Activation mechanism of PINK1. *Nature* 602, 328–335. doi: 10.1038/s41586-021-04340-2

Hatano, Y., Li, Y., Sato, K., Asakawa, S., Yamamura, Y., Tomiyama, H., et al. (2004). Novel PINK1 mutations in early-onset parkinsonism. *Ann. Neurol.* 56, 424–427. doi: 10.1002/ana.20251

Kakade, P., Ojha, H., Raimi, O. G., Shaw, A., Waddell, A. D., Ault, J. R., et al. (2022). Mapping of a N-terminal alpha-helix domain required for human PINK1 stabilization, Serine228 autophosphorylation and activation in cells. *Open Biol.* 12:210264. doi: 10.1098/rsob.210264

Leites, E. P., and Morais, V. A. (2021). The PINK1-mediated crosstalk between neural cells and the underlying link to Parkinson's Disease. *Cells* 10:10061395. doi: 10.3390/cells10061395

Li, J. Y., Li, N. N., Wang, L., Peng, J. X., Duan, L. R., Chen, C. L., et al. (2021). A compound heterozygous PINK1-associated juvenile Parkinson's disease with pregnancy in Chinese. *J. Neurol.* 268, 2223–2227. doi: 10.1007/s00415-021-10405-z

Li, J., Lai, M., Zhang, X., Li, Z., Yang, D., Zhao, M., et al. (2022). PINK1-parkin-mediated neuronal mitophagy deficiency in prion disease. *Cell Death Dis.* 13:162. doi: 10.1038/s41419-022-04613-2

Liu, Y., Guardia-Laguarta, C., Yin, J., Erdjument-Bromage, H., Martin, B., James, M., et al. (2017). The ubiquitination of PINK1 is restricted to its mature 52-kDa form. *Cell Rep.* 20, 30–39. doi: 10.1016/j.celrep.2017.06.022

Matsuda, S., Kitagishi, Y., and Kobayashi, M. (2013). Function and characteristics of PINK1 in mitochondria. *Oxid. Med. Cell Longev.* 2013:601587. doi: 10.1155/2013/601587

Pattingre, S., and Turtoi, A. (2022). BAG family members as mitophagy regulators in mammals. *Cells* 11:11040681. doi: 10.3390/cells11040681

Peviani, M., Kurosaki, M., Terao, M., Lidonnici, D., Gensano, F., Battaglia, E., et al. (2012). Lentiviral vectors carrying enhancer elements of Hb9 promoter drive selective transgene expression in mouse spinal cord motor neurons. *J. Neurosci. Methods* 205, 139–147. doi: 10.1016/j.jneumeth.2011.12.024

Qin, L. X., Tan, J. Q., Zhang, H. N., Rizwana, K., Lu, J. H., Tang, J. G., et al. (2017). BAG5 interacts with DJ-1 and inhibits the neuroprotective effects of DJ-1 to combat mitochondrial oxidative Damage. *Oxid. Med. Cell Longev.* 2017:5094934. doi: 10.1155/2017/5094934

Qin, L., Guo, J., Zheng, Q., and Zhang, H. (2016). BAG2 structure, function and involvement in disease. *Cell Mol. Biol. Lett.* 21:18. doi: 10.1186/s11658-016-0020-2

Rochet, J., Hay, B., and Guo, M. (2012). Molecular insights into Parkinson's disease. *Prog. Mol. Biol. Transl. Sci.* 2012, 125–188. doi: 10.1016/B978-0-12-385883-2.00011-4

Sekine, S. (2020). PINK1 import regulation at a crossroad of mitochondrial fate: the molecular mechanisms of PINK1 import. *J. Biochem.* 167, 217–224. doi: 10.1093/jb/mvz069

Valente, E. M., Abou-Sleiman, P. M., Caputo, V., Muqit, M. M., Harvey, K., Gispert, S., et al. (2004). Hereditary early-onset Parkinson's disease caused by mutations in PINK1. *Science* 304, 1158–1160. doi: 10.1126/science.1096284

Vizziello, M., Borellini, L., Franco, G., and Ardolino, G. (2021). Disruption of mitochondrial homeostasis: the role of PINK1 in parkinson's disease. *Cells* 10:10113022. doi: 10.3390/cells10113022

Voigt, A., Berlemann, L. A., and Winklhofer, K. F. (2016). The mitochondrial kinase PINK1: functions beyond mitophagy. *J. Neurochem.* 139, 232–239. doi: 10.1111/jnc.13655

Wang, P., Guo, Y., Song, C., Liu, Y., and Deng, H. (2018). PINK1 p.K520RfsX3 mutation identified in a Chinese family with early-onset Parkinson's disease. *Neurosci. Lett.* 676, 98–102. doi: 10.1016/j.neulet.2018.04.020

Wang, X., Guo, J., Fei, E., Mu, Y., He, S., Che, X., et al. (2014). BAG5 protects against mitochondrial oxidative damage through regulating PINK1 degradation. *PLoS One* 9:e86276. doi: 10.1371/journal.pone.0086276

Whiten, D. R., Cox, D., and Sue, C. M. (2021). PINK1 signalling in neurodegenerative disease. *Essays Biochem.* 65, 913–923. doi: 10.1042/EBC20210036

Ying, Z., Haiyan, G., and Haidong, G. (2013). BAG5 regulates PTEN stability in MCF-7 cell line. *BMB Rep.* 46, 490–494. doi: 10.5483/bmbrep.2013.46.10.268

Yuan, X., Guo, J., Shi, Z., Xiao, Z., Yan, X., Zhao, B., et al. (2010). R492X mutation in PTEN-induced putative kinase 1 induced cellular mitochondrial dysfunction and oxidative stress. *Brain Res.* 1351, 229–237. doi: 10.1016/j.brainres.2010.06.005

Conflict of Interest: The authors declare that the research was conducted in the absence of any commercial or financial relationships that could be construed as a potential conflict of interest.

Publisher's Note: All claims expressed in this article are solely those of the authors and do not necessarily represent those of their affiliated organizations, or those of the publisher, the editors and the reviewers. Any product that may be evaluated in this article, or claim that may be made by its manufacturer, is not guaranteed or endorsed by the publisher.

frontiers | Frontiers in Neuroscience

TYPE Review
PUBLISHED 28 July 2022
DOI 10.3389/fnins.2022.936760

OPEN ACCESS

EDITED BY
Zhi Sun,
First Affiliated Hospital of Zhengzhou University, China

REVIEWED BY
Jacopo Meldolesi,
Vita-Salute San Raffaele University, Italy
Pratibha Singh,
Rice University, United States

*CORRESPONDENCE
Ling Qiu
lingqiubj@163.com
Songlin Yu
yusonglinpku@163.com

SPECIALTY SECTION
This article was submitted to Neuropharmacology, a section of the journal Frontiers in Neuroscience

RECEIVED 05 May 2022
ACCEPTED 08 July 2022
PUBLISHED 28 July 2022

CITATION
Zou Y, Mu D, Ma X, Wang D, Zhong J, Gao J, Yu S and Qiu L (2022) Review on the roles of specific cell-derived exosomes in Alzheimer's disease. *Front. Neurosci.* 16:936760. doi: 10.3389/fnins.2022.936760

Review on the roles of specific cell-derived exosomes in Alzheimer's disease

Yutong Zou[1], Danni Mu[1], Xiaoli Ma[1,2], Danchen Wang[1], Jian Zhong[1], Jing Gao[3], Songlin Yu[1]* and Ling Qiu[1,4]*

[1]Department of Laboratory Medicine, Peking Union Medical College Hospital, Peking Union Medical College & Chinese Academy of Medical Science, Beijing, China, [2]Medical Science Research Center (MRC), Peking Union Medical College Hospital, Peking Union Medical College and Chinese Academy of Medical Science, Beijing, China, [3]Department of Neurology, Peking Union Medical College Hospital, Peking Union Medical College & Chinese Academy of Medical Sciences, Beijing, China, [4]State Key Laboratory of Complex Severe and Rare Diseases, Peking Union Medical College Hospital, Peking Union Medical College & Chinese Academy of Medical Sciences, Beijing, China

Alzheimer's disease (AD) is the sixth leading cause of death worldwide and cannot be effectively cured or prevented; thus, early diagnosis, and intervention are important. The importance of exosomes, membrane-bound extracellular vesicles produced in the endosome of eukaryotic cells, in the development, diagnosis, and treatment of AD has been recognized; however, their specific functions remain controversial and even unclear. With the development of exosome extraction, isolation, and characterization, many studies have focused on exosomes derived from different cells and body fluids. In this study, we summarized the roles of exosomes derived from different body fluids and cells, such as neuron, glial, stem, and endothelial cells, in the development, diagnosis, monitoring, and treatment of AD. We also emphasize the necessity to focus on exosomes from biological fluids and specific cells that are less invasive to target. Moreover, aside from the concentrations of classic and novel biomarkers in exosomes, the size and number of exosomes may also influence early and differential diagnosis of AD.

KEYWORDS

Alzheimer's disease, mild cognitive impairment, exosome, biomarkers, neuron, glial cells

Introduction

Alzheimer's disease (AD) is one of the leading causes of death worldwide and the most common form of dementia, comprising 60–80% of all cases (Landeiro et al., 2018). The global number of patients with AD is expected to rise to 65.7 million in 2030 and 115.4 million in 2050, at a rate of one new case every 3 s (Prince et al., 2013). AD is characterized by the accumulation of amyloid plaques formed by extracellular aggregates of the amyloid-β (Aβ) peptide, neurofibrillary tangles formed of intracellular hyperphosphorylated microtubule-associated tau proteins, and axonal degeneration. It can affect memory, use of language, and behavior and may develop into a severe disability, causing a huge burden to both families and society (Ghidoni et al., 2018). Currently, more than 99% of clinical trials for AD therapy have failed

(Cummings et al., 2014), and only seven FDA-approved palliative drugs are available. Therefore, timely diagnosis and intervention are important in the early stages of AD.

According to the 2011 guidelines from the National Institute on Aging and the Alzheimer's Association (Jack et al., 2011), reliable biomarkers for AD only included the levels of Aβ1-42, total tau, and phosphorylated tau in the cerebrospinal fluid (CSF), which are expensive, invasive, and infeasible for screening. It has been estimated that, even in high-income countries, only 20–50% of dementia cases were correctly recognized and documented in primary care (Zheng et al., 2016). However, neuropathological alterations in patients with AD were reported to begin 10–20 years before the development of clinical symptoms (Villemagne et al., 2013). Thus, it is necessary and meaningful to find reliable and feasible biomarkers to help effectively diagnose AD, especially in the early stages.

In the last decade, many studies have found that extracellular vehicles (EVs) play key roles in the management of normal physiological environments, including waste management, stem cell maintenance, and tissue repair, as well as in pathological processes, including AD (Ratajczak et al., 2006; Gatti et al., 2011; van der Pol et al., 2012; Watson et al., 2019). Exosomes, 30–150 nm in diameter, are main EVs that originate in the endosome, and can carry multifarious molecular cargo, such as nucleic acids, lipids, and proteins (DeLeo and Ikezu, 2018; Yokoi et al., 2019). In the central nervous system, exosomes are critical for intercellular communication, maintenance of myelination, synaptic plasticity, and trophic support of neurons (Hornung et al., 2020). Currently, exosomes play important roles in the development, diagnosis, and treatment of AD; however, their specific functions remain controversial and even unclear. For example, some study found that exosomes could help spread tau proteins and encourage Aβ aggregation (Song et al., 2020a; Ruan et al., 2021); however, other studies reported that neuronal exosomes could restrain Aβ oligomerization, accelerate Aβ fibril formation, and facilitate microglia-mediated Aβ clearance, implying that exosomes from different cell types might exhibit different effects on the development of AD (Yuyama et al., 2012, 2014; Asai et al., 2015; Dinkins et al., 2017). Since exosomes secreted from different cell types contain particular and different types of markers, it is possible to identify their origins and isolate them from a specific cell subgroup, and corresponding extraction and purification methods have also been developed in recent years (Goetzl et al., 2019; Hornung et al., 2020). Thus, it is feasible and meaningful to recognize, extract, and analyze specific cell-derived exosomes based on the features of the targeted diseases. Noticeably, because exosomes are the main type of EVs, many authors interchangeably used the terms EVs and exosomes (Hornung et al., 2020). Thus, we also include some important studies taking about EVs in this review. Moreover, it is still challenging for effective and specific extraction, isolation, and characterization of exosomes, thus, the mentioned exosomes in many cases could also contain small amounts of other EVs.

Considering the above and based on previous published studies, in this review we mainly discuss and summarize the roles of exosomes derived from different body fluids and cells in the development, diagnosis, monitoring, and treatment of AD, as well as the remaining challenges in this field.

Exosomes from various body fluids provide possibilities for the early diagnosis and intervention of Alzheimer's disease

Cerebrospinal fluid-derived exosomes

A review reported that a large percentage of modulated proteins originate from exosomes, most of which are involved in the growth, development, maturation, and migration of neurons and neurotransmitter-mediated cellular communication (Bastos et al., 2017). Thus, CSF-derived exosomes have been widely studied, and their proteome has been recognized as a potential new reservoir for biomarker discovery in neurological disorders, including AD (Street et al., 2012). It has also been reported that more than 400 unique proteins mainly involved in AD, as well as the aging and telomere length pathway, were considerably enriched in CSF-derived EVs (Muraoka et al., 2019), and some proteins such as HSPA1A, NPEPPS, and PTGFRN could be used to monitor the progression of mild cognitive impairment (MCI) converted to AD (Muraoka et al., 2020). Moreover, the levels of total tau and p-181-tau in CSF-derived EVs were not only positively correlated with, but also higher than those in total CSF in individuals with AD (Guix et al., 2018; Muraoka et al., 2019). Thus, CSF-derived exosomes (or EVs) play important roles in the early and differential diagnosis of AD. However, the techniques used to derive exosomes from CSF still require refinement to reduce volume and variability.

Blood-derived exosomes

Since the collection of exosomes from the CSF is invasive, it is necessary and urgent to find less or non-invasive biomarkers from other body fluids. Exosomes consist of a lipid bilayer encapsulating the cytosol and have an efficient capability to cross the blood-brain barrier without the loss of their biomarkers, thereby reaching many biological fluids, such as blood, urine, saliva, and synovial fluid (Colombo et al., 2012). Thus, the exosomes in these body fluids could dynamically reflect the pathological changes occurring in some inaccessible sites, such as the brain, making them promising biomarkers for the first step of multistage diagnoses.

Of these different body fluids, plasma and serum are the most widely used for the extraction of exosomes. Interestingly, previous studies have shown that the levels of exosome-bound Aβ could correlate better with PET imaging of brain amyloid plaques and differentiate various clinical stages of dementia compared to unbound or total circulating Aβ (Lim et al., 2019). Further extensive analyses of abnormal protein levels in neural cell-derived exosomes could identify patients with AD up to a decade ahead of clinically detectable cognitive losses (Goetzl, 2020). These reports imply that the levels of biomarkers in brain-derived, blood-borne exosomes can better reflect alterations occurring in the brain (Guix et al., 2018; Lim et al., 2019). It was also reported that the levels of Aβ1-42, total tau, p-181-tau, and p-S396-tau in neuron-derived exosomes (NDEs) from plasma were highly correlated with those in CSF and could differentiate patients with AD from those with MCI and/or controls with an accuracy of up to 96.4% (Fiandaca et al., 2015; Jia et al., 2019). Moreover, it was reported that patients who eventually developed AD had considerably higher levels of 181-tau and/or p-S396-tau in their NDEs compared to their plasma, even 10 years prior to diagnosis, compared to those who did not develop AD (Fiandaca et al., 2015; Winston et al., 2016).

Apart from the classic biomarkers, many other promising biomarkers such as lysosomal proteins, GAP43, neurogranin, SNAP25, and synaptotagmin 1 in NDEs from plasma could predict the development of AD at least 5 years before cognitive impairment and differentiate AD from frontotemporal dementia with 95.8% accuracy (Goetzl et al., 2015a; Jia et al., 2021). Another study also found that neuro-protective transcription factors such as repressor element 1 silencing transcription factor, low-density lipoprotein receptor-related protein 6, and heat shock factor 1 in NDEs from plasma decreased 2–10 years before the onset of clinical AD symptoms, implying a possible early pathogenic contribution of increased neuronal susceptibility to neurotoxic proteins in AD rather than higher levels of pathogenic proteins (Goetzl et al., 2015b). Furthermore, miRNAs such as miR-9-5p, miR-598, miR-125b, miR-29, miR-342-3p, and miR-193b, which are highly stable and resistant to degradation in exosomes, could be promising biomarkers for early clinical diagnosis and monitoring of AD (Riancho et al., 2017; Chen et al., 2019; Dong et al., 2020). Recently, a meta-analysis found that exosome-derived markers in serum had a higher diagnostic value for AD and MCI than those in plasma, implying that isolating exosomes from serum is a more accurate and non-invasive detection method (Xing et al., 2021).

Exosomes derived from urine and other body fluids

A pilot study found that the levels of Aβ1-42 and p-S396-tau in urinary exosomes were higher in patients with AD than in controls, suggesting that it is a promising non-invasive biomarker (Sun et al., 2019). Comprehensive proteomic profiling analysis identified 336 differentially expressed proteins, including 44 brain cell biomarkers in urinary exosomes, of which 22 were further verified. Notably, annexin 2 and clusterin were markedly decreased in AD mouse models compared to control mice (Song et al., 2020b). Moreover, 48 differentially expressed miRNAs in urinary exosomes, including 18 upregulated and 30 downregulated ones, were identified and verified prior to the identification of Aβ plaque deposition, which was predicted to display gene targets and important signaling pathways closely associated with AD pathogenesis (Song et al., 2021). Furthermore, other non-invasive body fluids, such as saliva-derived exosomes (Han et al., 2018; Rani et al., 2021) are also promising for the early diagnosis of AD. However, associated studies are limited and need to be further explored, and the collections of saliva samples needs to be further standardized in clinical application.

Exosomes derived from different cells play different roles in the development, diagnosis, and treatment of Alzheimer's disease

Exosomes derived from neural cells play multifaceted roles in the nervous system, including in synaptic plasticity, the neuron-glia interface, neuroregeneration, neuroprotection, and the dissemination of neuropathological molecules (Upadhya et al., 2020). It has also been reported that exosomes derived from various types of neural cells, including neurons, glia, stem cells and so on, play different roles in the development of AD (Figure 1) (Song et al., 2020a); therefore, it is vital to distinguish and analyze specific cell-derived exosomes.

Neuron-derived exosomes

As the basic structural and functional unit of the nervous system, neurons mediate various neural activities such as the conduction of excitation. Proteins in exosomes are released from affected neurons and propagate along neuroanatomically connected regions of the brain, leading to the spread of neurodegenerative diseases. Full-length tau proteins, which are more prone to aggregation, were found to be higher inside NDEs than in their free form (Guix et al., 2018), implying that NDEs could promote the transmission of tau. Moreover, the levels of P-S396-tau and P-T181-tau in NDEs can predict the development of AD up to 10 years before the clinical onset of sporadic AD (Fiandaca et al., 2015). Furthermore, a recent study demonstrated that NDEs, but not total exosomes, in plasma samples of AD patients could induce complement-mediated

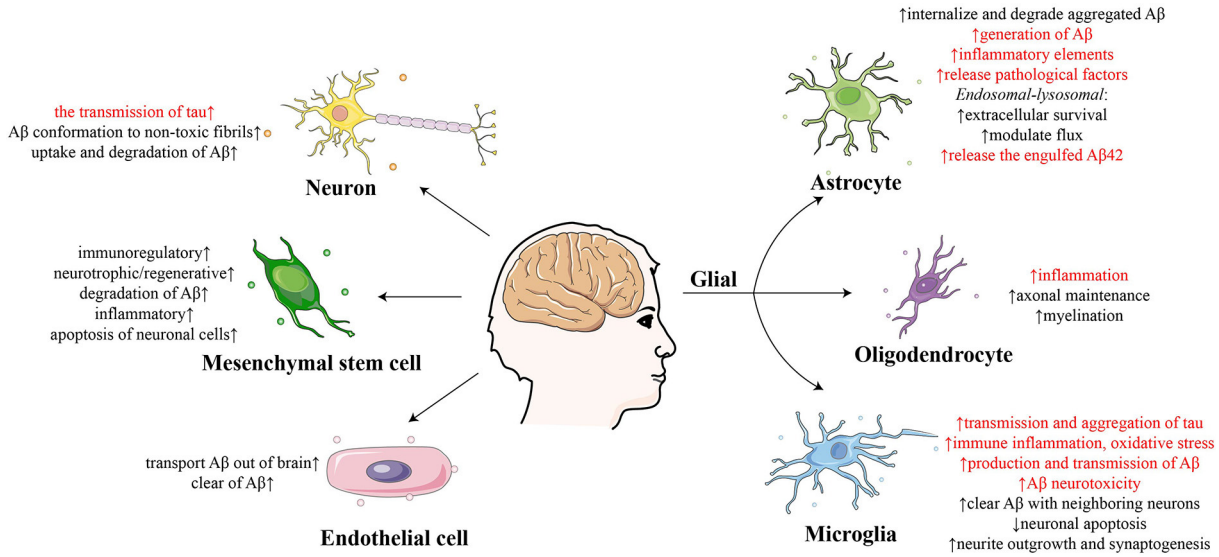

FIGURE 1
Summary of the effect of exosomes derived from different cells on the development of Alzheimer's disease.

neurotoxicity, leading to the decrease of cell viability (Nogueras-Ortiz et al., 2020).

However, beneficial effects of NDEs on extracellular Aβ have also been found. NDEs may drive conformational changes in Aβ to form non-toxic amyloid fibrils and promote uptake and degradation by microglia (Yuyama et al., 2012). With enriched expression of glycosphingolipids, ceramide, and the GPI-anchored protein PrPc, NDEs showed stronger affinity for Aβ than other origin-derived exosomes, such as those from glial cells (Joshi et al., 2015; Yuyama et al., 2015). Moreover, it was reported that intracerebral infusion of NDEs into mouse brains could decrease the levels of Aβ and attenuate Aβ-induced synaptic density toxicity in the hippocampus (Yuyama et al., 2014, 2015), which implies that supplementation or promotion of NDE generation could be a novel therapeutic approach for AD (Yuyama et al., 2019).

Moreover, NDEs can also be used to diagnose AD. A meta-analysis showed that the area under the curve (AUC, 95% confidence interval) of miRNA and other biomarkers in NDEs for the diagnosis of AD or MCI was up to 0.89 (0.86–0.92), and a sub-group analysis found that NDEs from plasma had a higher AUC value (Xing et al., 2021). Higher levels of alpha-globin, beta-globin, and delta-globin in NDEs were found in patients with AD compared to those in controls (Arioz et al., 2021). The levels of presynaptic proteins, including synaptotagmin and synaptophysin, as well as postsynaptic proteins, including synaptopodin and neurogranin, in plasma NDEs were reported to be markedly lower in patients with AD, which was also correlated with the extent of cognitive loss (Goetzl et al., 2016a, 2018a). Many other biomarkers in NDEs were also found to be markedly different between patients with AD and controls, such as the level of Ser/Tyr phosphorylation of the insulin receptor substrate 1 (indicating insulin resistance), lysosomal enzymes and ubiquitin (indicating lysosomal dysfunction), and cellular survival factors (indicating impaired cellular stress responses) (Goetzl et al., 2015a,b; Kapogiannis et al., 2015). Furthermore, with the specific expression of neuronal, L1, or neural cell adhesion molecules, NDEs could be effectively isolated from total plasma/serum exosomes using a precipitation or immunoaffinity method with according antibodies (Fiandaca et al., 2015). With this isolation method, NDEs were found to comprise up to 15% of total plasma exosomes (Kapogiannis et al., 2015).

Glial cell-derived exosomes

Brain function depends on coordinated interactions between neurons and glial cells, including astrocytes, microglia, and oligodendrocytes. However, the specific functions of glial cells and their derived exosomes remain controversial. For example, it has been reported that exosomes in glia could be transferred into neurons via cargo molecule-dependent and membrane contact-dependent mechanisms, which could benefit neurons or reversely disseminate the disease (Brites and Fernandes, 2015).

Astrocyte-derived exosomes

As the most abundant type of glial cells in the brain, astrocytes accumulate at sites of Aβ peptide deposition, internalizing and degrading aggregated peptides, which is considered a protective process (Wyss-Coray et al., 2003).

Cellular experiments have shown that Aβ1-42 can inhibit exosome release from astrocytes by activating the c-Jun N-terminal kinase signaling pathway, thereby increasing the levels of astrocyte-derived exosomes (ADEs) via ultrasound stimulation can reverse oligomeric Aβ-induced cytotoxicity and help the clearance of Aβ plaques *in vitro* (Abdullah et al., 2016; Deng et al., 2021). Moreover, neuroprotective proteins such as synapsin 1, angiogenesis-associated molecules such as vascular endothelial growth factor, and matrix metalloproteinases involved in extracellular matrix proteolysis have been found in ADEs or astrocyte-derived EVs (Proia et al., 2008; Sbai et al., 2010; Wang et al., 2011). ADEs could also prolong the extracellular survival of protective endosomal-lysosomal cargo, such as the cysteine-protease inhibitor cystatin C, with their limiting membrane (Mathews and Levy, 2019). Efficient exosome release would help modulate flux via the neuronal–endosomal pathway by decompressing potential "traffic jams" and contributing to the degradation of neuronal debris (Mathews and Levy, 2019).

However, when a large amount of Aβ accumulates within astrocytes for a prolonged period without degradation, severe endosomal–lysosomal defects would occur in the astrocytes. Astrocytes can then release engulfed Aβ1-42 protofibrils through exosomes, leading to severe neurotoxicity to neighboring neurons (Söllvander et al., 2016). Animal experiments have also revealed that Aβ and tau released into the serum are most likely from ADEs in the brain (Rosas-Hernandez et al., 2019). Moreover, reducing the secretion of ADEs by neutral sphingomyelinase 2 loss-of-function could improve pathology and cognition in the 5XFAD mouse model (Dinkins et al., 2016). Recently, it was reported that some subsets of astrocytes contain amyloid precursor proteins (APP), β-secretase, and γ-secretase, which are required for the generation of Aβ peptides. These components are increased by fibrillary Aβ1-42 and several inflammatory cytokines (Zhao et al., 2011; Goetzl et al., 2016b). Furthermore, certain inflammatory and neurodegenerative reactions would elicit a coordinated response, leading to astrocyte hyperplasia and their conversion into reactive phenotypes, which could increase the expression of pro-inflammatory elements and damage both synapses and neurons (Liddelow and Barres, 2017; Goetzl et al., 2018b). Astrocytes can also release pathological factors such as S100β, a protein enriched in the brain of patients with AD that contributes to peri-plaque pathology (Mrak et al., 1996). Recently, a deep RNA sequencing study reported that ADEs influence neurodegenerative diseases mainly through metabolic and ubiquitin-dependent protein balance (Xie et al., 2022). Therefore, it is hard to deem the effect of astrocytes and ADEs on the development of AD as either "protective" or "disruptive."

Currently, studies on the ability of classic biomarkers in ADEs to help in the diagnosis of AD are still lacking. The levels of complement proteins such as C1q, C3b, C3d, and cytokines including IL-6, TNF-α, and IL-1β in ADEs were found to be considerably different between patients with AD and controls, which could also distinguish between moderate and preclinical stage AD (Goetzl et al., 2018b; Goetzl, 2020). As components of neurotoxic neuroinflammation, complement proteins in plasma ADEs could be predictive biomarkers of patients with MCI progressing into AD, with considerably higher levels of C1q, C4b, factor D, fragment Bb, C5b, C3b, and C5b-C9 in converters within 3 years (Winston et al., 2019). The expression of the anti-human glutamine aspartate transporter has been widely used for the isolation of ADEs (Goetzl et al., 2018b). Moreover, plasma ADEs prominently express higher levels of glial fibrillary acidic protein and glutamine synthetase than NDEs, which could be used to distinguish between ADEs and NDEs (Goetzl et al., 2016b). Since, the cargos in exosomes derived from human neuron and astrocyte cells were mainly recognized as useful biomarkers for the diagnosis of AD, thus related results from previous studies were summarized in Table 1.

Microglia-derived exosomes

As the primary innate immune cells in the brain, microglia can detect tissue damage and microbial infection, and phagocytose not only dying cells and, protein aggregates, but living neurons, and synapses (Neumann et al., 2009; Schafer et al., 2012). It was also found that exosomes added to mixed brain cultures containing all major cell types were preferentially taken up by microglia (Fitzner et al., 2011). Moreover, microglial-derived EVs could influence neurite outgrowth and modulate neuronal activity (Delpech et al., 2019; Paolicelli et al., 2019). However, it is relatively difficult to define the function of microglia as "protective" or 'disruptive", because they can dynamically switch between different phenotypes depending on the stage of the disease (Guo et al., 2021).

Microglia can phagocytize tau-containing cytopathic neurons or synapses and efficiently transmit tau to neurons via phagocytosis and exosomes. Thus, microglia and microglia-derived exosomes (MDEs) are positively correlated with tau pathology, and their depletion dramatically suppresses the propagation of tau and reduces excitability in the dentate gyrus (Schafer et al., 2012; Asai et al., 2015; Ruan et al., 2020). When tau-containing MDEs are taken up by neurons, abnormal aggregation of tau is further triggered (Asai et al., 2015). Moreover, reactive microglia may release exosomes carrying the inflammatory markers, including iNOS, IL-1β, TNF-α, MHC class II, IL-6, miR-155, miR-146a and miR-124, and pro-resolving genes, including IL-10 and arginase 1, leading to a more damaging pro-inflammatory state throughout the brain (Frühbeis et al., 2013; Fernandes et al., 2018). Deep RNA sequencing also demonstrated that MDEs influence neurodegenerative diseases through immune inflammation and oxidative stress (Xie et al., 2022). Suppressing the expression of miR-21-5p is considered a promising novel strategy for the treatment of neuroinflammation (Yin et al., 2020). Furthermore,

TABLE 1 Exosomes derived from human neuron and astrocyte cells as AD biomarkers in previous studies.

	References	Disease group	Control group	Body fluid	Cell source	Isolation method	Validation techniques	Cargo change
1	Fiandaca et al. (2015)	AD, $n = 57$	Cognitively normal controls, $n = 57$	Serum	Neuron	anti-NCAM	ELISA	↑total tau, P-S396-tau, P-T181-tau, Aβ1-42
2	Goetzl et al. (2016a)	AD, $n = 24$	Cognitively normal (1–10 years before the diagnosis of AD), $n = 24$	EDTA plasma	Neuron	anti-L1CAM	ELISA	↑P-S396-tau, P-T181-tau, Aβ1-42
3	Winston et al. (2016)	AD, $n = 10$	Cognitively normal controls, $n = 10$	Plasma	Neuron	anti-L1CAM	ELISA	↑P-S396-tau, P-T181-tau, Aβ1-42 ↓neurogranin, repressor element 1-silencing transcription factor
		Progressed to AD within 36 months, $n = 20$	Stable MCI, $n = 20$					
4	Jia et al. (2019)	AD, $n = 28$	Amnestic MCI, $n = 15$; healthy controls, $n = 29$	Plasma	Neuron	anti-NCAM	ELISA	↑Aβ42, T-tau, P-T181-tau
5	Arioz et al. (2021)	AD, $n = 20$	Healthy controls, $n = 20$	Serum	Neuron	anti-L1CAM	LC-MS/MS	↑alpha-globin, beta-globin, delta-globin
6	Goetzl et al. (2017)	AD, $n = 28$	Cognitively normal controls, $n = 28$	EDTA plasma	Neuron	anti-L1CAM	ELISA	↓neuronal pentraxin 2, neurexin 2a, GluA4-containing glutamate receptor, neuroligin 1
		AD, $n = 18$	Cognitively normal (6–11 years before the diagnosis of AD), $n = 18$					neurexin 2a, GluA4-containing glutamate receptor, neuroligin 1
7	Goetzl et al. (2016b)	AD, $n = 12$	Cognitively normal controls, $n = 28$	EDTA plasma	Neuron	anti-L1CAM	ELISA	↓synaptophysin, synaptopodin, synaptotagmin, neurogranin, growth-associated protein 43
		AD, $n = 9$	Cognitively intact or with MCI (1–10 years before the diagnosis of AD), $n = 9$					
8	Kapogiannis et al. (2015)	AD, $n = 26$	AD normal controls, $n = 26$	Plasma	Neuron	anti-L1CAM	ELISA	↑P-serine 312-IRS-1 ↓P-pan-tyrosine-IRS-1
		AD, $n = 22$	Cognitively normal (1–10 years before the diagnosis of AD), $n = 22$					

(Continued)

10.3389/fnins.2022.936760

TABLE 1 Continued

	References	Disease group	Control group	Body fluid	Cell source	Isolation method	Validation techniques	Cargo change
9	Goetzl et al. (2015a)	AD, $n = 26$	AD normal controls, $n = 26$	Plasma	Neuron	anti-L1CAM	ELISA	↑cathepsin D, lysosome-associated membrane protein 1, ubiquitinylated proteins ↓heat-shock protein 70
		AD, $n = 20$	Cognitively normal (1–10 years before the diagnosis of AD), $n = 20$					
10	Goetzl et al. (2015b)	AD, $n = 24$	AD normal controls, $n = 24$	Heparin plasma	Neuron	anti-L1CAM	ELISA	↓low-density lipoprotein receptor-related protein 6, heat-shock factor-1, repressor element 1-silencing transcription factor
		Preclinical AD (1–10 years before diagnosis of AD), $n = 16$	Cognitively normal controls, $n = 16$					
11	Goetzl et al. (2016a)	Amnestic MCI or early AD, $n = 12$	Cognitively normal controls, $n = 10$	EDTA plasma	Astrocyte	anti-ACSA-1	ELISA	↑β-secretase 1, sAPPb, Aβ42 ↓septin-8, GDNF
12	Goetzl et al. (2018a)	Early AD, $n = 28$	Cognitively normal controls, $n = 28$	EDTA plasma	Astrocyte	anti-ACSA-1	ELISA	↑IL-6, TNF-α, IL-1β, C1q, C4b, factor B, factor D, Bb, C3b, C3d, C5b-C9 terminal complement complex ↓CR1, CD46, CD59, DAF
		AD, $n = 16$	Cognitively normal (5–12 years before the diagnosis of AD), $n = 16$					↑C4b, C3d, factor B, Bb, C3b, C5b-C9 terminal complement complex, TNF-α, IL-1β ↓CD59, DAF
13	Winston et al. (2019)	AD, $n = 20$	Cognitively normal controls, $n = 20$	EDTA plasma	Astrocyte	anti-ACSA-1	ELISA	↑C1q, C4b, factor D, Bb, C5b, C3b, C5b-C9
		Progressed to AD within 3 years, $n = 20$	Stable MCI during the 36-month study, $n = 20$					

AD, Alzheimer's disease; MCI, mild cognitive impairment; L1CAM, L1 cell adhesion molecule; NCAM, neural cell adhesion molecule; ACSA-1, human glutamine aspartate transporter.

10.3389/fnins.2022.936760

it was demonstrated that MDEs and microglia-derived EVs not only had higher APP and Aβ1-40 production, carried oligomeric Aβ, and mediated Aβ transmission, but also promoted the extracellular aggregation of Aβ1-42 to form small soluble neurotoxic species, which strongly increased Aβ neurotoxicity (Joshi et al., 2014; Fernandes et al., 2018; Gouwens et al., 2018). However, it has been reported that microglia and neighboring neurons could work together to clear Aβ peptides via exosomes (Guo et al., 2021). Microglia-depleted mice had increased levels of soluble Aβ in the brain, and statins could promote the degradation of extracellular Aβ by stimulating the secretion of MDE-associated insulin-degrading enzymes, indicating a beneficial role of microglia in the metabolism of extracellular Aβ (Fuhrmann et al., 2010; Tamboli et al., 2010). Furthermore, cargo molecules in microglia derived EVs, including trombospondin-1 and 4, can suppress neuronal apoptosis and promote neurite outgrowth and synaptogenesis, implying a neuroprotective role (Drago et al., 2017). Thus, further investigation of the roles of microglia and MDEs in central nervous system disorders is required.

Recently, advances in single-cell RNA sequencing have helped unravel some questions in the field of microglia through the discovery of a new phenotype called "disease-associated microglia." These accumulate around plaques and exhibit upregulated gene expression of apolipoprotein E (APOE) and trigger the receptors expressed on myeloid cells 2 (TREM2), which are considered genetic risk factors for AD (Keren-Shaul et al., 2017). However, another study found that TREM2 knockout ameliorated amyloid pathology in the early stages of AD, but exacerbated it later in the disease process (Jay et al., 2017), which highlights the roles of microglia and MDEs in AD pathology depending on the stage of the disease. Furthermore, a reproducible and efficient method for yielding purified primary microglia cells and effectively isolating and characterization of MDEs based on CD11b/c has been proposed in recent years (Murgoci et al., 2018), which is beneficial for further studies on MEDs.

Oligodendrocyte-derived exosomes

Although few studies have focused on the potential roles of oligodendrocytes in AD pathogenesis, some gene variants that increase the risk of AD have been found to be predominantly expressed in oligodendrocytes. Interact with axon, oligodendrocyte played an important role in neuronal integrity. Oligodendrocyte-derived exosomes (ODEs) may be internalized by neurons through endocytosis, which could contribute to neuroprotection and long-term axonal maintenance under normal, or oxygen and glucose-deprived conditions (Frühbeis et al., 2012; Fröhlich et al., 2014). Moreover, it was reported that markedly increased numbers of both newly generated and mature oligodendrocytes following treatment with mesenchymal stromal cell-derived exosomes considerably decreased amyloid-β precursor protein density and improved neurological outcomes (Zhang et al., 2021). ODEs can also participate in the management of oxidative stress by transferring human superoxide dismutase and catalase. When stress resistance occurs following ischemia, neurons take up more ODEs (Krämer-Albers et al., 2007). Notably, alterations in the composition of ODEs under some pathological conditions may switch immunologically inert exosomes into active ones, which may trigger inflammatory reactions in the brain. Furthermore, an immunocapture protocol based on common oligodendrocyte biomarkers, such as 2,3-cyclic nucleotide-3-phosphodiesterase, can extract and isolate ODEs for further study (Yu et al., 2020).

Stem cell-derived exosomes

Stem cell-derived exosomes play important roles in the therapy for AD (Vasic et al., 2019; Sivandzade and Cucullo, 2021). Compared with traditional stem cell transplantation, stem cell-derived exosomes are relatively easier to manage, have lower immunogenicity, and have a lower risk of tumor formation, making them a potential therapeutic method (Guo et al., 2020). When the unique functionalities of exosome-derived membranes are combined with synthetic gold nanoparticles (AuNPs), efficient brain targeting can be achieved (Khongkow et al., 2019). In 5xFAD accelerated transgenic mouse model of AD, human neural stem cell-derived EVs showed the regenerative potential on the neurocognitive and neuropathologic hallmarks, and significantly reduced dense core Aβ plaque accumulation and microglial activation in the AD brain (Apodaca et al., 2021).

Mesenchymal stem cells (MSCs), a type of adult pluripotent stem cell, are derived from connective tissue especially adipose tissue. MSCs can reduce the Aβ plaque burden by the internalization and degradation of Aβ oligomers via the endosomal-lysosomal pathway. Electron microscopy and proteomic analysis further revealed that the therapeutic effect of MSCs was due to their exosomes (Lai et al., 2010). With well-characterized immunoregulatory neurotrophic and regenerative properties, MSC-derived exosomes were considered as a promising candidate for AD therapy and most widely studied. In mouse models, MSC-derived exosome administration via the lateral ventricle or intravenous injection could reduce Aβ expression and improve AD-like behaviors (Chen et al., 2021; Liu et al., 2022). Enzymatically active neprilysin, the most important Aβ-degrading enzyme in the brain, is also found in MSC-derived exosomes (Joshi et al., 2015). Moreover, MSC-derived EVs were considered as the best cell-free candidates for promoting a reparative process by activating positive responses in the brain microenvironment via intercellular communication (Elia et al., 2019). MiRNA-22-loaded exosomes derived from adipose-derived MSCs can decrease the release of inflammatory

factors, thereby playing a synergetic therapeutic role in AD (Zhai et al., 2021). Moreover, miR-223 loaded MSC-derived exosomes protected neuronal cells from apoptosis via the PTEN-PI3K/AKT pathway, providing a potential therapeutic approach for AD (Wei et al., 2020). Furthermore, a previous study proved the safety of MSC-derived EVs (Nassar et al., 2016), and a clinical trial was conducted to evaluate their safety and effectiveness in patients with mild to moderate dementia (www.clinicaltrials.gov, NCT04388982). It is worth noting that the efficacy was dosage-dependent, and the lower dose of exosomes was found to be more neuroprotective (Venugopal et al., 2017). Moreover, specific MSC-related molecules, such as CD29, CD44, CD90, and CD73, could help recognize and isolate MSC-derived exosomes.

Noticeably, even if EVs derived from native stem cells have potential in the treatment of neurodegenerative diseases including AD, its clinical application is still limited due to the short half-life, limited targeting, rapid clearance after application, and insufficient payload (Bang and Kim, 2022). Some strategies such as engineered EVs by genetic modification could improve stability, targeting ability and EVs tracking (Lino et al., 2021), thus, associated technologies need to be further explored and developed to prompt the clinical therapeutic application of stem cell-derived exosomes.

Endothelial cell-derived exosomes

Exosomes derived from endothelial cells (EDEs) of the human brain microvasculature contain P-glycoprotein, a member of the ABC transporter family, which can effectively transport Aβ out of the brain. Thus, it has been reported that EDEs can greatly facilitate the cerebral clearance of Aβ and potently ameliorate cognitive dysfunction in AD mice (Pan et al., 2020). CD81-normalized levels of Aβ1-40 and Aβ1-42 in plasma EDEs were also found to be considerably higher in the preclinical AD/MCI group with small cerebral vascular disease than in controls, which often occurs before the presentation of neuronal and other cellular changes in AD (Abner et al., 2020). Moreover, endothelial proteins such as vascular cell adhesion molecule-1 and endothelial nitric oxide synthase can be used for the precipitation and enrichment of EDEs when using immune-specific absorption procedures for the analysis of cargo proteins (Goetzl et al., 2017).

The size and number of exosomes could be promising biomarkers for the diagnosis of AD

A recent study found that not only the constitution Aβ and p-S396-tau in exosomes markedly differed between patients with AD compared to the controls, but the exosomes from patients with AD were smaller and lower in quantity, as determined by transmission electron microscopy (TEM) and nanoparticle tracking analysis (NTA), contributing to the early diagnosis of AD (Sun et al., 2020). Since TEM and NTA technology are widely used to visualize and characterize extracted exosomes, it is feasible to combine information on the size and number of exosomes with biomarker levels for the early and differential diagnosis of AD (Szatanek et al., 2017).

The size of exosomes

One study reported that the size of plasma exosomes was smaller in an AD group than in the control group, which is beneficial for early diagnosis of AD (Sun et al., 2020). However, some studies found larger size of plasma EVs in patients with AD than in controls, which could be induced by the uptake and accumulation of Aβ (Longobardi et al., 2021). Moreover, in another study, no significant difference was observed in the diameters of EVs in the CSF between patients with AD and the controls (Saugstad et al., 2017). These inconsistent results are likely to be due to the differences in exosome types and sources. Thus, further studies need to be conducted to explore the roles of specific exosomes in the diagnosis of AD.

The number of exosomes

Some studies have reported markedly lower concentrations of plasma exosomes in patients with AD compared to those in controls (Sun et al., 2020; Longobardi et al., 2021). Considering both the size and concentration of exosomes, the diagnostic performance to distinguish between dementia and controls was high, with a sensitivity of 83.3% and specificity of 86.7% (Longobardi et al., 2021). Moreover, APOE4 was found to drive the downregulation of brain exosome biosynthesis and release, which plays an important role in endosomal and lysosomal deficits and could lead to a higher risk of AD development (Peng et al., 2019). However, other studies found that astrocytes in AD could induce an increased release of exosomes containing toxic proteins, and exposure to amyloid *in vitro* could increase the production of cell-derived exosomes (Dinkins et al., 2014; Chiarini et al., 2017). Another study found that the number of serum exosomes in transgenic mice with AD was considerably higher than that in wild-type mice, with increased ADEs and decreased EDEs (Rosas-Hernandez et al., 2019). Moreover, NDEs from participants with Down syndrome, who had characteristic neuropathological features of AD at the age of 40 years and eventually developed AD, had 39% higher levels of exosomes on average than those from the control group [(1,433 ± 87 pg/ml) vs. (1,027 ± 87 pg/ml)] (Hamlett et al., 2018). It was also reported that upregulation of exosome release was recognized as a useful mechanism to help clear these

deleterious proteins, which could also be recognized in urine samples (Sun et al., 2019). Furthermore, a basic study found that preventing exosome secretion could reduce the formation of amyloid plaques *in vivo*; thus, drugs interfering with exosome secretion, such as neutral nSMase2, could be used as potential drug targets in AD (Dinkins et al., 2014, 2015).

These inconsistent results could also be related to the differences in exosome types and sources, as well as different efficacies of extraction across different samples. Thus, more studies are needed to reach a definite conclusion in which the standardized process of exosome extraction, isolation, and characterization plays an important role. Moreover, the released exosomes were mostly recognized by the CD81 marker, which could be interfered with possible increased soluble CD81 levels per exosome. Thus, an accurate count of exosome numbers is important. NTA using ALIX as an exosome marker or other burgeoning high-sensitivity exosome-counting systems, such as Exo-counter and single molecule array, has been proven to be more accurate for the determination of exosome amounts (Fiandaca et al., 2015; Kapogiannis et al., 2015; Eitan et al., 2017; Yokose et al., 2020; Ter-Ovanesyan et al., 2021).

Conclusion

The role of specific cell-derived exosomes in the development, diagnosis, monitoring, and treatment of AD has attracted increasing attention in recent years. However, the conclusions of different studies are largely inconsistent and many mechanisms remain unclear. Thus, we summarize the roles of exosomes derived from different body fluids and cells in the development, diagnosis, monitoring, and treatment of AD in this study, and emphasize the necessity to focus on exosomes from specific cells and less-invasive biological fluids. Moreover, aside from the concentrations of classic and novel biomarkers in exosomes, we recognized and summarized the roles of the size and number of exosomes play in early and differential diagnosis of AD at first.

Interestingly, a recent study pointed out that a few proteins that had not yet been reported to be expressed in neurons were highly expressed in NDEs, implying that some NDEs may originate in non-neuronal tissues (Pulliam et al., 2019). Thus, the process and mechanism of specific cell-derived exosomes, from their origin, formation, and transportation to their ultimate roles in AD, still need to be further studied. Second, the standardization and automation of the whole process of extraction, isolation, and characterization, including the size and number of specific cell-derived exosomes, remain a challenge (Doyle and Wang, 2019; Guo et al., 2020; Hornung et al., 2020) and need to be developed and optimized. Moreover, methods which is time-saving, low-cost, and convenient, must be explored for clinical applications. Furthermore, it is crucial to accurately measure the levels of promising biomarkers in exosomes, particularly classical Aβ and tau, which are of great importance for their clinical application. The levels of Aβ1-42 in NDEs are $<$10 pg/ml, and that of p-181-tau is $\sim$100 pg/ml, which is difficult to accurately determine with the traditional ELISA method. Therefore, automatic detection platforms, such as electrochemiluminescence instruments and single molecule arrays, and technologies with stronger anti-interference abilities, such as mass spectra, need to be developed. Except for the exosomes in CSF, further studies should focus on specific cell-derived exosomes in plasma, urine, and other non-invasive fluids, considering not only their internal biomarkers, but also their sizes and numbers.

Author contributions

LQ and SY mainly guided the study. YZ mainly wrote this manuscript. DM mainly drawn the figure. XM, JZ, DW, and JG made suggestions for revision of the manuscript. All authors reviewed the manuscript and approved the submission.

Funding

This study was supported by National Key Research and Development Program of China (No. 2021YFC2009300/2021YFC2009302), National Key Research and Development Program of China (No. 2020YFA0804501), Education Reforming Funding of PUMC (10023201900101), and Beijing Key Clinical Specialty for Laboratory Medicine - Excellent Project (No. ZK201000).

Acknowledgments

The authors would like to acknowledge the language editing service provided by the ELSEVIER website.

Conflict of interest

The authors declare that the research was conducted in the absence of any commercial or financial relationships that could be construed as a potential conflict of interest.

Publisher's note

References

Abdullah, M., Takase, H., Nunome, M., Enomoto, H., Ito, J., Gong, J. S., et al. (2016). Amyloid-β reduces exosome release from astrocytes by enhancing JNK phosphorylation. *J. Alzheimers Dis.* 53, 1433–1441. doi: 10.3233/JAD-160292

Abner, E. L., Elahi, F. M., Jicha, G. A., Mustapic, M., Al-Janabi, O., Kramer, J. H., et al. (2020). Endothelial-derived plasma exosome proteins in Alzheimer's disease angiopathy. *FASEB J.* 34, 5967–5974. doi: 10.1096/fj.202000034R

Apodaca, L. A., Baddour, A. A. D., Garcia, C. Jr., Alikhani, L., Giedzinski, E., Ru, N., et al. (2021). Human neural stem cell-derived extracellular vesicles mitigate hallmarks of Alzheimer's disease. *Alzheimers Res. Ther.* 13:57. doi: 10.1186/s13195-021-00791-x

Arioz, B. I., Tufekci, K. U., Olcum, M., Durur, D. Y., Akarlar, B. A., Ozlu, N., et al. (2021). Proteome profiling of neuron-derived exosomes in Alzheimer's disease reveals hemoglobin as a potential biomarker. *Neurosci. Lett.* 755:135914. doi: 10.1016/j.neulet.2021.135914

Asai, H., Ikezu, S., Tsunoda, S., Medalla, M., Luebke, J., Haydar, T., et al. (2015). Depletion of microglia and inhibition of exosome synthesis halt tau propagation. *Nat. Neurosci.* 18, 1584–1593. doi: 10.1038/nn.4132

Bang, O. Y., and Kim, J. E. (2022). Stem cell-derived extracellular vesicle therapy for acute brain insults and neurodegenerative diseases. *BMB Rep.* 55, 20–29. doi: 10.5483/BMBRep.2022.55.1.162

Bastos, P., Ferreira, R., Manadas, B., Moreira, P. I., and Vitorino, R. (2017). Insights into the human brain proteome: Disclosing the biological meaning of protein networks in cerebrospinal fluid. *Crit. Rev. Clin. Lab. Sci.* 54, 185–204. doi: 10.1080/10408363.2017.1299682

Brites, D., and Fernandes, A. (2015). Neuroinflammation and depression: microglia activation, extracellular microvesicles and microRNA dysregulation. *Front. Cell. Neurosci.* 9:476. doi: 10.3389/fncel.2015.00476

Chen, J. J., Yang, G., Yan, Q. Q., Zhao, J., and Li, S. (2019). Exosome-encapsulated microRNAs as promising biomarkers for Alzheimer's disease. *Rev. Neurosci.* 31, 77–87. doi: 10.1515/revneuro-2019-0001

Chen, Y. A., Lu, C. H., Ke, C. C., Chiu, S. J., Jeng, F. S., Chang, C. W., et al. (2021). Mesenchymal stem cell-derived exosomes ameliorate Alzheimer's disease pathology and improve cognitive deficits. *Biomedicines* 9:594. doi: 10.3390/biomedicines9060594

Chiarini, A., Armato, U., and Gardenal, E., Gui, L., and Dal Prà, I. (2017). Amyloid β-exposed human astrocytes overproduce Phospho-Tau and overrelease it within exosomes, effects suppressed by calcilytic NPS 2143-further implications for Alzheimer's therapy. *Front. Neurosci.* 11:217. doi: 10.3389/fnins.2017.00217

Colombo, E., Borgiani, B., Verderio, C., and Furlan, R. (2012). Microvesicles: novel biomarkers for neurological disorders. *Front. Physiol.* 3:63. doi: 10.3389/fphys.2012.00063

Cummings, J. L., Morstorf, T., and Zhong, K. (2014). Alzheimer's disease drug-development pipeline: few candidates, frequent failures. *Alzheimers Res. Ther.* 6:37. doi: 10.1186/alzrt269

DeLeo, A. M., and Ikezu, T. (2018). Extracellular vesicle biology in Alzheimer's disease and related tauopathy. *J. Neuroimmune Pharmacol.* 13, 292–308. doi: 10.1007/s11481-017-9768-z

Delpech, J. C., Herron, S., Botros, M. B., and Ikezu, T. (2019). Neuroimmune crosstalk through extracellular vesicles in health and disease. *Trends Neurosci.* 42, 361–372. doi: 10.1016/j.tins.2019.02.007

Deng, Z., Wang, J., Xiao, Y., Li, F., Niu, L., Liu, X., et al. (2021). Ultrasound-mediated augmented exosome release from astrocytes alleviates amyloid-β-induced neurotoxicity. *Theranostics* 11, 4351–4362. doi: 10.7150/thno.52436

Dinkins, M. B., Dasgupta, S., Wang, G., Zhu, G., and Bieberich, E. (2014). Exosome reduction in vivo is associated with lower amyloid plaque load in the 5XFAD mouse model of Alzheimer's disease. *Neurobiol. Aging* 35, 1792–1800. doi: 10.1016/j.neurobiolaging.2014.02.012

Dinkins, M. B., Dasgupta, S., Wang, G., Zhu, G., He, Q., Kong, J. N., et al. (2015). The 5XFAD mouse model of Alzheimer's disease exhibits an age-dependent increase in anti-ceramide IgG and exogenous administration of ceramide further increases anti-ceramide titers and amyloid plaque burden. *J. Alzheimers Dis.* 46, 55–61. doi: 10.3233/JAD-150088

Dinkins, M. B., Enasko, J., Hernandez, C., Wang, G., Kong, J., Helwa, I., et al., (2016). Neutral Sphingomyelinase-2 deficiency ameliorates Alzheimer's disease pathology and improves cognition in the 5XFAD mouse. *J. Neurosci.* 36, 8653–8667. doi: 10.1523/JNEUROSCI.1429-16.2016

Dinkins, M. B., Wang, G., and Bieberich, E. (2017). Sphingolipid-enriched extracellular vesicles and Alzheimer's disease: a decade of research. *J. Alzheimers Dis.* 60, 757–768. doi: 10.3233/JAD-160567

Dong, X., Zheng, D., and Nao, J. (2020). Circulating Exosome microRNAs as diagnostic biomarkers of dementia. *Front. Aging Neurosci.* 12:580199. doi: 10.3389/fnagi.2020.580199

Doyle, L. M., and Wang, M. Z. (2019). Overview of extracellular vesicles, their origin, composition, purpose, and methods for exosome isolation and analysis. *Cells* 8:727. doi: 10.3390/cells8070727

Drago, F., Lombardi, M., Prada, I., Gabrielli, M., Joshi, P., Cojoc, D., et al. (2017). ATP modifies the proteome of extracellular vesicles released by microglia and influences their action on astrocytes. *Front. Pharmacol.* 8:910. doi: 10.3389/fphar.2017.00910

Eitan, E., Tosti, V., Suire, C. N., Cava, E., Berkowitz, S., Bertozzi, B., et al. (2017). In a randomized trial in prostate cancer patients, dietary protein restriction modifies markers of leptin and insulin signaling in plasma extracellular vesicles. *Aging Cell* 16, 1430–1433. doi: 10.1111/acel.12657

Elia, C. A., Losurdo, M., Malosio, M. L., and Coco, S. (2019). Extracellular vesicles from mesenchymal stem cells exert pleiotropic effects on Amyloid-β, inflammation, and regeneration: a spark of hope for Alzheimer's disease from tiny structures? *Bioessays* 41:e1800199. doi: 10.1002/bies.201800199

Fernandes, A., Ribeiro, A. R., Monteiro, M., Garcia, G., Vaz, A. R., and Brites, D. (2018). Secretome from SH-SY5Y APP(Swe) cells trigger time-dependent CHME3 microglia activation phenotypes, ultimately leading to miR-21 exosome shuttling. *Biochimie* 155, 67–82. doi: 10.1016/j.biochi.2018.05.015

Fiandaca, M. S., Kapogiannis, D., Mapstone, M., Boxer, A., Eitan, E., Schwartz, J. B., et al. (2015). Identification of preclinical Alzheimer's disease by a profile of pathogenic proteins in neurally derived blood exosomes: a case-control study. *Alzheimers Dement.* 11, 600–607.e1. doi: 10.1016/j.jalz.2014.06.008

Fitzner, D., Schnaars, M., van Rossum D, Krishnamoorthy G, Dibaj P, and Bakhti M, (2011). Selective transfer of exosomes from oligodendrocytes to microglia by macropinocytosis. *J. Cell Sci.* 124, 447–458. doi: 10.1242/jcs.074088

Fröhlich, D., Kuo, W. P., Frühbeis, C., Sun, J. J., Zehendner, C. M., Luhmann, H. J., et al. (2014). Multifaceted effects of oligodendroglial exosomes on neurons: impact on neuronal firing rate, signal transduction and gene regulation. *Philos. Trans. R. Soc. Lond. B. Biol. Sci.* 369:20130510. doi: 10.1098/rstb.2013.0510

Frühbeis, C., Fröhlich, D., and Krämer-Albers, E. M. (2012). Emerging roles of exosomes in neuron-glia communication. *Front. Physiol.* 3:119. doi: 10.3389/fphys.2012.00119

Frühbeis, C., Fröhlich, D., Kuo, W. P., Amphornrat, J., Thilemann, S., Saab, A. S., et al. (2013). Neurotransmitter-triggered transfer of exosomes mediates oligodendrocyte-neuron communication. *PLoS Biol.* 11:e1001604. doi: 10.1371/journal.pbio.1001604

Fuhrmann, M., Bittner, T., Jung, C. K., Burgold, S., Page, R. M., Mitteregger, G., et al. (2010). Microglial Cx3cr1 knockout prevents neuron loss in a mouse model of Alzheimer's disease. *Nat. Neurosci.* 13, 411–413. doi: 10.1038/nn.2511

Gatti, S., Bruno, S., Deregibus, M. C., Sordi, A., Cantaluppi, V., Tetta, C., et al. (2011). Microvesicles derived from human adult mesenchymal stem cells protect against ischaemia-reperfusion-induced acute and chronic kidney injury. *Nephrol. Dial. Transplant* 26, 1474–1483. doi: 10.1093/ndt/gfr015

Ghidoni, R., Squitti, R., Siotto, M., and Benussi, L. (2018). Innovative biomarkers for Alzheimer's disease: focus on the hidden disease biomarkers. *J. Alzheimers Dis.* 62, 1507–1518. doi: 10.3233/JAD-170953

Goetzl, E. J. (2020). Advancing medicine for Alzheimer's disease: a plasma neural exosome platform. *FASEB J.* 34, 13079–13084. doi: 10.1096/fj.202001655

Goetzl, E. J., Abner, E. L., Jicha, G. A., Kapogiannis, D., and Schwartz, J. B. (2018a). Declining levels of functionally specialized synaptic proteins in plasma neuronal exosomes with progression of Alzheimer's disease. *FASEB J.* 32, 888–893. doi: 10.1096/fj.201700731R

Goetzl, E. J., Boxer, A., Schwartz, J. B., Abner, E. L., Petersen, R. C., Miller, B. L., et al. (2015a). Altered lysosomal proteins in neural-derived plasma exosomes in preclinical Alzheimer disease. *Neurology* 85, 40–47. doi: 10.1212/WNL.0000000000001702

Goetzl, E. J., Boxer, A., Schwartz, J. B., Abner, E. L., Petersen, R. C., Miller, B. L., et al. (2015b). Low neural exosomal levels of cellular survival factors in Alzheimer's disease. *Ann. Clin. Transl. Neurol.* 2, 769–773. doi: 10.1002/acn3.211

Goetzl, E. J., Kapogiannis, D., Schwartz, J. B., Lobach, I. V., Goetzl, L., Abner, E. L., et al. (2016a). Decreased synaptic proteins in neuronal exosomes of frontotemporal dementia and Alzheimer's disease. *FASEB J.* 30, 4141–4148. doi: 10.1096/fj.201600816R

Goetzl, E. J., Mustapic, M., Kapogiannis, D., Eitan, E., Lobach, I. V., Goetzl, L., et al. (2016b). Cargo proteins of plasma astrocyte-derived exosomes in Alzheimer's disease. *FASEB J.* 30, 3853–3859. doi: 10.1096/fj.201600756R

Goetzl, E. J., Nogueras-Ortiz, C., Mustapic, M., Mullins, R. J., Abner, E. L., Schwartz, J. B., et al. (2019). Deficient neurotrophic factors of CSPG4-type neural cell exosomes in Alzheimer disease. *FASEB J.* 33, 231–238. doi: 10.1096/fj.201801001

Goetzl, E. J., Schwartz, J. B., Abner, E. L., Jicha, G. A., and Kapogiannis, D. (2018b). High complement levels in astrocyte-derived exosomes of Alzheimer disease. *Ann. Neurol.* 83, 544–552. doi: 10.1002/ana.25172

Goetzl, E. J., Schwartz, J. B., Mustapic, M., Lobach, I. V., Daneman, R., Abner, E. L., et al. (2017). Altered cargo proteins of human plasma endothelial cell-derived exosomes in atherosclerotic cerebrovascular disease. *FASEB J.* 31, 3689–3694. doi: 10.1096/fj.201700149

Gouwens, L. K., Ismail, M. S., Rogers, V. A., Zeller, N. T., Garrad, E. C., Amtashar, F. S., et al. (2018). Aβ42 protofibrils interact with and are trafficked through microglial-derived microvesicles. *ACS Chem. Neurosci.* 9, 1416–1425. doi: 10.1021/acschemneuro.8b00029

Guix, F. X., Corbett, G. T., Cha, D. J., Mustapic, M., Liu, W., Mengel, D., et al. (2018). Detection of aggregation-competent Tau in neuron-derived extracellular vesicles. *Int. J. Mol. Sci.* 19:663. doi: 10.3390/ijms19030663

Guo, M., Hao, Y., Feng, Y., Li, H., Mao, Y., Dong, Q., et al. (2021). Microglial exosomes in neurodegenerative disease. *Front. Mol. Neurosci.* 14:630808. doi: 10.3389/fnmol.2021.630808

Guo, M., Yin, Z., Chen, F., and Lei, P. (2020). Mesenchymal stem cell-derived exosome: a promising alternative in the therapy of Alzheimer's disease. *Alzheimers Res. Ther.* 12:109. doi: 10.1186/s13195-020-00670-x

Hamlett, E. D., Ledreux, A., Potter, H., Chial, H. J., Patterson, D., Espinosa, J. M., et al. (2018). Exosomal biomarkers in Down syndrome and Alzheimer's disease. *Free Radic. Biol. Med.* 114, 110–121. doi: 10.1016/j.freeradbiomed.2017.08.028

Han, Y., Jia, L., Zheng, Y., and Li, W. (2018). Salivary exosomes: emerging roles in systemic disease. *Int. J. Biol. Sci.* 14, 633–643. doi: 10.7150/ijbs.25018

Hornung, S., Dutta, S., and Bitan, G. (2020). CNS-derived blood exosomes as a promising source of biomarkers: opportunities and challenges. *Front. Mol. Neurosci.* 13:38. doi: 10.3389/fnmol.2020.00038

Jack, C. R. Jr., Albert, M. S., Knopman, D. S., McKhann, G. M., Sperling, R. A., Carrillo, M. C., et al. (2011). Introduction to the recommendations from the National Institute on Aging-Alzheimer's Association workgroups on diagnostic guidelines for Alzheimer's disease. *Alzheimers Dement.* 7, 257–262. doi: 10.1016/j.jalz.2011.03.004

Jay, T. R., Hirsch, A. M., Broihier, M. L., Miller, C. M., Neilson, L. E., Ransohoff, R. M., et al. (2017). Disease progression-dependent effects of TREM2 deficiency in a mouse model of Alzheimer's disease. *J. Neurosci.* 37, 637–647. doi: 10.1523/JNEUROSCI.2110-16.2016

Jia, L., Qiu, Q., Zhang, H., Chu, L., Du, Y., Zhang, J., et al. (2019). Concordance between the assessment of Aβ42, T-tau, and P-T181-tau in peripheral blood neuronal-derived exosomes and cerebrospinal fluid. *Alzheimers Dement.* 15, 1071–1080. doi: 10.1016/j.jalz.2019.05.002

Jia, L., Zhu, M., Kong, C., Pang, Y., Zhang, H., Qiu, Q., et al. (2021). Blood neuro-exosomal synaptic proteins predict Alzheimer's disease at the asymptomatic stage. *Alzheimers Dement.* 17, 49–60. doi: 10.1002/alz.12166

Joshi, P., Benussi, L., Furlan, R., Ghidoni, R., and Verderio, C. (2015). Extracellular vesicles in Alzheimer's disease: friends or foes? Focus on aβ-vesicle interaction. *Int. J. Mol. Sci.* 16, 4800–4813. doi: 10.3390/ijms16034800

Joshi, P., Turola, E., Ruiz, A., Bergami, A., Libera, D. D., Benussi, L., et al. (2014). Microglia convert aggregated amyloid-β into neurotoxic forms through the shedding of microvesicles. *Cell Death Differ.* 21, 582–593. doi: 10.1038/cdd.2013.180

Kapogiannis, D., Boxer, A., Schwartz, J. B., Abner, E. L., Biragyn, A., Masharani, U., et al. (2015). Dysfunctionally phosphorylated type 1 insulin receptor substrate in neural-derived blood exosomes of preclinical Alzheimer's disease. *FASEB J.* 29, 589–596. doi: 10.1096/fj.14-262048

Keren-Shaul, H., Spinrad, A., Weiner, A., Matcovitch-Natan, O., Dvir-Szternfeld, R., Ulland, T. K., et al. (2017). A unique microglia type associated with restricting development of Alzheimer's disease. *Cell* 169, 1276–1290.e17. doi: 10.1016/j.cell.2017.05.018

Khongkow, M., Yata, T., Boonrungsiman, S., Ruktanonchai, U. R., Graham, D., and Namdee, K. (2019). Surface modification of gold nanoparticles with neuron-targeted exosome for enhanced blood-brain barrier penetration. *Sci. Rep.* 9:8278. doi: 10.1038/s41598-019-44569-6

Krämer-Albers, E. M., Bretz, N., Tenzer, S., Winterstein, C., Möbius, W., Berger, H., et al. (2007). Oligodendrocytes secrete exosomes containing major myelin and stress-protective proteins: trophic support for axons? *Proteomics Clin. Appl.* 1, 1446–1461. doi: 10.1002/prca.200700522

Lai, R. C., Arslan, F., Lee, M. M., Sze, N. S., Choo, A., Chen, T. S., et al. (2010). Exosome secreted by MSC reduces myocardial ischemia/reperfusion injury. *Stem Cell Res.* 4, 214–222. doi: 10.1016/j.scr.2009.12.003

Landeiro, F., Walsh, K., Ghinai, I., Mughal, S., Nye, E., Wace, H., et al. (2018). Measuring quality of life of people with predementia and dementia and their caregivers: a systematic review protocol. *BMJ Open* 8:e019082. doi: 10.1136/bmjopen-2017-019082

Liddelow, S. A., and Barres, B. A. (2017). Reactive astrocytes: production, function, therapeutic potential. *Immunity* 46, 957–967. doi: 10.1016/j.immuni.2017.06.006

Lim, C. Z. J., Zhang, Y., Chen, Y., Zhao, H., Stephenson, M. C., Ho, N. R. Y., et al. (2019). Subtyping of circulating exosome-bound amyloid β reflects brain plaque deposition. *Nat. Commun.* 10:1144. doi: 10.1038/s41467-019-09030-2

Lino, M. M., Simões, S., Tomatis, F., Albino, I., Barrera, A., Vivien, D., et al. (2021). Engineered extracellular vesicles as brain therapeutics. *J. Control. Release* 338, 472–485. doi: 10.1016/j.jconrel.2021.08.037

Liu, S., Fan, M., Xu, J. X., Yang, L. J., Qi, C. C., Xia, Q. R., et al. (2022). Exosomes derived from bone-marrow mesenchymal stem cells alleviate cognitive decline in AD-like mice by improving BDNF-related neuropathology. *J. Neuroinflammation* 19:35. doi: 10.1186/s12974-022-02393-2

Longobardi, A., Benussi, L., Nicsanu, R., Bellini, S., Ferrari, C., Saraceno, C., et al. (2021). Plasma extracellular vesicle size and concentration are altered in Alzheimer's disease, dementia with Lewy bodies, frontotemporal dementia. *Front. Cell Dev. Biol.* 9:667369. doi: 10.3389/fcell.2021.667369

Mathews, P. M., and Levy, E. (2019). Exosome production is key to neuronal endosomal pathway integrity in neurodegenerative diseases. *Front. Neurosci.* 13:1347. doi: 10.3389/fnins.2019.01347

Mrak, R. E., Sheng, J. G., and Griffin, W. S. (1996). Correlation of astrocytic S100 beta expression with dystrophic neurites in amyloid plaques of Alzheimer's disease. *J. Neuropathol. Exp. Neurol.* 55, 273–279. doi: 10.1097/00005072-199603000-00002

Muraoka, S., Jedrychowski, M. P., Tatebe, H., DeLeo, A. M., Ikezu, S., Tokuda, T., et al. (2019). Proteomic profiling of extracellular vesicles isolated from cerebrospinal fluid of former national football league players at risk for chronic traumatic encephalopathy. *Front. Neurosci.* 13:1059. doi: 10.3389/fnins.2019.01059

Muraoka, S., Jedrychowski, M. P., Yanamandra, K., Ikezu, S., Gygi, S. P., and Ikezu, T. (2020). Proteomic profiling of extracellular vesicles derived from cerebrospinal fluid of Alzheimer's disease patients: a pilot study. *Cells* 9:1959. doi: 10.3390/cells9091959

Murgoci, A. N., Cizkova, D., Majerova, P., Petrovova, E., Medvecky, L., Fournier, I., et al. (2018). Brain-cortex microglia-derived exosomes: nanoparticles for glioma therapy. *Chemphyschem* 19, 1205–1214. doi: 10.1002/cphc.201701198

Nassar, W., El-Ansary, M., Sabry, D., Mostafa, M. A., Fayad, T., Kotb, E., et al. (2016). Umbilical cord mesenchymal stem cells derived extracellular vesicles can safely ameliorate the progression of chronic kidney diseases. *Biomater. Res.* 20:21. doi: 10.1186/s40824-016-0068-0

Neumann, H., Kotter, M. R., and Franklin, R. J. (2009). Debris clearance by microglia: an essential link between degeneration and regeneration. *Brain* 132, 288–295. doi: 10.1093/brain/awn109

Nogueras-Ortiz, C. J., Mahairaki, V., Delgado-Peraza, F., Das, D., Avgerinos, K., Eren, E., et al. (2020). Astrocyte- and Neuron-derived extracellular vesicles from Alzheimer's disease patients effect complement-mediated neurotoxicity. *Cells* 9:1618. doi: 10.3390/cells9071618

Pan, J., He, R., Huo, Q., Shi, Y., and Zhao, L. (2020). Brain Microvascular endothelial cell derived exosomes potently ameliorate cognitive dysfunction by enhancing the clearance of Aβ through up-regulation of P-gp in mouse model of AD. *Neurochem. Res.* 45, 2161–2172. doi: 10.1007/s11064-020-03076-1

Paolicelli, R. C., Bergamini, G., and Rajendran, L. (2019). Cell-to-cell communication by extracellular vesicles: focus on microglia. *Neuroscience* 405, 148–157. doi: 10.1016/j.neuroscience.2018.04.003

Peng, K. Y., Pérez-González, R., Alldred, M. J., Goulbourne, C. N., Morales-Corraliza, J., Saito, M., et al. (2019). Apolipoprotein E4 genotype compromises brain exosome production. *Brain* 142, 163–175. doi: 10.1093/brain/awy289

Prince, M., Bryce, R., Albanese, E., Wimo, A., Ribeiro, W., and Ferri, C. P. (2013). The global prevalence of dementia: a systematic review and metaanalysis. *Alzheimers Dement.* 9, 63–75.e2. doi: 10.1016/j.jalz.2012.11.007

Proia, P., Schiera, G., Mineo, M., Ingrassia, A. M., Santoro, G. G., Savettieri, G., et al. (2008). Astrocytes shed extracellular vesicles that contain fibroblast growth factor-2 and vascular endothelial growth factor. *Int. J. Mol. Med.* 21, 63–67. doi: 10.3892/ijmm.21.1.63

Pulliam, L., Sun, B., Mustapic, M., Chawla, S., and Kapogiannis, D. (2019). Plasma neuronal exosomes serve as biomarkers of cognitive impairment in HIV infection and Alzheimer's disease. *J. Neurovirol.* 25, 702–709. doi: 10.1007/s13365-018-0695-4

Rani, K., Rastogi, S., Vishwakarma, P., Bharti, P. S., Sharma, V., Renu, K., et al. (2021). A novel approach to correlate the salivary exosomes and their protein cargo in the progression of cognitive impairment into Alzheimer's disease. *J. Neurosci. Methods* 347:108980. doi: 10.1016/j.jneumeth.2020.108980

Ratajczak, J., Miekus, K., Kucia, M., Zhang, J., Reca, R., Dvorak, P., et al. (2006). Embryonic stem cell-derived microvesicles reprogram hematopoietic progenitors: evidence for horizontal transfer of mRNA and protein delivery. *Leukemia* 20, 847–856. doi: 10.1038/sj.leu.2404132

Riancho, J., Vázquez-Higuera, J. L., Pozueta, A., Lage, C., Kazimierczak, M., Bravo, M., et al. (2017). MicroRNA profile in patients with Alzheimer's disease: analysis of miR-9-5p and miR-598 in raw and exosome enriched cerebrospinal fluid samples. *J. Alzheimers Dis.* 57, 483–491. doi: 10.3233/JAD-161179

Rosas-Hernandez, H., Cuevas, E., Raymick, J. B., Robinson, B. L., Ali, S. F., Hanig, J., et al. (2019). Characterization of serum exosomes from a transgenic mouse model of Alzheimer's disease. *Curr. Alzheimer Res.* 16, 388–395. doi: 10.2174/1567205016666190321155422

Ruan, Z., Delpech, J. C., Venkatesan Kalavai, S., Van Enoo, A. A., Hu, J., Ikezu, S., et al. (2020). P2RX7 inhibitor suppresses exosome secretion and disease phenotype in P301S tau transgenic mice. *Mol. Neurodegener.* 15:47. doi: 10.1186/s13024-020-00396-2

Ruan, Z., Pathak, D., Venkatesan Kalavai, S., Yoshii-Kitahara, A., Muraoka, S., Bhatt, N., et al. (2021). Alzheimer's disease brain-derived extracellular vesicles spread tau pathology in interneurons. *Brain.* 144, 288–309. doi: 10.1093/brain/awaa376

Saugstad, J. A., Lusardi, T. A., Van Keuren-Jensen, K. R., Phillips, J. I., Lind, B., Harrington, C. A., et al. (2017). Analysis of extracellular RNA in cerebrospinal fluid. *J. Extracell. Vesicles* 6:1317577. doi: 10.1080/20013078.2017.1317577

Sbai, O., Ould-Yahoui, A., Ferhat, L., Gueye, Y., Bernard, A., Charrat, E., et al. (2010). Differential vesicular distribution and trafficking of MMP-2, MMP-9, and their inhibitors in astrocytes. *Glia* 58, 344–366. doi: 10.1002/glia.20927

Schafer, D. P., Lehrman, E. K., Kautzman, A. G., Koyama, R., Mardinly, A. R., Yamasaki, R., et al. (2012). Microglia sculpt postnatal neural circuits in an activity and complement-dependent manner. *Neuron* 74, 691–705. doi: 10.1016/j.neuron.2012.03.026

Sivandzade, F., and Cucullo, L. (2021). Regenerative stem cell therapy for neurodegenerative diseases: an overview. *Int. J. Mol. Sci.* 22:2153. doi: 10.3390/ijms22042153

Söllvander, S., Nikitidou, E., Brolin, R., Söderberg, L., Sehlin, D., Lannfelt, L., et al. (2016). Accumulation of amyloid-β by astrocytes result in enlarged endosomes and microvesicle-induced apoptosis of neurons. *Mol. Neurodegener.* 11:38. doi: 10.1186/s13024-016-0098-z

Song, Z., Qu, Y., Xu, Y., Zhang, L., Zhou, L., Han, Y., et al. (2021). Microarray microRNA profiling of urinary exosomes in a 5XFAD mouse model of Alzheimer's disease. *Anim. Model Exp. Med.* 4, 233–242. doi: 10.1002/ame2.12175

Song, Z., Xu, Y., Deng, W., Zhang, L., Zhu, H., Yu, P., et al. (2020a). Brain derived exosomes are a double-edged sword in Alzheimer's disease. *Front. Mol. Neurosci.* 13:79. doi: 10.3389/fnmol.2020.00079

Song, Z., Xu, Y., Zhang, L., Zhou, L., Zhang, Y., Han, Y., et al. (2020b). Comprehensive proteomic profiling of urinary exosomes and identification of potential non-invasive early biomarkers of Alzheimer's disease in 5XFAD mouse model. *Front. Genet.* 11:565479. doi: 10.3389/fgene.2020.565479

Street, J. M., Barran, P. E., Mackay, C. L., Weidt, S., Balmforth, C., Walsh, T. S., et al. (2012). Identification and proteomic profiling of exosomes in human cerebrospinal fluid. *J. Transl. Med.* 10:5. doi: 10.1186/1479-5876-10-5

Sun, R., Wang, H., Shi, Y., Gao, D., Sun, Z., Chen, Z., et al. (2019). A pilot study of urinary exosomes in Alzheimer's disease. *Neurodegener. Dis.* 19, 184–191. doi: 10.1159/000505851

Sun, R., Wang, H., Shi, Y., Sun, Z., Jiang, H., and Zhang, J. (2020). Changes in the morphology, number, and pathological protein levels of plasma exosomes may help diagnose Alzheimer's disease. *J. Alzheimers Dis.* 73, 909–917. doi: 10.3233/JAD-190497

Szatanek, R., Baj-Krzyworzeka, M., Zimoch, J., Lekka, M., Siedlar, M., and Baran, J. (2017). The methods of choice for Extracellular Vesicles (EVs) characterization. *Int. J. Mol. Sci.* 18:1153. doi: 10.3390/ijms18061153

Tamboli, I. Y., Barth, E., Christian, L., Siepmann, M., Kumar, S., Singh, S., et al. (2010). Statins promote the degradation of extracellular amyloid {beta}-peptide by microglia via stimulation of exosome-associated insulin-degrading enzyme (IDE) secretion. *J. Biol. Chem.* 285, 37405–37414. doi: 10.1074/jbc.M110.149468

Ter-Ovanesyan, D., Norman, M., Lazarovits, R., Trieu, W., Lee, J. H., Church, G., et al. (2021). Framework for rapid comparison of extracellular vesicle isolation methods. *Elife* 10:e70725. doi: 10.7554/eLife.70725.sa2

Upadhya, R., Zingg, W., Shetty, S., and Shetty, A. K. (2020). Astrocyte-derived extracellular vesicles: Neuroreparative properties and role in the pathogenesis of neurodegenerative disorders. *J. Control Release* 323, 225–239. doi: 10.1016/j.jconrel.2020.04.017

van der Pol, E., Böing, A. N., Harrison, P., Sturk, A., and Nieuwland, R. (2012). Classification, functions, and clinical relevance of extracellular vesicles. *Pharmacol. Rev.* 64, 676–705. doi: 10.1124/pr.112.005983

Vasic, V., Barth, K., and Schmidt, M. H. H. (2019). Neurodegeneration and Neuro-Regeneration-Alzheimer's disease and stem cell therapy. *Int. J. Mol. Sci.* 20:4272. doi: 10.3390/ijms20174272

Venugopal, C., Shamir, C., Senthilkumar, S., Babu, J. V., Sonu, P. K., Nishtha, K. J., et al. (2017). Dosage and passage dependent neuroprotective effects of exosomes derived from rat bone marrow mesenchymal stem cells: an *in vitro* analysis. *Curr. Gene Ther.* 17, 379–390. doi: 10.2174/1566523218666180125091952

Villemagne, V. L., Burnham, S., Bourgeat, P., Brown, B., Ellis, K. A., Salvado, O., et al. (2013). Amyloid β deposition, neurodegeneration, and cognitive decline in sporadic Alzheimer's disease: a prospective cohort study. *Lancet Neurol.* 12, 357–367. doi: 10.1016/S1474-4422(13)70044-9

Wang, S., Cesca, F., Loers, G., Schweizer, M., Buck, F., Benfenati, F., et al. (2011). Synapsin I is an oligomannose-carrying glycoprotein, acts as an oligomannose-binding lectin, and promotes neurite outgrowth and neuronal survival when released via glia-derived exosomes. *J. Neurosci.* 31, 7275–7290. doi: 10.1523/JNEUROSCI.6476-10.2011

Watson, L. S., Hamlett, E. D., Stone, T. D., and Sims-Robinson, C. (2019). Neuronally derived extracellular vesicles: an emerging tool for understanding Alzheimer's disease. *Mol. Neurodegener.* 14:22. doi: 10.1186/s13024-019-0317-5

Wei, H., Xu, Y., Chen, Q., Chen, H., Zhu, X., and Li, Y. (2020). Mesenchymal stem cell-derived exosomal miR-223 regulates neuronal cell apoptosis. *Cell Death Dis.* 11:290. doi: 10.1038/s41419-020-2490-4

Winston, C. N., Goetzl, E. J., Akers, J. C., Carter, B. S., Rockenstein, E. M., Galasko, D., et al. (2016). Prediction of conversion from mild cognitive impairment to dementia with neuronally derived blood exosome protein profile. *Alzheimers Dement.* 3, 63–72. doi: 10.1016/j.dadm.2016.04.001

Winston, C. N., Goetzl, E. J., Schwartz, J. B., Elahi, F. M., and Rissman, R. A. (2019). Complement protein levels in plasma astrocyte-derived exosomes are abnormal in conversion from mild cognitive impairment to Alzheimer's disease dementia. *Alzheimers Dement.* 11, 61–66. doi: 10.1016/j.dadm.2018.11.002

Wyss-Coray, T., Loike, J. D., Brionne, T. C., Lu, E., Anankov, R., Yan, F., et al. (2003). Adult mouse astrocytes degrade amyloid-beta *in vitro* and *in situ*. *Nat. Med.* 9, 453–457. doi: 10.1038/nm838

Xie, H. M., Su, X., Zhang, F. Y., Dai, C. L., Wu, R. H., Li, Y., et al. (2022). Profile of the RNA in exosomes from astrocytes and microglia using deep sequencing: implications for neurodegeneration mechanisms. *Neural Regen. Res.* 17, 608–617. doi: 10.4103/1673-5374.320999

Xing, W., Gao, W., Lv, X., Xu, X., Zhang, Z., Yan, J., et al. (2021). The diagnostic value of exosome-derived biomarkers in Alzheimer's disease and mild cognitive impairment: a meta-analysis. *Front. Aging Neurosci.* 13:637218. doi: 10.3389/fnagi.2021.637218

Yin, Z., Han, Z., Hu, T., Zhang, S., Ge, X., Huang, S., et al. (2020). Neuron-derived exosomes with high miR-21-5p expression promoted polarization of M1 microglia in culture. *Brain Behav. Immun.* 83, 270–282. doi: 10.1016/j.bbi.2019.11.004

Yokoi, A., Villar-Prados, A., Oliphint, P. A., Zhang, J., Song, X., De Hoff, P., et al. (2019). Mechanisms of nuclear content loading to exosomes. *Sci. Adv.* 5:eaax8849. doi: 10.1126/sciadv.aax8849

Yokose, T., Kabe, Y., Matsuda, A., Kitago, M., Matsuda, S., Hirai, M., et al. (2020). O-Glycan-Altered extracellular vesicles: a specific serum marker elevated in pancreatic cancer. *Cancers* 12:2469. doi: 10.3390/cancers12092469

Yu, Z., Shi, M., Stewart, T., Fernagut, P. O., Huang, Y., Tian, C., et al. (2020). Reduced oligodendrocyte exosome secretion in multiple system atrophy involves SNARE dysfunction. *Brain* 143, 1780–1797. doi: 10.1093/brain/awaa110

Yuyama, K., Sun, H., Mitsutake, S., and Igarashi, Y. (2012). Sphingolipid-modulated exosome secretion promotes clearance of amyloid-β by microglia. *J. Biol. Chem.* 287, 10977–10989. doi: 10.1074/jbc.M111.324616

Yuyama, K., Sun, H., Sakai, S., Mitsutake, S., Okada, M., Tahara, H., et al. (2014). Decreased amyloid-β pathologies by intracerebral loading of glycosphingolipid-enriched exosomes in Alzheimer model mice. *J. Biol. Chem.* 289, 24488–24498. doi: 10.1074/jbc.M114.577213

Yuyama, K., Sun, H., Usuki, S., Sakai, S., Hanamatsu, H., Mioka, T., et al. (2015). A potential function for neuronal exosomes: sequestering intracerebral amyloid-β peptide. *FEBS Lett*. 589, 84–88. doi: 10.1016/j.febslet.2014.11.027

Yuyama, K., Takahashi, K., Usuki, S., Mikami, D., Sun, H., Hanamatsu, H., et al. (2019). Plant sphingolipids promote extracellular vesicle release and alleviate amyloid-β pathologies in a mouse model of Alzheimer's disease. *Sci. Rep*. 9:16827. doi: 10.1038/s41598-019-53394-w

Zhai, L., Shen, H., Sheng, Y., and Guan, Q. (2021). ADMSC Exo-MicroRNA-22 improve neurological function and neuroinflammation in mice with Alzheimer's disease. *J. Cell. Mol. Med*. 25, 7513–7523. doi: 10.1111/jcmm.16787

Zhang, J., Buller, B. A., Zhang, Z. G., Zhang, Y., Lu, M., Rosene, D. L., et al. (2021). Exosomes derived from bone marrow mesenchymal stromal cells promote remyelination and reduce neuroinflammation in the demyelinating central nervous system. *Exp. Neurol*. 347:113895. doi: 10.1016/j.expneurol.2021.113895

Zhao, J., O'Connor, T., and Vassar, R. (2011). The contribution of activated astrocytes to Aβ production: implications for Alzheimer's disease pathogenesis. *J. Neuroinflammation* 8:150. doi: 10.1186/1742-2094-8-150

Zheng, J., Yan, H., Shi, L., Kong, Y., Zhao, Y., Xie, L., et al. (2016). The CYP19A1 rs3751592 variant confers susceptibility to Alzheimer disease in the Chinese Han population. *Medicine* 95:e4742. doi: 10.1097/MD.0000000000004742

frontiers | Frontiers in Pharmacology

TYPE Original Research
PUBLISHED 04 August 2022
DOI 10.3389/fphar.2022.940555

OPEN ACCESS

EDITED BY
Yi Wang,
Zhejiang University, China

REVIEWED BY
Ai-Jun Liu,
Second Military Medical University, China
Simone Brogi,
University of Pisa, Italy
Zhi Sun,
First Affiliated Hospital of Zhengzhou University, China

*CORRESPONDENCE
Zhan-Ying Hong,
hongzhy001@163.com

†These authors have contributed equally to this work

SPECIALTY SECTION
This article was submitted to Neuropharmacology, a section of the journal Frontiers in Pharmacology

RECEIVED 10 May 2022
ACCEPTED 04 July 2022
PUBLISHED 04 August 2022

CITATION
Wang H, Dai J-Y, He Y-Z, Xia Z-W, Chen X-F, Hong Z-Y and Chai Y-F (2022), Therapeutic effect and mechanism of Anemarrhenae Rhizoma on Alzheimer's disease based on multi-platform metabolomics analyses. *Front. Pharmacol.* 13:940555. doi: 10.3389/fphar.2022.940555

Therapeutic effect and mechanism of *Anemarrhenae Rhizoma* on Alzheimer's disease based on multi-platform metabolomics analyses

Hui Wang[1†], Jian-Ying Dai[2†], Yu-Zhen He[1], Zhe-Wei Xia[1], Xiao-Fei Chen[1], Zhan-Ying Hong[1*] and Yi-Feng Chai[1]

[1]Shanghai Key Laboratory for Pharmaceutical Metabolite Research, School of Pharmacy, Naval Medical University, Shanghai, China, [2]College of Pharmacy, Fujian University of Traditional Chinese Medicine, Fuzhou, China

Anemarrhenae Rhizoma (AR) has multiple pharmacological activities to prevent and treat Alzheimer's disease (AD). However, the effect and its molecular mechanism are not elucidated clear. This study aims to evaluate AR's therapeutic effect and mechanism on AD model rats induced by *D*-galactose and $AlCl_3$ with serum metabolomics. Behavior study, histopathological observations, and biochemical analyses were applied in the AD model assessment. Gas chromatography-mass spectrometry (GC-MS) and liquid chromatography-mass spectrometry (LC-QTOF/MS) were combined with multivariate statistical analysis to identify potential biomarkers of AD and evaluate the therapeutic effect of AR on AD from the perspective of metabolomics. A total of 49 biomarkers associated with the AD model were identified by metabolomics, and pathway analysis was performed to obtain the metabolic pathways closely related to the model. With the pre-treatment of AR, 32 metabolites in the serum of AD model rats were significantly affected by AR compared with the AD model group. The regulated metabolites affected by AR were involved in the pathway of arginine biosynthesis, arginine and proline metabolism, ether lipid metabolism, glutathione metabolism, primary bile acid biosynthesis, and steroid biosynthesis. These multi-platform metabolomics analyses were in accord with the results of behavior study, histopathological observations, and biochemical analyses. This study explored the therapeutic mechanism of AR based on multi-platform metabolomics analyses and provided a scientific basis for the application of AR in the prevention and treatment of AD.

KEYWORDS

Alzheimer's disease, metabolomics, *Anemarrhenae Rhizoma*, LC-QTOF/MS, GC-MS

Introduction

Alzheimer's disease (AD), the most common cause of dementia in people over 65, is rising as our population ages. The outbreak of COVID-19 has accelerated the progression to death in AD patients (Xia et al., 2021). AD is a slowly progressive brain disease that begins many years before symptoms emerge. The hallmark pathologies are the accumulation of the protein beta-amyloid outside neurons and twisted strands of the protein tau inside neurons in the brain. The current hypotheses of AD mainly include the amyloid cascade hypothesis, the tau protein hypothesis, the inflammation hypothesis, the iron dyshomeostasis, the ferroptosis hypothesis, and the oxidative stress hypothesis (Wang et al., 2022). The AD biomarkers, such as CSF measures of Aβ1-42, t-tau, and p-tau, can assess aged patients' overall health and diseased condition and the pathogenic processes and pharmacological effects of any therapy (Olsson et al., 2016). However, concerning invasive approaches and high cost, it is essential to identify new biomarkers in other less invasive and easily collectible body fluids like the serum, urine, and expiratory gas. As AD's pathogenesis and progression are not fully developed, no disease-modifying treatments are available for AD. Currently approved drugs, including inhibitors to cholinesterase enzyme and antagonists to N-methyl-d-aspartate acid (NMDA), can only provide symptomatic relief or delay the progression of the disease (Athar et al., 2021). Recently, owing to several failed attempts in AD drug development to act on one target, attention has been paid to multiple therapeutic strategies to design and develop drugs capable of hitting more than one target (Benek et al., 2020; Xie et al., 2020; Husain et al., 2021). In China, traditional Chinese medicine (TCM) has been frequently applied in treating AD, and extensive progress researches have shown exceptional advantages due to the multi-target, multi-system, and multi-pathway capacity (Chen et al., 2020).

Anemarrhenae Rhizoma (AR, "zhimu" in Chinese), derived from the rhizome of *Anemarrhena asphodeloides* Bunge., is frequently used as a traditional Chinese medicine to treat AD and other memory deficits associated with aging. AR and the components also have been demonstrated by excellent biological and pharmacological activity, such as immunomodulatory, anti-inflammatory, anti-diabetes, anti-tumor, anti-depression, anticoagulation, etc (Wang et al., 2018; Liu et al., 2021). Timosaponin A-III (TA-III) was screened and identified as a potentially active component for the anti-AD activity, and BACE1 was proven to be a potential high-affinity target (Wang et al., 2020). Previous researches have shown that Timosaponin-BII possesses a neuronal protective and anti-inflammatory effect, possibly by suppressing the production of pro-inflammatory factors IL-1, IL-6, and TNF-α(Hu et al., 2005; Li et al., 2007; Lu et al., 2009; Huang et al., 2012). Sarsasapogenin was proved to be a promising structural template for developing new anti-Alzheimer drug candidates and is a bioactive lead compound (Wang et al., 2018). Multiple studies reported that mangiferin had neuroprotective effects via the regulation of antioxidant and anti-inflammatory pathways and PI3K/Akt, Nrf2/HO-1, and ERK1/2 signaling pathways (Liu et al., 2021). Consequently, AR is a suitable candidate for the comprehensive treatment of AD. However, the effect of AR extract on AD and the therapeutic mechanism have not been thoroughly investigated *in vivo*.

Metabolomics, a snapshot of the complete set of small-molecule, is especially suitable to provide a comprehensive systems-level study of the relationship between metabolites, disease, and drugs for complicated, multi-pathway involved pathological systems such as AD (Badhwar et al., 2020). With the rapid progress in mass spectrometry, bioinformatics, and systems biology, metabolomics-based technology provides a high potential strategy for discovering diagnostic markers and studying the pathological mechanism for AD (Cuperlovic-Culf and Badhwar, 2020). In the past, numerous metabolomics studies were implemented to investigate the action mechanisms of TCMs on AD (Yi et al., 2017; Sun et al., 2018; Zhang et al., 2020). Nevertheless, the considerable heterogeneity and dynamism of the human metabolome make it impossible for a single analytical to simultaneously determine the entire set of metabolites from complex biological samples (Gonzalez-Dominguez et al., 2017). Hence, the complementary analytical platforms for metabolomics analysis to unravel the underlying pathology of AD are recommended urgently.

In the present paper, gas chromatography-mass spectrometry (GC-MS) and liquid chromatography-mass spectrometry (LC-QTOF/MS) were combined with multivariate statistical analysis to identify potential biomarkers of AD model rats induced by both *D*-galactose (*D*-Gal) and $AlCl_3$. Furthermore, the therapeutic effects of AR and the mechanism underlying the effects on the pathogenesis of AD were also explored using a metabolomics strategy. Also, the Morris water maze (MWM) test is processed to examine the memory and spatial learning ability of model rats and rats pre-treated by AR. In addition, we also perform antioxidant assays such as malondialdehyde (MDA), superoxide dismutase (SOD), and nitric oxide (NO) in the hippocampus of rats to study the mechanism of AD on oxidative stress and investigate the influence of AR in the rat model of AD. The workflow for therapeutic effect and mechanism analyses of AR on Alzheimer's disease is shown in Figure 1. Those studies provided theoretical basics for designing and developing novel drugs for AD.

Materials and methods

Chemicals and materials

AR was purchased from the Shanghai Leiyunshang pharmaceutical Company. The AR extract was prepared by ethanol reflux. AR powder was extracted by 95% ethanol and reflux for 4 hours, and then the filtered residue dregs were

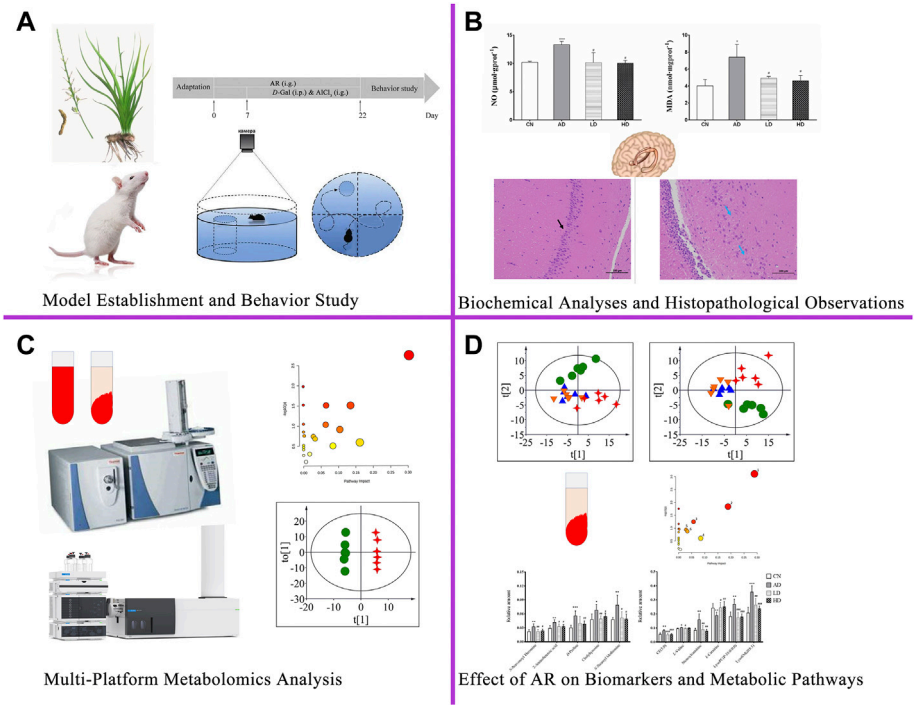

FIGURE 1
The workflow for therapeutic effect and mechanism analyses of AR on Alzheimer's disease. AR: *Anemarrhenae Rhizoma*.

decocted twice with water for 1 hour. All the filtrate was combined and concentrated to a proper amount in a vacuum. *D*-Gal and $AlCl_3$ were purchased from Sinopharm Chemical Regent Co., Ltd. (China). Methoxyamine hydrochloride, Pyridine, MSTFA, TMCS, Adonitol, and HPLC grade acetonitrile, methanol, and formic acid were obtained from Sigma-Aldrich (United States). 2-Chloro-L-Phenylalanine was purchased from Shanghai Yuanye Biotechnology Co., Ltd. The water was provided by Watsons (China). The ELISA kits of SOD, NO, and Ach were purchased from Nanjing Jiancheng Bioengineering Institute (China). Other reagents and solvents of analytical grade were provided by Sinopharm Chemical Regent Co., Ltd. (China).

Instruments

1290 Infinity UHPLC system (Agilent, United States), XSelect HSS T3 (2.1 × 100 mm, 2.5 μm, Waters, United States), 6530 QTOF/MS (Agilent, United States), Trace GC ultra-gas chromatograph (Thermo Fisher Scientific, United States), an Agilent DB-5MS column DSQ II mass spectrometer (Thermo Fisher Scientific, United States), Electronic balance (Switzerland Mettler company, Japan), high-speed freezing centrifuge (Thermo Fisher Scientific, United States), DZG-6020 vacuum drying oven (Shanghai Yiheng experimental instrument company, China). ZH-Mm Tis water maze equipment (Zhenghua biological instrument equipment company, China), Tecan infinite M200 pro multifunctional microplate reader (Switzerland), Vortex-6 vortex instrument (Macao slinberg Instrument Manufacturing Co., Ltd.); RVC2-18CD plus vacuum concentrator (Beijing gaodetong Technology Co., Ltd.).

Animals and modeling

Twenty-four male Sprague-Dawley rats (200 ± 20 g) were purchased from the JOINN Laboratories (China) Co., Ltd. Animal license number is SCXK (Hu) 2018–0006, animal certification number was 20180006032138. They were raised in an air-conditioned environment (temperature: 24 ± 2°C, humidity: 40%–77%) with a 12 h light-dark cycle, and food and water were available. The experiment begins after a week of adaptation. *D*-gal was dissolved in normal saline to obtain 30 mg/ml solution. $AlCl_3$ was dissolved in water to get a 60 mg/ml solution. The rats were randomly divided into four groups: the blank control group (CN), the AD model group (AD), the AR treatment group of low dosage (LD), and the AR treatment group of high dosage (HD), with six rats in each group.

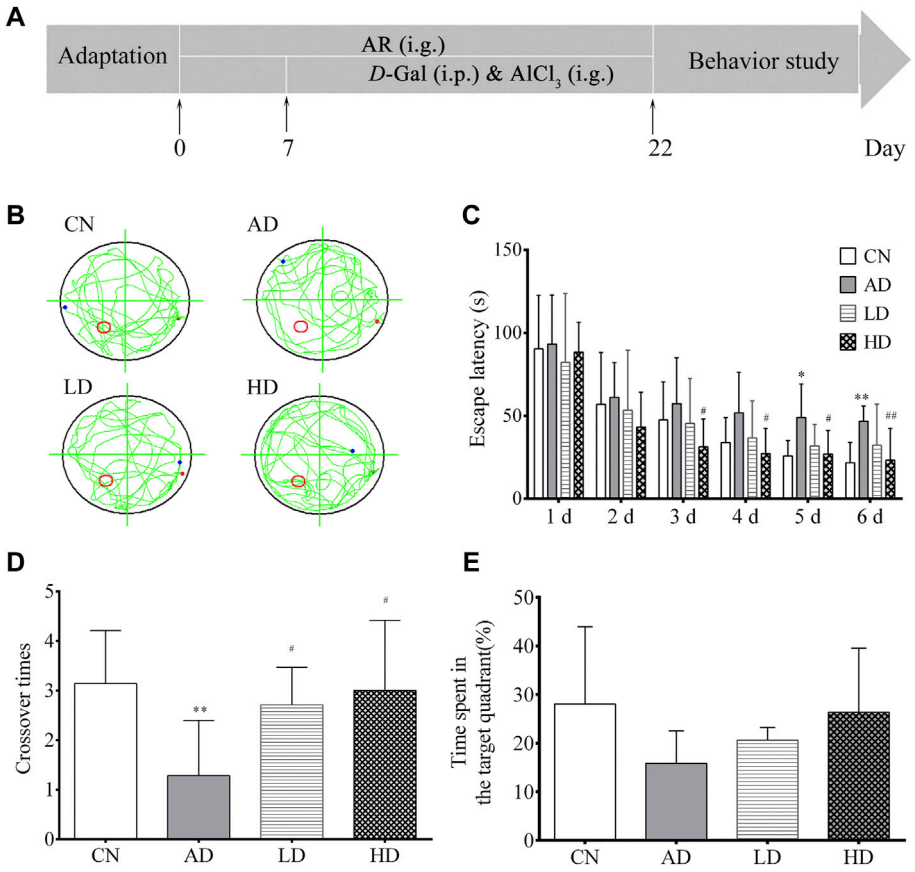

FIGURE 2
Effect of AR on AD model in MWM. **(A)** Schematic representation of the experimental procedure **(B)** Abridged general view of rat in testing, **(C)** Escape latency in location sailing test **(D)** Crossover times in spatial probe task, **(E)** Time in the target quadrant in spatial probe task. CN, the blank control group, AD, the AD model group, LD, the AR treatment group of low dosage (LD), HD, and the AR treatment group of high dosage (HD).*p < 0.05, **p < 0.01, compared with CN group; #p < 0.05, ##p < 0.01, compared with AD group).

The HD and LD groups were given AR solutions by intragastrical administration (i.g.,) at the dose of 200 mg·kg^{-1}and 100 mg kg^{-1} from the first day to the last days, respectively. In contrast, the blank control group and the AD model group were given equal volumes of distilled water. The AD model rats in the AD model group, the HD group, and the LD group were induced by intraperitoneal injection (i.p.) of *D*-Gal combined with intragastrical administration (i.g.) of $AlCl_3$ for 15 days from eighth days to twenty-second days, while the rats in the blank control group were given an equal volume of distilled water and saline. The whole modeling, drug administration, and behavior study procedure are shown in Figure 2A. All the operations had followed the guidelines of Animal Experimentation of Naval Medical University and were approved by the Animal Ethics Committee of the institution.

Behavior study of Alzheimer's disease model rats

The Morris water maze test (MWM) was conducted in a circular tank (diameter, 140 cm; height, 50 cm) filled with water (25 ± 2°C) to a depth of 35 cm, which was equipped with a submerged escape platform (10 × 10 cm) under the surface and located in a fixed position and surrounded by several spatial cues in a dimly-illuminated room. The water temperature was kept at 22–25°C. Spatial cues of different geometry were decorated by the

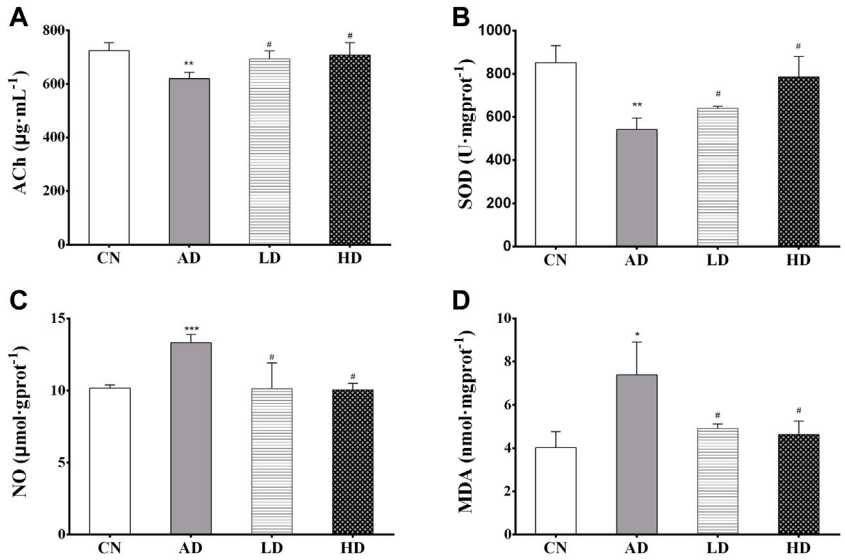

FIGURE 3
(A–D) The hippocampus levels of ACh, SOD, NO, and MDA. *$p < 0.05$, **$p < 0.01$, compared with CN group; #$p < 0.05$, ##$p < 0.01$, compared with AD group.

poolsides to help the rats recognize the platform position. The rats were individually handled for 3 min day every day for three consecutive days before the training. In the orientation navigation experiment, training was carried out twice daily for 5 days. In each trial, the animals were introduced into the pool at one of the four different starting positions around the pool in a random sequence. If the animal failed to escape within the 60 s, it would be guided to the platform and stay there for 20 s. The time for the rats to find the platform was called escape latency, and the path to the submerged escape platform was recorded. On day seven, the rats are submitted to a spatial probe test session 24 h after the last training session. The submerged platform was removed in the probe test, and the rats were placed in the water for 2 min. The number of crossing over the original position of the platform, the distance navigated, and time spent in the target quadrant, the effective platform quadrant, compared to the opposite quadrant were calculated.

Collection and processing of biological samples

The day after assessing MWM tests, rats were fasted overnight, with free access to water; blood samples were collected from the abdominal aorta of all groups just before sacrificing the rats by cervical decapitation. The fresh blood was centrifuged after 30 min (4°C, 4,000 rpm, 15 min), and the clear supernatant serum was stored in the refrigerator at −80°C.

After collecting the blood, the heads of the rats were moved onto the dry ice, and the hippocampus region was rapidly dissected on an ice-cooled glass plate, washed with saline, and divided into two portions. The first portion was homogenized with a homogenizer to give 10% (w/v) homogenate in the ice-cold medium in nine volumes of a 50 mM phosphate buffered saline (PBS, pH 7.0) containing 0.1 mmol/L ethylene-diamine-tetra-acetic acid (EDTA). The clear supernatants were prepared by centrifugation (4°C, 4,000 rpm, 30 min) for Ach, NO, and MDA assays. The second portion of the hippocampal was used for histopathological investigation.

Biochemical analysis and histopathological analysis

Hippocampus Ach levels, NO levels, SOD levels, and MDA levels were all measured using ELISA kits according to the manufacturer's instructions.

Every fresh rat hippocampus was placed in 4% paraformaldehyde as a fixative. Hematoxylin and Eosin (H&E) staining were performed to identify changes in hippocampus

CA1 formation and hippocampus CA3 formation. The histopathological alterations were then viewed and recorded under a light micro-scope at ×400 magnification.

Metabolite extraction, derivatization and GC–MS analysis

The metabolite extraction and derivatization method were based on the derivatization method by MSTFA. 200 μl of serum was accurately taken and added with 600 μl methanol with 2 μg/ml adonitol as an internal standard. After 3-min vortex and centrifugation at 4°C, 13,200 rpm for 25 min, 150 μl supernatant was separated and concentrated under a continuous gas nitrogen flow until the solvent was evaporated entirely. In a pyridine solution, the residue was dissolved in 75 μl of 20 mg/ml methoxyamine hydrochloride. After a 5-min vortex and oscillation at 70°C for 1 h, 75 μl of derivatization reagent MSTFA with 1% TMCS was precisely added. After a 5-min vortex and oscillation at 50°C for 1 h to full derivatization, 100 μl of n-heptane was added precisely. Finally, the supernatant was collected after centrifugation at 4°C, 13,200 rpm for 5 min. The quality control (QC) sample was prepared by mixing the supernatant of every sample and tested at regular intervals.

GC-MS analysis was undertaken on a Trace GC Ultra coupled to a Thermo DSQ II mass spectrometer. The metabolites were separated by a capillary gas chromatography column Agilent DB-5MS. The program was initially set to 70°C, maintained for 4 min, programmed to 220°C at a rate of 4°C min^{-1}, programmed to 310°C at a rate of 8°C min^{-1}, and then maintained for 4 min. Helium was used as carrier gas at a flow rate of 1.0 ml min^{-1}, and samples were injected in a 1:10 split ratio with the injector and transfer line isothermally at 260°C. The ion source temperature was maintained at 200°C for electron ionization, and the full scan mode with a mass range of m/z 50–650 was used after electron impact ionization. The solvent delay was set at 6 min.

Metabolite extraction and LC-QTOF/MS analysis

Three times the volume of the cold methanol with 2 μg/ml 2-Chloro-*L*-Phenylalanine as an internal standard was added to the serum samples. The mixture was centrifuged at 13,200 rpm for 25 min at 4°C, followed by vortexing for 3 min 150 μl supernatant was separated and concentrated under a continuous gas nitrogen flow until the solvent was evaporated entirely. The dried residue was dissolved in 200 μl methanol with 2 μg/ml 2-Chloro-*L*-Phenylalanine. After 15-min vortex and centrifugation at 13,200 rpm for 15 min at 4°, the supernatant was collected for test. The quality control (QC) sample was prepared as the procedure of GC-MS QC in part 2.7.

Chromatographic analysis was performed using Agilent 1290 Infinity UHPLC equipped with a Waters XSelect HSS T3. The mobile phase was composed of 0.1% formic acid in water (A) and 0.1% formic acid in acetonitrile (B) at a flow rate of 0.4 ml/min. The column was eluted with a gradient of 2% B at 0–2 min, 2%–98% B at 2–17 min, 98% B at 17–19 min. The column was maintained at 40°C, and the injection volume was 3 μl for each run. The LC-QTOF/MS metabolomics profiling analysis was performed on Agilent 6530 QTOF/MS in both positive electrospray ionization interface (ESI+) and negative electrospray ionization interface (ESI-). The MS parameters were set as follows: capillary voltage of 4.0 kV (ESI+)/3.5 kV (ESI-), fragmentor voltage of 120.0 V, drying gas flow of 11.0 L/min, the gas temperature of 350°C, and skimmer voltage of 60.0 V. The full-scan data were acquired from 50 to 1000 m/z over a run time of 19 min.

Data processing and statistical analysis

Both GC-MS data files and LC-QTOF/MS data files were processed by XCMS in R (v3.6.2) for peak finding, peak alignment, peak filtering, and the removal of isotope ions. For GC-MS, the method of target free filtration was adopted, in which only the ions with the most substantial peak value at the same retention time were retained (the retention time window is 0.01 min). The zero values were reduced, and the value count of the bucket required more than 80%. Then the individual bucket value was normalized according to the peak value of the internal standard. The processed LC-QTOF/MS and GC-MS data were then analyzed by multivariable analysis, including partial least square-discriminant analysis (PLS-DA) and Orthogonal Partial Least Squares Discrimination Analysis (OPLS-DA) by SIMCA software (version 14.0, Umetrics). The OPLS-DA of serum profiles was performed to screen the potential biomarkers of AD rats induced by $AlCl_3$/*D*-gal. Features with variable importance of projection (VIP) > 1.0 and $p < 0.05$ (Student's *t*-test) were selected as the potential differential metabolites for subsequent analysis. As to the LC-QTOF/MS, potential candidate biomarkers were further identified by comparing the accurate mass with standard substances of online databases, including HMDB, KEGG, and PubChem online. Then, the best-matching ions were used as candidate biomarkers. Similarly, as to the GC-MS potential differential metabolites, metabolite identification was performed by executing similarity searches in the NIST2017 mass spectral library (National Institute of Standards and Technology, Gaithersburg, United States) and metabolites with a NIST match factor (SI or RSI) of ≥600 were investigated. Analysis of metabolic pathways was performed using MetaboAnalyst and KEGG metabolic pathway database by the topological feature of the metabolic path.

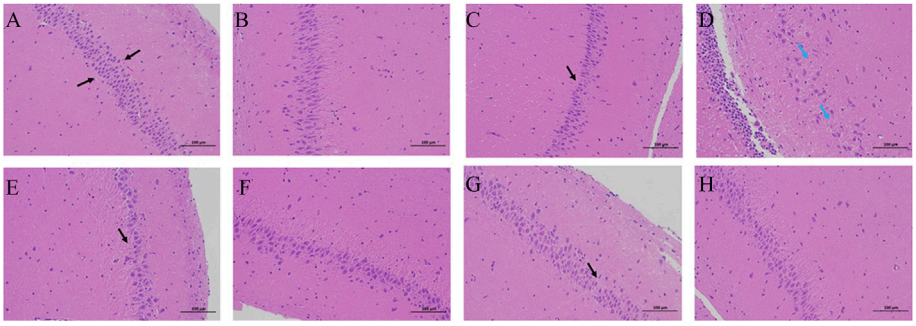

FIGURE 4
H&E staining in the therapeutic effect of AR against AD with a microscope. **(A,C,E,G)** the hippocampus CA1 of CN, AD, LD, and HD group **(B,D,F,H)** the hippocampus CA3 of CN, AD, LD, and HD group.

All statistical analysis was performed through the one-way ANOVA analysis and the Student's *t*-test, and all experimental data were expressed as mean ± standard deviation. Statistical significance was accepted if the *p*-value was less than 0.05.

Results

Behavior study results

In the orientation navigation experiment, with the increase of the trail times, all the rats' average escape latency decreased gradually over the training days. Furthermore, the escape latencies among the AD model group were longer than those of the blank control. To the rats in the LD and HD groups pre-treated with AR, their escape latency significantly decreased from the third day to the sixth day compared to the AD group. In the spatial probe test on day seven, both the number of crossing over the original position and the time spent in the target quadrant of the platform of the rats in the AD model group decreased noticeably compared to the blank control group. At the same time, a trend was reversed by pre-treatment with AR. All the MWM results shown in Figure 2 indicated the successful establishmentindicated the successful establishment of the AD model and AR could ameliorate the impairment of spatial learning and memory of AD model rats induced by *D*-Gal and $AlCl_3$ to some extent.

Biochemical analyses and histopathological observations

The results of the biochemical analyses are shown in Figure 3. Decreased ACh concentration ($p < 0.01$) and SOD activity ($p < 0.01$) in the hippocampus were found in the AD model group compared to the control group. Meanwhile, AR pre-treatment significantly increased ACh concentration and the SOD activity in the hippocampus compared with the AD model rats. Similarly, compared with the control group, the contents of NO, MDA in the hippocampus of the AD model group were significantly increased ($p < 0.005$ and $p < 0.05$), and significantly decreased contents ($p < 0.01$) were observed in the LD group and the HD group compared with AD model rats.

Neurons in the hippocampus CA1 region and hippocampus CA3 region are vulnerable to the memory circuit, and the degeneration is a major pathologic characteristic of AD. As shown in Figure 4, the pyramidal cells in the CA1 area were seen in about five layers. The pyramidal cells in CA1 and CA3 areas were neatly arranged and structurally intact, with the cytoplasm and nucleus clearly delineated. No apparent glial cell proliferation was found. However, sections from the hippocampus of AD group rats exhibited marked neuronal degeneration: the decreased number of surviving neurons, the sparsely disordered arrays of the neurons, the blurred cell boundaries, and the karyopyknotic phenomenon. Compared to the AD model rat brains, the damage to neurons was remarkably ameliorated in the hippocampus of the rats in the LD group and HD group.

The biochemical analysis results and H&E staining results indicated that AR could prevent and alleviate AD symptoms and slow down the progress.

Multi-platform metabolomics analysis

OPLS-DA focused on the inter-group difference between the AD and control groups, and both the LC-QTOF/MS and GC-MS results showed that the control and model groups were separated (Figure 5). With the LC-QTOF/MS metabolomics platform, we found the level of 39 metabolites significantly altered in the AD group

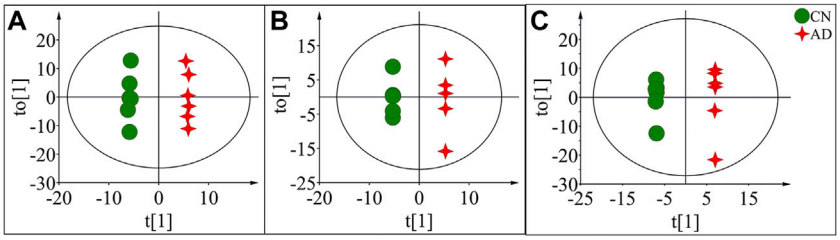

FIGURE 5
OPLS-DA score plots of potential biomarkers in the control group (CN) and AD model group (AD) in positive mode of LC-QTOF/MS **(A)**, negative mode of LC-QTOF/MS **(B)**, and in GC-MS **(C)**.

compared with the blank control group. The levels of 11 metabolites like retinyl ester and hypoxanthine were increased in the AD group, and those of 28 metabolites like *L*-Arginine and *L*-Valine were reduced in the AD group (Table 1). These regulated metabolites were involved in the pathway of retinol metabolism, cysteine and methionine metabolism, ether lipid metabolism, arginine biosynthesis, purine metabolism, arginine and proline metabolism, glutathione metabolism, glycerophospholipid metabolism, and tryptophan metabolism, et al. (Figure 6A). With the GC-MS metabolomics platform, we found the level of 11 metabolites significantly altered in the AD group compared with the blank control group, and the levels of these 11 metabolites like citrulline and L-ornithine were increased (Table 1). These regulated metabolites were involved in arginine biosynthesis, arginine and proline metabolism, primary bile acid biosynthesis, steroid biosynthesis, glutathione metabolism, steroid hormone biosynthesis, and butanoate metabolism, et al. (Figure 6B). All the regulated metabolites analyzed by the LC-QTOF/MS and GC-MS were involved in the pathway of arginine biosynthesis, retinol metabolism, arginine and proline metabolism, cysteine and methionine metabolism, ether lipid metabolism, purine metabolism, glutathione metabolism, primary bile acid biosynthesis, steroid biosynthesis, glycerophospholipid metabolism (Figure 6C).

Effect of *Anemarrhenae Rhizoma* on biomarkers and metabolic pathways

To characterize the efficacy of AR for preventing and treating AD, PLS-DA analyses of serum profiles obtained from the LC-QTOF/MS platform and GC-MS platform were performed to get a global overview of the response in the control group, AD model group, and oral administration AR group. The PLS-DA score plot (Figure 7) showed that the control group and AD group were separated, while the metabolic trajectory of rats pre-treated with AR moved to that of the control group while away from the AD model rats. These results indicated that AR could restore the pathological process of AD on a global metabolite level to prevent and treat AD. Furthermore, the relative amounts of the differential metabolites were compared among the blank control group, the AD model group, the LD group, and the HD group. 23 metabolites in the serum of rats pre-treated by AR in the LD group or the HD group tested by LC-QTOF/MS were significantly affected by AR compared with those in the AD model group ($p < 0.05$, Figure 8), and nine metabolites in the LD group or the HD group tested by GC-MS were significantly affected by AR compared with which in the AD model group ($p < 0.05$, Figure 8). Of note, all the regulated metabolites affected by AR were involved in the pathway of arginine biosynthesis, arginine and proline metabolism, ether lipid metabolism, glutathione metabolism, primary bile acid biosynthesis, steroid biosynthesis, et al. (Figure 6D), indicating that AR could partly correct the disturbed metabolic alterations in AD rats through these pathways.

Discussion

In this research, *D*-Gal and $AlCl_3$ were used to prepare the rat model of AD according to many previous investigations. We evaluated the AD model using a classical behavior study with the Morris water maze test, biochemical analysis, and histopathological observations. The results indicated that establishing the AD model with neuronal damage was successful, and AR could alleviate the symptoms of AD model rats induced by *D*-Gal/$AlCl_3$ and slow down the progress to some extent.

The difference in metabolic profiles of the AD model rats *in vivo* can be analyzed through the metabolomics method. In our study, an untargeted metabolomic method based on multi-platform analyses combining LC-QTOF/MS and GC-MS

TABLE 1 Major potential biomarkers of AD model group induced by *D*-Gal/$AlCl_3$ and related metabolic pathways.

No.	Metabolite	Exact mass	Formula	Adduct/ method	Trend	Related pathway
1	*L*-Carnitine	161.1052	$C_7H_{15}NO_3$	M + H	↓**	Carnitine synthesis
2	Cysteic acid	169.0045	$C_3H_7NO_5S$	M + FA-H	↑**	Taurine and hypotaurine metabolism
3	LysoPE (18:0/0:0)	481.3168	$C_{23}H_{48}NO_7P$	M + H	↑*	lysophospholipid
4	Cysteinylglycine	178.0412	$C_5H_{10}N_2O_3S$	M + Cl	↑**	Glutathione metabolism
5	*L*-Arginine	174.1117	$C_6H_{14}N_4O_2$	M + H	↑*	Aminoacyl-tRNA biosynthesis
6	Indoxyl sulfate	213.0096	$C_8H_7NO_4S$	M-H	↑*	neurotoxin
7	*L*-Methionine	149.051	$C_5H_{11}NO_2S$	M + H	↑*	Aminoacyl-tRNA biosynthesis
8	Stearoylcarnitine	427.3662	$C_{25}H_{49}NO_4$	M + K	↑**	Mitochondrial beta-oxidation of long chain saturated fatty acids
9	*L*-Valine	117.079	$C_5H_{11}NO_2$	M + K	↑*	Aminoacyl-tRNA biosynthesis
10	2-Aminobenzoic acid	137.0477	$C_7H_7NO_2$	M + H	↑**	Tryptophan metabolism
11	*D*-Proline	115.0633	$C_5H_9NO_2$	M + H	↑***	Cysteine and methionine metabolism
12	CE (5:0)	470.4124	$C_{32}H_{54}O_2$	M + K	↑**	Steroid biosynthesis
13	Retinyl ester	302.2246	$C_{20}H_{30}O_2$	M-H	↓**	Retinol metabolism
14	LysoSM(d18:1)	465.3457	$C_{23}H_{50}N_2O_5P$	M + NH4	↑***	lysophospholipid
15	LysoPC(22:5 (4*Z*,7*Z*,10*Z*,13*Z*,16*Z*)/0:0)	569.3481	$C_{30}H_{52}NO_7P$	M + FA-H	↓*	lysophospholipid
16	PC(18:1 (9Z)e/2:0)	549.3794	$C_{28}H_{56}NO_7P$	M + H	↑*	Ether lipid metabolism
17	LysoPC(P-18:0/0:0)	507.3689	$C_{26}H_{54}NO_6P$	M + H	↑**	lysophospholipid
18	Guanine	151.0494	$C_5H_5N_5O$	M + H	↑*	Purine metabolism
19	Xanthine	152.0334	$C_5H_4N_4O_2$	M-H20-H, M + Cl	↑*	Purine metabolism
20	DG (14:1n5/0:0/14:1n5)	508.4128	$C_{31}H_{56}O_5$	M + K	↓*	diglyceride
21	LysoPC(0:0/20:4 (5*Z*,8*Z*,11*Z*,14*Z*))	543.3325	$C_{28}H_{50}NO^7P$	M + FA-H	↑***	lysophospholipid
22	Cholic acid	408.2876	$C_{24}H_{40}O_5$	M-H	↑**	Primary bile acid biosynthesis
23	Methyl hippurate	193.0739	$C_{10}H_{11}NO_3$	M-H	↑*	fatty acid metabolism
24	2-Hydroxyvaleric acid	118.063	$C_5H_{10}O_3$	M-H	↑***	lactic acidosis
25	LysoPC(0:0/16:0)	495.3325	$C_{24}H_{50}NO_7P$	M + Cl	↓*	lysophospholipid
26	LysoPE (P-18:0/0:0)	465.3219	$C_{23}H_{48}NO_6P$	M-H	↑*	lysophospholipid
27	*N*-Stearoyl Methionine	415.312	$C_{23}H_{45}NO_3S$	M + Na	↑**	N-acylamides
28	*N*-Nervonoyl Threonine	467.3975	$C_{28}H_{53}NO_4$	M + K	↑**	N-acylamides
29	Cholyltyrosine	571.3509	$C_{33}H_{49}NO_7$	M + H	↑*	bile acid-amino acid conjugates
30	Cholylhistidine	545.3465	$C_{30}H_{47}N_3O_6$	M + H	↓**	bile acid-amino acid conjugates
31	PA (5-iso PGF2VI/8:0)	606.3169	$C_{29}H_{51}O_{11}P$	M-H	↓*	oxidized phosphatidic acid
32	DG (PGD2/0:0/10:0)	580.3975	$C_{33}H_{56}O_8$	M + Cl	↓*	triacylglycerol
33	DG (20:4 (7*E*,9*E*,11*Z*,13*E*)-3OH (5*S*,6*R*,15*S*)/0:0/8:0)	552.3662	$C_{31}H_{52}O_8$	M + Cl	↓**	triacylglycerol
34	DG (20:3 (8*Z*,11*Z*,14*Z*)-2OH (5,6)/0:0/8:0)	538.387	$C_{31}H_{54}O_7$	M + H	↑*	triacylglycerol
35	5-Methoxyindoleacetate	205.0739	$C_{11}H_{11}NO_3$	M-H20-H	↑**	Tryptophan metabolism
36	Prolylphenylalanine	262.1317	$C_{14}H_{18}N_2O_3$	M + Cl	↑**	dipeptide
37	Acetamidopropanal	115.0633	$C_5H_9NO_2$	M + H	↑***	polyamine metabolism
38	Hypoxanthine	136.0385	$C_5H_4N_4O$	M-H	↓*	Purine metabolism
39	LysoPC (0:0/20:4 (5*Z*,8*Z*,11*Z*,14*Z*))	543.3325	$C_{28}H_{50}NO_7P$	M + Cl	↓*	lysophospholipid
40	*L*-proline	115.0633	C_5 H_9 N O_2	GC-MS	↑***	Arginine and proline metabolism
41	Butanoic acid	117.0426	$C_4H_7NO_3$	GC-MS	↑**	Butanoate metabolism
42	Citrulline	175.0957	$C_6H_{13}N_3O_3$	GC-MS	↑***	Arginine biosynthesis
43	Acetylglycine	116.921	$C_4H_7NO_3$	GC-MS	↑*	Acetylglycine
44	*L*-Pyroglutamic acid	129.0426	$C_5H_7NO_3$	GC-MS	↑*	Glutathione metabolism
45	Methoxyacetic acid	90.0317	$C_3H_6O_3$	GC-MS	↑*	a secondary metabolite

(Continued on following page)

TABLE 1 (*Continued*) Major potential biomarkers of AD model group induced by *D*-Gal/$AlCl_3$ and related metabolic pathways.

No.	Metabolite	Exact mass	Formula	Adduct/ method	Trend	Related pathway
46	Urea	60.0324	CH_4N_2O	GC-MS	↑*	Arginine biosynthesis
47	Cholesterol	386.3549	$C_{27}H_{46}O$	GC-MS	↑*	Primary bile acid biosynthesis
48	3-Hydroxybutyric acid	248.1264	$C_4H_8O_3$	GC-MS	↑*	Butanoate metabolism
49	Lactic acid	90.0317	$C_3H_6O_3$	GC-MS	↑**	Glycolysis/Gluconeogenesis

Note, ↑ and ↓ values denote an increase and decrease, respectively. *$p < 0.05$, **$p < 0.01$, compared with the CN, group.

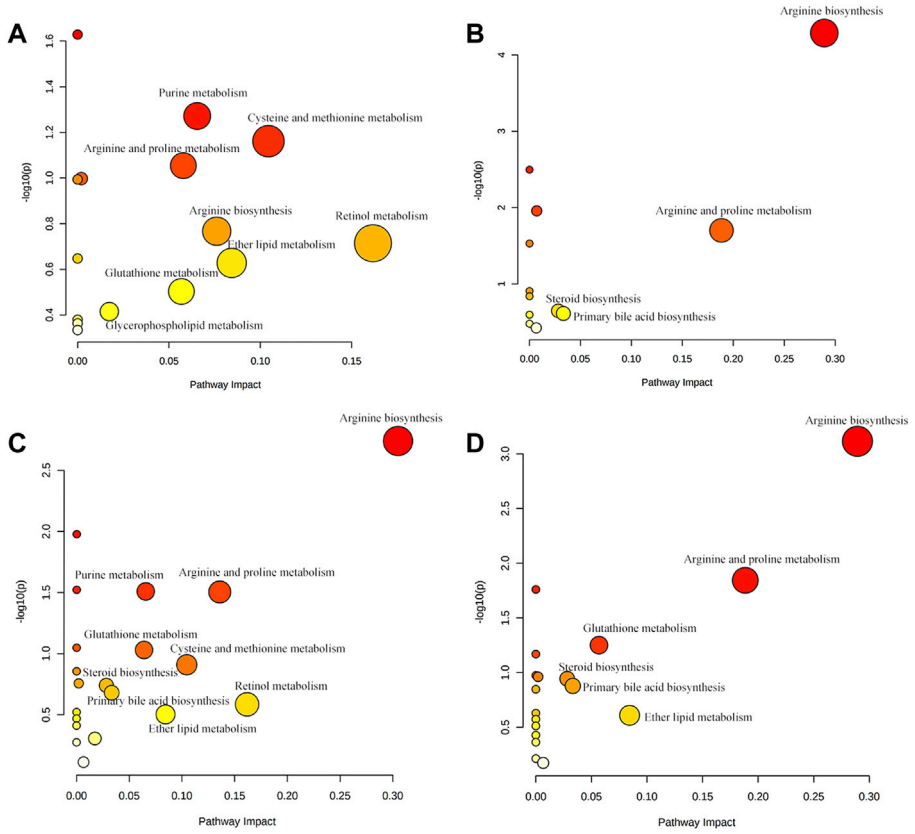

FIGURE 6
(A) Main metabolic pathways of potential biomarkers analyzed by LC-QTOF/MS. **(B)** Main metabolic pathways of potential biomarkers analyzed by GC-MS **(C)** The main metabolic pathways of potential biomarkers analyzed by LC-QTOF/MS and GC-MS. **(D)** Regulatory pathway analysis of AR treatment.

techniques was used to describe the characters of AD rats. Metabolites diversity and broad dynamic range in cellular abundance currently prohibit the possibility of using single-analysis procedures to measure all metabolites. Many combinations of analytical methods have been developed to achieve adequate metabolite coverage (Alseekh et al., 2021). GC-MS or LC-QTOF/MS in metabolomics analysis takes advantage of the high separation efficiency of the chromatographic system and the high sensitivity of MS detection (Kiseleva et al., 2021). Samples should be collected appropriately and extracted to maintain analyte yield in these two methods; however, samples for GC–MS must be performed an additional step, derivatization, to prevent degradation of the molecules at high temperatures and increase the volatility of the volatility metabolites (Zeki et al., 2020). In our study, a total of 39 metabolites were found significantly altered in the AD group with the LC-QTOF/MS metabolomics platform. With the continuous improvements in the related technologies, LC-

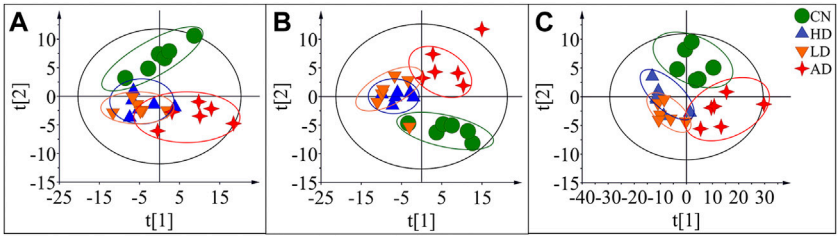

FIGURE 7
PLS-DA score plots of the serum samples from CN group, AD group, LD group, and HD group in positive mode of LC-QTOF/MS **(A)**, negative mode of LC-QTOF/MS **(B)**, and in GC-MS**(C)**.

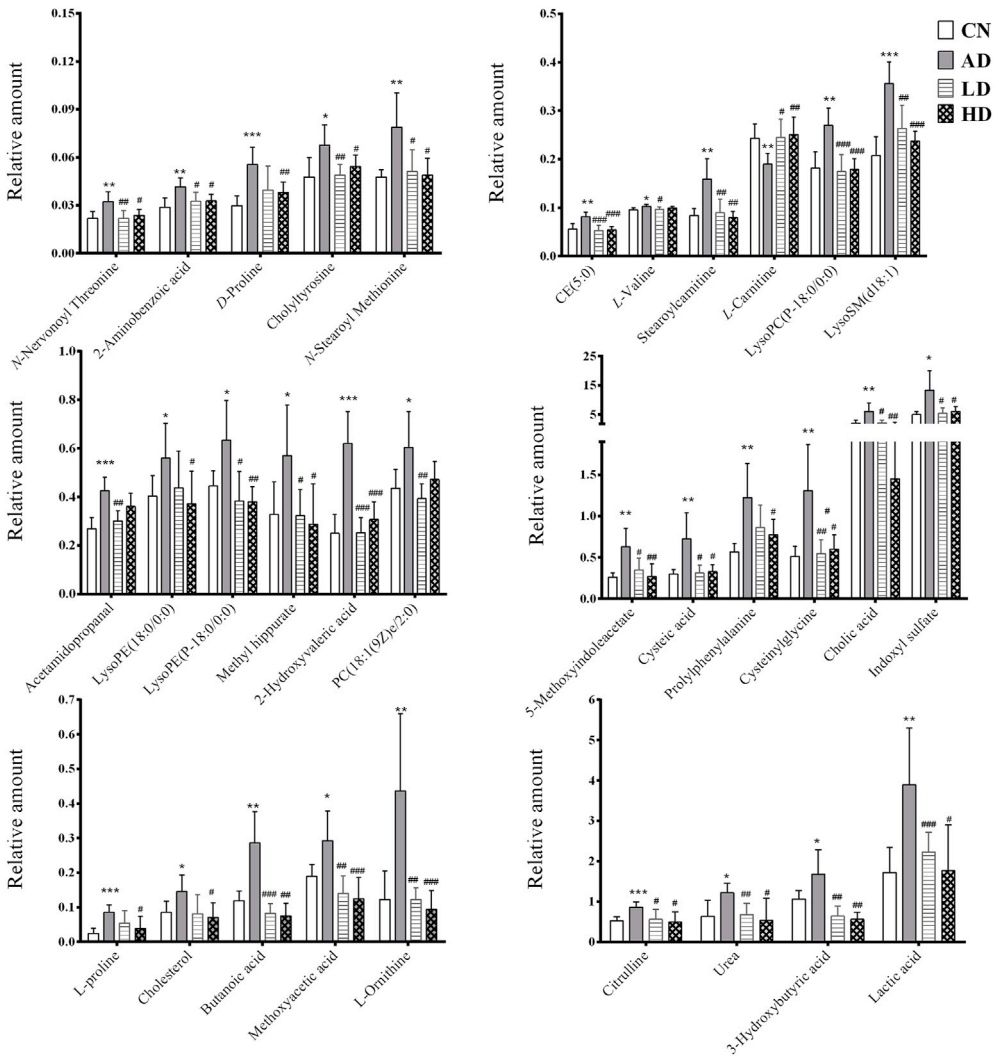

FIGURE 8
Potential biomarkers associated with AR pre-treatment in rat serum in positive mode of LC-QTOF/MS, negative mode of LC-QTOF/MS, and GC-MS. *$p < 0.05$, **$p < 0.01$, compared with CN group; #$p < 0.05$, ##$p < 0.01$, compared with AD group.

QTOF/MS has unequivocally become an established informative technique for metabolomics studies and has been utilized mostly (Khamis et al., 2017; Chaleckis et al., 2019). Previous studies have concluded that a vast number of metabolites studied using the LC-QTOF/MS platform could help shed light on alteration in the metabolic pathway in AD (Reveglia et al., 2021). Yet it is worth noting that, in this research, a total of 10 low molecular weight metabolites such as butanoic acid, citrulline, urea, cholesterol, and lactic acid were detected, and nine of which had not been identified by the LC-QTOF/MS method. GC-MS is the most suitable alternative for identifying volatile and semi-volatile metabolites. It has been widely employed to profile low molecular weight metabolites in AD research, such as free fatty acids, cholesterol derivatives neurotransmitters, and others (Luan et al., 2019; Kiseleva et al., 2021). In this research, the combination of GC-MS with LC-QTOF/MS also achieved a comprehensive pathway analysis result.

The development of proteinopathies, specifically the accumulation of the protein beta-amyloid and the cytotoxic aggregates of twisted tau protein, are the main features of AD. Without being sure of the mechanistic roles of the proteinopathies in the pathogenesis of AD, pathogenic protein aggregation remains strongly implicated in AD. Previous research elucidated that arginine could prevent the misfolding and aggregation of proteins and predicted that arginine might also prevent the aggregation and cytotoxicity of amyloidogenic proteins, particularly amyloid-beta and tau in AD (Mamsa and Meloni, 2021). However, accruing evidence suggests the alterations in polyamine homeostasis, such as the increase of arginine, are adaptive and beneficial when they follow a moderate temporary stimulus. In contrast, a maladaptive polyamine response will contribute to malfunction and degeneration (Polis et al., 2021). In our experiment, serum arginine level was found to be increased in the AD model group. And also, some metabolites such as arginine, citrulline, urea, proline, and some other metabolites related to arginine biosynthesis and metabolism were found to be altered in the AD model group. The pathways of arginine biosynthesis, arginine and proline metabolism were also concluded to be the top five crucial pathways with our pathway analysis. With the pre-treatment of AR, citrulline, urea, and proline were observed to correct to the control group. As some researches showed, there were AD- and age-related changes in the tissue concentrations of *L*-arginine and its downstream metabolites (*L*-citrulline, *L*-ornithine, glutamate, and glutamine, and some other metabolites) in a metabolite manner, which is in accord with our metabolomics results and the memory impairment of model mice in our behavior study (Liu et al., 2014).

Oxidative stress is one of the critical pathological events contributing to the degenerating cascades in AD (Ionescu-Tucker and Cotman, 2021). MDA is one of the best investigated products of oxidative stress, and the higher concentration of MDA is always measured in biological samples as biomarkers of lipid peroxidation (Tsikas, 2017). With the low antioxidant enzyme levels and high oxygen consumption, the central nervous system is vulnerable to oxidative stress (Kumar et al., 2017). Glutathione (GSH) is an essential antioxidant with important functions related to AD and is tightly linked to other redox mechanisms GSH, and GSH-associated metabolism represents the primary defense for the protection of cells from oxidative stress, while the extracellular redox state is mainly maintained by cysteine/cystine (Haddad et al., 2021). Pyroglutamic acid, also called 5-oxoproline, pyroglutamic acid, is a product of disordered glutathione metabolism, and elevated blood levels may be associated with problems of glutathione metabolism (Liss et al., 2013). Cysteinyl-glycine is a dipeptide composed of cysteine and glycine derived from the breakdown of GSH. In our experiment, both the serum levels of pyroglutamic acid and cysteinyl-glycine were found to be increased in the AD model group induced by *D*-Gal/$AlCl_3$, accompanying glutathione metabolism disorders in the AD model group. With the pre-treatment of AR, the glutathione metabolism pathway was regulated, and levels of cysteinyl-glycine decreased significantly. These results were in accord with biochemical analyses in which the contents of MDA in the hippocampus of the AD model group were significantly increased, and SOD levels in the hippocampus of the AD model group were decreased significantly, all of which were regulated by the pre-treatment of AR.

ACh is a signal transmitter of cholinergic neurons and has a vital role in cognitive processes. The metabolic process ACh is closely related to AD. ACh is involved in the modulation of acquisition, encoding, consolidation, reconsolidation, extinction, and memory retrieval (Ferreira-Vieira et al., 2016). It has been reported that the specific degeneration of cholinergic neurons occurs in AD and contributes to the memory loss exhibited by AD patients (Li et al., 2017). In this research, with the pre-treatment of AR, Ach was observed to correct to the control group. The behavior study results indicated that AR could prevent and ameliorate the impairment of spatial learning and memory of AD model rats induced by *D*-Gal and $AlCl_3$. NO is produced from the metabolism of *L*-arginine and is characterized as an unconventional neurotransmitter (Zuccarello et al., 2020). The role of NO in AD remains controversial since there are studies suggesting a neuroprotective function, while others support a neurotoxic action; however, abnormal NO signaling in the brain is one of AD's characteristics. It has been reported that excessive NO reacts with oxygen anion superoxide to form peroxynitrite and cause cellular damage (Calabrese et al., 2007). This research found increased NO concentration in the hippocampus in the AD model group compared to the control group, and AR pre-treatment decreased NO. The results indicated that NO in AD might remain a neurotoxic action and AR might havie neuroprotective function.

Conclusion

This research was undertaken to clarify AR's therapeutic effect and mechanism on AD based on multi-platform metabolomics analyses. The rat model of AD was established by *D*-galactose and $AlCl_3$. A serum metabolomics approach, combined with behavior study, histopathological observations, and biochemical analyses, was used to identify metabolic changes in AD model rats and to evaluate the effects of AR. A total of 49 metabolites related to the pathways of the arginine biosynthesis, arginine and proline metabolism, ether lipid metabolism, glutathione metabolism, and some other pathways were identified in the serum of AD rats. Biological interpretation of metabolite profiles illustrated that treatment with AR influenced arginine biosynthesis and metabolism, cysteine and methionine metabolism, purine metabolism, and glutathione metabolism the most in the pathogenesis of AD. The results that the cognitive dysfunctions, pathophysiological changes, and indexes of biochemical analyses of the AD model rat were reversed by pre-treatment with AR verified disturbance of pathways and the regulation of AR on AD. These results provide metabolomic evidence for the efficacy of AR in AD treatment. However, the mechanism of how AR influence these pathways and which active ingredients are absorbed into the blood and act on AD targets need validation. Validating these results and excavating the therapeutic mechanism of AR on AD intervention would be of considerable interest in the future.

Data availability statement

The original contributions presented in the study are included in the article/supplementary material, further inquiries can be directed to the corresponding authors.

Ethics statement

The animal study was reviewed and approved by Animal Ethics Committee of the institution of Naval Medical University.

Author contributions

Conceptualization, HW and J-YD; methodology, J-YD; software, HW; validation, Y-ZH, Z-WX, and X-FC; data curation, HW; writing—original draft preparation, HW and J-YD; writing—review and editing, Z-YH; supervision, Z-YH and Y-FC; project administration, Z-YH; funding acquisition, Z-YH. All authors have read and agreed to the published version of the manuscript.

Funding

This research was funded by National Natural Science Foundation of China, grant number 81872829 and 81673386.

Conflict of interest

The authors declare that the research was conducted in the absence of any commercial or financial relationships that could be construed as a potential conflict of interest.

The reviewer AL declared a shared affiliation, with the authors to the handling editor at the time of the review.

Publisher's note

References

Alseekh, S., Aharoni, A., Brotman, Y., Contrepois, K., D'Auria, J., Ewald, J., et al. (2021). Mass spectrometry-based metabolomics: a guide for annotation, quantification and best reporting practices. *Nat. Methods* 18 (7), 747–756. doi:10.1038/s41592-021-01197-1

Athar, T., Al Balushi, K., and Khan, S. A. (2021). Recent advances on drug development and emerging therapeutic agents for alzheimer's disease. *Mol. Biol. Rep.* 48 (7), 5629–5645. doi:10.1007/s11033-021-06512-9

Badhwar, A., McFall, G. P., Sapkota, S., Black, S. E., Chertkow, H., Duchesne, S., et al. (2020). A multiomics approach to heterogeneity in alzheimer's disease: focused review and roadmap. *Brain* 143 (5), 1315–1331. doi:10.1093/brain/awz384

Benek, O., Korabecny, J., and Soukup, O. (2020). A perspective on multi-target drugs for Alzheimer's disease. *Trends Pharmacol. Sci.* 41 (7), 434–445. doi:10.1016/j.tips.2020.04.008

Calabrese, V., Mancuso, C., Calvani, M., Rizzarelli, E., Butterfield, D. A., Stella, A. M., et al. (2007). Nitric oxide in the central nervous system: neuroprotection versus neurotoxicity. *Nat. Rev. Neurosci.* 8 (10), 766–775. doi:10.1038/nrn2214

Chaleckis, R., Meister, I., Zhang, P., and Wheelock, C. E. (2019). Challenges, progress and promises of metabolite annotation for LC-MS-based metabolomics. *Curr. Opin. Biotechnol.* 55, 44–50. doi:10.1016/j.copbio.2018.07.010

Chen, S. Y., Gao, Y., Sun, J. Y., Meng, X. L., Yang, D., Fan, L. H., et al. (2020). Traditional Chinese medicine: role in reducing beta-amyloid, apoptosis, autophagy, neuroinflammation, oxidative stress, and mitochondrial dysfunction of alzheimer's disease. *Front. Pharmacol.* 11, 497. doi:10.3389/fphar.2020.00497

Cuperlovic-Culf, M., and Badhwar, A. (2020). Recent advances from metabolomics and lipidomics application in alzheimer's disease inspiring drug discovery. *Expert Opin. Drug Discov.* 15 (3), 319–331. doi:10.1080/17460441.2020.1674808

Ferreira-Vieira, T. H., Guimaraes, I. M., Silva, F. R., and Ribeiro, F. M. (2016). Alzheimer's disease: Targeting the cholinergic system. *Curr. Neuropharmacol.* 14 (1), 101–115. doi:10.2174/1570159x13666150716165726

Gonzalez-Dominguez, R., Sayago, A., and Fernandez-Recamales, A. (2017). Metabolomics in alzheimer's disease: the need of complementary analytical platforms for the identification of biomarkers to unravel the underlying pathology. *J. Chromatogr. B Anal. Technol. Biomed. Life Sci.* 1071, 75–92. doi:10.1016/j.jchromb.2017.02.008

Haddad, M., Herve, V., Ben Khedher, M. R., Rabanel, J. M., and Ramassamy, C. (2021). Glutathione: an old and small molecule with great functions and new applications in the brain and in alzheimer's disease. *Antioxid. Redox Signal.* 35 (4), 270–292. doi:10.1089/ars.2020.8129

Hu, Y., Xia, Z., Sun, Q., Orsi, A., and Rees, D. (2005). A new approach to the pharmacological regulation of memory: Sarsasapogenin improves memory by elevating the low muscarinic acetylcholine receptor density in brains of memory-deficit rat models. *Brain Res.* 1060 (1-2), 26–39. doi:10.1016/j.brainres.2005.08.019

Huang, J. F., Shang, L., Liu, P., Zhang, M. Q., Chen, S., Chen, D., et al. (2012). Timosaponin-BII inhibits the up-regulation of BACE1 induced by ferric chloride in rat retina. *BMC Complement. Altern. Med.* 12, 189. doi:10.1186/1472-6882-12-189

Husain, A., Al Balushi, K., Akhtar, M. J., and Khan, S. A. (2021). Coumarin linked heterocyclic hybrids: a promising approach to develop multi target drugs for alzheimer's disease. *J. Mol. Struct.* 1241, 130618. doi:10.1016/j.molstruc.2021.130618

Ionescu-Tucker, A., and Cotman, C. W. (2021). Emerging roles of oxidative stress in brain aging and alzheimer's disease. *Neurobiol. Aging* 107, 86–95. doi:10.1016/j.neurobiolaging.2021.07.014

Khamis, M. M., Adamko, D. J., and El-Aneed, A. (2017). Mass spectrometric based approaches in urine metabolomics and biomarker discovery. *Mass Spectrom. Rev.* 36 (2), 115–134. doi:10.1002/mas.21455

Kiseleva, O., Kurbatov, I., Ilgisonis, E., and Poverennaya, E. (2021). Defining blood plasma and serum metabolome by GC-MS. *Metabolites* 12 (1), 15. doi:10.3390/metabo12010015

Kumar, A., Dhull, D. K., Gupta, V., Channana, P., Singh, A., Bhardwaj, M., et al. (2017). Role of Glutathione-S-transferases in neurological problems. *Expert Opin. Ther. Pat.* 27 (3), 299–309. doi:10.1080/13543776.2017.1254192

Li, T.-J., Qiu, Y., Yang, P.-Y., Rui, Y.-C., and Chen, W.-S. (2007). Timosaponin B-II improves memory and learning dysfunction induced by cerebral ischemia in rats. *Neurosci. Lett.* 421 (2), 147–151. doi:10.1016/j.neulet.2007.04.082

Li, Q., Yang, H., Chen, Y., and Sun, H. (2017). Recent progress in the identification of selective butyrylcholinesterase inhibitors for alzheimer's disease. *Eur. J. Med. Chem.* 132, 294–309. doi:10.1016/j.ejmech.2017.03.062

Liss, D. B., Paden, M. S., Schwarz, E. S., and Mullins, M. E. (2013). What is the clinical significance of 5-oxoproline (pyroglutamic acid) in high anion gap metabolic acidosis following paracetamol (acetaminophen) exposure? *Clin. Toxicol.* 51 (9), 817–827. doi:10.3109/15563650.2013.844822

Liu, P., Fleete, M. S., Jing, Y., Collie, N. D., Curtis, M. A., Waldvogel, H. J., et al. (2014). Altered arginine metabolism in alzheimer's disease brains. *Neurobiol. Aging* 35 (9), 1992–2003. doi:10.1016/j.neurobiolaging.2014.03.013

Liu, T., Song, Y., and Hu, A. (2021). Neuroprotective mechanisms of mangiferin in neurodegenerative diseases. *Drug Dev. Res.* 82 (4), 494–502. doi:10.1002/ddr.21783

Lu, W.-Q., Qiu, Y., Li, T.-J., Tao, X., Sun, L.-N., Chen, W.-S., et al. (2009). Timosaponin B-II inhibits pro-inflammatory cytokine induction by lipopolysaccharide in BV2 cells. *Arch. Pharm. Res.* 32 (9), 1301–1308. doi:10.1007/s12272-009-1916-4

Luan, H., Wang, X., and Cai, Z. (2019). Mass spectrometry-based metabolomics: Targeting the crosstalk between gut microbiota and brain in neurodegenerative disorders. *Mass Spectrom. Rev.* 38 (1), 22–33. doi:10.1002/mas.21553

Mamsa, S. S. A., and Meloni, B. P. (2021). Arginine and arginine-rich peptides as modulators of protein aggregation and cytotoxicity associated with alzheimer's disease. *Front. Mol. Neurosci.* 14, 759729. doi:10.3389/fnmol.2021.759729

Olsson, B., Lautner, R., Andreasson, U., Ohrfelt, A., Portelius, E., Bjerke, M., et al. (2016). CSF and blood biomarkers for the diagnosis of alzheimer's disease: a systematic review and meta-analysis. *Lancet. Neurol.* 15 (7), 673–684. doi:10.1016/S1474-4422(16)00070-3

Polis, B., Karasik, D., and Samson, A. O. (2021). Alzheimer's disease as a chronic maladaptive polyamine stress response. *Aging (Albany NY)* 13 (7), 10770–10795. doi:10.18632/aging.202928

Reveglia, P., Paolillo, C., Ferretti, G., De Carlo, A., Angiolillo, A., Nasso, R., et al. (2021). Challenges in LC-MS-based metabolomics for alzheimer's disease early detection: targeted approaches versus untargeted approaches. *Metabolomics.* 17 (9), 78. doi:10.1007/s11306-021-01828-w

Sun, L. M., Zhu, B. J., Cao, H. T., Zhang, X. Y., Zhang, Q. C., Xin, G. Z., et al. (2018). Explore the effects of Huang-Lian-Jie-Du-Tang on alzheimer's disease by UPLC-QTOF/MS-based plasma metabolomics study. *J. Pharm. Biomed. Anal.* 151, 75–83. doi:10.1016/j.jpba.2017.12.053

Tsikas, D. (2017). Assessment of lipid peroxidation by measuring malondialdehyde (MDA) and relatives in biological samples: analytical and biological challenges. *Anal. Biochem.* 524, 13–30. doi:10.1016/j.ab.2016.10.021

Wang, W., Wang, W., Yao, G., Ren, Q., Wang, D., Wang, Z., et al. (2018). Novel sarsasapogenin-triazolyl hybrids as potential anti-alzheimer's agents: design, synthesis and biological evaluation. *Eur. J. Med. Chem.* 151, 351–362. doi:10.1016/j.ejmech.2018.03.082

Wang, H. Q., Liu, M., Wang, L., Lan, F., Zhang, Y. H., Xia, J. E., et al. (2020). Identification of a novel BACE1 inhibitor, timosaponin A-III, for treatment of alzheimer's disease by a cell extraction and chemogenomics target knowledgebase-guided method. *Phytomedicine* 75, 153244. doi:10.1016/j.phymed.2020.153244

Wang, F., Wang, J., Shen, Y., Li, H., Rausch, W. D., Huang, X., et al. (2022). Iron dyshomeostasis and ferroptosis: a new alzheimer's disease hypothesis? *Front. Aging Neurosci.* 14, 830569. doi:10.3389/fnagi.2022.830569

Xia, X., Wang, Y., and Zheng, J. (2021). COVID-19 and alzheimer's disease: how one crisis worsens the other. *Transl. Neurodegener.* 10 (1), 15. doi:10.1186/s40035-021-00237-2

Xie, J., Liang, R., Wang, Y., Huang, J., Cao, X., Niu, B., et al. (2020). Progress in target drug molecules for alzheimer's disease. *Curr. Top. Med. Chem.* 20 (1), 4–36. doi:10.2174/1568026619666191203113745

Yi, L., Liu, W., Wang, Z., Ren, D., and Peng, W. (2017). Characterizing Alzheimer's disease through metabolomics and investigating anti-alzheimer's disease effects of natural products. *Ann. N. Y. Acad. Sci.* 1398 (1), 130–141. doi:10.1111/nyas.13385

Zeki, O. C., Eylem, C. C., Recber, T., Kir, S., and Nemutlu, E. (2020). Integration of GC-MS and LC-MS for untargeted metabolomics profiling. *J. Pharm. Biomed. Anal.* 190, 113509. doi:10.1016/j.jpba.2020.113509

Zhang, Z., Yi, P., Yang, J., Huang, J., Xu, P., Hu, M., et al. (2020). Integrated network pharmacology analysis and serum metabolomics to reveal the cognitive improvement effect of Bushen Tiansui formula on alzheimer's disease. *J. Ethnopharmacol.* 249, 112371. doi:10.1016/j.jep.2019.112371

Zuccarello, E., Acquarone, E., Calcagno, E., Argyrousi, E. K., Deng, S. X., Landry, D. W., et al. (2020). Development of novel phosphodiesterase 5 inhibitors for the therapy of alzheimer's disease. *Biochem. Pharmacol.* 176, 113818. doi:10.1016/j.bcp.2020.113818

frontiers | Frontiers in Pharmacology

TYPE Brief Research Report
PUBLISHED 27 September 2022
DOI 10.3389/fphar.2022.936632

OPEN ACCESS

EDITED BY
Yi Wang,
Zhejiang University, China

REVIEWED BY
Yule Wang,
Zhejiang University, China
Guang-Xian Zhang,
Thomas Jefferson University,
United States

*CORRESPONDENCE
Yanjie Tian,
tianyanjietongxun@163.com

†These authors have contributed equally to this work and share first authorship

SPECIALTY SECTION
This article was submitted to Neuropharmacology, a section of the journal Frontiers in Pharmacology

RECEIVED 05 May 2022
ACCEPTED 15 August 2022
PUBLISHED 27 September 2022

CITATION
Song Y, Wang M, Zhao S, Tian Y and Zhang C (2022), Matrine promotes mitochondrial biosynthesis and reduces oxidative stress in experimental optic neuritis.
Front. Pharmacol. 13:936632.
doi: 10.3389/fphar.2022.936632

Matrine promotes mitochondrial biosynthesis and reduces oxidative stress in experimental optic neuritis

Yifan Song[1,2†], Mengru Wang[3†], Suyan Zhao[1,2], Yanjie Tian[1,2*] and Chun Zhang[1,2]

[1]Department of Ophthalmology, Peking University Third Hospital, Beijing, China, [2]Beijing Key Laboratory of Restoration of Damaged Ocular Nerve, Peking University Third Hospital, Beijing, China, [3]Department of Pharmacology, School of Basic Medical Sciences, Zhengzhou University, Zhengzhou, China

Optic neuritis (ON), characterized by inflammation of the optic nerve and apoptosis of retinal ganglion cells (RGCs), is one of the leading causes of blindness in patients. Given that RGC, as an energy-intensive cell, is vulnerable to mitochondrial dysfunction, improving mitochondrial function and reducing oxidative stress could protect these cells. Matrine (MAT), an alkaloid derived from *Sophora flavescens*, has been shown to regulate immunity and protect neurons in experimental autoimmune encephalomyelitis (EAE), an animal model of multiple sclerosis and ON. However, the protective mechanism of MAT on RGCs is largely unknown. In this study, we show that MAT treatment significantly reduced the degree of inflammatory infiltration and demyelination of the optic nerve and increased the survival rate of RGCs. The expression of Sirtuin 1 (SIRT1), a member of an evolutionarily conserved gene family (sirtuins), was upregulated, as well as its downstream molecules Nrf2 and PGC-1α. The percentage of TOMM20-positive cells was also increased remarkably in RGCs after MAT treatment. Thus, our results indicate that MAT protects RGCs from apoptosis, at least in part, by activating SIRT1 to regulate PGC-1α and Nrf2, which, together, promote mitochondrial biosynthesis and reduce the oxidative stress of RGCs.

KEYWORDS

matrine, optic neuritis, mitochondrial biosynthesis, oxidative stress, SIRT1, PGC-1α, Nrf2

Introduction

Optic neuritis (ON), a common cause of visual defects in young people, is an inflammatory disease of the optic nerve, which is characterized by immune cell infiltration and subsequent demyelination (Kobayter and Chetty, 2019; Pihl-Jensen et al., 2021). Patients typically experience a sharp decrease in vision, orbital pain aggravated by eye movements, an afferent papillary defect, and dyschromatopsia, with

or without swelling of the optic nerve head. ON is the initial manifestation in approximately 20% of multiple sclerosis (MS) patients, and 50% of ON patients will develop MS during the disease (Kimura et al., 2017). Severe, even irreversible, visual loss can occur in ON, neuromyelitis optica (NMO), and experimental autoimmune encephalomyelitis (EAE), an animal model of MS (Azuchi et al., 2017).

There is increasing evidence that irreversible vision loss may result from inflammation of the optic nerve and apoptosis of the retinal ganglion cells (RGCs) (Liu et al., 2017; Zhang et al., 2020). Because the long axons of RGCs are vulnerable to lack of energy, they are highly reliant on mitochondria and are sensitive to mitochondrial dysfunction and oxidative stress (Lin and Kuang, 2014). Indeed, mitochondrial oxidative stress can induce neuronal damage in experimental ON (EON) (Qi et al., 2007). The activation of sirtuin 1 (SIRT1), a member of an evolutionarily conserved gene family (sirtuins) encoding NAD+ dependent deacetylases that regulates various components of cellular metabolism (Martin et al., 2015), can prevent RGC loss in ON by reducing oxidative stress and promoting mitochondrial function in neuronal cell lines (Khan et al., 2012). SIRT1 may function *via* regulating the expression of peroxisome proliferator-activated receptor γ coactivator-1α (PGC-1α), a metabolic coactivator that induces mitochondrial biogenesis and respiration by interacting with transcription factors (Finck and Kelly, 2006; Gerhart-Hines et al., 2007). SIRT1 also plays an important role in regulating the expression and activation of nuclear factor erythroid 2-related factor 2 (Nrf2) (Ding et al., 2016), a basic leucine zipper transcription factor that activates the gene network related to antioxidant defense and cell detoxification (Johnson and Johnson, 2015).

Matrine (MAT), a natural alkaloid component extracted from the herb Radix Sophorae Flavescentis, with a molecular weight (MW) of 258.43 (C15H24N2O), has been widely used in the clinical treatment of human hepatitis B and leukocytopenia with very few adverse reactions (Wang et al., 2017). Previous studies have shown that MAT can significantly improve the neural function of EAE and reduce central nervous system (CNS) and peripheral inflammatory responses (Kan et al., 2017; Zhang et al., 2017). Recent studies have shown that MAT can enhance mitochondrial function and inhibit oxidative stress in oligodendrocytes of EAE (Wang et al., 2019). In addition, we have conducted a preliminary exploration of the protective effect of MAT in RGCs in EON (Kang et al., 2021); however, the mechanism underlying this effect has not yet been elucidated. We focused on this issue in the present study and found that MAT regulates the expression and activation of PGC-1α and Nrf2 by activating SIRT1, promotes mitochondrial biosynthesis, and reduces oxidative stress, thus having a therapeutic effect on EON.

Materials and methods

Animals and EAE induction

Female Wistar rats (6–8 weeks old, 180–200 g) were purchased from the Jinan Pengyue Experimental Animal Breeding Co., Ltd., China, and raised under the condition of specific pathogens at the Laboratory Animal Center of the Henan Academy of Chinese Medicine, China. EAE was induced as described previously (Chu et al., 2021). Briefly, the spinal cord homogenate of guinea pigs (Jinan Jinfeng Experimental Animal Co., Ltd., China) was emulsified with the same volume of complete Freund's adjuvant (Sigma, St. Louis, MO, United States) containing 6 mg/ml Bacillus Calmette–Guérin vaccine (Solarbio Bio-Technology Co., Shanghai, China). Each rat was injected subcutaneously at four separate sites on the back with 0.5 ml of antigen emulsion.

Ethics approval and consent to participate

This study was approved by the Ethics Committee of Scientific Research of Henan Academy of Chinese Medicine; the ethical review number is HNTCMDW-20170601. All of the protocols were approved, and every effort was made to ensure minimal animal suffering.

MAT treatment and clinical scoring

The immunized rats were stochastically divided into three groups (n = 10, each group) (Kobayter and Chetty, 2019): EAE rats were injected intraperitoneally (i.p.) with 250 mg/kg/day MAT (Meilunbio, Dalian, China) (Kan et al., 2013) (Jiangsu Chia Tai-Tianqing Pharmaceutical Co. Ltd., Jiangsu, China), starting from day 11 after immunization (p.i.); EAE rats were injected intraperitoneally with the vehicle as a control group (Pihl-Jensen et al., 2021); and non-immunized rats i.p. injected with the vehicle were used as the naive control group (Kimura et al., 2017). From the date of immunization, changes in body weight, clinical signs, and neurological function scores were observed and recorded by two independent observers. The EAE model score uses the five-point scale: 0 = no clinical score; 1 = tail weakness; 2 = hind limb weakness; 3 = hind limb paralysis; 4 = forelimb paralysis; and 5 = moribund or death.

Histopathological evaluation

The rats were sacrificed on day 17 p.i. After extensive perfusion with physiological saline solution, the optic nerves and retinas were removed and post-fixed with FAS eyeball

fixative (Servicebio, Wuhan, China). The tissue was then embedded in paraffin and cut into 2–5 μm thick sections, dewaxed in xylene, and rehydrated. Hematoxylin–eosin (H&E) staining was used to detect inflammatory infiltration, and Luxol fast blue (LFB) staining was used to detect demyelination. The degree of infiltration of inflammatory cells and demyelination in the optic nerve was assessed by a double-blind investigator, similar to the open standard. For inflammation, 0 = no infiltration, 1 = a little cell infiltration of the optic nerve or optic nerve sheath, 2 = moderate infiltration, 3 = serious infiltration, and 4 = substantial infiltration. For demyelination, 0 = no demyelination, 1 = scattered demyelinating lesions, 2 = partial demyelinating lesion, and 3 = large number of demyelinating lesions. Scores of inflammation, infiltration, and demyelination were evaluated by Image-Pro Plus 6.0 software. Each experiment was repeated three times, and the results were averaged.

Immunofluorescence double labeling

Briefly, non-specific binding was blocked with 3% bovine serum albumin (BSA) (Serotec, United Kingdom) and permeabilized with 0.3% Triton X-100 in 1% BSA-PBS for 30 min. The sections were then incubated in blocking solution at 4°C overnight with primary antibodies specific for rabbit anti-Nrf2 (1:100), rabbit anti-SIRT1 (1:100), rabbit anti-PGC-1α (1:300), and rabbit anti-TOMM20 (1:250) (all from Abcam, Cambridge, United Kingdom) and then incubated with secondary antibody donkey anti-rabbit FITC (1:200; IgG; Proteintech, Wuhan, China) at room temperature (RT) for 2 h. After being permeabilized with 1% BSA-PBS for 3 × 5 min, the sections were incubated with rabbit anti-Brn3a (1:100; IgG; Bioss, Beijing, China) specific primary antibody in blocking solution overnight at 4°C, then incubated with secondary antibody donkey anti-rabbit Cy3 (1:200; IgG; Proteintech) at RT for 2 h, mounted with 4',6-diamidino-2-phenylindole (DAPI, 1:1,000; Roche, Basel, Switzerland), washed with PBS, cover-slipped, and examined under a fluorescence microscope (Leica Microsystem AG, Switzerland). As a negative control, additional sections were treated similarly, but the primary antibodies were omitted. All pictures were captured by a confocal microscope (Olympus Fluoview FV1000). For each group, ten sections were examined in a blinded fashion. Image-Pro Plus 6.0 software was used to calculate the quantification of target protein expression.

Cell Culture of RGC-5

Rat retinal ganglion cells (RGC-5) were purchased from iCell Bioscience Inc., Shanghai, China. Cells were maintained in Dulbecco's modified eagle medium (iCell Bioscience Inc., Shanghai) supplemented with 10% heat-inactivated fetal bovine serum (iCell Bioscience Inc., Shanghai) and in a humidified atmosphere containing 5% CO_2 at 37°C. RGC-5 cells were seeded into 6-well plates. Cells were treated in four groups: for the control group, 2 ml complete medium was added. For the TNF-α group, 2 ml of TNF-α (MedChemExpress, Shanghai, China) at a concentration of 50 ng/ml was added to the medium. For the MAT group, 2 ml (50 ng/ml) of TNF-α and 100 μM of MAT were added to the medium. For the MAT + Ex-527 group, 2 ml (50 ng/ml) of TNF-α, 100 μM of MAT, and 38 nM of EX527 (Beyotime Biotechnology, Shanghai, China) were added. All groups were cultured for 48 h before harvest.

Western Blot

After treatment, total protein from both cell lysate and the supernatant was isolated from N9 cells with RIPA lysis buffer (50 mM Tris-HCl, pH 7.4, 150 mM NaCl, 0.25% deoxycholic acid, 1% Nonidet P-40, one mM EDTA) including the protease and phosphatase inhibitor (Beyotime Biotechnology, Shanghai, China). For Western blot analysis, 8%–10% SDS-PAGE was used to resolve equal amounts of protein samples from both cell lysate and supernatant. The gel was transferred onto polyvinylidene fluoride (PVDF) membranes (Sigma-Aldrich, United States), and the membranes were blocked with 5% BSA in Tris-buffered saline containing 0.05% Tween-20 (TBST). Membranes were probed with primary antibodies at 4°C overnight. The following day, the incubated membranes were washed four times with TBST and then incubated with the horseradish peroxidase (HRP)-conjugated secondary antibodies. The antigen–antibody complex was screened by chemiluminescence using the Supersignal West Dura ECL reagent (Thermo Scientific, United States). Protein bands were detected with a densitometer (Bio-Rad, Shanghai). Band density analysis was performed with ImageJ software (National Institutes of Health, United States).

Measurement of mitochondrial membrane potential (ΔΨM)

For the measurement of mitochondrial membrane potential (ΔΨM), cells were harvested and stained with JC-1 (Beyotime Biotechnology, Shanghai, China) and Rhodamine 123 (Beyotime Biotechnology, Shanghai, China) and were quantified by flow cytometry analysis as described previously (Pal et al., 2020). JC-1 dye is a lipophilic, cationic dye developed to detect ΔΨM in healthy and apoptotic cells. After two washes with phosphate-buffered saline (PBS) to remove media, trypsin-treated cells were harvested, washed again with PBS, and then incubated in 500 μL JC-1 dye for 20 min. Samples were then washed with PBS once and analyzed immediately by an FACS analyzer (Luminex,

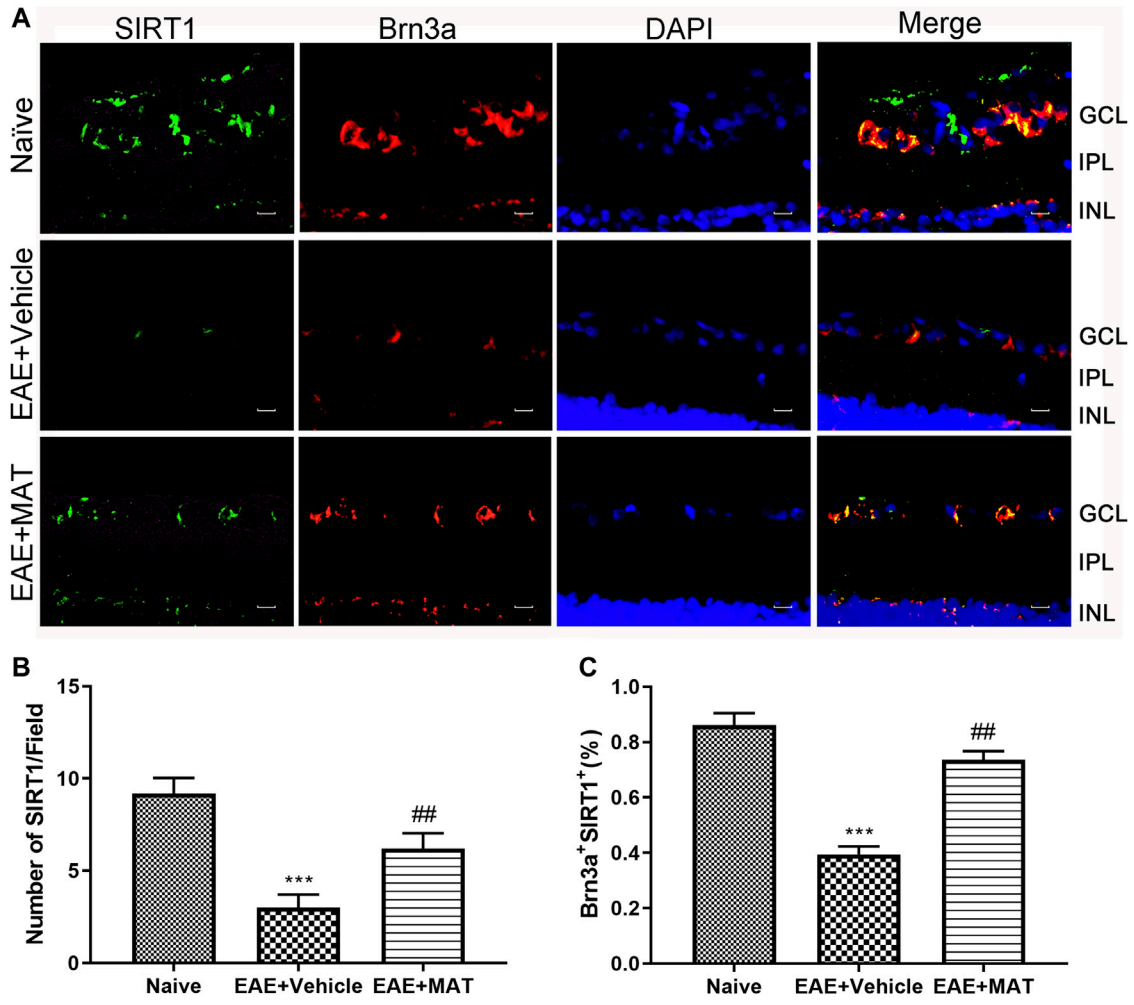

FIGURE 1
MAT promoted SIRT1 expression in RGCs. Eyeballs were harvested from naive rats, MAT- and vehicle-treated EAE rats. **(A)** Immunofluorescence double staining suggested that SIRT1 (FITC, green) were colocalized with Brn3a (Cy3, red) in the eyeball retina of EAE rats (200×). Scale bars, 10 μm. **(B)** Quantitative analysis of the number of positive cells. **(C)** Quantitative analysis of the rate of positive cells. Data represent mean ± SD; n = 10 rats per group. ** $p < 0.01$, *** $p < 0.001$, comparison between naive and vehicle-treated EAE groups. ## $p < 0.01$, comparison between vehicle- and MAT-treated EAE groups.

Guava® easyCyteTM). Rhodamine 123 is a cationic fluorescent dye. Treated cells were harvested and washed once with PBS and incubated with 500 μl of Rho123 dye (2 μM) for 30 min at a 37°C shaker incubator. After incubation, cells were washed with PBS and analyzed immediately by an FACS analyzer.

Statistical analyses

Multiple comparisons were performed using one-way ANOVA, followed by the Student–Newman–Keuls test. Clinical EAE scores and mean body weight were compared at individual time points between vehicle- and MAT-treated rats. Statistical software (GraphPad Prism 7.0, IBM SPSS Statistics 27) was used for statistical analyses; $p < 0.05$ was considered significant. Given that ON can occur bilaterally or unilaterally in either eye (Khan et al., 2017), each eye was used as an independent data point for all histological experiments.

Results

MAT alleviated the severity of optic neuropathology

As we reported before, MAT effectively suppresses CNS inflammation, demyelination, and axonal loss in optic nerves, as well as RGC apoptosis in EON (Kang et al., 2021). Briefly, we

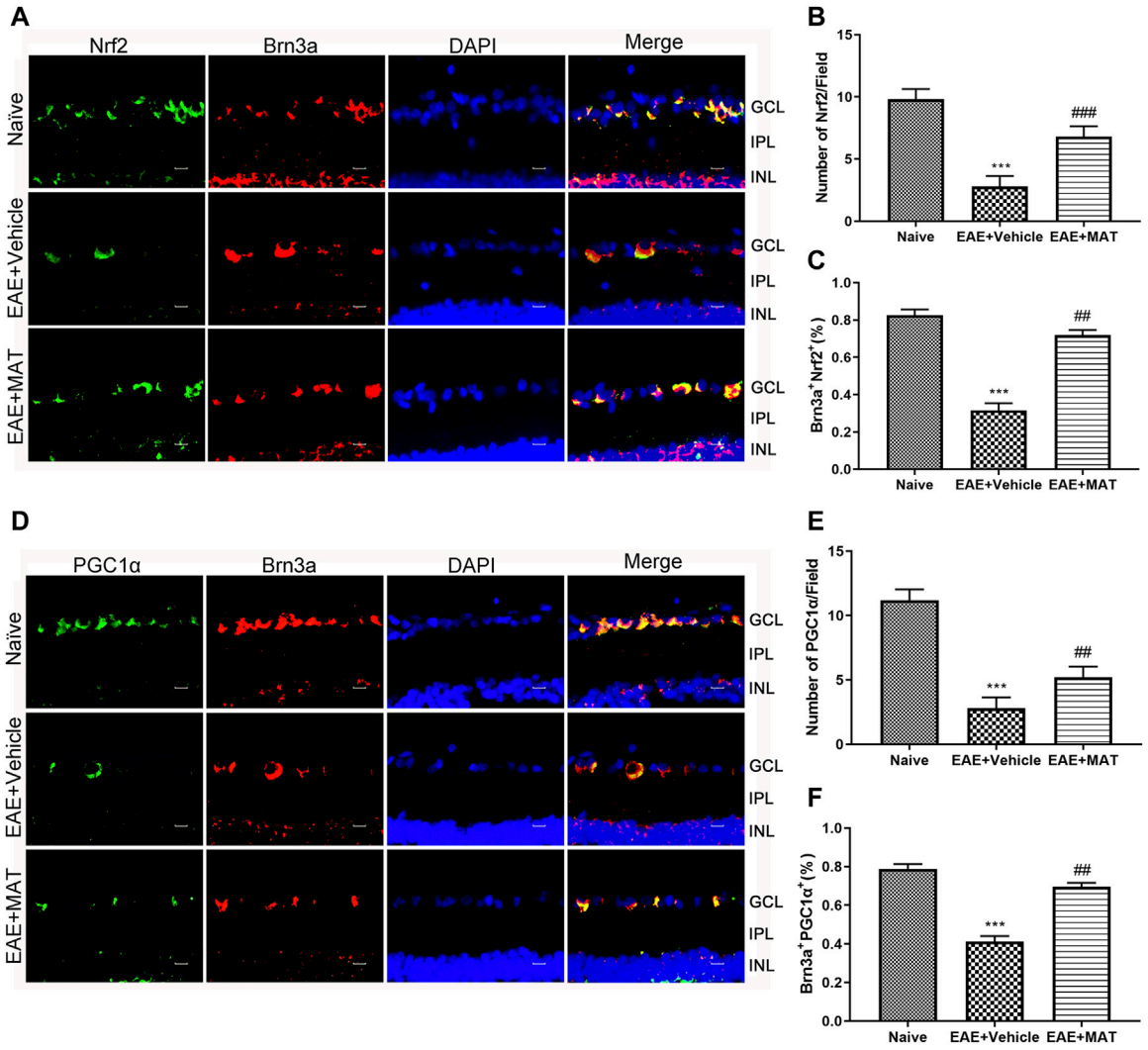

FIGURE 2
MAT elevated the expression of Nrf2 and PGC-1α. Eyeballs were harvested from naive rats, MAT- and vehicle-treated rats. **(A)** Immunofluorescence double staining suggested that Nrf2 (FITC, green) were colocalized with Brn3a (Cy3, red) (200×). Scale bars, 10 μm. **(B)** Quantitative analysis of the number of positive cells. **(C)** Quantitative analysis of the rate of positive cells. **(D)** Immunofluorescence double staining suggested that PGC-1α (FITC, green) were colocalized with Brn3a (Cy3, red) in the eyeball retina (200×). Scale bars, 10 μm. **(E)** Quantitative analysis of the number of positive cells. **(F)** Quantitative analysis of the rate of positive cells. Symbols represent mean ± SD; n = 10 rats per group. $^{**}p < 0.01$, $^{***}p < 0.001$, comparison between naive and vehicle-treated groups. $^{\#\#}p < 0.01$, comparison between vehicle- and MAT-treated EAE groups.

first induced an animal model of EON in Wister rats and then treated it from day 11 p.i., which resulted in a significant reduction in clinical scores for EAE and mitigation in weight loss in the MAT-treated group compared to saline-treated model rats. In order to verify the correlation between the clinical signs of EAE and EON, optic nerve transverses of all groups were examined by HE and LFB staining. Inflammatory infiltrates were diffusely distributed in the optic nerve of vehicle-treated rats, and this infiltration was significantly inhibited by MAT treatment. Furthermore, MAT treatment significantly reduced optic nerve demyelination compared to the EAE group (data shown in Supplementary Material).

MAT promoted SIRT1 expression in RGCs

To investigate the effect of MAT treatment on SIRT1 expression, we tested the number of cells that colocalized SIRT1 with Brn3a (RGCs marker) by immunofluorescence double staining. As shown in Figure 1A, it was observed on the paraffin section of the sagittal plane of the eye that the expression of SIRT1 was reduced in the vehicle-treated EAE rats compared with the naive rats. In contrast, its expression was significantly increased after treatment with MAT (Figures 1B,C). These results indicate an upregulating effect of MAT on the SIRT1 expression in RGCs.

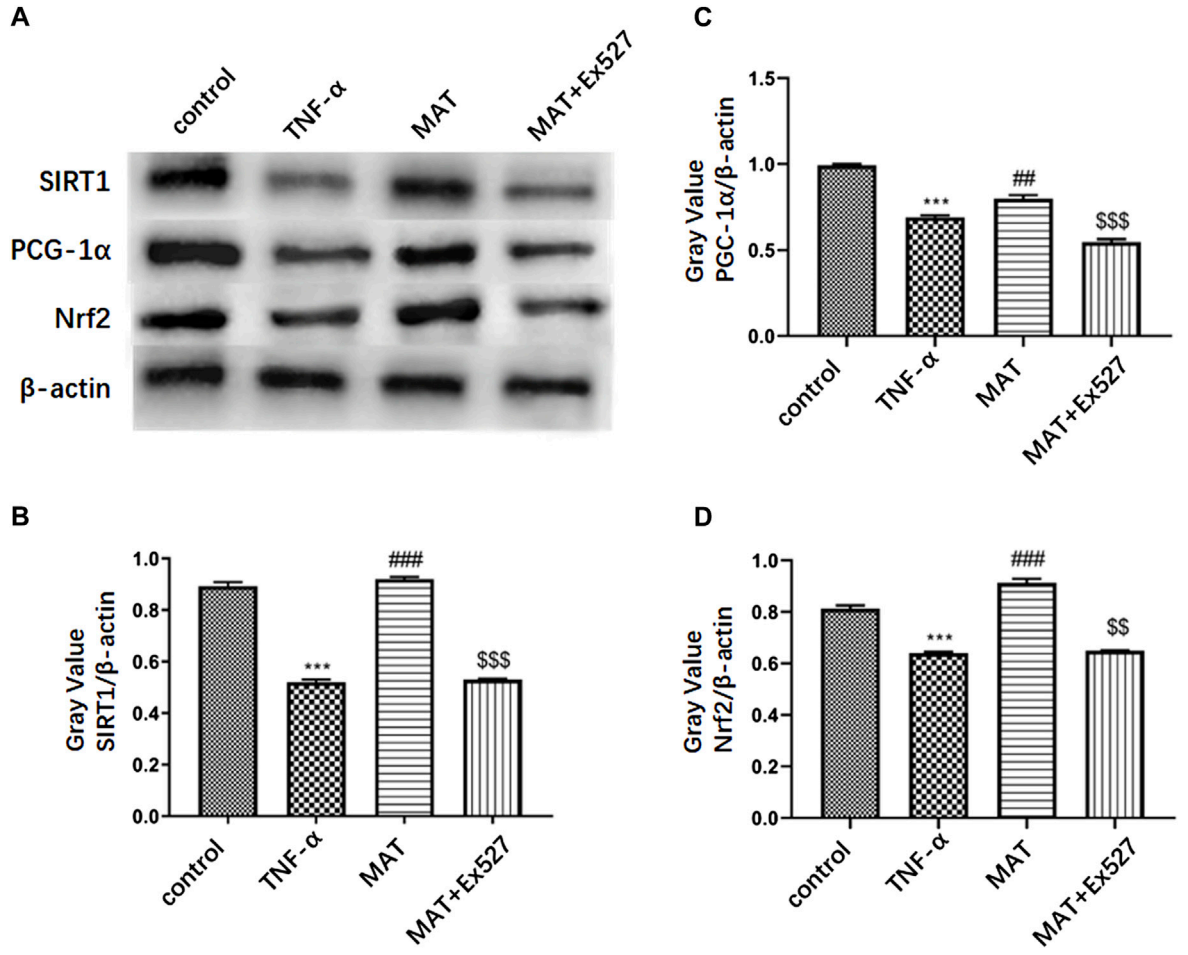

FIGURE 3
MAT could promote Nrf2/ PCG-1α expression in RGC-5 through upregulating SIRT1 expression. **(A)** PCG-1α and Nrf2 protein expression in RGC cells treated by TNF-α were attenuated compared to control group, as well as SIRT1 expression. MAT co-treatment could improve the expression of SIRT1, PCG-1α and Nrf2 significantly. This effect could be revised by EX527, an SIRT1 inhibitor. **(B-D)** Quantitative analysis of the relative expression of each molecule. Symbols represent mean ± SD; ** $p < 0.01$, ***$p < 0.001$, comparison between control and TNF-α groups. ##$p < 0.01$, ### $p < 0.001$, comparison between TNF-α and MAT groups. $$$p < 0.01$, $$$ $p < 0.001$ comparison between MAT and MAT+EX527 groups.

Increased expression of Nrf2 and PGC-1α by MAT treatment

Nrf2 is a key factor in the oxidative defense system, and SIRT1 is involved in the expression and activation of Nrf2. We, therefore, studied Nrf2 expression on the retina by immunofluorescence double staining to illustrate the effect of MAT on oxidative stress in ON (Figure 2A). The expression level of Nrf2 in the vehicle group was reduced compared to that in the naive group. This expression was significantly increased in the MAT-treated group compared to that in the vehicle-treated group (Figures 2B,C).

The PGC-1α expression has been considered to play a non-negligible role in mitochondrial biosynthesis. Therefore, we used immunofluorescence double staining to study the PGC-1α in the retina on the ON model (Figure 2D). Our results showed that the expression of PGC-1α in the immunized groups was significantly lower than in the normal group, whereas its expression in the MAT treatment group was markedly higher than in the vehicle-treated group (Figures 2E,F). These results indicate that MAT can promote the expression of PGC-1α.

MAT could promote Nrf2/PCG-1α expression in RGC-5 by upregulating the SIRT1 expression

To confirm that MAT could prevent RGC death through the SIRT1-PCG-1α/Nrf2 pathway, we used the RGC-5 cell line to perform the experiment. The PCG-1α and Nrf2 protein expression in RGC treated by TNF-α were attenuated

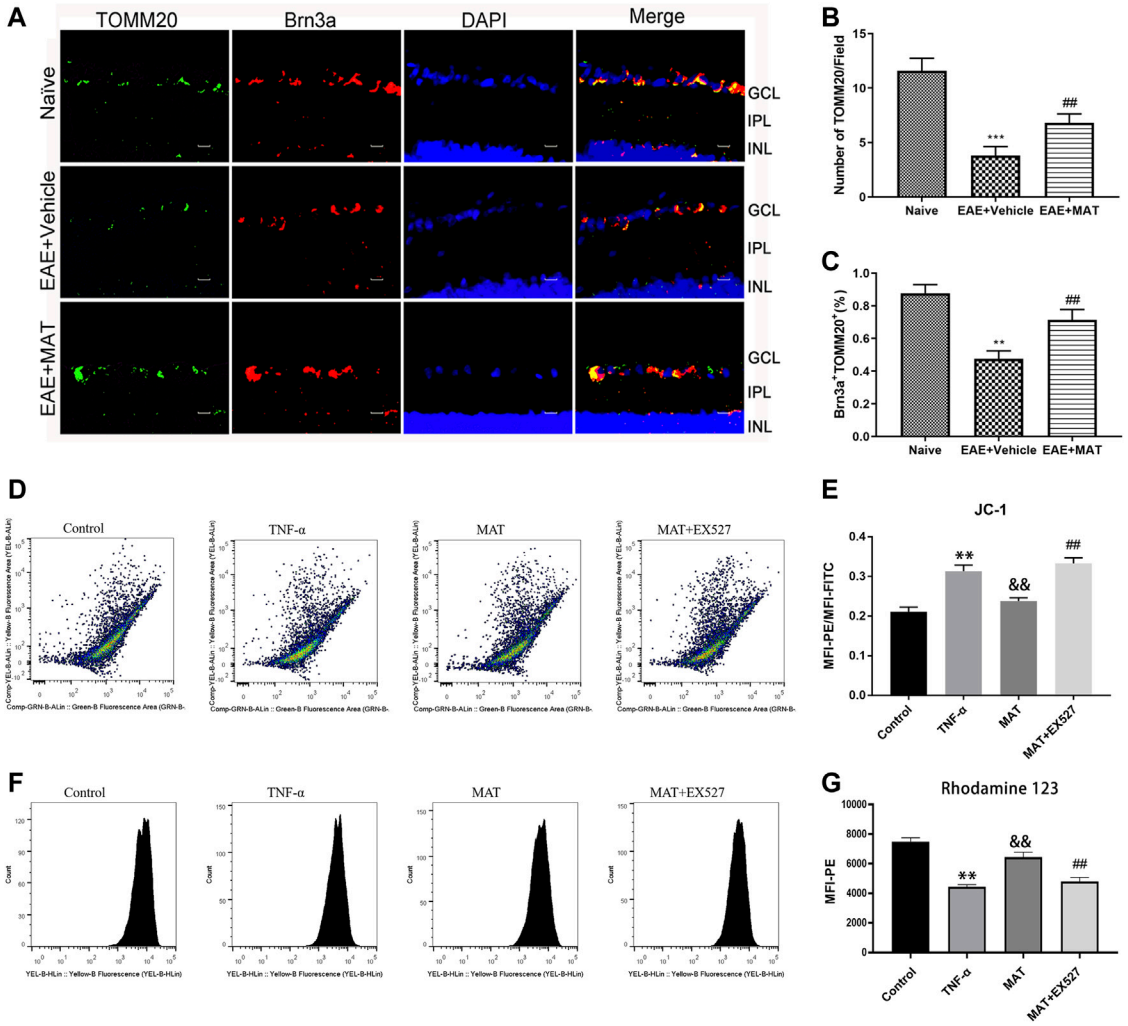

FIGURE 4
MAT motivated mitochondrial biosynthesis. Eyeballs were harvested from naive rats, MAT- and vehicle-treated EAE rats. **(A)** Immunofluorescence double staining suggested that TOMM20 (FITC, green) were colocalized with Brn3a (Cy3, red) in the eyeball retina of EAE rats. Scale bars, 10 μm. **(B)** Quantitative analysis of the number of positive cells. **(C)** Quantitative analysis of the rate of positive cells. Symbols represent mean ± SD; n = 10 rats per group. $^{**}p < 0.01$, $^{***}p < 0.001$, comparison between naive and vehicle-treated EAE groups. $\#\#p < 0.01$, comparison between vehicle- and MAT-treated EAE groups. **(D–G)** TNF-α expose increase in loss of mitochondrial membrane potential (ΔΨM) in retinal cells. FACS analysis using JC-1 dye and Rhodamine-123 dye showing increase in mitochondrial membrane potential ((ΔΨM) with MAT treatmen in RGC-5 cells and this effect could be attenuated by EX527. Symbols represent mean ± SD; $^{**}p < 0.01$, comparison between control and TNF-α groups. $\&\&p < 0.01$, comparison between TNF-α and MAT groups. $\#\#p < 0.01$ comparison between MAT and MAT+EX527 groups.

compared to the control group, as well as the SIRT1 expression. MAT co-treatment could improve the expression of SIRT1, PCG-1α, and Nrf2 significantly. This effect could be revised by EX527, a SIRT1 inhibitor (Figure 3).

MAT affected mitochondrial biosynthesis

Previous studies had shown that MAT protected mitochondrial membrane integrity by inhibiting cytochrome c (Cyt c) release (Wang et al., 2019). Therefore, we decided to explore the effects of MAT on mitochondria in the retina. We determined the expression of TOMM20, a mitochondrial outer membrane transporter commonly used to label mitochondria, in RGCs by immunofluorescence double staining (Figure 4A). The percentage of TOMM20+ Brn3a+ cells in the retina was remarkably reduced during the disease period. However, it was increased in the MAT treatment group (Figures 4B,C). Thus, MAT can enhance mitochondrial biosynthesis in the retina.

Mitochondrial membrane potential (ΔΨM) reflects the functional status of the mitochondrion. We used JC-1 and Rho123 for the qualitative measurement of ΔΨM in RGC-5 cells. Cells with healthy mitochondria show high ΔΨM, whereas cells with damaged mitochondria show low ΔΨM. FACS analysis showed that, with the exposure of TNF-α to RGC-5 cells for 48 h, a significant decrease in ΔΨM was observed, and this was revised by 100 μM MAT, whose effect could be attenuated by Ex527 (Figures 4D,E). To support these findings, we checked the ΔΨM level using Rho123 dye. There was a gradual decrease in the ΔΨM level in the TNF-α group. However, the decreased level of mitochondrial ΔΨM upon TNF-α exposure was revised after the treatment of MAT, and this effect could be attenuated by the SIRT1 inhibitor (Figures 4F,G).

Discussion

Axons of RGCs, which form the optic nerve, are demyelinated in various optic neuropathies, including ON (Wang et al., 2018), and have very limited spontaneous regeneration after injury (Benowitz et al., 2017). ON, which usually occurs in patients with MS and its animal model, EAE (Quinn et al., 2011; Murphy et al., 2020), can cause optic nerve damage and subsequently the death of RGCs (Moore and Goldberg, 2010). It has been recently shown that MAT can limit the inflammation and demyelination of the optic nerve and reduce RGCs apoptosis (Kang et al., 2021). However, the mechanism of this natural alkaloid during this process is still unclear. Herein, we show that the MAT treatment induces SIRT1, PGC-1α, and Nrf2 expression; promotes mitochondrial biosynthesis; and reduces oxidative stress, thereby preventing the loss of RGCs and exerting protective effects on the optic nerve in ON.

Mitochondria are cytoplasmic organelles responsible for producing adenosine triphosphate (ATP), and they play an important role in regulating cellular calcium metabolism, reactive oxygen species (ROS) production, and apoptosis (Mancini et al., 2018). It has been discussed that during the progression of optic neuritis, the oxidative injury to the mitochondrion began prior to inflammatory cell infiltration and continued (Guy, 2008). When the mitochondrial respiratory chain synthesizes ATP, it also produces ROS, mainly in the shape of superoxide, because of the leakage of electrons to oxygen molecules. The increase in mitochondrial electron transport chain activity usually increases the production of by-products ATP and ROS, while the amassing of superoxide in the mitochondria is noxious to cells (Packialakshmi and Zhou, 2018). Due to the central metabolic function of mitochondria and its involvement in the pathophysiology of neurodegenerative diseases, diabetes, and cancer, it has become the focus of basic and translational research (Kappler et al., 2019). Mitochondria are reported to be abundant in the RGCs, and the number of mitochondria in unmyelinated axons is higher than in myelinated axons (Kitaoka et al., 2013). Talla et al. also showed that the reduced activity of the optic nerve complex I in EAE mice increases mitochondrial oxidative stress, which leads to neurodegeneration related to permanent vision loss (Talla et al., 2015). Among molecules that regulate mitochondria function, the SIRT1 expression could prevent the loss of RGC by reducing oxidative stress and maintaining energy homeostasis (Munemasa and Kitaoka, 2015). Most capabilities of SIRT1 happen in the nucleus, where SIRT1 deacetylates histones or other proteins, such as transcription factors or chromatin remodeling proteins (Kim et al., 2015). Although SIRT1 is mostly located in the nucleus, the regulation of mitochondrial biogenesis and function primarily depends on the distribution of SIRT1 in the cytoplasm and mitochondria (Aquilano et al., 2013). Furthermore, SIRT1 regulates cell survival and apoptosis by mediating the deacetylation of p53 (Kulkarni et al., 2014; Yarahmadi et al., 2019), a tumor suppressor gene that contributes to the oligomerization of pro-apoptotic proteins in mitochondria through transcription-dependent and non-transcription-dependent pathways, which may induce mitochondrial outer membrane permeability and mitochondrial Cyt c release (Tu et al., 2018; Vidhyapriya et al., 2018). Our experimental results show significantly enhanced expression of SIRT1 in RGCs after MAT treatment both *in vivo* and *in vitro*, suggesting that MAT may regulate mitochondrial function by upregulating the SIRT1 expression of RGCs, thereby preventing their loss in ON.

Mitochondrial oxidative stress is generally considered to be the major agent of many neurodegenerative diseases such as MS and ON (Khan et al., 2017). Nrf2 is an important transcription factor of the mitochondrial endogenous antioxidant pathway, which affects the expression of multiple antioxidant pathways, including glutathione and cytoprotective genes (Osborne et al., 2016). Under redox-equilibrium cellular conditions, Nrf2 is sequestered in the cytoplasm and undergoes proteasome-mediated degradation (McMahon et al., 2003). During oxidative stress, modification of key binding proteins allows Nrf2 to dissociate and enter the nucleus, recruiting transcription mechanisms to participate in the antioxidant response elements (AREs) and stimulating transcription of target genes associated with antioxidant defense and cellular detoxification (Chen et al., 2015). In addition, the activation of the Nrf2 antioxidant pathway and nuclear accumulation are also regulated by SIRT1 (Zhao et al., 2019). Nrf2 is referred to as the molecular switch of Nrf2/Keap1/ARE signaling and is also a paramount part of the ROS signaling pathway, which can be activated by oxidative stress inducers (Liu et al., 2018). The activation of the Nrf2/ARE signaling pathway is also a self-defense and protection mechanism of cells in response to oxidative stress (Cheng et al., 2017; Yu et al., 2019) and has a neuroprotective effect in EAE-related ON (Larabee et al., 2016). To explore the effect of MAT on Nrf2 expression in RGCs of EAE rats, we found that the expression of Nrf2 was significantly increased upon MAT treatment, suggesting that MAT promotes mitochondrial biosynthesis and reduces oxidative stress, which may be related to the promotion of Nrf2 expression. Moreover, the Nrf2 expression was inhibited by EX527, a SIRT1 inhibitor, suggesting MAT upregulated the Nrf2 expression in RGCs by activating the SIRT1 pathway.

It has been shown that the activity of Nrf1 and Nrf2 can be induced by the PGC-1 transcriptional coactivators family, composed of PGC-1α, PGC-1β, and PGC-1-related coactivators. This activity leads to the transactivation of many genes encoding mitochondrial biogenic specific proteins (Selvakumar et al., 2018). PGC-1α is a major regulator of cellular metabolism and is involved in guiding the expression of nuclear regulatory genes related to mitochondrial biogenesis and antioxidant stress (St-Pierre et al., 2006). PGC-1α has no DNA binding activity of its own but can jointly activate a large number of transcription factors; for example, its interaction with NRFs can promote mitochondrial gene expression and proliferation (Bruns et al., 2019). Consequently, PGC-1α is an intermediary of oxidative phosphorylation and mitochondrial biogenesis and is generally considered the main regulator of mitochondrial function in mammals (LeBleu et al., 2014). The deacetylation state of PGC-1α is the activation state during mitochondrial biogenesis (Price et al., 2012). SIRT1 directly interacts with PGC-1α to regulate PGC-1α activity, and with the increase in the transcriptional activity of PGC-1α, mitochondrial gene transcription and mitochondrial biogenesis are also enhanced (Ma et al., 2017). By co-activating with Nrf2, PGC-1α modulates the expression of metabolic genes in the nuclear and mitochondrial genomes and thus serves as a crucial regulator of accommodative response to oxidative stress (Sharma et al., 2015). PGC-1α is also an important regulator of the mitochondrial endogenous antioxidant defense system, which works by regulating numerous antioxidant proteins, independent of Nrf2 (Osborne et al., 2016). Reduced PGC-1α expression in the retina is involved in all major processes of retinal damage and subsequent repair (Egger et al., 2012). Moreover, the PGC-1α signaling pathway is a significant regulator of astrocyte reactivity and RGC homeostasis as it adjusts the pathogenic sensitivity of the inner retina to metabolic and oxidative damage (Guo et al., 2014). Consistent with these observations, PGC-1α expression in the retina of ON rats and RGC-5 treated with TNF-α both were significantly increased after MAT treatment and could be attenuated by EX527, suggesting that MAT may promote mitochondrial biogenesis and maintain RGC homeostasis by SIRT1/PGC-1α pathway.

In conclusion, our study shows that MAT can effectively inhibit the disease progression of ON and protect RGCs. MAT activates the SIRT1, PGC-1α, and Nrf2 expression in the retina to promote mitochondrial biosynthesis and reduce oxidative stress, which could be revised by the SIRT1 inhibitor. Thus, we believe that MAT treatment could protect RGCs from apoptosis in ON by the SIRT1-PGC-1α/Nrf2 pathway.

Data availability statement

The raw data supporting the conclusions of this article will be made available by the authors without undue reservation.

Ethics statement

The animal study was reviewed and approved by the Ethics Committee of Scientific Research of Henan Academy of Chinese Medicine.

Author contributions

YS and CZ contributed to the conception and design of the study. YS and MW participated in the animal experiments and wrote the first draft of the manuscript. MW organized the database and performed the statistical analysis. SZ and YT helped revise the article. All authors contributed to manuscript revision and read and approved the submitted version.

Funding

This work was supported by grants from the National Natural Science Foundation of China (81970798).

Acknowledgments

We thank Katherine Regan for editorial assistance.

Conflict of interest

The authors declare that the research was conducted in the absence of any commercial or financial relationships that could be construed as a potential conflict of interest.

Publisher's note

Supplementary material

The Supplementary Material for this article can be found online at: https://www.frontiersin.org/articles/10.3389/fphar.2022.936632/full#supplementary-material

References

Aquilano, K., Baldelli, S., Pagliei, B., and Ciriolo, M. R. (2013). Extranuclear localization of SIRT1 and PGC-1α: An insight into possible roles in diseases associated with mitochondrial dysfunction. *Curr. Mol. Med.* 13 (1), 140–154. doi:10.2174/1566524011307010140

Azuchi, Y., Kimura, A., Guo, X., Akiyama, G., Noro, T., Harada, C., et al. (2017). Valproic acid and ASK1 deficiency ameliorate optic neuritis and neurodegeneration in an animal model of multiple sclerosis. *Neurosci. Lett.* 639, 82–87. doi:10.1016/j.neulet.2016.12.057

Benowitz, L. I., He, Z., and Goldberg, J. L. (2017). Reaching the brain: Advances in optic nerve regeneration. *Exp. Neurol.* 287, 365–373. doi:10.1016/j.expneurol.2015.12.015

Bruns, I., Sauer, B., Burger, M. C., Eriksson, J., Hofmann, U., Braun, Y., et al. (2019). Disruption of peroxisome proliferator-activated receptor γ coactivator (PGC)-1α reverts key features of the neoplastic phenotype of glioma cells. *J. Biol. Chem.* 294 (9), 3037–3050. doi:10.1074/jbc.RA118.006993

Chen, B., Lu, Y., Chen, Y., and Cheng, J. (2015). The role of Nrf2 in oxidative stress-induced endothelial injuries. *J. Endocrinol.* 225 (3), R83–R99. doi:10.1530/JOE-14-0662

Cheng, L. B., Li, K. R., Yi, N., Li, X. M., Wang, F., Xue, B., et al. (2017). miRNA-141 attenuates UV-induced oxidative stress via activating Keap1-Nrf2 signaling in human retinal pigment epithelium cells and retinal ganglion cells. *Oncotarget* 8 (8), 13186–13194. doi:10.18632/oncotarget.14489

Chu, Y., Jing, Y., Zhao, X., Wang, M., Zhang, M., Ma, R., et al. (2021). Modulation of the HMGB1/TLR4/NF-κB signaling pathway in the CNS by matrine in experimental autoimmune encephalomyelitis. *J. Neuroimmunol.* 352, 577480. doi:10.1016/j.jneuroim.2021.577480

Ding, Y. W., Zhao, G. J., Li, X. L., Hong, G. L., Li, M. F., Qiu, Q. M., et al. (2016). SIRT1 exerts protective effects against paraquat-induced injury in mouse type II alveolar epithelial cells by deacetylating NRF2 *in vitro*. *Int. J. Mol. Med.* 37 (4), 1049–1058. doi:10.3892/ijmm.2016.2503

Egger, A., Samardzija, M., Sothilingam, V., Tanimoto, N., Lange, C., Salatino, S., et al. (2012). PGC-1α determines light damage susceptibility of the murine retina. *PLOS ONE* 7 (2), e31272. doi:10.1371/journal.pone.0031272

Finck, B. N., and Kelly, D. P. (2006). PGC-1 coactivators: Inducible regulators of energy metabolism in health and disease. *J. Clin. Invest.* 116 (3), 615–622. doi:10.1172/JCI27794

Gerhart-Hines, Z., Rodgers, J. T., Bare, O., Lerin, C., Kim, S. H., Mostoslavsky, R., et al. (2007). Metabolic control of muscle mitochondrial function and fatty acid oxidation through SIRT1/PGC-1alpha. *EMBO J.* . 26 (7), 1913–1923. doi:10.1038/sj.emboj.7601633

Guo, X., Dason, E. S., Zanon-Moreno, V., Jiang, Q., Nahirnyj, A., Chan, D., et al. (2014). PGC-1α signaling coordinates susceptibility to metabolic and oxidative injury in the inner retina. *Am. J. Pathol.* 184 (4), 1017–1029. doi:10.1016/j.ajpath.2013.12.012

Guy, J. (2008). Optic nerve degeneration in experimental autoimmune encephalomyelitis. *Ophthalmic Res.* 40 (3-4), 212–216. doi:10.1159/000119879

Johnson, D. A., and Johnson, J. A. (2015). Nrf2--a therapeutic target for the treatment of neurodegenerative diseases. *Free Radic. Biol. Med.* 88, 253–267. doi:10.1016/j.freeradbiomed.2015.07.147

Kan, Q. C., Zhang, H. J., Zhang, Y., Li, X., Xu, Y. M., Thome, R., et al. (2017). Matrine treatment blocks NogoA-induced neural inhibitory signaling pathway in ongoing experimental autoimmune encephalomyelitis. *Mol. Neurobiol.* 54 (10), 8404–8418. doi:10.1007/s12035-016-0333-1

Kan, Q. C., Zhu, L., Liu, N., and Zhang, G. X. (2013). Matrine suppresses expression of adhesion molecules and chemokines as a mechanism underlying its therapeutic effect in CNS autoimmunity. *Immunol. Res.* 56 (1), 189–196. doi:10.1007/s12026-013-8393-z

Kang, J., Liu, S., Song, Y., Chu, Y., Wang, M., Shi, Y., et al. (2021). Matrine treatment reduces retinal ganglion cell apoptosis in experimental optic neuritis. *Sci. Rep.* 11 (1), 9520. doi:10.1038/s41598-021-89086-7

Kappler, L., Hoene, M., Hu, C., von Toerne, C., Li, J., Bleher, D., et al. (2019). Linking bioenergetic function of mitochondria to tissue-specific molecular fingerprints. *Am. J. Physiol. Endocrinol. Metab.* 317 (2), E374–E387. doi:10.1152/ajpendo.00088.2019

Khan, R. S., Dine, K., Geisler, J. G., and Shindler, K. S. (2017). Mitochondrial uncoupler prodrug of 2, 4-dinitrophenol, MP201, prevents neuronal damage and preserves vision in experimental optic neuritis. *Oxid. Med. Cell. Longev.* 2017, 7180632. doi:10.1155/2017/7180632

Khan, R. S., Fonseca-Kelly, Z., Callinan, C., Zuo, L., Sachdeva, M. M., and Shindler, K. S. (2012). SIRT1 activating compounds reduce oxidative stress and prevent cell death in neuronal cells. *Front. Cell. Neurosci.* 6, 63. doi:10.3389/fncel.2012.00063

Kim, S. Y., Sim, C. K., Tang, H., Han, W., Zhang, K., and Xu, F. (2015). Acetylome analysis identifies SIRT1 targets in mRNA-processing and chromatin-remodeling in mouse liver. *PLOS ONE* 10 (10), e0140619. doi:10.1371/journal.pone.0140619

Kimura, A., Namekata, K., Guo, X., Noro, T., Harada, C., and Harada, T. (2017). Targeting oxidative stress for treatment of glaucoma and optic neuritis. *Oxid. Med. Cell. Longev.*, 2817252. doi:10.1155/2017/2817252

Kitaoka, Y., Munemasa, Y., Kojima, K., Hirano, A., Ueno, S., and Takagi, H. (2013). Axonal protection by Nmnat3 overexpression with involvement of autophagy in optic nerve degeneration. *Cell. Death Dis.* 4, e860. doi:10.1038/cddis.2013.391

Kobayter, L., and Chetty, S. (2019). Management of optic neuritis in Ireland: A survey comparing the management practices of acute demyelinating optic neuritis amongst ophthalmologists and neurologists in Ireland. *Ir. J. Med. Sci.* 188 (1), 277–282. doi:10.1007/s11845-018-1817-y

Kulkarni, S. R., Donepudi, A. C., Xu, J., Wei, W., Cheng, Q. C., Driscoll, M. V., et al. (2014). Fasting induces nuclear factor E2-related factor 2 and ATP-binding Cassette transporters via protein kinase A and Sirtuin-1 in mouse and human. *Antioxid. Redox Signal.* 20 (1), 15–30. doi:10.1089/ars.2012.5082

Larabee, C. M., Desai, S., Agasing, A., Georgescu, C., Wren, J. D., Axtell, R. C., et al. (2016). Loss of Nrf2 exacerbates the visual deficits and optic neuritis elicited by experimental autoimmune encephalomyelitis. *Mol. Vis.* 22, 1503–1513.

LeBleu, V. S., O'Connell, J. T., Gonzalez, H. K., Wikman, H., Pantel, K., Haigis, M. C., et al. (2014). PGC-1α mediates mitochondrial biogenesis and oxidative phosphorylation in cancer cells to promote metastasis. *Nat. Cell. Biol.* 16 (10), 992–1003. doi:10.1038/ncb3039

Lin, W. J., and Kuang, H. Y. (2014). Oxidative stress induces autophagy in response to multiple noxious stimuli in retinal ganglion cells. *AUTOPHAGY* 10 (10), 1692–1701. doi:10.4161/auto.36076

Liu, Q., Li, H., Yang, J., Niu, X., Zhao, C., Zhao, L., et al. (2017). Valproic acid attenuates inflammation of optic nerve and apoptosis of retinal ganglion cells in a rat model of optic neuritis. *Biomed. Pharmacother.* 96, 1363–1370. doi:10.1016/j.biopha.2017.11.066

Liu, X. F., Zhou, D. D., Xie, T., Hao, J. L., Malik, T. H., Lu, C. B., et al. (2018). The Nrf2 signaling in retinal ganglion cells under oxidative stress in ocular neurodegenerative diseases. *Int. J. Biol. Sci.* 14 (9), 1090–1098. doi:10.7150/ijbs.25996

Ma, S., Zhao, Y., Sun, J., Mu, P., and Deng, Y. (2017). miR449a/SIRT1/PGC-1alpha is necessary for mitochondrial biogenesis induced by T-2 toxin. *Front. Pharmacol.* 8, 954.

Mancini, A., Tantucci, M., Mazzocchetti, P., de Iure, A., Durante, V., Macchioni, L., et al. (2018). Microglial activation and the nitric oxide/cGMP/PKG pathway underlie enhanced neuronal vulnerability to mitochondrial dysfunction in experimental multiple sclerosis. *Neurobiol. Dis.* 113, 97–108. doi:10.1016/j.nbd.2018.01.002

Martin, A., Tegla, C. A., Cudrici, C. D., Kruszewski, A. M., Azimzadeh, P., Boodhoo, D., et al. (2015). Role of SIRT1 in autoimmune demyelination and neurodegeneration. *Immunol. Res.* 61 (3), 187–197. doi:10.1007/s12026-014-8557-5

McMahon, M., Itoh, K., Yamamoto, M., and Hayes, J. D. (2003). Keap1-dependent proteasomal degradation of transcription factor Nrf2 contributes to the negative regulation of antioxidant response element-driven gene expression. *J. Biol. Chem.* 278 (24), 21592–21600. doi:10.1074/jbc.m300931200

Moore, D. L., and Goldberg, J. L. (2010). Four steps to optic nerve regeneration. *J. Neuroophthalmol.* 30 (4), 347–360. doi:10.1097/WNO.0b013e3181e755af

Munemasa, Y., and Kitaoka, Y. (2015). Autophagy in axonal degeneration in glaucomatous optic neuropathy. *Prog. Retin. Eye Res.* 47, 1–18. doi:10.1016/j.preteyeres.2015.03.002

Murphy, O. C., Kwakyi, O., Iftikhar, M., Zafar, S., Lambe, J., Pellegrini, N., et al. (2020). Alterations in the retinal vasculature occur in multiple sclerosis and exhibit novel correlations with disability and visual function measures. *Mult. Scler.* 26 (7), 815–828. doi:10.1177/1352458519845116

Osborne, N. N., Nunez-Alvarez, C., Joglar, B., and Del, O. S. (2016). Glaucoma: Focus on mitochondria in relation to pathogenesis and neuroprotection. *Eur. J. Pharmacol.* 787, 127–133. doi:10.1016/j.ejphar.2016.04.032

Packialakshmi, B., and Zhou, X. (2018). Experimental autoimmune encephalomyelitis (EAE) up-regulates the mitochondrial activity and manganese superoxide dismutase (MnSOD) in the mouse renal cortex. *PLOS ONE* 13 (4), e0196277. doi:10.1371/journal.pone.0196277

Pal, S., Rao, G. N., and Pal, A. (2020). High glucose-induced ROS accumulation is a critical regulator of ERK1/2-Akt-tuberin-mTOR signalling in RGC-5 cells. *Life Sci.* 256, 117914. doi:10.1016/j.lfs.2020.117914

Pihl-Jensen, G., Wanscher, B., and Frederiksen, J. L. (2021). Predictive value of optical coherence tomography, multifocal visual evoked potentials, and full-field visual evoked potentials of the fellow, non-symptomatic eye for subsequent multiple sclerosis development in patients with acute optic neuritis. *Mult. Scler.* 27 (3), 391–400. doi:10.1177/1352458520917924

Price, N. L., Gomes, A. P., Ling, A. J., Duarte, F. V., Martin-Montalvo, A., North, B. J., et al. (2012). SIRT1 is required for AMPK activation and the beneficial effects of resveratrol on mitochondrial function. *Cell. Metab.* 15 (5), 675–690. doi:10.1016/j.cmet.2012.04.003

Qi, X., Lewin, A. S., Sun, L., Hauswirth, W. W., and Guy, J. (2007). Suppression of mitochondrial oxidative stress provides long-term neuroprotection in experimental optic neuritis. *Invest. Ophthalmol. Vis. Sci.* 48 (2), 681–691. doi:10.1167/iovs.06-0553

Quinn, T. A., Dutt, M., and Shindler, K. S. (2011). Optic neuritis and retinal ganglion cell loss in a chronic murine model of multiple sclerosis. *Front. Neurol.* 2, 50. doi:10.3389/fneur.2011.00050

Selvakumar, G. P., Iyer, S. S., Kempuraj, D., Raju, M., Thangavel, R., Saeed, D., et al. (2018). Glia maturation factor dependent inhibition of mitochondrial PGC-1α triggers oxidative stress-mediated apoptosis in N27 rat dopaminergic neuronal cells. *Mol. Neurobiol.* 55 (9), 7132–7152. doi:10.1007/s12035-018-0882-6

Sharma, D. R., Sunkaria, A., Wani, W. Y., Sharma, R. K., Verma, D., Priyanka, K., et al. (2015). Quercetin protects against aluminium induced oxidative stress and promotes mitochondrial biogenesis via activation of the PGC-1α signaling pathway. *NEUROTOXICOLOGY* 51, 116–137. doi:10.1016/j.neuro.2015.10.002

St-Pierre, J., Drori, S., Uldry, M., Silvaggi, J. M., Rhee, J., Jager, S., et al. (2006). Suppression of reactive oxygen species and neurodegeneration by the PGC-1 transcriptional coactivators. *Cell.* 127 (2), 397–408. doi:10.1016/j.cell.2006.09.024

Talla, V., Koilkonda, R., Porciatti, V., Chiodo, V., Boye, S. L., Hauswirth, W. W., et al. (2015). Complex I subunit gene therapy with NDUFA6 ameliorates neurodegeneration in EAE. *Invest. Ophthalmol. Vis. Sci.* 56 (2), 1129–1140. doi:10.1167/iovs.14-15950

Tu, W., Zhang, Q., Liu, Y., Han, L., Wang, Q., Chen, P., et al. (2018). Fluoride induces apoptosis via inhibiting SIRT1 activity to activate mitochondrial p53 pathway in human neuroblastoma SH-SY5Y cells. *Toxicol. Appl. Pharmacol.* 347, 60–69. doi:10.1016/j.taap.2018.03.030

Vidhyapriya, P., Divya, D., Bala, M., and Sakthivel, N. (2018). Photoactivated [Mn(CO)3Br(mu-bpcpd)]2 induces apoptosis in cancer cells via intrinsic pathway. *J. Photochem Photobiol. B* 188, 28–41. doi:10.1016/j.jphotobiol.2018.08.021

Wang, F., Dang, Y., Wang, J., Zhou, T., and Zhu, Y. (2018). Gypenosides attenuate lipopolysaccharide-induced optic neuritis in rats. *Acta Histochem.* 120 (4), 340–346. doi:10.1016/j.acthis.2018.03.003

Wang, M. R., Zhang, X. J., Liu, H. C., Ma, W. D., Zhang, M. L., Zhang, Y., et al. (2019). Matrine protects oligodendrocytes by inhibiting their apoptosis and enhancing mitochondrial autophagy. *Brain Res. Bull.* 153, 30–38. doi:10.1016/j.brainresbull.2019.08.006

Wang, X., Lin, H., and Zhang, R. (2017). The clinical efficacy and adverse effects of interferon combined with matrine in chronic hepatitis B: A systematic review and meta-analysis. *Phytother. Res.* 31 (6), 849–857. doi:10.1002/ptr.5808

Yarahmadi, S., Abdolvahabi, Z., Hesari, Z., Tavakoli-Yaraki, M., Yousefi, Z., Seiri, P., et al. (2019). Inhibition of sirtuin 1 deacetylase by miR-211-5p provides a mechanism for the induction of cell death in breast cancer cells. *GENE* 711, 143939. doi:10.1016/j.gene.2019.06.029

Yu, J., Sun, W., Song, Y., Liu, J., Xue, F., Gong, K., et al. (2019). SIRT6 protects retinal ganglion cells against hydrogen peroxide-induced apoptosis and oxidative stress by promoting Nrf2/ARE signaling via inhibition of Bach1. *Chem. Biol. Interact.* 300, 151–158. doi:10.1016/j.cbi.2019.01.018

Zhang, H. K., Ye, Y., Li, K. J., Zhao, Z. N., and He, J. F. (2020). Gypenosides prevent H2O2-induced retinal ganglion cell apoptosis by concurrently suppressing the neuronal oxidative stress and inflammatory response. *J. Mol. Neurosci.* 70 (4), 618–630. doi:10.1007/s12031-019-01468-9

Zhang, M. L., Zhang, X. J., Kang, J., Zhang, H. J., Chen, X. L., Liu, N., et al. (2017). Matrine promotes NT3 expression in CNS cells in experimental autoimmune encephalomyelitis. *Neurosci. Lett.* 649, 100–106. doi:10.1016/j.neulet.2017.04.005

Zhao, X., Jin, Y., Li, L., Xu, L., Tang, Z., Qi, Y., et al. (2019). MicroRNA-128-3p aggravates doxorubicin-induced liver injury by promoting oxidative stress via targeting Sirtuin-1. *Pharmacol. Res.* 146, 104276. doi:10.1016/j.phrs.2019.104276

frontiers | Frontiers in Pharmacology

TYPE Original Research
PUBLISHED 28 September 2022
DOI 10.3389/fphar.2022.941656

OPEN ACCESS

EDITED BY
Erxi Wu,
Baylor Scott and White Health,
United States

REVIEWED BY
Dayalan Sampath,
Texas A&M University, United States
Sudhanshu P. Raikwar,
Barrow Neurological Institute (BNI),
United States
Dan Qi,
Baylor Scott and White Health,
United States

*CORRESPONDENCE
Bing Niu,
bingniu@shu.edu.cn
Cheng Li,
chengli_2017@tongji.edu.cn

†These authors have contributed equally to this work

SPECIALTY SECTION
This article was submitted to Neuropharmacology, a section of the journal Frontiers in Pharmacology

RECEIVED 11 May 2022
ACCEPTED 29 August 2022
PUBLISHED 28 September 2022

CITATION
Zhang H, Cao S, Xu Y, Sun X, Fei M, Jing Q, Xu X, Tang J, Niu B and Li C (2022), Landscape of immune infiltration in entorhinal cortex of patients with Alzheimer's disease. *Front. Pharmacol.* 13:941656. doi: 10.3389/fphar.2022.941656

Landscape of immune infiltration in entorhinal cortex of patients with Alzheimer's disease

Hui Zhang[1,2,3,4,5†], Silu Cao[1,2,3,4,5†], Yaru Xu[1,2,3,4,5], Xiaoru Sun[1,2,3,4], Miaomiao Fei[1,2,3,4], Qi Jing[1,2,3,4,5], Xiaodong Xu[1,2,3,4,5], Jinxuan Tang[1,2,3,4], Bing Niu[6*] and Cheng Li[1,2,3,4*]

[1]Department of Anesthesiology and Perioperative Medicine, Shanghai Fourth People's Hospital, School of Medicine, Tongji University, Shanghai, China, [2]Shanghai Key Laboratory of Anesthesiology and Brain Functional Modulation, Shanghai, China, [3]Translational Research Institute of Brain and Brain-like Intelligence, Shanghai Fourth People's Hospital, School of Medicine, Tongji University, Shanghai, China, [4]Clinical Research Center for Anesthesiology and Perioperative Medicine, Tongji University, Shanghai, China, [5]Department of Anesthesiology, Shanghai Tenth People's Hospital, School of Medicine, Tongji University, Shanghai, China, [6]School of Life Sciences, Shanghai University, Shanghai, China

Alzheimer's disease (AD) is one of the most common neurodegenerative diseases and manifests as progressive memory loss and cognitive dysfunction. Neuroinflammation plays an important role in the development of Alzheimer's disease and anti-inflammatory drugs reduce the risk of the disease. However, the immune microenvironment in the brains of patients with Alzheimer's disease remains unclear, and the mechanisms by which anti-inflammatory drugs improve Alzheimer's disease have not been clearly elucidated. This study aimed to provide an overview of the immune cell composition in the entorhinal cortex of patients with Alzheimer's disease based on the transcriptomes and signature genes of different immune cells and to explore potential therapeutic targets based on the relevance of drug targets. Transcriptomics data from the entorhinal cortex tissue, derived from GSE118553, were used to support our study. We compared the immune-related differentially expressed genes (irDEGs) between patients and controls by using the limma R package. The difference in immune cell composition between patients and controls was detected *via* the xCell algorithm based on the marker genes in immune cells. The correlation between marker genes and immune cells and the interaction between genes and drug targets were evaluated to explore potential therapeutic target genes and drugs. There were 81 irDEGs between patients and controls that participated in several immune-related pathways. xCell analysis showed that most lymphocyte scores decreased in Alzheimer's disease, including $CD4^+$ Tc, $CD4^+$ Te, Th1, natural killer (NK), natural killer T (NKT), pro-B cells, eosinophils, and regulatory T cells, except for Th2 cells. In contrast, most myeloid cell scores increased in patients, except in dendritic cells. They included basophils, mast cells, plasma cells, and macrophages. Correlation analysis suggested that 37 genes were associated with these cells involved in innate immunity, of which eight genes were drug targets. Taken together, these results delineate the profile of the immune components of the

entorhinal cortex in Alzheimer's diseases, providing a new perspective on the development and treatment of Alzheimer's disease.

KEYWORDS

Alzheimer's disease, entorhinal cortex, immune, transcriptomic, drug

Introduction

Alzheimer's disease (AD) is one of the most common neurodegenerative diseases (Jack et al., 2010). Approximately 50 million people worldwide suffer from dementia, and by 2050, more than 100 million people will experience dementia, which places a heavy economic burden on societies and families (Lane et al., 2018; Jing et al., 2021). The clinical features of AD include progressive memory loss and cognitive dysfunction. The main pathological changes in AD include β-amyloid deposition, neurofibrillary tangles, neuronal loss, synaptic dysfunction, and neuroinflammation in the brain (Serrano-Pozo et al., 2011; Jack et al., 2013; Spires-Jones & Hyman, 2014; Oliveros et al., 2022; Peng et al., 2022). Despite significant advancements in assessing AD, both from basic and clinical studies, there is currently no effective treatment to prevent or reverse AD. Therefore, the etiology and pathogenesis of the disease require further study and elucidation. Moreover, there is an urgent need for effective drugs to prevent and delay the progression of AD. In recent years, increasing research evidence has revealed that neuroinflammation plays a crucial role in AD (Heneka et al., 2015; Ransohoff, 2016; Lindestam Arlehamn et al., 2019). Central microglia, astrocytes, and peripheral monocytes are considered to be the main cells involved in neuroinflammation. Microglia can penetrate cell surface receptors and is hypothesized to play an important role in the inflammatory response in AD (Paresce et al., 1996; Bamberger et al., 2003; Liu et al., 2005; Stewart et al., 2010). The results from animal studies have suggested that peripheral mononuclear cell infiltration is associated with amyloid plaques (Simard et al., 2006). Furthermore, a mouse model demonstrated that peripheral mononuclear phagocytes play a critical role in reducing Aβ plaque accumulation (Simard et al., 2006). Pathological responses of astrocytes include reactive astrogliosis, a complex multistage pathologically specific response of astrocytes, which is usually considered to protect nerves and restore damaged nerve tissues (Sofroniew, 2009; Sofroniew & Vinters, 2010). Except for activated microglia, hypertrophic reactive astrocytes that accumulate around senile plaques are often observed both in postmortem human tissue from ADs (Medeiros & LaFerla, 2013) and in animal models with the disorder (Olabarria et al., 2010).

In addition to resident immune cells such as microglia and astrocytes, there are also infiltrating immune cells in the brain. Most infiltrating immune cells are mainly present in the border regions of the brain, and immune infiltrating cells are absent in the brain parenchyma under normal conditions (Cugurra et al., 2021). These border region cells can affect the brain by secreting cytokines, modulating adjacent epithelial and ependymal cells, and altering cerebrospinal fluid composition. These cells are involved in tissue homeostasis and may enter the brain parenchyma when an abnormality occurs; therefore, they may play a central role in promoting recovery and may also accelerate the pathological process. Many previous studies have concluded that inflammation has a damaging effect on neurons in the brains of patients with AD and the usage of anti-inflammatory drugs can reduce the risk of the disease (Aisen, 2002). In the past decade, there have been several reports of anti-inflammatory drugs, especially nonsteroidal anti-inflammatory drugs (NSAIDs), for the treatment of AD. Multiple meta-analyses have produced strong, generally consistent statistical evidence that the use of NSAIDs has resulted in a halved or even lower risk of developing AD (McGeer et al., 1996; Anthony et al., 2000). Therefore, exploring the immunological differences between patients with AD and controls may provide evidence for the treatment of AD.

The entorhinal cortex is a vital link between the cerebral cortex and hippocampus, and it plays a crucial role in the formation and retrieval of memory (de Calignon et al., 2012). The molecular mechanism of entorhinal cortex alterations is significant for the prevention and treatment of AD. Our study aimed to provide a landscape of different immune cell compositions in the entorhinal cortex between patients with AD and controls based on the transcriptomics and signature genes of different immune cells by using the xCell algorithm (Aran et al., 2017). Combined with correlation analysis, genes related to immune microenvironment differences and the potential therapeutic targets involved in therapy were further identified. These results provide evidence to comprehensively understand the association between immune infiltration and disease in the brain parenchyma of patients with AD and to obtain new ideas for its prevention and treatment.

Materials and methods

Data collection

The Gene Expression Omnibus (GEO) database is an international public repository that archives and freely distributes high-throughput gene expression and other

TABLE 1 Characteristics of the entorhinal cortex tissue in AD and control samples in the GSE118553 dataset.

	Controls	ADs	*p*
Age (=<80/> 80)	17/7	13/24	0.006
Sex (Male/Female)	12/12	14/23	0.348

functional genomics datasets (Clough & Barrett, 2016). It mainly refers to gene sequencing data, including microarray, second-generation sequencing, and third-generation sequencing data, which can be downloaded by using the GEOquery package in the R programming environment (Davis & Meltzer, 2007). The GSE118553 dataset contain transcriptomic data of the entorhinal cortex, temporal cortex, frontal cortex, and cerebellum brain region from controls, asymptomatic AD, and AD subjects. Neuropathological evaluation for neurodegenerative diseases was performed in accordance with standard criteria (Patel et al., 2019). Among them, transcriptomic data from the entorhinal cortex of controls and ADs were extracted to support this study. The characteristics of the entorhinal cortex tissue from ADs and control samples in the GSE118553 dataset are shown in Table 1. According to the data processing instructions, the expression matrix was maximum likelihood estimation background corrected by using the R package MBCB (Allen et al., 2009), log2 transformed, and robust spline normalization by using the R package Lumi (Du et al., 2008). The data were annotated by using the GPL10558 platform. For multiple probes corresponding to the same gene, the average value of all probes was used as the gene expression value. The characteristics, such as age and sex, were also obtained from the GSE118553 dataset. We turned age into a categorical variable based on the median of it to facilitate comparison of baseline differences between ADs and controls. The differences between the two groups were studied using Chi-square tests in R. Propensity score matching (PSM), performed with the matching package, was applied to eliminate baseline differences.

Immune-related differentially expressed genes between Alzheimer's diseases and controls

Differentially expressed genes (DEGs) between 37 ADs and 24 controls were detected with the limma package based on the cutoff criteria of a |log 2-fold change (FC)| > 0.5 and adjusted *p* value <0.05 (Ritchie et al., 2015). The immune-related gene (IRG) list was downloaded from ImmPort (https://www.immport.org/home) (Bhattacharya et al., 2018). Immune-related DEGs (irDEGs) were visualized using the Venn diagrams package (Nagpal et al., 2021), and the function of irDEGs was annotated by using Metascape (metascape.org), which is an online bioinformatic pipeline for multiple gene lists that allows effective gene function annotation and data-driven gene prioritization decisions (Zhou et al., 2019).

Immune cells in samples

xCell, using a set of 10,808 genes for calculating the score of 64 immune and stromal cell types based on a novel gene signature–based method, was used to calculate the scores for immune cell infiltration in the entorhinal cortex tissue of each sample (Aran et al., 2017). The gene markers of each cell type are displayed in Supplementary Table S1 (Aran et al., 2017). According to the cell gene markers, a total of 34 immune cell types can be scored with xCell. A total of 21 of all immune cell types were lymphoid cells. The different cell type scores between ADs and controls were estimated with the Mann–Whitney *U* test, and a *p* value <0.05 was considered statistically significant. t-Distributed stochastic neighbor embedding (tSNE) analyses were performed with all cell signature genes to visualize all samples in 2D maps by using the tSNE algorithm (Kobak & Berens, 2019). Cell signature differentially expressed genes (csDEGs) were selected and displayed with a percent stacked bar chart.

Correlation between cell signature genes and immune cells

To explore the gene potential causes of the differences in immune cells between ADs and controls, Pearson correlation analysis was used to assess the relationship between differentially expressed signature genes and corresponding cell scores, with a *p* value <0.05 considered statistically significant. The genes may play critical roles in causing cell differences between ADs and control. Similarly, the Pearson correlation analysis was performed to reveal the correlation between myeloid cells and lymphocytes in ADs, as well as the correlation between different cell types. Correlations between genes and each cell type were performed to detect potential genes that contribute to the association between cell types.

Drug-targeted immune gene identification and functional annotation

In this study, we used three properties to identify potential therapeutic target immune genes. First, the gene is an immune cell signature gene or associated with immune cells, which has been obtained in the aforementioned analysis; second, the gene is associated with AD, which can be determined with GeneCards inferred functionality scores higher than 40 by the GeneCards

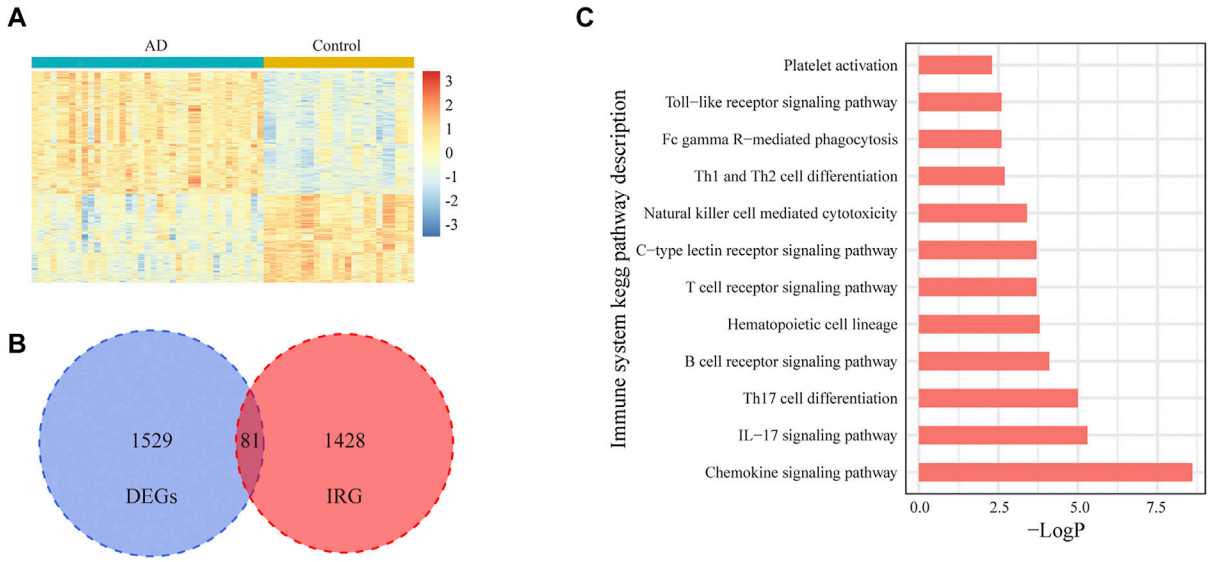

FIGURE 1
Expression of IRGs in the entorhinal cortex for AD and control samples in the GSE118553 dataset. **(A)**. Heatmap of 1,610 DEGs in the entorhinal cortex for AD and control samples in the GSE118553 dataset. The DEGs were filtered with |log2 fold change (FC)| > 0.5 and adjusted *p* value <0.05. **(B)**. In total, 81 IRGs in DEGs are displayed with a Venn diagram. **(C)**. In total, 12 immune system pathways were significantly enriched with 81 irDEGs.

database (https://www.genecards.org/); last, the gene is the target of drug action, which can be determined by the PharmGKB database (Hewett et al., 2002). The functions of target genes were annotated by Kyoto Encyclopedia of Genes and Genomes (KEGG) functional enrichment analysis. The expression of drug-targeted immune genes between the two groups is shown as a boxplot with ggplot2. Receiver operating characteristic (ROC) curves and areas under the ROC curve (AUCs) were examined by the pROC package to determine the predictive value of drug-targeted immune genes (Mandrekar, 2010). The relationship between potential targets and drugs was visualized by using Cytoscape 3.5.1 (Shannon et al., 2003).

Prediction of candidate miRNAs

MicroRNAs (miRNAs) are small noncoding RNAs that direct posttranscriptional repression of many mRNAs and thereby regulate -diverse biological processes from cell proliferation and apoptosis to organ development and immunity (Bartel, 2009). We selected candidate miRNAs whose expression levels were correlated with those potential therapeutic target immune genes by using the ENCORI database (https://starbase.sysu.edu.cn/). The miRNAs with clipExpNum higher than t times and that regulated more than two target immune genes were screened, and they were considered to play critical value in participating in the expression level of selected drug-targeted immune genes. The expression of predicted miRNAs was obtained from GSE48552, which includes early-stage and late-stage AD subjects. The DESeq2 package was applied to detect differentially expressed miRNAs at different stages and between females and males.

Results

irDEGs between patients with Alzheimer's disease and controls

In total, 31,426 mRNA expression profile data from 24 controls and 37 patients with AD in the GSE118553 dataset were used for this study. The characteristics of all samples are displayed in Table 1. There was a significant difference in age between the two groups (p = 0.006), whereas no significant difference was found in sex. The normalized mRNA expression levels in all samples are shown in Supplementary Figure S1. According to the screening criteria, 1,610 DEGs were detected between patients and controls. Among these genes, 81 DEGs were related to immunity. A heatmap of the differentially expressed genes and a Venn diagram of the irDEGs are shown in Figures 1A,B. A KEGG functional enrichment analysis of irDEGs in Metascape showed that these genes were significantly enriched in several immune system KEGG pathways, such as the chemokine signaling pathway, interleukin (IL)-17 signaling pathway, Th17 cell differentiation, B-cell receptor signaling pathway, hematopoietic cell lineage, T-cell receptor signaling pathway, C-type lectin

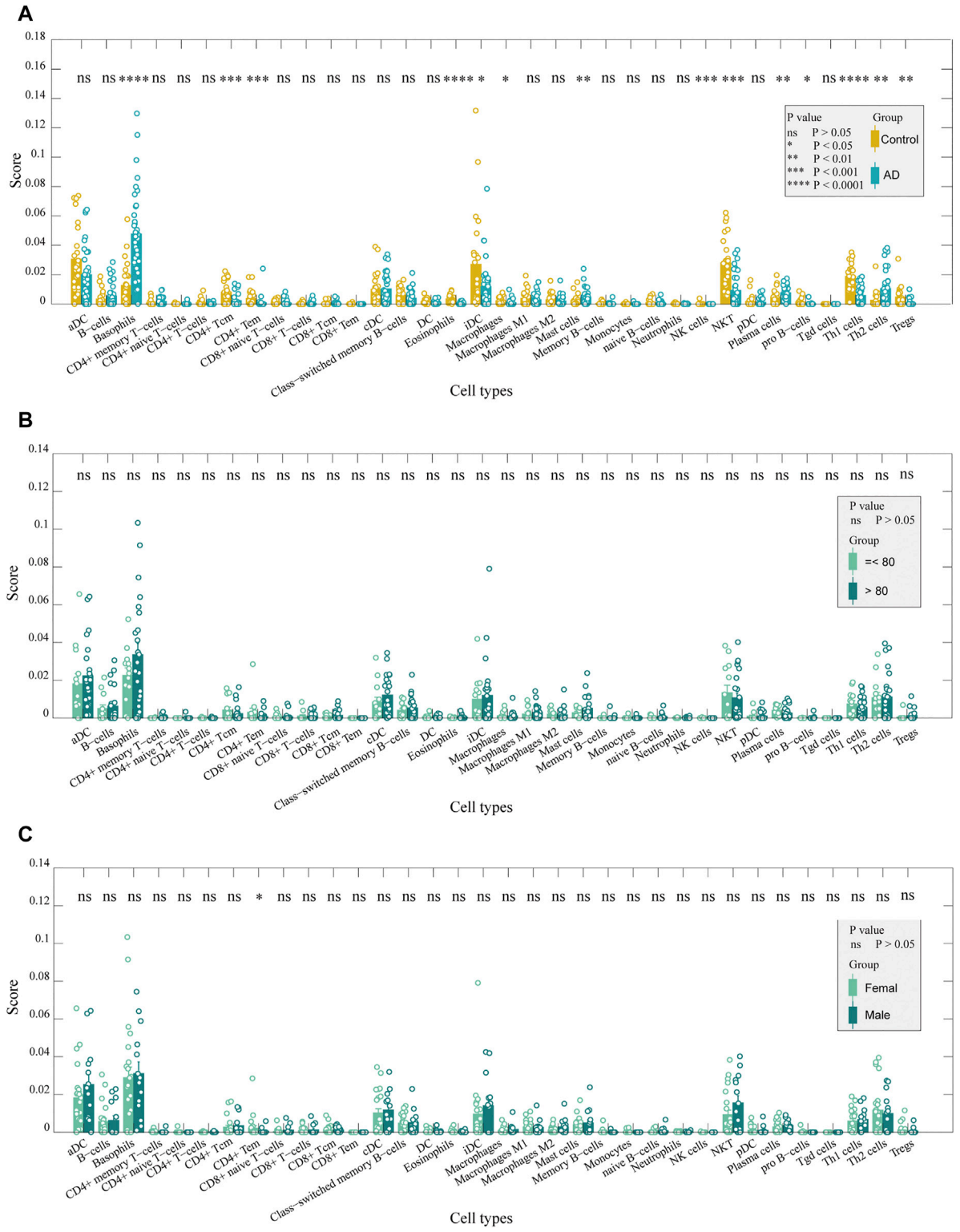

FIGURE 2
Immune cells in the entorhinal cortex between AD and control samples. **(A)**. Comparison of the scores of immune cells between AD and control samples: $CD4^+$ Tc, $CD4^+$ Te, Th1, NK, NKT, and pro-B cells, eosinophils, and Tregs were decreased in ADs ($p < 0.05$). In contrast, basophils, mast cells, plasma cells, and macrophages had elevated scores ($p < 0.05$). **(B)**. Comparison of immune cell scores between older and younger patients in AD samples: no significant difference was detected. **(C)**. Comparison of the score of immune cells between females and males in AD samples: only $CD4^+$ Tem was significantly different between the two groups ($p < 0.05$).

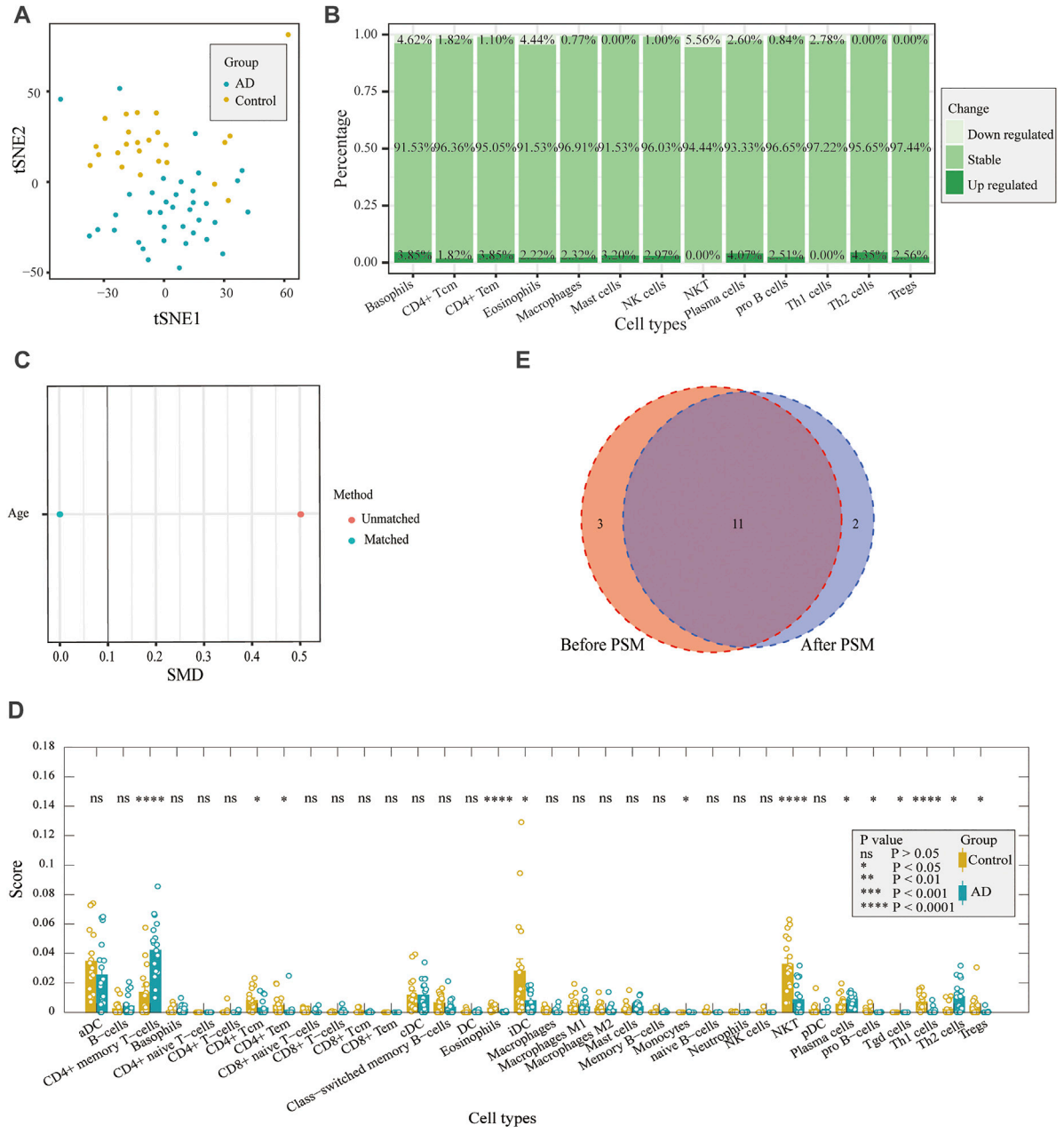

FIGURE 3
Correlation between differentially expressed marker genes and corresponding immune cells. **(A)** tSNE plot for AD and control individuals by using immune cell markers. **(B)**. DEG proportions in immune cell markers. **(C)** Difference in age was reduced after PSM. **(D)** Comparison of immune cell scores between AD and control samples after PSM. **(E)** Results both before PSM and after PSM are displayed with a Venn diagram. After PSM, changes in 11 immune cell scores were the same as before PSM.

receptor signaling pathway, natural killer cell–mediated cytotoxicity, Th1 and Th2 cell differentiation, Fc gamma R–mediated phagocytosis, Toll-like receptor signaling pathway, and platelet activation (Figure 1C). These results illustrate the involvement of immunity in AD progression at the transcriptome level.

Differences in immune cells between patients with Alzheimer's disease and controls

Gene expression data were analyzed according to the xCell algorithm to calculate 34 immune cell scores in each entorhinal

TABLE 2 Characteristics of the entorhinal cortex tissue in AD and control samples after propensity score matching.

	Controls	ADs	*p*
Age (=<80/> 80)	11/7	11/7	1
Sex (Male/Female)	11/7	8/10	0.317

cortex sample, and 14 immune cell scores differed between the two groups (Figure 2A). Among these immune cells, nine were lymphocytes, and the remaining five were myeloid cells. Overall, among the differential immune cell types, except for Th2 cells, which were elevated in patients, most of the lymphocyte scores decreased in ADs, including $CD4^+$ Tc, $CD4^+$ Te, Th1, natural killer (NK), NK T- and pro-B cells, eosinophils, and regulatory T cells. In contrast, most myeloid cells had elevated scores, except for interstitial dendritic cells (iDCs). They included basophils, mast cells, plasma cells, and macrophages. We also compared age and sex differences in immune cell scores in AD samples and found no significant differences in immune cell scores across age groups (Figure 2B). There were no significant differences in immune cell scores between sexes, except for $CD4^+$ Tem (Figure 2C). The results indicated that the immune differences may be independent of sex and age. Using t-distributed stochastic neighbor embedding (tSNE) to reduce the dimension of the data according to the expression of the marker genes in the two groups, patients and controls could be roughly distinguished. (Figure 3A). The ratio of differential genes to cell marker genes is shown in Figure 3B, and the number of csDEGs accounted for less than 10% of the corresponding cell marker genes.

Considering the age difference between the AD and control groups, we used PSM to perform 1:1 matching between the two groups to investigate whether there was an effect of age on immune infiltration. There were 18 samples in each group after matching (Table 2), and there was no difference in age (Figure 3C). We performed immune infiltration analysis using xCell and found that most of the results were consistent with those of prior matching (Figures 3D,E). The results were different for eosinophils, mast cells, and NK cells, in addition to significant differences in gamma delta T cells ($p < 0.05$) and monocytes ($p < 0.05$). Since most of the results did not significantly change after matching for age considering that the reduction in sample size may lead to poorer feasibility of the results, we used the data before matching for further analysis.

Correlation between csDEGs and immune cells

We explored whether the differences in immune cells were caused by differentially expressed marker genes. The DEGs in the different immune cells are shown in Figures 4A,B. In basophils, mast cells, macrophages, and Th2 cells, most of the differential marker genes were elevated in patients. This finding indicated that the differences in these cells in the AD group may be related to the different marker genes. We performed a correlation analysis between the expression levels of the different marker genes and the corresponding cell scores, and the results showed that *FBP2*, *GZMA*, *KCNJ9*, and *R3HDM1* were positively correlated with these cells, whereas *GRIN1*, *PMP2*, *ZMYND10*, *ADCY2*, *PNMA3*, *RASL12*, and *SLC24A2* were significantly negatively correlated (Figures 4C,D). The results also suggested that these genes may contribute to cellular differences between patients and controls.

Correlation in immune cells

To reveal the interrelationships between immune cells in AD samples, we performed the Pearson correlation analysis between intercellular scores in immune cells. The correlation between myeloid cells and lymphoid cells is shown in Figure 5A, and there was no significant correlation between myeloid cells and immune cells (cor = 0.3, $p = 0.07$). The correlation between immune cells is shown in Figure 5B. There was a close association between differential immune cells, most of which were positively correlated, such as basophils and iDCs, mast cells, NK cells, pro-B cells, eosinophils, iDCs, pro-B cells, and Th1 cells. In addition, Th2 cells were negatively correlated with NKT and Th1 cells. We further explored the potential genes leading to cell-to-cell correlation using the correlation analysis between marker genes and cell scores. A total of 51 marker genes were significantly associated with the differentially expressed cells (Figure 5C). Among these genes, 37 immune genes were associated with innate immunity.

Drug-targeted immune genes associated with innate immunity

In the GeneCards database, there are 3,676 genes related to AD according to the inferred functionality scores (>40). Moreover, 2,500 genes were identified as drug targets in the PharmGKB database. Through intersection analysis, we finally identified eight potential therapeutic target genes acting on innate immune cells: *GABRA1*, *GRIN1*, *GRM4*, *BMPR1A*, *GLB1*, *NTRK2*, *KCNN3*, and *TRPM3* (Figure 6A). According to the enrichment analysis results in Metascape, *BMPR1A* participated in cytokine–cytokine receptor interactions, fluid shear stress, and atherosclerosis, Hippo signaling pathway, signaling pathways regulating pluripotency of stem cells, and the tumor growth factor (TGF)-beta signaling pathway (Figure 6B). These pathways may play important roles in the association with immune cells involved. The expression

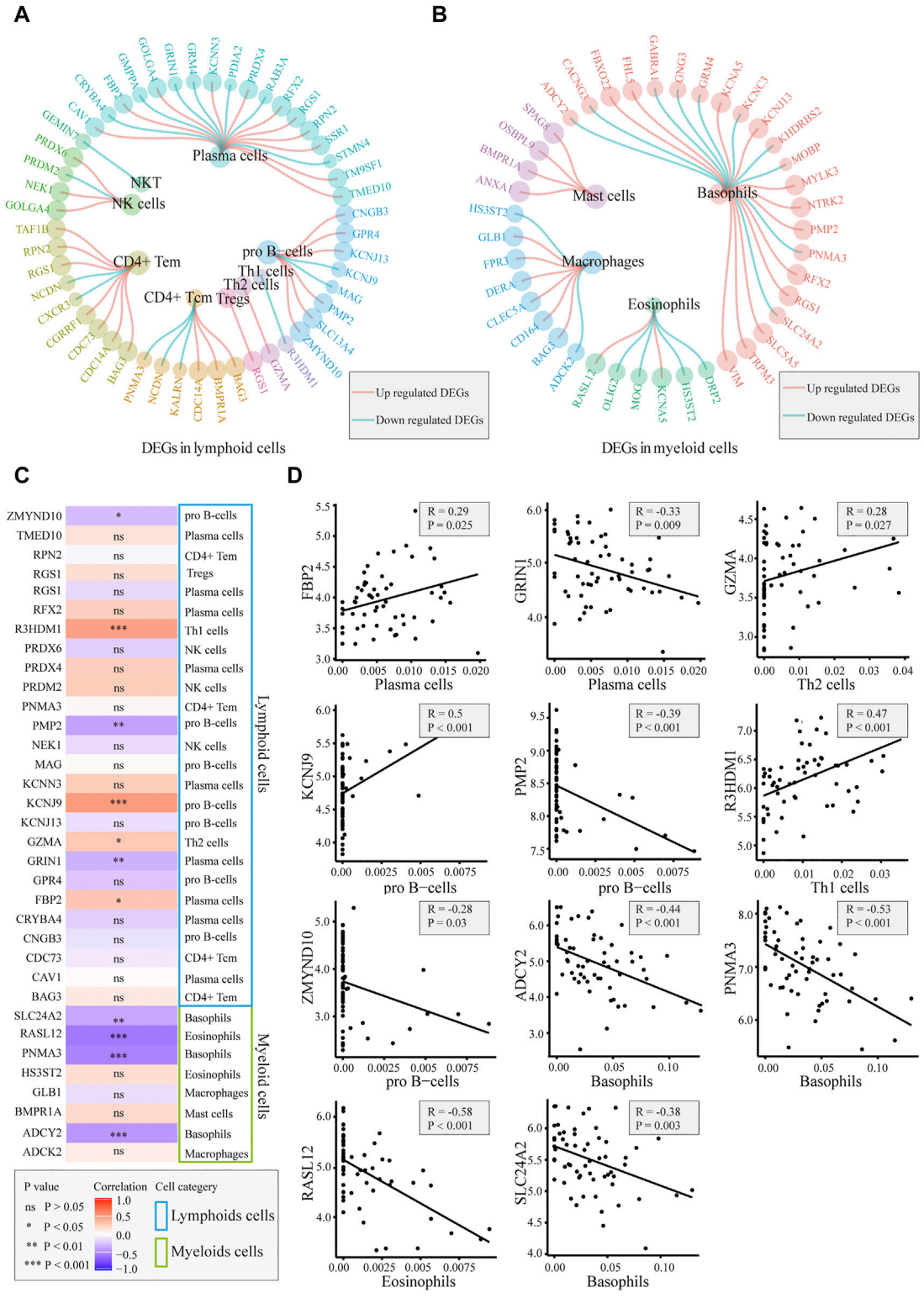

FIGURE 4
Correlation between immune cells and related gene detection. **(A)**. Differentially expressed marker genes in lymphoid cells. **(B)**. Differentially expressed marker genes in myeloid cells. **(C)**. Heatmap of the correlation between differentially expressed marker genes and corresponding immune cells. **(D)**. Plot of the correlation between differentially expressed marker genes and corresponding immune cells: *FBP2*, *GZMA*, *KCNJ9*, and *R3HDM1* are positively correlated with the corresponding cells. *GRIN1*, *PMP2*, *ZMYND10*, *ADCY2*, *PNMA3*, *RASL12*, and *SLC24A2* were significantly negatively correlated with the corresponding cells.

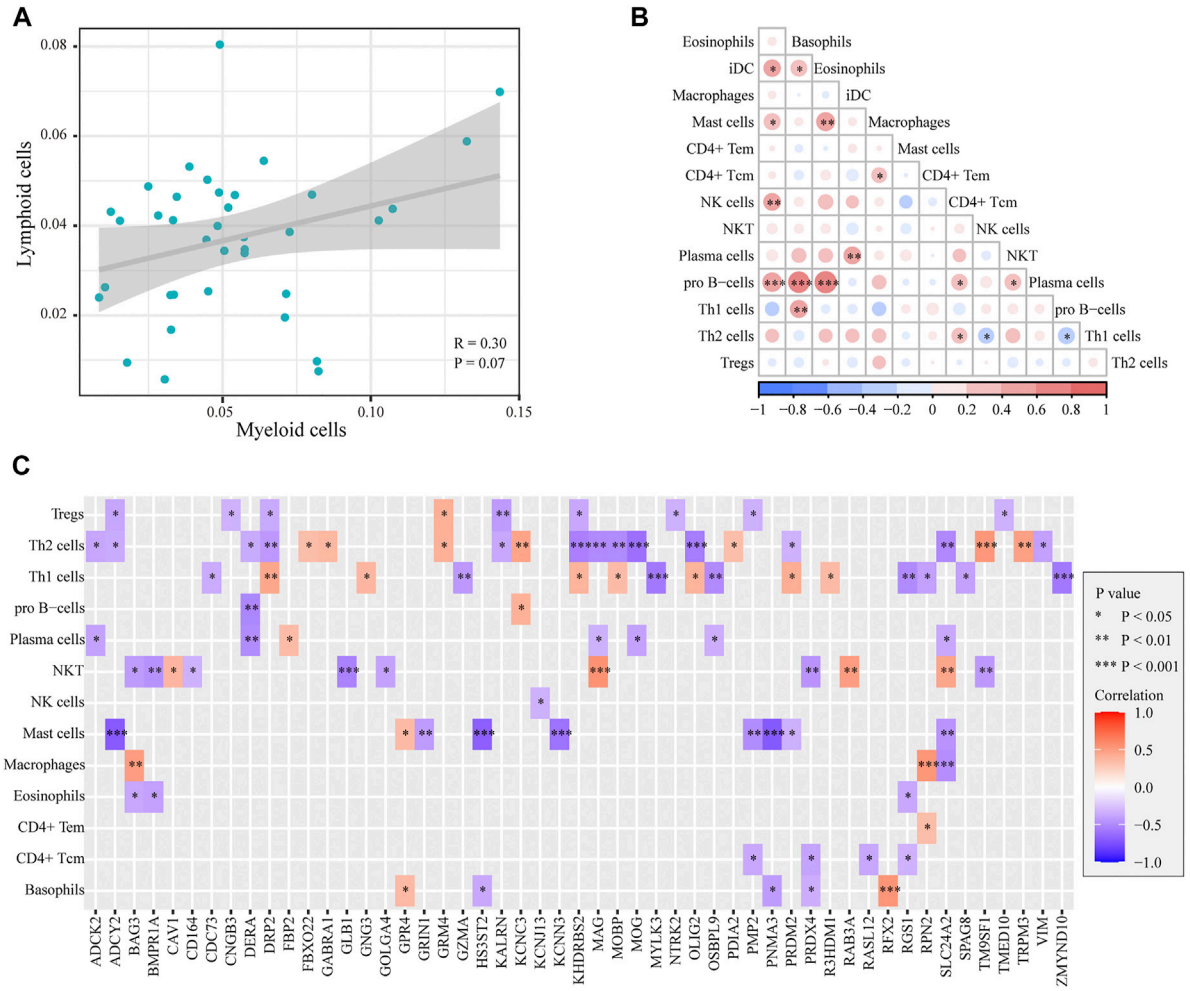

FIGURE 5
Correlation between myeloid cells and lymphoid cells in ADs. **(A)**. Plot of the correlation between myeloid cells and lymphoid cells: no significant difference was detected ($p = 0.07$). **(B)**. Heatmap of the correlation between immune cells: a close correlation between immune cells. **(C)**. Heatmap of the correlation between cell scores and genes: 51 marker genes were significantly associated with the differentially expressed cells.

levels of these eight genes in the AD and control groups are shown in Figure 6C. *GABRA1*, *GRIN1*, and *GRM4* were significantly increased in AD, whereas *BMPR1A*, *GLB1*, *NTRK2*, *KCNN3*, and *TRPM3* were significantly decreased (Figure 6C). The significant correlation between the eight genes and immune cells is displayed in Figure 7. We proceeded to test the diagnostic value of the gene expression levels to detect AD in our cohort using the ROC analysis. Almost all AUCs of genes were higher than 0.8, and the AUCs for *BMPR1A* and *TRPM3* were higher than 0.95, confirming that these genes can predict AD with high sensitivity and specificity, despite the small sample size (Figure 8). There were 36 drugs targeting these eight genes, including memantine, cycloserine, riluzole, and diclofenac sodium, which have been reported to be beneficial in reducing the incidence of AD (Figure 9).

Prediction of candidate miRNAs

miRNAs play a significant role in immune responses, such as maturation, proliferation, differentiation, and activation. Using the ENCORI database, we predicted miRNAs that may regulate the expression of drug-targeted genes. A total of 14 miRNAs, which may be involved in regulating gene expression and thus affecting immune infiltration, were screened as those with clipExpNum > 2 and that regulated > 2 target immune genes (Figure 10A). They participate in the regulation of immune infiltration by regulating the expression of *BMPR1A*, *GLB1*, *GRM4*, and *KCNN3*. In GSE48552, 10 miRNAs were detected from six early-stage AD patients and six late-stage AD patients, and four miRNAs had different expression levels in different disease states (Figure 10B). *hsa-miR-320c* was highly expressed in early-stage AD, whereas *hsa-miR-18a-5p*, *hsa-miR-18b-5p*, and

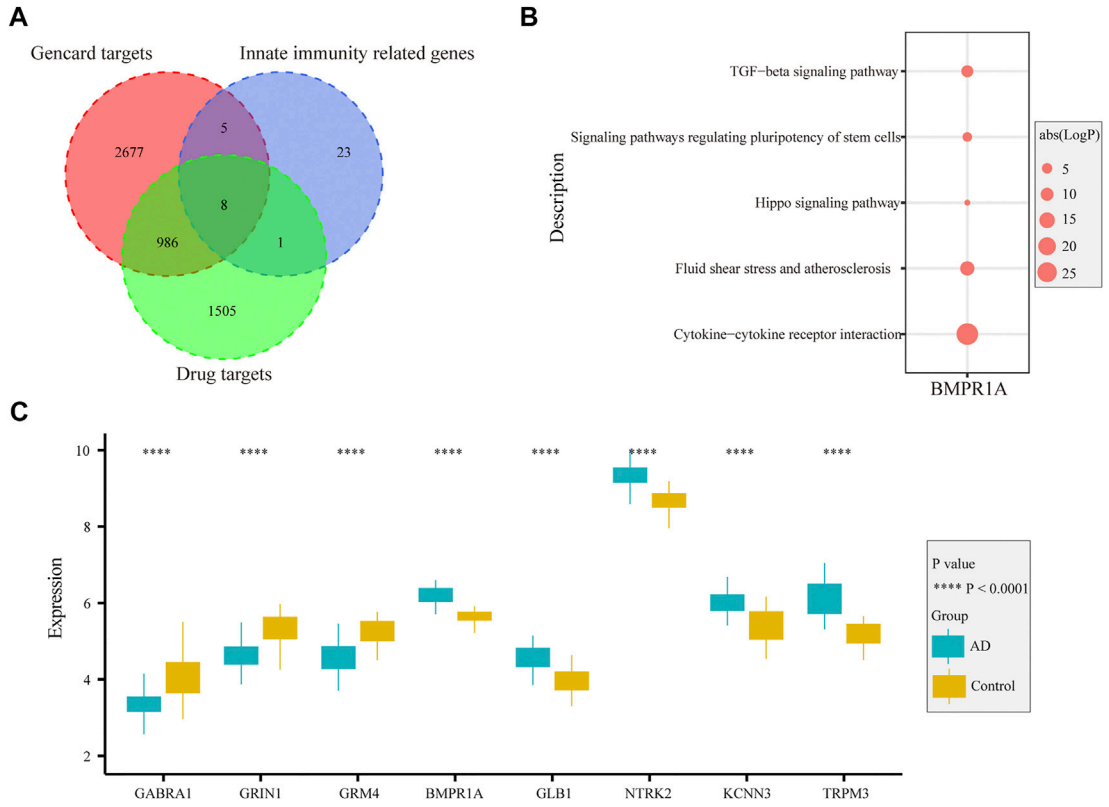

FIGURE 6
Function and expression of drug-targeted genes associated with myeloid cells in AD. **(A)**. Eight drug-targeted genes associated with myeloid cells for AD were selected. **(B)**. Pathways from KEGG analysis with 81 irDEGs associated with drug-targeted genes. **(C)**. Boxplot displaying the expression of eight drug-targeted genes in the entorhinal cortex between AD and control samples: *GABRA1*, *GRIN1*, and *GRM4* are significantly increased in AD samples, whereas *BMPR1A*, *GLB1*, *NTRK2*, *KCNN3*, and *TRPM3* are decreased in AD samples.

hsa-miR-491-5p were highly expressed in late-stage AD. We also assessed the expression of those miRNAs between sexes in AD, and no significant difference was detected (Figure 10C).

Discussion

In this study, we aimed to describe the immune cell landscape and related genes that cause specificity in the entorhinal cortex between patients with AD and control patients. We found that 81 irDEGs between patients with AD and controls, such as those involved in chemokine signaling, IL-17 signaling, Th17 cell differentiation, B-cell receptor signaling, hematopoietic cell differentiation, T-cell receptor signaling, C-type lectin receptor signaling, NK cell–mediated cytotoxicity, and Th1 and Th2 cell differentiation, were enriched in several immune system pathways. The immune cell landscape of brain tissues showed that several lymphocyte scores were decreased in AD, including $CD4^+$ Tc, $CD4^+$ Te, Th1, NK, NKT, pro-B cells, eosinophils, and Tregs. Significantly increased basophils, mast cells, and plasma cells, all of which are myeloid cells, were discovered in AD. The involvement of innate immunity in AD progression has been revealed at the transcriptomic level. In addition, the correlation between marker genes and immune cells detected potential genes that contributed to the immune specificity in the two groups. A close correlation was observed between the differentially scored immune cells. Finally, eight target genes and 36 drugs that may act on innate immunity were identified, which showed a high AUC in the identification of AD and may provide new strategies for AD treatment.

Neuroinflammation has a significant effect on the pathophysiology of AD (Heneka et al., 2015; Ransohoff, 2016; Lindestam Arlehamn et al., 2019). Infiltrating immune cells in border regions can affect the brain by secreting cytokines, modulating adjacent epithelial and ependymal cells, and altering cerebrospinal fluid composition (Cugurra et al., 2021). These cells are involved in tissue homeostasis, and they may enter the brain parenchyma when abnormalities occur. Studies have shown that impaired meningeal lymphatic function may be a factor in the aggravation of AD pathology (Louveau et al., 2016; Da Mesquita et al., 2018). Similarly, dysfunction of the meningeal lymphatic system has been implicated in the pathogenesis of

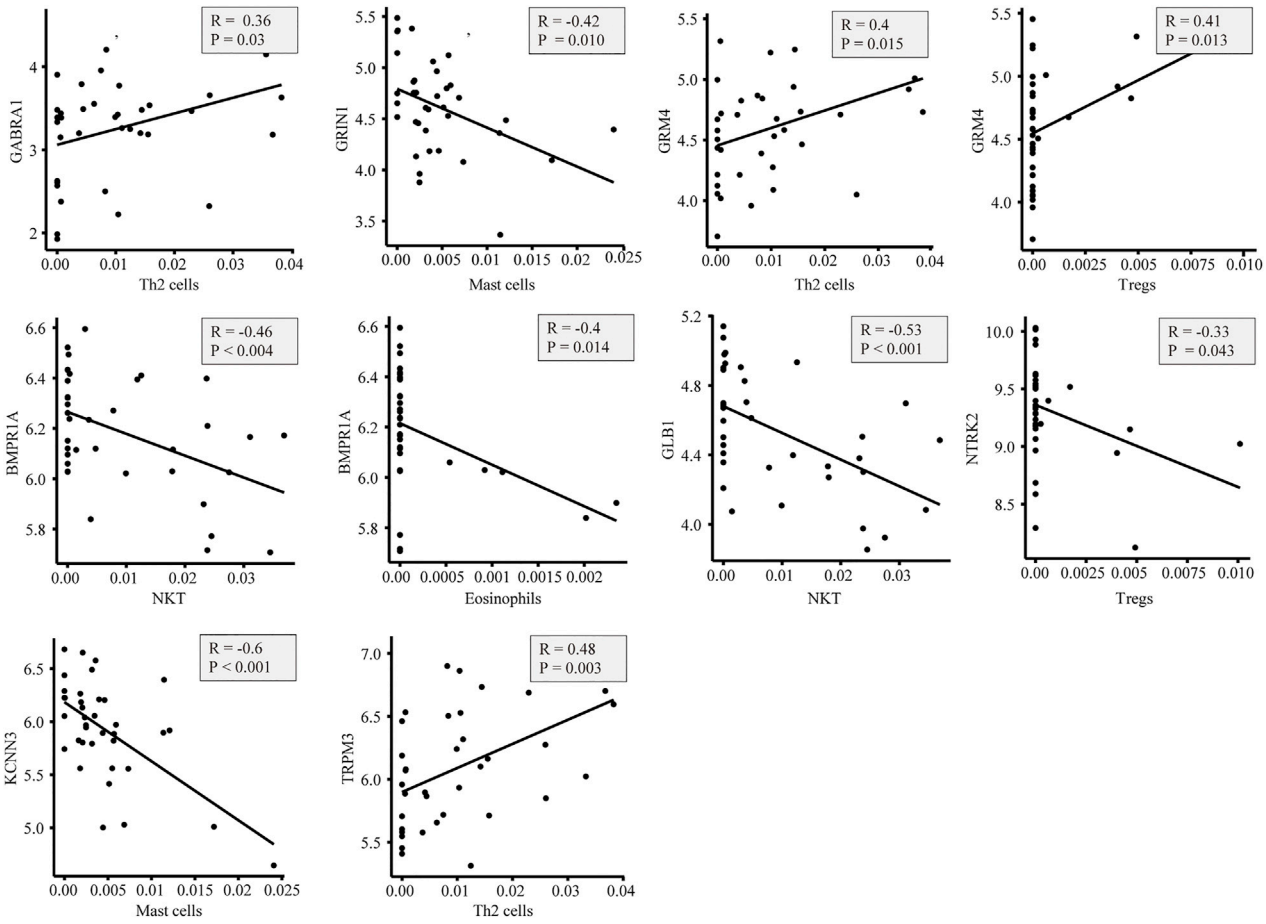

FIGURE 7
Plot of the correlation between eight genes associated with immune cells: there is a close correlation between genes and immune cells.

other classic autoimmune neurodegenerative diseases, such as multiple sclerosis and autoimmune encephalitis (Hsu et al., 2019; Schwartz et al., 2019). In AD, neuroinflammation is not a passive system activated by the emergence of senile plaques and neurofibrillary tangles but instead plays an equally (or greater) role in the pathogenesis of plaques and tangles themselves (Zhang et al., 2013). The important role of neuroinflammation is supported by the findings that immune receptor genes, such as *TREM22* and *CD33*, are associated with AD (Bradshaw et al., 2013; Griciuc et al., 2013; Guerreiro et al., 2013). Innate immunity plays a major immune role in AD (Heppner et al., 2015). Innate immune cell hyperexcitability was reported to be associated with cognitive decline (Nam et al., 2022). In a murine amyloidosis model, IFN-I signaling represents a critical module within the neuroinflammatory network of AD and prompts concerted cellular states that are detrimental to memory and cognition (Roy et al., 2022). Collective histological, bioinformatics and molecular analyses highlight the permanent activation of microglia, the brain's resident immune cells, and the association of many AD risk polymorphisms and rare variants with microglia and innate immunity (Zhang et al., 2013; Huang et al., 2017). Scientists have recognized these and have focused their efforts on therapies aimed at modulating innate immunity. In the present study, we found that the AD group had significantly lower scores for eosinophils, macrophages, NK, NKT, and Treg cells, while higher scores for basophils, mast cells, and macrophages in AD were detected. This result also supports the important role of innate immunity in the development of AD.

In addition to characterizing differences in immune cell profiles between patients with AD and controls, we identified eight genes with potential roles in innate immune cells and 36 drugs with potential therapeutic effects by correlation analysis and combining the GeneCards and PharmGKB databases. These genes and drugs may provide evidence for the treatment of AD. *BMPR1A* encodes a morphogenetic protein receptor. The ligands of these receptors are members of the TGF-β superfamily involved in the regulation of cell

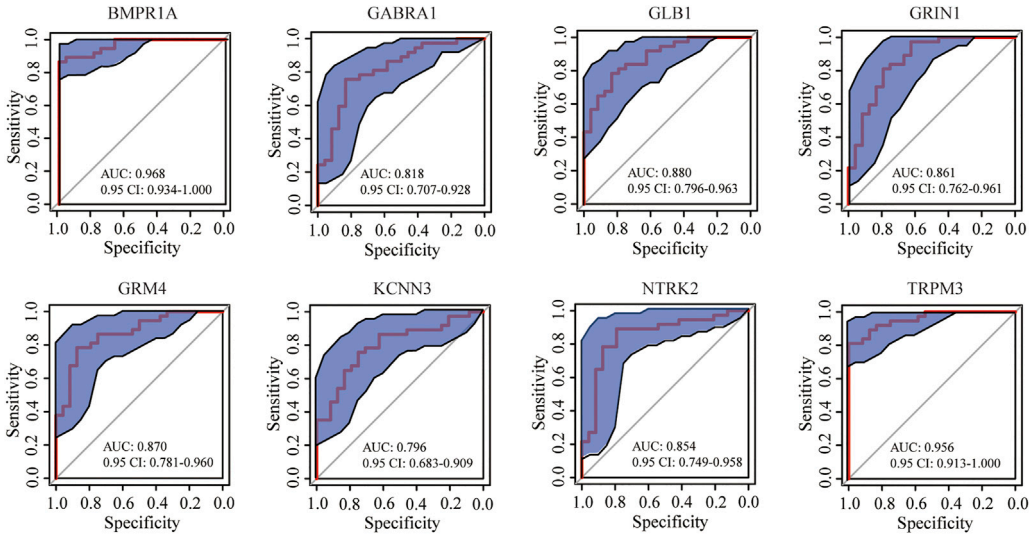

FIGURE 8
ROC curve of eight genes in predicting AD samples: blue area represents the 0.95 CI value of each gene for the prediction of AD; red curve is the ROC curve of eight genes in predicting AD; almost all AUCs of the gene were higher than 0.8, and the AUCs for *BMPR1A* and *TRPM3* were higher than 0.95.

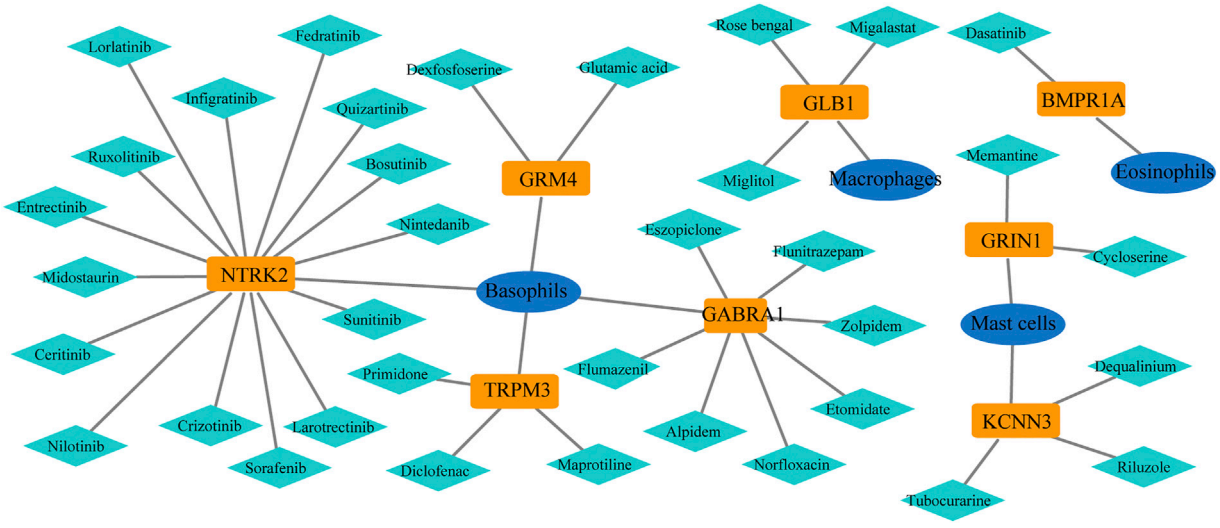

FIGURE 9
Potential drugs of selected genes from the PharmGKB database: 36 drugs targeted these eight genes.

proliferation, differentiation, and apoptosis and therefore play essential roles during embryonic development and pattern formation (Morikawa et al., 2016). TGF-β regulates a variety of important cell and tissue functions, such as cell growth and differentiation, angiogenesis, extracellular matrix production, immune function, cell chemotaxis, apoptosis, and hematopoiesis (Flanders et al., 1998). In this analysis, the TGF-β signaling pathway was significantly enriched in KEGG analysis, indicating its critical function in the neuroinflammation of AD. Chemokines are cytokines that orchestrate innate and adaptive immune responses and are differentially regulated in several neuroinflammatory disorders (Charo & Ransohoff, 2006). Our previous analysis provides evidence regarding viral infection in AD development (Sun et al., 2022). In our study, we found that the differential expression of *BMPR1* was significantly related to the occurrence of AD, which may

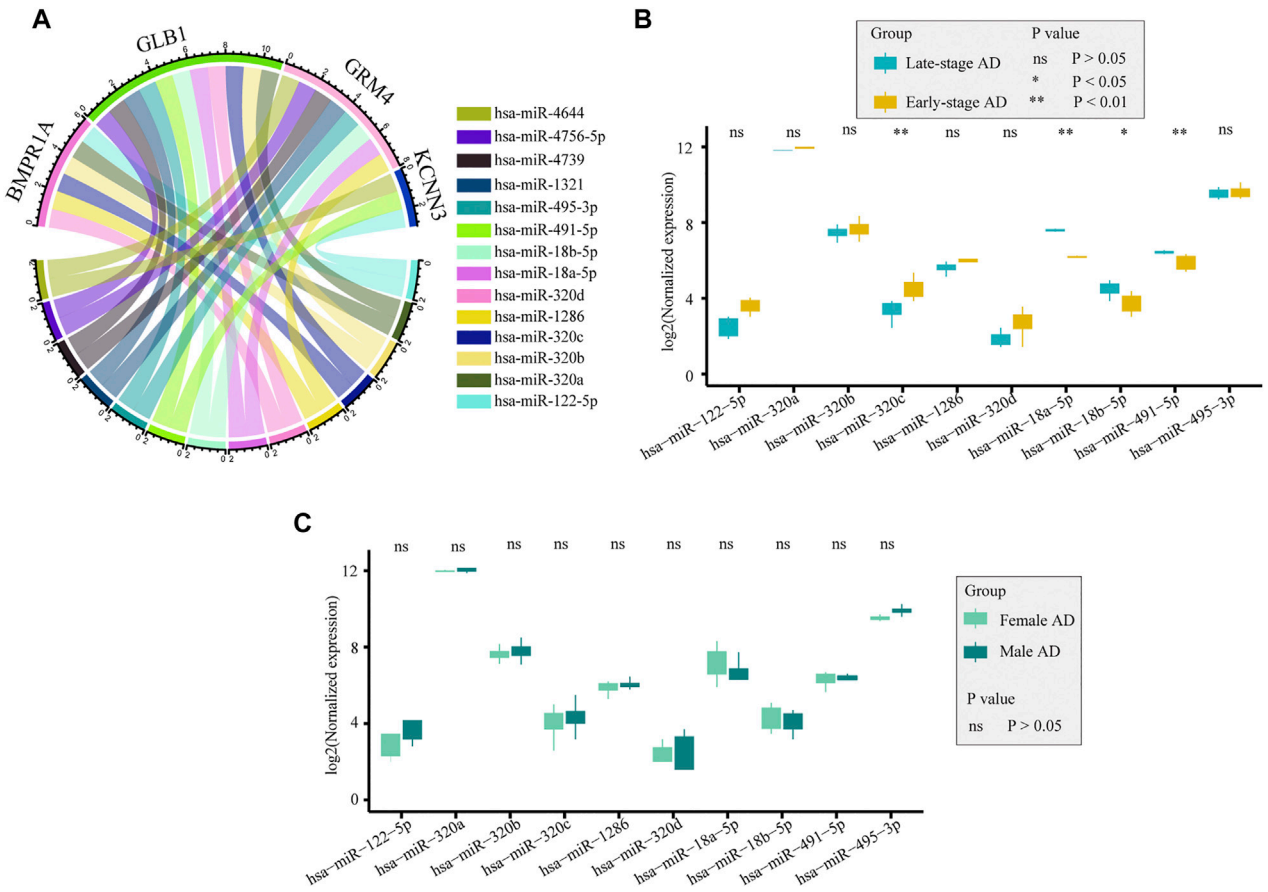

FIGURE 10
Potential miRNAs regulated selected genes. **(A)**. Potential miRNAs regulating selected genes were obtained from the ENCORI database. **(B)**. Expression of miRNAs between early-stage and late-stage ADs from GSE48552: *hsa-miR-320c*, *hsa-miR-18a-5p*, *hsa-miR-18b-5p*, and *hsa-miR-491-5p* were differentially expressed between the two groups. **(C)**. Expression of miRNAs between females and males ADs from GSE48552: no significant difference was detected between the two groups.

provide new evidence for the treatment of AD in the future. In our analysis, we also found that *NPC2*, *METTL7A*, and *ARL5A* were highly expressed in patients with AD compared to controls. According to previous reports, *NPC2* is considered to be closely related to lipid metabolism (Awan et al., 2022) and tumor metastasis (de Araujo et al., 2021). The relevance of *METTL7A* to lipid metabolism has also received attention (Yi et al., 2020). *APOE*, a key gene in the development of AD, encodes a multifunctional protein with central roles in lipid metabolism (Liu et al., 2013). These studies all indicate that lipid metabolism may play an important role in AD development. *ARL5A* belongs to the ARF family, which are members of the *Ras* gene superfamily of GTP-binding proteins that are involved in a variety of processes, such as cellular communication, endoplasmic reticulum binding, vesicle transport, and protein synthesis (Lin et al., 2002; Wang et al., 2005). The association between *ARL5A* and AD has not been reported and needs to be further studied.

These results suggest that a number of drugs act on innate immune cells through the eight immune genes identified and that they may play an important role in the prevention and treatment of AD. For example, memantine, cycloserine, riluzole, and diclofenac sodium have all been reported to have beneficial effects on reducing the incidence of AD. Memantine, an N-methyl-D-aspartate receptor (NMDAR) antagonist, is clinically quite effective for behavioral symptoms and is often added to cholinesterase inhibitors to enhance their effects, whereas aducanumab has recently been approved for amyloidosis (Langa et al., 2004; Giacobini et al., 2022). Aducanumab is used to mitigate the neurotoxicity associated with AD and other neurodegenerative disorders. Memantine blocks the NMDAR subtype of the glutamate receptor, preventing excessive activation of the glutamate receptor while allowing normal activity (Langa et al., 2004). Its blockade antagonizes the overactive glutaminergic system in the central nervous system (CNS), which is hypothesized to be involved in

the neurotoxicity of AD. NMDA encephalitis is an important autoimmune encephalitis, and its associated syndromes and immune-mediated mechanisms have been described (Muñoz-Lopetegi et al., 2020). Our results suggest that memantine may exert a therapeutic effect by affecting *GRIN1* expression in mast cells. These results may offer new perspectives for the treatment of NMDA autoimmune encephalitis and AD with memantine. D-cycloserine exhibits partial agonist activity at the glycine site of the NMDA subtype of the glutamate receptor, promoting receptor activation and improving cognition and memory, which has been validated as a cognitive benefit in patients with AD (Bowen et al., 1992; Tsai et al., 1999). Riluzole, the glutamate modulator, is FDA-approved for the treatment of amyotrophic lateral sclerosis, with potential benefits for cognition, aging, and structural and molecular markers of AD (Matthews et al., 2021). Diclofenac is chemically related to the finasteride class of NSAIDs and has been shown to improve cognition in two independent studies using mouse models of AD (Joo et al., 2006; Daniels et al., 2016). It is also associated with a reduced risk of developing AD (Stuve et al., 2020).

miRNAs play important gene regulatory roles in animals and plants by pairing with mRNAs of protein-coding genes to direct their posttranscriptional repression (Bartel, 2009). Therefore, we also predicted miRNAs that might regulate the expression of drug-targeted genes. We found that these 14 microRNAs might be involved in regulating gene expression, thereby affecting immune infiltration. *hsa-miR-320a*, *hsa-miR-495*, and *hsa-miR-122-5p* have been reported to be associated with autoimmune disease-related outcomes (Yao et al., 2019; Cordes et al., 2020; Ni & Leng, 2020; Fu et al., 2021). It is noteworthy that the reports for *hsa-miR-320a*, *hsa-miR-320b*, and *hsa-miR-320c* involved central immunity (Regev et al., 2018). Our results predict the important role of autoimmunity in AD development in the related assessment of miRNAs, and they reveal powerful new endogenous combinatorial therapeutic targets.

In conclusion, this study attempted to clarify the possible mechanism of the immune microenvironment involved in the occurrence and development of AD by analyzing the immune microenvironment of the entorhinal cortex of patients with AD and to describe the association between genes on drugs and immune cells. However, this study still has certain limitations. First, the application of drugs affects transcriptome expression, but we were not able to obtain reliable information on drug usage from GEO dataset. Second, age may have an effect on immune infiltration, but considering that the smaller sample size would lead to less reliable results, our study did not use age-matched data for analysis. Third, the results were not validated with biological experiments, which are strictly limited by ethics. In the future, we will further study the role of the immune microenvironment in the pathogenesis of AD using more samples and animal models. In conclusion, our study describes the specificity of the immune cell landscape and associated genes contributing to AD in the entorhinal cortex, which provides new insights into the treatment of AD.

Data availability statement

The datasets presented in this study can be found in online repositories. The names of the repository/repositories and accession number(s) can be found below: https://www.ncbi.nlm.nih.gov/geo/, GSE118553, GSE48552.

Author contributions

HZ and SC conducted the data in the study and draft the manuscript, and all authors took responsibility for the integrity of the data and accuracy of the data analysis. YX, XS, QJ, and MF conducted to plot the figure in the study. XX and JT conducted to collect the data from online database. BN and CL conceptualized and designed the study. All authors have reviewed and approved the final manuscript.

Funding

We acknowledge the Natural Science Foundation of Shanghai (grant number: 20ZR1442900) and Shanghai Fourth People's Hospital, School of Medicine, Tongji University (grant numbers: sykyqd01901 and SY-XKZT-2021-2001) for providing funding support to the current work.

Acknowledgments

The authors are grateful to the providers who submitted the data to the public databases. We acknowledge the Natural Science Foundation of Shanghai and Shanghai Fourth People's Hospital, School of Medicine, Tongji University for providing funding support for the current work.

Conflict of interest

The authors declare that the research was conducted in the absence of any commercial or financial relationships that could be construed as a potential conflict of interest.

Publisher's note

All claims expressed in this article are solely those of the authors and do not necessarily represent those of

their affiliated organizations, or those of the publisher, the editors and the reviewers. Any product that may be evaluated in this article, or claim that may be made by its manufacturer, is not guaranteed or endorsed by the publisher.

Supplementary material

The Supplementary Material for this article can be found online at: https://www.frontiersin.org/articles/10.3389/fphar.2022.941656/full#supplementary-material

References

Aisen, P. S. (2002). The potential of anti-inflammatory drugs for the treatment of Alzheimer's disease. *Lancet. Neurol.* 1, 279–284. doi:10.1016/s1474-4422(02)00133-3

Allen, J. D., Chen, M., and Xie, Y. (2009). Model-based background correction (MBCB): R methods and GUI for illumina bead-array data. *J. Cancer Sci. Ther.* 1, 25–27. doi:10.4172/1948-5956.1000004

Anthony, J. C., Breitner, J. C., Zandi, P. P., Meyer, M. R., Jurasova, I., Norton, M. C., et al. (2000). Reduced prevalence of AD in users of NSAIDs and H2 receptor antagonists: The cache county study. *Neurology* 54, 2066–2071. doi:10.1212/wnl.54.11.2066

Aran, D., Hu, Z., and Butte, A. J. (2017). xCell: digitally portraying the tissue cellular heterogeneity landscape. *Genome Biol.* 18, 220. doi:10.1186/s13059-017-1349-1

Awan, S., Lambert, M., Imtiaz, A., Alpy, F., Tomasetto, C., Oulad-Abdelghani, M., et al. (2022). Wnt5a promotes lysosomal cholesterol egress and protects against atherosclerosis. *Circ. Res.* 130, 184–199. doi:10.1161/circresaha.121.318881

Bamberger, M. E., Harris, M. E., McDonald, D. R., Husemann, J., and Landreth, G. E. (2003). A cell surface receptor complex for fibrillar beta-amyloid mediates microglial activation. *J. Neurosci.* 23, 2665–2674. doi:10.1523/jneurosci.23-07-02665.2003

Bartel, D. P. (2009). MicroRNAs: Target recognition and regulatory functions. *Cell* 136, 215–233. doi:10.1016/j.cell.2009.01.002

Bhattacharya, S., Dunn, P., Thomas, C. G., Smith, B., Schaefer, H., Chen, J., et al. (2018). ImmPort, toward repurposing of open access immunological assay data for translational and clinical research. *Sci. Data* 5, 180015. doi:10.1038/sdata.2018.15

Bowen, D. M., Francis, P. T., Pangalos, M. N., Stephens, P. H., and Procter, A. W. (1992). Treatment strategies for Alzheimer's disease. *Lancet* 339, 132–133. doi:10.1016/0140-6736(92)91050-i

Bradshaw, E. M., Chibnik, L. B., Keenan, B. T., Ottoboni, L., Raj, T., Tang, A., et al. (2013). CD33 alzheimer's disease locus: Altered monocyte function and amyloid biology. *Nat. Neurosci.* 16, 848–850. doi:10.1038/nn.3435

Charo, I. F., and Ransohoff, R. M. (2006). The many roles of chemokines and chemokine receptors in inflammation. *N. Engl. J. Med.* 354, 610–621. doi:10.1056/NEJMra052723

Clough, E., and Barrett, T. (2016). The gene expression Omnibus database. *Methods Mol. Biol.* 1418, 93–110. doi:10.1007/978-1-4939-3578-9_5

Cordes, F., Demmig, C., Bokemeyer, A., Brückner, M., Lenze, F., Lenz, P., et al. (2020). MicroRNA-320a monitors intestinal disease activity in patients with inflammatory bowel disease. *Clin. Transl. Gastroenterol.* 11, e00134. doi:10.14309/ctg.0000000000000134

Cugurra, A., Mamuladze, T., Rustenhoven, J., Dykstra, T., Beroshvili, G., Greenberg, Z. J., et al. (2021). Skull and vertebral bone marrow are myeloid cell reservoirs for the meninges and CNS parenchyma. *Science* 373, eabf7844. doi:10.1126/science.abf7844

Da Mesquita, S., Louveau, A., Vaccari, A., Smirnov, I., Cornelison, R. C., Kingsmore, K. M., et al. (2018). Functional aspects of meningeal lymphatics in ageing and Alzheimer's disease. *Nature* 560, 185–191. doi:10.1038/s41586-018-0368-8

Daniels, M. J., Rivers-Auty, J., Schilling, T., Spencer, N. G., Watremez, W., Fasolino, V., et al. (2016). Fenamate NSAIDs inhibit the NLRP3 inflammasome and protect against Alzheimer's disease in rodent models. *Nat. Commun.* 7, 12504. doi:10.1038/ncomms12504

Davis, S., and Meltzer, P. S. (2007). GEOquery: A bridge between the gene expression Omnibus (GEO) and BioConductor. *Bioinforma. Oxf. Engl.* 23, 1846–1847. doi:10.1093/bioinformatics/btm254

de Araujo, L. S., Ribeiro-Alves, M., Wipperman, M. F., Vorkas, C. K., Pessler, F., and Saad, M. H. F. (2021). Transcriptomic biomarkers for tuberculosis: Validation of NPC2 as a single mRNA biomarker to diagnose TB, predict disease progression, and monitor treatment response. *Cells* 10, 2704. doi:10.3390/cells10102704

de Calignon, A., Polydoro, M., Suárez-Calvet, M., William, C., Adamowicz, D. H., Kopeikina, K. J., et al. (2012). Propagation of tau pathology in a model of early Alzheimer's disease. *Neuron* 73, 685–697. doi:10.1016/j.neuron.2011.11.033

Du, P., Kibbe, W. A., and Lin, S. M. (2008). lumi: a pipeline for processing Illumina microarray. *Bioinforma. Oxf. Engl.* 24, 1547–1548. doi:10.1093/bioinformatics/btn224

Flanders, K. C., Ren, R. F., and Lippa, C. F. (1998). Transforming growth factor-betas in neurodegenerative disease. *Prog. Neurobiol.* 54, 71–85. doi:10.1016/s0301-0082(97)00066-x

Fu, S., Zheng, Y., Sun, Y., Lai, M., Qiu, J., Gui, F., et al. (2021). Suppressing long noncoding RNA OGRU ameliorates diabetic retinopathy by inhibition of oxidative stress and inflammation via miR-320/USP14 axis. *Free Radic. Biol. Med.* 169, 361–381. doi:10.1016/j.freeradbiomed.2021.03.016

Giacobini, E., Cuello, A. C., and Fisher, A. (2022). Reimagining cholinergic therapy for Alzheimer's disease. *Brain.* 145, 2250–2275. doi:10.1093/brain/awac096

Griciuc, A., Serrano-Pozo, A., Parrado, A. R., Lesinski, A. N., Asselin, C. N., Mullin, K., et al. (2013). Alzheimer's disease risk gene CD33 inhibits microglial uptake of amyloid beta. *Neuron* 78, 631–643. doi:10.1016/j.neuron.2013.04.014

Guerreiro, R., Wojtas, A., Bras, J., Carrasquillo, M., Rogaeva, E., Majounie, E., et al. (2013). TREM2 variants in Alzheimer's disease. *N. Engl. J. Med.* 368, 117–127. doi:10.1056/NEJMoa1211851

Heneka, M. T., Carson, M. J., El Khoury, J., Landreth, G. E., Brosseron, F., Feinstein, D. L., et al. (2015). Neuroinflammation in Alzheimer's disease. *Lancet. Neurol.* 14, 388–405. doi:10.1016/s1474-4422(15)70016-5

Heppner, F. L., Ransohoff, R. M., and Becher, B. (2015). Immune attack: The role of inflammation in alzheimer disease. *Nat. Rev. Neurosci.* 16, 358–372. doi:10.1038/nrn3880

Hewett, M., Oliver, D. E., Rubin, D. L., Easton, K. L., Stuart, J. M., Altman, R. B., et al. (2002). PharmGKB: The pharmacogenetics knowledge base. *Nucleic Acids Res.* 30, 163–165. doi:10.1093/nar/30.1.163

Hsu, M., Rayasam, A., Kijak, J. A., Choi, Y. H., Harding, J. S., Marcus, S. A., et al. (2019). Neuroinflammation-induced lymphangiogenesis near the cribriform plate contributes to drainage of CNS-derived antigens and immune cells. *Nat. Commun.* 10, 229. doi:10.1038/s41467-018-08163-0

Huang, K. L., Marcora, E., Pimenova, A. A., Di Narzo, A. F., Kapoor, M., Jin, S. C., et al. (2017). A common haplotype lowers PU.1 expression in myeloid cells and delays onset of Alzheimer's disease. *Nat. Neurosci.* 20, 1052–1061. doi:10.1038/nn.4587

Jack, C. R., Jr., Knopman, D. S., Jagust, W. J., Petersen, R. C., Weiner, M. W., Aisen, P. S., et al. (2013). Tracking pathophysiological processes in alzheimer's disease: An updated hypothetical model of dynamic biomarkers. *Lancet. Neurol.* 12, 207–216. doi:10.1016/s1474-4422(12)70291-0

Jack, C. R., Jr., Knopman, D. S., Jagust, W. J., Shaw, L. M., Aisen, P. S., Weiner, M. W., et al. (2010). Hypothetical model of dynamic biomarkers of the Alzheimer's pathological cascade. *Lancet. Neurol.* 9, 119–128. doi:10.1016/s1474-4422(09)70299-6

Jing, Q., Zhang, H., Sun, X., Xu, Y., Cao, S., Fang, Y., et al. (2021). A comprehensive analysis identified hub genes and associated drugs in alzheimer's disease. *Biomed. Res. Int.* 2021, 8893553. doi:10.1155/2021/8893553

Joo, Y., Kim, H. S., Woo, R. S., Park, C. H., Shin, K. Y., Lee, J. P., et al. (2006). Mefenamic acid shows neuroprotective effects and improves cognitive impairment in *in vitro* and *in vivo* Alzheimer's disease models. *Mol. Pharmacol.* 69, 76–84. doi:10.1124/mol.105.015206

Kobak, D., and Berens, P. (2019). The art of using t-SNE for single-cell transcriptomics. *Nat. Commun.* 10, 5416. doi:10.1038/s41467-019-13056-x

Lane, C. A., Hardy, J., and Schott, J. M. (2018). Alzheimer's disease. *Eur. J. Neurol.* 25, 59–70. doi:10.1111/ene.13439

Langa, K. M., Foster, N. L., and Larson, E. B. (2004). Mixed dementia: Emerging concepts and therapeutic implications. *Jama* 292, 2901–2908. doi:10.1001/jama.292.23.2901

Lin, C. Y., Li, C. C., Huang, P. H., and Lee, F. J. (2002). A developmentally regulated ARF-like 5 protein (ARL5), localized to nuclei and nucleoli, interacts with heterochromatin protein 1. *J. Cell Sci.* 115, 4433–4445. doi:10.1242/jcs.00123

Lindestam Arlehamn, C. S., Garretti, F., Sulzer, D., and Sette, A. (2019). Roles for the adaptive immune system in Parkinson's and Alzheimer's diseases. *Curr. Opin. Immunol.* 59, 115–120. doi:10.1016/j.coi.2019.07.004

Liu, C. C., Liu, C. C., Kanekiyo, T., Xu, H., and Bu, G. (2013). Apolipoprotein E and alzheimer disease: Risk, mechanisms and therapy. *Nat. Rev. Neurol.* 9, 106–118. doi:10.1038/nrneurol.2012.263

Liu, Y., Walter, S., Stagi, M., Cherny, D., Letiembre, M., Schulz-Schaeffer, W., et al. (2005). LPS receptor (CD14): A receptor for phagocytosis of alzheimer's amyloid peptide. *Brain* 128, 1778–1789. doi:10.1093/brain/awh531

Louveau, A., Da Mesquita, S., and Kipnis, J. (2016). Lymphatics in neurological disorders: A neuro-lympho-vascular component of multiple sclerosis and alzheimer's disease? *Neuron* 91, 957–973. doi:10.1016/j.neuron.2016.08.027

Mandrekar, J. N. (2010). Receiver operating characteristic curve in diagnostic test assessment. *J. Thorac. Oncol.* 5, 1315–1316. doi:10.1097/JTO.0b013e3181ec173d

Matthews, D. C., Mao, X., Dowd, K., Tsakanikas, D., Jiang, C. S., Meuser, C., et al. (2021). Riluzole, a glutamate modulator, slows cerebral glucose metabolism decline in patients with Alzheimer's disease. *Brain.* 144, 3742–3755. doi:10.1093/brain/awab222

McGeer, P. L., Schulzer, M., and McGeer, E. G. (1996). Arthritis and anti-inflammatory agents as possible protective factors for alzheimer's disease: A review of 17 epidemiologic studies. *Neurology* 47, 425–432. doi:10.1212/wnl.47.2.425

Medeiros, R., and LaFerla, F. M. (2013). Astrocytes: Conductors of the alzheimer disease neuroinflammatory symphony. *Exp. Neurol.* 239, 133–138. doi:10.1016/j.expneurol.2012.10.007

Morikawa, M., Derynck, R., and Miyazono, K. (2016). TGF-β and the TGF-β family: Context-dependent roles in cell and tissue physiology. *Cold Spring Harb. Perspect. Biol.* 8, a021873. doi:10.1101/cshperspect.a021873

Muñoz-Lopetegi, A., Graus, F., Dalmau, J., and Santamaria, J. (2020). Sleep disorders in autoimmune encephalitis. *Lancet. Neurol.* 19, 1010–1022. doi:10.1016/s1474-4422(20)30341-0

Nagpal, S., Kuntal, B. K., and Mande, S. S. (2021). NetSets.js: A JavaScript framework for compositional assessment and comparison of biological networks through venn-integrated network diagrams. *Bioinforma. Oxf. Engl.* 37, 580–582. doi:10.1093/bioinformatics/btaa723

Nam, H., Lee, Y., Kim, B., Lee, J. W., Hwang, S., An, H. K., et al. (2022). Presenilin 2 N141I mutation induces hyperactive immune response through the epigenetic repression of REV-ERBα. *Nat. Commun.* 13, 1972. doi:10.1038/s41467-022-29653-2

Ni, W. J., and Leng, X. M. (2020). Down-regulated miR-495 can target programmed cell death 10 in ankylosing spondylitis. *Mol. Med.* 26, 50. doi:10.1186/s10020-020-00157-3

Olabarria, M., Noristani, H. N., Verkhratsky, A., and Rodríguez, J. J. (2010). Concomitant astroglial atrophy and astrogliosis in a triple transgenic animal model of Alzheimer's disease. *Glia* 58, 831–838. doi:10.1002/glia.20967

Oliveros, G., Wallace, C. H., Chaudry, O., Liu, Q., Qiu, Y., Xie, L., et al. (2022). Repurposing ibudilast to mitigate Alzheimer's disease by targeting inflammation. *Brain.* 2022, awac136. doi:10.1093/brain/awac136

Paresce, D. M., Ghosh, R. N., and Maxfield, F. R. (1996). Microglial cells internalize aggregates of the Alzheimer's disease amyloid beta-protein via a scavenger receptor. *Neuron* 17, 553–565. doi:10.1016/s0896-6273(00)80187-7

Patel, H., Hodges, A. K., Curtis, C., Lee, S. H., Troakes, C., Dobson, R. J. B., et al. (2019). Transcriptomic analysis of probable asymptomatic and symptomatic alzheimer brains. *Brain Behav. Immun.* 80, 644–656. doi:10.1016/j.bbi.2019.05.009

Peng, L., Bestard-Lorigados, I., and Song, W. (2022). The synapse as a treatment avenue for Alzheimer's Disease. *Mol. Psychiatry* 27, 2940–2949. doi:10.1038/s41380-022-01565-z

Ransohoff, R. M. (2016). How neuroinflammation contributes to neurodegeneration. *Science* 353, 777–783. doi:10.1126/science.aag2590

Regev, K., Healy, B. C., Paul, A., Diaz-Cruz, C., Mazzola, M. A., Raheja, R., et al. (2018). Identification of MS-specific serum miRNAs in an international multicenter study. *Neurol. Neuroimmunol. Neuroinflamm.* 5, e491. doi:10.1212/nxi.0000000000000491

Ritchie, M. E., Phipson, B., Wu, D., Hu, Y., Law, C. W., Shi, W., et al. (2015). Limma powers differential expression analyses for RNA-sequencing and microarray studies. *Nucleic Acids Res.* 43, e47. doi:10.1093/nar/gkv007

Roy, E. R., Chiu, G., Li, S., Propson, N. E., Kanchi, R., Wang, B., et al. (2022). Concerted type I interferon signaling in microglia and neural cells promotes memory impairment associated with amyloid β plaques. *Immunity* 55, 879–894.e6. doi:10.1016/j.immuni.2022.03.018

Schwartz, N., Chalasani, M. L. S., Li, T. M., Feng, Z., Shipman, W. D., and Lu, T. T. (2019). Lymphatic function in autoimmune diseases. *Front. Immunol.* 10, 519. doi:10.3389/fimmu.2019.00519

Serrano-Pozo, A., Frosch, M. P., Masliah, E., and Hyman, B. T. (2011). Neuropathological alterations in Alzheimer disease. *Cold Spring Harb. Perspect. Med.* 1, a006189. doi:10.1101/cshperspect.a006189

Shannon, P., Markiel, A., Ozier, O., Baliga, N. S., Wang, J. T., Ramage, D., et al. (2003). Cytoscape: A software environment for integrated models of biomolecular interaction networks. *Genome Res.* 13, 2498–2504. doi:10.1101/gr.1239303

Simard, A. R., Soulet, D., Gowing, G., Julien, J. P., and Rivest, S. (2006). Bone marrow-derived microglia play a critical role in restricting senile plaque formation in Alzheimer's disease. *Neuron* 49, 489–502. doi:10.1016/j.neuron.2006.01.022

Sofroniew, M. V. (2009). Molecular dissection of reactive astrogliosis and glial scar formation. *Trends Neurosci.* 32, 638–647. doi:10.1016/j.tins.2009.08.002

Sofroniew, M. V., and Vinters, H. V. (2010). Astrocytes: Biology and pathology. *Acta Neuropathol.* 119, 7–35. doi:10.1007/s00401-009-0619-8

Spires-Jones, T. L., and Hyman, B. T. (2014). The intersection of amyloid beta and tau at synapses in Alzheimer's disease. *Neuron* 82, 756–771. doi:10.1016/j.neuron.2014.05.004

Stewart, C. R., Stuart, L. M., Wilkinson, K., van Gils, J. M., Deng, J., Halle, A., et al. (2010). CD36 ligands promote sterile inflammation through assembly of a Toll-like receptor 4 and 6 heterodimer. *Nat. Immunol.* 11, 155–161. doi:10.1038/ni.1836

Stuve, O., Weideman, R. A., McMahan, D. M., Jacob, D. A., and Little, B. B. (2020). Diclofenac reduces the risk of alzheimer's disease: A pilot analysis of NSAIDs in two US veteran populations. *Ther. Adv. Neurol. Disord.* 13, 1756286420935676. doi:10.1177/1756286420935676

Sun, X., Zhang, H., Yao, D., Xu, Y., Jing, Q., Cao, S., et al. (2022). Integrated bioinformatics analysis identifies hub genes associated with viral infection and alzheimer's disease. *J. Alzheimers Dis.* 85, 1053–1061. doi:10.3233/jad-215232

Tsai, G. E., Falk, W. E., Gunther, J., and Coyle, J. T. (1999). Improved cognition in Alzheimer's disease with short-term D-cycloserine treatment. *Am. J. Psychiatry* 156, 467–469. doi:10.1176/ajp.156.3.467

Wang, Z. X., Shi, L., Liu, J. F., An, X. M., Chang, W. R., and Liang, D. C. (2005). 2.0 A crystal structure of human ARL5-GDP3'P, a novel member of the small GTP-binding proteins. *Biochem. Biophys. Res. Commun.* 332, 640–645. doi:10.1016/j.bbrc.2005.04.168

Yao, Q., Wang, X., He, W., Song, Z., Wang, B., Zhang, J., et al. (2019). Circulating microRNA-144-3p and miR-762 are novel biomarkers of Graves' disease. *Endocrine* 65, 102–109. doi:10.1007/s12020-019-01884-2

Yi, X., Liu, J., Wu, P., Gong, Y., Xu, X., and Li, W. (2020). The key microRNA on lipid droplet formation during adipogenesis from human mesenchymal stem cells. *J. Cell. Physiol.* 235, 328–338. doi:10.1002/jcp.28972

Zhang, B., Gaiteri, C., Bodea, L. G., Wang, Z., McElwee, J., Podtelezhnikov, A. A., et al. (2013). Integrated systems approach identifies genetic nodes and networks in late-onset Alzheimer's disease. *Cell* 153, 707–720. doi:10.1016/j.cell.2013.03.030

Zhou, Y., Zhou, B., Pache, L., Chang, M., Khodabakhshi, A. H., Tanaseichuk, O., et al. (2019). Metascape provides a biologist-oriented resource for the analysis of systems-level datasets. *Nat. Commun.* 10, 1523. doi:10.1038/s41467-019-09234-6

frontiers | Frontiers in Pharmacology

TYPE Review
PUBLISHED 08 November 2022
DOI 10.3389/fphar.2022.1020918

OPEN ACCESS

EDITED BY
Yi Wang,
Zhejiang University, China

REVIEWED BY
Zili Zhang,
Nanjing University of Chinese Medicine, China
Ole Valente Mortensen,
Drexel University, United States

*CORRESPONDENCE
Kaidi Ren,
renkd006@163.com
Qi Feng,
fengqi2019@zzu.edu.cn
Yuming Xu,
xuyuming@zzu.edu.cn

SPECIALTY SECTION
This article was submitted to Neuropharmacology, a section of the journal Frontiers in Pharmacology

RECEIVED 16 August 2022
ACCEPTED 26 October 2022
PUBLISHED 08 November 2022

CITATION
Wei Z, Xie Y, Wei M, Zhao H, Ren K, Feng Q and Xu Y (2022), New insights in ferroptosis: Potential therapeutic targets for the treatment of ischemic stroke.
Front. Pharmacol. 13:1020918.
doi: 10.3389/fphar.2022.1020918

New insights in ferroptosis: Potential therapeutic targets for the treatment of ischemic stroke

Ziqing Wei[1,2,3], Yi Xie[1,2], Mingze Wei[4], Huijuan Zhao[5], Kaidi Ren[6,7,8]*, Qi Feng[9,10,11]* and Yuming Xu[1,2]*

[1]Department of Neurology, The First Affiliated Hospital of Zhengzhou University, Zhengzhou, China, [2]Henan Key Laboratory of Cerebrovascular Diseases, The First Affiliated Hospital of Zhengzhou University, Zhengzhou, China, [3]Clinical Systems Biology Laboratories, The First Affiliated Hospital of Zhengzhou University, Zhengzhou, China, [4]The Second Clinical Medical College, Harbin Medical University, Harbin, China, [5]Henan International Joint Laboratory of Thrombosis and Hemostasis, Basic Medical College, Henan University of Science and Technology, Luoyang, China, [6]Department of Pharmacy, The First Affiliated Hospital of Zhengzhou University, Zhengzhou, China, [7]Henan Key Laboratory of Precision Clinical Pharmacy, Zhengzhou, China, [8]Henan Engineering Research Center for Application & Translation of Precision Clinical Pharmacy, Zhengzhou University, Zhengzhou, China, [9]Research Institute of Nephrology, The First Affiliated Hospital of Zhengzhou University, Zhengzhou, China, [10]Department of Integrated Traditional and Western Nephrology, The First Affiliated Hospital of Zhengzhou University, Zhengzhou, China, [11]Henan Province Research Center for Kidney Disease, The First Affiliated Hospital of Zhengzhou University, Zhengzhou, China

Stroke is a common disease in clinical practice, which seriously endangers people's physical and mental health. The neurovascular unit (NVU) plays a key role in the occurrence and development of ischemic stroke. Different from other classical types of cell death such as apoptosis, necrosis, autophagy, and pyroptosis, ferroptosis is an iron-dependent lipid peroxidation-driven new form of cell death. Interestingly, the function of NVU and stroke development can be regulated by activating or inhibiting ferroptosis. This review systematically describes the NVU in ischemic stroke, provides a comprehensive overview of the regulatory mechanisms and key regulators of ferroptosis, and uncovers the role of ferroptosis in the NVU and the progression of ischemic stroke. We further discuss the latest progress in the intervention of ferroptosis as a therapeutic target for ischemic stroke and summarize the research progress and regulatory mechanism of ferroptosis inhibitors on stroke. In conclusion, ferroptosis, as a new form of cell death, plays a key role in ischemic stroke and is expected to become a new therapeutic target for this disease.

KEYWORDS

stroke, neurovascular unit (NVU), ferroptosis, inhibitors, therapeutic target

Introduction

Stroke is a common disease in clinical practice, which seriously endangers people's health and is mainly divided into two subtypes, including ischemic and hemorrhagic stroke (Peisker et al., 2017). Current evidence suggests that ischemic stroke accounts for approximately 85% of the morbidity of stroke (Benjamin et al., 2018), mainly due to cerebral blood circulation disorder, localized brain tissue necrosis or softening caused by

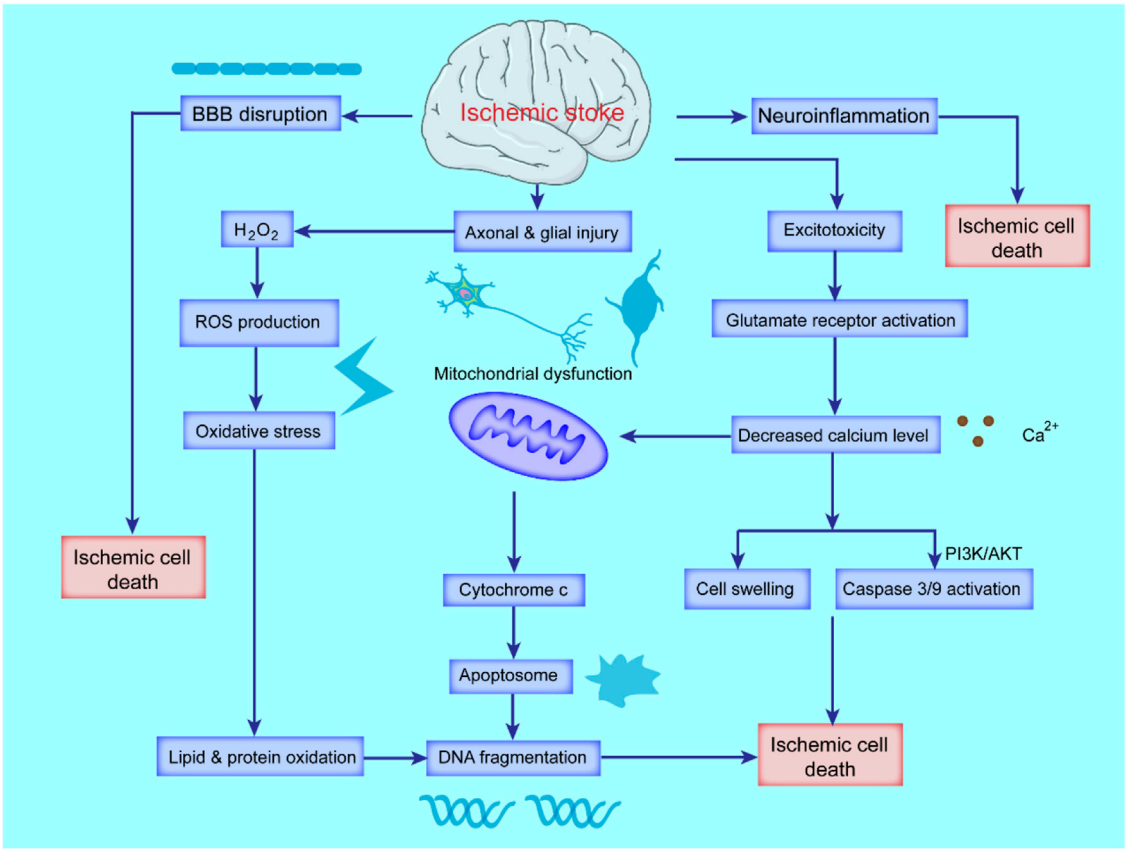

FIGURE 1
Schematic diagram of the pathological mechanism of ischemic stroke. Ischemic stroke triggers cascades of complex events that cause oxidative stress and excitotoxicity due to the accumulation of ROS and calcium (Ca^{2+}), blood-brain-barrier (BBB) breakdown and activated inflammatory responses. Excessive ROS and Ca^{2+} lead to mitochondrial dysfunction and activation of apoptotic factors, ultimately leading to apoptosis and necrotic cell death.

ischemia and hypoxia, leading to corresponding nervous system function defects (Sacco et al., 2013). Ischemic stroke is also a serious disease with high mortality, and the resulting severe cognitive and motor impairments can significantly burden families and society (Owolabi et al., 2015; Donkor, 2018). The post-ischemic brain is characterized by the accumulation of amyloid plaques and neurofibrillary tangles, followed by the development of dementia (Yang et al., 2019). Therefore, ischemic stroke increases the neurological deficits in dementia patients (Owolabi et al., 2015).

It is widely thought that the neurovascular unit (NVU) plays a crucial role in the occurrence and development of ischemic stroke (Iadecola, 2017), as well as in the remodeling of blood vessels and nerves after stroke (Leigh et al., 2018). The past decade has witnessed significant inroads in pathological research on ischemic stroke with the discovery of a new form of cell death in the NVU of ischemic stroke, namely ferroptosis (Doll et al., 2017; Magtanong and Dixon, 2018; Zhou et al., 2021).

In recent years, ferroptosis has become a research hotspot (Dixon et al., 2012). During ferroptosis, a high abundance of unsaturated fatty acids on the cell membrane undergo lipid peroxidation under ferrous iron or ester oxygenase, thereby inducing cell death (Yang et al., 2016). The occurrence and execution of ferroptosis depend on the interaction of amino acid, lipid and iron metabolism (Ursini and Maiorino, 2020), and its sensitivity is also regulated by several key pathways and processes (Chen et al., 2021a). Ferroptosis is associated with various diseases such as Parkinson's disease (Mahoney-Sanchez et al., 2021), tumor (Kim et al., 2016), and renal failure (Adedoyin et al., 2018), and the development of these diseases can be intervened by activating or inhibiting ferroptosis.

In ischemic stroke, pathological changes are closely related to ferroptosis, such as iron metabolism disorder, lipid peroxidation, and increased ROS (Hu et al., 2019; Ren et al., 2020). An increasing body of evidence from recently published studies substantiates the correlation between ferroptosis and stroke (Hu et al., 2019; Ren et al., 2020). This review provides a

comprehensive overview of the NVU of ischemic stroke and the role of ferroptosis in ischemic stroke, providing new insights into the application of ferroptosis in treating ischemic stroke.

NVU in ischemic stroke

Although significant progress has been made in better understanding the mechanism of neuron injury and repair after ischemia (Figure 1), there is still a lack of effective treatment for this disease (Chan, 1996; Hu et al., 2017; Yang et al., 2017). In the past, research on cerebral ischemic injury was mostly limited to neurons (Yang et al., 2019) or different cell groups and structures in the brain (Yang et al., 2017; Qin et al., 2019), ignoring the integrity of brain function and the interaction between different structures. Recently, the concept of the neurovascular unit as a new protective target for ischemic brain injury has been proposed (Cai et al., 2017; Zhao et al., 2020a).

The neurovascular unit is mainly composed of neurons, glial cells (including astrocytes, microglia, oligodendrocytes), and the blood-brain barrier (BBB, including vascular endothelial cells, astrocytic end-foot processes, basal lamina and pericytes) to maintain homeostasis of the central system (Pardridge, 1991), and extracellular matrix that maintains the integrity of the brain tissue environment (Lo and Rosenberg, 2009; Iadecola, 2017). The NVU maintains the normal physiological function of neurons and the repair of damaged neurons, which emphasizes the importance of the interconnection and mutual influence between neurons, glial cells and cerebrovascular (Stamatovic et al., 2008; Lo and Rosenberg, 2009) and provides the foothold for further study of neuron injury and protection mechanism. Overall, the NVU plays a key role in the clinical treatment of ischemic stroke and is increasingly valued by researchers and clinicians (Iadecola, 2017).

Neurons

It is well-established that neurons are most vulnerable to cerebral ischemia-reperfusion injury (CIRI) (Lo and Rosenberg, 2009) and are continuously affected by several pathological reactions such as inflammation, excitatory amino acid toxicity, and oxidative stress after CIRI (Rohnert et al., 2012). Among them, excitatory amino acids include glutamate and aspartate (Brann and Mahesh, 1994), glutamate is the main excitatory neurotransmitter in the mammalian central nervous system, which can have long-term effects on the structure and function of neurons, and glutamate-mediated excitatory signal transduction can affect mammalian brain functions, including cognition, memory and learning. The release of a large number of excitatory amino acids will activate plenty of ion channels and lead to persistent intracellular Ca^{2+} level increase, cell damage and death, which is called excitatory amino acid toxicity (Gillessen et al., 2002). While, this excitotoxicity caused by excitatory amino acids is one of the earliest and widely recognized molecular mechanisms of CIRI (Lai et al., 2014). When the brain is in a state of ischemia and hypoxia, the release of excitatory neurotransmitters is increased and reuptake is impaired due to metabolic disorders, and eventually the level of excitatory neurotransmitters in the ischemic region increases rapidly that leads to aberrant activation of many Ca^{2+}-dependent pathways and initiation of apoptosis, necroptosis and autophagy processes in the brain (Shen et al., 2022). Current evidence suggests that neuronal death accounts for the poor prognosis in ischemic stroke (Chen et al., 2020). Indeed, assessing the severity of an ischemic stroke and the cause of death depends largely on the number of neurons dying in the affected brain area (Lazarov and Hollands, 2016).

Microglia

Microglia are innate immune cells in the brain, accounting for approximately 5–20% of glial cells (Benveniste, 1997). The main functions of microglia are to recognize pathogens, phagocytose necrotic or apoptotic cells, remove damaged neurons, tissue fragments, small and inactive synapses, infected small molecules and macromolecules, regulate T cell response, and induce inflammatory process (Nimmerjahn et al., 2005). In addition, microglia have extensive connections with other NVU cells (Thurgur and Pinteaux, 2019), which can regulate the microenvironmental homeostasis of NVU, and have positive significance for maintaining the barrier function of BBB (Abdullahi et al., 2018). When an ischemic stroke occurs, neurons activate microglia to differentiate into M1-and M2-phenotypes by releasing certain soluble factors and intracellular components (Akhmetzyanova et al., 2019; Qin et al., 2019). It is well-established that M1-type microglia have a pro-inflammatory and deleterious effect on the ischemic brain (Yu et al., 2022), while M2-type microglia can reduce the inflammatory response and exert neuroprotective effects (Varin and Gordon, 2009; Soehnlein and Lindbom, 2010).

In addition, microglia can affect the activity of neurons by releasing ATP and stimulating astrocytes to release glutamate to increase the excitatory postsynaptic potential (Barakat and Redzic, 2016; Illes et al., 2021). After cerebral ischemia, microglia release many inflammatory factors (Soehnlein and Lindbom, 2010), destroy the normal function of neurons and damage vascular endothelial cells, thereby destroying the BBB structure and aggravating brain edema (Yenari et al., 2010).

Oligodendrocytes

Oligodendrocytes are the myelinating cells in the central nervous system (CNS) and originate from oligodendrocyte progenitor cells (OPCs). OPCs can differentiate into oligodendrocytes or astrocytes according to the environment

(Hughes et al., 1988). Endothelial cells promote the proliferation of OPCs by releasing trophic factors such as brain-derived neurotrophic factor (BDNF) and basic fibroblast growth factor (bFGF) (Dugas et al., 2008) and release vascular endothelial growth factor A (VEGF-A) to promote oligodendrocyte migration (Guo et al., 2008; Arai and Lo, 2009). The main function of oligodendrocytes is to form an insulating myelin sheath wrapping the axons in the CNS, assist in the efficient transmission of bioelectrical signals, and maintain and protect the normal function of neurons (Baumann and Pham-Dinh, 2001; Kuhn et al., 2019). Abnormalities in oligodendrocytes not only lead to demyelinating lesions of the CNS but also cause neuronal damage, psychiatric diseases, and even brain tumors (Kuhn et al., 2019). Under ischemic conditions, the expression of Nogo-A in oligodendrocytes is upregulated (Kern et al., 2013), thereby inhibiting axonal remodeling, impairing neuronal function, and triggering the early breakdown of BBB by secreting matrix metalloproteinase-9 (Mandai et al., 1997; Dewar et al., 2003).

Vascular endothelial cells

Vascular endothelial cells (VECs) constitute a monolayer of specialized cells strategically positioned between the vascular wall and the bloodstream (Kruger-Genge et al., 2019). Ischemic stroke results from a combination of factors such as platelet adhesion and aggregation and related release reactions (Del Zoppo, 1998), fibrin protease activation, and fibrin formation after vascular endothelial injury (Zhou et al., 2020). Under normal conditions, certain active factors released by VECs play a protective role in regulating vascular tension, coagulation, fibrinolysis, and maintaining normal blood pressure and hemodynamics (Sandoo et al., 2010). Once the vascular endothelium is damaged, the exposed subendothelial layer can cause platelet adhesion and aggregation, leading to thrombosis (Chen and Lopez, 2005). The stimulated VECs can also release tissue factors to promote the extrinsic coagulation process involving coagulation factor XII and accelerate thrombosis (Lopes-Bezerra and Filler, 2003). Notably, prolonged ischemia-hypoxia and ischemia-reperfusion (I/R) can damage VECs (Zhou et al., 2020). In addition, ischemia and hypoxia can induce the expression of VEGF (Ramakrishnan et al., 2014), which can promote the proliferation of VECs and participate in angiogenesis, thereby suppressing ischemic stroke and playing a neuroprotective role (Lopes-Bezerra and Filler, 2003; Zhou et al., 2020).

Astrocytes

In glial cells, astrocytes perform multiple homeostatic functions to maintain the survival and stability of the NVU (Becerra-Calixto and Cardona-Gomez, 2017), exerting neuroprotective, angiogenic, immunomodulatory, neurogenic, and antioxidant effects with the ability to modulate synaptic function (Daneman and Prat, 2015; Becerra-Calixto and Cardona-Gomez, 2017). Under physiological conditions, astrocytes release various neurotrophic factors, which can repair damage to neurons and VECs (Ye et al., 2018). During cerebral ischemia, the energy supply of brain cells is insufficient, resulting in the dysregulation of intracellular calcium and sodium pumps (Peng et al., 2019). Because of the extensive gap junctions and hemichannels in astrocytes, the gap junctions are destroyed, and Ca^{2+} and toxic substances are rapidly transmitted, causing astrocytes to release a large amount of glutamate to aggravate the excitatory amino acid toxicity (Lim et al., 2021). On the other hand, astrocytes are overactivated in the acute phase of ischemia, eventually forming a glial scar that hinders the repair of neurons (Sofroniew, 2009).

Pericytes

Brain pericytes are located in the center of the NVU and respond by receiving, integrating and processing signals from neighboring cells (Hamilton et al., 2010; Armulik et al., 2011; Winkler et al., 2011). They are critical in maintaining the normal function of the CNS and are involved in the formation and maintenance of BBB, cerebral blood flow (CBF) regulation, immunoregulation, angiogenesis, and stability. Overwhelming evidence substantiates that the dysfunction and loss of pericytes play a key role in the pathogenesis of various cerebrovascular diseases (Winkler et al., 2011). It has been shown that after ischemia, pericytes begin to detach from the cerebral microvessels (Zhou et al., 2022), which causes the destruction of tight junctions between cells, resulting in the destruction and leakage of the BBB (Bergers and Song, 2005). The platelet-derived growth factor receptor β (PDGFRβ) on pericytes is upregulated after cerebral ischemia and can combine with PDGFβ secreted by VECs to promote the recruitment and migration of pericytes for neovascularization to promote maturation (Makihara et al., 2015; Hutter-Schmid and Humpel, 2016). It has been shown that pericytes begin to secrete VEGF within 24 h after ischemic stroke, which promotes angiogenesis in the peri-infarct area by activating VEGFR in endothelial cells (Shibuya, 2011; Yang et al., 2017; Zhou et al., 2022). Under ischemic and hypoxic conditions, pericytes can exhibit pluripotent stem cell properties and participate in immune responses (Davidoff, 2019; Fernandez-Morales et al., 2019). A recent study found that TNF-α could promote the release of IL-6 from pericytes, which contributed to the activation of microglia (Matsumoto et al., 2018a).

This NVU theory emphasizes the important connection between neurons, glial cells and microvessels after cerebral

TABLE 1 The functions and regulators of NVU.

NVU components	Functions	Regulators	References
Neurons	Critical in the regulation of BBB function, innervate endothelial cells and their associated astrocytes. Maintain the homeostasis of the brain microenvironment, provide nutritional support for the brain*etc.*	Mcl-1/Bcl-2, OXR1, P53/Caspase-3, TRAF3, ADIPOR2*etc.*	Awooda et al. (Awooda et al., 2015) Anilkumar et al. (Anilkumar et al., 2020) Cregan et al. (Cregan et al., 1999)
Astrocytes	As a part of the blood-brain barrier, can connect capillaries and neurons, participate in the nutritional support of neurons and the regulation of electrophysiological activities, and can secrete a large number of neurotrophic factors and growth factors to maintain the stability of the microenvironment and repair after injury	AQP-4, TLR4, TGF-β, ADIPOR2, Nrf2, ApoE, MCSF, IL-6, MCP-1, MMP-9, GFAP, GLT-1, GLAST, PARS*etc.*	Becerra-Calixto et al. (Becerra-Calixto and Cardona-Gomez, 2017) Hiroko (Ikeshima-Kataoka, 2016) Cekanaviciute et al. (Cekanaviciute and Buckwalter, 2016)
Microglia	As an innate immune effector cell, microglia is necessary for the normal development of the nervous system	TLR, MHC-II, CD16/32, BDNF, GDNF, VEGF, BMP-7, TGF-β, CSF-1, TNF-α, TNF-β, IGF-1, NADPH oxidase, IL-1, IL-4, IL-5, IL-6, IL-8, IL-10, pro-MMP-9, NO, ROS*etc.*	Kim et al. (Kim and De Vellis, 2005) Hamel (Hamel, 2006) Colonna et al. (Colonna and Butovsky, 2017) Kang et al. (Kang et al., 2020)
Oligodendrocytes	Their main function is to wrap axons in the central nervous system, form an insulating myelin structure, assist in the efficient transmission of bioelectrical signals, maintain and protect the normal function of neurons	Nogo-A, CNTF, IGF-1, NT-3, PDGF*etc.*	Nave et al. (Nave and Werner, 2014) Plemel et al. (Plemel et al., 2014)
Vascular endothelia cells (VECs)	As the physical barrier of the BBB, VECs are formed by preventing cells and molecules from passively entering the brain through tight junctions between cells	NF-κB, NO, Prostacyclin, EDHF, Eicosanoids, TIMP-2, VCAM-1, ICAM-1, P-selectin, MMP*etc.*	Onat et al. (Onat et al., 2011) Henke et al. (Henke et al., 2007) Kathrina et al. (Marcelo et al., 2013)
Pericytes	Vital in the formation and maintenance of BBB integrity, angiogenesis, and removal of toxic substances	Angiopoientin-1, MIF, Occludin, SIPT1, MRP*etc.*	Rustenhoven et al. (Rustenhoven et al., 2017) Hori et al. (Hori et al., 2004)
Extracellular matrix (ECM)	Mediating cell differentiation, proliferation, adhesion, morphogenesis and phenotype	Collagen, Undulin, Tenascin, Fibronectin, Dermatan sulfate, Decorin*etc.*	Bonnans et al. (Bonnans et al., 2014) Zhang et al. (Zhang et al., 2021a)
Basal lamina	Located on the outside of the lumen of the cerebral microvascular endothelium, it is composed of extracellular matrix proteins secreted by VECs, pericytes, and astrocytes, and is involved in the regulation of vascular integrity	Collagen, Laminin, Fibronectin, Elastin, Proteoglycans, Merosin, Dystroglycan, Nidogen, Growth factors, MMP*etc.*	Hoshi et al. (Hoshi and Ushiki, 2004) Nguyen et al. (Nguyen et al., 2021)

ischemia, corroborating that all components of NVU are involved in the pathological process of cerebral ischemia injury (Stamatovic et al., 2008; Mcconnell et al., 2017). This connection is realized through cell-cell and cell-matrix interaction. There are many chemicals involved in the regulation of BBB permeability in different cell types of NVU. These regulatory chemicals fall into different categories, such as proinflammatory cytokines (e.g., TNF-α, IL-1, IL-6), neurotransmitters (e.g., NO), ROS and other substances (Table 1). Comprehensive treatment of NVU can effectively combat ischemic stroke. Therefore, NVU provides a theoretical basis for the current research and treatment of neurological diseases, and targeting NVU from a global perspective may bring new opportunities for treating ischemic stroke.

Mechanisms and key regulators of ferroptosis

Programmed cell death plays an important role in homeostasis and disease development. Among them, ferroptosis is a newly discovered form first proposed by Stockwell et al., in 2012 (Dixon et al., 2012). Ferroptosis is significantly different from other types of cell death such as apoptosis, necrosis, autophagy, and pyroptosis at the morphological, biochemical, and genetic levels (Dixon et al., 2012). The morphological features of ferroptosis are mainly manifested in mitochondria, including reduced volume, increased membrane density, and reduced numbers or absence (Chen et al., 2021a; Jiang et al., 2021). Regarding biochemical characteristics, ferroptosis manifests as glutathione depletion,

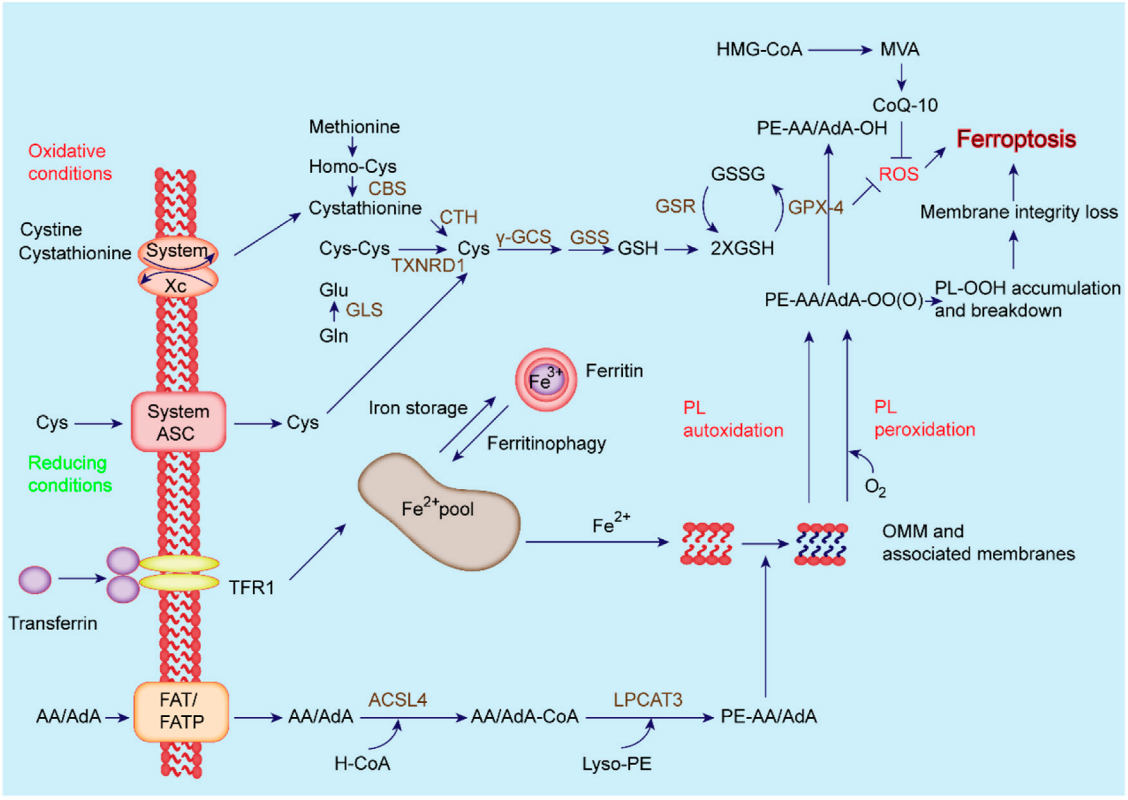

FIGURE 2
Regulatory mechanisms of ferroptosis. The primary metabolism involved in ferroptosis can be roughly divided into three categories: iron metabolism, System Xc^-/GSH/GPX4 pathway, and lipid peroxidation. Besides, the FSP1-CoQ_{10}-NAD(P)H pathway, which exists as an independent parallel system with GPX4 and GSH, inhibits phospholipid peroxidation and ferroptosis.

glutathione peroxidase 4 (GPX4) inactivation, and lipid peroxide accumulation (Chen et al., 2021a; Jiang et al., 2021).

It has been confirmed that ferroptosis is closely related to neurodegenerative diseases, tumors, cardiovascular and cerebrovascular diseases, and acute kidney injury (AKI) (Ward et al., 2014; Fang et al., 2019; Bao et al., 2021), and its inhibitors can effectively delay disease progression and improve clinical symptoms (Angeli et al., 2017). However, the regulatory mechanism of ferroptosis has not yet been fully elucidated. With significant progress achieved in the study of ferroptosis, various regulatory factors and mechanisms have been discovered, suggesting that it is mainly related to iron metabolism disorder, amino acid antioxidant system imbalance, and lipid peroxide accumulation (Figure 2) (Dixon et al., 2012; Chen et al., 2021a). When iron metabolism disorder causes the increase of intracellular free iron, iron catalyzes the production of ROS through the Fenton reaction, and ROS further promotes lipid peroxidation, causing the accumulation of lipid peroxides and inducing ferroptosis (Dixon et al., 2012; Stockwell et al., 2017; Chen et al., 2021a). Indeed, an in-depth study and elucidation of the pathophysiological mechanism of ferroptosis can provide new ideas and treatment methods for ferroptosis-related diseases.

Iron metabolism

Iron metabolism disorders, especially iron overload, are key to ferroptosis (Dixon et al., 2012). Fe^{3+} in the blood circulation is combined with transferrin and transported to the cell through transferrin receptor 1 (TFR1) on the cell membrane surface (Beguin et al., 2014). Then Fe^{3+} is reduced to Fe^{2+} and released into the labile iron pool (LIP) in the cytoplasm (Kakhlon and Cabantchik, 2002), while excess iron is stored in ferritin (Jacobs et al., 1972). During this process, nuclear receptor coactivator 4 (NCOA4) acts as an adaptor protein to mediate the targeted transport of ferritin to lysosomes for autophagic degradation, thereby releasing free Fe^{2+}, a process called ferritinophagy, mainly responsible for iron release and recovery (Mancias et al., 2014). Part of Fe^{2+} is transported out of cells through ferroportin1 (FPN1) on the cell membrane to ensure that the intracellular iron concentration is not excessively high under physiological conditions (Zhang et al., 2011; Zhang et al.,

2012). Current evidence suggests that iron metabolism disorders can increase intracellular LIP and cause an increase in intracellular free iron (Ravingerova et al., 2020).

Due to the instability and high reactivity of Fe^{2+}, hydroxyl radicals can be generated through the Fenton reaction (Thomas et al., 2009), which can directly react with polyunsaturated fatty acids (PUFAs) in the plasma membrane to generate a large amount of lipid ROS (Magtanong et al., 2016), and further promote lipid peroxidation and peroxide accumulation, inducing cell ferroptosis (Stockwell et al., 2017).

System Xc^-

The cystine-glutamate antiporter System Xc^- is widely distributed in the phospholipid bilayer of biological cells (Bannai, 1986; Sasaki et al., 2002; Bridges et al., 2012). It is a heterodimer composed of light chain solute carrier family seven member 11 (SLC7A11) and heavy chain solute carrier family three member 2 (SLC3A2) (Sato et al., 1999; Broer and Wagner, 2002; Verrey et al., 2004). The System Xc^- can export intracellular glutamate to the extracellular space while importing cystine into the cytoplasm, where cystine is reduced to cysteine, which is involved in glutathione (GSH) synthesis (Seib et al., 2011). Glutathione peroxidase (GPX), whose active center is selenocysteine, catalyzes the conversion of reduced GSH to oxidized glutathione (GSSG), converting toxic peroxides into hydroxyl compounds to protect cell membranes from oxidative stress damage (Guan et al., 2017).

GPX4 is the only enzyme found in the GPX family that can reduce peroxides in lipid membranes, and its antioxidant effect is significantly higher than other family members (Margis et al., 2008). In particular, GPX4 can degrade hydrogen peroxide and other small molecule peroxides induced by iron overload in cells, preventing ferroptosis caused by the accumulation of ROS (Borchert et al., 2018). The antioxidant activity of GPX4 depends on GSH, which acts as an electron donor and converts toxic lipid hydroperoxide into non-toxic lipid alcohol (L-OH) (Fei et al., 2020). When System Xc^- is blocked, glutamate and cystine cannot be exchanged, resulting in the accumulation of intracellular glutamate, decreased GSH synthesis and GPX4 activity, thereby increasing ROS in lipids and inducing cell ferroptosis (Forcina and Dixon, 2019).

Lipid peroxidation

Lipid peroxidation refers to the loss of hydrogen atoms of lipids under the action of free radicals or lipid peroxidase, resulting in the oxidation, fragmentation and shortening of lipid carbon chains and the production of lipid free radicals, lipid hydroperoxides (LOOH) and reactive aldehydes (such as malondialdehyde and 4-hydroxynonenal) and other cytotoxic substances, eventually cause lipid oxidative degradation reactions that damage cells (Ayala et al., 2014). ROS are a group of molecules with partially reduced oxygen, including peroxides, superoxides, singlet oxygen, free radicals, *etc.*, which cause cell death by damaging DNA, RNA and lipid molecules (Su et al., 2019; Villalpando-Rodriguez and Gibson, 2021). As a member of intracellular ROS, lipid peroxides are the ultimate executors of ferroptosis (Cheng et al., 2021). The deleterious effect of lipid peroxidation is mainly reflected in the oxidative degradation of two important biofilm components, including phosphatidylethanolamines (PEs) and PUFAs (Gaschler and Stockwell, 2017).

PUFA is the main component of phospholipids in cell and organelle membranes and is also an important substrate for the synthesis of PE (Stubbs and Smith, 1984). PUFA has a high affinity for free radicals, and the hydrogen atoms between its double bonds are easily oxidized by free radicals (Cunnane, 1994). The lipid peroxidation reaction of PUFA is roughly divided into two stages (Kanner et al., 1987; Girotti, 1998; Ayala et al., 2014). First, ROS acquire hydrogen atoms in PUFA to generate lipid radicals (Yin et al., 2011); subsequently, lipid radicals interact with oxygen molecules to generate lipid peroxyl radicals (LOO-) (Chamulitrat and Mason, 1989). LOO- can reportedly abstract hydrogen atoms from other PUFAs to form lipid radicals and lipid hydroperoxides (Chamulitrat and Mason, 1989; Girotti, 1998). Moreover, LOO- participates in the oxidation process of PUFAs, which ensures that the lipid peroxidation of PUFAs exhibits the characteristics of a cascade reaction (Yin et al., 2011).

However, the affinity between PE and free radicals is not high, and oxidation sites need to be formed under the action of two enzymes before lipid peroxidation occurs (Pratt et al., 2011). First, long-chain acyl-Coa synthetase-4 (ACSL4) utilizes arachidonic acid (AA) and adrenic acid (AdA) to synthesize arachidonoyl-CoA (AA-COA) and adrenoyl-CoA (AdA-COA) (Ma et al., 2021); then, AA/AdA-COA combines with PE to form PE-AA/AdA under the catalytic action of lysophosphatidylcholine acyltransferase 3 (LPCAT3) (Kagan et al., 2017).

PE-AA/AdA is easily oxidized to cytotoxic PE-AA/AdA-OOH by free radicals or Arachidonate 15-Lipoxygenase (ALOX15), which promotes ferroptosis (Kagan et al., 2017). LOX-mediated lipid hydroperoxide production has been suggested to be involved in ferroptosis (Shintoku et al., 2017). The accumulation of lipid peroxides, especially phospholipid peroxides, is a hallmark event of ferroptosis (Shintoku et al., 2017). High levels of ACSL4 and LPCAT3 have been detected in various tumors, such as renal and liver cancer cells (Luo et al., 2021). At present, the expression of these two enzymes has been used to assess the sensitivity of various tumor cells to ferroptosis (Yuan et al., 2016a; Doll et al., 2017; Kagan et al., 2017; Magtanong and Dixon, 2018).

Nrf2

Nuclear factor-E2-related factor 2 (Nrf2) is a transcription factor with a leucine zipper structure, which plays a key anti-oxidation role (Jaiswal, 2004). The activity of Nrf2 is strictly regulated by Kelch-like ECH-associated protein 1 (Keap1) (Kobayashi and Yamamoto, 2006). Under normal conditions, Nrf2 binds to Keap1 and is inactivated with ubiquitination and degradation in the proteasome (Zhang et al., 2004). Once in a state of oxidative stress, Keap1 is degraded by autophagy to release Nrf2 (Kaspar et al., 2009). Free Nrf2 rapidly translocates to the nucleus, which binds to antioxidant response elements (AREs) in the promoter region to drive antioxidant gene expression, balance oxidative stress and maintain cellular redox homeostasis (Kwak et al., 2007).

It is well-established that Nrf2 can regulate a variety of antioxidant enzymes, such as superoxide dismutase (SOD), catalase (CAT), glutathione peroxidase (GPX), glutathione reductase (GR), NAD(P)H quinine oxidoreductase (NQO1) and so on (Dhakshinamoorthy et al., 2000; Zhu et al., 2005). Therefore, Nrf2 is considered an important regulator of ferroptosis and a therapeutic target for tumors and neurodegenerative diseases highly associated with oxidative stress (Abdalkader et al., 2018; Song and Long, 2020).

P53

p53 has attracted much interest as a tumor suppressor molecule since its discovery (Harris, 1996). The p53 molecule can induce apoptosis and cell cycle arrest, exerting a strong tumor suppressor effect (Chen, 2016). In 2015, Jiang et al. linked p53 to ferroptosis for the first time (Jiang et al., 2015) and demonstrated that mutation of p53 can inhibit the activity of System Xc^-, downregulate the expression of SLC7A11 (Jiang et al., 2015), and reduce the activity of GPX4, thereby promoting lipid peroxidation and inducing ferroptosis (Jiang et al., 2015). It is widely thought that p53 is at the core of a powerful signaling network; it regulates the sensitivity of cells to ferroptosis in different cell types and under different stress factors through several independent signaling pathways (Harris and Levine, 2005; Huang, 2021).

In addition to increasing sensitivity to ferroptosis, p53 appears to have an opposing effect (Liu et al., 2020a). When cells undergo cysteine deprivation, another signaling pathway is activated, with increased expression of wild-type p53 to induce p21 transcription or inhibit DPP4 binding to NOX1, ultimately inhibiting cell susceptibility to ferroptosis (Wang et al., 2012; Badgley et al., 2020). These two functions seem contradictory, but they are unified in cells. On the one hand, ferroptosis, as a form of regulated cell death, has physiological significance in the evolution of species, and p53 can achieve the purpose of removing abnormal cells and inhibiting tumorigenesis by increasing the sensitivity of cells to ferroptosis (Jiang et al., 2015; Liu et al., 2020a); on the other hand, when metabolic stress occurs, p53 can reduce the sensitivity of cells to ferroptosis by enhancing the ability to regulate ROS level to help normal cells survive the damage induced by various stress factors and promote cell survival (Tarangelo et al., 2018). Overwhelming evidence substantiates that cell types and p53 mutation sites may influence the mechanism of p53 in regulating cell ferroptosis (Wynford-Thomas and Blaydes, 1998; Wang et al., 2008; Ji et al., 2022), although the specific underlying mechanism warrants further study.

FSP1

Previous studies suggested that GPX4 and free radical antioxidants regulate ferroptosis. Recently, Marcus Conrad and José Pedro Friedmann Angeli's team used a clonal expression strategy to screen for genes that can inhibit ferroptosis caused by loss of GPX4 in human cancer cells and found that *flavoprotein apoptosis-inducing factor mitochondria-related 2 (AIFM2)* is an anti-ferroptosis gene and renamed AIFM2 to ferroptosis suppressor protein 1 (FSP1). FSP1, originally described as a pro-apoptotic gene, showed the ability to inhibit ferroptosis induced by *GPX4* knockout (Doll et al., 2019). In addition, the researchers found that the main mechanism of FSP1 in inhibiting ferroptosis is to reduce Coenzyme Q_{10} (CoQ_{10}) with NAD(P)H, inhibit lipid peroxidation, and resist the occurrence of ferroptosis (Doll et al., 2019). The FSP1-CoQ_{10}-NAD(P)H pathway exists as an independent parallel system, which, together with GPX4 and glutathione, inhibits phospholipid peroxidation and ferroptosis (Bersuker et al., 2019; Doll et al., 2019). Their anti-ferroptosis properties have been widely used in the study of anti-tumor therapy (Bersuker et al., 2019). Growing evidence suggests that when GPX4 is inactivated, FSP1 can continue to maintain tumor growth *in vivo*, while deletion of *GPX4* and *FSP1* can inhibit tumor growth (Doll et al., 2019). As a novel ferroptosis inhibitor, FSP1 provides a new direction for disease research.

ACSL4

ACSL4 is a lipid metabolism enzyme required for lipid peroxidation and belongs to the ACSL family (Lopes-Marques et al., 2013). Current research suggests that PUFAs can be used as substrates for lipid peroxidation (Ayala et al., 2014), and their accumulation is a marker of ferroptosis; thus, the intracellular PUFAs content determines the development of ferroptosis and increased content can promote the progression of lipid peroxidation-induced ferroptosis (Das, 2019; Kuang et al., 2020). ACSL4 can activate free PUFAs and then complete the peroxidation process of membrane phospholipids with the participation of the other key enzymes, LPCAT3 and ALOX15 (Lee et al., 2021). Therefore, the ACSL4/LPCAT3/ALOX15 pathway can promote lipid peroxidation-induced

ferroptosis (Lee et al., 2021). Zhang et al. showed that PKCβII, one of the isoforms of PKC (Steinberg, 2008), is an important lipid peroxidation sensor activated by lipid peroxidation during ferroptosis that can phosphorylate ACSL4 to amplify the effect of lipid peroxidation, eventually inducing ferroptosis (Zhang et al., 2022). This study also confirmed that the PKCβII-ACSL4 mechanism affects the efficacy of cancer immunotherapy by regulating ferroptosis (Zhang et al., 2022).

Other regulatory mechanisms

Heat shock proteins (HSP) are a class of highly conserved molecular chaperones expressed in response to environmental stress and render cells resistant to different types of cell death (Feder and Hofmann, 1999). For example, HSPB1 can inhibit ferroptosis by reducing iron uptake (Sun et al., 2015); HSPA5 binds to and stabilizes GPX4, thereby indirectly avoiding the damage of lipid peroxidation in ferroptosis (Zhu et al., 2017); however, the HSP9 inhibitor CDDO can inhibit ferroptosis in tumor cells, suggesting that HSP90 may play a different role in ferroptosis (Qin et al., 2015).

Mitochondria have been reported to participate in the pathogenesis of ferroptosis (Gao et al., 2019). CDGSH iron-sulfur domain 1 (CISD1) is a class of mitochondrial iron-exporting proteins that inhibit ferroptosis by preventing the accumulation of iron and the production of ROS in mitochondria (Yuan et al., 2016b). In addition, voltage-dependent anion channels (VDACs) located in the mitochondrial outer membrane play an important regulatory role in ferroptosis (Lemasters, 2017). It has been shown that Erastin, a ferroptosis inducer (Shibata et al., 2019; Zhao et al., 2020b), can act on VDAC to promote the release of a large number of oxides, causing ROS-dependent mitochondrial dysfunction and bioenergy exhaustion to induce ferroptosis (Zhao et al., 2020b), while the reduction of VDAC expression can reduce the occurrence of Erastin-induced ferroptosis (Yang et al., 2020).

Epigenetics is a key factor in regulating gene expression, and more and more research results show that epigenetic regulation (e.g., DNA methylation, histone modification and miRNA) plays an important role in ferroptosis (Jaenisch and Bird, 2003; Wu et al., 2020). DNA methylation is the most widely studied epigenetic modification. Increased DNA methylation may lead to gene silencing, while decreased methylation activates gene expression (Newell-Price et al., 2000), and DNA methylation is closely related to iron metabolism and can control the expression of ferroptosis-related genes (e.g., *GPX4* and *SLC7A11*) to regulate ferroptosis (Zhao et al., 2022). Currently, DNA methylation is widely used as a diagnostic, predictive, and prognostic biomarker for multiple cancers (Huo et al., 2019). According to the histone modification studies, it was found that reducing histone 2A ubiquitination (H2Aub) on the *SLC7A11* promoter can downregulate SLC7A11 and prevent ferroptosis (Zhang et al., 2019a); the histone 2B monoubiquitination (H2Bub1) modification is significantly down-regulated during the induction of ferroptosis, and artificial inhibition of endogenous H2Bub1 can significantly increase the sensitivity of cells to the ferroptosis inducer Erastin (Wang et al., 2019); in addition, histone deacetylase (HDAC) can regulate iron metabolism by inhibiting *HAMP* gene expression (Sukiennicki et al., 2019). There are also many studies reporting that a large number of microRNAs (miRNAs) can regulate ROS metabolism and ferroptosis (Zhang et al., 2020a). Mitofusin (Mfn) is a key protein that maintains mitochondrial morphology, regulates cellular lipid metabolism, endoplasmic reticulum stress and ROS generation (Papanicolaou et al., 2011), and plays a potential role in ferroptosis (Wei et al., 2020). miR-195, miR-125a and miR-761 have all been reported to regulate the mitochondrial function and metabolism of breast cancer cells, pancreatic cancer cells and liver cancer cells by targeting *Mfn2*, respectively, and affect the growth of tumor cells (Guo et al., 2017; Pan et al., 2018; Purohit et al., 2019); miR-137 can negatively regulate ferroptosis by directly targeting glutamine transporter SLC1A5 in melanoma cells (Luo et al., 2018). These further reveal the miRNA regulation role in ferroptosis, which contributes to an in-depth understanding of the mechanism of ferroptosis.

Ferroptosis in ischemic stroke

An increasing body of evidence from recently published studies suggests that ferroptosis is closely related to various diseases, such as tumor and neurological diseases (Ward et al., 2014; Fang et al., 2019; Bao et al., 2021). On the one hand, ferroptosis inducers can induce ferroptosis in abnormal cells, and tumor cells are highly sensitive to ferroptosis (Wu et al., 2019). Accordingly, ferroptosis can be induced in tumor cells to treat tumors. Non-targeted strategies based on nanoparticles have been designed to deliver iron, peroxides and other toxic substances to kill tumor cells (Zhang et al., 2019b; Raj et al., 2021).

The discovery of various enzymes regulating ferroptosis has enabled the targeted therapy of tumors, the most prominent target being GPX4, which is expressed in most tumor cells and is important for cell survival (Zhang et al., 2020b). GPX4-deficient cancer cells can be efficiently eliminated by the FSP-specific inhibitor iFSP1, while in GPX4-expressing cancer cells, iFSP1 cooperates with RSL3 to induce cancer cell ferroptosis (Gaschler et al., 2018). Therefore, FSP1 inhibitors may have clinical applications, especially for treating drug-resistant tumors or tumors that exhibit de-differentiation characteristics (Wang et al., 2021a). In addition, pharmacological or genetic inhibition of system Xc^- to prevent the development and metastasis of various tumors has yielded good efficacy and low toxicity in mouse models (Zhu et al., 2019).

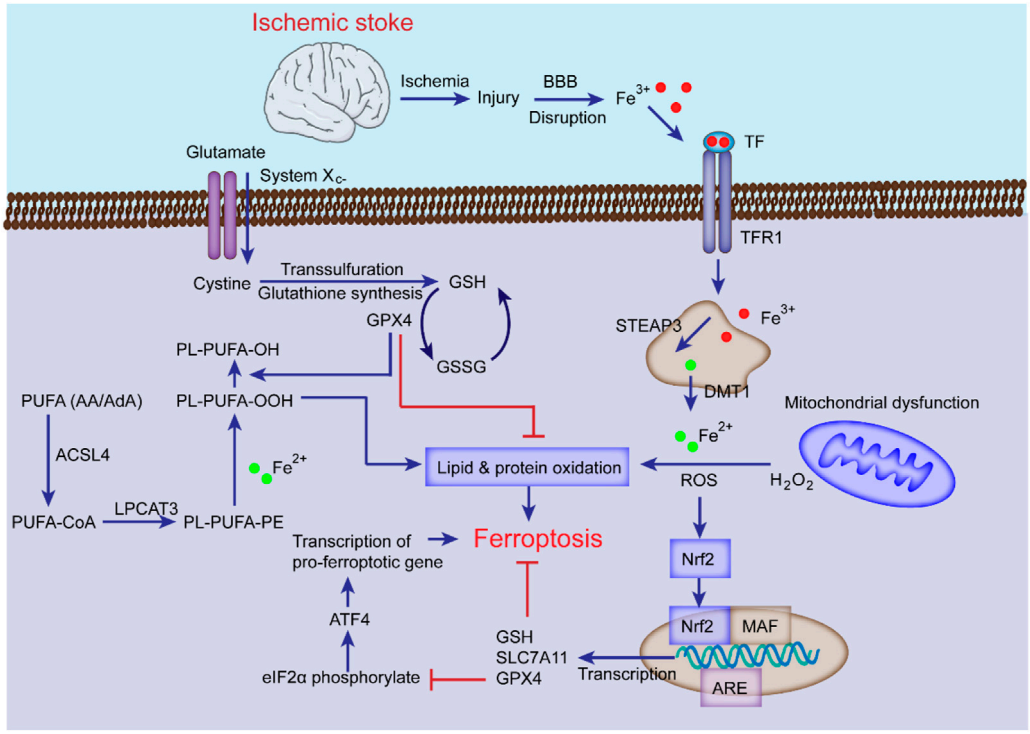

FIGURE 3
The mechanisms of ferroptosis in ischemic stroke. Following ischemic stroke, the BBB is disrupted, which allows Fe^{3+} in the blood to be released into cells through TF and TFR1, then stored in the endosome, where Fe^{3+} is converted into Fe^{2+} and transported to the cytoplasm by DMT1 with the cooperation of STEAP3. The excess Fe^{2+} generates ROS and participates in the synthesis of PUFA lipid peroxides (L-OOH), which can induce ferroptosis; System Xc^- is simultaneously impaired, which inhibits cystine-glutamate exchange and reduces the generation of GSH and GPX4, thereby inhibiting lipid alcohol (L-OH) production, ultimately leading to ferroptosis. Additionally, the Nrf2 pathway can inhibit ferroptosis and alleviate ischemic stroke injury by inducing GSH, SLC7A11, and GPX4 transcription.

On the other hand, ferroptosis inhibitors can inhibit ferroptosis in normal cells and can be used to prevent or treat neurological diseases (Angeli et al., 2017). Studies have found that ferroptosis is associated with *Parkinson*'s disease (Mahoney-Sanchez et al., 2021). Ferroptosis is an important cell death pathway of dopaminergic neurons (Do Van et al., 2016), and the ferroptosis inhibitor ferrostatin-1 can reportedly inhibit neuronal cell death *in vitro* and *in vivo* (Reichert et al., 2020). Interestingly, it has been reported that many pathological features of *Alzheimer*'s disease are associated with an imbalance in iron homeostasis, and iron overload in the brain may be responsible for the rapid cognitive decline in *Alzheimer*'s patients (Belaidi and Bush, 2016). Water maze experiments showed that mice with *GPX4* knockout in the cerebral cortex and hippocampal neurons showed significant cognitive impairment and degeneration of hippocampal neurons. The degree of neurodegeneration was reduced after treatment with Vitamin E or the ferroptosis inhibitor Liproxstatin-1 (Hambright et al., 2017; Lane et al., 2018). These studies suggest that ferroptosis is widely involved in regulating the functions of neurons related to learning and memory.

It has been established that the levels of intracellular lipid peroxides and Fe^{2+} are increased during stroke, and ferroptosis inhibitors can upregulate the levels of GSH, GPX4 or system Xc^- to alleviate brain damage, indicating that ferroptosis affects the progression of stroke (Magtanong and Dixon, 2018; Zhang et al., 2021b). Studies have shown that ferroptosis inhibitors protect mice from ischemia-reperfusion injury in a middle cerebral artery occlusion (MCAO) model (Tuo et al., 2017), suggesting that ferroptosis can lead to neuronal death and NVU damage after ischemic stroke (Xu et al., 2022). Understanding the roles of iron metabolism, amino acid metabolism, and lipid metabolism of ferroptosis in ischemic stroke provides theoretical support for treating this disease (Jiang et al., 2021). The following content specifically discusses the role of ferroptosis in ischemic stroke (Figure 3).

Iron metabolism and ischemic stroke

It is well-established that iron homeostasis in the brain is disrupted after ischemic stroke, which impedes NVU

recovery (Hu and Song, 2017). Intracellular iron overload is the main mechanism for inducing ferroptosis after cerebral ischemia, and the inhibition of iron overload can suppress ferroptosis in ischemic stroke and reduce damage (Fang et al., 2018). Under pathological conditions of ischemia and hypoxia, the expression of ferritin, transferrin, and TFR1 in the brain is increased, resulting in increased iron uptake by neurons and oligodendrocytes in the NVU (Kawabata, 2019; Ng et al., 2019). The acidic environment of ischemia and hypoxia can cause the overexpression of divalent metal-ion transporter 1 (DMT1) in microglia (Rotin et al., 1986; Chang et al., 2006), resulting in increased brain iron content (Cheli et al., 2018); meanwhile, ischemia can upregulate TFR1 levels, resulting in increased iron uptake (Chen et al., 2019; Tang et al., 2021).

There is a rich literature available suggesting that serum hepcidin and iron concentrations are elevated in patients with ischemic stroke, indicating that hepcidin is critical in cerebral ischemic iron overload (Davalos et al., 1994; Petrova et al., 2016). During ischemic stroke, the expression of interleukin-6 (IL-6) in cells increases hepcidin through the JAK/STAT3 pathway (Cojocaru et al., 2009), which causes FPN1 degradation, resulting in reduced iron release and thus intensified iron accumulation in cells (Cojocaru et al., 2009; Zhou et al., 2017). Therefore, the rational application of iron metabolism inhibitors, such as deferoxamine and iron chelators, to reduce the iron content in the brain after an ischemic stroke can reduce neuronal death and promote the recovery of NVU function after ischemic stroke (Jones et al., 2020; Roemhild et al., 2021; Yang et al., 2021).

In 2017, Tuo et al. revealed the relationship between Tau and ferroptosis and the role of ferroptosis in CIRI using the MCAO mouse model (Tuo et al., 2017). Tau can promote neuronal iron efflux and inhibit ferroptosis, which may be related to the reduction of tau caused by cerebral ischemia. Meanwhile, ferroptosis inhibitors liproxstatin-1 (Lip-1) or ferrostatin-1 (Fer-1) can significantly reduce neurological damage, indicating that ferroptosis can aggravate CIRI.

After ischemic stroke, the BBB is destroyed, leading to cerebral edema and aggravating brain tissue damage and neurological dysfunction (Abdullahi et al., 2018). Numerous studies have shown that systemic iron pools are transferred to neurons in the brain parenchyma when the BBB is disrupted, thereby exacerbating ferroptosis. Accordingly, changes in iron content in brain tissue reflect the degree of BBB dysfunction (Degregorio-Rocasolano et al., 2019). Iron accumulation accompanies the entire pathological process, and iron metabolism is considered an important pathophysiological factor involved in secondary injury after ischemic stroke (Waldvogel-Abramowski et al., 2014; Roemhild et al., 2021).

Amino acid metabolism and ischemic stroke

As the brain's most abundant excitatory neurotransmitter, glutamate is a critical regulator in maintaining neural function (Zhou and Danbolt, 2014). NVU damage and death caused by excessively high extracellular glutamate concentration is known as excitotoxicity (Yang et al., 2019). In ischemic stroke, when the brain is in a state of ischemia and hypoxia due to metabolic disorders, glutamate release is increased, and reuptake is hindered, resulting in a rapid increase in glutamate levels in the ischemic area of the brain (Castillo et al., 1996). Subsequent activation of glutamate receptors leads to abnormal activation of several signaling pathways and iron deposition to stimulate cell death (Griesmaier and Keller, 2012; Willard and Koochekpour, 2013). Therefore, glutamate excitotoxicity is widely thought to be one of the mechanisms of ferroptosis (Zhang et al., 2021c). Indeed, glutamate excitotoxicity after cerebral ischemia, described as ferroptosis, can be effectively suppressed by the ferroptosis inhibitor Fer-1 (Xie et al., 2022).

As mentioned above, system Xc^- has a positive effect on inhibiting ferroptosis; however, the increase of extracellular glutamate content caused by cerebral ischemia is mainly caused by system Xc^- (Ikeda et al., 1989), and inhibiting the expression of system Xc^- can hinder ferroptosis, thereby reducing cerebral ischemia damage (Vespa et al., 1998). Domercq et al. showed that system Xc^- was upregulated in astrocytes and microglia in a rat model of stroke, while its inhibition reduced inflammation and attenuated CIRI (Matute et al., 2006; Martin et al., 2018). It can be concluded that the increased expression of System Xc^- during cerebral ischemia does not inhibit but promote the occurrence of ferroptosis, which may be due to the upregulated expression of System Xc^-, leading to the excitotoxic effect caused by glutamate release exceeding its own antioxidant protective effect (Polewski et al., 2016).

In addition, GSH, as an endogenous inhibitor of ferroptosis, is reportedly related to ischemic stroke (Zhang et al., 2021b). Enhancing the expression of GPX4 and GSH synthesis can inhibit ferroptosis and reduce ischemic stroke injury (Zhang et al., 2021b). Increased lipid peroxidation levels and decreased GSH levels have been detected in an MCAO model (Liu et al., 2020b). Moreover, Edaravone has been proposed to counteract ferroptosis in various conditions, especially in cystine deficiency leading to decreased GSH content, and has been clinically approved for the treatment of acute ischemic stroke (Kikuchi et al., 2009; Matsumoto et al., 2018b). In addition, selenium (Se) can effectively enhance and maintain the activity of GPX4 (Ferguson et al., 2012; Liu et al., 2021). After ischemic stroke, Se supplementation can effectively inhibit GPX4-dependent ferroptosis and endoplasmic reticulum (ER) stress-induced cell death and improve NVU function by promoting GPX4 expression (Alim et al., 2019). In recent years, much

emphasis has been placed on understanding the direct effects of GPX4 and GSH on stroke.

Lipid metabolism and ischemic stroke

Lipid peroxidation is a key driver of ferroptosis, stimulated by oxidative stress (Lee et al., 2021). ROS can accumulate to toxic levels during oxidative stress, leading to cellular damage and dysfunction, whereas antioxidants can prevent cellular damage by converting ROS into harmless molecules (Conrad et al., 2018). ROS are produced in large quantities during ischemic stroke, along with decreased levels of endogenous antioxidants, leading to oxidative stress (Cadenas, 2018). For example, the 1,2,4-triazole derivative compound 11 can exert a neuroprotective effect by promoting the expression of Nrf2 and SOD to induce an antioxidant effect (Lao et al., 2022). During a stroke, AA and AdA on the cell membrane can generate lipid peroxides through a series of reactions (Mccall et al., 1987; Nishizawa et al., 2021). Growing evidence suggests that ACSL4 and LOX, especially 12/15-LOX, are increased in ischemic stroke (Jin et al., 2008; Singh and Rao, 2019).

LOX is a key enzyme that causes lipid peroxidation and induces ferroptosis (Shintoku et al., 2017). It has been reported that *12/15-Lox* gene deletion can reduce the infarct size after stroke (Singh and Rao, 2019). Additionally, 12/15-LOX were highly expressed in a cerebral ischemia model, and their inhibitors could inhibit the damage of ferroptosis to NVU cells (Jin et al., 2008). For example, the specific inhibitor ML351 has been reported to exert a protective effect against CIRI (Tourki et al., 2021). Moreover, ACSL4 participates in the synthesis and remodeling of PEs, thus affecting the synthesis of lipid peroxides, and upregulation of its expression can contribute to ferroptosis (Kuwata et al., 2019). It has been shown that in ischemic stroke, ACSL4 is upregulated and mediates neuronal death, ultimately leading to stroke injury (Li et al., 2019). Moreover, the ACSL4 inhibitor rosiglitazone can inhibit ferroptosis and protect brain function (Li et al., 2019). Cui et al. found that knockout of *ACSL4* protects mice from cerebral ischemia, whereas its overexpression can exacerbate brain damage (Cui et al., 2021). Other studies have found that the accumulation of Fe^{2+} and ROS decreased, the expression of ACSL4 and TFR decreased, and GPX4 and FTH1 increased in MCAO model cells treated with safflower flavin thus inhibiting neuronal ferroptosis in MCAO (Li et al., 2021).

These findings suggest that both ACSL4 and LOX involved in lipid metabolism can serve as innovative therapeutic targets for ischemic stroke (Cui et al., 2021), inhibiting ferroptosis by reducing ROS accumulation and lipid peroxidation, providing new ideas for the treatment of ischemic stroke (Li et al., 2021).

Additionally, mounting evidence suggests that Nrf2 is an important regulator of the cellular antioxidant defense system (Abdalkader et al., 2018), and its moderate activation is beneficial in alleviating cerebral ischemic injury (Lao et al., 2022). Although little evidence is available that changes in Nrf2 levels directly affect ferroptosis in stroke, several studies have suggested that the Nrf2 pathway can alleviate stroke injury (Shih et al., 2005; Liu et al., 2018; Lao et al., 2022). It has also been shown that Epicatechin can regulate oxidative stress through the Nrf2 pathway *via* penetrating the BBB, thus protecting against transient cerebral ischemic injury (Chang et al., 2014).

Treatment of ischemic stroke by targeting ferroptosis

With the gradual recognition of the role of ferroptosis in ischemic stroke, treating ischemic stroke by inhibiting ferroptosis has become a research hotspot. As the pathological stimulus signals of ischemic stroke, ischemia, hypoxia and hypertension can all lead to brain damage (Khoshnam et al., 2017), during which local brain tissue metabolism changes, such as the reduction of GSH, GPX4 and tau proteins, and the increase of lipoxygenase (LOX) and BBB permeability, specifically manifested as iron overload and the enhancement of lipid peroxidation, that boost the generation of ROS and ultimately trigger ferroptosis-related cell death (Magtanong and Dixon, 2018). In addition, the restoration of normal blood circulation after ischemic stroke for a period of time will lead to CIRI (Lo and Rosenberg, 2009). Cerebral ischemia-reperfusion will lead to the activation of a variety of cell death pathways, including ferroptosis (Chen et al., 2021b). The phenomenon of increased lipid peroxidation and increased intracellular iron levels contribute to amplify the cerebral oxidative stress and inflammatory response, that further aggravate neuronal injury during reperfusion. Therefore, ferroptosis mediates and aggravates ischemic stroke injury (Figure 4). Major therapeutic advances include ferroptosis inhibitors, iron homeostasis regulators, lipid peroxidation pathway inhibitors, and ROS generation inhibitors. Table 2 summarized some key factors related to regulating ferroptosis, as well as therapeutic reagents in stroke and their functional mechanisms.

Current evidence suggests that ferroptosis inhibitors Fer-1 or Lip-1 can effectively reduce brain damage after reperfusion in a mouse model of ischemic stroke (Tuo et al., 2017; Feng et al., 2019), and Edaravone can be used to treat patients with acute ischemic stroke (Enomoto et al., 2019; Kobayashi et al., 2019). Mechanistic studies have suggested that Edaravone can scavenge free radicals and inhibit lipid peroxidation, thereby inhibiting oxidative damage (Kikuchi et al., 2013). Moreover, the intravenous administration of Edaravone after I/R in rats prevented the progression of cerebral edema and cerebral infarction, alleviated the accompanying neurological symptoms, and inhibited delayed neuronal death (Watanabe et al., 2018). In recent years, iron chelation therapy has been shown to suppress ferroptosis in a CIRI model (Cappellini et al.,

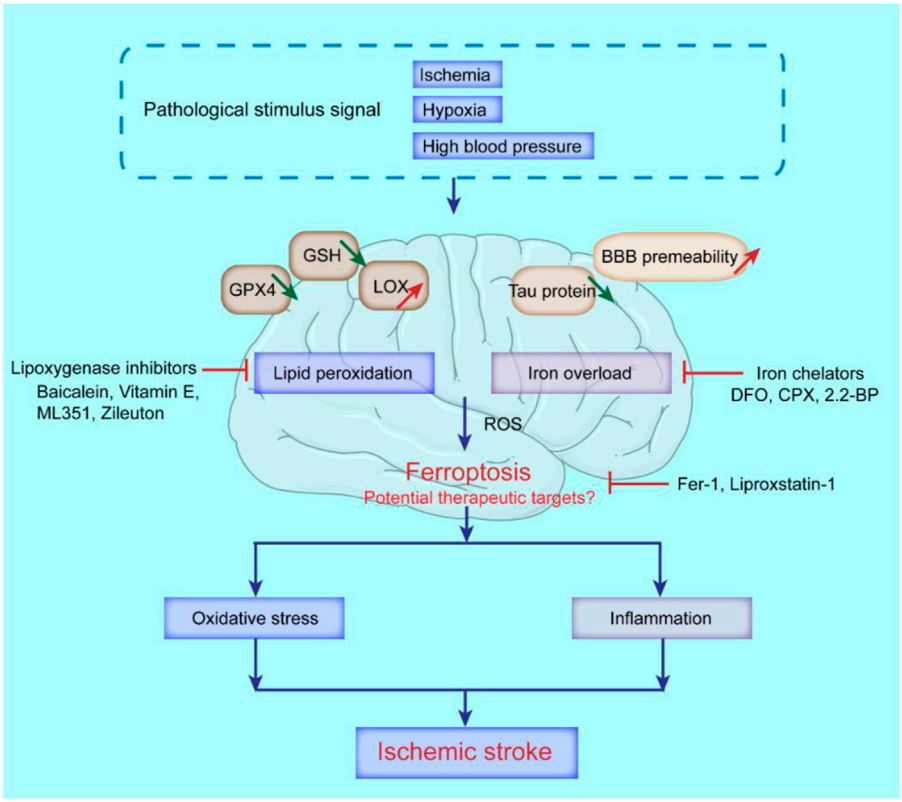

FIGURE 4
Possible molecular mechanisms of ferroptosis and potential therapeutic targets in ischemic stroke. The decrease of GSH, GPX4, tau protein, and the increase of lipoxygenase (LOX), and BBB permeability, can lead to the occurrence of ferroptosis in ischemic stroke. Iron chelators like deferoxamine (DFO), ciclopirox (CPX) and 2,2-bipyridyl (2,2-BP) can inhibit ferroptosis; Lipoxygenase inhibitors like Baicalein, Vitamin E, ML351 and Zileuton can suppress LOXs activity to rescue cells from ferroptosis; Ferrostatin-1 (Fer-1) and Liproxstatin-1 (Lip-1) inhibit radical-trapping antioxidants which activate LOXs to prevent ferroptosis in cells.

2006; Grignano et al., 2020). Deferoxamine (DFO), a high-affinity iron chelator with the ability to bind to free iron ions to form stable complexes that weaken the Fenton response, has been approved by the U.S. Food and Drug Administration (FDA) for the treatment of iron overload-related diseases (Hanson et al., 2009; Tevlin et al., 2021). The ferroptosis inhibitor deferoxamine, which also acts as an iron chelator, improved cognitive impairment after stroke in diabetic rats with MCAO (Hanson et al., 2009). In addition, CoQ_{10} was found to possess beneficial effects in a rat MCAO model and improved the prognosis of neurological impairment in patients with acute ischemic stroke (Nasoohi et al., 2019). Therefore, as an endogenous lipid-soluble antioxidant, CoQ_{10} can effectively inhibit lipid peroxidation and is expected to be a drug that hinders ferroptosis (Littarru and Tiano, 2007; Rizzardi et al., 2021). Another drug inhibiting ferroptosis during ischemic stroke is Se (Ramezani et al., 2021). Alim *et al.* found that Se supplementation activates GPX4 homeostatic transcription *in vivo*, inhibiting cellular ferroptosis and improving neurological function (Alim et al., 2019). Octreotide has anti-inflammatory and antioxidant effects and protects the brain from cerebral ischemic injury by activating the Nrf2/ARE pathway (Wang et al., 2015). In patients with cerebral ischemic injury, melatonin has been reported to reduce nerve cell ferroptosis by increasing Nrf2, and significantly improve the learning, memory and cognitive abilities (Koh, 2008).

Intriguingly, several traditional Chinese herbal medicines have also been shown to inhibit ferroptosis in ischemic stroke. The monoterpenoid phenol carvacrol has been reported to effectively reduce ROS expression, reduce iron deposition and elevate GPX4 levels, thereby protecting hippocampal neurons from CIRI (Friedman, 2014; Li et al., 2016). Galangin inhibition of ferroptosis by activating SLC7A11/GPX4 can reportedly attenuate CIRI (Guan et al., 2021). In addition, Naotaifang extract has been reported to inhibit neuronal ferroptosis by downregulating TFR1/DMT1 and upregulating the SCL7A11/GPX4 pathway, thereby improving neurological function in post-ischemic rats (Lan et al., 2020).

Although these traditional Chinese medicines have not been clinically validated to improve the condition of ischemic stroke

TABLE 2 Pharmacological research progress on ferroptosis in ischemic stroke.

Characteristics	Regulations	Reagents and mechanisms	
Morphological characteristics: Mitochondrial volume decreases, membrane density increases, and mitochondria decrease or disappear	Positive regulators: ACSL4, Hmox1, NCOA4	Inducers	Mechanism
		Erastin	Inactivates and decreases the level of GSH.
		RSL3	Inactivates GPX4 and causes accumulation of lipid hydroperoxides
		Inhibitors	
		Deferoxamine	As an iron chelator, it can prevent iron-dependent lipid peroxidation
		Liproxstatin-1	Inhibits mitochondrial lipid peroxidation and restores the expression of GSH, GPX4 and FSP1
Biochemical characteristics: Ferroptosis is manifested as GSH depletion, GXP4 inactivation, and lipid peroxide accumulation	Negative regulators: GPX4, Nrf2, HSPB1, SLC7A11, FSP1	Selenium	Protects GPX4 and upregulates GPX4 expression
		Ferrostatin-1	Prevents glutamate-induced neurotoxicity and inhibits lipid peroxidation
		Ceruloplasmin	Oxidizes ferrous ions to less toxic ferric forms
		N-Acetylcysteine (NAC)	Maintains intracellular GSH level and lower endogenous oxidant level
		Vitamin D	An antioxidant and a regulator of iron metabolism
		Vitamin E	inhibits LOX activity by competing at the substrate-binding site and by scavenging hydroxyl group radicals

patients, their safety and lack of toxicity may facilitate their clinical translation (Fung and Linn, 2015).

Outlook

Ischemic stroke is a common disease that seriously endangers human health, and its incidence has increased in recent years (Sacco et al., 2013). Its complex pathological process and related mechanisms have become a research hotspot (Peisker et al., 2017; Yang et al., 2019). Thrombolytic therapy for cerebral ischemic injury has been limited by the narrow therapeutic time window, CIRI induction, and a high risk of hemorrhagic transformation, emphasizing the need for new treatments (Ringleb et al., 2002; Schellinger and Warach, 2004).

As the concept of NVU was proposed, researchers began to assess the feasibility of treating ischemic stroke from multiple approaches and perspectives (Cai et al., 2017; Zhao et al., 2020a). Stroke caused by different causes was regarded as a reactive injury process involving brain NVU (Yenari et al., 2010; Hu et al., 2017; Iadecola, 2017). In the treatment after brain injury, it has been transformed from single neuron protection to more comprehensive and in-depth protection of NVU (Wang et al., 2021b). The pathophysiological changes of NVU are typically characterized by tissue hypoxia, inflammation, activation of angiogenesis, and complex interactions between various components of NVU, which together lead to increased BBB permeability, brain edema, neuronal dysfunction and injury (Stanimirovic and Friedman, 2012). Cerebral ischemic injury is an inflammatory stimulus response, and all cellular components and matrix components of NVU are involved and make related responses (Ishikawa et al., 2004). The research and development of traditional drugs is limited to a certain pathological link in the pathological process of NVU, so the effect is not ideal. Therefore, during the treatment, the overall structure of NVU should be targeted, and the dynamic changes of each component should be coordinated to reduce nerve damage and promote repair. Ferroptosis is a new cell death mode discovered in recent years, with the continuous research, it has been recognized that ferroptosis plays an important role in a wide range of biological processes, including normal physiology and various pathological conditions (Stockwell et al., 2017). At present, the morphology, biology, and mechanism pathways of ferroptosis are partially understood, but the process of ferroptosis involves a variety of mechanisms, which are precisely regulated by signaling pathways. Questions remain as to how ferroptosis is related to the occurrence of diseases and whether it is associated with other modes of cell death to mediate the progression of diseases. Therefore, further in-depth study of the mechanism of ferroptosis and its role in different disease types is of great significance for finding therapeutic targets for related diseases and the development of targeted drugs.

The pathogenesis of ischemic stroke is complicated, current evidence suggests that ferroptosis plays an important role in the progression of ischemic stroke, inhibiting ferroptosis can alleviate ischemic stroke injury (Li et al., 2019; Liu et al., 2020b; Zhang et al., 2021b). When ischemic stroke occurs, iron ion aggregation in neurons leads to iron overload, which causes ROS aggregation through Fenton reaction, and GSH level

is significantly reduced and lipid peroxidation increase in ischemic stroke mouse model (Liu et al., 2020b), indicating that ferroptosis is also a way of neurons death during the pathophysiological process of ischemic stroke. Ferroptosis inhibitors and iron chelators can effectively reduce the damage of neurons during ischemic brain death, suggesting that there are potential targets in the ferroptosis pathway to regulate ischemic stroke and its inhibition during ischemia has huge prospects for clinical application (Zhou et al., 2021).

However, investigating the role of ferroptosis in ischemic stroke is still in its preliminary stages, and many questions remain to be answered. For example, during ischemia and hypoxia, different cell types of NVU in brain tissue (Wang et al., 2021b), including neurons, microglia, astrocytes, oligodendrocytes, *etc.*, are stimulated and damaged (Cai et al., 2017), and ferroptosis occurs in these different cell types, although its role remains to be elucidated (Doll et al., 2017; Jiang et al., 2021; Lee et al., 2021; Nishizawa et al., 2021), warranting further studies. In the field of basic research, there is a lack of effective biomarkers for ferroptosis, such as caspase activation in apoptosis or autolysosome formation in autophagy (Earnshaw et al., 1999; Hundeshagen et al., 2011). Accordingly, exploring specific biomarkers of ferroptosis is urgent. Over the years, studies of the molecular mechanisms of ferroptosis in ischemic stroke have mostly focused on cell and animal models, indicating that more clinical studies on patients with ischemic stroke are required. In addition, drug development targeting ferroptosis in ischemic stroke is an important aspect of research. Among the ferroptosis inhibitors, only one drug, Edaraavone, is used to treat patients with acute ischemic stroke (Enomoto et al., 2019; Kobayashi et al., 2019). Other drugs have been found to be effective in animal and cell models of stroke (Hanson et al., 2009; Narayan et al., 2021). Therefore, there is an urgent need to develop and validate effective drugs in clinical treatment, including traditional Chinese medicine.

Although ferroptosis, as a new mode of cell death, plays a key role in ischemic stroke and is expected to become a new therapeutic target to improve the outcomes of this patient population, ischemic stroke is regulated by a variety of cell death pathways. Both ferroptosis and other programmed cell death modes (including cell apoptosis, necroptosis and autophagy) play an important role in the pathological process of ischemic stroke. More and more evidence has shown that there are interacting signaling pathways between these cell death modes with similar initial signals and molecular regulators. For example, p53, not only induces apoptosis, but also regulates ferroptosis (Hong et al., 2017). In the relationship between ferroptosis and necroptosis, iron overload leads to the opening of the mitochondrial permeability transition pore (MPTP), which exacerbates RIP1 phosphorylation and leads to cell necroptosis (Tian et al., 2020); HSP90 induces necroptosis and ferroptosis by promoting RIP1 phosphorylation and inhibiting GPX4 activation (Wang et al., 2018). In addition, research have shown that ferroptosis is an autophagic cell death process (Gao et al., 2016). Knockdown of autophagy-related *Atg5* and *Atg7* genes can limit Erastin-induced ferroptosis by reducing intracellular iron and lipid peroxidation, and knockdown of NCOA4 can inhibit ferritin degradation and prevent ferroptosis (Lu et al., 2017), however, the specific mechanism of autophagy mediated ferroptosis needs to be further explored. This evidence suggests a strong crosslink between them, combination therapy targeting different cell death pathways may be the most effective strategy for the treatment of ischemic stroke.

Author contributions

ZW, YX, MW, QF, and YX conceptualized and wrote the manuscript and created Figures. ZW, HZ, and KR contributed to the writing of the manuscript. ZW, MW, KR, QF, and YX reviewed and modified the manuscript. All authors approved the final version of the manuscript.

Funding

This work was supported by the National Natural Science Foundation of China (82204389), the Natural Science Foundation of Henan Province (222300420350) and the Henan Medical Science and Technique Foundation (LHGJ20200310, LHGJ20210351, LHGJ20190265), the Key R&D and promotion Special Projects of Henan Province (212102310194) and the Medical Science and Technology Research Project of Henan Province (SBGJ202102145).

Conflict of interest

The authors declare that the research was conducted in the absence of any commercial or financial relationships that could be construed as a potential conflict of interest.

Publisher's note

References

Abdalkader, M., Lampinen, R., Kanninen, K. M., Malm, T. M., and Liddell, J. R. (2018). Targeting Nrf2 to suppress ferroptosis and mitochondrial dysfunction in neurodegeneration. *Front. Neurosci.* 12, 466. doi:10.3389/fnins.2018.00466

Abdullahi, W., Tripathi, D., and Ronaldson, P. T. (2018). Blood-brain barrier dysfunction in ischemic stroke: Targeting tight junctions and transporters for vascular protection. *Am. J. Physiol. Cell Physiol.* 315 (3), C343–C356. doi:10.1152/ajpcell.00095.2018

Adedoyin, O., Boddu, R., Traylor, A., Lever, J. M., Bolisetty, S., George, J. F., et al. (2018). Heme oxygenase-1 mitigates ferroptosis in renal proximal tubule cells. *Am. J. Physiol. Ren. Physiol.* 314 (5), F702–F714. doi:10.1152/ajprenal.00044.2017

Akhmetzyanova, E., Kletenkov, K., Mukhamedshina, Y., and Rizvanov, A. (2019). Different approaches to modulation of microglia phenotypes after spinal cord injury. *Front. Syst. Neurosci.* 13, 37. doi:10.3389/fnsys.2019.00037

Alim, I., Caulfield, J. T., Chen, Y., Swarup, V., Geschwind, D. H., Ivanova, E., et al. (2019). Selenium drives a transcriptional adaptive program to block ferroptosis and treat stroke. *Cell* 177 (5), 1262–1279. doi:10.1016/j.cell.2019.03.032

Angeli, J. P. F., Shah, R., Pratt, D. A., and Conrad, M. (2017). Ferroptosis inhibition: Mechanisms and opportunities. *Trends Pharmacol. Sci.* 38 (5), 489–498. doi:10.1016/j.tips.2017.02.005

Anilkumar, U., Khacho, M., Cuillerier, A., Harris, R., Patten, D. A., Bilen, M., et al. (2020). MCL-1(Matrix) maintains neuronal survival by enhancing mitochondrial integrity and bioenergetic capacity under stress conditions. *Cell Death Dis.* 11 (5), 321. doi:10.1038/s41419-020-2498-9

Arai, K., and Lo, E. H. (2009). An oligovascular niche: Cerebral endothelial cells promote the survival and proliferation of oligodendrocyte precursor cells. *J. Neurosci.* 29 (14), 4351–4355. doi:10.1523/JNEUROSCI.0035-09.2009

Armulik, A., Genove, G., and Betsholtz, C. (2011). Pericytes: Developmental, physiological, and pathological perspectives, problems, and promises. *Dev. Cell* 21 (2), 193–215. doi:10.1016/j.devcel.2011.07.001

Awooda, H. A., Lutfi, M. F., Sharara, G. G., and Saeed, A. M. (2015). Oxidative/nitrosative stress in rats subjected to focal cerebral ischemia/reperfusion. *Int. J. Health Sci.* 9 (1), 17–24. doi:10.12816/0024679

Ayala, A., Munoz, M. F., and Arguelles, S. (2014). Lipid peroxidation: Production, metabolism, and signaling mechanisms of malondialdehyde and 4-hydroxy-2-nonenal. *Oxid. Med. Cell. Longev.* 2014, 360438. doi:10.1155/2014/360438

Badgley, M. A., Kremer, D. M., Maurer, H. C., DelGiorno, K. E., Lee, H. J., Purohit, V., et al. (2020). Cysteine depletion induces pancreatic tumor ferroptosis in mice. *Science* 368 (6486), 85–89. doi:10.1126/science.aaw9872

Bannai, S. (1986). Exchange of cystine and glutamate across plasma membrane of human fibroblasts. *J. Biol. Chem.* 261 (5), 2256–2263. doi:10.1016/s0021-9258(17)35926-4

Bao, W. D., Pang, P., Zhou, X. T., Hu, F., Xiong, W., Chen, K., et al. (2021). Loss of ferroportin induces memory impairment by promoting ferroptosis in Alzheimer's disease. *Cell Death Differ.* 28 (5), 1548–1562. doi:10.1038/s41418-020-00685-9

Barakat, R., and Redzic, Z. (2016). The role of activated microglia and resident macrophages in the neurovascular unit during cerebral ischemia: Is the jury still out? *Med. Princ. Pract.* 25, 3–14. doi:10.1159/000435858

Baumann, N., and Pham-Dinh, D. (2001). Biology of oligodendrocyte and myelin in the mammalian central nervous system. *Physiol. Rev.* 81 (2), 871–927. doi:10.1152/physrev.2001.81.2.871

Becerra-Calixto, A., and Cardona-Gomez, G. P. (2017). The role of astrocytes in neuroprotection after brain stroke: Potential in cell therapy. *Front. Mol. Neurosci.* 10, 88. doi:10.3389/fnmol.2017.00088

Beguin, Y., Aapro, M., Ludwig, H., Mizzen, L., and Osterborg, A. (2014). Epidemiological and nonclinical studies investigating effects of iron in carcinogenesis--a critical review. *Crit. Rev. Oncol. Hematol.* 89 (1), 1–15. doi:10.1016/j.critrevonc.2013.10.008

Belaidi, A. A., and Bush, A. I. (2016). Iron neurochemistry in alzheimer's disease and Parkinson's disease: Targets for therapeutics. *J. Neurochem.* 139, 179–197. doi:10.1111/jnc.13425

Benjamin, E. J., Virani, S. S., Callaway, C. W., Chamberlain, A. M., Chang, A. R., Cheng, S., et al. (2018). Heart disease and stroke statistics-2018 update: A report from the American heart association. *Circulation* 137 (12), e67–e492. doi:10.1161/CIR.0000000000000558

Benveniste, E. N. (1997). Role of macrophages/microglia in multiple sclerosis and experimental allergic encephalomyelitis. *J. Mol. Med.* 75 (3), 165–173. doi:10.1007/s001090050101

Bergers, G., and Song, S. (2005). The role of pericytes in blood-vessel formation and maintenance. *Neuro. Oncol.* 7 (4), 452–464. doi:10.1215/S1152851705000232

Bersuker, K., Hendricks, J. M., Li, Z., Magtanong, L., Ford, B., Tang, P. H., et al. (2019). The CoQ oxidoreductase FSP1 acts parallel to GPX4 to inhibit ferroptosis. *Nature* 575 (7784), 688–692. doi:10.1038/s41586-019-1705-2

Bonnans, C., Chou, J., and Werb, Z. (2014). Remodelling the extracellular matrix in development and disease. *Nat. Rev. Mol. Cell Biol.* 15 (12), 786–801. doi:10.1038/nrm3904

Borchert, A., Kalms, J., Roth, S. R., Rademacher, M., Schmidt, A., Holzhutter, H. G., et al. (2018). Crystal structure and functional characterization of selenocysteine-containing glutathione peroxidase 4 suggests an alternative mechanism of peroxide reduction. *Biochim. Biophys. Acta. Mol. Cell Biol. Lipids* 1863 (9), 1095–1107. doi:10.1016/j.bbalip.2018.06.006

Brann, D. W., and Mahesh, V. B. (1994). Excitatory amino acids: Function and significance in reproduction and neuroendocrine regulation. *Front. Neuroendocrinol.* 15 (1), 3–49. doi:10.1006/frne.1994.1002

Bridges, R. J., Natale, N. R., and Patel, S. A. (2012). System xc(-) cystine/glutamate antiporter: An update on molecular pharmacology and roles within the CNS. *Br. J. Pharmacol.* 165 (1), 20–34. doi:10.1111/j.1476-5381.2011.01480.x

Broer, S., and Wagner, C. A. (2002). Structure-function relationships of heterodimeric amino acid transporters. *Cell biochem. Biophys.* 36 (2-3), 155–168. doi:10.1385/CBB:36:2-3:155

Cadenas, S. (2018). ROS and redox signaling in myocardial ischemia-reperfusion injury and cardioprotection. *Free Radic. Biol. Med.* 117, 76–89. doi:10.1016/j.freeradbiomed.2018.01.024

Cai, W., Zhang, K., Li, P., Zhu, L., Xu, J., Yang, B., et al. (2017). Dysfunction of the neurovascular unit in ischemic stroke and neurodegenerative diseases: An aging effect. *Ageing Res. Rev.* 34, 77–87. doi:10.1016/j.arr.2016.09.006

Cappellini, M. D., Cohen, A., Piga, A., Bejaoui, M., Perrotta, S., Agaoglu, L., et al. (2006). A phase 3 study of deferasirox (ICL670), a once-daily oral iron chelator, in patients with beta-thalassemia. *Blood* 107 (9), 3455–3462. doi:10.1182/blood-2005-08-3430

Castillo, J., Davalos, A., Naveiro, J., and Noya, M. (1996). Neuroexcitatory amino acids and their relation to infarct size and neurological deficit in ischemic stroke. *Stroke* 27 (6), 1060–1065. doi:10.1161/01.str.27.6.1060

Cekanaviciute, E., and Buckwalter, M. S. (2016). Astrocytes: Integrative regulators of neuroinflammation in stroke and other neurological diseases. *Neurotherapeutics* 13 (4), 685–701. doi:10.1007/s13311-016-0477-8

Chamulitrat, W., and Mason, R. P. (1989). Lipid peroxyl radical intermediates in the peroxidation of polyunsaturated fatty acids by lipoxygenase. *J. Biol. Chem.* 264 (35), 20968–20973. doi:10.1016/s0021-9258(19)30031-6

Chan, P. H. (1996). Role of oxidants in ischemic brain damage. *Stroke* 27 (6), 1124–1129. doi:10.1161/01.str.27.6.1124

Chang, Y. Z., Ke, Y., Du, J. R., Halpern, G. M., Ho, K. P., Zhu, L., et al. (2006). Increased divalent metal transporter 1 expression might be associated with the neurotoxicity of L-DOPA. *Mol. Pharmacol.* 69 (3), 968–974. doi:10.1124/mol.105.017756

Chang, C. F., Cho, S., and Wang, J. (2014). (-)-Epicatechin protects hemorrhagic brain via synergistic Nrf2 pathways. *Ann. Clin. Transl. Neurol.* 1 (4), 258–271. doi:10.1002/acn3.54

Cheli, V. T., Santiago Gonzalez, D. A., Marziali, L. N., Zamora, N. N., Guitart, M. E., Spreuer, V., et al. (2018). The divalent metal transporter 1 (DMT1) is required for iron uptake and normal development of oligodendrocyte progenitor cells. *J. Neurosci.* 38 (43), 9142–9159. doi:10.1523/JNEUROSCI.1447-18.2018

Chen, J., and Lopez, J. A. (2005). Interactions of platelets with subendothelium and endothelium. *Microcirculation* 12 (3), 235–246. doi:10.1080/10739680590925484

Chen, J. (2016). The cell-cycle arrest and apoptotic functions of p53 in tumor initiation and progression. *Cold Spring Harb. Perspect. Med.* 6 (3), a026104. doi:10.1101/cshperspect.a026104

Chen, C., Liu, P., Duan, X., Cheng, M., and Xu, L. X. (2019). Deferoxamine-induced high expression of TfR1 and DMT1 enhanced iron uptake in triple-negative breast cancer cells by activating IL-6/PI3K/AKT pathway. *Onco. Targets. Ther.* 12, 4359–4377. doi:10.2147/OTT.S193507

Chen, Y. C., Ma, N. X., Pei, Z. F., Wu, Z., Do-Monte, F. H., Keefe, S., et al. (2020). A NeuroD1 AAV-based gene therapy for functional brain repair after ischemic injury through *in vivo* astrocyte-to-neuron conversion. *Mol. Ther.* 28 (1), 217–234. doi:10.1016/j.ymthe.2019.09.003

Chen, X., Li, J., Kang, R., Klionsky, D. J., and Tang, D. (2021). Ferroptosis: Machinery and regulation. *Autophagy* 17 (9), 2054–2081. doi:10.1080/15548627.2020.1810918

Chen, Y., Fan, H., Wang, S., Tang, G., Zhai, C., and Shen, L. (2021). Ferroptosis: A novel therapeutic target for ischemia-reperfusion injury. *Front. Cell Dev. Biol.* 9, 688605. doi:10.3389/fcell.2021.688605

Cheng, Y., Song, Y., Chen, H., Li, Q., Gao, Y., Lu, G., et al. (2021). Ferroptosis mediated by lipid reactive oxygen species: A possible causal link of neuroinflammation to neurological disorders. *Oxid. Med. Cell. Longev.* 2021, 5005136. doi:10.1155/2021/5005136

Cojocaru, I. M., Cojocaru, M., Tanasescu, R., Iliescu, I., Dumitrescu, L., and Silosi, I. (2009). Expression of IL-6 activity in patients with acute ischemic stroke. *Rom. J. Intern Med.* 47 (4), 393–396.

Colonna, M., and Butovsky, O. (2017). Microglia function in the central nervous system during health and neurodegeneration. *Annu. Rev. Immunol.* 35, 441–468. doi:10.1146/annurev-immunol-051116-052358

Conrad, M., Kagan, V. E., Bayir, H., Pagnussat, G. C., Head, B., Traber, M. G., et al. (2018). Regulation of lipid peroxidation and ferroptosis in diverse species. *Genes Dev.* 32 (9-10), 602–619. doi:10.1101/gad.314674.118

Cregan, S. P., Maclaurin, J. G., Craig, C. G., Robertson, G. S., Nicholson, D. W., Park, D. S., et al. (1999). Bax-dependent caspase-3 activation is a key determinant in p53-induced apoptosis in neurons. *J. Neurosci.* 19 (18), 7860–7869. doi:10.1523/jneurosci.19-18-07860.1999

Cui, Y., Zhang, Y., Zhao, X., Shao, L., Liu, G., Sun, C., et al. (2021). ACSL4 exacerbates ischemic stroke by promoting ferroptosis-induced brain injury and neuroinflammation. *Brain Behav. Immun.* 93, 312–321. doi:10.1016/j.bbi.2021.01.003

Cunnane, S. C. (1994). Antioxidants, free radicals and PUFA. *Prostagl. Leukot. Essent. Fat. Acids* 50 (6), 363–364. doi:10.1016/0952-3278(94)90248-8

Daneman, R., and Prat, A. (2015). The blood-brain barrier. *Cold Spring Harb. Perspect. Biol.* 7 (1), a020412. doi:10.1101/cshperspect.a020412

Das, U. N. (2019). Saturated fatty acids, MUFAs and PUFAs regulate ferroptosis. *Cell Chem. Biol.* 26 (3), 309–311. doi:10.1016/j.chembiol.2019.03.001

Davalos, A., Fernandez-Real, J. M., Ricart, W., Molins, A., Planas, E., and Genis, D. (1994). Iron-related damage in acute ischemic stroke. *Stroke* 25 (8), 1543–1546. doi:10.1161/01.str.25.8.1543

Davidoff, M. S. (2019). The pluripotent microvascular pericytes are the adult stem cells even in the testis. *Adv. Exp. Med. Biol.* 1122, 235–267. doi:10.1007/978-3-030-11093-2_13

Degregorio-Rocasolano, N., Marti-Sistac, O., and Gasull, T. (2019). Deciphering the iron side of stroke: Neurodegeneration at the crossroads between iron dyshomeostasis, excitotoxicity, and ferroptosis. *Front. Neurosci.* 13, 85. doi:10.3389/fnins.2019.00085

Del Zoppo, G. J. (1998). The role of platelets in ischemic stroke. *Neurology* 51, S9–S14. doi:10.1212/wnl.51.3_suppl_3.s9

Dewar, D., Underhill, S. M., and Goldberg, M. P. (2003). Oligodendrocytes and ischemic brain injury. *J. Cereb. Blood Flow. Metab.* 23 (3), 263–274. doi:10.1097/01.WCB.0000053472.41007.F9

Dhakshinamoorthy, S., Long, D. J., 2nd, and Jaiswal, A. K. (2000). Antioxidant regulation of genes encoding enzymes that detoxify xenobiotics and carcinogens. *Curr. Top. Cell. Regul.* 36, 201–216. doi:10.1016/s0070-2137(01)80009-1

Dixon, S. J., Lemberg, K. M., Lamprecht, M. R., Skouta, R., Zaitsev, E. M., Gleason, C. E., et al. (2012). Ferroptosis: An iron-dependent form of nonapoptotic cell death. *Cell* 149 (5), 1060–1072. doi:10.1016/j.cell.2012.03.042

Do Van, B., Gouel, F., Jonneaux, A., Timmerman, K., Gele, P., Petrault, M., et al. (2016). Ferroptosis, a newly characterized form of cell death in Parkinson's disease that is regulated by PKC. *Neurobiol. Dis.* 94, 169–178. doi:10.1016/j.nbd.2016.05.011

Doll, S., Freitas, F. P., Shah, R., Aldrovandi, M., da Silva, M. C., Ingold, I., et al. (2019). FSP1 is a glutathione-independent ferroptosis suppressor. *Nature* 575 (7784), 693–698. doi:10.1038/s41586-019-1707-0

Doll, S., Proneth, B., Tyurina, Y. Y., Panzilius, E., Kobayashi, S., Ingold, I., et al. (2017). ACSL4 dictates ferroptosis sensitivity by shaping cellular lipid composition. *Nat. Chem. Biol.* 13 (1), 91–98. doi:10.1038/nchembio.2239

Donkor, E. S. (2018). Stroke in the 21(st) century: A snapshot of the burden, epidemiology, and quality of life. *Stroke Res. Treat.* 2018, 3238165. doi:10.1155/2018/3238165

Dugas, J. C., Mandemakers, W., Rogers, M., Ibrahim, A., Daneman, R., and Barres, B. A. (2008). A novel purification method for CNS projection neurons leads to the identification of brain vascular cells as a source of trophic support for corticospinal motor neurons. *J. Neurosci.* 28 (33), 8294–8305. doi:10.1523/JNEUROSCI.2010-08.2008

Earnshaw, W. C., Martins, L. M., and Kaufmann, S. H. (1999). Mammalian caspases: Structure, activation, substrates, and functions during apoptosis. *Annu. Rev. Biochem.* 68, 383–424. doi:10.1146/annurev.biochem.68.1.383

Enomoto, M., Endo, A., Yatsushige, H., Fushimi, K., and Otomo, Y. (2019). Clinical effects of early edaravone use in acute ischemic stroke patients treated by endovascular reperfusion therapy. *Stroke* 50 (3), 652–658. doi:10.1161/STROKEAHA.118.023815

Fang, S., Yu, X., Ding, H., Han, J., and Feng, J. (2018). Effects of intracellular iron overload on cell death and identification of potent cell death inhibitors. *Biochem. Biophys. Res. Commun.* 503 (1), 297–303. doi:10.1016/j.bbrc.2018.06.019

Fang, X., Wang, H., Han, D., Xie, E., Yang, X., Wei, J., et al. (2019). Ferroptosis as a target for protection against cardiomyopathy. *Proc. Natl. Acad. Sci. U. S. A.* 116 (7), 2672–2680. doi:10.1073/pnas.1821022116

Feder, M. E., and Hofmann, G. E. (1999). Heat-shock proteins, molecular chaperones, and the stress response: Evolutionary and ecological physiology. *Annu. Rev. Physiol.* 61, 243–282. doi:10.1146/annurev.physiol.61.1.243

Fei, W., Chen, D., Tang, H., Zheng, W., Chen, F., Chen, F., et al. (2020). Targeted GSH-exhausting and hydroxyl radical self-producing manganese-silica nanomissiles for MRI guided ferroptotic cancer therapy. *Nanoscale* 12 (32), 16738–16754. doi:10.1039/d0nr02396e

Feng, Y., Madungwe, N. B., Imam Aliagan, A. D., Tombo, N., and Bopassa, J. C. (2019). Liproxstatin-1 protects the mouse myocardium against ischemia/reperfusion injury by decreasing VDAC1 levels and restoring GPX4 levels. *Biochem. Biophys. Res. Commun.* 520 (3), 606–611. doi:10.1016/j.bbrc.2019.10.006

Ferguson, L. R., Karunasinghe, N., Zhu, S., and Wang, A. H. (2012). Selenium and its' role in the maintenance of genomic stability. *Mutat. Res.* 733 (1-2), 100–110. doi:10.1016/j.mrfmmm.2011.12.011

Fernandez-Morales, J. C., Hua, W., Yao, Y., and Morad, M. (2019). Regulation of Ca(2+) signaling by acute hypoxia and acidosis in cardiomyocytes derived from human induced pluripotent stem cells. *Cell Calcium* 78, 1–14. doi:10.1016/j.ceca.2018.12.006

Forcina, G. C., and Dixon, S. J. (2019). GPX4 at the crossroads of lipid homeostasis and ferroptosis. *Proteomics* 19 (18), e1800311. doi:10.1002/pmic.201800311

Friedman, M. (2014). Chemistry and multibeneficial bioactivities of carvacrol (4-isopropyl-2-methylphenol), a component of essential oils produced by aromatic plants and spices. *J. Agric. Food Chem.* 62 (31), 7652–7670. doi:10.1021/jf5023862

Fung, F. Y., and Linn, Y. C. (2015). Developing traditional Chinese medicine in the era of evidence-based medicine: Current evidences and challenges. *Evid. Based. Complement. Altern. Med.* 2015, 425037. doi:10.1155/2015/425037

Gao, M., Monian, P., Pan, Q., Zhang, W., Xiang, J., and Jiang, X. (2016). Ferroptosis is an autophagic cell death process. *Cell Res.* 26 (9), 1021–1032. doi:10.1038/cr.2016.95

Gao, M., Yi, J., Zhu, J., Minikes, A. M., Monian, P., Thompson, C. B., et al. (2019). Role of mitochondria in ferroptosis. *Mol. Cell* 73 (2), 354–363. doi:10.1016/j.molcel.2018.10.042

Gaschler, M. M., Andia, A. A., Liu, H., Csuka, J. M., Hurlocker, B., Vaiana, C. A., et al. (2018). FINO2 initiates ferroptosis through GPX4 inactivation and iron oxidation. *Nat. Chem. Biol.* 14 (5), 507–515. doi:10.1038/s41589-018-0031-6

Gaschler, M. M., and Stockwell, B. R. (2017). Lipid peroxidation in cell death. *Biochem. Biophys. Res. Commun.* 482 (3), 419–425. doi:10.1016/j.bbrc.2016.10.086

Gillessen, T., Budd, S. L., and Lipton, S. A. (2002). Excitatory amino acid neurotoxicity. *Adv. Exp. Med. Biol.* 513, 3–40. doi:10.1007/978-1-4615-0123-7_1

Girotti, A. W. (1998). Lipid hydroperoxide generation, turnover, and effector action in biological systems. *J. Lipid Res.* 39 (8), 1529–1542. doi:10.1016/s0022-2275(20)32182-9

Griesmaier, E., and Keller, M. (2012). Glutamate receptors - prenatal insults, long-term consequences. *Pharmacol. Biochem. Behav.* 100 (4), 835–840. doi:10.1016/j.pbb.2011.04.011

Grignano, E., Birsen, R., Chapuis, N., and Bouscary, D. (2020). From iron chelation to overload as a therapeutic strategy to induce ferroptosis in leukemic cells. *Front. Oncol.* 10, 586530. doi:10.3389/fonc.2020.586530

Guan, T., Song, J., Wang, Y., Guo, L., Yuan, L., Zhao, Y., et al. (2017). Expression and characterization of recombinant bifunctional enzymes with glutathione peroxidase and superoxide dismutase activities. *Free Radic. Biol. Med.* 110, 188–195. doi:10.1016/j.freeradbiomed.2017.06.005

Guan, X., Li, Z., Zhu, S., Cheng, M., Ju, Y., Ren, L., et al. (2021). Galangin attenuated cerebral ischemia-reperfusion injury by inhibition of ferroptosis through activating the SLC7A11/GPX4 axis in gerbils. *Life Sci.* 264, 118660. doi:10.1016/j.lfs.2020.118660

Guo, S., Kim, W. J., Lok, J., Lee, S. R., Besancon, E., Luo, B. H., et al. (2008). Neuroprotection via matrix-trophic coupling between cerebral endothelial cells and neurons. *Proc. Natl. Acad. Sci. U. S. A.* 105 (21), 7582–7587. doi:10.1073/pnas.0801105105

Guo, G. C., Wang, J. X., Han, M. L., Zhang, L. P., and Li, L. (2017). microRNA-761 induces aggressive phenotypes in triple-negative breast cancer cells by repressing TRIM29 expression. *Cell. Oncol.* 40 (2), 157–166. doi:10.1007/s13402-016-0312-6

Hambright, W. S., Fonseca, R. S., Chen, L., Na, R., and Ran, Q. (2017). Ablation of ferroptosis regulator glutathione peroxidase 4 in forebrain neurons promotes cognitive impairment and neurodegeneration. *Redox Biol.* 12, 8–17. doi:10.1016/j.redox.2017.01.021

Hamel, E. (2006). Perivascular nerves and the regulation of cerebrovascular tone. *J. Appl. Physiol. (1985)* 100 (3), 1059–1064. doi:10.1152/japplphysiol.00954.2005

Hamilton, N. B., Attwell, D., and Hall, C. N. (2010). Pericyte-mediated regulation of capillary diameter: A component of neurovascular coupling in health and disease. *Front. Neuroenergetics* 2, 5. doi:10.3389/fnene.2010.00005

Hanson, L. R., Roeytenberg, A., Martinez, P. M., Coppes, V. G., Sweet, D. C., Rao, R. J., et al. (2009). Intranasal deferoxamine provides increased brain exposure and significant protection in rat ischemic stroke. *J. Pharmacol. Exp. Ther.* 330 (3), 679–686. doi:10.1124/jpet.108.149807

Harris, C. C. (1996). p53 tumor suppressor gene: from the basic research laboratory to the clinic--an abridged historical perspective. *Carcinogenesis* 17 (6), 1187–1198. doi:10.1093/carcin/17.6.1187

Harris, S. L., and Levine, A. J. (2005). The p53 pathway: Positive and negative feedback loops. *Oncogene* 24 (17), 2899–2908. doi:10.1038/sj.onc.1208615

Henke, N., Schmidt-Ullrich, R., Dechend, R., Park, J. K., Qadri, F., Wellner, M., et al. (2007). Vascular endothelial cell-specific NF-kappaB suppression attenuates hypertension-induced renal damage. *Circ. Res.* 101 (3), 268–276. doi:10.1161/CIRCRESAHA.107.150474

Hong, S. H., Lee, D. H., Lee, Y. S., Jo, M. J., Jeong, Y. A., Kwon, W. T., et al. (2017). Molecular crosstalk between ferroptosis and apoptosis: Emerging role of ER stress-induced p53-independent PUMA expression. *Oncotarget* 8 (70), 115164–115178. doi:10.18632/oncotarget.23046

Hori, S., Ohtsuki, S., Hosoya, K., Nakashima, E., and Terasaki, T. (2004). A pericyte-derived angiopoietin-1 multimeric complex induces occludin gene expression in brain capillary endothelial cells through Tie-2 activation *in vitro*. *J. Neurochem.* 89 (2), 503–513. doi:10.1111/j.1471-4159.2004.02343.x

Hoshi, O., and Ushiki, T. (2004). Neutrophil extravasation in rat mesenteric venules induced by the chemotactic peptide N-formyl-methionyl-luecylphenylalanine (fMLP), with special attention to a barrier function of the vascular basal lamina for neutrophil migration. *Arch. Histol. Cytol.* 67 (1), 107–114. doi:10.1679/aohc.67.107

Hu, H. J., and Song, M. (2017). Disrupted ionic homeostasis in ischemic stroke and new therapeutic targets. *J. Stroke Cerebrovasc. Dis.* 26 (12), 2706–2719. doi:10.1016/j.jstrokecerebrovasdis.2017.09.011

Hu, X., De Silva, T. M., Chen, J., and Faraci, F. M. (2017). Cerebral vascular disease and neurovascular injury in ischemic stroke. *Circ. Res.* 120 (3), 449–471. doi:10.1161/CIRCRESAHA.116.308427

Hu, X., Wu, D., He, X., Zhao, H., He, Z., Lin, J., et al. (2019). circGSK3β promotes metastasis in esophageal squamous cell carcinoma by augmenting β-catenin signaling. *Mol. Cancer* 18 (1), 160. doi:10.1186/s12943-019-1095-y

Huang, J. (2021). Current developments of targeting the p53 signaling pathway for cancer treatment. *Pharmacol. Ther.* 220, 107720. doi:10.1016/j.pharmthera.2020.107720

Hughes, S. M., Lillien, L. E., Raff, M. C., RoHrer, H., and SendtnerM. (1988). Ciliary neurotrophic factor induces type-2 astrocyte differentiation in culture. *Nature* 335 (6185), 70–73. doi:10.1038/335070a0

Hundeshagen, P., Hamacher-Brady, A., Eils, R., and Brady, N. R. (2011). Concurrent detection of autolysosome formation and lysosomal degradation by flow cytometry in a high-content screen for inducers of autophagy. *BMC Biol.* 9, 38. doi:10.1186/1741-7007-9-38

Huo, X., Sun, H., Cao, D., Yang, J., Peng, P., Yu, M., et al. (2019). Identification of prognosis markers for endometrial cancer by integrated analysis of DNA methylation and RNA-Seq data. *Sci. Rep.* 9 (1), 9924. doi:10.1038/s41598-019-46195-8

Hutter-Schmid, B., and Humpel, C. (2016). Platelet-derived growth factor receptor-beta is differentially regulated in primary mouse pericytes and brain slices. *Curr. Neurovasc. Res.* 13 (2), 127–134. doi:10.2174/1567202613666160219120411

Iadecola, C. (2017). The neurovascular unit coming of age: A journey through neurovascular coupling in health and disease. *Neuron* 96 (1), 17–42. doi:10.1016/j.neuron.2017.07.030

Ikeda, M., Nakazawa, T., Abe, K., Kaneko, T., and Yamatsu, K. (1989). Extracellular accumulation of glutamate in the hippocampus induced by ischemia is not calcium dependent--*in vitro* and *in vivo* evidence. *Neurosci. Lett.* 96 (2), 202–206. doi:10.1016/0304-3940(89)90058-x

Ikeshima-Kataoka, H. (2016). Neuroimmunological implications of AQP4 in astrocytes. *Int. J. Mol. Sci.* 17 (8), E1306. doi:10.3390/ijms17081306

Illes, P., Verkhratsky, A., and Tang, Y. (2021). Surveilling microglia dampens neuronal activity: Operation of a purinergically mediated negative feedback mechanism. *Signal Transduct. Target. Ther.* 6 (1), 160. doi:10.1038/s41392-021-00586-4

Ishikawa, M., Zhang, J. H., Nanda, A., and Granger, D. N. (2004). Inflammatory responses to ischemia and reperfusion in the cerebral microcirculation. *Front. Biosci.* 9, 1339–1347. doi:10.2741/1330

Jacobs, A., Miller, F., Worwood, M., and Wardrop, C. A. (1972). Ferritin in the serum of normal subjects and patients with iron deficiency and iron overload. *Br. Med. J.* 4 (5834), 206–208. doi:10.1136/bmj.4.5834.206

Jaenisch, R., and Bird, A. (2003). Epigenetic regulation of gene expression: How the genome integrates intrinsic and environmental signals. *Nat. Genet.* 33, 245–254. doi:10.1038/ng1089

Jaiswal, A. K. (2004). Nrf2 signaling in coordinated activation of antioxidant gene expression. *Free Radic. Biol. Med.* 36 (10), 1199–1207. doi:10.1016/j.freeradbiomed.2004.02.074

Ji, H., Wang, W., Li, X., Han, X., Zhang, X., Wang, J., et al. (2022). p53: A double-edged sword in tumor ferroptosis. *Pharmacol. Res.* 177, 106013. doi:10.1016/j.phrs.2021.106013

Jiang, L., Kon, N., Li, T., Wang, S. J., Su, T., Hibshoosh, H., et al. (2015). Ferroptosis as a p53-mediated activity during tumour suppression. *Nature* 520 (7545), 57–62. doi:10.1038/nature14344

Jiang, X., Stockwell, B. R., and Conrad, M. (2021). Ferroptosis: Mechanisms, biology and role in disease. *Nat. Rev. Mol. Cell Biol.* 22 (4), 266–282. doi:10.1038/s41580-020-00324-8

Jin, G., Arai, K., Murata, Y., Wang, S., Stins, M. F., Lo, E. H., et al. (2008). Protecting against cerebrovascular injury: Contributions of 12/15-lipoxygenase to edema formation after transient focal ischemia. *Stroke* 39 (9), 2538–2543. doi:10.1161/STROKEAHA.108.514927

Jones, G., Goswami, S. K., Kang, H., Choi, H. S., and Kim, J. (2020). Combating iron overload: A case for deferoxamine-based nanochelators. *Nanomedicine (Lond)* 15, 1341–1356. doi:10.2217/nnm-2020-0038

Kagan, V. E., Mao, G., Qu, F., Angeli, J. P. F., Doll, S., Croix, C. S., et al. (2017). Oxidized arachidonic and adrenic PEs navigate cells to ferroptosis. *Nat. Chem. Biol.* 13 (1), 81–90. doi:10.1038/nchembio.2238

Kakhlon, O., and Cabantchik, Z. I. (2002). The labile iron pool: Characterization, measurement, and participation in cellular processes(1). *Free Radic. Biol. Med.* 33 (8), 1037–1046. doi:10.1016/s0891-5849(02)01006-7

Kang, R., Gamdzyk, M., Lenahan, C., Tang, J., Tan, S., and Zhang, J. H. (2020). The dual role of microglia in blood-brain barrier dysfunction after stroke. *Curr. Neuropharmacol.* 18 (12), 1237–1249. doi:10.2174/1570159X18666200529150907

Kanner, J., German, J. B., and Kinsella, J. E. (1987). Initiation of lipid peroxidation in biological systems. *Crit. Rev. Food Sci. Nutr.* 25 (4), 317–364. doi:10.1080/10408398709527457

Kaspar, J. W., Niture, S. K., and Jaiswal, A. K. (2009). Nrf2:INrf2 (Keap1) signaling in oxidative stress. *Free Radic. Biol. Med.* 47 (9), 1304–1309. doi:10.1016/j.freeradbiomed.2009.07.035

Kawabata, H. (2019). Transferrin and transferrin receptors update. *Free Radic. Biol. Med.* 133, 46–54. doi:10.1016/j.freeradbiomed.2018.06.037

Kern, F., Stanika, R. I., Sarg, B., Offterdinger, M., Hess, D., Obermair, G. J., et al. (2013). Nogo-A couples with Apg-1 through interaction and co-ordinate expression under hypoxic and oxidative stress. *Biochem. J.* 455 (2), 217–227. doi:10.1042/BJ20130579

Khoshnam, S. E., Winlow, W., Farzaneh, M., Farbood, Y., and Moghaddam, H. F. (2017). Pathogenic mechanisms following ischemic stroke. *Neurol. Sci.* 38 (7), 1167–1186. doi:10.1007/s10072-017-2938-1

Kikuchi, K., Tancharoen, S., Matsuda, F., Biswas, K. K., Ito, T., Morimoto, Y., et al. (2009). Edaravone attenuates cerebral ischemic injury by suppressing aquaporin-4. *Biochem. Biophys. Res. Commun.* 390 (4), 1121–1125. doi:10.1016/j.bbrc.2009.09.015

Kikuchi, K., Tancharoen, S., Takeshige, N., Yoshitomi, M., Morioka, M., Murai, Y., et al. (2013). The efficacy of edaravone (radicut), a free radical scavenger, for cardiovascular disease. *Int. J. Mol. Sci.* 14 (7), 13909–13930. doi:10.3390/ijms140713909

Kim, S. E., Zhang, L., Ma, K., Riegman, M., Chen, F., Ingold, I., et al. (2016). Ultrasmall nanoparticles induce ferroptosis in nutrient-deprived cancer cells and

suppress tumour growth. *Nat. Nanotechnol.* 11 (11), 977–985. doi:10.1038/nnano.2016.164

Kim, S. U., and De Vellis, J. (2005). Microglia in health and disease. *J. Neurosci. Res.* 81 (3), 302–313. doi:10.1002/jnr.20562

Kobayashi, M., and Yamamoto, M. (2006). Nrf2-Keap1 regulation of cellular defense mechanisms against electrophiles and reactive oxygen species. *Adv. Enzyme Regul.* 46, 113–140. doi:10.1016/j.advenzreg.2006.01.007

Kobayashi, S., Fukuma, S., Ikenoue, T., and Fukuhara, S. (2019). Effect of edaravone on neurological symptoms in real-world patients with acute ischemic stroke. *Stroke* 50 (7), 1805–1811. doi:10.1161/STROKEAHA.118.024351

Koh, P. O. (2008). Melatonin attenuates the focal cerebral ischemic injury by inhibiting the dissociation of pBad from 14-3-3. *J. Pineal Res.* 44 (1), 101–106. doi:10.1111/j.1600-079X.2007.00495.x

Kruger-Genge, A., Blocki, A., Franke, R. P., and Jung, F. (2019). Vascular endothelial cell biology: An update. *Int. J. Mol. Sci.* 20 (18), E4411. doi:10.3390/ijms20184411

Kuang, F., Liu, J., Tang, D., and Kang, R. (2020). Oxidative damage and antioxidant defense in ferroptosis. *Front. Cell Dev. Biol.* 8, 586578. doi:10.3389/fcell.2020.586578

Kuhn, S., Gritti, L., Crooks, D., and Dombrowski, Y. (2019). Oligodendrocytes in development, myelin generation and beyond. *Cells* 8 (11), E1424. doi:10.3390/cells8111424

Kuwata, H., Nakatani, E., Shimbara-Matsubayashi, S., Ishikawa, F., Shibanuma, M., Sasaki, Y., et al. (2019). Long-chain acyl-CoA synthetase 4 participates in the formation of highly unsaturated fatty acid-containing phospholipids in murine macrophages. *Biochim. Biophys. Acta. Mol. Cell Biol. Lipids* 1864 (11), 1606–1618. doi:10.1016/j.bbalip.2019.07.013

Kwak, M. K., Cho, J. M., Huang, B., Shin, S., and Kensler, T. W. (2007). Role of increased expression of the proteasome in the protective effects of sulforaphane against hydrogen peroxide-mediated cytotoxicity in murine neuroblastoma cells. *Free Radic. Biol. Med.* 43 (5), 809–817. doi:10.1016/j.freeradbiomed.2007.05.029

Lai, T. W., Zhang, S., and Wang, Y. T. (2014). Excitotoxicity and stroke: Identifying novel targets for neuroprotection. *Prog. Neurobiol.* 115, 157–188. doi:10.1016/j.pneurobio.2013.11.006

Lan, B., Ge, J. W., Cheng, S. W., Zheng, X. L., Liao, J., He, C., et al. (2020). Extract of Naotaifang, a compound Chinese herbal medicine, protects neuron ferroptosis induced by acute cerebral ischemia in rats. *J. Integr. Med.* 18 (4), 344–350. doi:10.1016/j.joim.2020.01.008

Lane, D. J. R., Ayton, S., and Bush, A. I. (2018). Iron and alzheimer's disease: An update on emerging mechanisms. *J. Alzheimers Dis.* 64, S379–S395. doi:10.3233/JAD-179944

Lao, Y., Wang, Y., Chen, J., Huang, P., Su, R., Shi, J., et al. (2022). Synthesis and biological evaluation of 1, 2, 4-triazole derivatives as potential Nrf2 activators for the treatment of cerebral ischemic injury. *Eur. J. Med. Chem.* 236, 114315. doi:10.1016/j.ejmech.2022.114315

Lazarov, O., and Hollands, C. (2016). Hippocampal neurogenesis: Learning to remember. *Prog. Neurobiol.* 138-140, 1–18. doi:10.1016/j.pneurobio.2015.12.006

Lee, J. Y., Kim, W. K., Bae, K. H., Lee, S. C., and Lee, E. W. (2021). Lipid metabolism and ferroptosis. *Biol. (Basel)* 10 (3), 184. doi:10.3390/biology10030184

Leigh, R., Knutsson, L., Zhou, J., and van Zijl, P. C. (2018). Imaging the physiological evolution of the ischemic penumbra in acute ischemic stroke. *J. Cereb. Blood Flow. Metab.* 38 (9), 1500–1516. doi:10.1177/0271678X17700913

Lemasters, J. J. (2017). Evolution of voltage-dependent anion channel function: From molecular sieve to governator to actuator of ferroptosis. *Front. Oncol.* 7, 303. doi:10.3389/fonc.2017.00303

Li, Z., Hua, C., Pan, X., Fu, X., and Wu, W. (2016). Carvacrol exerts neuroprotective effects via suppression of the inflammatory response in middle cerebral artery occlusion rats. *Inflammation* 39 (4), 1566–1572. doi:10.1007/s10753-016-0392-5

Li, Y., Feng, D., Wang, Z., Zhao, Y., Sun, R., Tian, D., et al. (2019). Ischemia-induced ACSL4 activation contributes to ferroptosis-mediated tissue injury in intestinal ischemia/reperfusion. *Cell Death Differ.* 26 (11), 2284–2299. doi:10.1038/s41418-019-0299-4

Li, X., Ma, N., Xu, J., Zhang, Y., Yang, P., Su, X., et al. (2021). Targeting ferroptosis: Pathological mechanism and treatment of ischemia-reperfusion injury. *Oxid. Med. Cell. Longev.* 2021, 1587922. doi:10.1155/2021/1587922

Lim, S., Kim, T. J., Kim, Y. J., Kim, C., Ko, S. B., and Kim, B. S. (2021). Senolytic therapy for cerebral ischemia-reperfusion injury. *Int. J. Mol. Sci.* 22 (21), 11967. doi:10.3390/ijms222111967

Littarru, G. P., and Tiano, L. (2007). Bioenergetic and antioxidant properties of coenzyme Q10: Recent developments. *Mol. Biotechnol.* 37 (1), 31–37. doi:10.1007/s12033-007-0052-y

Liu, L., Vollmer, M. K., Fernandez, V. M., Dweik, Y., Kim, H., and Dore, S. (2018). Korean red ginseng pretreatment protects against long-term sensorimotor deficits after ischemic stroke likely through Nrf2. *Front. Cell. Neurosci.* 12, 74. doi:10.3389/fncel.2018.00074

Liu, J., Zhang, C., Wang, J., Hu, W., and Feng, Z. (2020). The regulation of ferroptosis by tumor suppressor p53 and its pathway. *Int. J. Mol. Sci.* 21 (21), E8387. doi:10.3390/ijms21218387

Liu, J., Guo, Z. N., Yan, X. L., Huang, S., Ren, J. X., Luo, Y., et al. (2020). Crosstalk between autophagy and ferroptosis and its putative role in ischemic stroke. *Front. Cell. Neurosci.* 14, 577403. doi:10.3389/fncel.2020.577403

Liu, L., Wang, M., Gong, N., Tian, P., and Deng, H. (2021). Se improves GPX4 expression and SOD activity to alleviate heat-stress-induced ferroptosis-like death in goat mammary epithelial cells. *Anim. Cells Syst.* 25 (5), 283–295. doi:10.1080/19768354.2021.1988704

Lo, E. H., and Rosenberg, G. A. (2009). The neurovascular unit in health and disease: Introduction. *Stroke* 40 (3), S2–S3. doi:10.1161/STROKEAHA.108.534404

Lopes-Bezerra, L. M., and Filler, S. G. (2003). Endothelial cells, tissue factor and infectious diseases. *Braz J. Med. Biol. Res.* 36 (8), 987–991. doi:10.1590/s0100-879x2003000800004

Lopes-Marques, M., Cunha, I., Reis-Henriques, M. A., Santos, M. M., and Castro, L. F. C. (2013). Diversity and history of the long-chain acyl-CoA synthetase (Acsl) gene family in vertebrates. *BMC Evol. Biol.* 13, 271. doi:10.1186/1471-2148-13-271

Lu, B., Chen, X. B., Ying, M. D., He, Q. J., Cao, J., and Yang, B. (2017). The role of ferroptosis in cancer development and treatment response. *Front. Pharmacol.* 8, 992. doi:10.3389/fphar.2017.00992

Luo, M., Wu, L., Zhang, K., Wang, H., Zhang, T., Gutierrez, L., et al. (2018). miR-137 regulates ferroptosis by targeting glutamine transporter SLC1A5 in melanoma. *Cell Death Differ.* 25 (8), 1457–1472. doi:10.1038/s41418-017-0053-8

Luo, W., Wang, J., Dai, X., Zhang, H., Qu, Y., Xiao, W., et al. (2021). ACSL4 expression is associated with CD8+ T cell infiltration and immune response in bladder cancer. *Front. Oncol.* 11, 754845. doi:10.3389/fonc.2021.754845

Ma, Y., Zhang, X., Alsaidan, O. A., Yang, X., Sulejmani, E., Zha, J., et al. (2021). Long-chain acyl-CoA synthetase 4-mediated fatty acid metabolism sustains androgen receptor pathway-independent prostate cancer. *Mol. Cancer Res.* 19 (1), 124–135. doi:10.1158/1541-7786.MCR-20-0379

Magtanong, L., and Dixon, S. J. (2018). Ferroptosis and brain injury. *Dev. Neurosci.* 40 (5-6), 382–395. doi:10.1159/000496922

Magtanong, L., Ko, P. J., and Dixon, S. J. (2016). Emerging roles for lipids in non-apoptotic cell death. *Cell Death Differ.* 23 (7), 1099–1109. doi:10.1038/cdd.2016.25

Mahoney-Sanchez, L., Bouchaoui, H., Ayton, S., Devos, D., Duce, J. A., and Devedjian, J. C. (2021). Ferroptosis and its potential role in the physiopathology of Parkinson's Disease. *Prog. Neurobiol.* 196, 101890. doi:10.1016/j.pneurobio.2020.101890

Makihara, N., Arimura, K., Ago, T., Tachibana, M., Nishimura, A., Nakamura, K., et al. (2015). Involvement of platelet-derived growth factor receptor beta in fibrosis through extracellular matrix protein production after ischemic stroke. *Exp. Neurol.* 264, 127–134. doi:10.1016/j.expneurol.2014.12.007

Mancias, J. D., Wang, X., Gygi, S. P., Harper, J. W., and Kimmelman, A. C. (2014). Quantitative proteomics identifies NCOA4 as the cargo receptor mediating ferritinophagy. *Nature* 509 (7498), 105–109. doi:10.1038/nature13148

Mandai, K., Matsumoto, M., Kitagawa, K., Matsushita, K., OhTsuki, T., Mabuchi, T., et al. (1997). Ischemic damage and subsequent proliferation of oligodendrocytes in focal cerebral ischemia. *Neuroscience* 77 (3), 849–861. doi:10.1016/s0306-4522(96)00517-9

Marcelo, K. L., Goldie, L. C., and Hirschi, K. K. (2013). Regulation of endothelial cell differentiation and specification. *Circ. Res.* 112 (9), 1272–1287. doi:10.1161/CIRCRESAHA.113.300506

Margis, R., Dunand, C., Teixeira, F. K., and Margis-Pinheiro, M. (2008). Glutathione peroxidase family - an evolutionary overview. *FEBS J.* 275 (15), 3959–3970. doi:10.1111/j.1742-4658.2008.06542.x

Martin, A., Domercq, M., and Matute, C. (2018). Inflammation in stroke: The role of cholinergic, purinergic and glutamatergic signaling. *Ther. Adv. Neurol. Disord.* 11, 1756286418774267. doi:10.1177/1756286418774267

Matsumoto, J., Dohgu, S., Takata, F., Machida, T., Bolukbasi Hatip, F. F., Hatip-Al-Khatib, I., et al. (2018). TNF-α-sensitive brain pericytes activate microglia by releasing IL-6 through cooperation between IκB-NFκB and JAK-STAT3 pathways. *Brain Res.* 1692, 34–44. doi:10.1016/j.brainres.2018.04.023

Matsumoto, S., Murozono, M., Kanazawa, M., Nara, T., Ozawa, T., and Watanabe, Y. (2018). Edaravone and cyclosporine A as neuroprotective agents for acute ischemic stroke. *Acute Med. Surg.* 5 (3), 213–221. doi:10.1002/ams2.343

Matute, C., Domercq, M., and Sanchez-Gomez, M. V. (2006). Glutamate-mediated glial injury: Mechanisms and clinical importance. *Glia* 53 (2), 212–224. doi:10.1002/glia.20275

Mccall, J. M., Braughler, J. M., and Hall, E. D. (1987). Lipid peroxidation and the role of oxygen radicals in CNS injury. *Acta Anaesthesiol. belg.* 38 (4), 373–379.

Mcconnell, H. L., Kersch, C. N., Woltjer, R. L., and Neuwelt, E. A. (2017). The translational significance of the neurovascular unit. *J. Biol. Chem.* 292 (3), 762–770. doi:10.1074/jbc.R116.760215

Narayan, S. K., Grace Cherian, S., Babu Phaniti, P., Babu Chidambaram, S., Rachel Vasanthi, A. H., and Arumugam, M. (2021). Preclinical animal studies in ischemic stroke: Challenges and some solutions. *Anim. Model. Exp. Med.* 4 (2), 104–115. doi:10.1002/ame2.12166

Nasoohi, S., Simani, L., Khodagholi, F., Nikseresht, S., Faizi, M., and Naderi, N. (2019). Coenzyme Q10 supplementation improves acute outcomes of stroke in rats pretreated with atorvastatin. *Nutr. Neurosci.* 22 (4), 264–272. doi:10.1080/1028415X.2017.1376928

Nave, K. A., and Werner, H. B. (2014). Myelination of the nervous system: Mechanisms and functions. *Annu. Rev. Cell Dev. Biol.* 30, 503–533. doi:10.1146/annurev-cellbio-100913-013101

Newell-Price, J., Clark, A. J., and King, P. (2000). DNA methylation and silencing of gene expression. *Trends Endocrinol. Metab.* 11 (4), 142–148. doi:10.1016/s1043-2760(00)00248-4

Ng, S. W., Norwitz, S. G., and Norwitz, E. R. (2019). The impact of iron overload and ferroptosis on reproductive disorders in humans: Implications for preeclampsia. *Int. J. Mol. Sci.* 20 (13), E3283. doi:10.3390/ijms20133283

Nguyen, B., Bix, G., and Yao, Y. (2021). Basal lamina changes in neurodegenerative disorders. *Mol. Neurodegener.* 16 (1), 81. doi:10.1186/s13024-021-00502-y

Nimmerjahn, A., Kirchhoff, F., and Helmchen, F. (2005). Resting microglial cells are highly dynamic surveillants of brain parenchyma *in vivo*. *Science* 308 (5726), 1314–1318. doi:10.1126/science.1110647

Nishizawa, H., Matsumoto, M., Chen, G., Ishii, Y., Tada, K., Onodera, M., et al. (2021). Lipid peroxidation and the subsequent cell death transmitting from ferroptotic cells to neighboring cells. *Cell Death Dis.* 12 (4), 332. doi:10.1038/s41419-021-03613-y

Onat, D., Brillon, D., Colombo, P. C., and Schmidt, A. M. (2011). Human vascular endothelial cells: A model system for studying vascular inflammation in diabetes and atherosclerosis. *Curr. Diab. Rep.* 11 (3), 193–202. doi:10.1007/s11892-011-0182-2

Owolabi, M. O., Akarolo-Anthony, S., Akinyemi, R., Arnett, D., Gebregziabher, M., Jenkins, C., et al. (2015). The burden of stroke in africa: A glance at the present and a glimpse into the future. *Cardiovasc. J. Afr.* 26, S27–S38. doi:10.5830/CVJA-2015-038

Pan, L., Zhou, L., Yin, W., Bai, J., and Liu, R. (2018). miR-125a induces apoptosis, metabolism disorder and migrationimpairment in pancreatic cancer cells by targeting Mfn2-related mitochondrial fission. *Int. J. Oncol.* 53 (1), 124–136. doi:10.3892/ijo.2018.4380

Papanicolaou, K. N., Khairallah, R. J., Ngoh, G. A., Chikando, A., Luptak, I., O'Shea, K. M., et al. (2011). Mitofusin-2 maintains mitochondrial structure and contributes to stress-induced permeability transition in cardiac myocytes. *Mol. Cell. Biol.* 31 (6), 1309–1328. doi:10.1128/MCB.00911-10

Pardridge, W. M. (1991). Advances in cell biology of blood-brain barrier transport. *Semin. Cell Biol.* 2 (6), 419–426.

Peisker, T., Koznar, B., Stetkarova, I., and Widimsky, P. (2017). Acute stroke therapy: A review. *Trends cardiovasc. Med.* 27 (1), 59–66. doi:10.1016/j.tcm.2016.06.009

Peng, L., Zhao, Y., Li, Y., Zhou, Y., Li, L., Lei, S., et al. (2019). Effect of DJ-1 on the neuroprotection of astrocytes subjected to cerebral ischemia/reperfusion injury. *J. Mol. Med.* 97 (2), 189–199. doi:10.1007/s00109-018-1719-5

Petrova, J., Manolov, V., Vasilev, V., Tzatchev, K., and Marinov, B. (2016). Ischemic stroke, inflammation, iron overload - connection to a hepcidin. *Int. J. Stroke* 11 (1), NP16–17. doi:10.1177/1747493015607509

Plemel, J. R., Keough, M. B., Duncan, G. J., Sparling, J. S., Yong, V. W., Stys, P. K., et al. (2014). Remyelination after spinal cord injury: Is it a target for repair? *Prog. Neurobiol.* 117, 54–72. doi:10.1016/j.pneurobio.2014.02.006

Polewski, M. D., Reveron-Thornton, R. F., Cherryholmes, G. A., Marinov, G. K., Cassady, K., and Aboody, K. S. (2016). Increased expression of system xc- in glioblastoma confers an altered metabolic state and temozolomide resistance. *Mol. Cancer Res.* 14 (12), 1229–1242. doi:10.1158/1541-7786.MCR-16-0028

Pratt, D. A., Tallman, K. A., and Porter, N. A. (2011). Free radical oxidation of polyunsaturated lipids: New mechanistic insights and the development of peroxyl radical clocks. *Acc. Chem. Res.* 44 (6), 458–467. doi:10.1021/ar200024c

Purohit, P. K., Edwards, R., Tokatlidis, K., and Saini, N. (2019). MiR-195 regulates mitochondrial function by targeting mitofusin-2 in breast cancer cells. *RNA Biol.* 16 (7), 918–929. doi:10.1080/15476286.2019.1600999

Qin, D. J., Tang, C. X., Yang, L., Lei, H., Wei, W., Wang, Y. Y., et al. (2015). Hsp90 is a novel target molecule of CDDO-me in inhibiting proliferation of ovarian cancer cells. *PLoS One* 10 (7), e0132337. doi:10.1371/journal.pone.0132337

Qin, C., Zhou, L. Q., Ma, X. T., Hu, Z. W., Yang, S., Chen, M., et al. (2019). Dual functions of microglia in ischemic stroke. *Neurosci. Bull.* 35 (5), 921–933. doi:10.1007/s12264-019-00388-3

Raj, S., Khurana, S., Choudhari, R., Kesari, K. K., Kamal, M. A., Garg, N., et al. (2021). Specific targeting cancer cells with nanoparticles and drug delivery in cancer therapy. *Semin. Cancer Biol.* 69, 166–177. doi:10.1016/j.semcancer.2019.11.002

Ramakrishnan, S., Anand, V., and Roy, S. (2014). Vascular endothelial growth factor signaling in hypoxia and inflammation. *J. Neuroimmune Pharmacol.* 9 (2), 142–160. doi:10.1007/s11481-014-9531-7

Ramezani, M., Simani, L., Abedi, S., and Pakdaman, H. (2021). Is selenium supplementation beneficial in acute ischemic stroke? *Neurologist* 27 (2), 51–55. doi:10.1097/NRL.0000000000000365

Ravingerova, T., Kindernay, L., Bartekova, M., Ferko, M., Adameova, A., Zohdi, V., et al. (2020). The molecular mechanisms of iron metabolism and its role in cardiac dysfunction and cardioprotection. *Int. J. Mol. Sci.* 21 (21), E7889. doi:10.3390/ijms21217889

Reichert, C. O., De Freitas, F. A., Sampaio-Silva, J., Rokita-Rosa, L., Barros, P. d. L., Levy, D., et al. (2020). Ferroptosis mechanisms involved in neurodegenerative diseases. *Int. J. Mol. Sci.* 21 (22), E8765. doi:10.3390/ijms21228765

Ren, X., Hu, H., Farooqi, I., and Simpkins, J. W. (2020). Blood substitution therapy rescues the brain of mice from ischemic damage. *Nat. Commun.* 11 (1), 4078. doi:10.1038/s41467-020-17930-x

Ringleb, P. A., Schellinger, P. D., Schranz, C., and Hacke, W. (2002). Thrombolytic therapy within 3 to 6 hours after onset of ischemic stroke: Useful or harmful? *Stroke* 33 (5), 1437–1441. doi:10.1161/01.str.0000015555.21285.db

Rizzardi, N., Liparulo, I., Antonelli, G., Orsini, F., Riva, A., Bergamini, C., et al. (2021). Coenzyme Q10 phytosome formulation improves CoQ10 bioavailability and mitochondrial functionality in cultured cells. *Antioxidants* 10 (6), 927. doi:10.3390/antiox10060927

Roemhild, K., Von Maltzahn, F., Weiskirchen, R., Knuchel, R., von Stillfried, S., and Lammers, T. (2021). Iron metabolism: Pathophysiology and pharmacology. *Trends Pharmacol. Sci.* 42 (8), 640–656. doi:10.1016/j.tips.2021.05.001

Rohnert, P., Schroder, U. H., Ziabreva, I., Tager, M., Reymann, K. G., and Striggow, F. (2012). Insufficient endogenous redox buffer capacity may underlie neuronal vulnerability to cerebral ischemia and reperfusion. *J. Neurosci. Res.* 90 (1), 193–202. doi:10.1002/jnr.22754

Rotin, D., Robinson, B., and Tannock, I. F. (1986). Influence of hypoxia and an acidic environment on the metabolism and viability of cultured cells: Potential implications for cell death in tumors. *Cancer Res.* 46 (6), 2821–2826.

Rustenhoven, J., Jansson, D., Smyth, L. C., and Dragunow, M. (2017). Brain pericytes as mediators of neuroinflammation. *Trends Pharmacol. Sci.* 38 (3), 291–304. doi:10.1016/j.tips.2016.12.001

Sacco, R. L., Kasner, S. E., Broderick, J. P., Caplan, L. R., Connors, J. J. B., Culebras, A., et al. (2013). An updated definition of stroke for the 21st century: A statement for healthcare professionals from the American heart association/American stroke association. *Stroke* 44 (7), 2064–2089. doi:10.1161/STR.0b013e318296aeca

Sandoo, A., Van Zanten, J. J., Metsios, G. S., Carroll, D., and Kitas, G. D. (2010). The endothelium and its role in regulating vascular tone. *Open cardiovasc. Med. J.* 4, 302–312. doi:10.2174/1874192401004010302

Sasaki, H., Sato, H., Kuriyama-Matsumura, K., Maebara, K., Wang, H., Tamba, M., et al. (2002). Electrophile response element-mediated induction of the cystine/glutamate exchange transporter gene expression. *J. Biol. Chem.* 277 (47), 44765–44771. doi:10.1074/jbc.M208704200

Sato, H., Tamba, M., Ishii, T., and Bannai, S. (1999). Cloning and expression of a plasma membrane cystine/glutamate exchange transporter composed of two distinct proteins. *J. Biol. Chem.* 274 (17), 11455–11458. doi:10.1074/jbc.274.17.11455

Schellinger, P. D., and Warach, S. (2004). Therapeutic time window of thrombolytic therapy following stroke. *Curr. Atheroscler. Rep.* 6 (4), 288–294. doi:10.1007/s11883-004-0060-3

Seib, T. M., Patel, S. A., and Bridges, R. J. (2011). Regulation of the system x(C)-cystine/glutamate exchanger by intracellular glutathione levels in rat astrocyte primary cultures. *Glia* 59 (10), 1387–1401. doi:10.1002/glia.21176

Shen, Z., Xiang, M., Chen, C., Ding, F., Wang, Y., Shang, C., et al. (2022). Glutamate excitotoxicity: Potential therapeutic target for ischemic stroke. *Biomed. Pharmacother.* 151, 113125. doi:10.1016/j.biopha.2022.113125

Shibata, Y., Yasui, H., Higashikawa, K., Miyamoto, N., and Kuge, Y. (2019). Erastin, a ferroptosis-inducing agent, sensitized cancer cells to X-ray irradiation via glutathione starvation *in vitro* and *in vivo*. *PLoS One* 14 (12), e0225931. doi:10.1371/journal.pone.0225931

Shibuya, M. (2011). Vascular endothelial growth factor (VEGF) and its receptor (VEGFR) signaling in angiogenesis: A crucial target for anti- and pro-angiogenic therapies. *Genes Cancer* 2 (12), 1097–1105. doi:10.1177/1947601911423031

Shih, A. Y., Li, P., and Murphy, T. H. (2005). A small-molecule-inducible Nrf2-mediated antioxidant response provides effective prophylaxis against cerebral ischemia *in vivo*. *J. Neurosci.* 25 (44), 10321–10335. doi:10.1523/JNEUROSCI.4014-05.2005

Shintoku, R., Takigawa, Y., Yamada, K., Kubota, C., Yoshimoto, Y., Takeuchi, T., et al. (2017). Lipoxygenase-mediated generation of lipid peroxides enhances ferroptosis induced by erastin and RSL3. *Cancer Sci.* 108 (11), 2187–2194. doi:10.1111/cas.13380

Singh, N. K., and Rao, G. N. (2019). Emerging role of 12/15-Lipoxygenase (ALOX15) in human pathologies. *Prog. Lipid Res.* 73, 28–45. doi:10.1016/j.plipres.2018.11.001

Soehnlein, O., and Lindbom, L. (2010). Phagocyte partnership during the onset and resolution of inflammation. *Nat. Rev. Immunol.* 10 (6), 427–439. doi:10.1038/nri2779

Sofroniew, M. V. (2009). Molecular dissection of reactive astrogliosis and glial scar formation. *Trends Neurosci.* 32 (12), 638–647. doi:10.1016/j.tins.2009.08.002

Song, X., and Long, D. (2020). Nrf2 and ferroptosis: A new research direction for neurodegenerative diseases. *Front. Neurosci.* 14, 267. doi:10.3389/fnins.2020.00267

Stamatovic, S. M., Keep, R. F., and Andjelkovic, A. V. (2008). Brain endothelial cell-cell junctions: How to "open" the blood brain barrier. *Curr. Neuropharmacol.* 6 (3), 179–192. doi:10.2174/157015908785777210

Stanimirovic, D. B., and Friedman, A. (2012). Pathophysiology of the neurovascular unit: Disease cause or consequence? *J. Cereb. Blood Flow. Metab.* 32 (7), 1207–1221. doi:10.1038/jcbfm.2012.25

Steinberg, S. F. (2008). Structural basis of protein kinase C isoform function. *Physiol. Rev.* 88 (4), 1341–1378. doi:10.1152/physrev.00034.2007

Stockwell, B. R., Friedmann Angeli, J. P., Bayir, H., Bush, A. I., Conrad, M., Dixon, S. J., et al. (2017). Ferroptosis: A regulated cell death nexus linking metabolism, redox biology, and disease. *Cell* 171 (2), 273–285. doi:10.1016/j.cell.2017.09.021

Stubbs, C. D., and Smith, A. D. (1984). The modification of mammalian membrane polyunsaturated fatty acid composition in relation to membrane fluidity and function. *Biochim. Biophys. Acta* 779 (1), 89–137. doi:10.1016/0304-4157(84)90005-4

Su, L. J., Zhang, J. H., Gomez, H., Murugan, R., Hong, X., Xu, D., et al. (2019). Reactive oxygen species-induced lipid peroxidation in apoptosis, autophagy, and ferroptosis. *Oxid. Med. Cell. Longev.* 2019, 5080843. doi:10.1155/2019/5080843

Sukiennicki, G. M., Marciniak, W., Muszynska, M., Baszuk, P., Gupta, S., Bialkowska, K., et al. (2019). Iron levels, genes involved in iron metabolism and antioxidative processes and lung cancer incidence. *PLoS One* 14 (1), e0208610. doi:10.1371/journal.pone.0208610

Sun, X., Ou, Z., Xie, M., Kang, R., Fan, Y., Niu, X., et al. (2015). HSPB1 as a novel regulator of ferroptotic cancer cell death. *Oncogene* 34 (45), 5617–5625. doi:10.1038/onc.2015.32

Tang, L. J., Zhou, Y. J., Xiong, X. M., Li, N. S., Zhang, J. J., Luo, X. J., et al. (2021). Ubiquitin-specific protease 7 promotes ferroptosis via activation of the p53/TfR1 pathway in the rat hearts after ischemia/reperfusion. *Free Radic. Biol. Med.* 162, 339–352. doi:10.1016/j.freeradbiomed.2020.10.307

Tarangelo, A., Magtanong, L., Bieging-Rolett, K. T., Li, Y., Ye, J., Attardi, L. D., et al. (2018). p53 suppresses metabolic stress-induced ferroptosis in cancer cells. *Cell Rep.* 22 (3), 569–575. doi:10.1016/j.celrep.2017.12.077

Tevlin, R., Longaker, M. T., and Wan, D. C. (2021). Deferoxamine to minimize fibrosis during radiation therapy. *Adv. Wound Care* 11, 548–559. doi:10.1089/wound.2021.0021

Thomas, C., Mackey, M. M., Diaz, A. A., and Cox, D. P. (2009). Hydroxyl radical is produced via the Fenton reaction in submitochondrial particles under oxidative stress: Implications for diseases associated with iron accumulation. *Redox Rep.* 14 (3), 102–108. doi:10.1179/135100009X392566

Thurgur, H., and Pinteaux, E. (2019). Microglia in the neurovascular unit: Blood-brain barrier-microglia interactions after central nervous system disorders. *Neuroscience* 405, 55–67. doi:10.1016/j.neuroscience.2018.06.046

Tian, Q., Qin, B., Gu, Y., Zhou, L., Chen, S., Zhang, S., et al. (2020). ROS-mediated necroptosis is involved in iron overload-induced osteoblastic cell death. *Oxid. Med. Cell. Longev.* 2020, 1295382. doi:10.1155/2020/1295382

Tourki, B., Black, L. M., Kain, V., and Halade, G. V. (2021). Lipoxygenase inhibitor ML351 dysregulated an innate inflammatory response leading to impaired cardiac repair in acute heart failure. *Biomed. Pharmacother.* 139, 111574. doi:10.1016/j.biopha.2021.111574

Tuo, Q. Z., Lei, P., Jackman, K. A., Li, X. L., Xiong, H., Li, X. L., et al. (2017). Tau-mediated iron export prevents ferroptotic damage after ischemic stroke. *Mol. Psychiatry* 22 (11), 1520–1530. doi:10.1038/mp.2017.171

Ursini, F., and Maiorino, M. (2020). Lipid peroxidation and ferroptosis: The role of GSH and GPx4. *Free Radic. Biol. Med.* 152, 175–185. doi:10.1016/j.freeradbiomed.2020.02.027

Varin, A., and Gordon, S. (2009). Alternative activation of macrophages: Immune function and cellular biology. *Immunobiology* 214 (7), 630–641. doi:10.1016/j.imbio.2008.11.009

Verrey, F., Closs, E. I., Wagner, C. A., Palacin, M., Endou, H., and Kanai, Y. (2004). CATs and HATs: The SLC7 family of amino acid transporters. *Pflugers Arch.* 447 (5), 532–542. doi:10.1007/s00424-003-1086-z

Vespa, P., Prins, M., Ronne-Engstrom, E., CaronM.Shalmon, E., Hovda, D. A., et al. (1998). Increase in extracellular glutamate caused by reduced cerebral perfusion pressure and seizures after human traumatic brain injury: A microdialysis study. *J. Neurosurg.* 89 (6), 971–982. doi:10.3171/jns.1998.89.6.0971

Villalpando-Rodriguez, G. E., and Gibson, S. B. (2021). Reactive oxygen species (ROS) regulates different types of cell death by acting as a rheostat. *Oxid. Med. Cell. Longev.* 2021, 9912436. doi:10.1155/2021/9912436

Waldvogel-Abramowski, S., Waeber, G., Gassner, C., Buser, A., Frey, B. M., Favrat, B., et al. (2014). Physiology of iron metabolism. *Transfus. Med. Hemother.* 41 (3), 213–221. doi:10.1159/000362888

Wang, Y., Dai, S. D., Qi, F. J., Xu, H. T., and Wang, E. H. (2008). p53 protein expression and genetic mutation in two primary cell types in pulmonary sclerosing haemangioma. *J. Clin. Pathol.* 61 (2), 192–196. doi:10.1136/jcp.2007.050401

Wang, H., Zhou, W., Zheng, Z., Zhang, P., Tu, B., He, Q., et al. (2012). The HDAC inhibitor depsipeptide transactivates the p53/p21 pathway by inducing DNA damage. *DNA Repair (Amst)* 11 (2), 146–156. doi:10.1016/j.dnarep.2011.10.014

Wang, J., Sun, Z., Shen, J., Wu, D., Liu, F., Yang, R., et al. (2015). Octreotide protects the mouse retina against ischemic reperfusion injury through regulation of antioxidation and activation of NF-κB. *Oxid. Med. Cell. Longev.* 2015, 970156. doi:10.1155/2015/970156

Wang, Z., Guo, L. M., Wang, Y., Zhou, H. K., Wang, S. C., Chen, D., et al. (2018). Inhibition of HSP90α protects cultured neurons from oxygen-glucose deprivation induced necroptosis by decreasing RIP3 expression. *J. Cell. Physiol.* 233 (6), 4864–4884. doi:10.1002/jcp.26294

Wang, Y., Yang, L., Zhang, X., Cui, W., Liu, Y., Sun, Q. R., et al. (2019). Epigenetic regulation of ferroptosis by H2B monoubiquitination and p53. *EMBO Rep.* 20 (7), e47563. doi:10.15252/embr.201847563

Wang, H., Lin, D., Yu, Q., Li, Z., Lenahan, C., Dong, Y., et al. (2021). A promising future of ferroptosis in tumor therapy. *Front. Cell Dev. Biol.* 9, 629150. doi:10.3389/fcell.2021.629150

Wang, L., Xiong, X., Zhang, L., and Shen, J. (2021). Neurovascular unit: A critical role in ischemic stroke. *CNS Neurosci. Ther.* 27 (1), 7–16. doi:10.1111/cns.13561

Ward, R. J., Zucca, F. A., Duyn, J. H., Crichton, R. R., and Zecca, L. (2014). The role of iron in brain ageing and neurodegenerative disorders. *Lancet. Neurol.* 13 (10), 1045–1060. doi:10.1016/S1474-4422(14)70117-6

Watanabe, K., Tanaka, M., Yuki, S., Hirai, M., and Yamamoto, Y. (2018). How is edaravone effective against acute ischemic stroke and amyotrophic lateral sclerosis? *J. Clin. Biochem. Nutr.* 62 (1), 20–38. doi:10.3164/jcbn.17-62

Wei, S., Qiu, T., Wang, N., Yao, X., Jiang, L., Jia, X., et al. (2020). Ferroptosis mediated by the interaction between Mfn2 and IREα promotes arsenic-induced nonalcoholic steatohepatitis. *Environ. Res.* 188, 109824. doi:10.1016/j.envres.2020.109824

Willard, S. S., and Koochekpour, S. (2013). Glutamate, glutamate receptors, and downstream signaling pathways. *Int. J. Biol. Sci.* 9 (9), 948–959. doi:10.7150/ijbs.6426

Winkler, E. A., Bell, R. D., and Zlokovic, B. V. (2011). Central nervous system pericytes in health and disease. *Nat. Neurosci.* 14 (11), 1398–1405. doi:10.1038/nn.2946

Wu, J., Minikes, A. M., Gao, M., Bian, H., Li, Y., Stockwell, B. R., et al. (2019). Intercellular interaction dictates cancer cell ferroptosis via NF2-YAP signalling. *Nature* 572 (7769), 402–406. doi:10.1038/s41586-019-1426-6

Wu, Y., Zhang, S., Gong, X., Tam, S., Xiao, D., Liu, S., et al. (2020). The epigenetic regulators and metabolic changes in ferroptosis-associated cancer progression. *Mol. Cancer* 19 (1), 39. doi:10.1186/s12943-020-01157-x

Wynford-Thomas, D., and Blaydes, J. (1998). The influence of cell context on the selection pressure for p53 mutation in human cancer. *Carcinogenesis* 19 (1), 29–36. doi:10.1093/carcin/19.1.29

Xie, Z., Xu, M., Xie, J., Liu, T., Xu, X., Gao, W., et al. (2022). Inhibition of ferroptosis attenuates glutamate excitotoxicity and nuclear autophagy in a CLP septic mouse model. *Shock* 57 (5), 694–702. doi:10.1097/SHK.0000000000001893

Xu, Y., Liu, Y., Li, K., Yuan, D., Yang, S., Zhou, L., et al. (2022). COX-2/PGE2 pathway inhibits the ferroptosis induced by cerebral ischemia reperfusion. *Mol. Neurobiol.* 59 (3), 1619–1631. doi:10.1007/s12035-021-02706-1

Yang, W. S., Kim, K. J., Gaschler, M. M., Patel, M., Shchepinov, M. S., and Stockwell, B. R. (2016). Peroxidation of polyunsaturated fatty acids by lipoxygenases drives ferroptosis. *Proc. Natl. Acad. Sci. U. S. A.* 113 (34), E4966–E4975. doi:10.1073/pnas.1603244113

Yang, S., Jin, H., Zhu, Y., Wan, Y., Opoku, E. N., Zhu, L., et al. (2017). Diverse functions and mechanisms of pericytes in ischemic stroke. *Curr. Neuropharmacol.* 15 (6), 892–905. doi:10.2174/1570159X15666170112170226

Yang, Q., Huang, Q., Hu, Z., and Tang, X. (2019). Potential neuroprotective treatment of stroke: Targeting excitotoxicity, oxidative stress, and inflammation. *Front. Neurosci.* 13, 1036. doi:10.3389/fnins.2019.01036

Yang, Y., Luo, M., Zhang, K., Zhang, J., Gao, T., Connell, D. O., et al. (2020). Nedd4 ubiquitylates VDAC2/3 to suppress erastin-induced ferroptosis in melanoma. *Nat. Commun.* 11 (1), 433. doi:10.1038/s41467-020-14324-x

Yang, F., Wu, Z., Dai, D., Zhang, L., Zhang, X., Zhang, X., et al. (2021). The iron chelator deferoxamine decreases myeloma cell survival. *J. Int. Med. Res.* 49 (1), 300060520987396. doi:10.1177/0300060520987396

Ye, J., Sun, Z., and Hu, W. (2018). Roles of astrocytes in cerebral infarction and related therapeutic strategies. *Zhejiang Da Xue Xue Bao Yi Xue Ban.* 47 (5), 493–498. doi:10.3785/j.issn.1008-9292.2018.10.08

Yenari, M. A., Kauppinen, T. M., and Swanson, R. A. (2010). Microglial activation in stroke: Therapeutic targets. *Neurotherapeutics* 7 (4), 378–391. doi:10.1016/j.nurt.2010.07.005

Yin, H., Xu, L., and Porter, N. A. (2011). Free radical lipid peroxidation: Mechanisms and analysis. *Chem. Rev.* 111 (10), 5944–5972. doi:10.1021/cr200084z

Yu, S. S., Li, Z. Y., Xu, X. Z., Yao, F., Luo, Y., Liu, Y. C., et al. (2022). M1-type microglia can induce astrocytes to deposit chondroitin sulfate proteoglycan after spinal cord injury. *Neural Regen. Res.* 17 (5), 1072–1079. doi:10.4103/1673-5374.324858

Yuan, H., Li, X., Zhang, X., Kang, R., and Tang, D. (2016). Identification of ACSL4 as a biomarker and contributor of ferroptosis. *Biochem. Biophys. Res. Commun.* 478 (3), 1338–1343. doi:10.1016/j.bbrc.2016.08.124

Yuan, H., Li, X., Zhang, X., Kang, R., and Tang, D. (2016). CISD1 inhibits ferroptosis by protection against mitochondrial lipid peroxidation. *Biochem. Biophys. Res. Commun.* 478 (2), 838–844. doi:10.1016/j.bbrc.2016.08.034

Zhang, D. D., Lo, S. C., Cross, J. V., Templeton, D. J., and Hannink, M. (2004). Keap1 is a redox-regulated substrate adaptor protein for a Cul3-dependent ubiquitin ligase complex. *Mol. Cell. Biol.* 24 (24), 10941–10953. doi:10.1128/MCB.24.24.10941-10953.2004

Zhang, Z., Zhang, F., An, P., Guo, X., Shen, Y., Tao, Y., et al. (2011). Ferroportin1 deficiency in mouse macrophages impairs iron homeostasis and inflammatory responses. *Blood* 118 (7), 1912–1922. doi:10.1182/blood-2011-01-330324

Zhang, Z., Zhang, F., Guo, X., An, P., Tao, Y., and Wang, F. (2012). Ferroportin1 in hepatocytes and macrophages is required for the efficient mobilization of body iron stores in mice. *Hepatology* 56 (3), 961–971. doi:10.1002/hep.25746

Zhang, Y., Koppula, P., and Gan, B. (2019). Regulation of H2A ubiquitination and SLC7A11 expression by BAP1 and PRC1. *Cell Cycle* 18 (8), 773–783. doi:10.1080/15384101.2019.1597506

Zhang, C., Yan, L., Gu, Z., and Zhao, Y. (2019). Strategies based on metal-based nanoparticles for hypoxic-tumor radiotherapy. *Chem. Sci.* 10 (29), 6932–6943. doi:10.1039/c9sc02107h

Zhang, X., Wang, L., Li, H., Zhang, L., Zheng, X., and Cheng, W. (2020). Crosstalk between noncoding RNAs and ferroptosis: New dawn for overcoming cancer progression. *Cell Death Dis.* 11 (7), 580. doi:10.1038/s41419-020-02772-8

Zhang, X., Sui, S., Wang, L., Li, H., Zhang, L., Xu, S., et al. (2020). Inhibition of tumor propellant glutathione peroxidase 4 induces ferroptosis in cancer cells and enhances anticancer effect of cisplatin. *J. Cell. Physiol.* 235 (4), 3425–3437. doi:10.1002/jcp.29232

Zhang, W., Liu, Y., and Zhang, H. (2021). Extracellular matrix: An important regulator of cell functions and skeletal muscle development. *Cell Biosci.* 11 (1), 65. doi:10.1186/s13578-021-00579-4

Zhang, Y., Lu, X., Tai, B., Li, W., and Li, T. (2021). Ferroptosis and its multifaceted roles in cerebral stroke. *Front. Cell. Neurosci.* 15, 615372. doi:10.3389/fncel.2021.615372

Zhang, X., Yu, K., Ma, L., Qian, Z., Tian, X., Miao, Y., et al. (2021). Endogenous glutamate determines ferroptosis sensitivity via ADCY10-dependent YAP suppression in lung adenocarcinoma. *Theranostics* 11 (12), 5650–5674. doi:10.7150/thno.55482

Zhang, H. L., Hu, B. X., Li, Z. L., Du, T., Shan, J. L., Ye, Z. P., et al. (2022). PKCβII phosphorylates ACSL4 to amplify lipid peroxidation to induce ferroptosis. *Nat. Cell Biol.* 24 (1), 88–98. doi:10.1038/s41556-021-00818-3

Zhao, Y., Yang, J., Li, C., Zhou, G., Wan, H., Ding, Z., et al. (2020). Role of the neurovascular unit in the process of cerebral ischemic injury. *Pharmacol. Res.* 160, 105103. doi:10.1016/j.phrs.2020.105103

Zhao, Y., Li, Y., Zhang, R., Wang, F., Wang, T., and Jiao, Y. (2020). The role of erastin in ferroptosis and its prospects in cancer therapy. *Onco. Targets. Ther.* 13, 5429–5441. doi:10.2147/OTT.S254995

Zhao, Q., Ge, Z., Fu, S., Wan, S., Shi, J., Wu, Y., et al. (2022). DNA methylation plays an important role in iron-overloaded Tibetans. *Genes Genet. Syst.* 97 (2), 55–66. doi:10.1266/ggs.21-00006

Zhou, S., Du, X., Xie, J., and Wang, J. (2017). Interleukin-6 regulates iron-related proteins through c-Jun N-terminal kinase activation in BV2 microglial cell lines. *PLoS One* 12 (7), e0180464. doi:10.1371/journal.pone.0180464

Zhou, S., Gao, B., Sun, C., Bai, Y., Cheng, D., Zhang, Y., et al. (2020). Vascular endothelial cell-derived exosomes protect neural stem cells against ischemia/reperfusion injury. *Neuroscience* 441, 184–196. doi:10.1016/j.neuroscience.2020.05.046

Zhou, Y., Liao, J., Mei, Z., Liu, X., and Ge, J. (2021). Insight into crosstalk between ferroptosis and necroptosis: Novel therapeutics in ischemic stroke. *Oxid. Med. Cell. Longev.* 2021, 9991001. doi:10.1155/2021/9991001

Zhou, S. Y., Guo, Z. N., Zhang, D. H., Qu, Y., and Jin, H. (2022). The role of pericytes in ischemic stroke: Fom cellular functions to therapeutic targets. *Front. Mol. Neurosci.* 15, 866700. doi:10.3389/fnmol.2022.866700

Zhou, Y., and Danbolt, N. C. (2014). Glutamate as a neurotransmitter in the healthy brain. *J. Neural Transm.* 121 (8), 799–817. doi:10.1007/s00702-014-1180-8

Zhu, H., Itoh, K., Yamamoto, M., Zweier, J. L., and Li, Y. (2005). Role of Nrf2 signaling in regulation of antioxidants and phase 2 enzymes in cardiac fibroblasts: Protection against reactive oxygen and nitrogen species-induced cell injury. *FEBS Lett.* 579 (14), 3029–3036. doi:10.1016/j.febslet.2005.04.058

Zhu, S., Zhang, Q., Sun, X., Zeh, H. J., Lotze, M. T., Kang, R., et al. (2017). HSPA5 regulates ferroptotic cell death in cancer cells. *Cancer Res.* 77 (8), 2064–2077. doi:10.1158/0008-5472.CAN-16-1979

Zhu, T., Shi, L., Yu, C., Dong, Y., Qiu, F., Shen, L., et al. (2019). Ferroptosis promotes photodynamic therapy: Supramolecular photosensitizer-inducer nanodrug for enhanced cancer treatment. *Theranostics* 9 (11), 3293–3307. doi:10.7150/thno.32867

frontiers | Frontiers in Pharmacology

TYPE Original Research
PUBLISHED 21 December 2022
DOI 10.3389/fphar.2022.1076960

OPEN ACCESS

EDITED BY
Yi Wang,
Zhejiang University, China

REVIEWED BY
Hecheng Wang,
Dalian University of Technology, China
Raúl González-Domínguez,
Universidad de Cádiz, Spain

*CORRESPONDENCE
Li-Hua Zuo,
zuolihua2013@126.com

SPECIALTY SECTION
This article was submitted to Neuropharmacology, a section of the journal Frontiers in Pharmacology

RECEIVED 22 October 2022
ACCEPTED 12 December 2022
PUBLISHED 21 December 2022

CITATION
Liu L-W, Yue H-Y, Zou J, Tang M, Zou F-M, Li Z-L, Jia Q-Q, Li Y-B, Kang J and Zuo L-H (2022), Comprehensive metabolomics and lipidomics profiling uncovering neuroprotective effects of *Ginkgo biloba* L. leaf extract on Alzheimer's disease.
Front. Pharmacol. 13:1076960.
doi: 10.3389/fphar.2022.1076960

Comprehensive metabolomics and lipidomics profiling uncovering neuroprotective effects of *Ginkgo biloba* L. leaf extract on Alzheimer's disease

Li-Wei Liu[1,2,3], He-Ying Yue[1,2,3], Jing Zou[1,2,3], Meng Tang[4], Fan-Mei Zou[1,2,3], Zhuo-Lun Li[1,2,3], Qing-Quan Jia[1,2,3], Yu-Bo Li[5], Jian Kang[1,2,3] and Li-Hua Zuo[1,2,3]*

[1]Department of Pharmacy, the First Affiliated Hospital of Zhengzhou University, Zhengzhou, Henan Province, China, [2]Henan Key Laboratory of Precision Clinical Pharmacy, Zhengzhou, Henan Province, China, [3]Henan Engineering Research Center of Clinical Mass Spectrometry for Precision Medicine, Zhengzhou, Henan Province, China, [4]The First Department of Orthopaedics, Zhengzhou Central Hospital Affiliated to Zhengzhou University, Zhengzhou, Henan Province, China, [5]Tianjin University of Traditional Chinese Medicine, Tianjin, China

Introduction: *Ginkgo biloba* L. leaf extract (GBLE) has been reported to be effective for alleviating cognitive and memory impairment in Alzheimer's disease (AD). Nevertheless, the potential mechanism remains unclear. Herein, this study aimed to explore the neuroprotective effects of GBLE on AD and elaborate the underlying therapeutic mechanism.

Methods: Donepezil, the most widely prescribed drug for AD, was used as a positive control. An integrated metabolomics and lipidomics approach was adopted to characterize plasma metabolic phenotype of APP/PS1 double transgenic mice and describe the metabolomic and lipidomic fingerprint changes after GBLE intervention. The Morris water maze test and immunohistochemistry were applied to evaluate the efficacy of GBLE.

Results: As a result, administration of GBLE significantly improved the cognitive function and alleviated amyloid beta (Aβ) deposition in APP/PS1 mice, showing similar effects to donepezil. Significant alterations were observed in metabolic signatures of APP/PS1 mice compared with wild type (WT) mice by metabolomic analysis. A total of 60 markedly altered differential metabolites were identified, including 28 lipid and lipid-like molecules, 13 organic acids and derivatives, 11 organic nitrogen compounds, and 8 other compounds, indicative of significant changes in lipid metabolism of AD. Further lipidomic profiling showed that the differential expressed lipid metabolites between APP/PS1 and WT mice mainly consisted of phosphatidylcholines, lysophosphatidylcholines, triglycerides, and ceramides. Taking together all the data, the plasma metabolic signature of APP/PS1 mice was primarily characterized by disrupted sphingolipid metabolism, glycerophospholipid metabolism, glycerolipid metabolism, and amino acid metabolism. Most of the disordered metabolites were ameliorated after GBLE treatment, 19 metabolites and 24 lipids of which were significantly reversely regulated (adjusted-p<0.05), which were

considered as potential therapeutic targets of GBLE on AD. The response of APP/PS1 mice to GBLE was similar to that of donepezil, which significantly reversed the levels of 23 disturbed metabolites and 30 lipids.

Discussion: Our data suggested that lipid metabolism was dramatically perturbed in the plasma of APP/PS1 mice, and GBLE might exert its neuroprotective effects by restoring lipid metabolic balance. This work provided a basis for better understanding the potential pathogenesis of AD and shed new light on the therapeutic mechanism of GBLE in the treatment of AD.

KEYWORDS

Ginkgo biloba **L. leaf extract, Alzheimer's disease, metabolomics, lipidomics, neuroprotective effects**

1 Introduction

Alzheimer's disease (AD) is the dominant type of dementia and manifests a progressive decline in memory and cognitive function in parallel with behavioral disorders (Knopman et al., 2021). It is characterized by classical pathophysiological hallmarks of extracellular accumulating beta-amyloid (Aβ) and intraneuronal tau-laden neurofibrillary tangles (Breijyeh and Karaman, 2020). As the fifth leading cause of death in the elderly, AD has become one of the most important public health issues (GBD 2016 Dementia Collaborators, 2019). At present, there are approximately 50 million AD cases worldwide and this number is projected to triple by 2050 with the growth of geriatric population (Scheltens et al., 2021), causing enormous burden for the public health system in the world (Wong, 2020). However, there are no cures for this disease up till now. Therefore, it is urgent and significant to decode the mechanisms of AD and discover new strategies for AD therapy. Traditional Chinese medicine (TCM), with characteristics of multi-components and multi-targets, has been applied in clinical practice for thousands of years. It has attracted increasing attention for the treatment of AD, due to the comparable efficacy and fewer side effects than conventional drugs (Sun et al., 2013). Some novel natural compounds isolated from herbs have shown neuroprotective effects and are regarded as potential anti-AD drugs (Andrade et al., 2019; Suresh et al., 2022).

As one of the most universal herbal supplements, *Ginkgo biloba* L. and its different preparations have been utilized to treat neurological and cardiovascular disorders for millennia with good effectiveness on blood stasis and chest stuffiness (Tabassum et al., 2022). It is considered to possess the efficacies of promoting blood circulation to remove blood stasis and obstacles in the channels, increasing cerebral bloodflow, and protecting nerve cells (Li et al., 2018). A standard *Ginkgo biloba* L. leaf extract (GBLE), EGb761, demonstrated significant symptomatic improvement in cognitive function and behavior in patients with mild-to-moderate dementia, and was listed in local clinical guidelines in Switzerland, Germany, and some Asian countries (Savaskan et al., 2018). Promising chemical components identified in GBLE mainly include flavonoids, terpenoids, biflavonoids, and organic acids, exhibiting a variety of pharmacological activities, such as preventing oxidative stress, increasing cerebral blood flow, protecting Aβ toxicity, affecting neurotransmission and neuroplasticity (Tabassum et al., 2022). Accumulating clinical evidence has shown the therapeutic effects of GBLE on behavioral and psychological symptoms in AD patients (Nowak et al., 2021). Despite definite efficacy of GBLE, the underlying mechanism remains enigmatic, especially its effects on metabolic alterations of AD.

Evidences have suggested that metabolic dysregulation plays an important role in the pathophysiology of AD (Poddar et al., 2021). The lipid-related abnormalities were observed in the initial report of neuropathology (Alzheimer et al., 1995), and the lipid dyshomeostasis became a focus of AD research until recent decades. Both animal and clinical studies demonstrated that disrupted lipid metabolism was closely related to the pathogenesis and progression of AD (Touboul and Gaudin, 2014; Peña-Bautista et al., 2022). However, the impact of GBEL on plasma metabolome and lipidome in AD has not been investigated. Comprehensive metabolomic analysis can holistically detect the endogenous metabolic changes in biological systems, providing a powerful approach for understanding mechanism of disease and its response to TCM. Lipidomics, an important branch of metabolomics, focuses on identifying and characterizing lipid classes, subclasses and molecular species. An integration of metabolomics with lipidomics offers a global atlas of the metabolic landscape, which is becoming an emerging tool to evaluate therapeutic effects and reveal potential mechanism of TCM.

Herein, an ultra-high-performance liquid chromatography-mass spectrometry- (UHPLC-MS-) based metabolomic and lipidomic profiling analysis was performed in the plasma of wild-type and amyloid precursor protein (APP)/presenilin-1

(PS1) double-transgenic mice, a prominent mouse model of AD. It is the first exploratory investigation on the plasma metabolome and lipidome of APP/PS1 mice treated with GBLE. This study may provide a novel insight into the neuroprotective effects of GBLE and the potential mechanisms of ameliorating AD pathology, which are significant for improving clinical outcome and development of new drugs from *Ginkgo biloba* L. for AD.

2 Materials and methods

2.1 Materials and chemicals

The standardized GBLE drops (Ginaton®) were manufactured by Dr. Willmar Schwabe GmbH & Co KG (Karlsruhe, Germany, batch number: 0190321), containing 40 mg/ml of a standardized dry extract of Ginkgo biloba (EGb 761®). The ginkgo flavone glycosides account for 24% of the exact and terpenelactones for 6%. The chemical profiling of GBLE was analyzed using ultra-high performance liquid chromatography coupled with a Q Exactive hybrid quadrupole-orbitrap high resolution mass spectrometry (UHPLC-Q-Orbitrap HRMS, Thermo Fisher Scientific, San Jose, CA, United States). The chromatographic separation was performed on an ACQUITY UPLC BEH C18 column (100 mm × 2.1 mm, 1.7 μm, Waters, United States) maintained at 40°C with a flow rate of 0.20 ml/min. The mobile phase consisted of solvent A (ultra-pure water containing 0.1% formic acid) and solvent B (acetonitrile). The gradient elution was as follows: 5% B at 0–4 min, 5%–10% B at 4–15 min, 10%–20% B at 15–30 min, 20%–40% B at 30–45 min, 40%–100% B at 45–51 min, 100% B at 51–56 min, 100%–5% B at 56–56.2 min, 5% B at 56.2–60 min. The injection volume was set to 5 μl.

A total of 21 chemical constituents in GBLE were purchased from Chengdu Must Bio-technology Co., Ltd. (Sichuan, China), with the purities ≥98%. The endogenous metabolite standards were offered by Sigma-Aldrich (St Louis, MO, United States) and J&K Scientific Ltd. (Beijing, China). Rabbit anti-Aβ anti-body was purchased from Wuhan Servicebio Technology CO, LTD. (GB111197, Wuhan, China). HPLC-grade acetonitrile, methanol and isopropanol were obtained from Fisher Scientific (Fair Lawn, NJ, United States). Donepezil hydrochloride and methyl *tert*-butyl ether (MTBE) were bought from J&K Scientific Ltd. (Beijing, China). Formic acid of chromatographic grade was supplied by Aladdin Industrial Co., Ltd. (Shanghai, China). Ammonium formate was purchased from Sigma-Aldrich (St Louis, MO, United States). Deionized water was prepared by the Milli-Q water purification system (Millipore, Shanghai, China). Other chemicals and reagents were all of analytical purity.

2.2 Animals and experimental design

The six-month-old male APP/PS1 double transgenic mice (B6C3-Tg) and wild type (WT) littermates were purchased from Huachuang Sino Pharmaceutical Technology Co., LTD. (Jiangsu, China). After 7 days of acclimation, the APP/PS1 mice were randomly divided into APP/PS1 group (n = 10), APP/PS1+Donepezil group (n = 10), and APP/PS1+GBLE group (n = 10). The littermate wild-type mice were served as WT group (n = 10). Mice in the APP/PS1+GBLE group were given GBLE by gavage at a dose of 50 mg/kg (10 mg/ml) daily for 90 consecutive days. The dosage was determined based on the dose conversion coefficient between mouse and human in line with previous studies (Yu et al., 2021). Mice in the APP/PS1+ Donepezil group were given donepezil orally (1 mg/kg/day) for 90 days. Mice in the APP/PS1 group and WT group were intragastrically administrated with saline solution (5 ml/kg/day) for 90 days. Design of animal experiment was shown in Supplementary Figure S1. All animal studies were conducted in accordance with the National Institutes of Health Guidelines for the Care and Use of Laboratory Animals, and the experiments were approved by the Animal Ethics Committee of Zhengzhou University (ZZU-LAC20220225[13]).

2.3 Morris water maze test

The Morris water maze (MWM) test is one of the most common behavioral tests to assess spatial learning and memory abilities of mice. At the last week of administration in this study, the MWM test was carried out in a circular tank (diameter, 120 cm; height, 40 cm) filled with opaque water, and a hidden platform (diameter, 12 cm) was placed about 1 cm below the water surface (Figure 1A). The procedures were conducted according to previous studies with minor modifications (Yi et al., 2020).

Overall, this experiment lasted for 6 days, including place navigation test and spatial probe test (Figure 1B). In the place navigation test, mice were subjected to a spatial acquisition experiment to evaluate their spatial learning ability during a 5-day training period, and each mouse was trained to find the hidden platform twice a day with a 1-h interval. Subsequent spatial probe test was performed on the sixth day to assess spatial memory retention ability of mice, during which the mice were released into water to swim freely for 60 s after removing the submerged platform. The following data were recorded: 1) Escape latency, defined as the time for the mice to find the hidden platform area for the first time; 2) The number of crossing over the original position of platform; 3) The distance and time spent in the target quadrant for the mice. SANS video tracking system (SA201, Jiangsu, China) was applied to record and analyze the experimental data.

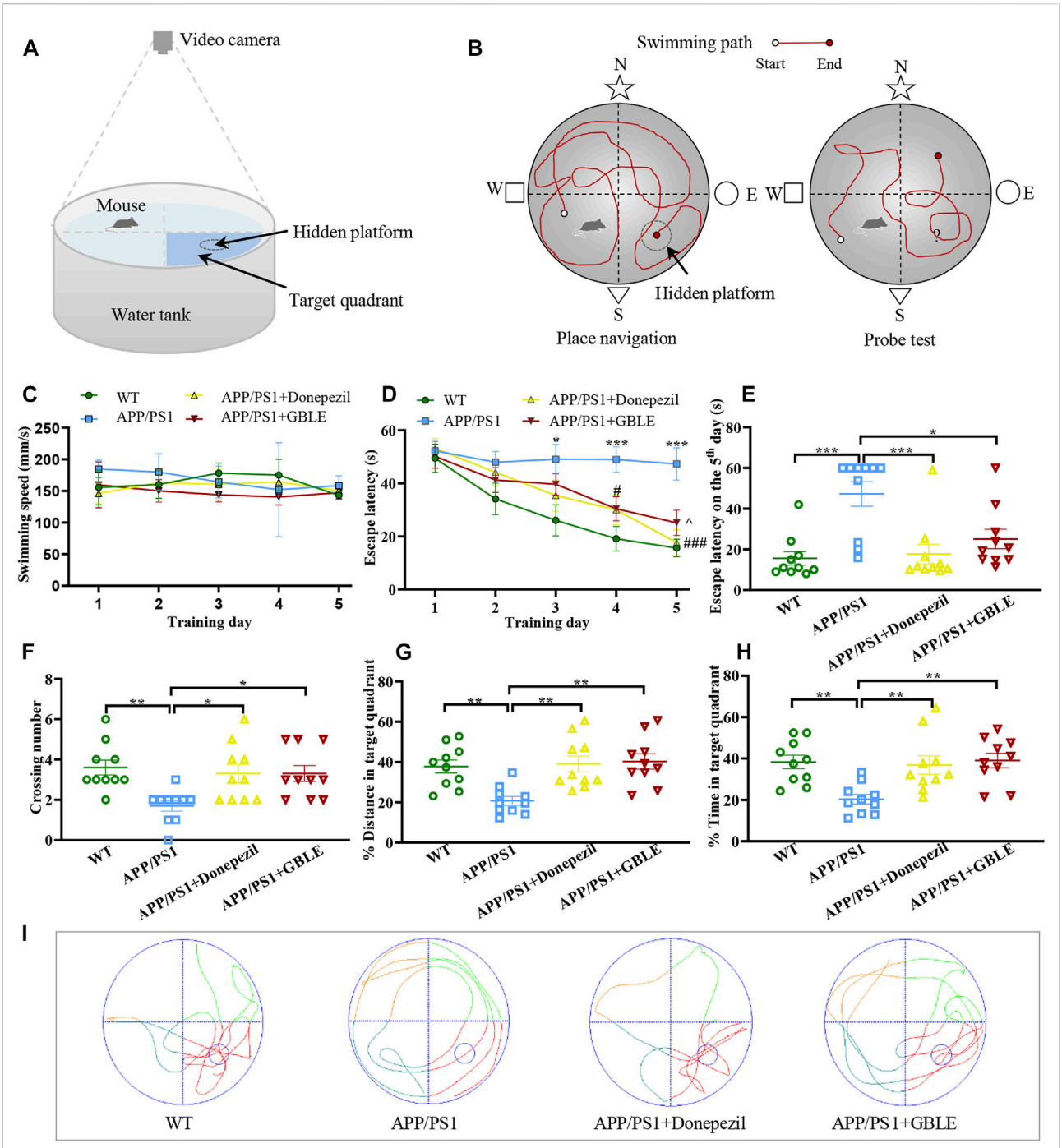

FIGURE 1
The performance of mice in Morris water maze (MWM) test. **(A)** Schematic diagram of MWM equipment. **(B)** Illustration of place navigation test and probe test in MWM. **(C)** The swimming speeds of mice in different groups during five consecutive training days. **(D)** The escape latencies of mice in different groups during five consecutive training days. *: $p < 0.05$, ***: $p < 0.001$ for APP/PS1 group *versus* WT group; $^{\#}$: $p < 0.05$, $^{\#\#\#}$: $p < 0.001$ for APP/PS1+Donepezil group *versus* APP/PS1 group; $^{\wedge}$ $p < 0.05$ for APP/PS1+GBLE group *versus* APP/PS1 group. **(E)** The escape latencies of mice in different groups on the 5th day. **(F)** The average crossing number over the platform during the probe test. **(G)** The percentage of distance in target quadrant during the probe test. **(H)** The percentage of time spent in target quadrant during the probe test. Data were presented as mean ± SEM. *: $p < 0.05$, **: $p < 0.01$, ***: $p < 0.001$. **(I)** Representative swimming paths of mice in the four groups during the probe trial.

2.4 Sample collection

Two days after the MWM test, the blood samples were collected in anti-coagulation tubes by cardiac puncture and mice were sacrificed by cervical dislocation. After centrifuging at 3000 rpm at 4°C for 10 min, the supernatant plasma was transferred and stored at −80°C until metabolomic and lipidomic analysis. The brain was dissected from skull and immerged in 4% paraformaldehyde (PFA) for further immunohistochemistry assays.

2.5 Immunohistochemistry

The brain tissue samples were embedded in paraffin blocks, and then sectionalized at a thickness of 5 μm. The paraffin sections were deparaffinized in xylene and rehydrated in gradient ethanol. Antigen retrieval was achieved by immersing the sections in a repair box filled with citric acid buffer (PH 6.0) in a microwave oven. Subsequently, sections were sealed with 3% H_2O_2 to block the activity of endogenous peroxidase. The brain sections were then incubated with rabbit anti-beta-amyloid antibody diluted at 1:500 at 4 °C overnight. After washing with PBS (PH 7.4) three times for 5 min each, sections were incubated with goat anti-rabbit IgG (1:200, HRP labeled) for 50 min at room temperature. DAB color developing solution was added to the sections, and the positive showed brownish yellow. Sections were then counterstained with hematoxylin. The Images and representative photos were acquired under a microscope.

2.6 Untargeted metabolomic experiments

2.6.1 Sample preparation

Sample preparation and data acquisition were performed according to previously published work (Liu et al., 2020). Analytes were extracted from plasma by protein precipitation with methanol for metabolomics studies. Ketoprofen and 2-chloro-L-phenylalanine were used as internal standards for the ESI^- and ESI^+ modes respectively on the basis of literature (Huang et al., 2019). A 150 μL aliquot of ice-cold methanol containing 500 ng/ml ketoprofen and 50 ng/ml 2-chloro-L-phenylalanine was added to 50 μL plasma. After being vortexed for 60 s, the mixture was centrifuged at 13,000 rpm for 10 min at 4 °C. Subsequently, the supernatant was carefully transferred to a sample vial for further UHPLC-Q-Orbitrap HRMS analysis. To evaluate the robustness of analytical platform, pooled quality control (QC) sample was prepared by mixing an equal volume of each plasma sample.

2.6.2 LC-MS/MS analysis

Untargeted metabolomics analysis was performed on Thermo Scientific UltiMate 3000 UHPLC system coupled to a Q-Exactive Hybrid Quadrupole-Orbitrap high resolution mass spectrometer (Thermo Scientific, San Jose, United States) equipped with a heated electrospray ionization source operating in both positive and negative ion modes as previously described (Liu et al., 2020). Chromatographic separation was achieved on a Waters ACQUITY UPLC HSS T3 column (2.1 × 100 mm, 1.8 μm), while the column oven temperature was maintained at 40 °C. The ultra-pure water containing 0.1% (v/v) formic acid (A) and acetonitrile (B) were used as mobile phase and eluted at a flow rate of 0.3 ml/min. The gradient elution was set as follows: 0–1 min, 5% B; 1–9 min, 5%–100% B; 9–12 min, 100% B; 12–12.1 min, 100%–5% B; 12.1–15 min, 5% B, and the injection volume was 5 μl. The optimized MS parameters were: ion spray voltage, 3.5 kV (+) and 2.8 kV (−); capillary temperature, 320 °C; ion source temperature, 350°C; sheath gas flow rate, 40 arb (+) and 38 arb (−); auxiliary gas flow rate, 10 arb; collision energy, 20, 40, and 60 eV. The resolution was 70,000 for full MS scan and 17,500 for dd-MS2 scan, and the scan range was performed at 80–1,200 m/z, both in positive and negative ion modes. The samples were injected in random order, and a QC sample was analyzed every five sample runs in the analytical batch. All the raw data were acquired and processed using Thermo Xcalibur 3.0 software (Thermo Scientific, San Jose, United States).

2.7 Lipidomic experiments

2.7.1 Sample preparation

The preparation of plasma samples followed the previous publications with minor modification (Matyash et al., 2008; Chen et al., 2021). In general, aliquots of 50 μl plasma samples were pipetted into 2 ml Eppendorf tubes. A total of 300 μl pre-chilled methanol was added to each sample and vortexed for 1 min. Then, 1 ml of MTBE was added and the mixture was incubated in a shaker at room temperature for 60 min to extract the lipids. Phase separation was induced by adding 250 μl of distilled water to the mixture, followed by votexing for 30 s. After storing at room temperature for 10 min, the mixture was centrifuged at 13,000 rpm for 10 min at 4°C. Subsequently, 2 × 400 μl of the upper phase were transferred into two Eppendorf tubes respectively and dried in a vacuum centrifuge. Finally, the residues were reconstituted with 70 μl of isopropanol/acetonitrile (9:1, v/v) for LC-MS/MS analysis.

2.7.2 LC-MS/MS analysis

Lipidomic analysis was also performed on Thermo Scientific UltiMate 3000 UHPLC system coupled to Q-Exactive Hybrid Quadrupole-Orbitrap high resolution mass spectrometer (Thermo Scientific, San Jose, United States). The lipid compounds separation was achieved on an ACQUITY UPLC® CSH C18 column (1.7 mm × 100 mm, 1.8 μm) maitained at 40°C with a flow rate of 0.3 ml/min. The mobile phase consisted of

water/acetonitrile (4:6, v/v) for solvent A and isopropanol/acetonitrile (9:1, v/v) for solvent B, with both A and B containing 10 mM ammonium formate. Analysis was carried out under gradient elution condition as follows: 0–2 min, 30%B; 2–25 min, 30%–100% B; 25–30 min, 100% B. The injection volume of each sample was 5 μl. Data was acquired using full MS/dd-MS2 approach in positive and negative ion modes, respectively. The MS parameters were the same as that of metabolomic analyses. The QC sample process identical to that of metabolomic experiment was also performed in the lipidomic analysis.

2.8 Data processing and statistical analysis

For the animal experiments, data was analyzed by SPSS 22.0 software (IBM Corp, Armonk, NY, United States) and GraphPad Prism 9.4.1 software (GraphPad Software Inc, San Diego, United States). Student's t-test was used for comparisons between two groups, whereas one-way ANOVA was conducted for comparisons among groups. The data are presented as means ± standard error of the mean (SEM). A p-value less than 0.05 was considered statistically significant.

For the metabolomic analysis, LC-MS/MS raw data was preprocessed using Compound Discoverer (CD) 3.3 software (Thermo Fisher Scientific, San Jose, CA, United States). The workflow incorporated several defined steps, such as noise filtering, peak detection, retention time (RT) alignment, and feature annotation. The spectra were selected from raw data and then aligned with mass error of 5 ppm and RT tolerance of 0.2 min. QC samples were used for compound annotation based on fragment matching with public databases as well as additional RT against our in-house library. The mzCloud and mzVault databases were applied for compound annotation on MS/MS level with a mass tolerance of 10 ppm. ChemSpider, Human Metabolome Database (HMDB), Kyoto Encyclopedia of Genes and Genomes (KEGG), and MassList (CD internal database for endogenous metabolites) were used to annotate features based on exact mass with a mass tolerance of 5 ppm. Compound peak areas were normalized to the constant sum using embedded function before statistical analysis (Hao et al., 2018).

A data matrix including retention time (t_R), mass-to-charge ratio (m/z) values, and peak area was generated from CD3.3 software, and the 80% rule was employed to handle missing values in the dataset. Then, the resulting three-dimensional matrix was imported into SIMICA software (version 14.1, Umetrics, Sweden) for multivariate statistical analysis, including principal component analysis (PCA) and orthogonal partial least-squares discriminant analysis (OPLS-DA). Each metabolite variable was scaled to unit variance prior to performing PCA and OPLS-DA. PCA was conducted to evaluate the overall distribution of data, evaluate reproducibility and stability of QC samples, and explore outliers. OPLS-DA was applied to screen differential features between comparable groups, and model validity was assessed by permutation test (200 permutations). Benjamini–Hochberg false discovery rate (FDR) procedure was employed for the multiple test adjustments, and adjusted-p values <0.05 were considered statistically significant. The differential features were selected with variable importance in the projection (VIP) value >1.0 and adjusted-p value <0.05. Differential metabolites were identified by searching ChemSpider, HMDB, KEGG, MassList, mzCloud, mzVault, as well as in-house-built spectral libraries based on the accurate mass, MS/MS fragments, and isotope pattern matching, and further confirmed using available reference standards.

For the lipidomic analysis, acquired MS/MS data were processed using Thermo Scientific LipidSearch 4.2 software for peak detection, lipid annotation, peak alignment, and relative quantitation (Bhawal et al., 2021). The main parameters were set as follows: precursor tolerance, 5 ppm; product tolerance, 5 ppm; intensity threshold for product ion, 5.0%. The search results from individual files were aligned using a 0.25 min tolerance window and the data merged for each annotated lipid. Subsequently, the data obtained from LipidSearch software were subjected to multivariate statistical analysis including PCA and OPLS-DA using SIMICA 14.1 software. The FDR-adjusted p values and fold change (FC) values were calculated according to peak areas. The differential lipids were selected based on the following criteria: VIP value >1.0 and adjusted-p value <0.05.

After that, the significantly altered metabolites and lipids were imported into MetaboAnalyst 5.0 software (https://www.metaboanalyst.ca/) for further analyses. Hierarchical clustering heatmaps were generated using ward's cluster method and Euclidean distance type. Pearson correlation analyses were performed to measure the strength of associations between metabolites. The altered metabolic pathways were determined by "Pathway Analysis" module based on the *Mus musculus* KEGG pathway library, and the results from pathway enrichment analysis were combined with pathway topology analysis. Finally, a global perturbed pathway network formed with differential metabolites and lipids was depicted to reflect the overall metabolic disturbance in APP/PS1 mice and the effects of GBLE.

3 Results

3.1 Chemical composition of GBLE

The total ion chromatograms (TIC) of GBLE in positive ion mode and negative ion mode were shown in

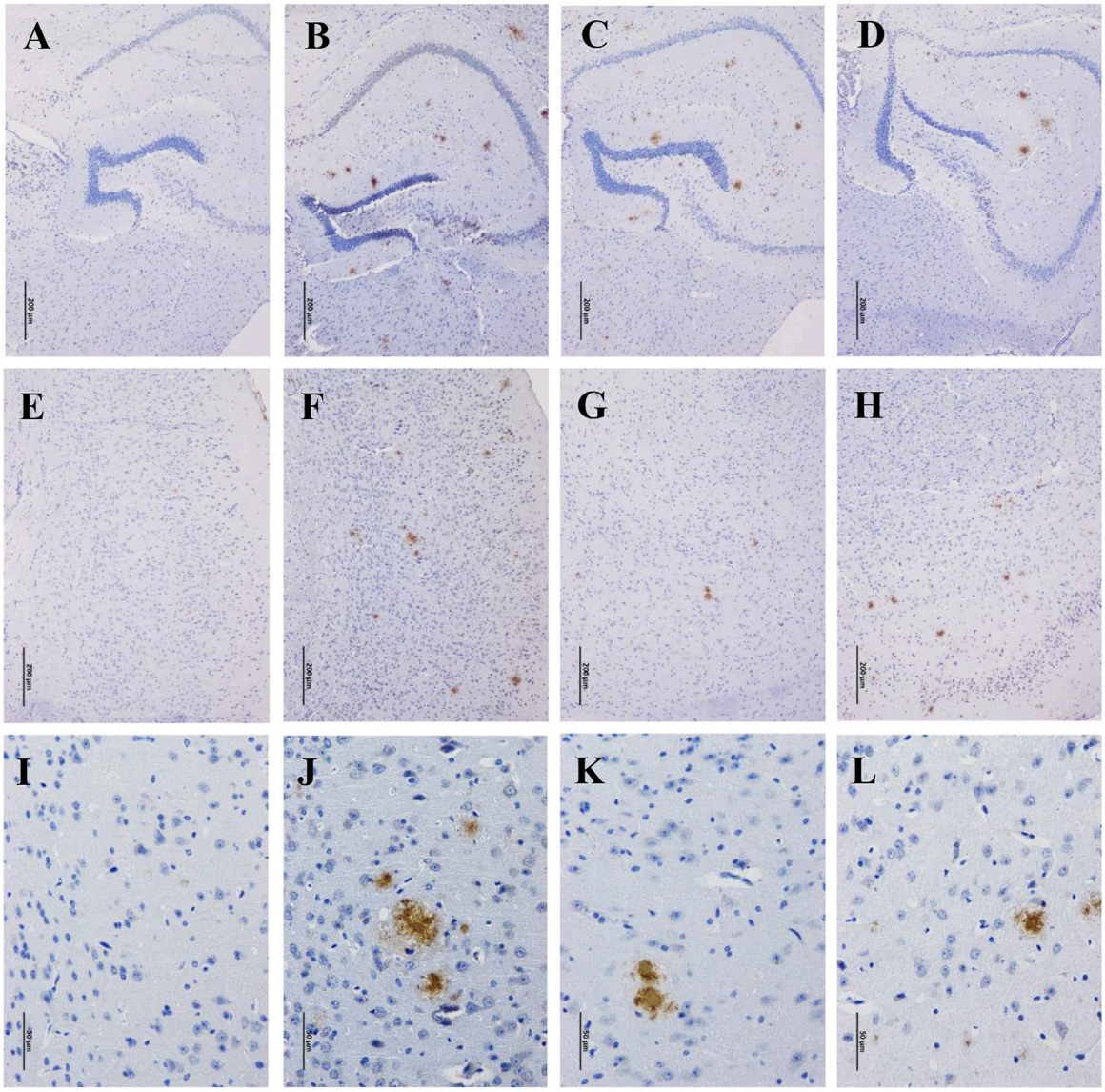

FIGURE 2
Effects of GBLE on the expression of β-amyloid in hippocampus and cortex by immunohistochemistry. **(A–D)** Immunohistochemical staining of β-amyloid plaques in hippocampus (100×) of WT, APP/PS1, APP/PS1+ Donepezil, and APP/PS1+GBLE groups, respectively. **(E–H)** Immunohistochemical staining of β-amyloid plaques in cortex (100×) for each group. **(I–L)** Immunohistochemical staining of β-amyloid plaques in cortex (400×) for each group.

Supplementary Figure S2. A total of 81 components were identified, including 54 flavonoids and their glycosides, 13 terpenoids, 10 carboxylic acids, and 4 other compounds, 21 compounds of which were confirmed by comparison with reference standards. The chemical information of these constituents was described in Supplementary Table S1. The results showed that flavonoids and terpenoids are the main compositions in GBLE, and these components exhibited higher response in negative ion mode.

3.2 Effects of GBLE on the cognitive behavior and brain pathology of APP/PS1 mice

3.2.1 GBLE ameliorates learning and memory impairments in APP/PS1 mice

MWM test was conducted to evaluate the neuroprotective effect of GBLE on the learning and memory deficits in APP/PS1 mice. There was no significant difference in swimming speed among all groups (Figure 1C). As shown in Figure 1D, gradually

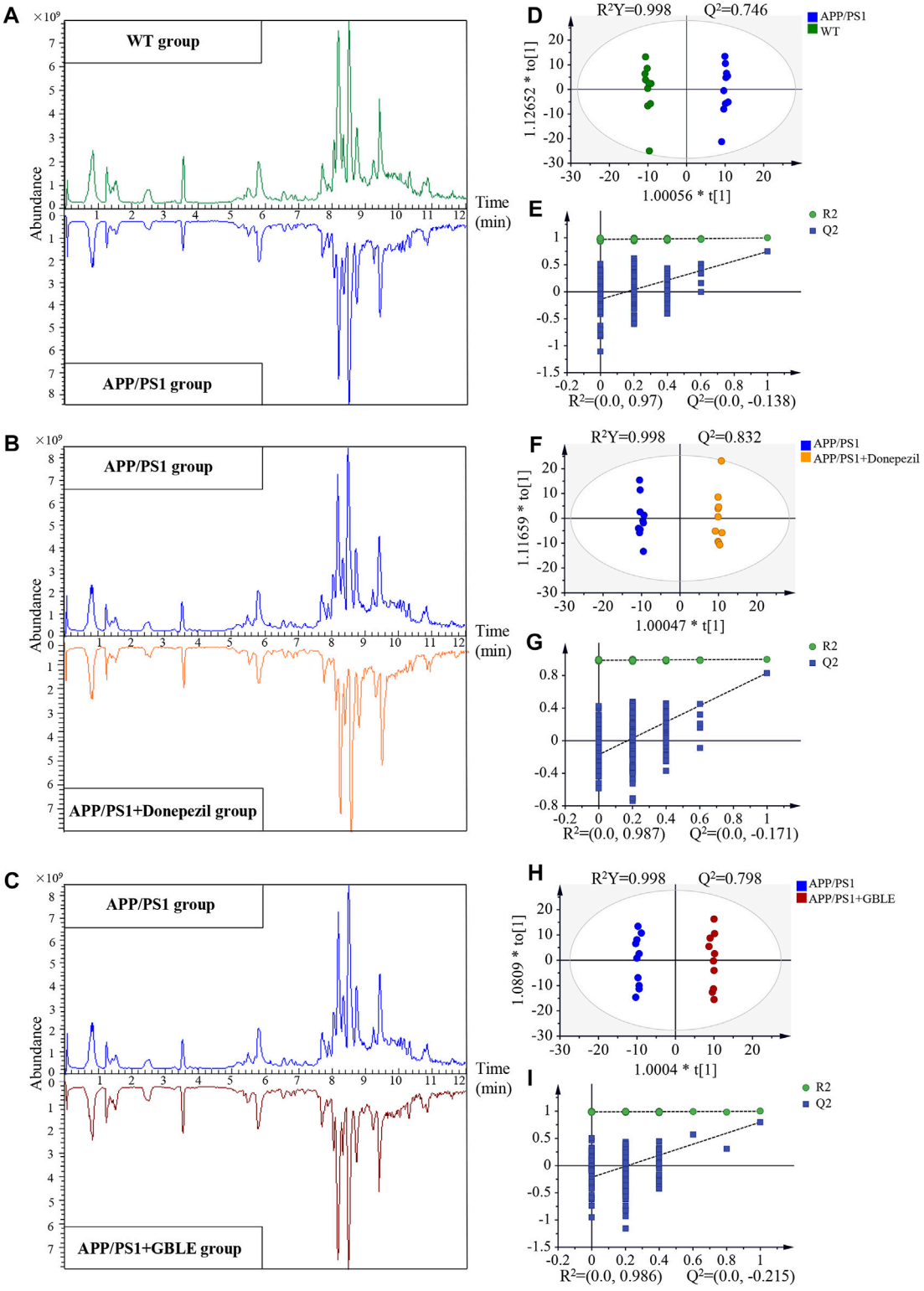

FIGURE 3
UHPLC-Q-Orbitrap HRMS-based untargeted metabolomic analysis. **(A,B,C)** Comparisons of representative total ion chromatograms for plasma samples from WT, APP/PS1, APP/PS1+Donepezil, and APP/PS1+GBLE groups in positive ion mode. **(D,E)** OPLS-DA score plots and corresponding permutation tests for APP/PS1 vs. WT in positive ion mode. **(F,G)** OPLS-DA score plots and corresponding permutation tests for APP/PS1+Donepezil vs. APP/PS1 in positive ion mode. **(H,I)** OPLS-DA score plots and corresponding permutation tests for APP/PS1+GBLE vs. APP/PS1 in positive ion mode.

decreased escape latencies were observed over time during the five consecutive days of place navigation period for the mice in WT group, APP/PS1+Donepezil group, and APP/PS1+GBLE group. In contrast, the mice in APP/PS1 group showed no improvement in finding the hidden platform, indicating a learning impairment. Treatment with donepezil or GBLE dramatically improved their spatial learning ability after training, especially on the fifth day (Figure 1E), and GBLE exhibited a similar effect to donepezil. Evidently, the escape latency of APP/PS1 mice treated with GBLE decreased to 50.1% on the fifth day with the value of 25.14 ± 4.54 s, compared with the first day. In the probe test (without the platform), APP/PS1 mice crossed the original position of platform fewer times and spent less time in the target quadrant than WT mice, suggesting memory decline in the AD model. At the same time, treatment with GBLE significantly attenuated memory impairment of APP/PS1 mice as evidenced by increased number of crossing the original position of missing platform, elevated % distance and % time spent in the target quadrant (Figures 1F–H). In addition, Figure 1I demonstrated the typical swimming paths for different groups in the probe test on the 6th day. Together, these results indicated that GBLE treatment could noticeably ameliorate the cognitive deficits of APP/PS1 mice.

3.2.2 GBLE disaggregates Aβ plaques in the brain of APP/PS1 mice

Accumulation of β-amyloid aggregates in the brain is considered to be associated with cognitive impairment of AD. Therefore, the Aβ levels in the hippocampus and cortex of the mice were examined through immunohistochemistry staining. There were no Aβ deposits detected in the hippocampus and cortex of WT mice (Figures 2A,E,I), while robust Aβ plaques were clearly observed in that of APP/PS1 mice (Figures 2B,F,J). By contrast, the Aβ plaques were significantly disaggregated after 90 days of GBLE treatment (Figures 2C,G,K), exhibiting a similar result as the mice of APP/PS1+Donepezil group (Figures 2D,H,L). These results demonstrated that GBLE could alleviate Aβ accumulation and aggregate in the brain of APP/PS1 mice.

3.3 Global metabolic alterations in plasma samples of APP/PS1 mice and the protective effects of GBLE treatment

3.3.1 Reliability Assessment of the analytical method

Representative typical total ion chromatograms of plasma samples obtained from UHPLC-Q-Orbitrap HRMS analysis for different groups were shown in Figures 3A–C. QC samples and internal standards were applied in the current research to assess the reproducibility and stability of analytical strategy. Unsupervised PCA models for the whole dataset were generated to explore the clustering trend of all the samples. As shown in Supplementary Figures S3A,B, the tightly clustered QC samples in the PCA score plots both in positive and negative ion modes confirmed stability of LC-MS system and high reliability of acquired data throughout the run. In addition, over 90% (93.34% for positive ion mode and 96.82% for negative ion mode) of the ion features possessed relative standard deviation (RSD) values ≤30% across the QC samples, providing further evidence for the robustness of analytical method (Supplementary Figures S3C,D). Meantime, RSD values for the internal standards were also calculated across all the samples, and the values were 4.9% for 2-chloro-L-phenylalanine and 6.5% for ketoprofen. Supplementary Figures S3E,F represent variations of relative abundance with injection order for the ESI^+ and ESI^- internal standards, respectively. The results demonstrated satisfactory stability and high reproducibility of analytical strategy in this study.

3.3.2 Plasma metabolomic profiling distinguished APP/PS1 mice from WT group

Significant discriminations in plasma metabolic phenotypes between APP/PS1 and WT groups were observed by OPLS-DA models from data produced by ESI^+ ($R^2Y = 0.998$ and $Q^2 = 0.746$, Figure 3D) and ESI^- mode ($R^2Y = 0.998$ and $Q^2 = 0.518$, Supplementary Figure S4A), respectively. Furthermore, permutation tests of 200 cross-validation were performed to validate each OPLS-DA model, and the results suggested high goodness of fit and good predictive capability of the constructed models (Figure 3E, Supplementary Figure S4B). After combining positive and negative data, 305 ion features that significantly contributed to the metabolic distinction between the two groups were screened. The volcano plot graphically depicts −log10 (*p*-value) *versus* log2 (FC) for ion features between the comparison (Figure 4A).

As shown in Table 1, a total of 60 differential metabolites (43 metabolites detected in positive ion mode and 17 metabolites in negative mode) were identified between APP/PS1 and WT groups according to accurate *m/z* and MS/MS fragments, and 11 metabolites of which were confirmed by reference standards. Wherein the levels of 31 metabolites obviously increased in APP/PS1 mice compared with WT group, mainly including oleamide, sphinganine, linoleamide, ketosphingosine, sphingosine, and sphingosine 1-phosphate, while 29 metabolites such as 3-hydroxytetradecanoic acid, 5′-methylthioadenosine, adenosine, palmitic amide, and Cer(d18:0/14:0) exhibited significant down-regulated trends. Metabolite set enrichment analysis on the basis of a library containing 464 main chemical class metabolite sets showed that fatty amides, sphingoid bases, amino acids and peptides, amines, and fatty acids and conjugates were notably affected in APP/PS1 group (Figure 4B). The differential metabolites were classified based on HMDB database. As illustrated in Figure 5A, different colors of each pie represent

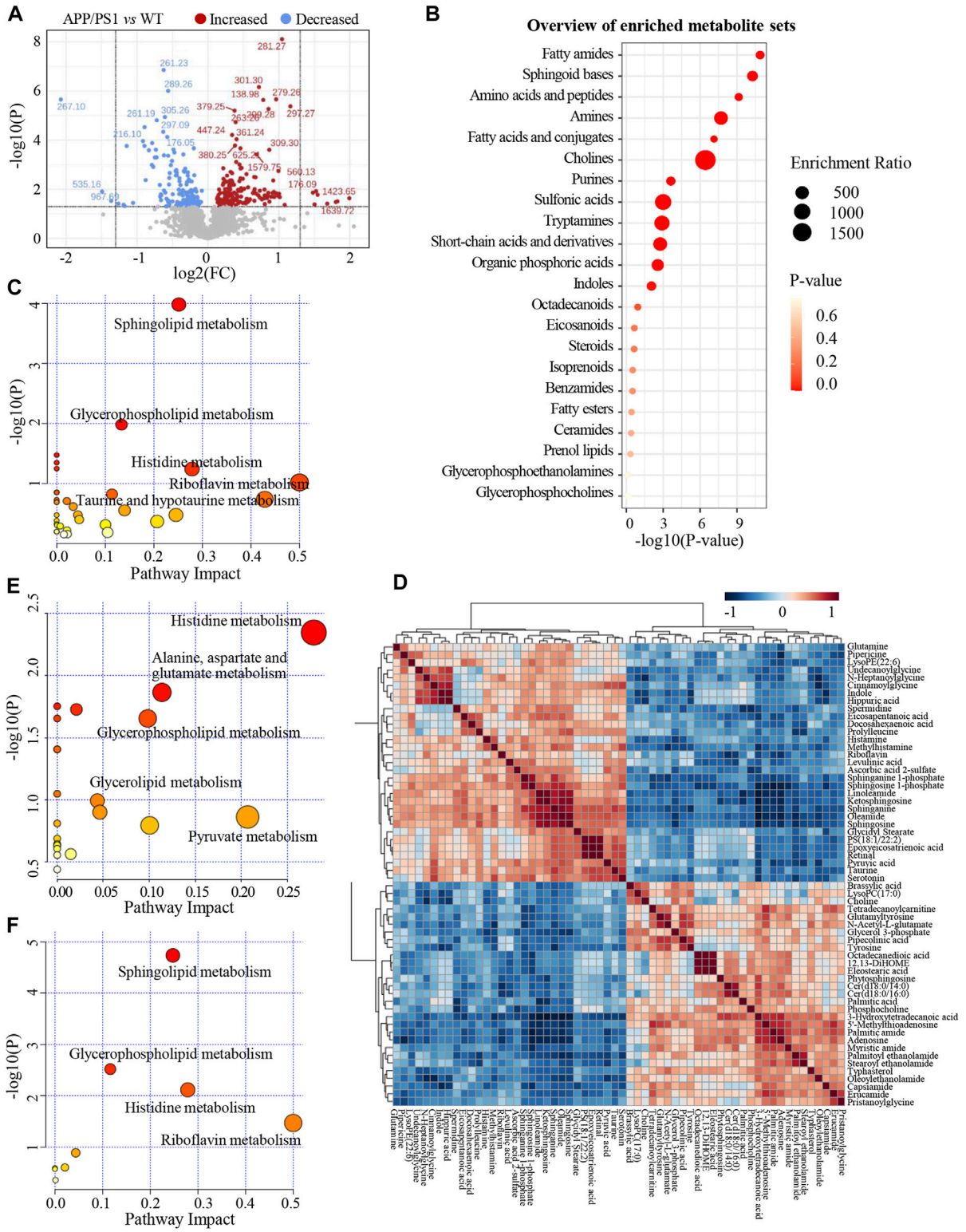

FIGURE 4
(A) The volcano plot of ion features for the comparison between APP/PS1 group vs. WT group. **(B)** Overview of enriched differential metabolite sets. **(C)** Metabolic pathways enrichment analysis on the basis of differential metabolites between APP/PS1 vs. WT group. **(D)** Heatmap of Pearson correlation matrix between the 60 differential metabolites. **(E)** Metabolic pathways enrichment analysis on the basis of differential metabolites between APP/PS1+GBLE vs. APP/PS1 group. **(F)** Metabolic pathways enrichment analysis on the basis of differential metabolites between APP/PS1+Donepezil vs. APP/PS1 group.

TABLE 1 Differential metabolites between the comparison of APP/PS1 and WT groups and the change trends in response to GBLE treatment.

No	Differential metabolites	m/z	Rt (min)	Formula	Ion mode	APP/PS1 vs. WT			APP/PS1+Donepezil vs. APP/PS1		APP/PS1+GBLE vs. APP/PS1	
						VIP	Adjusted-*p* value	FC	Adjusted-*p* value	FC	Adjusted-*p* value	FC
1	Spermidine	146.16513	0.67	$C_7H_{19}N_3$	P	1.39	4.26E-02	1.20 ↑[a]	9.69E-02	0.83 ↓	9.32E-01	0.98 ↓
2	Methylhistamine	126.10269	0.68	$C_6H_{11}N_3$	P	1.80	1.21E-02	1.59 ↑[a]	4.47E-02	0.66 ↓[a]	2.44E-02	0.63 ↓[a]
3	Histamine[b]	112.08716	0.68	$C_5H_9N_3$	P	1.34	4.10E-02	1.35 ↑[a]	1.63E-03	0.56 ↓[c]	4.50E-02	0.71 ↓[a]
4	Pipecolinic acid[b]	130.08627	0.71	$C_6H_{11}NO_2$	P	1.39	4.26E-02	0.80 ↓[a]	1.31E-01	1.20 ↑	2.52E-02	1.19 ↑[a]
5	Choline[b]	104.10720	0.82	$C_5H_{13}NO$	P	1.33	4.28E-02	0.91 ↓[a]	1.14E-02	1.23 ↑[a]	1.54E-01	1.08 ↑
6	Glutamine[b]	147.07627	0.85	$C_5H_{10}N_2O_3$	P	1.36	4.28E-02	1.12 ↑[a]	7.38E-01	1.02 ↑	2.58E-02	0.87 ↓[a]
7	Taurine[b]	124.00612	0.87	$C_2H_7NO_3S$	N	1.97	1.78E-02	1.29 ↑[a]	7.58E-01	1.03 ↑	7.63E-01	0.96 ↓
8	Prolylleucine	229.15440	0.88	$C_{11}H_{20}N_2O_3$	P	1.54	2.94E-02	1.31 ↑[a]	3.86E-01	0.88 ↓	6.71E-01	0.93 ↓
9	Ascorbic acid 2-sulfate	254.98130	0.89	$C_6H_8O_9S$	N	1.64	3.69E-02	1.26 ↑[a]	4.95E-01	0.91 ↓	9.32E-01	1.02 ↑
10	Pyruvic acid	87.00742	0.95	$C_3H_4O_3$	N	1.86	2.81E-02	1.57 ↑[a]	1.97E-01	0.78 ↓	3.44E-02	0.65 ↓[a]
11	Glycerol 3-phosphate	171.00533	0.96	$C_3H_9O_6P$	N	2.10	1.22E-02	0.69 ↓[a]	2.45E-03	1.68 ↑[c]	4.50E-02	1.27 ↑[a]
12	Adenosine	268.10368	1.33	$C_{10}H_{13}N_5O_4$	P	2.48	2.67E-05	0.24 ↓[c]	4.32E-03	3.09 ↑[c]	9.84E-02	3.00 ↑
13	N-Acetyl-L-glutamate	188.05560	1.34	$C_7H_{11}NO_5$	N	1.79	2.99E-02	0.63 ↓[a]	5.91E-01	1.11 ↑	3.10E-01	0.82 ↓
14	Tyrosine[b]	180.06571	1.36	$C_9H_{11}NO_3$	N	1.62	3.88E-02	0.74 ↓[a]	7.66E-01	0.95 ↓	8.78E-01	0.97 ↓
15	Serotonin[b]	177.10216	1.92	$C_{10}H_{12}N_2O$	P	1.57	2.81E-02	2.88 ↑[a]	2.62E-01	0.63 ↓	5.76E-01	0.77 ↓
16	Levulinic acid	115.03884	2.50	$C_5H_8O_3$	N	1.47	4.49E-02	1.24 ↑[a]	3.54E-01	0.87 ↓	4.43E-01	1.11 ↑
17	Glutamyltyrosine	311.12348	2.96	$C_{14}H_{18}N_2O_6$	P	1.46	3.69E-02	0.63 ↓[a]	6.04E-01	1.14 ↑	6.84E-01	0.92 ↓
18	5′-Methylthioadenosine	298.09662	3.50	$C_{11}H_{15}N_5O_3S$	P	2.31	3.06E-04	0.65 ↓[c]	8.32E-05	1.58 ↑[c]	6.85E-03	1.74 ↑[c]
19	Riboflavin[b]	377.14523	4.10	$C_{17}H_{20}N_4O_6$	P	1.37	3.87E-02	1.16 ↑[a]	4.12E-02	0.88 ↓[a]	8.78E-01	1.02 ↑
20	Hippuric acid[b]	180.06544	4.19	$C_9H_9NO_3$	P	1.42	3.69E-02	1.48 ↑[a]	3.21E-01	0.85 ↓	9.84E-02	1.44 ↑
21	Indole	118.06525	4.20	C_8H_7N	P	1.40	3.74E-02	1.58 ↑[a]	4.70E-01	0.86 ↓	7.87E-02	1.50 ↑
22	N-Heptanoylglycine	186.11273	4.44	$C_9H_{17}NO_3$	N	2.02	1.45E-02	1.19 ↑[a]	7.09E-02	0.86 ↓	4.96E-02	0.86 ↓[a]
23	Cinnamoylglycine	204.06582	5.15	$C_{11}H_{11}NO_3$	N	1.68	3.50E-02	1.78 ↑[a]	6.62E-01	0.87 ↓	9.32E-01	0.97 ↓
24	3-Hydroxytetradecanoic acid	262.23719	5.18	$C_{14}H_{28}O_3$	P	2.61	4.20E-06	0.65 ↓[c]	3.63E-02	1.24 ↑[a]	1.90E-02	1.26 ↑[a]

(Continued on following page)

10.3389/fphar.2022.1076960

TABLE 1 (*Continued*) Differential metabolites between the comparison of APP/PS1 and WT groups and the change trends in response to GBLE treatment.

No	Differential metabolites	m/z	Rt (min)	Formula	Ion mode	APP/PS1 vs. WT			APP/PS1+Donepezil vs. APP/PS1		APP/PS1+GBLE vs. APP/PS1	
						VIP	Adjusted-*p* value	FC	Adjusted-*p* value	FC	Adjusted-*p* value	FC
25	Undecanoylglycine	266.17200	6.18	$C_{13}H_{25}NO_3$	P	1.60	2.81E-02	1.29 ↑[a]	7.39E-02	0.78 ↓	4.04E-01	0.86 ↓
26	Palmitic acid	274.27325	6.56	$C_{16}H_{32}O_2$	P	1.64	2.81E-02	0.83 ↓[a]	5.38E-01	1.08 ↑	2.58E-02	1.29 ↑[a]
27	Phytosphingosine	318.29944	6.60	$C_{18}H_{39}NO_3$	P	1.42	3.82E-02	0.85 ↓[a]	7.55E-01	1.03 ↑	7.29E-02	1.26 ↑
28	Brassylic acid	243.15975	6.96	$C_{13}H_{24}O_4$	N	1.77	3.26E-02	0.85 ↓[a]	5.65E-01	1.05 ↑	6.85E-03	1.24 ↑[c]
29	Linoleamide	280.26292	7.02	$C_{18}H_{33}NO$	P	2.51	2.67E-05	1.95 ↑[c]	8.32E-05	0.54 ↓[c]	1.90E-02	0.66 ↓[a]
30	Ketosphingosine	298.27348	7.02	$C_{18}H_{35}NO_2$	P	2.47	4.21E-05	2.24 ↑[c]	6.01E-04	0.53 ↓[c]	1.90E-02	0.61 ↓[a]
31	Oleamide	282.27854	7.42	$C_{18}H_{37}NO$	P	2.70	4.70E-07	2.06 ↑[c]	2.57E-05	0.55 ↓[c]	7.87E-02	0.70 ↓
32	Sphingosine	300.28910	7.42	$C_{18}H_{37}NO_2$	P	2.45	4.62E-05	1.81 ↑[c]	1.59E-03	0.62 ↓[c]	1.50E-01	0.74 ↓
33	Sphinganine	302.30458	7.57	$C_{18}H_{39}NO_2$	P	2.53	1.39E-05	1.65 ↑[c]	1.59E-03	0.69 ↓[c]	9.39E-01	1.01 ↑
34	Sphingosine 1-phosphate	378.24130	7.63	$C_{18}H_{38}NO_5P$	N	2.80	4.74E-05	1.30 ↑[c]	5.69E-04	0.72 ↓[c]	2.38E-01	0.89 ↓
35	Eleostearic acid	279.23118	7.77	$C_{18}H_{30}O_2$	P	1.50	3.26E-02	0.63 ↓[a]	7.09E-02	1.67 ↑	7.63E-01	1.10 ↑
36	Octadecanedioic acid	337.23409	7.77	$C_{18}H_{34}O_4$	P	1.43	3.69E-02	0.68 ↓[a]	7.09E-02	1.62 ↑	9.36E-01	1.02 ↑
37	12,13-DiHOME	313.23823	7.78	$C_{18}H_{34}O_4$	N	1.54	4.28E-02	0.69 ↓[a]	1.06E-01	1.66 ↑	8.63E-01	1.07 ↑
38	Sphinganine 1-phosphate	382.27086	7.81	$C_{18}H_{40}NO_5P$	P	1.91	6.74E-03	1.39 ↑[c]	3.63E-02	0.78 ↓[a]	3.93E-01	1.28 ↑
39	LysoPE (22:6)	526.29159	8.17	$C_{27}H_{44}NO_7P$	P	1.69	1.78E-02	1.23 ↑[a]	3.63E-02	0.82 ↓[a]	4.47E-01	0.93 ↓
40	Docosahexaenoic acid[b]	327.23255	8.20	$C_{22}H_{32}O_2$	N	2.06	1.45E-02	1.18 ↑[a]	9.69E-02	0.87 ↓	2.38E-01	1.13 ↑
41	Phosphocholine[b]	184.07265	8.56	$C_5H_{14}NO_4P$	P	1.45	3.82E-02	0.68 ↓[a]	3.63E-02	1.64 ↑[a]	1.36E-01	1.46 ↑
42	Tetradecanoylcarnitine	372.31015	8.91	$C_{21}H_{41}NO_4$	P	1.49	3.58E-02	0.85 ↓[a]	3.63E-02	1.13 ↑[a]	5.68E-01	1.06 ↑
43	Retinal	285.22070	8.91	$C_{20}H_{28}O$	P	1.53	3.26E-02	1.99 ↑[a]	9.58E-01	0.98 ↓	8.63E-01	0.89 ↓
44	PS(18:1/22:2)	840.57575	8.92	$C_{46}H_{84}NO_{10}P$	N	1.80	3.23E-02	1.74 ↑[a]	5.91E-01	1.15 ↑	8.63E-01	1.10 ↑
45	Epoxyeicosatrienoic acid	319.22738	8.93	$C_{20}H_{32}O_3$	N	1.75	3.29E-02	2.02 ↑[a]	9.12E-01	0.97 ↓	9.32E-01	0.96 ↓
46	LysoPC(17:0)	510.35456	8.98	$C_{25}H_{52}NO_7P$	P	1.33	4.51E-02	0.82 ↓[a]	2.36E-01	1.15 ↑	1.90E-02	1.33 ↑[a]
47	Glycidyl Stearate	341.30430	9.24	$C_{21}H_{40}O_3$	P	1.41	3.69E-02	1.21 ↑[a]	7.47E-01	0.97 ↓	9.32E-01	0.99 ↓
48	Cer(d18:0/14:0)	512.50289	9.68	$C_{32}H_{65}NO_3$	P	1.84	9.36E-03	0.69 ↓[c]	7.69E-01	0.96 ↓	8.05E-02	1.29 ↑

(Continued on following page)

10.3389/fphar.2022.1076960

TABLE 1 (*Continued*) Differential metabolites between the comparison of APP/PS1 and WT groups and the change trends in response to GBLE treatment.

No	Differential metabolites	m/z	Rt (min)	Formula	Ion mode	APP/PS1 vs. WT			APP/PS1+Donepezil vs. APP/PS1		APP/PS1+GBLE vs. APP/PS1	
						VIP	Adjusted-*p* value	FC	Adjusted-*p* value	FC	Adjusted-*p* value	FC
49	Pipericine	336.32532	9.78	$C_{22}H_{41}NO$	P	1.78	1.45E-02	1.89 ↑[a]	3.63E-02	0.56 ↓[a]	3.93E-01	0.81 ↓
50	Eicosapentanoic acid	301.21712	9.85	$C_{20}H_{30}O_2$	N	2.31	5.38E-03	1.36 ↑[c]	4.32E-03	0.72 ↓[c]	4.50E-02	0.82 ↓[a]
51	Palmitoyl ethanolamide	300.28907	9.86	$C_{18}H_{37}NO_2$	P	1.78	1.45E-02	0.82 ↓[a]	3.63E-02	1.37 ↑[a]	1.90E-02	1.25 ↑[a]
52	Oleoyl ethanolamide	326.30463	10.05	$C_{20}H_{39}NO_2$	P	1.87	1.10E-02	0.82 ↓[a]	1.89E-02	1.45 ↑[a]	3.88E-04	1.55 ↑[c]
53	Cer(d18:0/16:0)	540.53402	10.06	$C_{34}H_{69}NO_3$	P	1.37	4.10E-02	0.77 ↓[a]	1.93E-01	0.83 ↓	4.43E-01	1.12 ↑
54	Pristanoylglycine	356.31512	10.20	$C_{21}H_{41}NO_3$	P	1.53	3.26E-02	0.83 ↓[a]	5.91E-01	1.09 ↑	2.38E-01	1.10 ↑
55	Myristic amide	228.23177	10.42	$C_{14}H_{29}NO$	P	1.61	2.81E-02	0.66 ↓[a]	3.63E-02	1.36 ↑[a]	3.44E-02	1.33 ↑[a]
56	Capsiamide	270.27852	10.46	$C_{17}H_{35}NO$	P	1.60	2.81E-02	0.84 ↓[a]	5.65E-01	1.09 ↑	2.91E-01	1.11 ↑
57	Stearoyl ethanolamide	328.32032	10.73	$C_{20}H_{41}NO_2$	P	1.48	3.68E-02	0.82 ↓[a]	4.88E-01	1.12 ↑	4.43E-01	1.10 ↑
58	Typhasterol	447.34780	10.81	$C_{28}H_{48}O_4$	N	1.82	2.81E-02	0.77 ↓[a]	9.79E-01	1.00 ↓	1.51E-01	1.21 ↑
59	Erucamide	338.34090	10.85	$C_{22}H_{43}NO$	P	1.92	9.36E-03	0.82 ↓[c]	5.65E-01	1.09 ↑	1.59E-01	1.07 ↑
60	Palmitic amide	256.26292	11.24	$C_{16}H_{33}NO$	P	2.24	4.46E-04	0.67 ↓[c]	8.43E-02	1.15 ↑	5.64E-03	1.24 ↑[c]

[a]Adjusted-*p* values <0.05.

[b]Metabolites were identified by reference standards.

[c]Adjusted-*p* values <0.01; Rt, retention time; VIP, variable importance in the projection obtained from APP/PS1 group vs. WT group; 12,13-DiHOME, 12,13-dihydroxy-9-octadecenoic acid; LysoPE, lysophosphatidylethanolamine; PS, phosphatidylserine; LysoPC, lysophosphatidylcholine; Cer, ceramide; P, positive ion mode; N, negative ion mode.

10.3389/fphar.2022.1076960

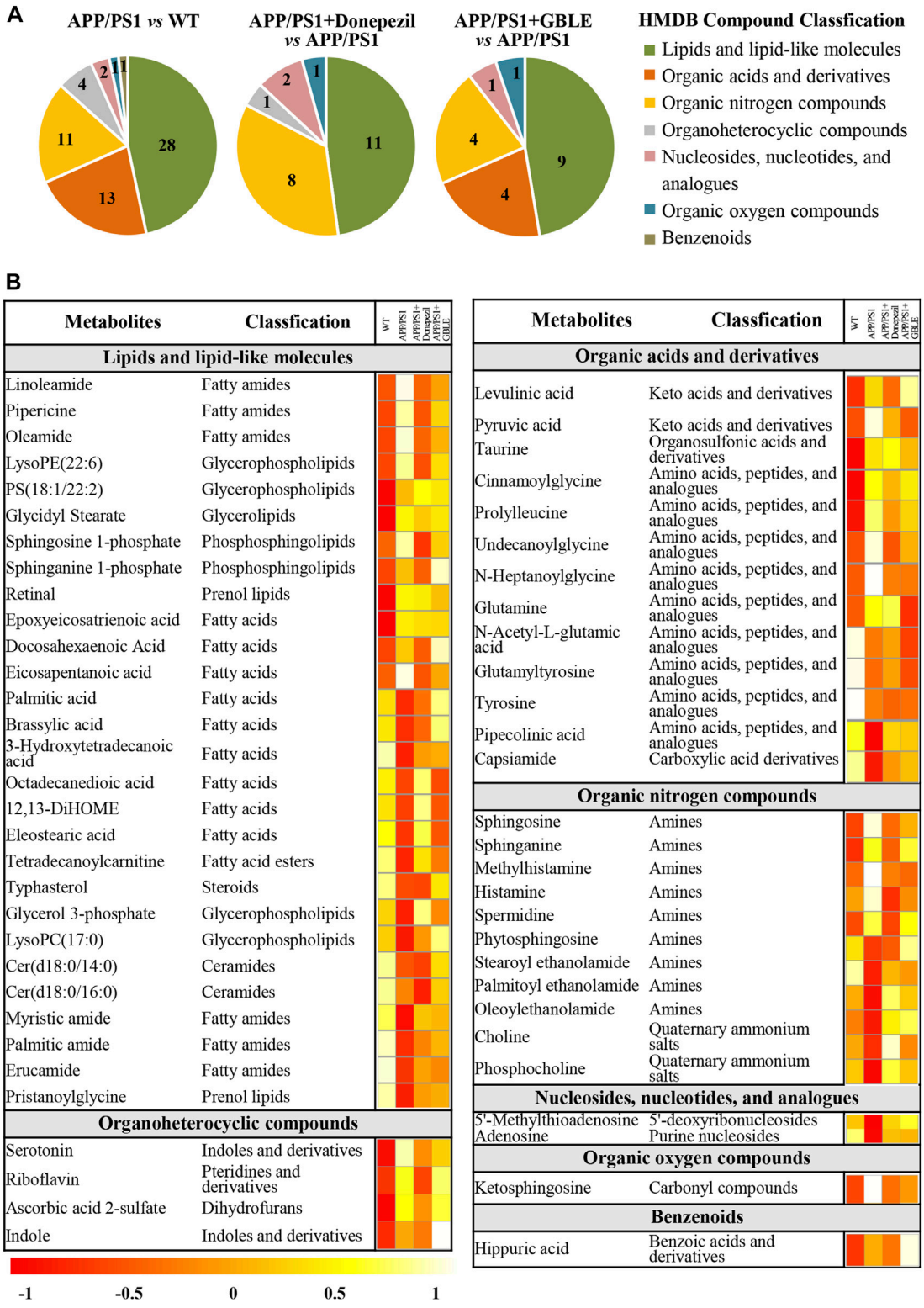

FIGURE 5
Classification and heatmap analysis of differential metabolites. **(A)** Pie charts showing the HMDB compound classification of disorded metabolites in APP/PS1 and regulated metabolites by Donepezil and GBLE, respectively. **(B)** Heat map showing the average levels of metabolites in each group. The colors from red to white in the heatmap indicate higher levels of metabolites.

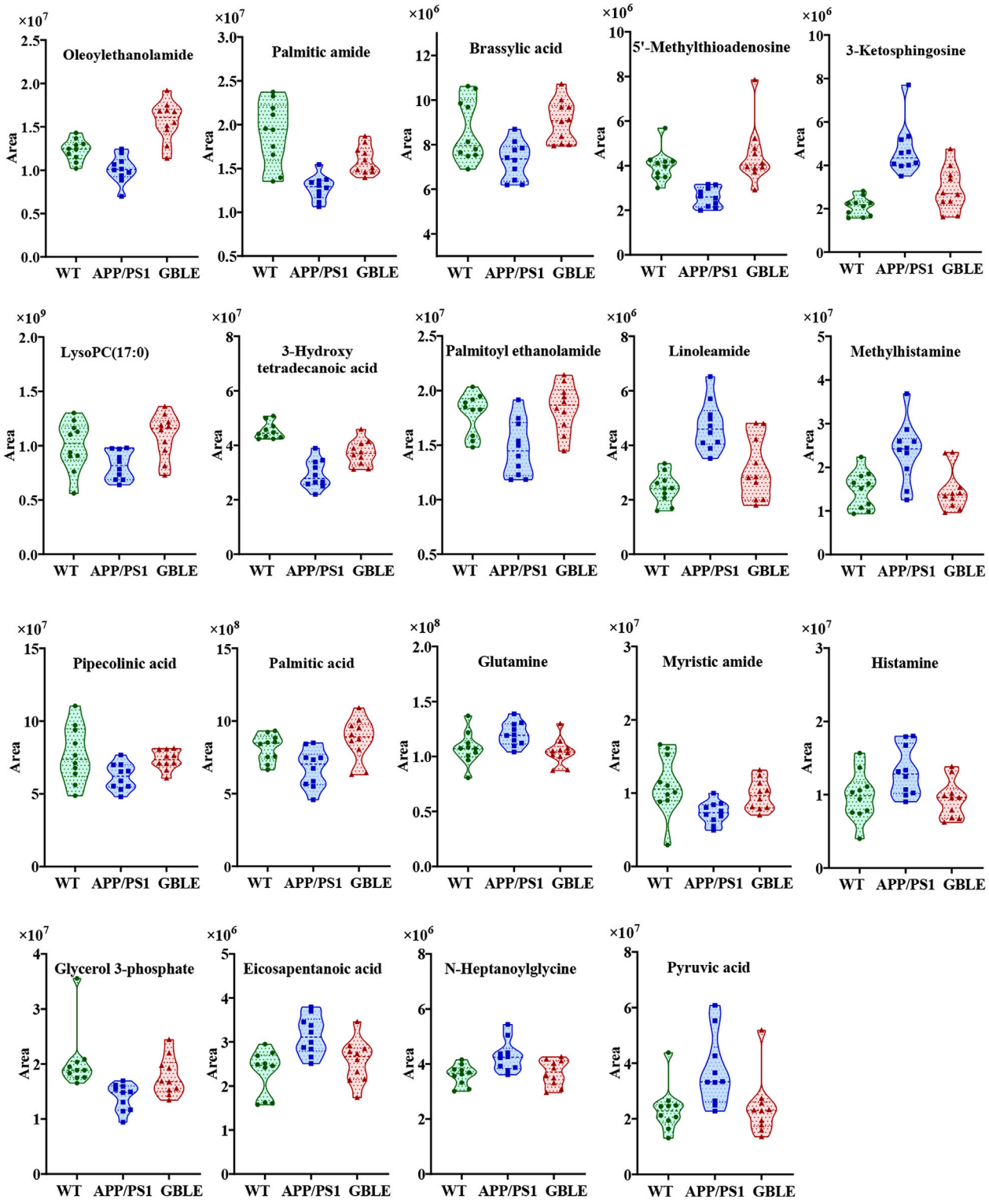

FIGURE 6
Violin plots showing the average peak area changes of each metabolite significantly ameliorated by GBLE.

different HMDB classification. The results demonstrated that these metabolites consisted of 28 lipid and lipid-like molecules, 13 organic acids and derivatives, 11 organic nitrogen compounds, and 8 other compounds, indicative of significant changes in lipid metabolism of AD.

Subsequently, metabolic pathway enrichment analysis was performed to further investigate the potential pathogenesis of AD. These significantly altered metabolites in plasma of APP/PS1 mice were mainly involved in sphingolipid metabolism, glycerophospholipid metabolism, histidine metabolism, riboflavin metabolism, and taurine and hypotaurine metabolism (Figure 4C). Additionally, the correlation heatmap displays relationships between the 60 differential metabolites (Figure 4D). It was shown that the levels of unsaturated fatty amides and metabolites related to sphingolipid metabolism correlated negatively with saturated fatty amides and fatty acyl ethanolamides.

3.3.3 Effect of GBLE treatment on the metabolic abnormality of APP/PS1 mice

The OPLS-DA models were also established for the comparisons between APP/PS1+Donepezil/GBLE group and APP/PS1 group based on the LC-MS/MS data derived from positive and negative ion mode, respectively (Figures 3F–I, Supplementary Figures S4C–F). Analogously, the score plots both revealed remarkable separations for the two comparisons. To probe the influence of GBLE on the metabolic aberration of AD, the metabolic signatures of WT, APP/PS1, APP/PS1+ Donepezil, and APP/PS1+GBLE groups were compared by focusing on the levels of the above differential metabolites. It was noteworthy that the vast majority of these 60 metabolites showed opposite trends for APP/PS1 vs. WT and APP/PS1+GBLE vs. APP/PS1, and 19 metabolites of which were significantly reversely regulated by GBLE, mainly including oleoyl ethanolamide, palmitic amide, brassylic acid, 5′-methylthioadenosine, ketosphingosine, and lysoPC(17:0) (Table 1). For the positive control group, 23 disordered metabolites were significantly reversed by donepezil. The effect of GBLE on regulating metabolic disturbance in APP/PS1 mice was similar to but slightly weaker than that of donepezil, and the regulated metabolites were somewhat different in the two groups. The HMDB classification for the obviously regulated metabolites was displayed in Figure 5A, and the area of each pie chart represented the relative proportion for each class of metabolites. This figure illustrated that most of the altered metabolites after GBLE intervention were classified as lipids and lipid-like molecules.

The relative levels of these differential metabolites across different groups were visualized in a heat map based on the average of each group. As shown in Figure 5B, the color discrimination between APP/PS1 group and WT group was obvious, indicating the metabolic disturbance in AD. Most metabolites were reversibly regulated after GBLE and donepezil treatment as reflected by the change trends of colors. Furthermore, the violin plot visually exhibited the levels of 19 significantly altered metabolites in three different groups (Figure 6), and the impact of GBLE on the perturbed metabolites was evident. Metabolic pathway analysis was conducted to explore the underlying mechanism of GBLE in ameliorating AD. The 19 differential metabolites between APP/PS1+GBLE and APP/PS1 group were primarily associated with histidine metabolism, alanine, aspartate and glutamate metabolism, glycerophospholipid metabolism, glycerolipid metabolism, and pyruvate metabolism (Figure 4E). The impacts of major metabolic pathways were slightly different from that of donepezil treatment (Figure 4F).

3.4 Lipid signatures of APP/PS1 mice and the regulation effects of GBLE treatment on abnormal lipid metabolites

3.4.1 Lipid identification

Plasma untargeted metabolomic profiling suggested that the disordered metabolites and disturbed metabolic pathways in APP/PS1 mice mainly related to lipid metabolism. In line with this, the lipidomic analysis was further performed using UHPLC-Q-Orbitrap HRMS. In total, 1,116 and 513 lipid features covering varies subclasses were detected in positive and negative ion modes, respectively (Figure 7A and Figure 7B). After combining data derived from the two different ion modes and removing duplicated lipids, 1,175 lipid metabolites in six major categories were obtained, including 687 glycerophospholipids, 329 glycerolipids, 103 sphingolipids, 28 saccharolipids, 21 sterol lipids, and seven fatty acyls. Figure 7C delineates the number of every lipid subclass belonging in each category.

3.4.2 Characterization of differential lipid metabolites in plasma samples between APP/PS1 and WT groups and the role of GBLE in regulation of lipids

The unsupervised PCA analysis was carried out, and there was a clear trend towards separation for APP/PS1 vs. WT group and APP/PS1+Donepezil/GBLE vs. APP/PS1 group as presented in the 3D score plot (Figure 8A). Additionally, it was noteworthy that QC samples were clustered in the center of the score plot, confirming the good reproducibility of instrument and high reliability of lipidomic data. Moreover, the OPLS-DA score plots showed complete separations between APP/PS1 and WT groups (R^2Y = 0.999, Q^2 = 0.807; Figure 8B), between APP/PS1+Donepezil and APP/PS1 groups (R^2Y = 0.943, Q^2 = 0.757; Figure 8C), and between APP/PS1+GBLE and APP/PS1 groups (R^2Y = 0.961, Q^2 = 0.833; Figure 8D).

The differential expressed lipid metabolites between APP/PS1 and WT mice were determined conforming to VIP

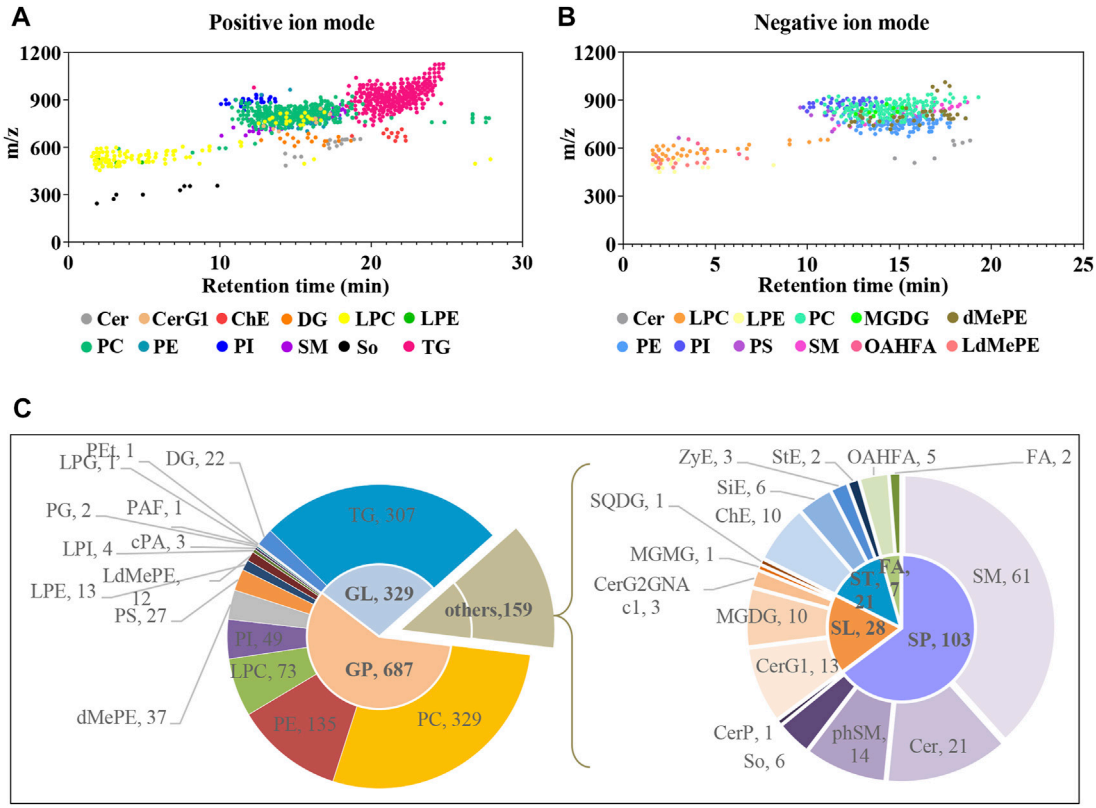

FIGURE 7
Delineation of plasma lipids detected by UHPLC-Q-Orbitrap HRMS. **(A,B)** Scatter plots of lipid features detected in positive and negative ion modes, respectively. **(C)** Pie charts showing the number of every lipid subclass belonging in each category. Cer, ceramides; CerG1, monoglycosylceramide; ChE, cholesteryl ester; DG, diglyceride; LPC, lysophosphatidylcholine; LPE, lysophosphatidylethanolamine; PC, phosphatidylcholine; PE, phosphatidylethanolamine; PI, phosphatidylinositol; SM, sphingomyelin; So, sphingoshine; TG, triglyceride; MGDG, monogalactosyldiacylglycerol; dMePE, dimethylphosphatidylethanolamine; PS, phosphatidylserine; OAHFA (O-acyl)-1-hydroxy fatty acid; LdMePE, Lysodimethylphosphatidylethanolamine; PG, phosphatidylglycerol; LPG, lysophosphatidylglycerol; PEt, phosphatidylethanol; PAF, platelet-activating factor; cPA, cyclic phosphatidic acid; SQDG, sulfoquinovosyldiacylglycerol; ZyE, zymosteryl; SiE, sitosteryl ester; MGMG, monogalactosylmonoacylglycerol; CerP, ceramides phosphate; phSM, phytosphingosine; StE, stigmasteryl ester; GP, glycerophospholipids; GL, glycerolipids; SP, sphingolipids; SL, saccharolipids; ST, sterol lipids; FA, fatty acyls.

scores >1.0 and adjusted-*p* values <0.05. Of the 68 altered lipids, 49 were significantly increased in APP/PS1 group mainly belonging to triglycerides (TG), lyso-phosphatidylcholines (LPC), phosphatidylcholines (PC), and sphingomyelins (SM) subclasses, while 19 were decreased mainly including phosphatidylinositols (PI), lyso-phosphatidylinositols (LPI), phosphatidylethanolamines (PE), and a fraction of PC and LPC (Figure 8E).

Taking the above disturbed lipid metabolites as the evaluation indices of therapeutic effect, the role of GBLE treatment on the plasma lipid fingerprint of AD was investigated through a comparison of APP/PS1+GBLE group vs. APP/PS1 group. As shown in Figure 8F, a number of differential lipids exhibited obvious recovery trend after treatment with GBLE. The effect of GBLE on lipid metabolism disorder in APP/PS1 mice was similar to but slightly weaker than that of donepezil. The result indicated that a lipid disorder occurred in APP/PS1 mice, and this abnormality could be ameliorated by GBLE administration. In general, GBLE showed significant effect on lipid metabolism in APP/PS1 mice.

4 Discussion

In the present study, an integrated metabolomics and lipidomics approach was adopted to characterize the metabolomic phenotype of APP/PS1 mice and describe the metabolic fingerprint change after GBLE intervention. Taking together all the data, here, we delineated a metabolic correlation network based on the differential metabolites and lipids, and proposed several significant metabolic pathways in response to GBLE treatment for APP/PS1 mice (Figure 9). The major findings of this work are summarized as follows: 1)

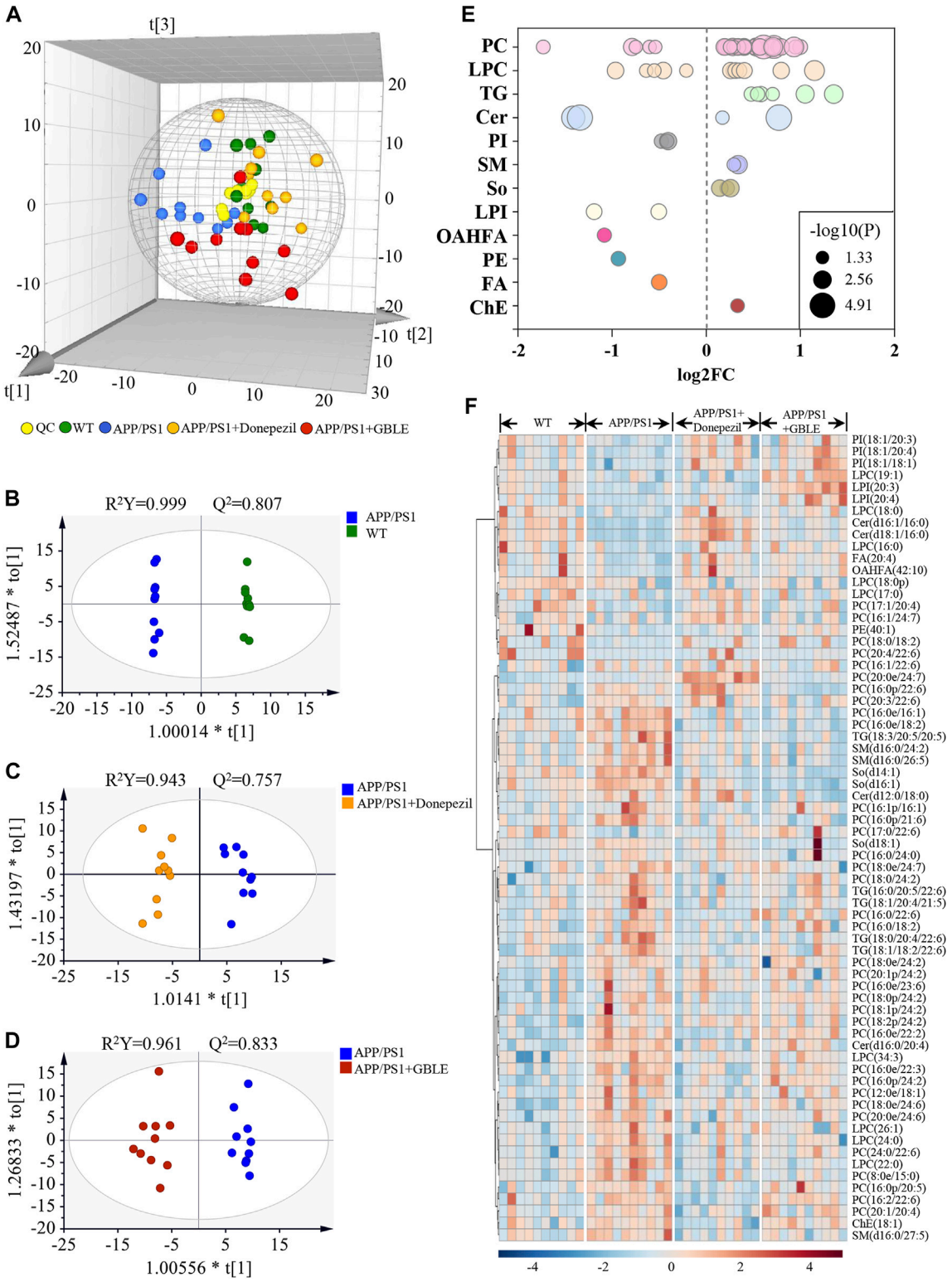

FIGURE 8
UHPLC-Q-Orbitrap HRMS-based lipidomic analysis. **(A)** Three dimensional PCA plot of all the plasma samples from different groups. **(B)** OPLS-DA score plot for APP/PS1 vs. WT group. **(C)** OPLS-DA score plot for APP/PS1+Donepezil vs. APP/PS1 group. **(D)** OPLS-DA score plot for APP/PS1+GBLE vs. APP/PS1 group. **(E)** Bubble chart of differential lipids for APP/PS1 vs. WT group. **(F)** Heatmap of the 68 differential lipids among the WT, APP/PS1, APP/PS1+Donepezil, and APP/PS1+GBLE groups. The colors from blue to red indicates the elevation of lipid metabolites.

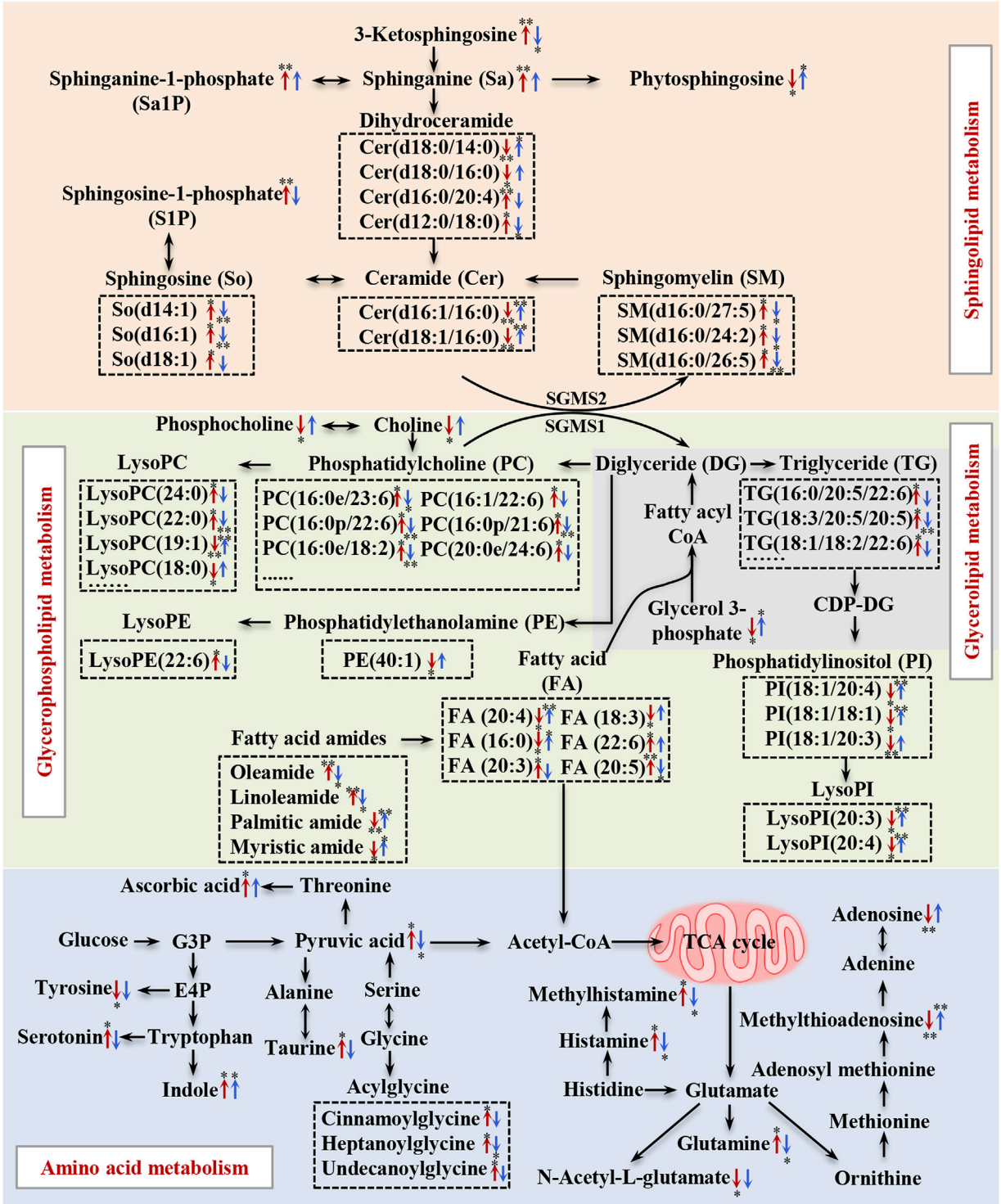

FIGURE 9
Disturbed metabolic pathway network in APP/PS1 mice and the interventional effects of GBLE by integrating metabolomics and lipidomics data. The red arrows represent altered metabolites in APP/PS1 mice compared with WT group, and the blue arrows represent the regulated metabolites by GBLE treatment. *: adjusted-p < 0.05, **: adjusted-p < 0.01.

Administration of GBLE significantly improved the cognitive function and alleviated Aβ deposition in APP/PS1 mice. 2) The plasma metabolic signature of APP/PS1 mice was primarily characterized by disrupted sphingolipid metabolism, glycerophospholipid metabolism, glycerolipid metabolism, and amino acid metabolism. 3) GBLE treatment could reverse the disturbance of many key endogenous metabolites and regulate abnormal metabolism in APP/PS1 mice, particularly lipid dishomeostasis. The results may be helpful in understanding the potential pathogenesis of AD and shed new light on the therapeutic mechanism of GBLE in the treatment of AD.

In recent years, metabolomics has been widely employed to characterize the metabolic alterations of diseases and provides a potential approach to explore the complex action modes of TCMs. During the past 10 years, over hundreds of metabolomics studies have been conducted to uncover the metabolic changes in multiple biological matrices including plasma, serum, cerebrospinal fluid, urine, feces, and tissues of different AD animal models and patients (González-Domínguez et al., 2018; Dai et al., 2022). These studies demonstrated disturbances of energy-related metabolism, fatty acid metabolism, nitrogen metabolism, amino acid metabolism, and many others related to AD. Similarly to previous studies, significant alterations were observed in levels of glycerophospholipids, sphingolipids, glycerolipids, fatty acids, amino acids, and nucleotides in the present work. Lipidomics analysis showed significant changes in the levels of PCs, LPCs, PEs, Cers, SMs and some other lipids, corroborating the pivotal role of lipid metabolism in the pathogenesis of AD, despite not entirely consistent change with previous literatures on AD-related lipidome and phospholipidome (González-Domínguez et al., 2014a; González-Domínguez et al., 2014b).

Lipids, the essential components of cellular membranes, play crucial roles in many biological processes, such as maintenance of cell structure and function, energy storage, signal transduction and regulation of gene expression (Brügger, 2014; Han, 2016). The lipids have been classified into eight categories: fatty acyls, glycerolipids, glycerophospholipids, sphingolipids, sterol lipids, saccharolipids, prenol lipids, and polyketides (Fahy et al., 2005), and each category consists of further lipid subclasses. Among these lipids, glycerophospholipids, sphingolipids, and cholesterol are mainly localized in neuronal membranes and myelin (Wang et al., 2021). Abnormal lipid metabolism is closely correlated with neurological diseases and affects cognitive function (Wong et al., 2017). It is widely accepted that the accumulation of Aβ is strongly associated with cognitive dysfunction of AD. Lipid rafts, enriched in sphingolipids and glycerophospholipids, not only promote the generation of Aβ peptides and facilitate the formation of toxic oligomers, but also host specific neuronal receptors which participate in the signal transduction of neuropathological events. A wealth of evidence has unambiguously linked lipid rafts to neurodegenerative diseases, including AD (Mesa-Herrera et al., 2019). Previous studies have shown significant alterations in molecular structure and functionality of lipid rafts in the frontal cortex of brains in AD patients (Rushworth and Hooper, 2010). Therefore, we speculated that the metabolic disorder of sphingolipids and glycerophospholipids induced the abnormal expression of Aβ *via* breaking down the lipid rafts homeostasis. Nevertheless, it is still no consensus on the change trends of various lipids for AD from previous studies.

In this work, one of the most changes was observed in sphingolipid metabolism in the plasma of APP/PS1 mice. Compared with WT mice, the levels of sphingosine, sphinganine, 3-ketosphingosine, sphingosine-1-phosphate (S1P), sphinganine-1-phosphate and sphingomyelins (SM) were significantly increased in APP/PS1 mice, while ceramides presented both negative and positive associations with AD. Ceramides, with the structure containing a long-chain sphingoid base and one N-acylated fatty acid, are central molecules in the biosynthesis and catabolism of sphingolipids (Pralhada Rao et al., 2013). According to the fatty acids contained in the structure, previous study demonstrated that the increase of ceramides containing very long fatty acids was more pronounced in AD (Cutler et al., 2004), which was associated with the elevated expression of long-chain ceramide synthase (Katsel et al., 2007). It was corroborated by the increased level of Cer (d16:0/20:4) in APP/PS1 mice in this work. Some previous researches have demonstrated that upregulated ceramides can promote aggregation of Aβ through the effect on lipid rafts (Badawy et al., 2018). On the other hand, the increased level of unsaturated fatty acid-containing ceramide (Cer d16:0/20:4) together with a significant decrease in several saturated fatty acids-containing ceramides (Cer d16:1/16:0, Cer d18:1/16:0, Cer d18:0/14:0, and Cer d18:0/16:0) were observed in APP/PS1 mice. The results could be consequent with the elevated activity of stearoyl-CoA desaturase, which was associated with AD (Astarita et al., 2011). Our results were consistent with a recent study (Huynh et al., 2020). In addition, SM may be another specific biomarker for AD, which increased the risk of AD in previous clinical studies (Varma et al., 2018). Toledo reported that increase in levels of SMs in AD patients was related to cognitive decline and brain atrophy (Toledo et al., 2017). Kosicek found significantly increased SMs levels in the cerebrospinal fluid in patients with AD compared with healthy controls (Kosicek et al., 2012). In accordance with this, here we showed that APP/PS1 mice displayed elevated levels of SM(d16:0/27:5), SM(d16:0/24:2), and SM(d16:0/26:5) in plasma. S1P, a signaling molecule, is produced by ceramides *via* ceramidase and subsequent sphingosine kinase. Previous studies have reported that ceramidase is up-regulated in AD (He et al., 2010), as well as the activity of sphingosine kinase 2 (Takasugi et al., 2011), which could be responsible for the significantly increased levels of S1P in APP/PS1 mice in the present study. Excitingly, our results suggested that GBLE showed significant improvement in the

disturbed sphingolipid metabolism, and sphingolipids may serve as putative therapeutic targets of GBLE on AD.

The results also suggested significant alterations in glycerophospholipids and glycerolipids for APP/PS1 mice, such as PCs, LPCs, PEs, LPEs, PIs, LPIs, and TGs. Glycerol 3-phosphate, a key molecule in the initial step of glycerolipid and glycerophospholipids metabolism, was significantly lower in APP/PS1 mice when compared with WT group, which is in agreement with a recent research (Watanabe et al., 2021). Previously published researches supported possible associations between glycerophospholipids and amyloid deposits related to pathology of AD (Whiley et al., 2014). Huo et al. discovered that increased levels of some PCs were related to cognitive impairment (Huo et al., 2020). Toledo reported that the levels of PCs were elevated in the cerebrospinal fluid of AD patients and associated with aberrant Aβ1-42 (Toledo et al., 2017). Similar to these results, most PCs were upregulated in the plasma of APP/PS1 mice in the present study. In fact, researches on the levels of PCs in AD were not uniform and the results were somewhat controversial (Toledo et al., 2017; Huo et al., 2020; Bhawal et al., 2021). These contrary findings could arise by diverse functions of different PCs, which can be responsible for the minority of decreased PCs in our study. Our results implicated that specific PCs, rather than PCs as a whole, might play important roles in AD. LPCs serve as mediators in multiple neuronal pathways involved in neurobiology of AD (Frisardi et al., 2011), and previous studies have reported decreased levels of LPCs in AD (González-Domínguez et al., 2014b). However, in the present work, it was observed that the levels of LPCs containing fatty acids with carbon atoms <20 were decreased, while those with carbon atoms >20 were increased in the plasma of APP/PS1 mice, which might be worthy to be studied further. In addition, numerous studies reported reduced levels of PEs (Igarashi et al., 2011; González-Domínguez et al., 2014b), as confirmed in our data. As for glycerolipids, the levels of TGs were markedly increased in APP/PS1 mice, and our findings were consistent with a related study in which a higher level of TG was observed in the serum of AD patients (Berezhnoy et al., 2022). Notably, most of these changes showed a significant correction after GBLE administration. The close relationship between these molecules and AD may provide a new strategy for further research on the treatment of this disease.

Besides, we observed a dramatic disorder in the fatty amides levels in the plasma of APP/PS1 mice. In a recent study on AD biomarker discovery, the plasma fatty amides were demonstrated to be associated with brain amyloid burden, hippocampal volume, and memory (Kim et al., 2019). Palmitic amide is a primary fatty acid amide and plays a pivotal role in cellular signal transduction. Decreased serum palmitic amide in AD was reported earlier (Chu et al., 2016). Oleamide has been early identified in the brains of sleep-deprived mice and cats (Cravatt et al., 1995) and is a vital regulatory lipid in central nervous system. Kim M. et al. Identified significantly higher levels of oleamide and linoleamide in the plasma of AD patients (Kim et al., 2019). These findings agreed with our results, and we found that the saturated fatty amides seemed decreased while unsaturated fatty amides were increased in APP/PS1 mice. The opposite directions could be attributed to increased desaturase activity in AD. Indeed, so far very little is known about the biological function of fatty amides, which may be key therapeutical targets in the treatment of AD.

Additionally, the APP/PS1 mice showed perturbed amino acid metabolism, tricarboxylic acid (TCA) cycle and fatty acids oxidation, and these alterations were ameliorated following 3-month GBLE administration. The dyshomeostasis of aromatic amino acids and the synthesis of neurotransmitters was associated with AD (González-Domínguez et al., 2021), which was corroborated by the altered tyrosine and serotonin in the present work. Histamine and methylhistamine were significantly elevated in APP/PS1 mice, and previous evidence suggested that neurotransmitter systems including neuronal histamine could contribute to the development and maintenance of AD-related cognitive deficits (Zlomuzica et al., 2016). Acylglycines are produced through the action of glycine N-acyltransferase and they are normally minor metabolites of fatty acids. Elevated levels of acylglycines (cinnamoylglycine, heptanoylglycine, and undecanoylglycine) appeared in the plasma of APP/PS1 mice, indicating a disordered fatty acid oxidation in AD. The increased level of pyruvate was related to dysregulated TCA cycle, which was consistent with previous studies (Rushworth and Hooper, 2010). In this work, we also found APP/PS1 mice displayed a declined level of acylcarnitine, which was not merely a cofactor in β-oxidation, but also had beneficial effects in the treatment of neurological diseases (Jones et al., 2010). Various studies have reported important deregulations in the metabolism of purines and pyrimidines (González-Domínguez et al., 2021). Adenosine, an important neuroprotective factor (Rahman, 2009), was dramatically decreased in APP/PS1 mice and upregulated by GBLE intervention, as well as methylthioadenosine.

Of note, in addition to AD, GBLE is also used for prevention and therapy of myocardial ischemia. A metabolomics study demonstrated that the cardioprotective effect of GBLE was achieved through comprehensive regulation of multiple metabolic pathways covering lipid, energy, amino acid and nucleotide metabolism (Wang et al., 2016). The similar regulating effect of GBLE on different diseases seems to reflect the strategy of "homotherapy for heteropathy" for TCM.

To sum up, we comprehensively described the metabolic signatures of AD and evaluated the effects of GBLE on plasma metabolome and lipidome in APP/PS1 mice. However, this work has some limitations worth noting. Firstly, the metabolomic and lipidomic profiles were obtained only based on the plasma samples. Characterizing the metabolic signatures of brain tissues is needed in future studies, and a comprehensive research through combining the data from plasma and brain

tissue is crucial for unveiling the pathological mechanisms of AD and therapeutic targets of GBLE. Secondly, we observed that numerous endogenous metabolites were regulated by GBLE. However, the molecular mechanisms are still not well understood. It is essential to further explore the causality and investigate the biological context in which theses metabolites operate by integrating additional information such as protein and gene expression in the future. Besides, this study only includes male mice, and it is uncertain whether the effect of GBLE is the same in female mice. Nevertheless, this study provides a better understanding on the metabolism-based neuroprotective effects of GBLE on AD.

5 Conclusion

In conclusion, we delineated the metabolic disturbance in the plasma of APP/PS1 mice and investigated the overall therapeutic effect of GBLE on AD through UHPLC-MS/MS-based metabolomic and lipidomic approach. The metabolic perturbation in APP/PS1 mice was primarily related to sphingolipid metabolism, glycerophospholipid metabolism, glycerolipid metabolism, and amino acid metabolism, and this dyshomeostasis could be ameliorated by GBLE treatment. These results deepen our knowledge about the pathophysiological mechanisms of AD, provide available evidence for the neuroprotective effect of GBLE administration, and reveal the characteristic of multiple components, targets and pathways for traditional Chinese medicines.

Data availability statement

The original contributions presented in the study are included in the article/Supplementary Materials, further inquiries can be directed to the corresponding author.

Ethics statement

The animal study was reviewed and approved by the Animal Ethics Committee of Zhengzhou University.

Author contributions

L-HZ and L-WL contributed to the original idea and design of this study. L-WL, H-YY, JZ, F-MZ, and Q-QJ performed the experiments. L-WL and Z-LL conducted data analysis. L-WL and MT drafted the manuscript. Y-BL and JK revised the manuscript. All authors have read and approved the final manuscript.

Funding

This study was supported by the National Natural Science Foundation of China (82003921), the National Natural Science Foundation of Henan Province (222300420303), the National Key R&D Program of China (2021YFC2401105), the Key Research and Promotion Project of Henan Province (222102310082), the Joint Project of Medical Science and Technology of Henan Province (LHGJ20190280, LHGJ20220418), and Open Foundation of Key Laboratory of Digital Technology in Medical Diagnostics of Zhejiang Province (SZZD202216).

Conflicts of interest

The authors declare that the research was conducted in the absence of any commercial or financial relationships that could be construed as a potential conflict of interest.

Publisher's note

All claims expressed in this article are solely those of the authors and do not necessarily represent those of their affiliated organizations, or those of the publisher, the editors and the reviewers. Any product that may be evaluated in this article, or claim that may be made by its manufacturer, is not guaranteed or endorsed by the publisher.

Supplementary material

The Supplementary Material for this article can be found online at: https://www.frontiersin.org/articles/10.3389/fphar.2022.1076960/full#supplementary-material

SUPPLEMENTARY FIGURE S1
The animal experiment schedule.

SUPPLEMENTARY FIGURE S2
The total ion chromatograms of GBLE in **(A)** positive ion mode and **(B)** negative ion mode.

SUPPLEMENTARY FIGURE S3
Reliability assessment of the analytical method by the performance of QC samples and internal standard responses. **(A,B)** PCA score plots of all the samples in positive and negative ion modes. **(C,D)** Relative standard deviation (RSD) distribution of metabolic ion features for QC samples detected in positive and negative ion modes. **(E,F)** Relative abundance variabilities of 2-chloro-L-phenylalanine (ESI^+ internal standard) and ketoprofen (ESI^- internal standard) with respect to the injection order.

SUPPLEMENTARY FIGURE S4
The OPLS-DA score plots and corresponding permutation tests for **(A,B)** APP/PS1 *vs.* WT, **(C,D)** APP/PS1+Donepezil *vs.* APP/PS1 and **(E,F)** APP/PS1+GBLE *vs.* APP/PS1 in negative ion mode.

References

Alzheimer, A., Stelzmann, R. A., Schnitzlein, H. N., and Murtagh, F. R. (1995). An English translation of Alzheimer's 1907 paper, "Uber eine eigenartige Erkankung der Hirnrinde. *Clin. Anat.* 8, 429–431. doi:10.1002/ca.980080612

Andrade, S., Ramalho, M. J., Loureiro, J. A., and Pereira, M. D. C. (2019). Natural compounds for Alzheimer's disease therapy: A systematic review of preclinical and clinical studies. *Int. J. Mol. Sci.* 20, 2313. doi:10.3390/ijms20092313

Astarita, G., Jung, K. M., Vasilevko, V., Dipatrizio, N. V., Martin, S. K., Cribbs, D. H., et al. (2011). Elevated stearoyl-CoA desaturase in brains of patients with Alzheimer's disease. *PLoS One* 6, e24777. doi:10.1371/journal.pone.0024777

Badawy, S. M. M., Okada, T., Kajimoto, T., Hirase, M., Matovelo, S. A., Nakamura, S., et al. (2018). Extracellular α-synuclein drives sphingosine 1-phosphate receptor subtype 1 out of lipid rafts, leading to impaired inhibitory G-protein signaling. *J. Biol. Chem.* 293, 8208–8216. doi:10.1074/jbc.RA118.001986

Berezhnoy, G., Laske, C., and Trautwein, C. (2022). Quantitative NMR-based lipoprotein analysis identifies elevated HDL-4 and triglycerides in the serum of Alzheimer's disease patients. *Int. J. Mol. Sci.* 23, 12472. doi:10.3390/ijms232012472

Bhawal, R., Fu, Q., Anderson, E. T., Gibson, G. E., and Zhang, S. (2021). Serum metabolomic and lipidomic profiling reveals novel biomarkers of efficacy for Benfotiamine in Alzheimer's disease. *Int. J. Mol. Sci.* 22, 13188. doi:10.3390/ijms222413188

Breijyeh, Z., and Karaman, R. (2020). Comprehensive review on Alzheimer's disease: Causes and treatment. *Molecules* 25, 5789. doi:10.3390/molecules25245789

Brügger, B. (2014). Lipidomics: Analysis of the lipid composition of cells and subcellular organelles by electrospray ionization mass spectrometry. *Annu. Rev. Biochem.* 83, 79–98. doi:10.1146/annurev-biochem-060713-035324

Chen, Q. Q., Wang, F. X., Cai, Y. Y., Zhang, Y. K., Fang, J. K., Qi, L. W., et al. (2021). Untargeted metabolomics and lipidomics uncovering the cardioprotective effects of Huanglian Jiedu Decoction on pathological cardiac hypertrophy and remodeling. *J. Ethnopharmacol.* 270, 113646. doi:10.1016/j.jep.2020.113646

Chu, H., Zhang, A., Han, Y., Lu, S., Kong, L., Han, J., et al. (2016). Metabolomics approach to explore the effects of Kai-Xin-San on Alzheimer's disease using UPLC/ESI-Q-TOF mass spectrometry. *J. Chromatogr. B Anal. Technol. Biomed. Life Sci.* 1015-1016, 50–61. doi:10.1016/j.jchromb.2016.02.007

Cravatt, B. F., Prospero-Garcia, O., Siuzdak, G., Gilula, N. B., Henriksen, S. J., Boger, D. L., et al. (1995). Chemical characterization of a family of brain lipids that induce sleep. *Science* 268, 1506–1509. doi:10.1126/science.7770779

Cutler, R. G., Kelly, J., Storie, K., Pedersen, W. A., Tammara, A., Hatanpaa, K., et al. (2004). Involvement of oxidative stress-induced abnormalities in ceramide and cholesterol metabolism in brain aging and Alzheimer's disease. *Proc. Natl. Acad. Sci.* 101, 2070–2075. doi:10.1073/pnas.0305799101

Dai, Z., Hu, T., Su, S., Liu, J., Ma, Y., Zhuo, Y., et al. (2022). Comparative metabolomics analysis reveals key metabolic mechanisms and protein biomarkers in Alzheimer's disease. *Front. Pharmacol.* 13, 904857. doi:10.3389/fphar.2022.904857

Fahy, E., Subramaniam, S., Brown, H. A., Glass, C. K., Merrill, A. H., Jr, Murphy, R. C., et al. (2005). A comprehensive classification system for lipids. *J. Lipid Res.* 46, 839–861. doi:10.1194/jlr.E400004-JLR200

Frisardi, V., Panza, F., Seripa, D., Farooqui, T., and Farooqui, A. A. (2011). Glycerophospholipids and glycerophospholipid-derived lipid mediators: A complex meshwork in Alzheimer's disease pathology. *Prog. Lipid Res.* 50, 313–330. doi:10.1016/j.plipres.2011.06.001

GBD 2016 Dementia Collaborators (2019). Global, regional, and national burden of Alzheimer's disease and other dementias, 1990–2016: A systematic analysis for the global burden of disease study 2016. *Lancet Neurol.* 18, 88–106. doi:10.1016/S1474-4422(18)30403-4

González-Domínguez, R., García-Barrera, T., and Gómez-Ariza, J. L. (2014a). Combination of metabolomic and phospholipid-profiling approaches for the study of Alzheimer's disease. *J. Proteomics* 104, 37–47. doi:10.1016/j.jprot.2014.01.014

González-Domínguez, R., García-Barrera, T., and Gómez-Ariza, J. L. (2014b). Metabolomic study of lipids in serum for biomarker discovery in Alzheimer's disease using direct infusion mass spectrometry. *J. Pharm. Biomed. Anal.* 98, 321–326. doi:10.1016/j.jpba.2014.05.023

González-Domínguez, R., González-Domínguez, Á., Sayago, A., González-Sanz, J. D., Lechuga-Sancho, A. M., and Fernández-Recamales, Á. (2021). Mechanistic insights into Alzheimer's disease unveiled through the investigation of disturbances in central metabolites and metabolic pathways. *Biomedicines* 9, 298. doi:10.3390/biomedicines9030298

González-Domínguez, R., Sayago, A., and Fernández-Recamales, Á. (2018). High-throughput direct mass spectrometry-based metabolomics to characterize metabolite fingerprints associated with Alzheimer's disease pathogenesis. *Metabolites* 8, 52. doi:10.3390/metabo8030052

Han, X. (2016). Lipidomics for studying metabolism. *Nat. Rev. Endocrinol.* 12, 668–679. doi:10.1038/nrendo.2016.98

Hao, L., Wang, J., Page, D., Asthana, S., Zetterberg, H., Carlsson, C., et al. (2018). Comparative evaluation of MS-based metabolomics software and its application to preclinical Alzheimer's disease. *Sci. Rep.* 8, 9291. doi:10.1038/s41598-018-27031-x

He, X., Huang, Y., Li, B., Gong, C. X., and Schuchman, E. H. (2010). Deregulation of sphingolipid metabolism in Alzheimer's disease. *Neurobiol. Aging* 31, 398–408. doi:10.1016/j.neurobiolaging.2008.05.010

Huang, F. Q., Li, J., Jiang, L., Wang, F. X., Alolga, R. N., Wang, M. J., et al. (2019). Serum-plasma matched metabolomics for comprehensive characterization of benign thyroid nodule and papillary thyroid carcinoma. *Int. J. Cancer* 144, 868–876. doi:10.1002/ijc.31925

Huo, Z., Yu, L., Yang, J., Zhu, Y., Bennett, D. A., and Zhao, J. (2020). Brain and blood metabolome for Alzheimer's dementia: Findings from a targeted metabolomics analysis. *Neurobiol. Aging* 86, 123–133. doi:10.1016/j.neurobiolaging.2019.10.014

Huynh, K., Lim, W. L. F., Giles, C., Jayawardana, K. S., Salim, A., Mellett, N. A., et al. (2020). Concordant peripheral lipidome signatures in two large clinical studies of Alzheimer's disease. *Nat. Commun.* 11, 5698. doi:10.1038/s41467-020-19473-7

Igarashi, M., Ma, K., Gao, F., Kim, H. W., Rapoport, S. I., and Rao, J. S. (2011). Disturbed choline plasmalogen and phospholipid fatty acid concentrations in Alzheimer's disease prefrontal cortex. *J. Alzheimers Dis.* 24, 507–517. doi:10.3233/JAD-2011-101608

Jones, L. L., McDonald, D. A., and Borum, P. R. (2010). Acylcarnitines: Role in brain. *Prog. Lipid Res.* 49, 61–75. doi:10.1016/j.plipres.2009.08.004

Katsel, P., Li, C., and Haroutunian, V. (2007). Gene expression alterations in the sphingolipid metabolism pathways during progression of dementia and Alzheimer's disease: A shift toward ceramide accumulation at the earliest recognizable stages of Alzheimer's disease? *Neurochem. Res.* 32, 845–856. doi:10.1007/s11064-007-9297-x

Kim, M., Snowden, S., Suvitaival, T., Ali, A., Merkler, D. J., Ahmad, T., et al. (2019). Primary fatty amides in plasma associated with brain amyloid burden, hippocampal volume, and memory in the European Medical Information Framework for Alzheimer's Disease biomarker discovery cohort. *Alzheimers Dement.* 15, 817–827. doi:10.1016/j.jalz.2019.03.004

Knopman, D. S., Amieva, H., Petersen, R. C., Chetelat, G., Holtzman, D. M., Hyman, B. T., et al. (2021). Alzheimer disease. *Nat. Rev. Dis. Prim.* 7, 33. doi:10.1038/s41572-021-00269-y

Kosicek, M., Zetterberg, H., Andreasen, N., Peter-Katalinic, J., and Hecimovic, S. (2012). Elevated cerebrospinal fluid sphingomyelin levels in prodromal Alzheimer's disease. *Neurosci. Lett.* 516, 302–305. doi:10.1016/j.neulet.2012.04.019

Li, M. Z., Zhang, Y., Zou, H. Y., Ouyang, J. Y., Zhan, Y., Yang, L., et al. (2018). Investigation of Ginkgo biloba extract (EGb 761) promotes neurovascular restoration and axonal remodeling after embolic stroke in rat using magnetic resonance imaging and histopathological analysis. *Biomed. Pharmacother.* 103, 989–1001. doi:10.1016/j.biopha.2018.04.125

Liu, L. W., Shi, Y. Y., Li, Z. L., Zuo, L. H., Tang, M., Jing, Z. W., et al. (2020). Metabolomic insights into the synergistic effect of biapenem in combination with Xuebijing injection against sepsis. *Front. Pharmacol.* 11, 502. doi:10.3389/fphar.2020.00502

Matyash, V., Liebisch, G., Kurzchalia, T. V., Shevchenko, A., and Schwudke, D. (2008). Lipid extraction by methyl-tert-butyl ether for high-throughput lipidomics. *J. Lipid Res.* 49, 1137–1146. doi:10.1194/jlr.D700041-JLR200

Mesa-Herrera, F., Taoro-González, L., Valdés-Baizabal, C., Diaz, M., and Marín, R. (2019). Lipid and lipid raft alteration in aging and neurodegenerative diseases: A window for the development of new biomarkers. *Int. J. Mol. Sci.* 20, 3810. doi:10.3390/ijms20153810

Nowak, A., Kojder, K., Zielonka-Brzezicka, J., Wróbel, J., Bosiacki, M., Fabiańska, M., et al. (2021). The use of Ginkgo biloba L. as a neuroprotective agent in the Alzheimer's disease. *Front. Pharmacol.* 12, 775034. doi:10.3389/fphar.2021.775034

Peña-Bautista, C., Álvarez-Sánchez, L., Roca, M., García-Vallés, L., Baquero, M., and Cháfer-Pericás, C. (2022). Plasma lipidomics approach in early and specific Alzheimer's disease diagnosis. *J. Clin. Med.* 11, 5030. doi:10.3390/jcm11175030

Poddar, M. K., Banerjee, S., Chakraborty, A., and Dutta, D. (2021). Metabolic disorder in Alzheimer's disease. *Metab. Brain Dis.* 36, 781–813. doi:10.1007/s11011-021-00673-z

Pralhada Rao, R., Vaidyanathan, N., Rengasamy, M., Mammen Oommen, A., Somaiya, N., and Jagannath, M. R. (2013). Sphingolipid metabolic pathway: An overview of major roles played in human diseases. *J. Lipids* 2013, 178910. doi:10.1155/2013/178910

Rahman, A. (2009). The role of adenosine in Alzheimer's disease. *Curr. Neuropharmacol.* 7, 207–216. doi:10.2174/157015909789152119

Rushworth, J. V., and Hooper, N. M. (2010). Lipid rafts: Linking Alzheimer's amyloid-β production, aggregation, and toxicity at neuronal membranes. *Int. J. Alzheimers Dis.* 2011, 603052. doi:10.4061/2011/603052

Savaskan, E., Mueller, H., Hoerr, R., von Gunten, A., and Gauthier, S. (2018). Treatment effects of ginkgo biloba extract EGb 761® on the spectrum of behavioral and psychological symptoms of dementia: meta-analysis of randomized controlled trials. *Int. Psychogeriatr.* 30, 285–293. doi:10.1017/S1041610217001892

Scheltens, P., De Strooper, B., Kivipelto, M., Holstege, H., Chételat, G., Teunissen, C. E., et al. (2021). Alzheimer's disease. *Lancet* 397, 1577–1590. doi:10.1016/S0140-6736(20)32205-4

Sun, Z. K., Yang, H. Q., and Chen, S. D. (2013). Traditional Chinese medicine: A promising candidate for the treatment of Alzheimer's disease. *Transl. Neurodegener.* 2, 6. doi:10.1186/2047-9158-2-6

Suresh, S., Begum, R. F., Singh, S. A., and Chitra, V. (2022). Anthocyanin as a therapeutic in Alzheimer's disease: A systematic review of preclinical evidences. *Ageing Res. Rev.* 76, 101595. doi:10.1016/j.arr.2022.101595

Tabassum, N-E., Das, R., Lami, M. S., Chakraborty, A. J., Mitra, S., Tallei, T. E., et al. (2022). Ginkgo biloba: A treasure of functional phytochemicals with multimedicinal applications. *Evid. Based Complement. Altern. Med.* 2022, 8288818. doi:10.1155/2022/8288818

Takasugi, N., Sasaki, T., Suzuki, K., Osawa, S., Isshiki, H., Hori, Y., et al. (2011). BACE1 activity is modulated by cell-associated sphingosine-1-phosphate. *J. Neurosci.* 31, 6850–6857. doi:10.1523/JNEUROSCI.6467-10.2011

Toledo, J. B., Arnold, M., Kastenmüller, G., Chang, R., Baillie, R. A., Han, X., et al. (2017). Metabolic network failures in Alzheimer's disease: A biochemical road map. *Alzheimers Dement.* 13, 965–984. doi:10.1016/j.jalz.2017.01.020

Touboul, D., and Gaudin, M. (2014). Lipidomics of Alzheimer's disease. *Bioanalysis* 6, 541–561. doi:10.4155/bio.13.346

Varma, V. R., Oommen, A. M., Varma, S., Casanova, R., An, Y., Andrews, R. M., et al. (2018). Brain and blood metabolite signatures of pathology and progression in alzheimer disease: A targeted metabolomics study. *PLoS Med.* 15, e1002482. doi:10.1371/journal.pmed.1002482

Wang, Y. Y., Sun, Y. P., Luo, Y. M., Peng, D. H., Li, X., Yang, B. Y., et al. (2021). Biomarkers for the clinical diagnosis of Alzheimer's disease: Metabolomics analysis of brain tissue and blood. *Front. Pharmacol.* 12, 700587. doi:10.3389/fphar.2021.700587

Wang, Z., Zhang, J., Ren, T., and Dong, Z. (2016). Targeted metabolomic profiling of cardioprotective effect of Ginkgo biloba L. extract on myocardial ischemia in rats. *Phytomedicine* 23, 621–631. doi:10.1016/j.phymed.2016.03.005

Watanabe, Y., Kasuga, K., Tokutake, T., Kitamura, K., Ikeuchi, T., and Nakamura, K. (2021). Alterations in glycerolipid and fatty acid metabolic pathways in Alzheimer's disease identified by urinary metabolic profiling: A pilot study. *Front. Neurol.* 12, 719159. doi:10.3389/fneur.2021.719159

Whiley, L., Sen, A., Heaton, J., Proitsi, P., García-Gómez, D., Leung, R., et al. (2014). Evidence of altered phosphatidylcholine metabolism in Alzheimer's disease. *Neurobiol. Aging* 35, 271–278. doi:10.1016/j.neurobiolaging.2013.08.001

Wong, M. W., Braidy, N., Poljak, A., Pickford, R., Thambisetty, M., and Sachdev, P. S. (2017). Dysregulation of lipids in Alzheimer's disease and their role as potential biomarkers. *Alzheimers Demen* 13, 810–827. doi:10.1016/j.jalz.2017.01.008

Wong, W. (2020). Economic burden of Alzheimer disease and managed care considerations. *Am. J. Manag. Care* 26, S177–S183. doi:10.37765/ajmc.2020.88482

Yi, M., Zhang, C., Zhang, Z., Yi, P., Xu, P., Huang, J., et al. (2020). Integrated metabolomic and lipidomic analysis reveals the neuroprotective mechanisms of Bushen Tiansui formula in an Aβ1-42-induced rat model of Alzheimer's Disease. *Oxid. Med. Cell Longev.* 2020, 5243453. doi:10.1155/2020/5243453

Yu, D., Zhang, P., Li, J., Liu, T., Zhang, Y., Wang, Q., et al. (2021). Neuroprotective effects of Ginkgo biloba dropping pills in Parkinson's disease. *J. Pharm. Anal.* 11, 220–231. doi:10.1016/j.jpha.2020.06.002

Zlomuzica, A., Dere, D., Binder, S., De Souza Silva, M. A., Huston, J. P., and Dere, E. (2016). Neuronal histamine and cognitive symptoms in Alzheimer's disease. *Neuropharmacology* 106, 135–145. doi:10.1016/j.neuropharm.2015.05.007

frontiers | Frontiers in Pharmacology

TYPE Original Research
PUBLISHED 11 January 2023
DOI 10.3389/fphar.2022.1104954

OPEN ACCESS

EDITED BY
Yi Wang,
Zhejiang University, China

REVIEWED BY
Yue Ding,
Shanghai University of Traditional Chinese Medicine, China
Ran Liu,
Shenzhen Polytechnic, China

*CORRESPONDENCE
Lihua Zuo,
zuolihua2013@126.com

†These authors have contributed equally to this work

SPECIALTY SECTION
This article was submitted to Neuropharmacology, a section of the journal Frontiers in Pharmacology

RECEIVED 22 November 2022
ACCEPTED 30 December 2022
PUBLISHED 11 January 2023

CITATION
Zhou S, Liu L, Zhang Y, Zhang Z, Li H, Fan F, He J, Kang J and Zuo L (2023), Integrated untargeted and targeted metabolomics to reveal therapeutic effect and mechanism of *Alpiniae oxyphyllae* fructus on Alzheimer's disease in APP/PS1 mice. *Front. Pharmacol.* 13:1104954. doi: 10.3389/fphar.2022.1104954

Integrated untargeted and targeted metabolomics to reveal therapeutic effect and mechanism of *Alpiniae oxyphyllae* fructus on Alzheimer's disease in APP/PS1 mice

Shengnan Zhou[1,2,3†], Liwei Liu[1,2,3†], Yuanyuan Zhang[1,2,3], Zhibo Zhang[1,2,3], Hanbing Li[4], Feng Fan[5], Jiuming He[6], Jian Kang[1,2,3] and Lihua Zuo[1,2,3*]

[1]Department of Pharmacy, The First Affiliated Hospital of Zhengzhou University, Zhengzhou, Henan, China, [2]Henan Key Laboratory of Precision Clinical Pharmacy, Zhengzhou, Henan, China, [3]Henan Engineering Research Center of Clinical Mass Spectrometry for Precision Medicine, Zhengzhou, Henan, China, [4]College of Pharmacy, Henan University of Traditional Chinese Medicine, Zhengzhou, Henan, China, [5]Department of Neurointerventional radiology, The First Affiliated Hospital of Zhengzhou University, Zhengzhou, Henan, China, [6]State Key Laboratory of Bioactive Substance and Function of Natural Medicines, Institute of Materia Medica, Chinese Academy of Medical Sciences and Peking Union Medical College, Beijing, China

Introduction: *Alpiniae oxyphyllae* Fructus (AOF) has been abundantly utilized for the treatment of diarrhea, dyspepsia, kidney asthenia, and abdominal pain in China. AOF is effective for treating AD in clinical trials, but its exact mode of action is yet unknown.

Methods: In this study, metabolomics was combined to ascertain the alterations in plasma metabolism in APP/PS1 transgenic mice, the therapy of AOF on model mice, and the dynamic variations in 15 bile acids (BAs) concentration.

Results: 31 differential biomarkers were finally identified in APP/PS1 group vs. the WT group. The levels of 16 metabolites like sphinganine (Sa), lyso PE (20:2), lysoPC (17:0), glycocholic acid (GCA), deoxycholicacid (DCA) were increased in APP/PS1 group, and those of 15 metabolites like phytosphingosine, cer (d18:0/14:0), and fumaric acid were reduced in APP/PS1 group. After AOF treatment, 29 of the 31 differential metabolites showed a tendency to be back-regulated, and 15 metabolites were significantly back-regulated, including sphinganine (Sa), lyso PE (20:2), glycocholic acid (GCA), deoxycholic acid (DCA). The relationship between BAs level and AD had been received increasing attention in recent years, and we also found notable differences between DCA and GCA in different groups. Therefore, a BAs-targeted metabonomic way was established to determine the level of 15 bile acids in different groups. The consequence demonstrated that primary BAs (CA, CDCA) declined in APP/PS1 model mice. After 3 months of AOF administration, CA and CDCA levels showed an upward trend. Conjugated primary bile acids (TCA, GCA, TCDCA, GCDCA), and secondary bile acids (DCA, LCA, GDCA, TDCA, TLCA GLCA) ascended in APP/PS1 group. After 3 months of AOF treatment, the levels of most BAs decreased to varying degrees. Notably, the metabolic performance of DCA and GCA in different groups was consistent with the predictions of untargeted metabolomics, validating the correctness of untargeted metabolomics.

Discussion: According to metabolic pathways of regulated metabolites, it was prompted that AOF ameliorated the symptom of AD mice probably by regulating

bile acids metabolism. This study offers a solid foundation for further research into the AOF mechanism for the therapy of AD.

KEYWORDS

Alpiniae oxyphyllae fructus, alzheimer's disease, untargeted metabolomics, targeted metabolomics, bile acids

1 Introduction

Alzheimer's disease (AD) is a neurodegenerative illness with recollection loss and cognitive abnormalities as typical symptoms (Lane et al., 2018; Weller and Budson, 2018). In recent years, the number of AD patients and the fatality rate have risen year by year. It is challenging for ordinary households to afford the treatment of AD patients (Scheltens et al., 2021). Corresponding to this severe form, the drugs currently exploited to treat AD can only relieve the syndrome and cannot be cured (Li et al., 2021). The familiar pathological features of AD include abnormal accumulation of Aβ protein, hyperphosphorylation of tau protein, and synaptic dysfunction (Ju and Tam, 2022). The chemicals of traditional Chinese medicine (TCM) are plentiful and can act on multi-targets and multi-pathways (Li et al., 2021). In the treatment of AD, TCM has received more and more attention.

Alpiniae oxyphyllae fructus (AOF), which is the dry grown-up fruit of *Alpinia oxyphylla* Miq. Has a long history of application in traditional clinical Chinese medicine (Yang et al., 2020). In traditional medicine, AOF has been widely utilized for treatment of emesis, diarrhea, frequent urination, spermatorrhea and so on (Li R. et al., 2022). Modern pharmacological research manifested that AOF had anti-oxidant (Bian et al., 2013), anti-inflammatory (Qi et al., 2019), neuroprotective (Liu et al., 2020), anti-AD (Bian et al., 2021), and other effects. AOF contains a variety of chemical components, including sesquiterpenes, volatile oils, flavonoids, diarylheptanoids, steroids, and glycosides (Chen et al., 2013; Zhang et al., 2018). At present, the efficacy of AOF in AD is remarkable, but its potential therapeutic mechanism is not clear.

By using high-throughput data analysis, metabolomics seeks to keep track of how endogenous metabolites respond dynamically to external perturbations (Nielsen, 2017). Therefore, metabolomics is often used to observe the progression of diseases and to provide information on the relationship between diseases, drugs, and metabolites. Ultra high-performance liquid chromatography-quadrupole/orbitrap high-resolution mass spectrometry (UHPLC-Q-Orbitrap HRMS) is regarded as a suitable platform for metabolomic research. The mechanism of TCM therapy for AD had been extensively explained in recent years using untargeted metabolomics (Zhang et al., 2020; Chen et al., 2022; Wang et al., 2022). Targeted metabolomics characterize high sensitivity and quantitative precision, which focuses on a particular class of metabolites. In additon, the concept of the brain-gut axis has opened up a new perspective for the prevention and treatment of AD in recent years (Cryan et al., 2019; Doifode et al., 2021). Some scholars even claim that the gut was the "second brain". The contact between the brain and the gut may be accomplished by BAs metabolism (Mulak, 2021). So, in comprehensive metabolomics, it is essential to pay attention to changes in typical BAs.

In the present study, the Morris Water Maze (MWM) test and immunohistochemical (IHC) test were utilized to evaluate the therapeutic effect of AOF on AD from behavioral and pathological perspectives, respectively. After that, the untargeted metabolomics based on UHPLC-Q-orbitrap HRMS discovered that the treatment of AD by AOF may be related to bile acid metabolism. In addition, 15 bile acids were quantified using targeted metabonomics analysis. The specific operation process of this study is shown in Figure 1. Untargeted and targeted metabolomics work together produced a highly accurate prediction of the mechanism of action of AOF in the treatment of AD. In conclusion, this study offeres additional proof that AOF can reduce AD symptoms, indicating that it may be used as a medicine to treat AD in the future.

2 Material and methods

2.1 Chemicals and materials

Alpiniae Oxyphyllae Fructus was obtained from the Henan Tongrentang Drug Co., Ltd. (Zhengzhou, China), which was authenticated by Professor Hanbing Li (Henan University of Chinese Medicine). The reference substances of oplopanone, nootkatone, and valencene were acquired from J&K Scientific Co., Ltd. (Beijing, China). The references of 15 bile acids and its isotope internal standard were purchased from Bazoe Medical Co., Ltd., containing cholic acid (CA), chenodeoxycholic acid (CDCA), taurocholic acid (TCA), glycocholic acid (GCA), taurochenodeoxycholic acid (TCDCA), glycoursodeoxycholic acid (GCDCA), deoxycholic acid (DCA), ursodeoxycholic acid (UDCA), lithocholic acid (LCA), taurodeoxycholic acid (TDCA), tauroursodeoxycholic acid (TUDCA), Glycoursodeoxycholic acid (GUDCA), Glycolithocholic acid (GLCA), taurolithocholic acid (TLCA), CA-d4, DCA-d4, LCA-d4, GLCA-d4, TCA-d5, TLCA-d5, TCDCA-d5 and GCA-d4. Purity of all standards is more than 98%. Donepezil hydrochloride were purchased from J&K Scientific Co., Ltd. (Beijing, China). The HPLC grade acetonitrile and methanol were obtained from Fisher Scientific (Pittsburgh, PA, United States of America). HPLC-grade formic acid was obtained from the Aladdin Industrial Corporation (Shanghai, China). There were also other analytical-grade chemicals and reagents.

2.2 Animals

APP/PS1 male mice (B6C3-Tg) and wild type (WT) littermates (both were 6 months old, 30–40 g in weight) were acquired from Huachuang Sino Pharmaceutical Technology Co., LTD. (Jiangsu, China). For 1 week before the experiment, all animals were kept at a constant temperature of 25°C, 65% humidity, and a 12-h light/dark cycle. After 7 days, the APP/PS1 mice were erratically separated into APP/PS1 ($n = 6$), APP/PS1+Donepezil ($n = 6$), APP/PS1+AOF ($n = 6$). The littermate wild-type mice served as the WT group ($n = 6$). Mice in the APP/PS1+Donepezil group were given donepezil orally (1 mg/kg) for 3 months. The APP/PS1+AOF group and was administrated with AOF at 0.5 g/kg for 3 months. In this work, the dosage was established

using the dose conversion coefficient between mice and humans (Zuo et al., 2021). Saline solution (5 mL/kg/d) was intragastrically administered to the APP/PS1 group and the WT group for 3 months. All animal experimentation protocols adhered to the Experimental Animal Administration Regulations, and the operations were assented to by the Animal Ethics Committee of Zhengzhou University (No. ZZU-LAC20220225 [13]).

2.3 Preparation of AOF extract

AOF was elaborated by refluxing extraction way. The AOF was crushed and then passed through a 40-mesh sieve. 100 g AOF powder was precisely weighed, 10 times 95% ethanol was added, soaked for 1 h, and extracted at reflux for 1 h. The residue was extracted twice with 95% ethanol. Then the combined extracts were filtered, mixed, and dried under low pressure after being evaporated. The solution (1.0 g/mL) was made by adding methanol with the necessary amount of freeze-dried AOF powder and then put into an ultrasonic disperser for 10 min. The prepared solution was filtered by 0.22 μm membrane before entering to UHPLC-MS/MS system.

2.4 Morris water maze test

The MWM studies were conducted to assess the mice in each group's capacity for spatial learning and memory following the final treatment (Li et al., 2022a). The experimental apparatus consists of a circular pool filled with opaque water (diameter 120, height 40), a circular target platform, and an image acquisition system. The target platform should be positioned in the middle of one of the pool's four identically sized quadrants. Before the start of the experiment, opaque water 2 cm higher than the target platform was injected into the pool, and the water temperature was maintained at about 25°C ± 2°C. The MWM experiment is divided into two parts: the positioning and navigation test and the space exploration test. The day before the test, mice were arbitrarily swum in water for 3 min to adapt to the environment. The positioning and navigation experiment lasted for 5 days. Each mouse was placed in the water from two different quadrants every day, allowing it to freely find the target platform. Calculate the escape latency time by timing how long each mouse took to find the platform. On the sixth day, a space exploration experiment was carried out to investigate the memory ability of each group of mice. The platform was removed and the mice were forced to swim from two different quadrants. The time spent in the target quadrant and crossing times were recorded and analyzed by the SANS video tracking system (SA201, Jiangsu, China). Continuous intragastric administration during this experiment. Finally, all experimental data of MWM were statistically analyzed by GraphPad Prism 9.4.1 software. The Student's t-test was employed to compare the two groups, while the ANOVA was utilized to compare multiple groups. All data were displayed in means ± standard deviation (Mean ± SD). $p < 0.05$ was treated as a statistically observable difference.

2.5 Sample collection

The animals underwent a one-night fast, anesthesia, heart puncture blood collection, and 5% sodium heparin anticoagulation after the MWM experiment. After centrifuging at 3500 rpm for 10 min by 4°C centrifuge, the supernatant plasma was transferred for metabolomic analysis. After the blood is taken, the skull is opened and the whole brain is removed, immersed in 4% paraformaldehyde (PFA) for further immunohistochemistry (IHC) assay.

2.6 Immunohistochemistry

Immunohistochemistry (IHC) was used to assess pathological alterations in the mouse's brain's cortex and hippocampus. The brain tissue was sectioned and fixed in paraffin. Then gradually started the following operations. 1) Paraffin sections were dewaxed and hydrated by xylene and gradient ethanol. 2) To repair the antigens, the sections were submerged in citric acid (pH 6.0) antigen repair solution. 3) 3% H_2O_2 was added to block endogenous peroxidase. 4) The tissue was uniformly covered with 3% BSA in the tissue ring and closed at room temperature for 30min. 5) Add 1:500 diluted rabbit anti-beta-amyloid dropwise. 6) Slides were washed 3 times with shaking in PBS (pH 7.4) for 5 min each time. Subsequently, goat anti-rabbit IgG (1:200, HRP labeled) was added to the circle, and incubate at room temperature for 50min. 7) Add DAB coloring solution, positive for brownish yellow. 8) The cell nucleus was restained with hematoxylin and dehydrated. 9) Microscopic examination, image collection, and analysis.

2.7 Plasma untargeted metabolomics

2.7.1 UHPLC-Q-orbitrap HRMS method

In the qualitative profiling of AOF extracts and plasma untargeted metabolomics, an UHPLC-Q-orbitrap HRMS system was utilized. The column adopted a Waters ACQUITY UPLC HSS T3 column (2.1 × 100 mm, 1.8 μm) adhered to 40°C of the column oven temperature. The mobile phase consisted of pure water with 0.1% (v/v) formic acid A) and acetonitrile B). The gradient elution was set as follows: For qualitative profiling of AOF extracts 0–3.0 min, 5% B; 3.0–35 min, 5.0%–25% B; 35–43 min, 25%–40% B; 43–53 min, 40%–100% B; 53–57 min, 100% B; 57.1–60 min, 5% B; For plasma untargeted metabolomics: 0–1.0 min, 5% B; 1.0–9.0 min, 5%–100% B; 9.0–12.0 min, 100% B, 12.0–12.1, 100%–5% B, 12.1–15 min, 5% B; The flow rate and injection volume were 0.3 mL/min and 5 μl, respectively.

The optimized MS function was as follows: ion spray voltage, +3.5 kV and −2.8 kV; the ion source temperature was 350°C; the capillary mperature was 320°C; auxiliary gas flow rate, 10 arb; the sheath gas flow rate, +40 arb and -38 arb; the scan range was from 80 to 1200 m/*z* in all ion modes. The resolution of full MS scan and dd-MS^2 scan were 70,000 and 17,500, respecively. Nitrogen as the collision gas was used to stabilize the spray.

2.7.2 Blood sample preparation

The plasma samples were taken out of the −80°C refrigerator and melted on ice. The 150 μl aliquot of ice-cold methanol (containing 500 ng/mL, ketoprofen +50 ng/mL, 2-chloro-L-phenylalanine) was deposited with a 50 μl plasma sample. Then the mixture was vortexed for 1 min and centrifuged for 10 min at 13,300 rpm. Finally, transferred the supernatant to the sample vial. The order of injection of samples was random. The QC sample was collected from an equal volume of each plasma sample. And every five sample runs in the analytical batch, a QC sample was examined to evaluate the robustness of the analytical platform.

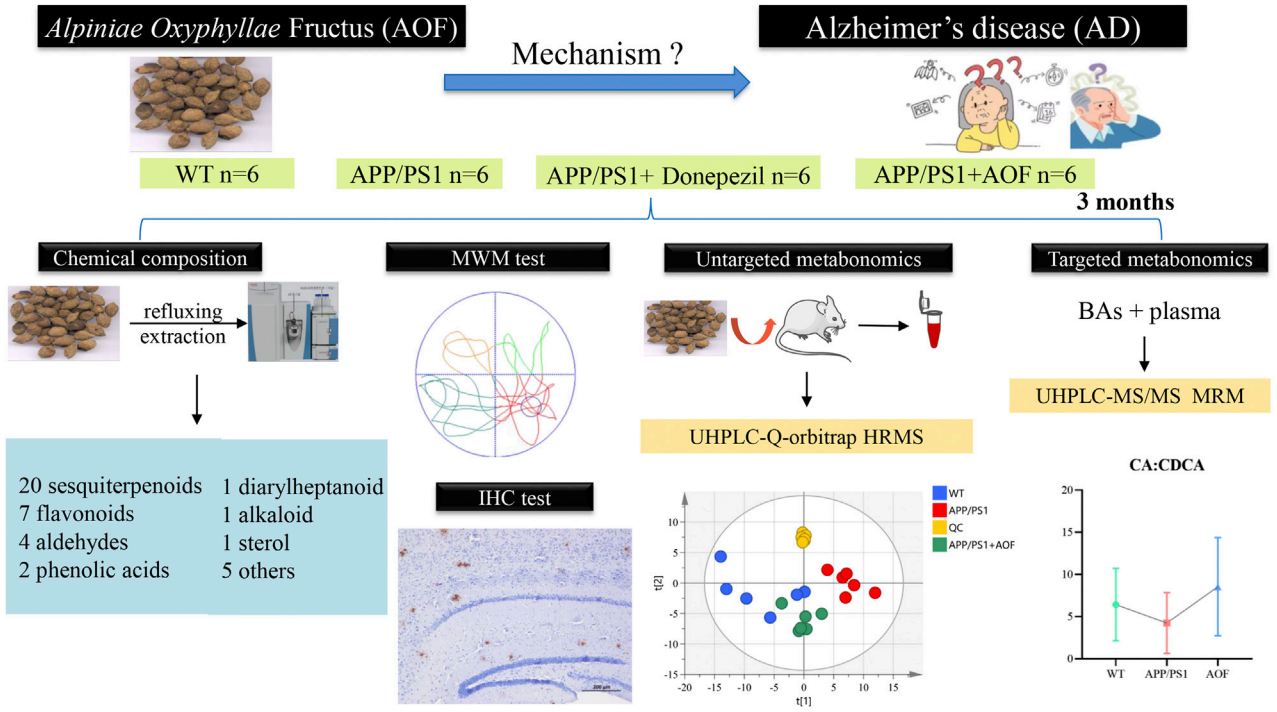

FIGURE 1
The flow chart of the whole experiment.

2.7.3 Data processing and statistical analysis

For the untargeted metabolomic analysis, UHPLC-Q-orbitrap HRMS data was processed by Compound Discoverer (CD) 3.3 software for peak alignment. CD provided a data matrix containing retention time, accurate relative molecular mass, and peak area of each compound. Subsequently, this data matrix was used for multivariate statistical analysis by SIMICA software (version 14.1, Umetrics, Sweden). To understand the changes in overall metabolism, evaluate the stability of QC samples, and filtered out the outliers, PCA analysis was used to process the data matrix. The OPLS-DA was used to specifically observe the separation between the two groups. 200 permutations test was utilized to appraise the validity of the OPLS-DA model. The features with variable importance in the projection (VIP) > 1.0 and p-value <0.05 were deemed as potential differential metabolites.

2.8 Targeted metabolomics analysis of bile acids

2.8.1 UHPLC-MS/MS -MRM method

In the quantitative analysis of fifteen bile acids, an UHPLC-MS/MS system was employed. Chromatographic separation occurred in a Waters ACQUITY UPLC® BEH C_{18} column (2.1 mm × 50 mm, 1.7 μm). The flow rate was 0.6 mL/min. A (water) and a mixture of B (acetonitrile containing 2% water, 0.2% ammonium formate (1 mol/L), and 0.05% ammonia water) made up the mobile phase. The gradient elution procedure was as follows: 30% B (0–0.6 min), 30%–40% B (0.6–2.6 min), 40%–95% B (2.6–3.0 min), 95% B (3.0–3.5 min), 95%–24.5% B (3.5–3.8 min), and continuing at 24.5% B up to 7.0 min. For all samples and standard solutions, the injection volume was 5 μl.

The AB SCIEX™ × 3200 spectrometer (Foster City, CA) equipped with a Shimadzu Prominence UHPLC (Pleasanton, CA). The mass spectrometer was run in the ESI^- mode with multiple reaction monitoring (MRM). The column temperature and sample tray temperature were 55°C and 8°C. The parameters were as follows: ion spray voltage was set at −4.5 kV, source temperature maintained at 500°C, and the flow of ion source gas1 (GS1) and ion source gas2 (GS2) were 40 L/h and 60 L/h, respectively. The transitions and collision energy levels of 15 BAs are lsited in Supplementary Table S2.

2.8.2 Standard stock solutions preparation

Each bile acid was individually dissolved in the suitable ratio of 50% methanol to produce the stock standard solutions (1.0 mg/mL). The final mixed standard solution was created by combining each stock solution with 50% methanol. The mixture of standard solutions was successively diluted with 50% methanol to generate several working standard solutions. The middle solution was then constantly diluted in 50% acetonitrile to obtain working solutions involving 80, 160, 320, 640, 1280, 2560, and 5120 ng/mL of CA, DCA, CDCA, LCA, GCA, GLCA, GCDCA, TLCA, TDCA, TCDCA, TUDCA; Low, medium and high concentrations of these acids were 480, 960, and 1920 ng/mL 40, 80, 160, 320, 640, 1280, and 2560 ng/mL of GUDCA, UDCA, GDCA, and TCA; Low, medium, and high concentrations of these bile acids were 240, 480, and 960 ng/mL.

2.8.3 Data acquisition and processing

The Analyst® 1.6.2 application (AB SCIEX™, Foster City, CA) was used for acquiring and integrating data. The software allows the exported data to be saved in the proper folder.

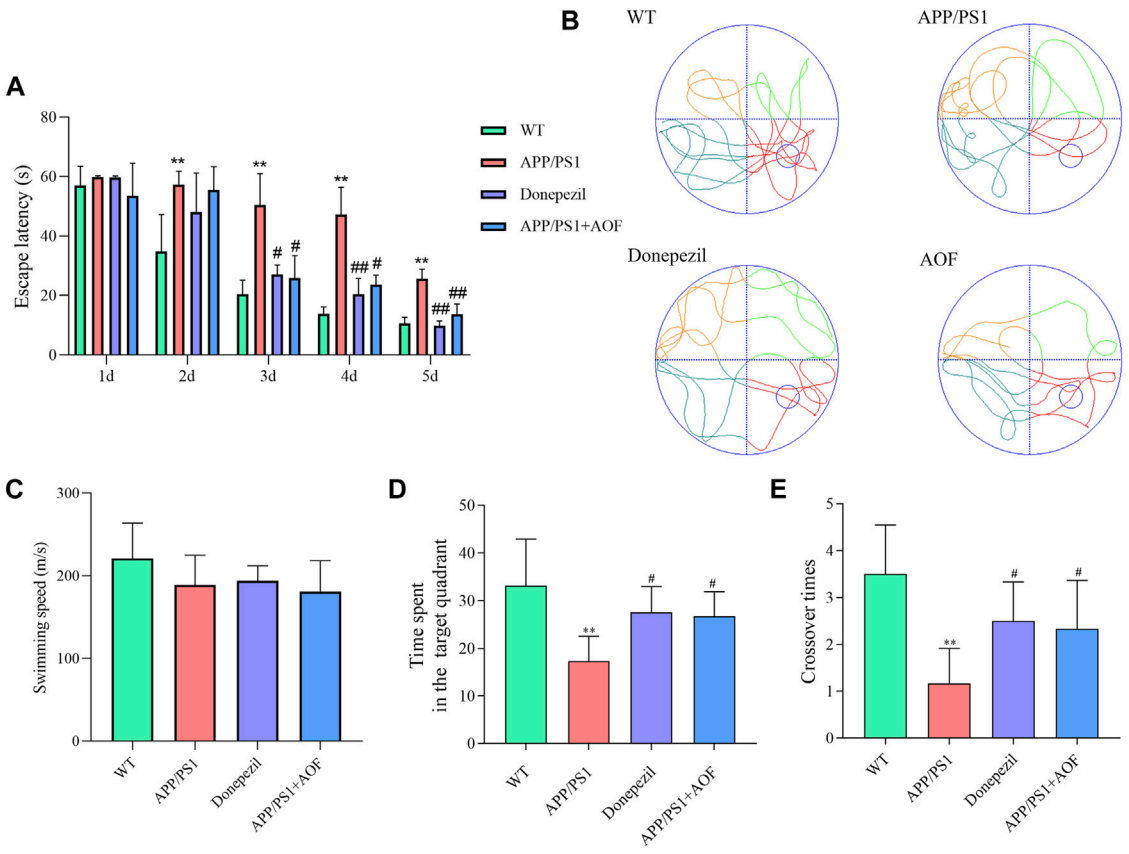

FIGURE 2
Effect of AOF on APP/PS1 mice in MWM. **(A)** Escape latency in directional navigation experiment. **(B)** Representative images of swimming trajectories. **(C)** The swimming speeds of mice in different groups **(D)** Time in the target quadrant in spatial probe task. **(E)** Number of platform crossings in spatial probe task. $^{*}p < 0.05$, $^{**}p < 0.01$, compared with WT group; $^{\#}p < 0.05$, $^{\#\#}p < 0.01$, compared with APP/PS1 group.

3 Results

3.1 Identification of the chemical composition of AOF

The base peak intensity (BPI) chromatograms demonstrate in Supplementary Figure S1. A total of 41 compounds were identified from AOF (Supplementary Table S1), including 20 sesquiterpenoids, seven flavonoids, 4 aldehydes, 2 phenolic acids, 1 diarylheptanoid, 1 alkaloid, 1 sterol, and 5 others. As the main characteristic chemical components of AOF, sesquiterpenoids are closely related to the neuroprotective effect. The 20 sesquiterpenoids found in this study included seven eudesmane sesquiterpenoids, seven eremophilane sesquiterpenoids, 5 cadinane sesquiterpenoids, and 1 oplopanone sesquiterpenoids.

3.2 AOF improves learning and memorizing abilities of APP/PS1 model mice

To investigate the influence of AOF on learning and memorizing abilities in AD mice, MWM was carried out 3 months after administration. As shown in Figure 2A, in the previous directional navigation experiment, with the extension of training days, the escape latency of all groups gradually declines. In addition, from the day 2, the escape latency of the APP/PS1 model group was longer than that of the WT group ($p < 0.01$).

On the day 3, compared with APP/PS1 model group, the escape latency of the APP/PS1+Donepezil group and APP/PS1+AOF began to decrease ($p < 0.05$). The escape latency of the APP/PS1+Donepezil group significantly decreased on days 4 and 5 of treatment ($p < 0.01$). Although the effect of AOF on the escape latency was not as fast as the positive drug, but the escape latency of APP/PS1+AOF was also observably decreased on the day 5 ($p < 0.01$). As shown in Figure 2B, the swimming trajectories of the WT group were complex, but the APP/PS1 group was single and clear. There was no difference in average swimming speed among all groups (Figure 2C). In the spatial probe task, compared with the WT group, the time spent in the target quadrant and the number of platform crossings of the APP/PS1 model group were markedly reduced ($p < 0.01$). After AOF treatment, both indicators of model mice were improved ($p < 0.05$). To sum up, these results proved that oral AOF can alleviate cognitive impairment in APP/PS1 mice.

3.3 AOF relieves the Aβ deposition in the brain of APP/PS1 mice

After the MWM experiment, all brain tissues were collected for the IHC test. The expressions of Aβ proteins in the

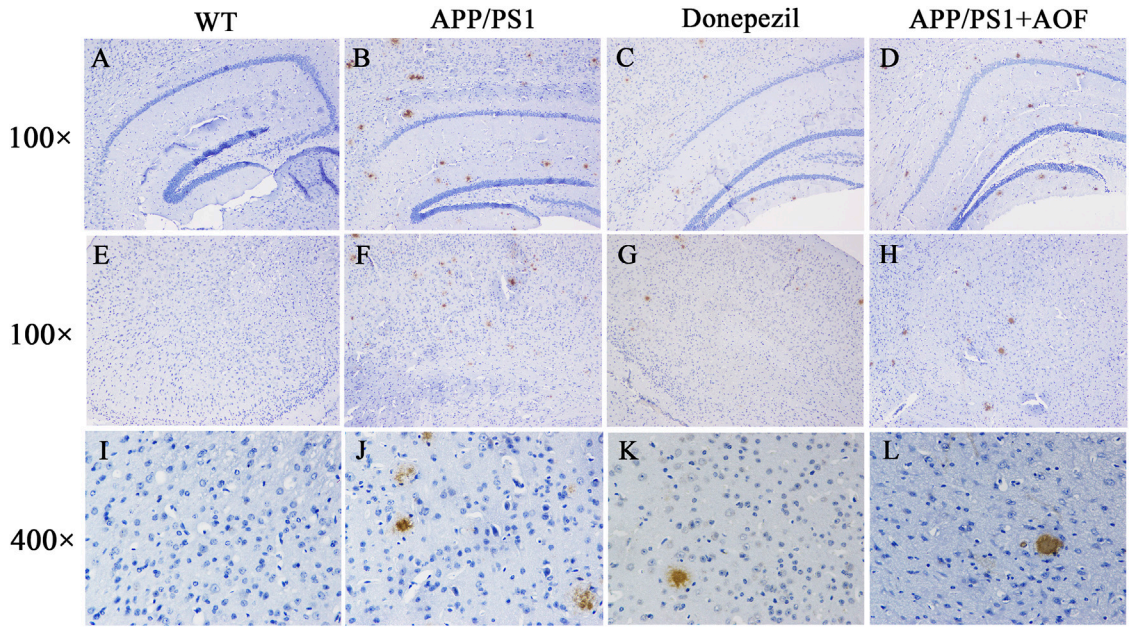

FIGURE 3
Effect of AOF on APP/PS1 mice in IHC test. **(A–D)** DAB-stained Aβ plaques in the hippocampal region (100×) of WT, APP/PS1, APP/PS1+ Donepezil, APP/PS1+AOF groups. **(E–H)** DAB-stained Aβ plaques in the cortex (100×) of WT, APP/PS1, APP/PS1+ Donepezil, APP/PS1+AOF groups. **(I–L)** Amplified views (400×) of the cortex in each group. WT, APP/PS1, APP/PS1+ Donepezil, APP/PS1+AOF groups.

hippocampus and cerebral cortex of 4 groups were observed and compared by IHC. As shown in Figure 3 (AB, DE, IJ), compared with the WT group, Aβ plaques were clearly increased in the hippocampus and cortex of the APP/PS1 group. After AOF treatment in 3 months, The Aβ plaques of brain tissue were significantly reduced Figure 3 (BD, FH, JL), displaying an alike result as the mice of APP/PS1+Donepezil group.

3.4 Untargeted plasma metabonomics results

3.4.1 Multivariate statistical analysis of plasma metabolites

UHPLC-Q-Orbitrap HRMS was utilized to explore the plasma metabolic profiles of WT, APP/PS1, and AOF mice in ESI^+ and ESI^- modes. To study the changes in the overall metabolism of each group, unsupervised PCA analysis was firstly used to evaluate the mass spectrometry data. As shown inSupplementary Figure S2**,** the WT group, APP/PS1 group, and AOF group showed a significant tendency of separation. The QC samples are clustered together, which indicates the stability of the analytical instrument. Then, we used OPLS-DA to specifically observe the separation between the two groups. As shown in an OPLS-DA score, there was a clear separation in APP/PS1 group vs. WT group (Figures 4A,B) and AOF group vs. APP/PS1 group (Figures 4E,F). In addition, 200 permutation tests were utilized to check the above OPLS-DA model, and the outcomes demonstrate that the model has an excellent fitting degree and excellent prediction ability (Figures 4C,D; Figure 4 G, H).

3.4.2 Differential metabolite identification and analysis

With the UHPLC-Q-Orbitrap HRMS metabolomics platform, 115 ion peaks were found in APP/PS1 group vs. the WT group by VIP values >1.0 and p values <0.05. Subsequently, 31 endogenous differential metabolites were defined in APP/PS1 group vs. WT group (Table 1). The levels of 16 metabolites like sphinganine, and lyso PE (20:2), lysoPC(17:0), glycocholic acid (GCA), deoxycholic acid (DCA) were increased in APP/PS1 group, and those of 15 metabolites like phytosphingosine, cer (d18:0/14:0), and fumaric acid were reduced in APP/PS1 group. As shown in Table 1, when AOF was administered for 3 months, 94% (29/31) of the metabolites had a tendency to retract and 48% (15/31) had a significant retract ($p < 0.05$).

To more vividly show the changes of metabolites in plasma between different groups, Origin 2021 was used for heat mapping (Figure 5). The difference between the groups is obvious according to the color. Compared with the WT group, the metabolites of the APP/PS1 group displayed a different color trend. It is worth noting that most of the dysregulated metabolites were improved after the administration of AOF. The above differential metabolite results indicated that AOF could reverse the metabolic abnormalities in model mice.

Furthermore, the differential metabolites were classified by HMDB. The classification results are displayed in pie charts. As shown in Figure 6A and Table 2, the different colors and areas represent different HMDB classifications and metabolite numbers. The results demonstrated that the 31 differential metabolites included 17 lipids and lipid-like molecules, 9 organic acids and derivatives, 2 organoheterocyclic compounds, 2 organic nitrogen compounds, 1 nucleosides, nucleotides, and analogues. The pie chart of the

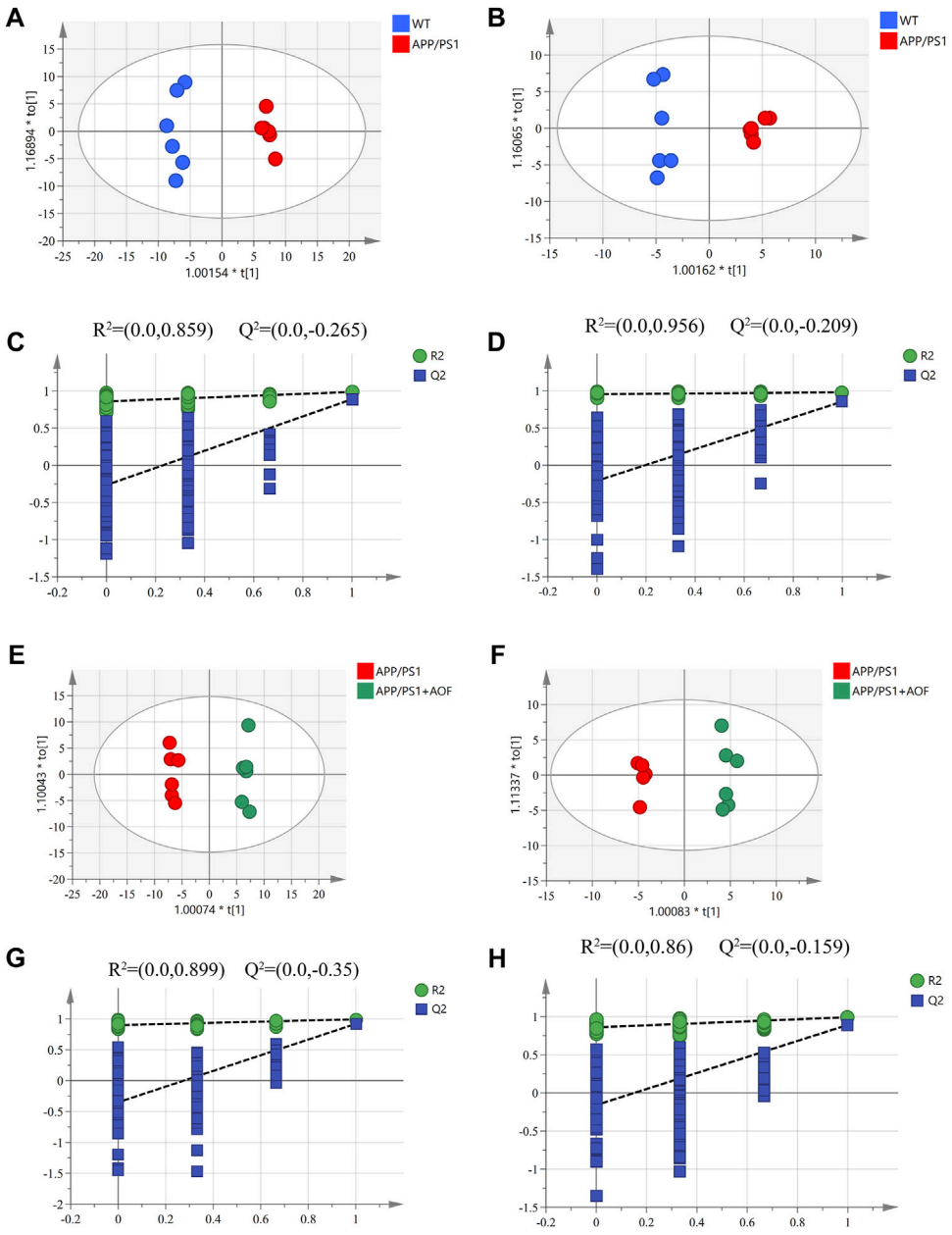

FIGURE 4
Multivariate statistical analysis of the plasma metabolites. (**A–B**) OPLS-DA score plots for APP/PS1 vs. WT in ESI$^+$ and ESI$^-$ ion mode. (**C–D**) 200 permutation tests for APP/PS1 vs. WT in ESI$^+$ and ESI$^-$ ion mode. (**E–F**) OPLS-DA score plots for APP/PS1+AOF vs. APP/PS1 in ESI$^+$ and ESI$^-$ ion mode. (**G–H**) 200 permutation tests for APP/PS1+AOF vs. APP/PS1 in ESI$^+$ and ESI$^-$ ion mode.

15 metabolites significantly regulated by AOF was shown in Figure 6B. Of the 15 metabolites significantly regulated by AOF, 2 metabolites (DCA, GCA) were classified as bile acids, alcohols and derivatives.

3.4.3 Metabolic pathway analysis

To explore the potential mechanism of AOF in alleviating AD symptoms, the differential metabolites in each group were introduced into Metabo Analyst 5.0 for further biological analysis. The 31 differential metabolites in APP/PS1 vs. WT were mainly enriched in sphingolipid metabolism, phenylalanine, tyrosine and tryptophan biosynthesis, tyrosine metabolism, TCA cycle, lysine degradation, glycerophospholipid metabolism, primary bile acid biosynthesis (Figure 7A). Compared with the APP/PS1 group, significantly callback metabolites in the APP/PS1+AOF group were mainly participate in sphingolipid metabolism, TCA cycle, glycerophospholipid metabolism, tyrosine metabolism, and primary bile acid biosynthesis (Figure 7B). Subsequently, the information on differential metabolites and metabolic pathways was integrated to construct a comprehensive network metabolic map for the AOF treatment of AD (Figure 8). This figure clearly shows the changes and associations of various metabolites in APP/PS1 vs. WT, and APP/PS1+AOF vs. APP/PS1. It should be noted that the metabolic disorders and the improvement of AOF were closely related to the metabolic pathway of BAs.

10.3389/fphar.2022.1104954

TABLE 1 Differential metabolites between APP/PS1 vs. WT and the callback function of AOF.

Ion mode	Metabolite	Formula	ppm	*m/z*	Rt	APP/PS1/WT	AOF/ApP/PS1
ESI+	3-Oxalomalic acid	$C_6H_6O_8$	2.44	206.0068	0.809	↑*	↓
	Aminoadipic acid	$C_6H_{11}NO_4$	−0.16	161.0688	0.868	↓*	↑
	N6-Acetyl-L-lysine	$C_8H_{16}N_2O_3$	−1.24	188.1159	1.272	↓*	↑
	Nicotinic acid	$C_6H_5NO_2$	0.58	123.0321	1.273	↓*	↑#
	Adenine	$C_5H_5N_5$	2.17	135.0548	1.329	↓*	↑#
	Adenosine	$C_{10}H_{13}N_5O_4$	−1.13	267.0965	1.331	↓*	↑#
	Aspartyl-Leucine	$C_{10}H_{18}N_2O_5$	−0.52	246.12144	2.258	↓*	↑
	Phytosphingosine	$C_{18}H_{39}NO_3$	-2.41	317.2922	7.258	↓*	↑
	Sphinganine	$C_{18}H_{39}NO_2$	−2.29	301.2974	7.565	↑*	↓##
	Sphinganine 1-phosphate	$C_{18}H_{40}NO_5P$	−1.97	381.2637	7.811	↑**	↓
	LysoPE (20:2)	$C_{25}H_{48}NO_7P$	1.61	505.3177	8.383	↑*	↓##
	LysoPC(17:0)	$C_{25}H_{52}NO_7P$	−0.52	509.3479	9.667	↑*	↓#
	Cer(d18:0/14:0)	$C_{32}H_{65}NO_3$	−1.34	511.4958	9.675	↓*	↑
	Linoleamide	$C_{18}H_{33}NO$	−1.95	279.2557	9.784	↑**	↓##
	Oleamide	$C_{18}H_{35}NO$	−1.99	281.2713	10.35	↑*	↓##
	Hexadecanamide	$C_{16}H_{33}NO$	−2.05	255.2557	11.103	↓*	↓
ESI-	Fumaric acid	$C_4H_4O_4$	−10.46	116.0097	0.929	↓*	↑#
	N-Acetyl-L-glutamic acid	$C_7H_{11}NO_5$	−4.16	189.0629	1.363	↓*	↑
	Tyrosine	$C_9H_{11}NO_3$	−4.77	181.073	1.383	↓*	↓
	2-methylcitric acid	$C_7H_{10}O_7$	−2.98	206.042	1.392	↓*	↑
	L-gamma-Glutamyl-L-leucine	$C_{11}H_{20}N_2O_5$	−0.47	260.1371	3.565	↓*	↑
	Thromboxane B2	$C_{20}H_{34}O_6$	−0.01	370.2355	6.086	↑*	↓#
	Glycocholic acid	$C_{26}H_{43}NO_6$	−0.27	465.3089	6.369	↑*	↓##
	Sphingosine 1-phosphate	$C_{18}H_{38}NO_5P$	−0.15	379.2487	7.642	↑**	↓#
	LysoPE (22:6)	$C_{27}H_{44}NO_7P$	−1.09	525.285	8.189	↑*	↓#
	Docosahexaenoic Acid	$C_{22}H_{32}O_2$	−1.01	328.2399	8.204	↑*	↓#
	Deoxycholic acid	$C_{24}H_{40}O_4$	-0.66	392.2924	8.259	↑*	↓##
	Palmitic acid	$C_{16}H_{32}O_2$	−1.94	256.2397	8.392	↑**	↓
	Stearic acid	$C_{18}H_{36}O_2$	−1.16	284.2712	9.306	↑*	↓
	Eicosapentanoic acid	$C_{20}H_{30}O_2$	−0.32	302.2245	9.851	↑**	↓
	Tiaprost	$C_{20}H_{28}O_6S$	−1.44	396.1601	10.383	↓*	↑

3.5 Targeted metabolomics

To assess the intimacy between changes in BAs metabolism and the relief of AD symptoms by AOF, we performed targeted quantitative validation of the bile acid profile by UHPLC-MS/MS-MRM method. Primary BAs (CA, CDCA) come from cholesterol in the liver. GCA and TCA are glycine-conjugate and taurine-conjugate of CA respectively. Similarly, GCDCA and TCDCA are glycine-conjugate and taurine-conjugate of CDCA. Under the action of anaerobic bacteria, CA is converted to secondary bile acids DCA, and CDCA is converted to secondary bile acids LCA and UDCA. DCA, UDCA, and LCA are coupled with glycine and taurine to form GDCA, TDCA, GUDCA, TUDCA, GLCA, and TLCA, respectively.

In this study, a significant downward trend (($p < 0.01$)) of CA and CDCA was also found in APP/PS1 model mice (Figures 9A,B). After 3 months of AOF administration, CA and CDCA levels of APP/PS1 mice showed an upward ($p < 0.05$) trend. Conjugated primary bile acids TCA (Figure 9C, $p < 0.05$), GCA (Figure 9D, $p < 0.05$), TCDCA (Figure 9E, $p < 0.01$), GCDCA (Figure 9F, $p < 0.01$) had an upward trend in APP/PS1 group. After 3 months of AOF treatment, the metabolic disorders of TCA, GCA, TCDCA, and

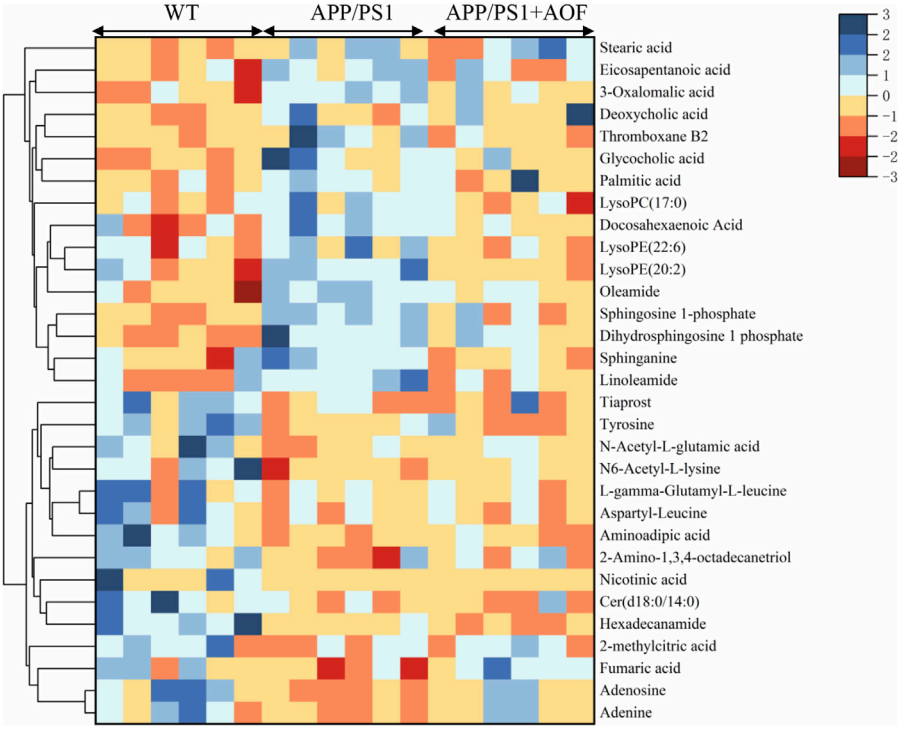

FIGURE 5
Heat map of differential metabolites in the plasma.

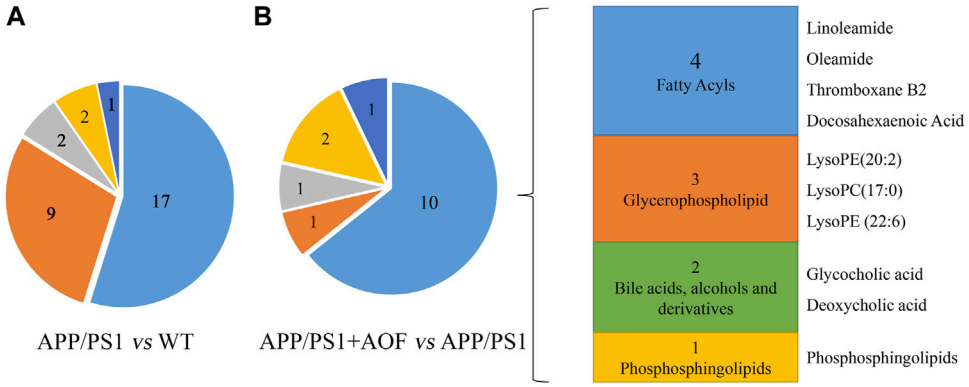

FIGURE 6
Differential metabolites were classified by HMDB database. **(A)** Differential metabolites were classified for APP/PS1 vs. WT. **(B)** Differential metabolites were classified for APP/PS1+AOF vs. APP/PS1.

GCDCA were all alleviated to different degrees. Similarly, secondary bile acids DCA (Figure 9G, $p < 0.05$), LCA (Figure 9I, $p < 0.01$), and correspondingly conjugated bile acids GDCA (Figure 9K, $p < 0.01$), TDCA (Figure 9J, $p < 0.01$), TLCA (Figure 9N, $p < 0.01$), GLCA (Figure 9O, $p < 0.05$) were elevated in the APP/PS1 group and declined in the APP/PS1+AOF group. Notably, the metabolic performance of DCA and GCA in different groups was consistent with the predictions of untargeted metabolomics, validating the correctness of untargeted metabolomics.

To explore which enzymatic processes play a key role in bile acid metabolism, we explored seven bile acid ratios in different groups of mice (Figure 10). The ratios of primary BAs to primary BAs (CA: CDCA) can reflect changes in the classical and alternative metabolic pathways of liver BAs (MahmoudianDehkordi et al., 2019). As shown in Figure 10A, CA: CDCA ratio had no significant change in the WT group and APP/PS1 group, and the callback effect was not obvious after AOF treatment. DCA: CA and LCA: CDCA is a common form of secondary bile acids: primary bile acids that reflect changes in gut microbiome enzymes. Among them,

TABLE 2 Detailed classification of differential metabolites.

A		
Linoleamide	Lipids and lipid-like molecules	Fatty Acyls
Oleamide	Lipids and lipid-like molecules	Fatty Acyls
Hexadecanamide	Lipids and lipid-like molecules	Fatty Acyls
Thromboxane B2	Lipids and lipid-like molecules	Fatty Acyls
Docosahexaenoic Acid	Lipids and lipid-like molecules	Fatty Acyls
Palmitic acid	Lipids and lipid-like molecules	Fatty Acyls
Stearic acid	Lipids and lipid-like molecules	Fatty Acyls
Eicosapentanoic acid	Lipids and lipid-like molecules	Fatty Acyls
Tiaprost	Lipids and lipid-like molecules	Fatty Acyls
LysoPE (20:2)	Lipids and lipid-like molecules	Glycerophospholipid
LysoPC(17:0/0:0)	Lipids and lipid-like molecules	Glycerophospholipid
LysoPE (22:6)	Lipids and lipid-like molecules	Glycerophospholipid
Glycocholic acid	Lipids and lipid-like molecules	Bile acids, alcohols and derivatives
Deoxycholic acid	Lipids and lipid-like molecules	Bile acids, alcohols and derivatives
Sphingosine 1-phosphate	Lipids and lipid-like molecules	Phosphosphingolipids
Dihydrosphingosine 1 phosphate	Lipids and lipid-like molecules	Phosphosphingolipids
Cer(d18:0/14:0)	Lipids and lipid-like molecules	Ceramides
B		
3-Oxalomalic acid	Organic acids and derivatives	Carboxylic acids and derivatives
L-gamma-Glutamyl-L-leucine	Organic acids and derivatives	Carboxylic acids and derivatives
Aminoadipic acid	Organic acids and derivatives	Carboxylic acids and derivatives
N6-Acetyl-L-lysine	Organic acids and derivatives	Carboxylic acids and derivatives
Aspartyl-Leucine	Organic acids and derivatives	Carboxylic acids and derivatives
2-methylcitric acid	Organic acids and derivatives	Carboxylic acids and derivatives
Fumaric acid	Organic acids and derivatives	Carboxylic acids and derivatives
N-Acetyl-L-glutamic acid	Organic acids and derivatives	Amino acids, peptides, and analogues
Tyrosine	Organic acids and derivatives	Amino acids, peptides, and analogues
C		
Sphinganine	Organic nitrogen compounds	Amines
Phytosphingosine	Organic nitrogen compounds	Amines
D		
Nicotinic acid	Organoheterocyclic compounds	Pyridinecarboxylic acids and derivatives
Adenine	Organoheterocyclic compounds	Purines and purine derivatives
E		
Adenosine	Nucleosides, nucleotides, and analogues	Purine nucleosides

DCA: CA is significantly related to the diagnosis of human Alzheimer's disease (Nho et al., 2019). In this study, significant differences in DCA: CA (Figure 10B) and LCA: CDCA (Figure 10C) values were found in plasma samples from different groups of mice. AOF can reduce DCA: CA and LCA: CDCA values in APP/PS1 mice, suggesting that AOF may slow down the progression of AD from the bile acid metabolism pathway. Finally, we investigated the effect of the combination of taurine and glycine on the dysmetabolism of secondary bile acids (Figures 10D–G). Except for TLCA: LCA, GDCA: DCA, TDCA: DCA, and GLCA: LCA had no significant association with AD, and AOF failed to significantly alter the metabolic disorder of bile acids, although there was a trend of correction.

4 Discussion

This research was the first to confirm the anti-AD effect of AOF and explore its potential mechanism by combining the overall behavioral performance, brain plaque deposition, plasma

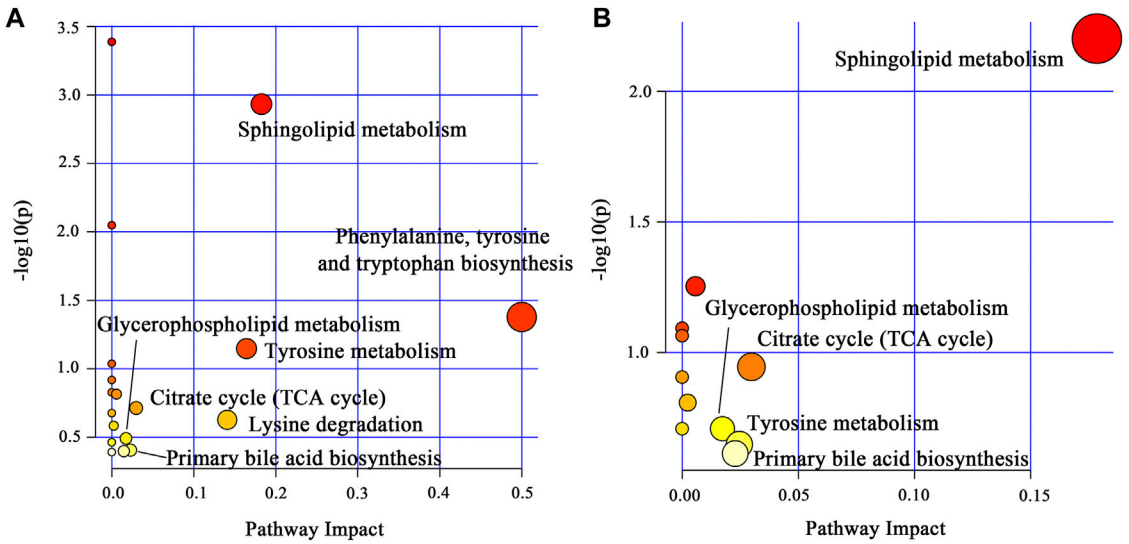

FIGURE 7
(A) Main metabolic pathways of the differential metabolites for APP/PS1 vs. WT. **(B)** Main metabolic pathways of the differential metabolites for APP/PS1+AOF vs. APP/PS1.

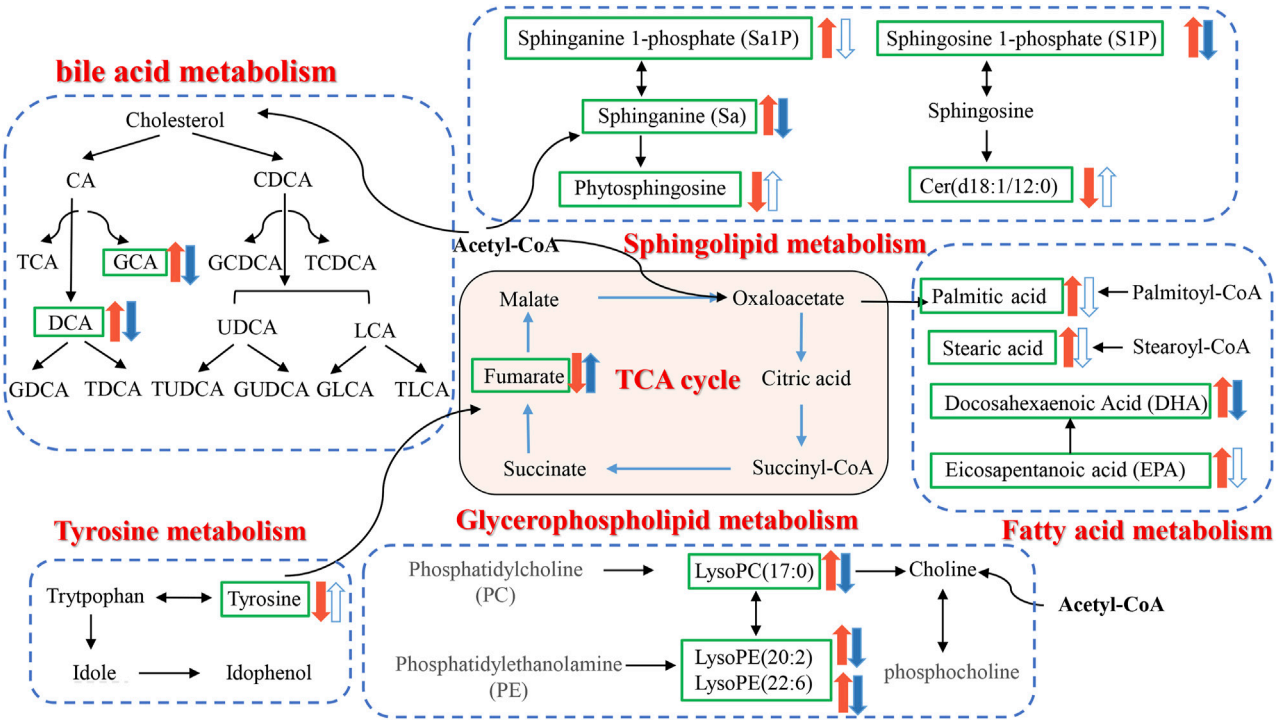

FIGURE 8
Disorder metabolic network in APP/PS1 mice and the interventional effect of AOF.

untargeted metabolomics, and targeted metabolomics results of transgenic mice. In this study, UHPLC-Q-Orbitrap HRMS was utilized to qualitatively analyze AOF, and 20 sesquiterpenoids were identified. As a characteristic component of AOF, sesquiterpenoids had been shown to play a neuroprotective role by alleviating oxidative stress, and have significant effects on amyloid-β-triggered cognitive impairment and neuronal abnormalities (Shi et al., 2014; Zhang et al., 2018). In addition, kaempferol (Li et al., 2019), 5-HMF (Liu et al., 2014), and chrysin (Talebi et al., 2021) had been proved to have anti-AD potential. The

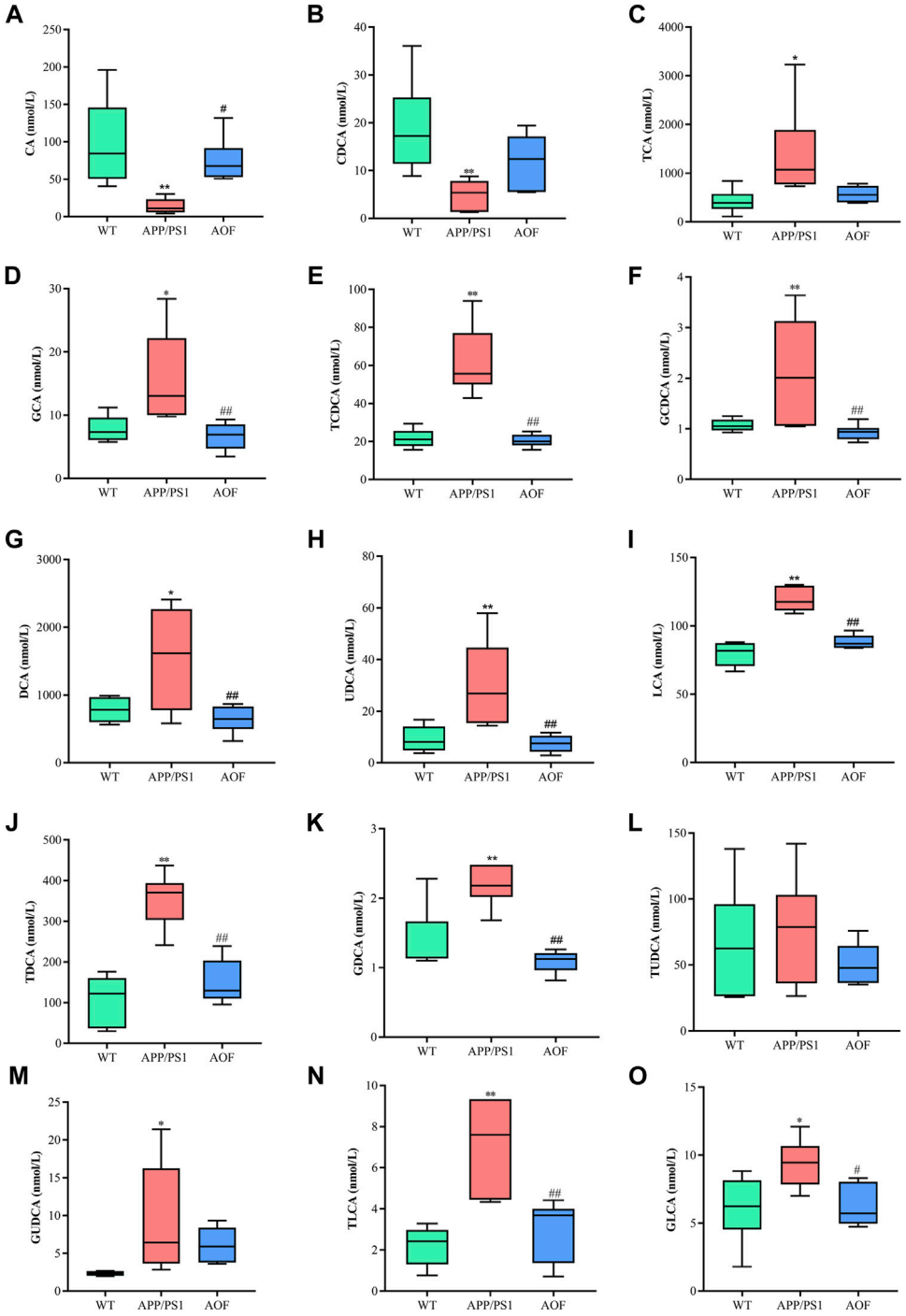

FIGURE 9
AOF reversed most BAs levels in different groups of APP/PS1 mice. **(A–O)** CA, CDCA, TCA, GCA, TCDCA, GCDCA, DCA, UDCA, LCA, TDCA, GDCA, TUDCA, GUDCA, TLCA, and GLCA, respectively. Data are presented as mean ± SEM (n = 6). *p < 0.05, **p < 0.01, compared with WT group; $^{\#}p$ < 0.05, $^{\#\#}p$ < 0.01, compared with APP/PS1 group.

above studies on the material basis of AOF suggested the therapeutic potential and value of AOF for AD.

The classic pathological feature of AD is the abnormal deposition of Aβ in the brain forming a large number of Aβ plaques (Ballard et al., 2011). Mutations in APP and PS1 genes lead to excessive deposition of $A\beta_{42}$ for the purpose of simulating the pathological features of AD (Vassar, 2004), and therefore APP/PS1 mode is recognized worldwide as a transgenic animal model for exploring AD. MWM, the gold standard of AD behavior, is commonly utilized to test the memory and learning ability of rodents. The MWM experiment demonstrated that AOF could improve the learning and memory impairment of APP/PS1 model mice. IHC was used to compare the expression levels of Aβ

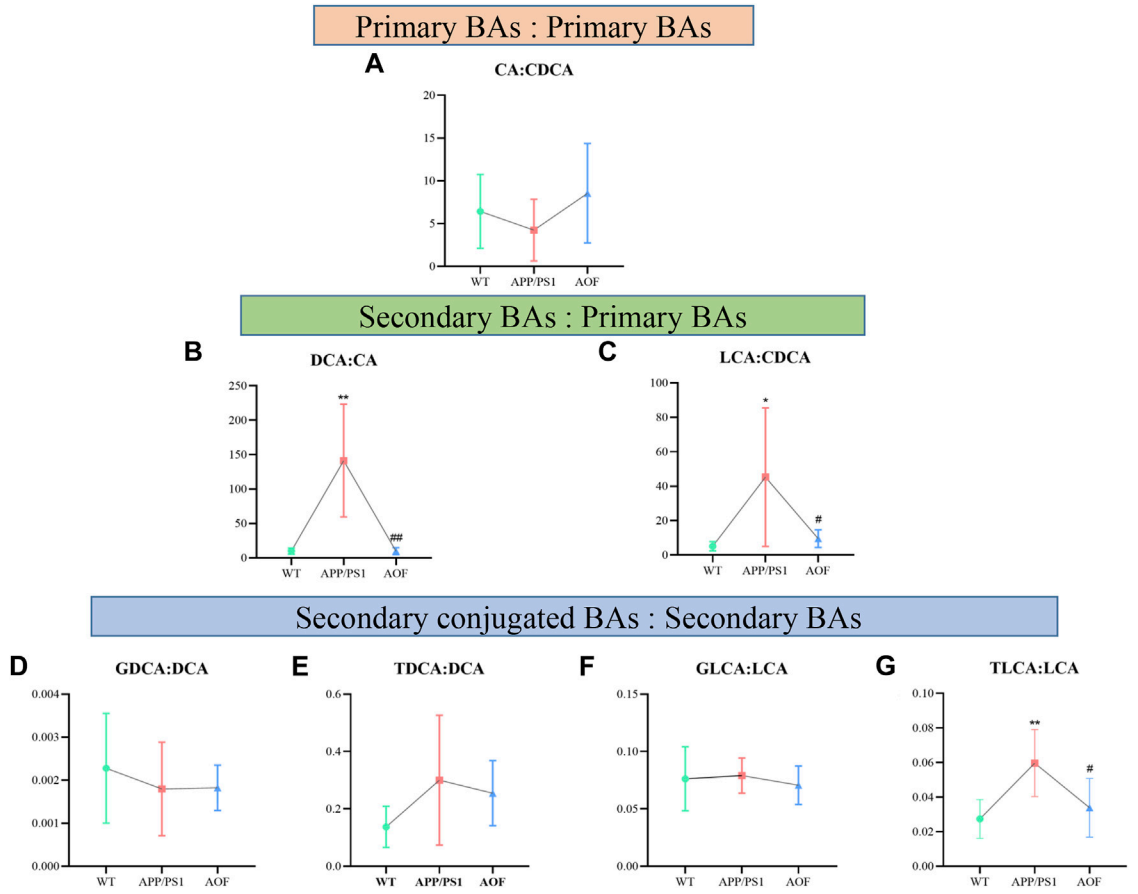

FIGURE 10
Ratios of primary and secondary BAs in different groups of APP/PS1 mice. **(A–G)** CA: CDCA, DCA: CA, LCA: CDCA, GDCA: DCA, TDCA: DCA, GLCA: LCA, and TLCA: LCA, respectively. Data are presented as mean ± SEM (n = 6). *p < 0.05, **p < 0.01, compared with WT group; $^{\#}p$ < 0.05, $^{\#\#}p$ < 0.01, compared with APP/PS1 group.

in the hippocampus and cortex of different groups of mice. The yellow-brown plaques in the APP/PS1 group were considerably more than in other groups. After AOF treatment, the plaques became less numerous and lighter in color. These results suggested that AOF may treat AD by reducing the expression of Aβ. In conclusion, AOF could adjust the behavioral characteristics and reduced the abnormal accumulation of Aβ in the hippocampus and cortex, which provided an experimental basis for the clinical use of AOF in the therapy of AD.

The etiology of AD is complex, and AOF has been commonly used to treat forgetfulness since ancient times. This study attempted to explain the therapeutic effect of AOF in terms of the disturbance and back regulation of potential differential metabolites in plasma. 31 plasma differential metabolites were found between the APP/PS1 and WT groups, 15 of which could be significantly back-regulated by AOF. It mainly involved sphingolipid metabolism, TCA cycle, glycerophospholipid metabolism, tyrosine metabolism, and primary bile acid biosynthesis. Lipids are critical components for maintaining normal cell structure and function, storing energy, and conducting signals (Gaschler and Stockwell, 2017; Wong et al., 2017). Dysregulation of lipid homeostasis is highly associated with neurodegenerative disease AD (Kao et al., 2020). In our study, AOF might improve AD symptoms through sphingolipid, glycerophospholipid, fatty acid, and bile acid metabolic pathways.

Sphinganine (Sa), sphinganine-1-phosphate (Sa1P), sphingosine-1-phosphate (S1P), ceramide (Cer), and phytosphingosine located in the sphingolipid metabolism pathway were all differential metabolites of WT and APP/PS1 groups. Compared with the WT group, Sa, Sa1P, and S1P levels in APP/PS1 group were significantly upregulated. After 3 months of AOF treatment, Sa1P showed a downward trend, and Sa and S1P considerably decreased. Ceramides are sphingolipids with a wide range of biological activities (Di Pardo and Maglione, 2018). Our data showed that the levels of phytosphingosine and cer (d18:0/14:0) in the APP/PS1 group decreased significantly, and the concentration of cer (d18:0/14:0) showed an upward trend after AOF treatment. Previous studies have shown that glycerophospholipid metabolism is closely related to the pathogenesis of AD (Kalli, 2020). Phosphatidylcholine (PC), phosphatidylethanolamine (PE), lysoPC, and lysoPE were located in glycerophospholipid metabolism. It found that increased lysoPC intensifies Aβ deposition and induces neurotoxicity (Sheikh et al., 2015). In our study, lysoPC(17:0), lysoPE (20:2), and lysoPE (22:6) levels increased observably in the APP/PS1 group and decreased markedly after AOF treatment. In the fatty acid metabolic pathway, the levels of palmitic acid, stearic acid, docosahexaenoic acid (DHA), and eicosapentanoic acid (EPA) all prominently escalate in APP/PS1 groups.

After AOF treatment, palmitic acid, stearic acid, and EPA showed a downward trend, while DHA was significantly improved. Palmitic acid and stearic acid have been proven to increase amyloid protein in cortical neurons and promote tau hyperphosphorylation. DHA (Bazan et al., 2011; Petermann et al., 2022) and EPA (Shahidi, 2018) are unique polyunsaturated fatty acids, which can regulate synaptic function and improve salient transmission, and have great significance in neurodegenerative diseases.

BAs eliminate liver cholesterol, a crucial factor in AD. In the liver, cholesterol is converted into the primary bile acids CDCA and CA. Secondary bile acids (DCA, UDCA, LCA) are produced by the dehydrogenation of primary bile acids by 7α-dihydroxylation. AOF might improve AD symptoms because it could regulate probiotics and inhibit pathogenic bacteria. The link between the brain and the gut might be liaised by BAs metabolism.

5 Conclusion

AD is a complex neurodegenerative disease. In this work, we come to three conclusions. 1) AOF could correct the behavior of model mice and reduce the deposition of AB in the brain. 2) Untargeted metabolomics showed that 15 plasma metabolites were significantly back-regulated by AOF, mainly involving the sphingolipid, glycerophospholipid, fatty acid, and bile acid metabolic pathways. 3) After AOF treatment, all BAs showed a correction trend, and most of the metabolites went back significantly. In summary, our study explored the mechanism of action of AOF in treating AD, and provided evidence for BAs as a potential diagnostic indicator for AD.

Data availability statement

The original contributions presented in the study are included in the article/Supplementary Material, further inquiries can be directed to the corresponding author.

Ethics statement

The animal research was approved by The Animal Ethics Committee of Zhengzhou University.

Author contributions

LZ designed the research; SZ, LL, YZ, and ZZ fulfilled the majority of the experiment; SZ wrote the manuscript; HL completed the identification of AOF; FF and JH assisted in completing several experiments; KJ amended the manuscript. All authors have approved the final manuscript.

Funding

This study was supported by the National Natural Science Foundation of China (No.82003921), the National Key R&D Program of China (2021YFC2401105), the National Natural Science Foundation of Henan Province (222,300,420,303), the key research and promotion project of Henan province (222102310082), the Joint project of medical science and technology of Henan Province (LHGJ20190280 and LHGJ20220418), the Open Foundation of Key Laboratory of Digital Technology in Medical Diagnostics of Zhejiang Province (SZZD202216), the key scientific research project of Henan institution of higher education (No. 21A320057), the Joint Construction Project of Henan Medical Science Project (No.SBGJ22002078), and Health Science and Technology Innovation Excellent Talents Training Project for Young and Middle-aged in Henan Province (No.YXKC2020058) and the Foundation of Basic Research for young Teachers of Zhengzhou University (No.JC22862049).

Conflict of interest

The authors declare that the research was conducted in the absence of any commercial or financial relationships that could be construed as a potential conflict of interest.

Publisher's note

All claims expressed in this article are solely those of the authors and do not necessarily represent those of their affiliated organizations, or those of the publisher, the editors and the reviewers. Any product that may be evaluated in this article, or claim that may be made by its manufacturer, is not guaranteed or endorsed by the publisher.

Supplementary material

The Supplementary Material for this article can be found online at: https://www.frontiersin.org/articles/10.3389/fphar.2022.1104954/full#supplementary-material

References

Ballard, C., Gauthier, S., Corbett, A., Brayne, C., Aarsland, D., and Jones, E. (2011). Alzheimer's disease. *Lancet* 377, 1019–1031. doi:10.1016/S0140-6736(10)61349-9

Bazan, N. G., Molina, M. F., and Gordon, W. C. (2011). Docosahexaenoic acid signalolipidomics in nutrition: Significance in aging, neuroinflammation, macular degeneration, Alzheimer's, and other neurodegenerative diseases. *Annu. Rev. Nutr.* 31, 321–351. doi:10.1146/annurev.nutr.012809.104635

Bian, Q. Y., Wang, S. Y., Xu, L. J., Chan, C. O., Mok, D. K. W., and Chen, S. B. (2013). Two new antioxidant diarylheptanoids from the fruits of *Alpinia oxyphylla*. *J. Asian Nat. Prod. Res.* 15, 1094–1099. doi:10.1080/10286020.2013.816297

Bian, Y., Chen, Y., Wang, X., Cui, G., Ung, C. O. L., Lu, J. H., et al. (2021). Oxyphylla A ameliorates cognitive deficits and alleviates neuropathology via the Akt-GSK3β and Nrf2-Keap1-HO-1 pathways *in vitro* and *in vivo* murine models of Alzheimer's disease. *J. Adv. Res.* 34, 1–12. doi:10.1016/j.jare.2021.09.002

Chen, F., Li, H., Li, Y. H., Tan, Y. F., and Zhang, J. Q. (2013). Quantitative analysis of the major constituents in Chinese medicinal preparation SuoQuan formulae by ultra fast high performance liquid chromatography/quadrupole tandem mass spectrometry. *Chem. Central J.* 7, 131. doi:10.1186/1752-153X-7-131

Chen, J., Hao, W., Zhang, C., Cui, M., Sun, Y., Zhang, Y., et al. (2022). Explore the therapeutic composition and mechanism of schisandra chinensis-acorus tatarinowii schott on Alzheimer's disease by using an integrated approach on chemical profile, network pharmacology, and UPLC-QTOF/MS-Based metabolomics analysis. *Oxidative Med. Cell. Longev.* 2022, 6362617–6362620. doi:10.1155/2022/6362617

Cryan, J. F., O Riordan, K. J., Cowan, C. S. M., Sandhu, K. V., Bastiaanssen, T. F. S., Boehme, M., et al. (2019). The microbiota-gut-brain Axis. *Physiol. Rev.* 99, 1877–2013. doi:10.1152/physrev.00018.2018

Di Pardo, A., and Maglione, V. (2018). Sphingolipid metabolism: A new therapeutic opportunity for brain degenerative disorders. *Front. Neurosci.* 12, 249. doi:10.3389/fnins.2018.00249

Doifode, T., Giridharan, V. V., Generoso, J. S., Bhatti, G., Collodel, A., Schulz, P. E., et al. (2021). The impact of the microbiota-gut-brain axis on Alzheimer's disease pathophysiology. *Pharmacol. Res.* 164, 105314. doi:10.1016/j.phrs.2020.105314

Gaschler, M. M., and Stockwell, B. R. (2017). Lipid peroxidation in cell death. *Biochem. Biophysical Res. Commun.* 482, 419–425. doi:10.1016/j.bbrc.2016.10.086

Ju, Y., and Tam, K. Y. (2022). Pathological mechanisms and therapeutic strategies for Alzheimer's disease. *Neural Regen. Res.* 17, 543–549. doi:10.4103/1673-5374.320970

Kalli, E. (2020). "Nutritional lipidomics in Alzheimer's disease,". GeNeDis 2018 *advances in experimental medicine and biology*. Editor P. Vlamos (Cham: Springer International Publishing), 95–104. doi:10.1007/978-3-030-32633-3_14

Kao, Y. C., Ho, P. C., Tu, Y. K., Jou, I. M., and Tsai, K. J. (2020). Lipids and Alzheimer's disease. *IJMS* 21, 1505. doi:10.3390/ijms21041505

Lane, C. A., Hardy, J., and Schott, J. M. (2018). Alzheimer's disease. *Eur. J. Neurol.* 25, 59–70. doi:10.1111/ene.13439

Li, H., Tan, Y., Cheng, X., Zhang, Z., Huang, J., Hui, S., et al. (2022a). Untargeted metabolomics analysis of the hippocampus and cerebral cortex identified the neuroprotective mechanisms of Bushen Tiansui formula in an aβ25-35-induced rat model of Alzheimer's disease. *Front. Pharmacol.* 13, 990307. doi:10.3389/fphar.2022.990307

Li, J., Du, Q. Z., Li, N., Du, S. Z., and Sun, Z. (2021). Alpiniae oxyphyllae Fructus and Alzheimer's disease: An update and current perspective on this traditional Chinese medicine. *Biomed. Pharmacother.* 135, 111167. doi:10.1016/j.biopha.2020.111167

Li, R., Wang, L., Zhang, Q., Duan, H., Qian, D., Yang, F., et al. (2022b). Alpiniae oxyphyllae fructus possesses neuroprotective effects on H_2O_2 stimulated PC_{12} cells via regulation of the PI3K/Akt signaling Pathway. *Front. Pharmacol.* 13, 966348. doi:10.3389/fphar.2022.966348

Li, W. H., Cheng, X., Yang, Y. L., Liu, M., Zhang, S. S., Wang, Y. H., et al. (2019). Kaempferol attenuates neuroinflammation and blood brain barrier dysfunction to improve neurological deficits in cerebral ischemia/reperfusion rats. *Brain Res.* 1722, 146361. doi:10.1016/j.brainres.2019.146361

Liu, A., Zhao, X., Li, H., Liu, Z., Liu, B., Mao, X., et al. (2014). 5-Hydroxymethylfurfural, an antioxidant agent from Alpinia oxyphylla Miq. improves cognitive impairment in Aβ1–42 mouse model of Alzheimer's disease. *Int. Immunopharmacol.* 23, 719–725. doi:10.1016/j.intimp.2014.10.028

Liu, H., Wang, X., Shi, Q., Li, L., Zhang, Q., Wu, Z. L., et al. (2020). Dimeric diarylheptanoids with neuroprotective activities from rhizomes of *Alpinia officinarum*. *ACS Omega* 5, 10167–10175. doi:10.1021/acsomega.0c01019

MahmoudianDehkordi, S., Moseley, M. A., Thompson, J. W., St John Williams, L., Tenenbaum, J. D., Xie, G., et al. (2019). Altered bile acid profile associates with cognitive impairment in Alzheimer's disease—an emerging role for gut microbiome. *Alzheimer's Dementia* 15, 76–92. doi:10.1016/j.jalz.2018.07.217

Mulak, A. (2021). Bile acids as key modulators of the brain-gut-microbiota Axis in Alzheimer's disease. *JAD* 84, 461–477. doi:10.3233/JAD-210608

Nho, K., Kueider-Paisley, A., MahmoudianDehkordi, S., Arnold, M., Risacher, S. L., Louie, G., et al. (2019). Altered bile acid profile in mild cognitive impairment and Alzheimer's disease: Relationship to neuroimaging and CSF biomarkers. *Alzheimer's Dementia* 15, 232–244. doi:10.1016/j.jalz.2018.08.012

Nielsen, J. (2017). Systems biology of metabolism. *Annu. Rev. Biochem.* 86, 245–275. doi:10.1146/annurev-biochem-061516-044757

Petermann, A. B., Reyna-Jeldes, M., Ortega, L., Coddou, C., and Yévenes, G. E. (2022). Roles of the unsaturated fatty acid docosahexaenoic acid in the central nervous system: Molecular and cellular insights. *IJMS* 23, 5390. doi:10.3390/ijms23105390

Qi, Y., Cheng, X., Jing, H., Yan, T., Xiao, F., Wu, B., et al. (2019). Effect of Alpinia oxyphylla—schisandra chinensis herb pair on inflammation and apoptosis in Alzheimer's disease mice model. *J. Ethnopharmacol.* 237, 28–38. doi:10.1016/j.jep.2019.03.029

Scheltens, P., De Strooper, B., Kivipelto, M., Holstege, H., Chételat, G., Teunissen, C. E., et al. (2021). Alzheimer's disease. *Lancet* 397, 1577–1590. doi:10.1016/S0140-6736(20)32205-4

Shahidi, F., and Ambigaipalan, P. (2018). Omega-3 polyunsaturated fatty acids and their Health benefits. *Annu. Rev. Food Sci. Technol.* 9, 345–381. doi:10.1146/annurev-food-111317-095850

Sheikh, A. Md., Michikawa, M., Kim, S. U., and Nagai, A. (2015). Lysophosphatidylcholine increases the neurotoxicity of Alzheimer's amyloid β1-42 peptide: Role of oligomer formation. *Neuroscience* 292, 159–169. doi:10.1016/j.neuroscience.2015.02.034

Shi, S. H., Zhao, X., Liu, B., Li, H., Liu, A. J., Wu, B., et al. (2014). The effects of sesquiterpenes-rich extract of *Alpinia oxyphylla* Miq. On amyloid-β-induced cognitive impairment and neuronal abnormalities in the cortex and Hippocampus of mice. *Oxidative Med. Cell. Longev.* 2014, 451802–451811. doi:10.1155/2014/451802

Talebi, M., Talebi, M., Farkhondeh, T., Kopustinskiene, D. M., Simal-Gandara, J., Bernatoniene, J., et al. (2021). An updated review on the versatile role of chrysin in neurological diseases: Chemistry, pharmacology, and drug delivery approaches. *Biomed. Pharmacother.* 141, 111906. doi:10.1016/j.biopha.2021.111906

Vassar, R. (2004). BACE1: The β-secretase enzyme in Alzheimer's disease. *JMN* 23, 105–114. doi:10.1385/JMN:23:1-2:105

Wang, H., Dai, J. Y., He, Y. Z., Xia, Z. W., Chen, X. F., Hong, Z. Y., et al. (2022). Therapeutic effect and mechanism of Anemarrhenae Rhizoma on Alzheimer's disease based on multi-platform metabolomics analyses. *Front. Pharmacol.* 13, 940555. doi:10.3389/fphar.2022.940555

Weller, J., and Budson, A. (2018). Current understanding of Alzheimer's disease diagnosis and treatment. *F1000Res* 7, F1000 Faculty Rev-1161. doi:10.12688/f1000research.14506.1

Wong, M. W., Braidy, N., Poljak, A., Pickford, R., Thambisetty, M., and Sachdev, P. S. (2017). Dysregulation of lipids in Alzheimer's disease and their role as potential biomarkers. *Alzheimer's Dementia* 13, 810–827. doi:10.1016/j.jalz.2017.01.008

Yang, X., Yang, Y., Chen, H., Xu, T., Li, C., Zhou, R., et al. (2020). Extraction, isolation, immunoregulatory activity, and characterization of Alpiniae oxyphyllae fructus polysaccharides. *Int. J. Biol. Macromol.* 155, 927–937. doi:10.1016/j.ijbiomac.2019.11.051

Zhang, Q., Zheng, Y., Hu, X., Hu, X., Lv, W., Lv, D., et al. (2018). Ethnopharmacological uses, phytochemistry, biological activities, and therapeutic applications of Alpinia oxyphylla miquel: A review. *J. Ethnopharmacol.* 224, 149–168. doi:10.1016/j.jep.2018.05.002

Zhang, Z., Yi, P., Yang, J., Huang, J., Xu, P., Hu, M., et al. (2020). Integrated network pharmacology analysis and serum metabolomics to reveal the cognitive improvement effect of Bushen Tiansui formula on Alzheimer's disease. *J. Ethnopharmacol.* 249, 112371. doi:10.1016/j.jep.2019.112371

Zuo, L., Li, J., Xue, L., Jia, Q., Li, Z., Zhang, M., et al. (2021). Integrated UPLC-MS/MS and UHPLC-Q-orbitrap HRMS analysis to reveal pharmacokinetics and metabolism of five terpenoids from Alpiniae oxyphyllae fructus in rats. *CDM* 22, 70–82. doi:10.2174/1389200221666201217154219

Frontiers in Pharmacology

Explores the interactions between chemicals and living beings

The most cited journal in its field, which advances access to pharmacological discoveries to prevent and treat human disease.

Discover the latest Research Topics

See more →

Frontiers

Avenue du Tribunal-Fédéral 34
1005 Lausanne, Switzerland
frontiersin.org

Contact us

+41 (0)21 510 17 00
frontiersin.org/about/contact